UNIVERSITY OF LONDON THESIS

Degree PhD Year 2007 Name of Author GUETTLER, Sebastian

Regulation of the SRF cofactor MAL by actin

Sebastian Guettler

This thesis is submitted in partial fulfilment of the requirements for the degree of Doctor of Philosophy from the University of London.

2007

Transcription Laboratory
Cancer Research UK London Research Institute
44 Lincoln's Inn Fields
London
WC2A 3PX

University College London
Gower Street
London
WC1E 6BT

ProQuest LLC
789 East Eisenhower Parkway
P.O. Box 1346
Ann Arbor, MI 48106-1346

Declaration

Part of the work presented in this thesis was performed in collaboration:

Fluorescence loss in photobleaching (FLIP) and Förster resonance energy transfer (FRET) analyses presented in Figures 3.5, 3.6, 4.3, 4.4 and 4.11 are the work of Maria Vartiainen.

The CD spectroscopy data shown in Figure 2.6 were kindly provided by Bernard O'Hara, Birkbeck College, London.

The structural analysis presented in Chapters 5 and 6 is the result of a collaboration with Stéphane Mouilleron from Neil McDonald's laboratory at the Institute. Of the work presented, I established and routinely prepared MAL/RPEL-actin complexes for crystallisation and was involved in the initial screens. Stéphane performed the majority of the crystallisation screens, all of the optimisation work at the crystallisation stage, collected the X-ray diffraction data and solved the crystal structures. The structures were interpreted together. Where analyses were done primarily by Stéphane, this is indicated in the legends. Stéphane also gave much-appreciated assistance in preparing structural representations shown in this thesis.

All other experiments presented in this thesis were performed by the author.

Sebastian Güttler

September 2007

Abstract

Serum Response Factor (SRF) is controlled by actin dynamics at many of its target genes: Rho-induced depletion of G-actin is sensed by MAL, a member of the myocardin family of SRF coactivators. MAL binds G-actin via its N-terminus, the "RPEL domain", containing three RPEL motifs. MAL rapidly circulates between nucleus and cytoplasm in resting NIH3T3 fibroblasts. It accumulates in the nucleus and activates SRF upon serum stimulation, which alters interactions between G-actin and the RPEL domain. In contrast, myocardin (MC) itself is constitutively nuclear and active when expressed in fibroblasts, suggesting that it is not controlled through Rho. This thesis addresses the mode and functions of actin binding by myocardin-family proteins.

Actin binding targets MAL for efficient CRM1-mediated nuclear export. Nuclear accumulation of MAL is not sufficient for activation of SRF-mediated transcription unless an inhibitory MAL-actin interaction in the nucleus is released. Actin therefore fulfils a dual role in MAL regulation by controlling MAL localisation as well as activity.

The MAL RPEL domain is sufficient to confer actin-regulated nucleocytoplasmic trafficking and binds multiple actin molecules, efficiently sequestering them from polymerisation. Actin-binding toxins directly interfere with the MAL-actin complex. The RPEL motif represents an actin-binding unit: affinities of MAL RPEL motifs 1 and 2 for actin are relatively high while RPEL3 binds actin weakly. RPEL motifs cooperate to regulate MAL. The regulatory contribution of an RPEL3-actin interaction depends on actin binding by the RPEL1-2 unit, differences in which account for differential regulation of MAL and MC, which binds actin weakly. A model of MAL regulation by differential actin occupancy of multiple RPEL motifs is proposed.

Crystal structures of MAL RPEL motifs 1 and 2 bound to G-actin were obtained. RPEL motifs maintain hydrophobic interactions with a hydrophobic cleft at the subdomain 1-3 interface of actin and a "platform" on subdomain 3, both at the "base" of the actin molecule in its conventional view (Kabsch et al., 1990). The RPEL motif also establishes critical polar interactions with actin. Conservation of the RPEL motif reflects actin binding. The structures rationalise RPEL-actin affinities and competition of actin-binding toxins and profilin with MAL. A crystal structure of the MAL RPEL domain bound to three actin molecules revealed an additional actin-binding site within the RPEL1-2 linker and actin-actin contacts in the RPEL domain-actin complex.

To my parents and grandparents

Acknowledgements

I thank Richard for giving me the opportunity to work in his lab, for his supervision, creativity and continuous support.

I thank Maria, whom it was great to work with, for teaching me the mysteries of actin and for having the nose for the right experiment.

Many thanks go to Stéphane for a very enjoyable collaboration, interesting discussions, help with figures and everything he taught me about structural biology.

I thank everyone in the lab for making the past four years happy and instructive. Thanks to Rob for his great help in the day-to-day lab business, for solving (almost) every problem, just like MacGyver, and for fruitful conversations about biochemistry, Guido for helping me to get started in the lab and Cisco for his insights. Special thanks go to Fiona for her invaluable assistance. I also thank Patrick, Alexia, Souhila, Tamara, Anastasia, Cristina, Masafumi, Jane, Sara and past members of the lab. I thank Tamara, Maria, Souhila, Carola and Rafal for comments on various bits and pieces of the following pages.

Many thanks go to Neil for his support and advice and helpful comments on Chapters 5 and 6 of this thesis, and his group, especially Phil, John, Rachel, Maureen, Becky and Andy for help and reagents. I also thank Michael and Caroline and their labs for critical and constructive discussions and helpful advice.

A big 'thank you' to Nicola O'Reilly and the peptide synthesis lab for outstanding work and everyone in the Equipment Park for their expert assistance. I thank Bernhard O'Hara for the CD spectroscopy experiment and Rose Watson for the electron micrographs of actin. Many thanks also to the London Research Institute services, who facilitated this work tremendously.

Thanks to the many friends who made working here special, including Thomas for thesis-writing pub lunches on Saturdays, Julia for the music and Andreas for the side project of figuring out where our cycling routes intersect.

Most importantly, I am grateful to my family for all their support over the years, especially my parents and grandparents and my twin brother Thomas.

I thank Cancer Research UK and the Boehringer Ingelheim Fonds for enabling and funding this work. Special thanks to the B.I.F. for their much-appreciated personal assistance! I also thank the "Studienstiftung des deutschen Volkes" for giving me the chance to participate in their student meetings.

Publications

Some of the results described in this thesis have been presented in the following publications:

Posern, G., Miralles, F., Guettler, S., and Treisman, R. (2004). Mutant actins that stabilise F-actin use distinct mechanisms to activate the SRF coactivator MAL. Embo J *23*, 3973-3983.

Vartiainen, M. K.*, Guettler, S.*, Larijani, B., and Treisman, R. (2007). Nuclear actin regulates dynamic subcellular localization and activity of the SRF cofactor MAL. Science *316*, 1749-1752.

Guettler, S., Vartiainen, M. K., Miralles, F., Larijani, B., and Treisman, R. (2007). RPEL motifs link the SRF cofactor MAL but not myocardin to Rho signalling via actin binding. *accepted (Molecular and Cellular Biology, MCB; 2 Nov 2007)*

A manuscript addressing the structural basis of RPEL-actin interactions is in preparation.

Abbreviations

α-	anti- (in Western blotting)
aa	amino acid
ADF	actin-depolymerising factor
ADP	adenosine diphosphate
APS	ammonium persulfate
Arp	actin-related protein
ATP	adenosine triphosphate
bp	base pair
BSA	bovine serum albumin
BSAC	basic, SAP, and coiled-coil domain
BTP	3-bis[tris(hydroxymethyl)methylamino]propane
cAMP	cyclic adenosine monophosphate
C_c	critical concentration of actin
CD	cytochalasin D (also circular dichroism)
cDNA	complementary DNA
ChIP	chromatin immunoprecipitation
CIP	calf intestinal phosphatase
cpm	counts per minute
CRM1	Chromosome Region Maintenance (Exportin 1)
C_T	threshold cycle
Da	Dalton
CV	column volume
DBP	vitamin-D binding protein
DMEM	Dulbecco/Vogt Modified Eagle's minimal media
DMF	dimethyl formamide
DMSO	dimethyl sulfoxide
DNA	deoxyribonucleic acid
DNase	deoxyribonuclease
dNTP	deoxy-nucleotide triphosphate
DTT	dithiothreitol
E	embryonic (day)
ECL	enhanced chemoluminescence
EDTA	ethylendiaminotetraacetic acid

EGTA	ethylenbis(oxyethylnitrilo)tetraacetic acid
EMSA	electrophoretic mobility shift assay
Ena/VASP	enabled / vasodilator-stimulated phosphoprotein
ES	embryonic stem (cell)
ESRF	European Synchrotron Radiation Facility
FA	fluorescence anisotropy
F-actin	filamentous actin
FCS	foetal calf serum
FITC	fluorescein
FLIM	fluorescence lifetime imaging
FLIP	fluorescence loss in photobleaching
FPLC	fast protein liquid chromatography
FRET	Förster resonance energy transfer
G-actin	globular (monomeric) actin
Gapdh	glyceraldehyde-3-phosphate dehydrogenase
GFP	green fluorescent protein
GST	glutathione S-transferase
GTP	guanosine triphosphate
GTPase	GTP hydrolase
HA	hemagglutinin
HEPES	4-(2-hydroxyethyl)-1-piperazineethanesulfonic acid
HRP	horseradish peroxidase
IP	immunoprecipitation
IPTG	isopropyl β-D-1-thiogalactopyranoside
Jasp	jasplakinolide
K_d	dissociation constant
LatA	latrunculin A
LatB	latrunculin B
LB	Luria-Bertaini (media)
LIMK	LIM kinase
LMB	leptomycin B
MADS	MCM1, AG, DEFA, SRF (founding members; see p. 59)
MAL	Megakaryocytic Acute Leukaemia
MAPK	mitogen-activated protein kinase
MKL	Megakaryoblastic Leukaemia

MC	myocardin
MCS	multiple cloning site
MEF2	myocyte enhancer factor 2
MEM	Modified Eagle's minimal media
MES	2-(n-morpholino)-ethanesulfonic acid
MIM	Missing-In-Metastasis
MME	monomethyl ether
MOPS	3-N-morpholinopropanesulphonic acid
mRNA	messenger RNA
mRNP	messenger ribonucleoprotein particle
MRTF	myocardin-related transcription factor
MWCO	molecular weight cutoff
NP40	Nonidet P40
NPF	nucleation-promoting factor

Nucleotides:

A	adenosine
C	cytosine
G	guanosine
N	nucleotide
T	thymidine

OD	optical density
PAGE	polyacrylamide gel electrophoresis
PBS	phosphate-buffered saline
PCR	polymerase chain reaction
PEG	polyethylene glycol
PES	polyethersulfone
PFAM	protein family database (http://pfam.sanger.ac.uk/)
$PI(4,5)P_2$	phosphatidylinositol(4,5)-bisphosphate
PK	pyruvate kinase
PMSF	phenylmethylsulfonyl fluoride
RNA	ribonucleic acid
ROCK	Rho kinase or Rho-associated coiled-coil-containing protein kinase

RPEL	motif name (RPxxxEL); PFAM 02755
rpm	revolutions per minute
Scar/WAVE	suppressor of cAMP receptor / WASP-family verprolin homologous protein
SD	standard deviation
SDS	sodium dodecyl sulfate
SEM	standard error mean
SRE	Serum Response Element
SRF	Serum Response Factor
SwA	swinholide A
TBE	Tris – boric acid – EDTA
TCF	Ternary Complex Factor
TE	Tris – EDTA
TEMED	N,N,N',N'-tetramethylethylenediamine
TEN	Tris – EDTA – NaCl
TMR	tetramethylrhodamine
Tris	2-amino-2-hydroxymethyl-1,3-propanediol
TX-100	triton X-100
U	unit
UTR	untranslated region
VASP	vasodilator-stimulated phosphoprotein
VCA	verprolin homology (=WH2); connecting or cofilin-like; acidic
v/v	volume to volume
WASP	Wiskott-Aldrich Syndrome protein
WAVE	WASP-family verprolin homologous protein
WB	Western blot
WH2	WASP-homology 2
WIP	WASP-interacting protein
WT	wild-type
w/v	weight to volume

The standard single-letter amino-acid code and the International System of units (SI) were used.

Table of contents

List of figures

List of tables

1 Introduction

1.1 Regulation of transcription in response to signals

Cells respond to specific extracellular and intracellular signals, frequently within minutes, by initiating specific signalling pathways, many of which control gene expression at the level of transcription. Fast and coordinated responses require sensitive and efficient machineries that can be activated in a reversible fashion. In eukaryotic cells, commonly employed regulatory principles include nucleocytoplasmic transport of gene-regulatory proteins, posttranslational modification resulting in inhibition or activation, controlled proteolytic degradation, liberation from sequestering compartments, for example by regulated proteolysis of their anchor, *de-novo* synthesis and cell-lineage specific expression of transcriptional regulators. In this section, I will briefly present examples of these recurring modes of transcriptional control.

1.1.1 Regulation of transcription factors and their regulators by nucleocytoplasmic transport

The access of numerous transcriptional regulators to chromatin is controlled at the level of nuclear localisation. Gene-regulatory proteins can be excluded from the cell nucleus in their inactive state and allowed access only when their activity is needed.

1.1.1.1 Mechanism of nucleocytoplasmic transport

Proteins of about 30-40 kDa or larger require an active transport machinery to traverse the nuclear pores embedded within the nuclear envelope, although proteins that are smaller than that are frequently transported in an active, regulated fashion (reviewed in Görlich and Kutay, 1999). Dedicated nuclear transport receptors, either importins or exportins, mediate the transport of cargo proteins into or out of the nucleus, respectively. They achieve this by overcoming the permeability barrier imposed by the nuclear pore. According to one model, transport receptors "melt" their way through the nuclear pore by competing with hydrophobic contacts that occur within a gel-like meshwork of phenylalanine-glycine rich (FG-) repeats formed by nuclear pore components (Frey et al., 2006). Most import and export receptors are members of the importin β family (reviewed in Görlich and Kutay, 1999). While importins bind their

cargo in the cytoplasm and release it in the nucleus, exportins do the reverse. In both cases, transport receptors have to relocate into their original compartment to engage in another transport cycle.

Coordinated transport requires directionality information as well as energy. Both are provided by the small GTPase Ran: energy is released by hydrolysis of GTP whereas directionality is conferred by a gradient of Ran-GTP with its highest concentrations in the cell nucleus and its lowest in the cytoplasm. The Ran gradient has been visualised using FRET-based biosensors (Kalab et al., 2002). The gradient is brought about by RCC1 (regulator of chromosome condensation), a Ran-GEF (guanine nucleotide exchange factor) associated with chromatin in the cell nucleus and Ran-GAP (GTPase-activating protein) in the cytoplasm. Exportins require an interaction with Ran-GTP for productive, cooperative binding of their cargo in the cell nucleus. Following their passage through the nuclear pore, trimeric export complexes are disassembled in the cytoplasm by the activation of the GTPase activity of Ran through a Ran-GAP. Importins are able to bind their cargo within the cytoplasm without the need of Ran. In the cell nucleus, Ran-GTP binds to the importin, thereby dissociating the import complex (reviewed in Görlich and Kutay, 1999).

Cofactor-mediated nuclear import and export depends on targeting sequences within the transport substrates. These signals are generally thought to consist of small signal peptides that can confer their transport properties on heterologous proteins (reviewed in Weis, 2003). Lysine-rich nuclear localisation signals (NLSs), originally identified in the SV40 large T antigen (Kalderon et al., 1984; Lanford and Butel, 1984), are substrates of the importin α/β dimer (reviewed in Görlich and Kutay, 1999). Leucine-rich nuclear export signals (NESs), originally identified in the HIV Rev protein and PKI (Fischer et al., 1995; Wen et al., 1995), are recognised by the export receptor exportin 1 / CRM1 (reviewed in Görlich and Kutay, 1999). STAT1, for example, is a substrate for both importin-α5 (McBride et al., 2002) and CRM1 (Marg et al., 2004) (see below). Smad4 is exported by CRM1 (Pierreux et al., 2000; Watanabe et al., 2000, and see below).

It was proposed that some signalling molecules are imported into the nucleus by importin-independent mechanisms (reviewed in Xu and Massague, 2004). This proposal is based on experiments with digitonin-permeabilised cells, in which nuclear import does not require the addition of cytosolic extract as a source of import factors (reviewed in Xu and Massague, 2004). Examples include β-catenin (Yokoya et al., 1999), Smad2,

3 and 4 (Xu et al., 2003; Xu et al., 2000), ERK2 (Matsubayashi et al., 2001; Whitehurst et al., 2002) and STAT proteins (see below). While the exact mechanism of their passage through the nuclear pore is unclear, it is thought that they can directly interact with nucleoporins without the assistance of a transport receptor.

1.1.1.2 Nucleocytoplasmic shuttling of STATs

STAT proteins (signal transducers and activators of transcription) represent one example of regulated nucleocytoplasmic transport of transcriptional regulators. In resting cells, STATs appear cytoplasmic. Instead of being statically anchored in the cytoplasm in their resting state, STATs constantly shuttle between nucleus and cytoplasm, and their localisation is determined by the steady state of nuclear import and export (reviewed in Meyer and Vinkemeier, 2004). Upon cytokine or growth-factor stimulation, receptor-associated Janus kinases (JAKs) phosphorylate a single tyrosine residue at the C-terminus of STAT proteins recruited to the membrane receptors (Shuai et al., 1993). STATs then form dimers by reciprocal engagement of their SH2 domains with their phosphotyrosine sites *in trans*. Phosphorylated, dimeric STATs accumulate in the cell nucleus, where they bind so-called gamma-activated sites (GAS) in the promoters of cytokine-responsive genes (reviewed in Levy and Darnell, 2002; Meyer and Vinkemeier, 2004). STATS are *bona-fide* transcription factors that activate these genes.

Nucleocytoplasmic shuttling of STATs occurs via different mechanisms. Irrespectively of cytokine stimulation, cycling of unphosphorylated STATs is maintained, in part, by a carrier-independent mechanism. Additionally, nuclear export of unphosphorylated STATs can occur in a constitutive, CRM1-dependent fashion (reviewed in Meyer and Vinkemeier, 2004). A carrier-dependent nuclear import pathway for STATs becomes operational upon activation of JAK-STAT signalling and STAT dimerisation: nuclear import of tyrosine-phosphorylated and therefore dimeric STATs requires the Ran-dependent importin α - importin β system (Sekimoto et al., 1997; Sekimoto et al., 1996). A nuclear localisation signal of tyrosine-phosphorylated STATs, located within the DNA-binding domain, is specific to the STAT dimer (Fagerlund et al., 2002; McBride et al., 2002). Despite this additional mechanism of nuclear import, carrier-independent transport of STATs remains operational even in

stimulated cells as only about 30% of the STAT pool become tyrosine-phosphorylated upon induction of signalling (reviewed in Meyer and Vinkemeier, 2004).

Interestingly, cytokine stimulation results in nuclear retention of STAT dimers rather than a change of nuclear import kinetics despite the switch in the import mechanism (reviewed in Meyer and Vinkemeier, 2004). Tyrosine-phosphorylated, and therefore dimeric, STATs are not exported from the nucleus (Meyer et al., 2004; Meyer et al., 2003). However, nuclear, tyrosine-phosphorylated STATs are rapidly dephosphorylated by a nuclear phosphatase, and this renders STATs capable of exiting the nucleus again (Meyer et al., 2003; reviewed in Meyer and Vinkemeier, 2004). DNA-bound STATs are resistant to dephoshorylation; hence, the rate of de-phosphorylation of STATs is determined by the off-rate of DNA binding.

The example of STAT regulation illustrates how phosphorylation and dephosphorylation can control nucleocytoplasmic transport and activity of a class of transcription factors.

1.1.1.3 Nucleocytoplasmic shuttling of Smads

Transforming growth factor β (TGF-β) signalling holds another example of localisation-controlled transcriptional regulators (reviewed in Shi and Massague, 2003). TGF-β signals through type II and type I receptors with serine/threonine-kinase activity. Ligand binding assembles the TGF-β type I receptor with the constitutively active type II receptor. The type I receptor becomes phosphorylated and activated through phosphorylation by the type II receptor and subsequently recruits and phosphorylates cytoplasmic, receptor-regulated R-Smad proteins such as Smad2 and Smad3. R-Smad recruitment can be facilitated by the auxiliary protein SARA (Smad anchor for receptor activation), which targets R-Smads to the membrane and the type II receptor (Tsukazaki et al., 1998). Phosphorylated R-Smads form complexes with Smad4, which can be dimeric or trimeric. These complexes accumulate in the nucleus, where they control gene transcription via different transcription factors, coactivators and corepressors in a context- and cell-type specific manner (reviewed in Derynck and Zhang, 2003 and ten Dijke and Hill, 2004).

Regulatory principles similar to those seen in the case of STATs appear to operate in the control of Smad nucleocytoplasmic transport. Although in quiescent cells Smads appear predominantly cytoplasmic, they constantly shuttle between nucleus and cytoplasm, and likewise their steady-state localisation is a consequence of a dynamic

equilibrium (Inman et al., 2002). Smads retain shuttling behaviour upon activation of TGF-β signalling (Inman et al., 2002). Nuclear accumulation of Smad2 results exclusively from decreased nuclear export rather than a change in nuclear import, presumably by nuclear trapping of the phosphorylated, complexed protein (Schmierer and Hill, 2005).

In both the STAT and the Smad examples, constant nucleocytoplasmic shuttling enables these signal transducers to monitor the activation state of their upstream receptors. Therefore, nuclear events remain sensitive to the activity of membrane receptors.

1.1.2 Regulation by combinatorial interactions of transcriptional regulators

1.1.2.1 The interferon-β enhanceosome

A classical and well-understood example of combinatorial transcriptional regulation is given by the assembly of an active transcription-factor complex on the enhancer of the interferon-β (IFN-β) gene in response to virus infection (see Panne et al., 2007, and references therein). The IFN-β enhancer contains three distinct positive regulatory elements for different transcription factors: NF-κB (nuclear factor-κB), IRF (interferon regulatory factor) family members and the heterodimer of ATF-2 (activating transcription factor-2) and c-Jun. Each of these transcription factors controls distinct transcriptional programmes, but in concert, they strongly activate the IFN-β gene (Thanos and Maniatis, 1995). Concurrent DNA binding and interaction between the transcription factors result in a high degree of positive cooperativity in the formation of a stable nucleoprotein complex termed "enhanceosome" (Panne et al., 2007). Loss of any of the interactions greatly impairs activation of the IFN-β gene.

1.1.2.2 Other examples

Smads (discussed above in Section 1.1.1.3) bind DNA weakly or not at all and therefore do not represent autonomous transcriptional regulators. Instead, they act as co-regulators of multiple sequence-specific transcription factors, coactivators and co-repressors (reviewed in Derynck and Zhang, 2003), and this contributes to the many

context- and cell-type-specific Smad-mediated programmes of TGF-β signalling (see Shi and Massague, 2003).

The interaction of Serum Response Factor (SRF) with at least two classes of cofactors, which are regulated by different signalling pathways, represents another example for how specificity is conferred to transcriptional responses (see below in Section 1.3.5).

1.1.3 Activation or inhibition of transcriptional regulators by phosphorylation

Phosphorylation is a heavily employed mechanism of cell signalling as highlighted by the fact that the human genome encodes 518 putative protein kinases (Manning et al., 2002). Protein phosphorylation can occur on serine or threonine, tyrosine and histidine residues. Modification of serine/threonine represents the most abundant type of protein phosphorylation, followed by tyrosine phosphorylation. Little is known about phosphorylation at histidine residues, which has been described in prokaryotes, lower eukaryotes and plants and is known to occur in mammals as well (Besant et al., 2003). Phosphorylation can regulate transcription factors either positively or negatively by multiple mechanisms.

1.1.3.1 Phosphorylation-controlled nucleocytoplasmic transport

Phosphorylation is frequently seen to control nucleocytoplasmic transport of transcriptional regulators, as illustrated above by the examples of STATs and Smads (see Section 1.1.1). In the case of STATs, phosphorylation not only impinges on nucleocytoplasmic transport but also enables STATs to bind DNA through inducing their dimerisation.

1.1.3.2 Phosphorylation-induced degradation of inhibitors

Phosphorylation can target proteins that, by physical interaction, keep transcriptional regulators in an inhibited state. A classical example is the control of NF-κB (reviewed in Hayden and Ghosh, 2004). The five mammalian NF-κB proteins form homo- or heterodimers in unstimulated cells, whose steady-state cytoplasmic

localisation is achieved by interaction with IκB (inhibitory κB) family proteins. Extracellular signals, for example tumour necrosis factor α (TNFα), stimulate the activity of the IKK (IκB kinase) complex, which phosphorylates IκB, thereby targeting it for polyubiquitination and proteasomal degradation (DiDonato et al., 1997). NF-κB is then allowed to accumulate in the nucleus and activate transcription of numerous genes. The presence of accessible nuclear import and export signals in at least some IκB-NF-κB complexes allows them to dynamically shuttle between nucleus and cytoplasm, even in the uninduced state. Signal-induced nuclear accumulation of NF-κB is conferred by changes in the import-export balance upon removal of IκB, which exposes the second nuclear localisation signal of the NF-κB dimer (reviewed in Hayden and Ghosh, 2004).

1.1.3.3 Activation of DNA-bound transcriptional regulators by phosphorylation

Phosphorylation can also activate transcription factors already bound to DNA. Ternary complex factors (TCFs), co-activators of SRF, receive activating signals through growth-factor stimulated, MAP-kinase (mitogen-activated protein kinase) mediated serine/threonine phosphorylation at their C-termini (see Section 1.3.6).

The transcription factor CREB (cAMP response element-binding protein) becomes phosphorylated by a multitude of kinases in various signalling pathways, including protein kinase A (PKA) in cAMP-induced signalling (reviewed in De Cesare et al., 1999). This triggers the recruitment of the CBP and p300 coactivators, which exhibit histone-acetyl transferase activity.

1.1.3.4 Inhibition of transcriptional regulators by phosphorylation

An example of a transcriptional activator that is inhibited by phosphorylation is Yorki (Yki; mammalian orthologue Yes-activated protein, YAP), the transcriptional coactivator of the novel, tumour-suppressive Hippo signalling pathway (reviewed in Edgar, 2006 and Harvey and Tapon, 2007). Yki promotes the expression of genes that serve proliferative and anti-apoptotic functions. The most downstream kinase in the Hippo pathway, Wts/Lats (Warts / Large Tumour Suppressor), phosphorylates and thereby inactivates Yki (Huang et al., 2005). Phosphorylation of Yki promotes its cytoplasmic localisation (Dong et al., 2007).

1.1.4 Stabilisation of transcriptional regulators

β-catenin is an Armadillo-repeat protein which fulfils multiple roles in the regulation of the actin cytoskeleton, cell adhesion and transcription mediated by TCF/Lef (T-cell factor / lymphoid enhancer-binding factor) transcription factors (reviewed in Kobielak and Fuchs, 2004 and Reya and Clevers, 2005). In unstimulated cells, newly synthesised β-catenin is sequestered by a multiprotein "destruction" complex, which contains the scaffold proteins adenomatous polyposis coli (APC) and axin (Rubinfeld et al., 1996). Kinases in the destruction complex, glycogen synthase kinase 3 (GSK3) and casein kinase I (CKI), phosphorylate β-catenin and thereby target it for proteasomal degradation (Aberle et al., 1997). Activation of Wnt signalling results in the disassembly and consequential stabilisation of β-catenin, which accumulates in the nucleus and activates TCF/Lef-mediated transcription.

1.1.5 Release of immobilised transcriptional regulators

Generally speaking, maintenance of cytoplasmic localisation constitutes an example of spatial sequestration of signalling molecules in their inactive state (see Section 1.1.1). In addition, gene regulators can be immobilised on certain cytoplasmic compartments. This occurs, for example, in the case of one branch of the unfolded protein response (UPR; reviewed in Bernales et al., 2006). The UPR provides an intracellular homeostasis mechanism that elicits a transcriptional programme upon accumulation of unfolded proteins in the endoplasmic reticulum (ER). The UPR modulates the capacity of the ER according to the cell's needs. The basic leucine zipper (bZIP) transcription factor ATF6 (activating transcription factor 6) is synthesised as an ER-resident integral membrane protein. Upon induction of the UPR, ATF6 is sorted into the Golgi apparatus via the secretory pathway. There, its cytosolic portion, which contains the transcription factor activity, is released by proteolytic cleavage (Ye et al., 2000). The now mobile ATF6 fragment accumulates in the nucleus and activates transcription of genes containing the ER stress response elements (ERSEs) (reviewed in Bernales et al., 2006).

1.1.6 *De-novo* synthesis of transcriptional regulators

Two further branches of the UPR provide examples for signal-induced *de-novo* synthesis of transcription factors, either through the control of translation or

unconventional mRNA splicing. Both processes are mediated by kinases that are anchored to the ER by a single-pass transmembrane domain, PERK (pancreatic ER kinase) and Ire1 (inositol-requiring enzyme 1). Both become activated upon the accumulation of unfolded proteins in the ER lumen (reviewed in Bernales et al., 2006).

Active PERK phosphorylates and inactivates the translation initiation factor eIF2α (Harding et al., 1999). This not only results in a general decrease in the activity of protein synthesis but also in the preferential translation of mRNAs that contain small upstream open reading frames or internal ribosome entry sites (IRESs). One of these mRNAs is that of ATF4, a UPR transcription factor (reviewed in Bernales et al., 2006).

Active Ire1 displays site-specific endoribonuclease activity and removes an unconventional intron from cytoplasmic *Hac1* mRNA (Cox and Walter, 1996; Sidrauski and Walter, 1997). Following fusion of the two exons by tRNA ligase (Sidrauski et al., 1996), *Hac1* mRNA, whose translation is blocked when it is unspliced, can now be translated. The protein product Hac1 is a transcription factor that controls UPR target genes (reviewed in Bernales et al., 2006).

1.1.7 Tissue-specific expression of transcriptional regulators

Tissue- or cell-lineage specific expression of transcriptional regulators can activate specialised transcriptional programmes required for cell differentiation and function. One example is the transcription factor Pax5, which is essential for B-cell development (reviewed in Cobaleda et al., 2007; Urbanek et al., 1994). Pax5 activates genes required for the commitment to the B-cell lineage while repressing lineage-inappropriate genes.

1.2 The actin cytoskeleton

In this thesis, I address the regulation of the transcription factor SRF by a signalling pathway which involves small GTP-binding proteins of the Rho family and the actin cytoskeleton. In this section, I will introduce the actin cytoskeleton, principles of its control and give examples for cytoskeletal and non-cytoskeletal, "unconventional" roles of actin. I will subsequently introduce SRF and its cofactors and describe how actin dynamics impinge on regulation of SRF via its coactivator MAL.

1.2.1 Actin

Actin is almost certainly the most abundant intracellular protein of mammalian cells with estimates for its concentration ranging from 65 to 300 μM in non-muscle cells (reviewed in dos Remedios et al., 2003). Furthermore, it is also one of the most conserved protein across all phyla in which actin is present, and actin-like proteins with a similar fold to actin exist even in bacteria (reviewed in dos Remedios et al., 2003). Actin is best known as the major constituent of the microfilament system, which is vital for processes such as cell motility, cell adhesion, cytokinesis, vesicular transport and their associated macroscopic phenomena, for example tissue morphogenesis during development and regeneration. The remarkable diversity of functions of actin is largely a consequence of its vast structural versatility.

1.2.1.1 Monomeric and filamentous actin

Monomeric actin is a globular protein of 42 kDa that is stabilised by an adenine nucleotide, either ATP or ADP (Figure 1.1 A). Actin monomers (G-actin) can polymerise to form filaments (F-actin) with a two-stranded, right-handed helical arrangement of actin protomers and two distinct ends owing to the asymmetry of the actin molecules, which are incorporated into the filament with identical directionality (see Section 1.2.1.4 for actin filament models; Figure 1.1 A). When actin filaments are decorated with myosin sub-fragment 1, actin appears as arrowhead-like structure. The opposite ends of the actin filament are therefore referred to as barbed and pointed ends (Huxley, 1963; Moore et al., 1970). Actin polymerisation and de-polymerisation forms, together with actomyosin contractility, the mechanistic basis underlying the abovementioned cellular processes. Due to its large structural versatility, actin can present a variety of distinct surfaces to actin-binding proteins that control or exploit assembly and disassembly of actin filaments.

Actin polymerisation can be reconstituted with the purified protein. Under low-salt conditions, actin exists in its monomeric form, that is as G-actin. Addition of physiological concentrations of monovalent and divalent cations, which occupy low-affinity binding sites on actin, induces actin polymerisation (reviewed in Carlier, 1991; Korn, 1982). Polymerisation is rapid once the rate-limiting nucleation step, the formation of an actin trimer (Sept and McCammon, 2001), has been overcome, occurring with a concentration-dependent rate constant of 11 monomers μM^{-1} s^{-1} at the

barbed end of the filament (Pollard, 1986). The associated increase in viscosity can be followed by viscometry or visually if the protein concentration allows (Figure 1.1 B). Once a balance between G- and F-actin is reached, addition and dissociation of monomers resumes although number and length of the actin filaments do not change. The concentration of G-actin that exchanges with the filament at steady state is known as the critical concentration (C_c) and is determined by the ratio of the rate constants for dissociation and association of actin monomers. The critical concentration at the barbed end of the filament (0.1 μM) is lower than at the pointed end (0.7 μM) (reviewed in Pollard and Borisy, 2003). Therefore, at steady state, addition of monomers to the barbed end occurs faster than addition to the pointed end of the filament. The barbed or fast-growing end is hence called the (+)-end while the pointed or slow-growing end is referred to as the (-)-end. The different properties of the actin filament ends result in the phenomenon known as actin treadmilling.

1.2.1.2 ATP binding and hydrolysis by actin

Although both ATP-actin and ADP-actin can polymerise, hydrolysis of the coordinated ATP regulates filament dynamics. ATP-actin incorporates into the elongating barbed end. Actin irreversibly hydrolyses ATP to ADP and phosphate with a half time of 2 s upon polymerisation (Blanchoin and Pollard, 2002; Carlier et al., 1988). ATP-actin and ADP-P_i-actin are functionally indistinguishable. Once the γ-phosphate group has dissociated, which occurs with a half time of about 350 s (Carlier and Pantaloni, 1986), the off-rate of ADP-actin increases, and actin monomers eventually dissociate (reviewed in Pollard and Borisy, 2003). Due to the higher concentration of ATP than ADP in the cell and the larger affinity of actin for ATP, ADP is readily replaced by ATP, and actin monomers can undergo another cycle of polymerisation. Note that this view is based on studies with skeletal-muscle α actin and that no delay in phosphate release upon ATP hydrolysis is observed for polymerising β actin, at least *in vitro* (Nyman et al., 2002; see Section 1.2.1.5 for actin isoforms). Nucleotide exchange on actin is catalysed by the abundant actin-binding protein profilin (see Section 1.2.2.1). The presence of ATP-actin at the barbed end of the filament but ADP-actin at its pointed end provides the explanation for different critical concentrations at the filament ends and the treadmilling phenomenon. The nucleotide status of actin is believed to act as a timer indicating the age of the filament and to initiate active disassembly of actin

filaments in cells, although this view may be challenged by the different behaviours α and β actin regarding γ-phosphate release.

1.2.1.3 Atomic structure of actin

Actin polymerisation represents a major obstacle for the crystallisation of actin. The first crystal structure of the actin molecule at atomic resolution was solved in 1990 (Kabsch et al., 1990). Kabsch *et al.* overcame the problem of actin polymerisation by generating an actin-DNaseI complex, which is incompatible with actin filament formation but able to crystallise (see also Section 1.2.2.5 Mannherz et al., 1977). Crystallisation of actin in the absence of any actin-binding protein was first reported in 1977 (Oriol et al., 1977), but it took another 28 years until a crystal structure of uncomplexed actin could be obtained (Otterbein et al., 2001).

Actin is folded into two domains, with the adenine nucleotide bound to a deep cleft between them (Figure 1.1 A). The two domains are defined as consisting of two subdomains each, so actin is usually described as an assembly of subdomains 1-4. The N- and C-termini of actin lie closely together in subdomain 1. The two actin domains are connected to each other by two helices between subdomains 1 and 3. This connection defines the "hinge", "propeller" motion around which causes the nucleotide cleft to open and close (Page et al., 1998; Tirion et al., 1995). The adenine nucleotide is coordinated with nanomolar affinity via a divalent cation, predominantly Mg^{2+} *in vivo* (reviewed in dos Remedios et al., 2003). The open and closed states of the actin molecule are visible in two different structures of actin with the actin-binding protein profilin (Chik et al., 1996; Schutt et al., 1993; Figure 1.1 B). In the open conformation, ATP is more solvent-exposed than in the closed conformation. Comparison of the actin protomer conformations in ATP- and ADP-actin filaments with known crystal structures suggests that the ATP-bound state of actin corresponds to the closed while the ADP-bound state corresponds to the open conformation of the actin monomer (Sablin et al., 2002). A "γ-phosphate sensing" mechanism reminiscent of that of other NTPases has been proposed for actin (Sablin et al., 2002). Two side chains, S14 and G158, from two different loops in the nucleotide-binding site of actin coordinate the γ-phosphate in the closed state of actin. It is thought that these interactions are coupled to the overall conformation of the actin molecule through a network of interactions that amplify the conformational subtleties of the nucleotide-binding site. In the open state,

coordination of the γ-phosphate is lost (discussed in Sablin et al., 2002). Actin filaments consist of ATP-actin, ADP-P_i-actin and ADP-actin. The nucleotide status represents a molecular timer of actin filaments and hence a γ-phosphate-controlled conformation of actin would play a vital role in the turnover of actin filaments in the cell (see Sections 1.2.1.1 and 1.2.2.3).

1.2.1.4 Models of the actin filament

The incompatibility of actin crystallisation and polymerisation has so far occluded first-hand observation of actin filaments at atomic resolution. However, crystal structures of unpolymerised actin and fibre diffraction studies of the actin filament have been used to derive models for the actin filament: the Holmes model (Holmes et al., 1990; Lorenz et al., 1993), in which actin protomers assume a closed conformation and a distinct model based on actin-actin crystal contacts in the profilin-actin co-crystal (Schutt et al., 1993). Insights from electron microscopy studies of actin filaments are consistent with the closed Holmes model (Bremer et al., 1994; Holmes et al., 2003). An electron microscopy study of an actin mutant (V159N), which adopts an open, ADP-P_i-like conformation in the ADP-bound form, has provided evidence for a Holmes-like open model (Belmont et al., 1999). Small-angle X-ray scattering studies of F-actin are under way (Oda et al., 2001; Popp et al., 1987).

According to the Holmes model of the actin filament, the arrangement of actin monomers can be described either as a single-start, tightly wound, left-handed helix or two-start, long-pitch, right-handed helix (Holmes et al., 1990). Since the longitudinal contacts between actin protomers are likely to be stronger than the interactions between the strands, F-actin is usually described as two-start helix. This helix has a half-pitch of 360-390, containing 12-14 monomers per half turn.

A different actin filament model was proposed based on crystallographic actin-actin contacts in the profilin-β-actin structure (Schutt et al., 1993). Actin molecules in the ribbon are related by a 2_1-screw axis with profilin intercalating between adjacent actin protomers on the same side of the screw axis. While the ribbon is not thought to represent a model for filamentous actin alone, Schutt *et al.* propose that actin molecules in the ribbon might be reoriented to form helical F-actin (Schutt et al., 1993; Schutt et al., 1995).

1.2.1.5 Actin isoforms, processing and modification

In mammals, actin is found in three groups of isoforms, α, β and γ, that can be separated by isoelectric focusing. Alpha actin, the most acidic isoform, is restricted to muscle cells, where it represents the most abundant isoform and a major component of the contractile apparatus. There are three α actins: smooth-muscle, cardiac-muscle and skeletal-muscle α actin. Cytoplasmic β and γ are more basic and found in non-muscle cells, where their relative abundance varies depending on the cell type. Smooth-muscle γ actin is thought to be specific to the urogenital tract (Kim et al., 1989). The differences between actin isoforms at the sequence level are small and are not expected to have major structural effects on the general actin fold (Figure 1.2). Differences are concentrated at the negatively charged N-terminus. However, smooth-muscle γ actin has a divergent C-terminal region.

The functional significance of different actin isoforms is not well understood. Cytoplasmic β and γ actins are differentially localised with β actin being more abundant at the leading edge of the cell and γ actin showing relative enrichment in the cell body and stress fibres (reviewed in Kashina, 2006; e.g., Otey et al., 1986). Targeting of the β actin message to the cellular periphery and regulation of its translation by zipcode binding protein 1 (ZBP1) contributes to enrichment of β actin at the leading edge (see Section 1.2.7) The actin aminotermini are target to processing and posttranslational modification, namely acetylation of the α amino group of the N-terminal residue and its removal in nonmuslce actins. In muscle actins, the first two amino acids are removed and the third one acetylated (reviewed in Kashina, 2006). A recent study demonstrates that β-, but not γ-actin, becomes arginylated at its N-terminus and that arginylation regulates cell spreading, lamella formation and β-actin localisation (Karakozova et al., 2006; reviewed in Kashina, 2006).

1.2.2 Actin-binding proteins

The cellular concentration of actin is about 300- to 400-fold higher that its critical concentration, yet the cell maintains pools of both G- and F-actin. Moreover, while treadmilling of purified actin is relatively slow, polymerisation and depolymerisation of actin can occur astonishingly rapidly within cells. An impressive example for rapid actin dynamics is given by Vaccinia virus, which hijacks the actin cytoskeleton to facilitate its spread to neighbouring cells (Frischknecht et al., 1999). Clearly, actin

polymerisation in the cell has to be regulated to account for fast actin-mediated processes such as this. The cell controls the state of the actin cytoskeleton by virtue of various actin-binding proteins, which fall into about 60 classes and can be catalogued by their functions (Siripala and Welch, 2007a; Siripala and Welch, 2007b). Actin binding proteins can sequester actin monomers, nucleate, stabilise, cap, cross-link, sever or travel along filaments.

One prominent example for cooperation of actin regulators is the protrusion of the leading edge in motile cells in response to extracellular signals (Figure 1.3, Pollard and Borisy, 2003). The machinery controlling this process is employed in numerous actin-mediated activities, including the control of SRF by the RhoA-actin pathway, which is the focus of this thesis.

In the following sections, I will introduce some of the recurring players in actin regulation and additional actin-binding proteins, whose crystal structures teach us about common and specific modes by which actin-binding proteins interact with actin.

1.2.2.1 Profilin

Profilins are small (about 15 kDa) proteins found throughout eukaryotes (reviewed in Witke, 2004). In humans, there are four profilin genes (reviewed in Polet et al., 2007). Profilin is highly abundant (20-100 μM, Buss et al., 1992). Its role in the regulation of actin assembly is two-sided: on the one hand, profilin blocks actin polymerisation, on the other, in the presence of thymosin β4, it promotes assembly of actin filaments (Pantaloni and Carlier, 1993; reviewed in Yarmola and Bubb, 2006).

The first structural insights into profilin functions came form crystals of bovine β-actin complexed with bovine profilin (Figure 1.4 B, Schutt et al., 1993), but numerous profilin-actin structures have been determined as of today. Profilin forms two α-helical assemblies separated by a 7-stranded β sheet. It sequesters actin monomers (Carlsson et al., 1977) by binding to the base of actin subdomains 1 and 3, occupying a surface area of 2,250 $Å^2$ (Schutt et al., 1993). The binding site of profilin on actin illustrates how profilin can inhibit spontaneous actin nucleation and prevent addition of actin monomers to the pointed end of actin filaments while allowing G-actin binding to the barbed end of growing filaments. Once profilin-actin has been added to a filament end, it has to rapidly dissociate to allow for the addition of the next actin molecule. This

might occur through a conformational change in ATP-actin upon filament binding (see dos Remedios et al., 2003).

By affecting the hinge between the two actin domains, profilin potently promotes nucleotide release from actin (Goldschmidt-Clermont et al., 1991). Given the high (millimolar) concentration of ATP in the cell and actin's higher affinity for ATP, profilin maintains a pool of ATP-actin ready to be incorporated into actin filaments (see Figure 1.3). In addition, profilin displays a higher affinity for ATP-actin monomers (0.1-0.5 μM for Mg^{2+}-ATP-G-actin and 5 μM for Mg^{2+}-ADP-G-actin) and inhibits ATP hydrolysis by actin (reviewed in dos Remedios et al., 2003; Tobacman and Korn, 1982). Profilin was also reported to decrease the critical concentration of actin, although the mechanism underlying this observation is still being investigated (Pantaloni and Carlier, 1993; discussed in Yarmola and Bubb, 2006).

Interaction of profilin with phosphatidylinositol(4,5)-bisphosphate, $PI(4,5)P_2$, efficiently dissociates profilin-actin complexes (Lassing and Lindberg, 1985), offering a potential mechanism for regulation of actin assembly by phospholipid signalling. $PI(4,5)P_2$ binding might induce a conformational change within profilin that results in dissociation of the profilin-actin complex (Raghunathan et al., 1992). There is evidence for a second $PI(4,5)P_2$ binding site in profilin that is compatible with actin binding (Skare and Karlsson, 2002). The ability of profilin to bind poly-L-proline stretches (Tanaka and Shibata, 1985) is required for its assistance in actin filament nucleation by formin proteins (see Section 1.2.3.2). Profilin is also an important cofactor for nuclear export of actin (see Section 1.2.5.1). The crystal structure of profilin with β-actin served as a basis for the ribbon model of the actin filament (see Section 1.2.1.4).

In the first actin-profilin structure, actin assumes a closed conformation (Schutt et al., 1993). In another profilin-actin structure, determined at 2.65 Å resolution from crystals obtained under different conditions, the profilin-actin contacts appear very similar, but actin is seen in an open conformation (Chik et al., 1996, see Figure 1.1 A). The significance of these two states of actin is discussed in Section 1.2.1.3.

1.2.2.2 Thymosin and WH2 motifs

Interaction of actin monomers with thymosin β4, a 5-kDa protein, provides a second actin buffering system found in higher eukaryotes (Safer et al., 1991; Safer et

al., 1990). Mammalian cells express three isoforms of thymosin β: β4, β10 and β15, which display a similarity of 70% (reviewed in Paunola et al., 2002). Thymosin β4, which is ubiquitously expressed, can be highly abundant, and concentrations of up to 500 μM have been reported (reviewed in dos Remedios et al., 2003). Like profilin, thymosin β4 displays a preference for ATP-actin: it binds ATP-G-actin (K_d = 1.7 μM) 50 times more strongly than ADP-actin (K_d = 80 μM) (reviewed in dos Remedios et al., 2003). Thymosin β4 binding blocks all actin assembly. Both profilin and thymosin β4 bind actin dynamically. According to the classical textbook model, profilin and thymosin β4 compete with each other for actin binding, and, because profilin has a higher affinity for actin monomers than thymosin β4 (profilin: K_d = 0.1-0.5 μM, reviewed in dos Remedios et al., 2003), profilin can efficiently maintain a polymerisation-competent pool of monomeric actin. A recent study has challenged this view, revealing that profilin, thymosin β4 and actin can form a ternary complex at physiological protein concentrations (Yarmola et al., 2001). Observations of competition between profilin and thymosin β4 might be due to allosteric effects. Indeed, thymosin β4 was reported to affect the conformation of actin (De La Cruz et al., 2000; Dedova et al., 2006). The regulation of the ternary complex to allow for actin polymerisation is currently unclear. Effects of molecular crowding, which could induce secondary structure in thymosin β4 facilitating or compromising actin binding have been proposed (Yarmola and Bubb, 2006). Some lower eukaryotes lack thymosin and entirely rely on profilin as an actin-monomer buffering agent.

Thymosins are frequently placed into larger family containing one or more copies of the WH2- (Wiskott-Aldrich Syndrome protein (WASP) homology 2-) motif, frequently referred to as 'WH2 domain'. (See Section 1.2.3.1 for more information on WASP-family proteins.) The WH2 motif is a short stretch of approximately 35 amino acids (reviewed in Paunola et al., 2002). Humans, for example, have 18 different WH2-motif containing proteins; plants, however, appear to have none. WH2-motif containing proteins include WASPs, β thymosins, ciboulots, verprolins, and Srv2/CAP (adenylyl-cyclase associated protein) (reviewed in Paunola et al., 2002). WH2 motifs comprise an N-terminal, well-conserved region, which forms an α helix, and C-terminal segment that is less well conserved (Chereau et al., 2005; reviewed in Paunola et al., 2002).

Several structural studies suggest that thymosin β4 is essentially unstructured in solution except for a small α helix in its N-terminus (Czisch et al., 1993; Domanski et al., 2004; Safer et al., 1997). When bound to actin, the α-helical content of thymosin β4 increases (Domanski et al., 2004; Safer et al., 1997). Using chemical cross-linking, the binding sites of thymosin β4 were mapped to a region in actin subdomains 1 and 3 and subdomain 2, and the distance between these sites is consistent with thymosin β4 being largely unstructured and extended (Safer et al., 1997). Direct crystallographic insights into thymosin β4 are limited. However, the use of a chimaeric protein containing gelsolin segment 1 (see Section 1.2.2.4 for gelsolin) and the C-terminal part of thymosin β4 (Figure 1.4 E, Irobi et al., 2004) and a related WH2-motif protein, *Drosophila* ciboulot (Figure 1.4 F, Hertzog et al., 2004), have allowed for further insights into the structure of the WH2 motif. Ciboulot contains three WH2 motifs, but forms a 1:1 complex with G-actin and promotes actin polymerisation at the barbed filament end, unlike thymosin β4 (Boquet et al., 2000). The activity of ciboulot is contained within the first one of its WH2 motifs (Hertzog et al., 2004).

The ciboulot crystal structure shows that its first WH2 motif, which is very similar to that of thymosin β4, forms an amphipathic α helix that engages with a hydrophobic cleft present between subdomains 1 and 3 of actin (Figure 1.4 F, Hertzog et al., 2004). It was proposed that, by interaction with the hydrophobic interdomain cleft of actin, thymosin β4 can sense the shear motion around the hinge imposed on actin by ATP hydrolysis, which opens the nucleotide-binding cleft (see Section 1.2.1.3) (Hertzog et al., 2004). This might explain the preference of thymosin β4 for ATP-actin.

In the gelsolin segment 1-thymosin β4 fusion protein, residues following the globular portion of segment 1 bind the "front" of actin (according to the view in Figure 1.1 A) in an extended conformation, reaching up to the interface formed between actin subdomains 2 and 4, where a short α helix caps the pointed end of actin (Figure 1.4 E). Along its trajectory, the extended chain forms two β strands that engage in sheet-like interactions with strands of actin subdomain 1 (Irobi et al., 2004). It appears clear from these structures and the filament model (see Section 1.2.1.4) that both the N- and the C-terminal halves of thymosin β4 contribute to inhibition of actin assembly. Models of the

entire thymosin β4 molecule with actin have been proposed on the basis of biochemical, NMR and crystallographic data (Hertzog et al., 2004; Xue et al., 2007).

It is curious that thymosin β4, which contains a single WH2 motif, inhibits actin filament assembly while other proteins of this family such as WASP, N-WASP (neural WASP) and WAVE (WASP family verprolin homologous protein), all of which are comprised of multiple WH2 motifs, promote actin polymerisation. Hertzog *et al.* exchanged residues of thymosin β4 for the equivalent ones of ciboulot. They identified thymosin β4 derivatives that, instead of sequestering actin monomers, promote actin filament assembly *in vitro*, very much like ciboulot (Hertzog et al., 2004). The critical residues lie in the extended region of thymosin β4 that binds the "front" of actin (according to the view in Figure 1.1 A) and the helix capping the pointed end (Hertzog et al., 2004). NMR studies demonstrated that ciboulot and the ciboulot-like thymosin-β4 derivative display weakened interactions with actin in the regions outside the N-terminal helix that binds the cleft. The identities of the critical amino acids in WH2-motif containing proteins correlate with their functions as either actin-sequestering or actin assembly-promoting factors (Hertzog et al., 2004).

1.2.2.3 ADF/Cofilin

Actin turnover relies on recycling of actin monomers from filaments. Unassisted depolymerisation of actin as it occurs *in vitro* would be too slow to account for the fast dynamics of actin *in vivo*. ADF (actin-depolymerising factor)/cofilins, small (15-20 kDa) proteins that bind both G- and F-actin, are important players in the G-actin recycling machinery (reviewed in dos Remedios et al., 2003). Binding of ADF/cofilin to actin filaments enhances the rate of monomer dissociation from the filament pointed end up to about 25-fold (Carlier et al., 1997). With a preference for ADP-F-actin rather than ATP-F-actin on the scale of 2 orders of magnitude, ADF/cofilin targets "aged" portions of the filament (Carlier et al., 1997, see Figure 1.3). This is likely to be a consequence of different conformations of the actin protomers in their ATP/ADP-P_i- and ADP-bound states (see Section 1.2.1.3). A preference of ADF/cofilin for actin monomers is thought to drive the depolymerisation reaction. Although referred to as an actin filament severing protein, ADF/cofilin does not actively break up the filaments. Instead, it changes the twist of the actin filament by binding cooperatively with each ADF/cofilin protein bridging two longitudinally oriented actin protomers in the filament

(McGough et al., 1997). The associated increase of strain within the filament is thought to be responsible for the increased off-rate of actin monomers from the pointed end but also an increased likelihood of filament breakage through increased thermal instability. This actin filament severing activity is weak and not observed under all experimental conditions (Carlier et al., 1997; Du and Frieden, 1998; Ichetovkin et al., 2000; Maciver et al., 1998).

The role of ADF/cofilin in the regulation of actin dynamics is likely to be more complex. Filament severing by ADF/cofilin generates free barbed ends that are thought to function as nuclei for actin polymerisation. ADF/cofilin has been shown to locally promote actin polymerisation through the generation of short actin filaments at the leading edge, for example after EGF stimulation of MTLn3 rat mammary adenocarcinoma cells (Chan et al., 2000) or targeted and local activation of caged cofilin (Ghosh et al., 2004). The latter study has demonstrated a role of ADF/cofilin in controlling directionality of cell migration. How the different functions of ADF/cofilin are coordinated is still unclear, and reports on ADF/cofilin activities are contradicting. In a recent report, Adrianantoandro and Pollard conclude from real-time microscopy assays that cofilins sever actin filaments at low concentrations and inhibit depolymerisation at barbed ends but do not accelerate subunit dissociation from pointed filament ends (Andrianantoandro and Pollard, 2006). Furthermore, the authors observed increased filament nucleation at cofilin concentrations at which actin monomer binding by cofilins can be detected.

ADF/cofilin itself is regulated through serine phosphorylation at its aminoterminus by members of the LIM and TESK (testicular protein kinase) family kinases (Arber et al., 1998; reviewed in Bamburg, 1999; Yang et al., 1998). Phosphorylation abolishes actin binding and consequentially any actin-regulatory activity of ADF/cofilin. Phosphorylation of LIMKs and therefore ADF/cofilin occurs downstream of active Rho family GTPases (see Section 1.2.4.2). Phospho-ADF/cofilin is dephosphorylated and activated by slingshot family protein phosphatases (Niwa et al., 2002).

1.2.2.4 Gelsolin

Gelsolin severs F-actin and caps actin filaments by binding to the barbed filament end in response to signal-induced hydrolysis of membrane-bound $PI(4,5)P_2$ and elevated Ca^{2+} levels (reviewed in dos Remedios et al., 2003). Filaments that are

capped can be rapidly degraded through the action of ADF/cofilin (see Section 1.2.2.3). Furthermore, filaments can be uncapped locally by a membrane rich in $PI(4,5)P_2$, and this event is thought to trigger actin polymerisation at the cell periphery (Allen, 2003, see Figure 1.3). Gelsolin is a critical regulator of intracellular actin dynamics, but one gelsolin isoform is secreted and acts in the bloodstream as component of the actin scavenger system (see Section 1.2.2.6).

Gelsolin consists of two similar halves with three domains each. The domains are named, from N- to C-terminus, segments 1-6. In isolation, a fragment comprising segments 1-3 has F-actin severing activity and is able to bind to two actin monomers. A construct spanning segments 4-6 binds a single actin monomer (reviewed in dos Remedios et al., 2003). Ca^{2+}-binding sites are present in each of the six segments, but their affinities vary, and they are thought to become occupied in distinct, Ca^{2+}-concentration dependent steps within the gelsolin activation process (discussed in Burtnick et al., 2004). While the functions of segments 1-3 do not require Ca^{2+} *per se*, actin binding by segments 4-6 is strictly dependent on Ca^{2+}. However, the activity of the N-terminal half of gelsolin can be modulated by physiological Ca^{2+} concentrations. In the context of the full-length protein, both halves of gelsolin contribute to its activity.

In a structure of gelsolin without actin and in the absence of Ca^{2+}, the six segments of gelsolin are arranged in a closed, globular assembly with the actin binding sites buried (Burtnick et al., 1997). According to a current model of gelsolin activation, at least two Ca^{2+}-dependent steps are required to release the activity of gelsolin through disengaging these intramolecular interactions. Binding of gelsolin to actin filaments occurs rapidly, but severing activity is low until further Ca^{2+}-induced conformational changes fully activate gelsolin (discussed in Burtnick et al., 2004).

Several crystal structures of gelsolin-actin complexes were determined to-date, including one with gelsolin segment 1 (McLaughlin et al., 1993), another one with segments 4-6 (Figure 1.4 C, Robinson et al., 1999) and one with the N-terminal half of gelsolin, segments 1-3 (Figure 1.4 D, Burtnick et al., 2004).

Gelsolin segment 1 forms a globular domain, which contacts actin by inserting its longest α helix into a hydrophobic cleft formed between subdomains 1 and 3 of actin

(Figure 1.4 D, Burtnick et al., 2004; McLaughlin et al., 1993). The linker connecting segments 1 and 2 interacts with the "front" of the actin molecule, directing gelsolin segment 2 to its interaction site on actin subdomain 2. A partially α-helical linker positions segment 3 to interact with actin subdomain 1 (Burtnick et al., 2004).

A structure of gelsolin segments 4-6 in the presence of Ca^{2+} demonstrates that calcium opens the assembly of segments, priming the C-terminal half of gelsolin for actin binding (Kolappan et al., 2003). The crystal structure of gelsolin segments 4-6 in complex with actin shows that segment 4 interacts with the hydrophobic cleft between actin subdomains 1 and 3 via its longest helix, very similar to the mode of binding observed for gelsolin segment 1 (Figure 1.4 C, Robinson et al., 1999). Gelsolin segment 6 makes some contacts with actin subdomain 3, whereas segment 5 does not contact actin directly.

1.2.2.5 DNaseI

The ability of DNaseI to inhibit actin polymerisation has been exploited to obtain the first actin crystal structure, that of rabbit skeletal-muscle actin (see Section 1.2.1.3, Figure 1.4 A, Kabsch et al., 1985). The functional significance of the actin-DNaseI interaction is not clear, although the ability of actin to inhibit DNaseI activity has been used for analytical purposes (Blikstad et al., 1978; Lazarides and Lindberg, 1974). DNaseI is a globular protein of 31 kDa. It binds with very high affinity (0.05 nM, Mannherz et al., 1980) to a loop in actin subdomain 2, which is hence termed the DNaseI-binding loop or D-loop. Actin and DNaseI share a surface area of 1830 $Å^2$. The DNaseI binding loop is almost devoid of secondary structure in the complex.

1.2.2.6 Vitamin-D binding protein

Besides acting as a carrier for vitamin D in the bloodstream, vitamin-D binding protein (DBP) is an essential component for the so-called actin scavenger system. This system ensures that actin released into the bloodstream following tissue necrosis or injury is depolymerised and cleared before it can obstruct organ function. DBP cooperates with gelsolin, an F-actin severing protein (see Section 1.2.2.4). DBP forms a high-affinity 1:1 complex (K_d = 1 nM) with actin, thereby sequestering actin from polymerisation (see Otterbein et al., 2002).

The crystal structures of uncomplexed DBP and the DBP-actin complex have been determined (Figure 1.4 G, Otterbein et al., 2002). DBP has three homologous, α-helical domains that are structurally related to those in human serum albumin, however, their relative arrangement is completely different in DBP. Differences between two independent molecules in the asymmetric unit of the crystal suggest a certain degree of conformational flexibility between the domains. DBP mainly contacts actin subdomain 3, but also makes some interaction with subdomain 1. The assembly of all three domains of DBP clamps around and engulfs nearly half of subdomain 3, burying an enormous surface area of 3454 $Å^2$. No major structural changes in actin are necessary to coordinate DBP, which, together with the large common surface between the two proteins, explains the high binding affinity.

1.2.2.7 A common theme in actin binding

The examples for actin complexes discussed above illustrate that every subdomain of actin can serve as a binding platform for actin-binding proteins. However, many actin-binding proteins engage with subdomains 1 and 3 of the actin molecule or, more precisely, with a hydrophobic cleft present at the interface between them. This has been proposed as a conserved mode of binding for many G-actin binding proteins (Dominguez, 2004). Besides gelsolin, the WH2 motif and DBP, ADF/cofilin and actin itself are thought to bind to the cleft via amphipathic helices. Furthermore, the actin-binding drugs swinholide A (see Section 1.2.6.3) and kabiramide C (Klenchin et al., 2003) target this region of actin (see Dominguez, 2004). This binding mode will be further discussed in Chapters 5 and 6.

1.2.3 Regulation of de-novo actin polymerisation

Spontaneous nucleation of actin filaments is the rate-limiting step during polymerisation of purified actin due to the high instability of actin dimers and trimers, which are thought to represent early steps in actin polymerisation (Sept and McCammon, 2001). In the cell, free G-actin is buffered by actin-monomer binding proteins profilin and thymosin β4 (see Sections 1.2.2.1 and 1.2.2.2). The cell employs actin-filament nucleation machineries to overcome this obstacle in several ways (reviewed in Pollard, 2007, see also Figure 1.3). Arp (Actin-related protein)2/3-complex and formin-mediated actin polymerisation are ubiquitous (with the exception of algae,

microsporidia and apicomplexa, which do not possess the Arp2/3 complex, Muller et al., 2005). A recent study described the protein Spire, representing a third family of actin nucleators, which is absent in protozoa but highly conserved in metazoans (reviewed in Kerkhoff, 2006; Quinlan et al., 2005). The activity of actin nucleators is regulated both by extracellular and intracellular signals.

1.2.3.1 The Arp2/3 complex

Activity of the Arp2/3 complex is thought to generate dendritic networks of branched actin filaments at the leading edge of motile cells (see Figure 1.3). The Arp2/3 complex nucleates new filaments at the side of existing ones in a characteristic 70° angle (Amann and Pollard, 2001; Blanchoin et al., 2000; Mullins et al., 1998). However, one should note that the so-called "dendritic nucleation model" of actin organisation at the leading edge of motile cells is still being debated since actin filament branches can arise during sample preparation for electron microscopy (Resch et al., 2002a; Resch et al., 2002b).

The Arp2/3 complex caps the pointed of an actin filament, anchors it laterally to the filament while actin monomers are added to the barbed end until it is capped. The Arp2/3 complex is a seven-subunit complex: the two actin-related protein components, Arp2 and Arp3, are stabilised in an inactive conformation by 5 other subunits (ARPC1 to ARPC5) (Machesky et al., 1994). Inhibitory interactions within the Arp2/3 complex are released through the cooperative action of nucleation-promoting factors (NPFs), actin filaments and actin monomers (Higgs et al., 1999; reviewed in Welch and Mullins, 2002). It is believed that the Arps form the first two subunits in a newly generated actin filament, but the crystal structure of the inactive Arp2/3 complex shows that the Arps are too distant to form a nucleus for actin polymerisation (Robinson et al., 2001). Generation of an active Arp2/3 complex requires a conformational change that orients the Arps such that they assume a similar relative orientation as two actin protomers along the short-pitch helix of an actin filament (Robinson et al., 2001).

NPFs include WASP (Wiskott-Aldrich syndrome protein), N-WASP (neural Wiskott-Aldrich syndrome protein) and Scar/WAVE (suppressor of cAMP receptor / WASP family verprolin homologous protein) family proteins. The activity of NPFs depends on the so-called VCA region (V for verprolin homology, also called WH2 motif for WASP homology 2; C for connecting or cofilin-like; A for acidic) that

juxtapositions the Arp2/3 complex and the first actin monomer to be incorporated into the filament (reviewed in Pollard, 2007). The VCA regions in WASP and N-WASP are targets for regulation: they are occluded in the autoinhibited, closed conformations through an intramolecular interaction of the C motif with the GTPase binding domain (GBD). Binding of the small GTPases Cdc42 or Rac to the GBD, interaction of phosphatidylinositol(4,5)-bisphosphate ($PI(4,5)P_2$) with a poly-basic region and binding of SH3-domain proteins to a proline-rich region cooperate to release the autoinhibitory conformation and make the VCA region accessible for the Arp2/3 complex and actin (reviewed in Pollard, 2007). In contrast, Scar/WAVE proteins are not autoinhibited but regulated in trans by a larger protein complex, the WAVE complex (reviewed in Disanza et al., 2005; Machesky et al., 1999).

1.2.3.2 Formins

Formin proteins (see inset in Figure 1.3) nucleate and support the polymerisation of linear, unbranched actin filaments (Pruyne et al., 2002; Sagot et al., 2002). These include actin fibres of filopodia and actin filaments within the contractile ring formed during cytokinesis (reviewed in Wallar and Alberts, 2003). Formins are homodimers characterised by an actin-binding FH2 (formin homology 2) domain that is preceded by an FH1 domain, which contains proline-rich motifs that recruit profilin-actin complexes (Chang et al., 1997). Theoretical models and experimental data suggest that FH2 domains promote actin filament nucleation by stabilising actin dimers (Pring et al., 2003). Two FH2 subunits form an antiparallel ring that embraces the barbed end of the actin filament (Xu et al., 2004). The two elongated actin-binding domains are stably tethered by flexible linkers. The association of formins with the actively growing barbed filament end might seem curious at first (Pruyne et al., 2002). However, formins act as leaky capping proteins that allow for the rapid elongation of barbed filament ends while preventing binding of genuine capping proteins (Zigmond et al., 2003). Therefore, formin-mediated actin filament elongation is highly processive. Structural and *in vitro* actin assembly assays have led to a model in which formins stair-step on a growing barbed end (Xu et al., 2004; Zigmond et al., 2003). Isolated FH2 domains or FH1-FH2 domain units slow filament elongation at the barbed end. The FH1 domain recruits profilin-actin complexes, and the presence of profilin can accelerate the elongation rate up to 15-fold *in vitro* (Kovar et al., 2006; Romero et al., 2004; Vavylonis et al., 2006). The FH1 domain is thought to maintain a high local concentration of actin at the

growing barbed end. Cells possess various formin proteins, some with very specialised function (reviewed in Higgs, 2005). Vertebrates, for example, have 15 formin proteins.

Like the Arp2/3 complex, formins are regulated to ensure spatial and temporal control of actin polymerisation. Mammalian diaphanous-related formin proteins (DRFs) assume an autoinhibitory intramolecular interaction reminiscent of that occurring in WASP and N-WASP. The GTPase binding domain (GBD) N-terminal to the FH1 domain interacts with the Diaphanous autoregulatory domain (DAD) C-terminal to the FH2 domain (Alberts, 2001; Watanabe et al., 1999). This autoinhibitory conformation is released by binding of active Rho GTPases to the GBD.

1.2.3.3 Spire

Spire is required for axis determination in *Drosophila* oocytes and the developing embryo (Manseau and Schupbach, 1989). Spire proteins assemble actin filaments by a mechanism that is distinct from that of the Arp2/3 complex and formins (Quinlan et al., 2005). Four WH2 motifs, frequently associated with a block of spontaneous actin polymerisation (see 1.2.2.2), recruit 4 actin monomers that are subsequently positioned to form a nucleus for actin polymerisation. A model was proposed in which dimerisation of actin monomers bound to the most C-terminal WH2 motifs is promoted by a linker connecting these two motifs. Actin monomers recruited by the remaining two WH2 motifs are thought to be assembled onto this actin prenucleus, resulting in a longitudinal actin tetramer that serves as a nucleus for actin polymerisation (discussed in Kerkhoff, 2006; Quinlan et al., 2005).

1.2.3.4 Control of F-actin assembly by barbed-end capping of actin filaments

Once actin polymerisation is initiated, it proceeds until the barbed filament end is capped. Gelsolin, discussed above in Section 1.2.2.4, can function as a barbed-end capping protein. The most abundant barbed-end capping protein, however, is capping protein / CapZ (Isenberg et al., 1980, see Figure 1.3). CapZ is a heterodimer that binds the barbed filament end with high affinity ($K_d \approx 1$ nM) and 1:1 stoichiometry, thereby blocking addition and loss of actin monomers (Caldwell et al., 1989; Narita et al., 2006; reviewed in Wear and Cooper, 2004). Since the presence of barbed filament ends largely determines whether filament growths occurs or not (Pollard and Borisy, 2003),

CapZ is a critical regulator of actin polymerisation, playing a major role in maintaining a pool of unpolymerised actin. Therefore, localised generation of only a few free barbed filament ends can efficiently direct actin polymerisation to control cell motility though directional protrusion (Pollard and Borisy, 2003, see Figure 1.3).

CapZ activity, like that of numerous other actin binding proteins, is regulated by phosphatidylinositol(4,5)-bisphosphate ($PI(4,5)P_2$) (Heiss and Cooper, 1991). Another way of controlling capping protein is by competition with other barbed-end binding proteins that promote F-actin assembly. Two examples are formin proteins (see Section 1.2.3.2) and vasodilator-stimulated phosphoprotein (Ena/VASP). Ena/VASP family proteins are multi-domain proteins that promote F-actin assembly and were proposed to bind at or near actin filament barbed ends to protect them from becoming capped by CapZ (Bear et al., 2002; reviewed in Krause et al., 2003).

1.2.4 Control of the actin cytoskeleton by Rho-family GTPases

The actin regulators introduced in the previous sections constantly remodel the actin cytoskeleton. This does not occur randomly but in a highly coordinated fashion and in response to extracellular and intracellular signals (see Figure 1.3). In the present section, I will illustrate how small GTPases of the Rho family orchestrate the actin cytoskeleton.

Rho-family GTPases are pivotal players in the control of actin dynamics and other processes, including the control of cell polarity, vesicular transport, the cell cycle, cell adhesion, microtubule dynamics, and cell death (reviewed in Etienne-Manneville and Hall, 2002). They are members of the Ras superfamily, which also includes the Ras, Rab, Arf and Ran (see Section 1.1.1.1) families (see Wennerberg et al., 2005). In mammals, 22 genes encoding Rho GTPases were identified: RhoA, B and C, Rac1, 2 and 3, Cdc42, RhoD, Rnd1, Rnd2, RhoE/Rnd3, RhoG, TC10, TCL, RhoH/TTF, Chp, Wrch-1, Rif, RhoBTB1 and 2, and Miro-1 and 2 (reviewed in Jaffe and Hall, 2005; Wennerberg and Der, 2004). Rho-family GTPases are characterised by their Rho-type GTPase-like domain that contains a Rho-specific insert (reviewed in Wennerberg and Der, 2004). The best-studied members are RhoA, Rac1 and Cdc42. In terms of actin restructuring, Rho, Rac, and Cdc42 activities are associated with stress fibres, lamellipodia and filopodia formation, respectively (Kozma et al., 1995; Nobes and Hall,

1995; Ridley and Hall, 1992; Ridley et al., 1992). Given that Rho GTPases regulate multiple processes implicated in cancer biology, they and their effectors constitute potential targets for therapeutic intervention (reviewed in Sahai and Marshall, 2002).

1.2.4.1 Regulation of Rho-family GTPases

Like all GTPases, Rho GTPases are biological switches that cycle between GDP-bound inactive and GTP-bound active conformations. In their active conformation, Rho GTPases interact with and activate downstream effector proteins. The intrinsic GTPase activity of many Rho GTPases is extremely low and requires the action of GTPase-activating proteins (GAPs), which increase the hydrolysis rate by several orders of magnitude (reviewed in Bos et al., 2007). Since the nucleotide binds to GTPases with high, nanomolar to picomolar affinity, nucleotide release necessitates guanine nucleotide exchange factors (GEFs), which catalyse nucleotide release by lowering the affinity for GDP. The higher cellular concentration of GTP as compared with GDP results in the generation of a GTP-bound pool of GTPases (reviewed in Bos et al., 2007; Schmidt and Hall, 2002). Activity of Rho and Rab family GTPases is further modulated by guanine nucleotide dissociation inhibitors (GDIs). GDIs usually target the GDP-bound form of the GTPase, preventing GEF-catalysed nucleotide exchange and therefore locking the GTPase in its inactive form. There are, however, examples of GDIs targeting the GTP-bound form of the GTPase, further lowering intrinsic nucleotide hydrolysis activity and preventing the interaction with GAPs and downstream effector targets (reviewed in DerMardirossian and Bokoch, 2005). GDIs also control subcellar and membrane localisation of Rho GTPases, which is critical for their function. They achieve this by shielding the C-terminal lipid moiety, thereby sequestering Rho GTPases from membranes (reviewed in DerMardirossian and Bokoch, 2005; Wennerberg and Der, 2004).

Direct phosphorylation (Lang et al., 1996) and ubiquitin-mediated, proteasome-dependent degradation (Wang et al., 2003a) constitute additional levels of control for Rho GTPases, at least in specific cases. In addition to the regulation of specific GEFs and GAPs, specificity of Rho-GTPase signalling can be achieved by scaffold proteins (reviewed in Marinissen and Gutkind, 2005).

1.2.4.2 Rho-GTPase effector proteins

More than 50 effector proteins have been identified for Rho, Rac and Cdc42, and these include serine/threonine and tyrosine kinases, lipid kinases, oxidases, lipases, and scaffold proteins (reviewed in Jaffe and Hall, 2005). A number of effector proteins mediate actin-based processes. Activation of any Rho GTPase is associated with an accumulation of F-actin at the expense of G-actin. Active forms of Cdc42 and Rac activate Scar/Wave proteins and WASP, which stimulate Arp2/3-mediated nucleation of branched actin filament networks (see Section 1.2.3.1). Direct interaction of Rho with formins releases the autoinhibited state of these proteins, which in turn promote the assembly of linear actin filaments (see Section 1.2.3.2).

A direct effector target of Rho is Rho kinase (ROCK). ROCK stimulates myosin-light chain (MLC) phosphorylation, both by directly phosphorylating MLC and through inactivating the myosin-binding subunit of myosin phosphatase (reviewed in Fukata et al., 2001). ROCK therefore promotes actomyosin-mediated contraction and stress-fibre formation.

Another group of ROCK substrates are the LIM kinases (LIMKs), which are activated when ROCK phosphorylates a threonine residue within their activation loop (Maekawa et al., 1999; Ohashi et al., 2000; Sumi et al., 2001). LIMKs phosphorylate and inactivate ADF/cofilin, thereby stabilising actin filaments (see Section 1.2.2.3).

Other kinases that phosphorylate and activate LIMKs are PAK (p21-activated kinase) and MRCK (myotonin-related Cdc42-binding kinase). PAKs are effectors of Cdc42 and Rac whereas MRCK was described as a Cdc42 effector (reviewed in Zhao and Manser, 2005).

1.2.4.3 Regulation of Rho GTPases by extracellular signals

Rho-family GTPases are activated downstream of cell surface receptors, which include cell-adhesion molecules, receptor tyrosine kinases and G-protein coupled receptors (GPCRs). The activity of guanine nucleotide exchange factors (GEFs) is coupled to receptor-mediated signalling. GEFs are multidomain proteins that can be controlled by interactions with regulatory proteins, lipids and second messengers as well as posttranslational modification. These can recruit GEFs to specific subcellular compartments, release them from an autoinhibitory conformation, or allosterically activate their catalytic function (reviewed in Bos et al., 2007 and Rossman et al., 2005).

1.2.5 "Unconventional" functions of actin in gene expression

Besides its well-established cytoskeletal functions, surprising roles of actin in nuclear architecture and nuclear processes such as chromatin remodelling, transcription and RNA export are becoming increasingly appreciated (reviewed in Bettinger et al., 2004). In this section, I will summarise some recent insights into the control of nuclear processes, especially transcription, by actin in the cell nucleus.

1.2.5.1 Nuclear actin concentrations are generally low

Given the small size of sequestered actin monomer complexes close to the exclusion limit of nuclear pores (see Section 1.1.1.1), cytoplasmic and nuclear actin pools are thought to communicate with each other. Actin is efficiently exported from the nucleus of most cells by exportin 6, which appears to be an export receptor solely dedicated to maintaining low levels of nuclear actin (Stuven et al., 2003). Exportin 6 specifically recognises profilin-actin complexes, revealing yet another role of profilin (see Section 1.2.2.1 for profilin functions). The efficiency of exportin 6 is high, as indicated by the finding that visible nuclear accumulation of actin in *Drosophila* Schneider cells requires an RNAi-mediated knockdown at the exportin-6 protein level of more than 90% (Stuven et al., 2003). Yet, the exportin system would account for a residual nuclear concentration of its substrates of about 1% relative to their total concentrations, which means that nuclear actin could be present at the low micromolar range (discussed in Bohnsack et al., 2006; Görlich et al., 2003). Interestingly, the exportin-6 pathway is inactive in the giant *Xenopus* oocytes, which require an intranuclear F-actin meshwork to support their large nuclei (Bohnsack et al., 2006). Injection of exportin 6 into these oocytes dramatically destabilises their cell nuclei. Exportin-6 expression in *Xenopus* is activated translationally upon induction of meiotic maturation, coinciding with germinal vesicle breakdown (GVBD; nuclear envelope breakdown) (Bohnsack et al., 2006).

Given the action of exportin 6 in somatic cells, it is clear that low concentrations of nuclear actin must suffice for any of its tasks.

A previous report has implicated the nuclear export receptor CRM1 in nuclear export of actin (Wada et al., 1998), however, this does not appear to represent a ubiquitous mechanism (Posern et al., 2002; Stuven et al., 2003).

1.2.5.2 Nuclear actin in basal transcription

Functions of nuclear actin in basal transcription were proposed in the early 1980s, based on interference with transcription by injection of actin-binding proteins and anti-actin antibodies into nuclei of amphibian oocytes (Scheer et al., 1984). More recently, actin was found to be bound to all three eukaryotic RNA polymerases (reviewed in Miralles and Visa, 2006).

RNA polymerase I can be co-immunoprecipitated in a complex with nuclear myosin I (NMI) and actin, and NMI localises to nucleoli, sites of active rDNA transcription (Fomproix and Percipalle, 2004). RNA-polymerase I activity requires nuclear myosin I (NMI) and actin, both *in vivo* and *in vitro* (Philimonenko et al., 2004). Antibodies against actin or NM1 block rDNA transcription from both naked DNA and chromatin. *In-vitro* transcription assays suggest that actin is required for steps that follow transcription initiation (Philimonenko et al., 2004). Actin and NMI were found in a complex with RNA polymerase I. Chromatin immunoprecipitation demonstrated that actin is associated with both the promoter and coding region of the 28S rRNA gene. In contrast, NMI only associates with the promoter region, suggesting an early role of NMI in rDNA transcription (Philimonenko et al., 2004). Indeed, NMI binds TIF-1A, a basal transcription-initiation factor, through which it might be recruited into the PolI complex (Philimonenko et al., 2004).

Antibodies against β actin inhibit transcription *in vivo*, as shown by microinjection into the nuclei of mammalian cells, and RNA-polymerase II mediated transcription initiation *in vitro* (Hofmann et al., 2004). Beta actin co-purifies with RNA polymerase II and is present in pre-initiation complexes assembled *in vitro*. Antibody competition experiments established that β actin is required for incorporation of RNA polymerase II into pre-initiation complexes. Beta actin is recruited to the promoters of interferon-inducible genes upon induction (Hofmann et al., 2004). Another study showed that actin binds the ribonucleoprotein hnRNP U, and that disruption of this interaction by peptide competition blocks RNA-polymerase II mediated transcription *in vivo* and *in vitro* (Kukalev et al., 2005).

Lastly, actin also associates with RNA polymerase III and can be detected on the promoter of an actively transcribed U6 snRNA (small nuclear RNA) gene (Hu et al., 2004). Actin can be dissociated from the PolIII complex by treatment with methane

methylsulfonate (MMS), which blocks PolIII-mediated transcription. PolIII obtained from MMS-treated cells is inactive in *in vitro* transcription assays, but its activity can be restored by addition of β actin (Hu et al., 2004).

1.2.5.3 Nuclear actin in chromatin remodelling complexes

Chromatin remodelling complexes are multi-protein machines that alter the structure of chromatin in an ATP-dependent manner to allow for gene transcription to take place. Actin and actin-related proteins (Arps) have been identified as components of chromatin remodelling complexes in *Saccharomyces cerevisiae*, *Drosophila melanogaster* and mammalian cells (reviewed in Blessing et al., 2004). So far, actin and Arps were found in three families of chromatin remodelling complexes, these containing ATPases of the SWI2/SNF2, INO80 or SWR1 families. Actin and Arps are stably associated, stoichiometric components of these complexes (reviewed in Olave et al., 2002). To give two examples, Arp9 and Arp7 are clearly enriched during purification of the 11-subunit *Saccharomyces cerevisiae* SWI/SNF complex, and deletion of their genes causes phenotypes characteristic of SWI/SNF inactivation (Peterson et al., 1998). The interation of actin and BAF53 (Arp4) with the BAF complex, a vertebrate SWI2/SNF2 family complex, was shown to be highly specific (Zhao et al., 1998). Actin binding binding to Brg1, the SWI2/SNF2 ATPase, could only be abolished by strongly denaturing conditions (Zhao et al., 1998). Electron microscopy showed that the BAF complex binds actin-filament pointed ends *in vitro* (Rando et al., 2002).

The mechanism of actin and Arp functions for actin/Arp-containing chromatin remodelling complexes is currently unclear. It was speculated that actin and Arps might target these complexes to histones or mediate interactions between chromatin remodelling complexes (discussed in Blessing et al., 2004).

1.2.5.4 Actin in RNA complexes

Actin was demonstrated to be a component of pre-mRNPs (messenger ribonucleoprotein particles) (reviewed in Miralles and Visa, 2006). Actin associates with Hrp65-2, a Balbiani ring protein from *Chironomus tentans*, and abolishment of this interaction by peptide competition blocks RNA-polymerase II mediated transcription both *in vivo* and *in vitro*. Nuclear run-on transcription studies suggest that actin is

required for productive transcription elongation (Percipalle et al., 2003). A later study suggests that the actin-Hrp65-2 interaction recruits p2D10, a histone acetyl transferase, into pre-mRNPs (Sjolinder et al., 2005). This observation substantiates the role of actin at multiple levels of the transcription process.

In summary, it is clear that actin is a critical component in all RNA polymerase and chromatin remodelling complexes. However, the molecular interactions of actin in these transcription complexes remain unknown, as does its polymerisation state. Two recent studies implicate the Arp2/3 complex and its regulator N-WASP in RNA-polymerase II mediated transcription, suggesting that F-actin might serve a nuclear function (Wu et al., 2006; Yoo et al., 2007). A fluorescence recovery after photobleaching (FRAP) study suggests that about 20% of nuclear actin are polymerised and turn over rapidly (McDonald et al., 2006). It is currently difficult to reconcile the presence of F-actin with exportin-6 mediated nuclear export of actin (see Section 1.2.5.1). Exportin-6 activity might prevent polymerisation of bulk actin in the nucleus by reducing the nuclear actin concentration to the low micromolar range, at which, however, actin might still be capable of polymerising.

Besides "conventional" G- and F-actin, actin can occur in various "unconventional" oligomeric states and conformations, and these may occur selectively or play specific roles in the cell nucleus (discussed in Jockusch et al., 2006). Nucleus-specific conformations or assemblies of actin were proposed based on studies with actin antibodies that preferentially stain nuclear structures (reviewed in Jockusch et al., 2006). States of actin specific to the nuclear compartment may be induced by actin-binding proteins present in the nucleus, such as components of the nuclear lamina or nuclear Arps or be intrinsic to actin itself. An example of an "unusual" actin-actin contact is the "lower dimer", in which the two actin molecules are arranged in an antiparallel fashion (discussed in Jockusch et al., 2006; see also Pederson and Aebi, 2002).

1.2.6 Actin-binding toxins as probes of actin function

The universal use of the microfilament system makes actin an ideal target for the defence against predators. Actin-binding toxins are widely used in studying the actin cytoskeleton and were employed extensively for the work presented in this thesis.

1.2.6.1 Latrunculins

Latrunculins, 16- or 14-membered macrolides, were first isolated from the Red Sea sponge *Latrunculia magnifica* (Spector et al., 1983). Latrunculins A and B bind actin monomers with a 1:1 stoichiometry and prevent their re-incorporation into actin filaments (Coue et al., 1987). Structural insights of latrunculin binding were obtained upon soaking crystals containing rabbit skeletal-muscle actin bound to gelsolin subdomain 1 with latrunculin A (Morton et al., 2000). Latrunculin A occupies the nucleotide-binding cleft of actin and is likely to inhibit nucleotide exchange through restricting movement between actin subdomains 2 and 4 (see Figure 1.4 F for a representation of latrunculin A-actin). Moreover, latrunculin A appears to restrict mobility of 2 loops in subdomains 2 and 4 that are thought to become ordered in the actin filament. Latrunculin A is somewhat more potent than latrunculin B (Spector et al., 1989), binding G-actin with a dissociation constant of 0.2 μM (Coue et al., 1987). Latrunculin B is structurally very similar to latrunculin A, and both drugs bind actin in very similar ways (Morton et al., 2000).

1.2.6.2 Cytochalasin D

Cytochalasins are a group of fungal macrocyclic metabolites, most of which have aromatic side groups. The way by which cytochalasins exert their effect on the actin cytoskeleton is complex. Though classically used as actin de-polymerising agents, cytochalasins have been reported to bind barbed ends of actin filaments, nucleate actin polymerisation by stabilising actin dimers, stimulate ATP hydrolysis on G-actin and shorten filaments via an unknown mechanism (discussed in Cooper, 1987; Sampath and Pollard, 1991).

1.2.6.3 Swinholide A

Swinholide A, a macrolide of 44 carbons and 2-fold symmetrical structure, was isolated from the marine sponge *Theonella swinhoei*. Swinholide A sequesters actin as dimers (Bubb et al., 1995). Its crystal structure with rabbit skeletal-muscle actin shows that swinholide A occupies two sites on actin (Klenchin et al., 2005): the macrolide ring contacts a hydrophobic patch on the surface of actin while its side chain inserts into a hydrophobic cleft between subdomains 1 and 3 of actin. The symmetry of swinholide A causes it to bridge 2 actin molecules facing each other. Except for a single salt bridge,

no actin-actin contacts are observed in the swinholide A-induced dimer (Klenchin et al., 2005).

1.2.6.4 Jasplakinolide

Jasplakinolide, a cyclic peptide isolated from the marine sponge *Jaspis johnstoni*, strongly binds to and stabilises actin filaments (Bubb et al., 1994).

1.2.6.5 Phalloidin

Phalloidin is a bicyclic peptide, which is isolated from the green deathcap toadstool *Amanita phalloides*. Phalloidin binds to and stabilises actin filaments (Lengsfeld et al., 1974).

1.2.7 Regulation of actin expression

Regulated synthesis of actin occurs in coordination with the state of the actin cytoskeleton via an autoregulatory feedback mechanism. A number of studies have shown that actin levels increase upon treatment of cells with actin-binding drugs which decrease the level of monomeric actin or stabilise actin filaments (Bershadsky et al., 1995; Reuner et al., 1995; Serpinskaya et al., 1990). Comparison of the effects of latrunculin A and swinholide A (see Section 1.2.6) on actin mRNA and protein levels demonstrated that the actin homeostasis mechanism responds to the levels of monomeric actin (G-actin) (Lyubimova et al., 1997).

Actin regulation occurs both transcriptionally and post-transcriptionally: transcription of the *β-actin* gene is enhanced upon growth-factor stimulation (Elder et al., 1984; Greenberg et al., 1985; Greenberg et al., 1986). Treatment of hepatocytes with the F-actin stabilising drug phalloidin increases *actin* transcription while block of actin polymerisation by *Clostridium botulinum* C2 toxin results in a markedly decreased half life of the *actin* mRNA without any effect on *actin* transcription (Bershadsky et al., 1995; Reuner et al., 1995). Downregulation of *actin*-mRNA levels is maintained in enucleated cells, adding further support to a non-transcriptional component of actin-expression control (Bershadsky et al., 1995). Post-transcriptional regulation of actin synthesis is mediated by the 3'-untranslated region (3'-UTR) of the *β-actin* mRNA

(Lyubimova et al., 1999). Loss of the 3'-UTR results in actin overproduction (Lyubimova et al., 1999).

The mechanism by which the 3'-UTR restrains translation of the *β-actin* mRNA is attributable to zipcode binding protein 1 (ZBP1), which binds to a 54-nucleotide "zipcode" within the 3'-UTR (Huttelmaier et al., 2005; Kislauskis et al., 1994; Ross et al., 1997). ZBP1 targets the *β-actin* mRNA to the leading edge of primary fibroblasts and actin-rich protrusions of neurons, and its function is required for normal cell motility and polarisation (Farina et al., 2003; Kislauskis et al., 1994; Ross et al., 1997). ZBP1 binds *β-actin* mRNA in the nucleus, preventing its translation in the cytoplasm until the RNA reaches the cell periphery, where Src-mediated tyrosine phosphorylation dissociates ZBP1 from the RNA and local translation can proceed (Huttelmaier et al., 2005).

CArG-boxes, binding sites of the transcription factor SRF, are present in the gene-regulatory regions of all *actin* genes (Minty and Kedes, 1986; Sun et al., 2006a). Indeed, SRF-mediated control of cardiac α (Boxer et al., 1989; Chen et al., 1996; Muscat et al., 1988), smooth-muscle α (Mack and Owens, 1999), skeletal-muscle α (Lee et al., 1991; Muscat et al., 1988), and smooth-muscle γ actin (Carson et al., 2000) was demonstrated. These and other studies indicate that cell-type specific actin isoform expression is achieved by several transcription factor complexes, which can act positively or negatively (see, for example, Moss et al., 1994). Recent large-scale expression profiling has confirmed the regulation of actin genes by SRF (Philippar et al., 2004; Selvaraj and Prywes, 2004). No expression of cardiac, smooth or skeletal-muscle α actins was detectable in $Srf^{-/-}$ knockout mice at E7.5-E9.5 (Arsenian et al., 1998). Total actin expression was strongly decreased but not abolished in different $Srf^{-/-}$ embryonic stem cell clones (Schratt et al., 2002). Given that β actin and cytoskeletal γ actin are the most abundant actin isoforms in non-muscle cells (see Section 1.2.1.5), genes encoding these actin isoforms appear to be SRF targets. Indeed, transient expression of SRF-VP16 but not its derivative lacking most of the MADS box resulted in elevated *β-actin* mRNA levels in SRF knockout ($Srf^{-/-}$) embryonic stem cells (Schratt et al., 2002). Loss of actin expression might contribute to the gastrulation defect of these mice (see Section1.3.4, discussed in Arsenian et al., 1998).

The control of SRF by actin dynamics offers a model for homeostasis of actin expression at the transcriptional level (see Section 1.4.1).

In the following section, I will introduce SRF and the mode by which different competing cofactors control its activity.

1.3 Serum Response Factor (SRF)

The transcription factor serum response factor (SRF) is a well-studied paradigm for growth-factor regulated gene expression by transcription factor complexes. Its mechanisms of control embody several of the regulatory principles outlined in Section 1.1, including interaction with cofactors that are regulated by phosphorylation and subcellular localisation.

SRF was first identified on the basis of its interaction with the promoter of the *Fos* proto-oncogene (Gilman et al., 1986; Norman et al., 1988; Prywes and Roeder, 1986; Prywes and Roeder, 1987; Treisman, 1986). The *Fos* gene had previously been classified as immediate early gene as it does not require new protein synthesis for its rapid and transient activation upon serum stimulation of quiescent cells in culture (Greenberg and Ziff, 1984). SRF is conserved throughout the animal kingdom with orthologues in nematodes, arthropods and chordates.

1.3.1 MADS-box transcription factors

SRF is part of a larger family of MADS-box transcription factors, named after its founding members, the yeast transcription factor MCM1 (Minichromosome maintanance 1, Passmore et al., 1989), yeast ARG80/ARGR1 (Arginine requiring, Dubois et al., 1987) or plant Agamous (Yanofsky et al., 1990), plant Deficiens (Sommer et al., 1990) and animal SRF. MADS-box transcription factors include metazoan MEF2 (Myocyte Enhancer Factor 2) and numerous plant transcription factors. MADS-box transcription factors control diverse processes in various biological systems, including floral organ development in plants, mating-type specification, stress responses, metabolism and cell-cycle progression in yeast and immediate-early and muscle-specific gene expression in mammals (reviewed in Messenguy and Dubois, 2003).

MADS-box transcription factors share similar core DNA-binding domains consisting of an N-terminal 56-amino acid MADS box and a C-terminal extension of about 30 amino acids (reviewed in Shore and Sharrocks, 1995). A phylogenetic analysis

of the MADS box and the C-terminal sequences defined two lineages of MADS-box proteins, which were named type I and type II (Alvarez-Buylla et al., 2000). The type-I lineage includes transcription factors similar to SRF whereas type-II MADS box proteins comprise MEF2-like and plant MIKC (for MADS, intervening, keratin-like and C-terminal domains) subfamilies. Characteristics of both groups appear across plants, fungi and animals today, suggesting that gene duplication has occurred ancestral to the divergence of plant and animal kingdoms. Plants have another group of MADS-box genes that cannot be clearly placed into the type-I or type-II groups and might have arisen from recombination between the two lineages (Alvarez-Buylla et al., 2000).

1.3.2 DNA binding by SRF

MADS-box proteins bind DNA as dimers. This is reflected in the dyad-symmetry of their DNA-binding sites, which are about 10 bp long with an A/T-rich core flanked by C/G-rich sequences. As expected from the conservation of their DNA-binding domains, DNA-binding sites are similar but nonetheless distinct (reviewed in Shore and Sharrocks, 1995).

The SRF DNA-binding site in the *Fos* promoter was identified by studying the responsiveness of heterologous promoters to serum and named accordingly as Serum Response Element (SRE) (Treisman, 1985). Similar regulatory elements were described at the same time in the gene encoding cardiac α actin in different species and termed CArG (CC A-rich GG) box, based on its A/T-rich sequence flanked by G-C basepairs (Minty and Kedes, 1986). CArG boxes of these genes were shown to bind SRF (Mohun et al., 1987). Biochemical studies, including electrophoretic mobility shift assays, footprinting experiments and *in-vitro* site selection, identified the SRE consensus essentially as $CC(A/T)_2A(A/T)_3GG$ (Pollock and Treisman, 1990; Treisman, 1986).

1.3.3 SRF target genes

Following the identification of the SRE in the *Fos* gene, SRF-binding sites were identified in numerous other immediate early genes such as *Egr1*, *Vcl* (vinculin) and *Cyr61* (reviewed in Treisman, 1995).

As of today, several large-scale expression profiling studies by microarray (Philippar et al., 2004; Selvaraj and Prywes, 2004; Tullai et al., 2004) or chromatin immunoprecipitation (Zhang et al., 2005) have very much expanded the list of SRF target genes and point toward a strong involvement of SRF in actin-mediated processes. Besides actin genes, whose regulation by SRF is discussed in Section 1.2.7, and the gene for vinculin, cytoskeletal genes include those for gelsolin, zyxin and tropomyosin, to name a few examples. Using a genome-wide *in silico* search for the theoretically 1216-degenerate CArG box (here defined as $CC(A/T)_6GG$), more than 100 hypothetical SRF target genes, including 10 that were previously described, were identified in the mouse genome (Sun et al., 2006a). These included further genes encoding actin cytoskeletal regulators, such as Arp3, RhoE, cofilin 1, cofilin 2, coronin 1, destrin, Ena, filamin A and C, profilin I, and talin 1. Thus, it is clear that SRF is heavily implicated in cytoskeletal processes, which is also reflected by *Srf* knockout phenotypes (see Section 1.3.4).

SRF controls the expression of numerous muscle-specific genes such as those encoding smooth-muscle α actin, SM22, smooth-muscle myosin light chain, smooth-muscle myosin light chain kinase, α-myosin heavy chain, the transcription factor Nkx2.5, and atrial natriuretic factor (ANF) (Wang et al., 2001a; Wang et al., 2003b). Many muscle-specific genes contain two SREs as opposed to a single SRE in the *Fos* gene (see Wang et al., 2003b). Interestingly, SRF adds to the transcriptional programme of cardiac development not only by controlling protein-coding genes: SRF regulates the heart-specific microRNAs *miR-1* and *miR-2*. *MiR-1* targets the mRNA of *Hand2*, a transcription factor that promotes the proliferation of ventricular cardiomyocytes (Zhao et al., 2005).

In summary, most SRF target genes are functionally linked to processes such as cell proliferation, myogenesis and the regulation of the actin cytoskeleton. It appears that SRF can mediate a switch between the fundamentally different programmes of cell proliferation and differentiation (reviewed in Miano et al., 2007).

1.3.4 SRF knockout phenotypes

SRF is essential for the formation of mesoderm, and a homozygous null mutation of *Srf* results in embryonic lethality during the gastrulation stage of mouse development

at embryonic day 7.5 (E7.5) (Arsenian et al., 1998). *Srf*$^{-/-}$ embryonic stem (ES) cells can, however, differentiate into mesodermal cells *in vitro* in response to external factors and form mesoderm-derived structures *in vivo*, demonstrating that the block of mesodermal differentiation arises from a non-cell-autonomous effect of SRF loss (Weinhold et al., 2000). However, *Srf*$^{-/-}$ ES cells show impairments in spreading, adhesion and migration due to severe disruption of normal function of the actin cytoskeleton (Schratt et al., 2002). These include reduced expression and mislocalisation of focal adhesion proteins such as β1-integrin, talin, vinculin and zyxin, impaired activation of focal adhesion kinase (FAK), and an overall reduction in actin expression (Schratt et al., 2002). Surprisingly, although the immediate-early gene response is dependent on SRF, proliferation of *Srf*$^{-/-}$ ES cells is not impaired, and mice develop normally up to E6.5 (Arsenian et al., 1998; Schratt et al., 2001). This was in contrast to previous cell-based assays, which have suggested a requirement of SRF for proliferation of myoblasts (Soulez et al., 1996).

Given the embryonic lethality of SRF, the approach of conditional knockout has shed light on the roles of SRF in later stages of development. Conditional knockout of SRF in the cardiovascular system (Miano et al., 2004) or the heart (Niu et al., 2005; Parlakian et al., 2004) of mice results in embryonic lethality between E10.5 and E13.5. Hearts of mutant mice are generally disorganised, show strong defects in trabeculation and lack the regular, parallel sarcomeric organisation found in the heart of wild-type animals. Smooth-muscle cells lack the characteristic bundles of actin and intermediate filaments, and their recruitment to the dorsal aorta is impaired (Miano et al., 2004). Deletion of SRF from skeletal muscle adult in adult mice results in a strong reduction of muscle mass and muscle regenerative potential and a disruption of sarcomeric architecture (Charvet et al., 2006).

The role of SRF in the nervous system has been studied extensively. Deletion of SRF from hippocampal or cortical neurons in the adult brain strongly impairs immediate-early gene expression, which is induced following exposure of mice to a novel environment, and long-term synaptic plasticity (Ramanan et al., 2005). Deletion of SRF in the adult forebrain of mice results in defects of hippocampus-dependent spatial memory; mutant mice therefore lack any sign of habituation when placed into a new environment (Etkin et al., 2006). On the cellular phenotypic level, these mice display severe neurite outgrowth and neuronal pathfinding defects in their hippocampi

(Knoll et al., 2006). Conditional knockout of SRF in the subventricular zone (SVZ), a neurogenic region of the brain, results in aberrant migration of cells of the SVZ along the rostral migratory stream into the olfactory bulb (Alberti et al., 2005). This cell-migration defect can be recapitulated *in vitro* and is therefore cell-autonomous.

SRF is also expressed in developing and mature lymphocytes and its conditional knockout in these cells affects both T- and B-cell development (Fleige et al., 2007). T-cell differentiation is dependent on SRF (see also Section 1.3.6.1), whereas its contribution to B-cell development is less critical. Loss of SRF in the B-cell compartment results in reduced B-cell numbers, absence of marginal zone B-cells, which populate a specific area in the spleen, and a decrease in a specific B-cell population.

1.3.4.1 SRF inactivation in non-vertebrates

SRF inactivation studies are not restricted to mice. In the amoeba *Dictyostelium discoideum*, SRF is required for spore maturation (Escalante and Sastre, 1998). In the nematode *Caenorhabditis elegans*, SRF (gene name *unc-120*) inactivation results in an "uncoordinated" (unc) phenotype from muscular defects (http://www.wormbase.org, Fraser et al., 2000).

SRF in the fruit fly *Drosophila melanogaster*, DSRF, is defined by several mutant alleles: *pruned*, a loss-of-function mutation induced by insertion of a P-element (Affolter et al., 1994; Guillemin et al., 1996) and classical mutations in the *blistered* allele (Fristrom et al., 1994; Montagne et al., 1996). Although different in severity, all mutations were later shown to affect the same gene (Montagne et al., 1996). *Pruned* mutants lack terminal branches of the tracheal system and are not viable (Affolter et al., 1994; Guillemin et al., 1996). The mutation results in the failure of terminal cells to form cytoplasmic projections, which in normal cells proceed to develop into tubular structures (Guillemin et al., 1996). The *blistered* mutations result in ectopic vein formation and "blistering" of the wing due to defective adhesion between the two epithelial cell layers of the wings (Fristrom et al., 1994; Montagne et al., 1996). DSRF is expressed in regions of wing imaginal discs that go on to develop intervein tissues, and its function appears to be the suppression of wing vein differentiation.

In summary, a recurring observation is the connection of SRF activity and cytoskeleton-mediated activities such as cell morphology, motility/contractility and adhesion in the various systems and organisms in which SRF was studied. While SRF appears essential for these processes, it is dispensable for cell proliferation *in vivo*. The extensive complement of SRF target genes reflects the role of SRF as a master regulator of the actin cytoskeleton (reviewed in Miano et al., 2007, and see Section 1.3.3).

1.3.5 Specificity of SRF-mediated gene expression

SRF is the product of a single gene with no apparent paralogues, widely expressed, constitutively nuclear in most cell types (Gauthier-Rouviere et al., 1991) and has a relatively weak transactivation domain (Johansen and Prywes, 1993). Yet, SRF efficiently activates a diverse range of transcriptional programmes in response to extracellular signals (see Section 1.3.3 for SRF target genes). These observations raise the questions of how signal-induced SRF activity and specificity of gene expression are achieved.

Dissection of the signalling requirements for SRF-mediated transcription defined two classes of SRF target genes in the fibroblast model: those that are preferentially controlled by Ras-Mitogen-Activated Protein (MAP) kinase signalling and those that require RhoA-actin signalling (Gineitis and Treisman, 2001). Sensitivity to different signalling pathways reflects differential recruitment of competing cofactors to the DNA-binding domain of SRF (Figure 1.5). The MAP-kinase dependent class of SRF target genes is controlled by members of the ternary complex (TCF) family of transcription factors (see Section 1.3.6) while the RhoA-dependent class is subject to regulation by the myocardin family of transcriptional coactivators (see Section 1.3.7) (reviewed in Posern and Treisman, 2006). The myocardin family contains myocardin, a cardiac- and smooth-muscle specific SRF coactivator, and the myocardin-related transcription factors (MRTFs), which include MAL.

Other potential SRF cofactors include homeodomain proteins such as the Nkx transcription factors, the GATA family of zinc-finger proteins and the MyoD family of basic-helix-loop-helix transcription factors, all of which cooperate with SRF in activation of transcription (reviewed in Posern et al., 2002 and Zaromytidou, 2007).

An example for an inhibitory SRF cofactor is provided by the heart-enriched LIM-only protein FHL2 (four-and-a-half LIM-domain protein 2; Philippar et al., 2004). FHL2 expression is a target of RhoA-actin-MAL signalling. FHL2 specifically antagonises MAL activity, directly competing with MAL for SRF binding, and thereby establishes a negative feedback mechanism (Philippar et al., 2004).

Phosphorylation of the SRF MADS box may modulate differential cofactor recruitment to SRF and thereby contribute to SRF regulation (Iyer et al., 2003; Iyer et al., 2006), but much remains to be learned about this (discussed in Posern and Treisman, 2006).

In the following section, I will introduce the SRF cofactors of the TCF and myocardin families before presenting the link of the MRTF subclass of myocardin-family proteins to actin dynamics in the subsequent section.

1.3.6 Ternary Complex Factors (TCFs)

TCF proteins, SAP-1 (Dalton and Treisman, 1992), Elk-1 (Shaw et al., 1989), and Net (also called SAP-2 or ERP) (Giovane et al., 1994; Lopez et al., 1994; Price et al., 1995), represent one class of SRF cofactors (reviewed in Treisman, 1994; see also Figure 1.5). All three TCF family members can form ternary complexes with SRF and DNA, but binding efficiencies and responsiveness to different signals vary (Price et al., 1995).

TCFs are members of the ETS domain family of transcription factors, which share a conserved N-terminal ETS domain that binds to DNA containing a central GGA motif (reviewed in Sharrocks, 2001). In SRF-TCF target genes, ETS DNA binding sites are located adjoining the SRE. In addition to the ETS domain, TCFs also possess a conserved central, hydrophilic B box and a C-terminal C box. The B box is critical for TCF interaction with SRF, but ternary complex formation also depends on DNA contacts by the ETS domain (Dalton and Treisman, 1992; Janknecht and Nordheim, 1992; Shore and Sharrocks, 1994). Therefore, the ETS domain and B box cooperate in ternary complex formation. The C box and the C-terminus contain several (S/T)P phosphorylation sites important for regulated transcriptional activation. It is through these sites that TCFs link SRF to upstream MAP kinase signalling (Gille et al., 1992;

Hill et al., 1993; Janknecht et al., 1993; Marais et al., 1993; Price et al., 1995; Zinck et al., 1993).

In-vitro studies addressing the question of whether C-terminal phosphorylation of TCFs is required for ternary-complex formation with SRF and DNA have led to contradicting views (discussed in Treisman, 1994). However, *in-vivo* genomic footprinting shows that TCFs occupy DNA in unstimulated cells (Herrera et al., 1989). SRF-TCF target genes can be recovered by chromatin immunoprecipitation of SAP-1 or Elk-1 in unstimulated thymocytes (Costello et al., 2004) or Elk-1 in fibroblasts (Li et al., 2003a). Moreover, fusion of the constitutively active activation domain of VP16 to the C-terminus of SAP-1 or Elk-1 resulted in SRF activation without the need of stimulation (Dalton and Treisman, 1992; discussed in Treisman, 1994). Therefore, MAP-kinase mediated TCF phosphorylation is likely to regulate ternary-complex activity rather than its assembly.

1.3.6.1 TCF knockout phenotypes

Inactivation of different TCFs in mice has begun to unravel their biological roles. Mice expressing a Net variant that lacks the ETS domain up-regulate *Egr1*, exhibit dilated lymphatic vessels in the thorax and die shortly after birth from respiratory failure resulting from accumulation of chyle in the thoracic cavity (Ayadi et al., 2001). Mice lacking SAP-1 display a drastic defect in positive selection of double-positive ($CD4^+/CD8^+$) thymocytes (Costello et al., 2004). *Sap1*$^{-/-}$ mice develop a phenotype similar to Castleman's disease when kept in non-sterile conditions (Costello et al., 2004). There clearly appears to be some degree of functional redundancy between different TCFs. Phenotypically, Elk1-knockout mice are largely indistinguishable from their wild-type littermates, except for some changes in *Fos* expression in certain regions of the brain following the induction of seizures (Cesari et al., 2004). The other two TCFs, Sap-1 or Net, might functionally compensate for the loss of Elk1. A full understanding of redundant and specific TCF functions will require the combined inactivation of different TCFs in mice.

1.3.7 Myocardin-related transcription factors (MRTFs)

A *Fos* promoter with an abolished Ets site remains responsive to serum, its major mitogenic component lysophosphatidic acid (LPA), or AlF_4^-, but not TPA (tetradecanoylphorbol-13-acetate), CSF1 (colony-stimulating factor 1), PDGF (platelet-derived growth factor), EGF (epidermal growth factor) or UV-C, suggesting that SRF is either directly modified in response to the previous group of signals or controlled by a growth-factor responsive SRF cofactor distinct from the TCFs (Graham and Gilman, 1991; Hill et al., 1994; Hill et al., 1995). In the absence of growth-factor induced phosphorylation of the SRF DNA-binding domain, the cofactor model remained most plausible. Further work established that the TCF-independent pathway involves Rho-family GTPases. RhoA is required for serum-, LPA- or AlF_4^--induced SRF activity, while two other Rho family GTPases, Rac1 and Cdc42, can also potentiate SRF-mediated transcription but are not required for serum induction in NIH3T3 fibroblasts (Hill et al., 1995).

The discovery of myocardin as a potent heart- and smooth-muscle specific SRF coactivator catalysed the identification of the unknown cofactor in the Rho pathway (Wang et al., 2001a, see Figure 1.5). Ubiquitously expressed MAL/MKL1 (Megakaryocytic Acute Leukaemia / Megakaryoblastic Leukaemia 1) was identified as a fusion partner of RBM15 (RNA-binding motif protein-15) in the t(1;22)(p13,q13) chromosomal translocation that occurs in acute megakaryoblastic leukaemia (AML) (Ma et al., 2001; Mercher et al., 2001). Another MAL protein, MAL16, was found to be encoded on chromosome 16 in humans (Mercher et al., 2001). Gene-trapping experiments affecting the *MAL16* locus in the mouse genome resulted in perinatal lethality (Skarnes et al., 1992). A splice variant of MAL, called BSAC (basic, SAP, and coiled-coil domain), was identified in a screen for antiapoptotic factors (Sasazuki et al., 2002). MAL was cloned and demonstrated to function as SRF-coactivator in the Rho pathway (Miralles et al., 2003). These proteins, MAL/MKL1/MRTF-A and MAL16/MKL2/MRTF-B, constitute the family of myocardin-related transcription factors (MRTFs).

The present thesis focuses on the myocardin family of SRF cofactors, particularly the control of MAL. A more detailed introduction to the biological roles and control of myocardin-family proteins will be given in Section 1.4.3.

1.3.8 Revealing the basis of cofactor recruitment: structural biology of SRF

1.3.8.1 Structure of the SRF core bound to DNA

The X-ray crystal structure of the SRF DNA binding domain (amino acids 132-223) in complex with a consensus SRE DNA provided first the structural insights into how this small domain simultaneously accomplishes dimerisation, sequence-specific DNA binding and co-factor recruitment (Pellegrini et al., 1995; Figure 1.6 A). The SRF homodimer forms a three-layered structure in which each structural element in a monomer interacts with the identical element in the other monomer. Two amphipathic α-helices, one contributed by the central region of the MADS box of each monomer, form an antiparallel coiled coil that contacts the minor groove of the DNA (Figure 1.6 A). Onto the coiled coil face opposite to the DNA packs a four-stranded antiparallel β-sheet formed by the C-terminal part of each MADS box. Sequences C-terminal to the MADS-box form an irregularly coiled pair of helices with a pair of short α-helices on top of this. The DNA is bent around the protein by 72°, and unusual groove widths compared to B-DNA reflect its distortion. This bending allows the basic N-termini of the MADS-box helices and loops at the edges of the β-sheet structure to contact the major grooves of each half site. The extended regions N-terminal to the MADS-box helices reach around the DNA and bind the minor grooves on the opposite side, inserting conserved arginine residues in an extended conformation. These contacts explain the different sequence specificities of the MADS-box transcription factors SRF, MCM1 and MEF2A (Nurrish and Treisman, 1995; Sharrocks et al., 1993).

Contact sites for SRF accessory factors of the TCF family (Treisman, 1994), previously identified by mutagenesis in SRF and comparison with ARG80 (Mueller and Nordheim, 1991), mainly map on the solvent-exposed helical region atop the β-sheet. The expanded major groove opposite the coiled-coil DNA interaction of SRF, which lies in the centre of the CArG-box consensus, is largely exposed and might therefore allow other cofactors to bind simultaneously, as proposed for Phox1 (Grueneberg et al., 1992; Simon et al., 1997).

1.3.8.2 Structure of the SAP1-SRF-DNA ternary complex

The structure of the ternary complex of the TCF SAP-1a, SRF and DNA was solved by X-ray crystallography (Hassler and Richmond, 2001), using the same SRF DNA-binding domain employed in the SRF-DNA study (see Section 1.3.8.1 and

Pellegrini et al., 1995) and a SAP-1a construct spanning the region from its DNA-binding domain to the B-box domain (Figure 1.6 B). The 26-bp DNA fragment included an ETS binding site (GGA core) 5' to the CArG box with 3 bp in between as in the *Fos* promoter. The structure illuminates the mechanism of cooperative binding of TCF proteins to SRF and DNA (Treisman et al., 1992). The proteins make extensive contacts over the entire length of this DNA fragment. Given the spacing of the binding sites, SRF and the ETS domain of SAP-1a are bound to opposite sides of the DNA molecule with the ETS domain occupying the major groove. The linker between the ETS domain and B-box is not resolved, suggesting that it is flexible (Figure 1.6 B). The B-box forms a 3_{10}-helix/β-strand/3_{10}-helix structure that contacts all three structural layers of one SRF molecule (see Section 1.3.8.1) and the DNA in its major groove. Extensive hydrophobic contacts mediated by residues in the 3_{10} helix and the β-strand of the B-box orient the β-strand to join the β-sheet that is provided by the SRF dimer in an antiparallel fashion. The structure confirms previous models regarding the role of the B box in ternary complex formation (Hill et al., 1993).

In the given spacing of the DNA-binding sites, the N-terminus of the αI helix of the TCF-proximal SRF molecule and the C-terminus of the SAP-1a α3 helix interact directly via hydrophobic surfaces, although the contribution to complex formation is not large. A larger spacing of the DNA binding sites as seen in many genes would abolish this interaction while a smaller spacing would block simultaneous binding of SRF and SAP-1a. In fact, both Elk-1 and SAP-1 display a high degree of flexibility in their DNA binding characteristics with SRF (Treisman et al., 1992). Cooperative formation of ternary complexes occurs even when the SRE and ETS sites are inverted relative to each other or separated by two helical turns of DNA.

1.4 The Rho-actin-MAL-SRF signalling pathway

1.4.1 Actin dynamics link SRF to Rho signalling

The variety of signalling events occurring downstream of active Rho GTPases (see Section 1.2.4.2) posed the question of which of the various Rho effectors connect RhoA to SRF-mediated transcription. A cDNA screen identified the LIM kinase-1 as one component of this link (Sotiropoulos et al., 1999, Figures 1.3 and 1.7). LIMK-1 is a target of the Rho effector Rho kinase (ROCK; see Section 1.2.4.2 and Figure 1.3). The ability of LIMK-1 to activate SRF depends on its effect on actin dynamics

(Sotiropoulos et al., 1999): LIM kinases phosphorylate and thereby inactivate ADF/cofilin, thereby achieving a stabilisation of actin filaments (see Sections 1.2.2.3 and 1.2.4.2). In addition to the RhoA-ROCK-LIMK-cofilin pathway, formin-mediated assembly of actin filaments provides a further input for SRF activity in the RhoA-actin pathway (Geneste et al., 2002, see Section 1.2.3.2 and Figure 1.7).

The contributions of both of the LIMK- and formin-mediated RhoA effector branches to SRF regulation differ between cell types (Geneste et al., 2002). TCF-independent SRF activation in NIH3T3 fibroblasts, requires mDia1 effector activity (Tominaga et al., 2000) but not ROCK-LIMK (Sahai et al., 1998; Sahai et al., 1999; Sotiropoulos et al., 1999). The ROCK-LIMK-cofilin pathway is, however, required for serum-induced activation of SRF in neuronal (PC12 phaeochromocytoma, SKNMC and Neuro2A) cells (Geneste et al., 2002). In PC12 cells, both effector pathways cooperate with each other for SRF activation, consistent with a model in which ROCK-LIMK-cofilin signalling stabilises actin filaments generated by mDia (Geneste et al., 2002).

1.4.2 Control of SRF by the G-actin pool

Interference with the actin polymerisation cycle in various ways demonstrated that signals which activate SRF independently of TCFs converge at the level of actin dynamics (Sotiropoulos et al., 1999). Agents that were used to interfere with actin polymerisation include *Clostridium botulinum* C2 toxin, which ADP-ribosylates G-actin at R177 and blocks its polymerisation, actin-binding toxins (see Section 1.2.6) and transiently expressed regulators of actin dynamics. Assembly of actin filaments by overexpression of VASP, WASP, N-WASP, the VCA region of N-WASP, or constitutively active forms of the formins mDia1 and mDia2 activates SRF (Sotiropoulos et al., 1999).

SRF might either respond to increased F-actin levels, a changed F:G-actin ratio or decreased G-actin levels. The actin-binding toxins swinholide A and cytochalasin D activate SRF without increasing the amount of F-actin as in the case of jasplakinolide (see Section 1.2.6 for mechanisms of actin-binding toxins). Overexpression of β actin or treatment with the G-actin sequestering toxin latrunculin B (see Section 1.2.6.1) inhibits SRF activation by serum. Beta actin overexpression increased the G-actin pool without affecting the F:G-actin ratio (Posern et al., 2002). Therefore, SRF is likely to respond to

a depletion of G-actin following the activation of RhoA. This observation is in agreement with the earlier notion that the G-actin pool controls actin expression (see Section 1.2.7).

These observations may be explained by an effect of these manipulations on the actin polymerisation cycle or a direct role of actin in signalling to SRF (Sotiropoulos et al., 1999). Actin mutants were studied to resolve this question (Posern et al., 2002). Expression of non-polymerisable mutant derivatives of β actin, G13R, R62D or an actin-VP16 fusion effectively blocked SRF activity. Conversely, actin mutants that stabilise F-actin, V159N or S14C, activate SRF in the absence of upstream stimuli. The observation that actin does not need to participate in the polymerisation cycle to affect SRF activity strongly suggests a direct role of actin in SRF regulation. However, a direct interaction between actin and SRF could not be detected (Posern et al., 2002). Recent work identified MAL as a G-actin binding SRF coactivator, which communicates the status of the actin cytoskeleton to SRF (Miralles et al., 2003).

In the following section, I will introduce in detail functions, topology and regulation of the myocardin family of SRF coactivators, which MAL is part of.

1.4.3 The myocardin family of SRF cofactors

The myocardin family (reviewed in Pipes et al., 2006 and Posern and Treisman, 2006) is a group of SRF cofactors that is distinct from the TCFs. It is represented by myocardin itself (Wang et al., 2001a) and the myocardin-related transcription factors (MRTFs) MAL and MAL16 (Miralles et al., 2003; Selvaraj and Prywes, 2003; Wang et al., 2002; Figure 1.8; also see Section 1.3.5 for an introduction to SRF cofactors and Section 1.3.7 for MRTFs in particular). Alternative splicing and translation start sites account for different isoforms with deviating N-termini. An overview of the myocardin-family proteins and their sequence relationships is given in Figure 1.8.

Note that, although the common nomenclature of MRTFs as "transcription factors" suggests otherwise, no MRTF-autonomous transcriptional activity has been reported. While both myocardin and MRTFs are coactivators of SRF, myocardin was also reported to potentiate MEF2-mediated transcription (Creemers et al., 2006). SRF and MEF2 are likely to compete for myocardin.

1.4.3.1 Steady-state localisation of myocardin-family proteins

MAL and MAL16 are cytoplasmic in serum-starved NIH3T3 fibroblasts, but accumulate in the nucleus and potentiate SRF-mediated transcription upon serum stimulation (Du et al., 2004; Kuwahara et al., 2005; Miralles et al., 2003). These localisation properties of MAL are, however, not observed in all cell lines. The BSAC splice variant of MAL localises similarly to MAL in NIH3T3 fibroblasts (Miralles et al., 2003) but was found nuclear in HeLa cells (Sasazuki et al., 2002). MAL localises to the nucleus of both serum-starved and -stimulated primary rat aortic and A7r5 smooth-muscle cells (Du et al., 2004). Moreover, in serum-starved MDA-MB-231 human breast cancer cells, a significant proportion of MAL appears nuclear, although it is likely that MAL is not transcriptionally active under these conditions (Cristina Perez-Sanchez and Souhila Medjkane, personal communication).

Conversely, the cardiac- and smooth-muscle specific SRF coactivator myocardin (MC), was never observed to localise to the cytoplasm and appears constitutively nuclear and active when expressed in NIH3T3 fibroblasts, 10T1/2 fibrobasts and COS cells (Kuwahara et al., 2005; Wang et al., 2001a; Wang et al., 2003b).

1.4.3.2 Domain organisation of myocardin family proteins

Myocardin-family proteins are about 1,000-amino acids in size and share a similar domain organisation (Figure 1.8).

1.4.3.2.1 The RPEL domain

The N-terminus of myocardin-family proteins contains a repeat of three RPEL motifs (PFAM 02755, http://pfam.sanger.ac.uk/, Finn et al., 2006), constituting the "RPEL domain" (Figure 1.8; see Figure 2.1 in Chapter 2 for a sequence alignment of myocardin-family RPEL domains). According to the PFAM database at the onset of the studies described here, RPEL motifs are 22-amino acid sequences of unknown function, containing an RPxxxEL core. RPEL motifs are found in multicellular fungi, nematodes, arthropods and chordates (Interpro IPR004018, Zdobnov and Apweiler, 2001). All three RPEL motifs in MAL contain this core with the exception of RPEL1, in which the first and most conserved R residue is followed by another R (RRxxxEL). The RPEL domain is required for binding of G-actin by MAL (Miralles et al., 2003; Posern et al., 2004, see

Chapter 2). Sequences of different RPEL motifs vary within and between myocardin-family members (Figure 1.8; see Figure 2.1 in Chapter 2 for sequence alignment). Initially, a methionine at the end of RPEL1, M92, was predicted to represent the translation start site of MAL. The resulting protein, termed MAL(met), lacks RPEL1 but is regulated similarly to the full-length variant that contains all three RPEL motifs (Miralles et al., 2003; Posern et al., 2004). Mutant derivatives of MAL(met) in which the P residues in the RPEL motifs are mutated to A display reduced actin binding affinity as assessed by co-immunoprecipitation, GST affinity sedimentation and yeast-two-hybrid assays (Miralles et al., 2003; Posern et al., 2004). Exchange of the R residues of the RPEL motifs in MAL(met) for D, generating charge reversals, also reduces actin binding in GST affinity sedimentation assays (Posern et al., 2004). Whether the RPEL motifs provide a structural framework of the RPEL domain that is necessary for actin binding or whether they represent the actin-binding elements themselves has remained unclear. Furthermore, it remained unknown whether the MAL-actin interaction is direct or indirect. Given the additive nature in the effect of RPEL motif mutations toward actin binding in the yeast-two-hybrid analysis, it is likely that multiple actin molecules interact with MAL (Posern et al., 2004). However, the effect might also be due to synergistic loss of secondary or tertiary structure with the introduction of further mutations.

Since myocardin appears constitutively active and is not subject to regulated nuclear localisation (see Section 1.4.3.1), the contribution of its RPEL motifs to regulation is unclear (Kuwahara et al., 2005; Wang et al., 2001a; Wang et al., 2003b). Myocardin RPEL motifs deviate from those in MAL and might therefore have different functions. Alternative splicing and differential translation start sites generate different isoforms of myocardin. A cardiac-enriched isoform, which contains all three RPEL motifs, interacts with and activates MEF2 (Creemers et al., 2006, see Figure 1.8). MEF2 activation depends on a region comprising the N-terminal half of RPEL1 and a short, myocardin-specific segment just N-terminal to it. An isoform of myocardin prevalent in smooth muscle lacks RPEL1 and most of RPEL2, and is therefore not able to activate MEF2-dependent transcription (Creemers et al., 2006).

1.4.3.2.1.1 A second family of RPEL-motif containing proteins

Besides myocardin-family proteins, a second protein family whose members contain RPEL motifs exists in metazoans. This family contains 4 proteins, named Phactrs (protein phosphatase 1 and actin regulatory proteins) 1-4 (Allen et al., 2004) or RPEL A, B, CL ("long") and CS ("short") (Favot et al., 2005). The proteins contain a cluster of three RPEL motifs at their C-termini and a single RPEL motif at their N-termini. All of them bind actin in co-immunoprecipitation experiments or can be targeted to the nucleus by co-expression of NLS-β actin (Sara Ellis, personal communication; Allen et al., 2004; Favot et al., 2005). Actin-binding activity of Phactr proteins is further supported by the observation that their overexpression in C2C12 cells results in cell shape alterations. The functions of Phactrs and the role of actin binding are currently unknown. Transiently expressed Phactr proteins localise to both nucleus and cytoplasm. They show a differential expression in different murine organs (Allen et al., 2004; Favot et al., 2005) and distinct distribution patterns in the rat brain (Allen et al., 2004). Phactr1 inhibits the *in-vitro* activity of protein phosphatase 1 (PP1), which it interacts with via a C-terminal site distinct from the RPEL motifs (Allen et al., 2004).

1.4.3.2.2 Putative nuclear localisation signals of MAL

The RPEL domain contains a basic region of 9 amino acids, termed B2 (Miralles et al., 2003). Deletion of the B2 region in the context of full-length MAL blocks nuclear accumulation of MAL, indicating that it represents a basic nuclear import signal (Vartiainen et al., 2007, see Section 1.1.1.1). However, deletion of the B2 region is not sufficient to block nuclear accumulation in the context of MAL(met), and additional deletion of a further basic region, B1, C-terminal of the RPEL motifs is required. A MAL mutant lacking the first 172 amino acids and therefore all sequences N-terminal and including the N-terminal half of RPEL3 (MAL ΔN) appears constitutively nuclear. Nuclear localisation of MAL ΔN is dependent on the B1 region (Miralles et al., 2003; Zaromytidou et al., 2006). The role of B1 in nuclear import of full-length MAL remains uncertain since its deletion in this context does not appear to change the nuclear accumulation kinetics of MAL (Maria Vartiainen, personal communication). Both basic regions are conserved in myocardin (see sequence alignment in Figure 2.1, Chapter 2).

1.4.3.2.2.1 The B1 and Q regions in MAL-SRF interaction and nuclear localisation

The B1 box is essential for ternary complex formation between MAL, SRF and DNA (Miralles et al., 2003). Residues in the C-terminal half of B1, especially hydrophobic and positively charged ones, appear more critical for ternary complex formation than residues in the N-terminal half, and a seven-residue sequence (LKYHQYI) within this region is required and sufficient for ternary complex formation (Zaromytidou et al., 2006). The nuclear localisation and SRF-interaction functions are separable as numerous point mutations that abolish ternary complex formation, mainly involving hydrophobic or aromatic amino acids such as two Y residues, do not affect nuclear localisation of MAL ΔN or signal-induced nuclear accumulation of MAL (Zaromytidou et al., 2006).

A 22-amino acid Q-rich region termed the Q-box appears to counteract MAL nuclear accumulation since its deletion results in increased nuclear localisation of MAL in the absence of stimuli (Miralles et al., 2003). Furthermore, deletion of the Q-box reduces ternary complex formation, implicating the Q-box in SRF binding (Miralles et al., 2003). A more detailed analysis demonstrated that the Q-box enhances SRF interaction, mainly through hydrophobic interactions involving the Q-box core (Zaromytidou et al., 2006). However, mutation of these residues did not significantly affect the ability of MAL ΔN to activate the SRF reporter, underlining that the Q-box is not critical for SRF binding *in vivo* (Zaromytidou et al., 2006).

Ternary complex factors (TCFs) and MAL compete for SRF, suggesting that they interact with a common surface on SRF (Miralles et al., 2003; Murai and Treisman, 2002; Wang et al., 2004). Mutagenesis of SRF indicated that both MAL and Elk-1 interact with a hydrophobic groove on SRF, to which the βII-strand of SRF contributes (see Section 1.3.8.2 for structure). However, the extents of how ternary complex formation is affected by point mutations of this region differ for MAL and Elk-1 for several residues, exchange of some of which had opposite effects (Zaromytidou et al., 2006). Therefore, MAL and Elk-1 bind SRF in somewhat different modes. Mutations in the αI helix of SRF (see Figure 1.6 B), which affect DNA bending by SRF, specifically compromise ternary complex formation with MAL but not Elk-1 (Zaromytidou et al., 2006). However, αI-helix mutations do not affect DNA distorsion in the ternary complex of MAL. This indicates that MAL makes direct contacts with DNA sequences flanking the SRE site. Indeed, MAL-SRF interaction is greatly facilitated by SRE DNA

in co-immunoprecipitation assays. MAL protects nucleotides at positions +16 through +22 and -16 through -22 relative to the SRE dyad from DNaseI (Zaromytidou et al., 2006). These flanking regions are required for efficient MAL-SRF-DNA ternary complex formation as shortening them to 16 nucleotides or less (relative to the SRE dyad) virtually abolishes MAL binding without affecting the SRF-DNA interaction. Whether MAL displays any DNA sequence preference is currently unknown.

In summary, the data suggest that MAL binds SRF by adding a β strand to the β-sheet region of SRF, similarly to the ternary complex factors (see Section 1.3.8.2 and Figure 1.6 B) and support a model in which direct contacts between MAL and DNA are facilitated by SRF-mediated DNA bending (Zaromytidou et al., 2006).

1.4.3.2.3 The SAP domain

SAP (SAF-A/B, Acinus, Pias) domains are 35-amino acid motifs predicted to contain two amphipathic helices; they occur in several DNA-binding proteins, but their functions are poorly understood. Proteins containing SAP domains regulate transcription, mRNA splicing, DNA repair, chromatin organisation and chromatin degradation in apoptosis (reviewed in Aravind and Koonin, 2000). Deletion of or mutations in the SAP domain of myocardin-family proteins do not affect ternary complex formation with SRF (Miralles et al., 2003; Wang et al., 2001a). However, mutation of the SAP domain strongly impairs the ability of myocardin to activate a reporter gene under control of the atrialnatriuretic factor (*ANF*) promoter (Wang et al., 2001a). Deletion of the SAP domain reduces the myogenic activity of myocardin in 10T1/2 fibroblasts by about 50%, as judged by the expression of smooth-muscle myosin heavy chain (Wang et al., 2003b). The SAP domain may function in a promoter-specific manner in the context of chromatin.

1.4.3.2.4 The leucine zipper motif

Myocardin-family proteins contain leucine-zipper like motifs, and these mediate homo-dimerisation both in MAL, MAL16 and myocardin (Miralles et al., 2003; Selvaraj and Prywes, 2003; Wang et al., 2003b), although MC homodimerisation is much weaker than that of MAL (Zaromytidou, 2007).

Leucine zipper motifs, which are frequently found in gene-regulatory proteins, form amphipathic helices with leucines in a regular 7-amino acid spacing, therefore extending from one side of the helix. The helices engage in a coiled coil by hydrophobic interactions (Landschulz et al., 1988).

MAL can form heterodimers with MAL16 (Selvaraj and Prywes, 2003) or myocardin (Zaromytidou, 2007). Although MAL dimerises in the context of the ternary complex with SRF and DNA, MC does not (Miralles et al., 2003; Wang et al., 2003b; Zaromytidou, 2007). Nevertheless, the leucine zipper is required for the full transactivation potential of myocardin, indicating that it is relevant *in vivo* (Du et al., 2004; Wang et al., 2003b). Leucine zipper functionality might be context-dependent since the leucine zipper of myocardin can mediate relatively strong homodimerisation of a MAL chimaera containing an ectopic myocardin leucine zipper (Zaromytidou, 2007).

1.4.3.2.5 The transcription activation domain

A C-terminal domain is required for the transactivation potential of myocardin-family proteins (Miralles et al., 2003; Wang et al., 2001a). Consistent with the C-terminus of MAL acting as a transcription activation domain, its fusion to the LexA-DNA binding domain confers transcription activation to a LexA reporter gene (Miralles et al., 2003). MRTF derivatives lacking the TAD act in a dominant-negative manner (Selvaraj and Prywes, 2003).

1.4.3.3 Biological functions of the myocardin family

1.4.3.3.1 Myocardin-family target genes

Activation of MAL by swinholide-A treatment induces its association with the promoters of *Cyr61*, *Srf* and *Vcl* but not *Egr1* or *Fos* (Miralles et al., 2003), indicating that MRTFs control a subset of SRF target genes defined previously (Gineitis and Treisman, 2001, see Section 1.3.3). MRTFs require SRF for DNA binding. They do not engage with DNA-binding sites distinct to the SRE as do TCFs, but the direct interaction of MAL with sequences flanking the SRE raises the question whether certain DNA sequences define a subset of SRF target genes that is preferentially controlled by MRTFs (Zaromytidou et al., 2006). Competition between TCFs and myocardin-family

proteins certainly represents one mechanism by which SRF target gene specificity is achieved (Wang et al., 2004; Zaromytidou et al., 2006; see also Section 1.3.5).

In a microarray analysis employing a cell line that expresses a dominant negative MAL derivative lacking the C-terminus including its transcription activation domain, serum-induction of 28 out of 150 SRF target genes required MAL (Selvaraj and Prywes, 2004). MAL-dependently activated genes included regulators of cell proliferation, transcription factors and regulators of the actin cytoskeleton. Comparison of available SRE sequences between MAL-dependent and MAL-independent genes identified no apparent DNA binding preference for MAL.

Since the dominant-negative approach in this study might also affect TCF-dependent genes, it is difficult to draw a clear boundary between genes found to be MAL-dependent and those that appeared MAL-independent. Future studies should target both MAL genes, which can be expected to be at least partially redundant, by RNA interference.

Myocardin controls smooth- and cardiac-muscle specific genes (see Section 1.3.3). While MAL and MAL16 are ubiquitously expressed (Du et al., 2004; Mercher et al., 2001; Selvaraj and Prywes, 2003; Wang et al., 2002), myocardin is restricted to smooth and cardiac muscle (Wang et al., 2001a). How is specificity between MAL/MAL16 and myocardin achieved? Numerous muscle-specific genes contain two SREs rather than a single one. In the absence of detectable leucine-zipper mediated myocardin dimerisation in ternary complexes with SRF on a single SRE, myocardin molecules on different SREs have been proposed to dimerise. The evidence for such a model is weak and largely based on the observation that the leucine zipper in myocardin is required for maximal SRF activation. It is more likely that myocardin, which activates SRF very strongly, is controlled by its expression in certain stages of development and competition with other SRF cofactors.

A cardiac-enriched isoform of myocardin can act as a coactivator of MEF2, another MADS-box transcription factor that controls a set of growth-associated and muscle-specific genes distinct from those regulated by SRF (Creemers et al., 2006, also see Section 1.4.3.2.1).

In addition to controlling a subset of growth-factor responsive immediate early genes, MAL proteins were also implicated in muscle development. When

overexpressed, MAL and MAL16 activate reporter genes driven by smooth- or cardiac-muscle gene promoters in non-muscle cells (Du et al., 2004; Selvaraj and Prywes, 2003; Wang et al., 2002) or endogenous smooth-muscle specific genes in undifferentiated *Srf*$^{-/-}$ embryonic stem cells (Du et al., 2004). Conversely, expression of dominant negative MAL or MAL16 suppresses activation of such reporter genes (Selvaraj and Prywes, 2003) or the endogenous *smooth-muscle α actin* gene (Selvaraj and Prywes, 2004).

1.4.3.3.2 Function of MAL in skeletal-muscle differentiation

MAL and MAL16 were also implicated in the differentiation of striated (skeletal and cardiac) muscle (Selvaraj and Prywes, 2003). Interestingly, C2C12 skeletal myoblasts lack myocardin, but express MAL and MAL16 in their undifferentiated state and after induction of differentiation (Selvaraj and Prywes, 2003). Expression of dominant negative MAL16 blocks differentiation-induced expression of skeletal-muscle α actin and α myosin heavy chain proteins and differentiation of C2C12 myoblasts to myotubes *in vitro*.

MAL/MAL16 activity in muscle cells might be activated by the cardiac-and skeletal-muscle specific protein STARS (striated muscle activator of Rho signalling) (Arai et al., 2002; Kuwahara et al., 2005). STARS is present in sarcomeric structures of cardiomyocytes and co-localises with actin filaments in stress fibres and the cell cortex in transfected COS cells. STARS potentiates basal activity of an *SM22*-promoter driven reporter gene and also synergises with induction of this reporter by cytochalasin-D treatment or overexpression of RhoA, MAL or MAL16 (Arai et al., 2002; Kuwahara et al., 2005). STARS-induced transcriptional activity depends on functional Rho (Arai et al., 2002) and MAL/MAL16 activation (Kuwahara et al., 2005). MAL/MAL16 activation by STARS is likely to occur through stablisation of actin filaments by STARS at basal Rho activity (Kuwahara et al., 2005), although in striated muscle, where actin filaments are generally stabilised, this mechanism is currently unclear. Knockdown of STARS by RNA interference reduces SRF activity in both undifferentiated and differentiated C2C12 cardiomyocytes and primary myoblasts (Kuwahara et al., 2005).

STARS may modulate the response of the heart to stress signalling induced by pathological situations such as cardiac hypertrophy (Kuwahara et al., 2007).

1.4.3.3.3 Activation of MAL in response to mechanical force

Application of exogenous force to cultured cells results in the activation of Rho GTPases (Smith et al., 2003; Wojciak-Stothard and Ridley, 2003). A recent study demonstrated that force-induced smooth-muscle α actin expression occurs via Rho-actin-dependent activation of MAL but not MAL16 (Zhao et al., 2007). The activation of MAL by tension applied to cells appears conserved in *Drosophila* (see Section 1.4.3.3.7).

1.4.3.3.4 MAL and MAL16 knockout phenotypes

Two groups have independently generated MAL knockout mice homozygous for a MAL mutant lacking the B1 and Q boxes and the SAP domain (Li et al., 2006) or, additionally, the leucine zipper and part of the transcription activation domain (Sun et al., 2006b). MAL knockout mice are viable but display mammary gland defects and therefore fail to nurse their offspring. Myoepithelial cells, which are required for milk ejection, de-differentiate and undergo apoptosis. This is a surprisingly specific phenotype given the ubiquitous expression of MAL, suggesting that other MRTFs or TCFs functionally substitute for MAL-dependent transcription. Although MAL16 is also expressed in mammary myoepithelial cells, it cannot compensate the loss of MAL. This might be due to *bona-fide* specialised functions of MAL and MAL16 or a dose-dependent defect (Li et al., 2006; Sun et al., 2006b).

MAL16 was inactivated in mice by homozygous deletion of its C-terminus including the transcription activation domain (Oh et al., 2005) or an enhancer-trap approach generating a fusion protein with β-galactosidase in place of the C-terminus (Li et al., 2005). MAL16 inactivation results in embryonic lethality between E13.5 and E14.5 (Oh et al., 2005) or perinatal lethality between E17.5 and postnatal day 1 (Li et al., 2005). Mutant mice display severe cardiovascular defects and show no differentiation of neural-crest derived smooth muscle cells. The somewhat less severe defect observed in the enhancer-trap study might be due to a 5% proportion of residual wild-type MAL16 mRNA (Li et al., 2005).

1.4.3.3.5 Myocardin is sufficient for smooth-muscle gene expression

Ectopic expression of myocardin in the *Xenopus* embryo is sufficient to activate cardiac genes (Small et al., 2005). Expression of myocardin in various non-muscle cells (10T1/2, NIH3T3, 3T3-L1, primary rat cardiac, and primary human mesenchymal stem cells and foreskin fibroblasts) results in activation of numerous smooth-muscle but few cardiac-muscle specific genes (van Tuyn et al., 2005; Wang et al., 2003b). 10T1/2 cells adopted a myocyte-like morphology upon forced myocardin expression (Wang et al., 2003b). Similarly, overexpression of myocardin and SRF in undifferentiated *Srf*$^{-/-}$ embryonic stem cells results in expression of smooth-muscle cell markers SM22α and smooth muscle myosin heavy chain (Du et al., 2004). Therefore, myocardin represents a master regulator of smooth-muscle gene expression.

1.4.3.3.6 Myocardin loss-of-function phenotypes

Mice homozygous for a myocardin derivative that lacks the B1 and Q boxes and part of the SAP domain die at E10.5 (Li et al., 2003b). Mutant embryos appear normal up to E8.0 but show a lack of blood vessels at E9.5. While they display normal endothelial cell differentiation, they lack smooth-muscle α actin positive vascular smooth-muscle cells. However, mutant mice show normal smooth-muscle α actin expression in the heart and normal cardiac development.

The defect resulting from inactivation of the *myocardin* gene is, however, not cell-autonomous, as cells derived from *myocardin*$^{-/-}$ cells can differentiate into vascular smooth muscle cells in a wild-type background (Pipes et al., 2005).

Other factors, possibly MAL or MAL16, might functionally compensate for the loss of myocardin in the heart. The situation is different in *Xenopus*, where myocardin is critical for cardiac gene expression and development (Small et al., 2005; Wang et al., 2001a).

Comparison of the myocardin-family knockout phenotypes to those observed upon inactivation of SRF in mice (see Section 1.3.4) reveals the important contribution of myocardin-family proteins to SRF-mediated expression of muscle-specific genes and genes associated with the regulation of the actin cytoskeleton.

1.4.3.3.7 *Functions of MAL in* Drosophila

The *Drosophila melanogaster* genome encodes a single MAL protein, termed DMRTF (*Drosophila* MRTF) or MAL-D (Han et al., 2004; Somogyi and Rorth, 2004). Like its mammalian ortologues, it also strongly activates SRF-mediated transcription (Han et al., 2004). DMRTF is ubiquitously expressed throughout *Drosophila* embryogenesis. Homozygous inactivation of DMRTF is lethal during larval development. Larvae display defects in tracheal branching that are similar but less severe to those induced by the *pruned* mutation, which inactivates SRF (see Section1.3.4, Affolter et al., 1994; Guillemin et al., 1996). This suggests that loss of DMRTF affects SRF activity (Han et al., 2004). Interference with maternal and zygotic DMRTF expression by RNAi increased the penetrance of the tracheal phenotype (Han et al., 2004).

Expression of dominant negative forms of DMRTF lacking the C-terminus in the developing mesoderm resulted in impaired migration of mesoderm-derived cells from dorsal to ventral. Conversely, expression of a constitutively active DMRTF derivative lacking the N-terminus caused a more pronounced migration of mesoderm-derived cells. In both cases, mesoderm-derived structures such as the heart tube or muscle did not develop properly (Han et al., 2004). Ectopic expression of the same set of DMRTF derivatives in the tracheal system confirmed the role of DMRTF in promoting outgrowth of tracheal branches. Their expression in the developing wing demonstrated that DMRTF promotes the formation of intervein tissue and suppresses generation of wing veins. Dominant negative DMRTF variants also resulted in defective fusion of the two wing layers, giving rise to the *blistered* phenotype observed in the SRF mutant (see Section 1.3.4, Fristrom et al., 1994; Han et al., 2004; Montagne et al., 1996).

Border cells are a cluster of motile cells invading the germline tissue and migrating toward the developing oocyte during *Drosophila* oogenesis (see Somogyi and Rorth, 2004). Their migratory behaviour is strongly impaired in DMRTF-mutant flies, where the cluster of border cells disintegrates, most likely due to defects in the actin cytoskeleton. Cytoskeletal defects are further documented by abnormalities in bristle morphology and decreased amounts of F-actin in cells of the follicular epithelium; conversely, overexpression of DMRTF or its hyperactive derivative lacking the N-terminus in follicle cells results in accumulation of F-actin (Somogyi and Rorth, 2004).

During migration, some but not all border cells display nuclear accumulation of DMRTF, and it is those who appear stretched that do. Actively migrating border cells accumulate DMRTF in the nucleus, but also those, which are "dragged along" with the border-cell cluster, even when their ability to migrate autonomously has been abolished by inactivation of *slbo*, a transcription factor required for border-cell migration (Somogyi and Rorth, 2004). Thus, the simplest interpretation of these data is that DMRTF, like MAL in mammalian cells, can be activated by external mechanical force (see Section 1.4.3.3.3). These observations also highlight the conservation of the MRTF-SRF system in controlling cytoskeletal gene expression.

1.4.3.4 Regulation of MAL activity

1.4.3.4.1 MAL inhibition by interaction with G-actin

Previous work has established that SRF responds to a depletion of the G-actin pool (see Section 1.4.2), strongly suggesting that a G-actin sensing system is operational, the molecular basis of which remained elusive until the discovery of MAL.

MAL fulfils the properties of the predicted SRF coactivator that communicates the status of the actin cytoskeleton to SRF (Miralles et al., 2003). MAL appears cytoplasmic in serum-starved cells, but depletion of the cellular G-actin pool by a variety of means discussed above (see Section 1.4.2) results in nuclear accumulation of MAL (Miralles et al., 2003; Posern et al., 2004) (see Section 1.4.3.1; Figure 1.9). Conversely, abrogation of Rho-GTPase activity or overexpression of wild-type or non-polymerisable actin block serum-induced nuclear accumulation of MAL.

MAL binds to G-actin via its RPEL domain, as demonstrated by co-immunoprecipitation assays with both wild-type and non-polymerisable (R62D) β-actin and the use of latrunculin B, which sequesters monomers (Miralles et al., 2003, see Section 1.4.3.2.1). MAL does not appear associated with actin filaments as it is readily extracted by detergents. MAL activity is negatively regulated by actin binding since loss of actin binding by interference with RPEL-domain function results in nuclear accumulation of MAL and activation of SRF-mediated transcription without the need of a stimulus. Co-immunoprecipitation experiments and, more recently, Förster resonance energy transfer (FRET) / fluorescence lifetime imaging (FLIM) suggest that the MAL-actin complex dissociates upon serum stimulation (Miralles et al., 2003; Vartiainen et

al., 2007). Although these experiments cannot resolve the precise kinetics of MAL-actin complex disassembly, they strongly suggest that actin dissociates from MAL only transiently with a minimum of MAL-actin interaction detected between 10 and 30 min upon serum stimulation. After this, the MAL-actin interaction recovers. Many immediate early genes, including some known MAL target genes, are transcribed transiently upon acute stimulation, including *Fos*, *Srf* and *Vcl* (Gineitis and Treisman, 2001; Greenberg and Ziff, 1984). The transient nature of MAL-actin complex dissociation might reflect a transient activation of its target genes.

1.4.3.4.2 MAL phosphorylation

MAL displays some basal phosphorylation but is further phosphorylated in response to serum stimulation, as shown by a phosphatase-sensitive shift of its mobility in SDS-PAGE (Miralles et al., 2003). Both Rho and MEK-ERK contribute to MAL phosphorylation, as indicated by the sensitivity of phosphorylation to co-expressed C3 transferase, which inactivates Rho by ADP-ribosylation, or the MEK inhibitor U0126. Most serum-induced phosphorylation events occur in the C-terminus of MAL, although N-terminal phosphoacceptor sites exist as well (Miralles et al., 2003 and Francesc Miralles, personal communication). One of these occurs in within the RPEL domain of MAL at S98 between RPEL motifs 1 and 2 (Francesc Miralles, personal communication). The functional role of MAL phosphorylation is currently being investigated.

1.4.3.4.3 Nucleocytoplasmic shuttling of MAL

Cytoplasmic localisation of MAL might reflect static anchoring of MAL in the cytoplasm or the steady state of a dynamic MAL localisation. The latter was confirmed recently by Maria Vartiainen: application of the antifungal antibiotic leptomycin B (LMB), which specifically blocks the nuclear export receptor CRM1 (Ossareh-Nazari et al., 1997), to serum-starved cells results in nuclear accumulation of MAL, occurring with an astonishingly short half time of about 50 s (Vartiainen et al., 2007). Therefore, MAL constantly circulates between the cell nucleus and the cytoplasm, similarly to other transcriptional regulators such as STATs, Smads and NF-κB described above (see Section 1.1.1). The rapid nuclear accumulation kinetics indicate that nuclear import rates of MAL are very high and, as apparent from the cytoplasmic localisation of MAL

in serum-starved cells, must be even exceeded by the nuclear export rates prevailing in uninduced cells. The observation that nuclear accumulation of MAL is similarly rapid upon application of serum indicates that very efficient mechanisms operate to control MAL subcellular localisation upon serum-induced signalling.

1.4.3.5 The titration model for MAL regulation by actin and open questions

The association of MAL with G-actin suggests a model for how MAL senses and responds to changes in the cellular G-actin concentration (Figure 1.9). The MAL-actin interaction accomplishes cytoplasmic steady-state localisation of MAL and inhibition of its transcriptional activity in unstimulated cells. Actin may control functional elements of MAL that are required for MAL activity. According to a titration model, growth-factor induced and Rho-mediated depletion of G-actin results in a net-dissociation of MAL-actin complexes, which allows for MAL nuclear accumulation and activation of SRF-mediated transcription (Figure 1.9).

Given that the interaction with G-actin controls MAL activity, what are the levels of control? Does actin binding affect nuclear import or nuclear export of MAL? Since nucleocytoplasmic shuttling implies the constant presence of low amounts of MAL in the nucleus, how do cells ensure that SRF-mediated transcription is not potentiated "accidentally", in the absence of the corresponding signal? How does MAL interact with actin, efficiently competing with other, abundant G-actin binding proteins such as profilin? According to the titration model, signal-dependent changes in the MAL-actin interaction achieve a switch from cytoplasmic and inactive to nuclear and active MAL within minutes upon induction, at least in NIH3T3 fibroblasts. When regarded with respect to individual MAL proteins, this regulatory mechanism implies that an analog input signal (G-actin concentration) is translated into a digital response (nuclear accumulation and SRF activation). How could the MAL-actin interaction achieve such a switch behaviour? What is the basis for Rho-independent, constitutive activity of myocardin?

The present thesis addresses a number of these questions.

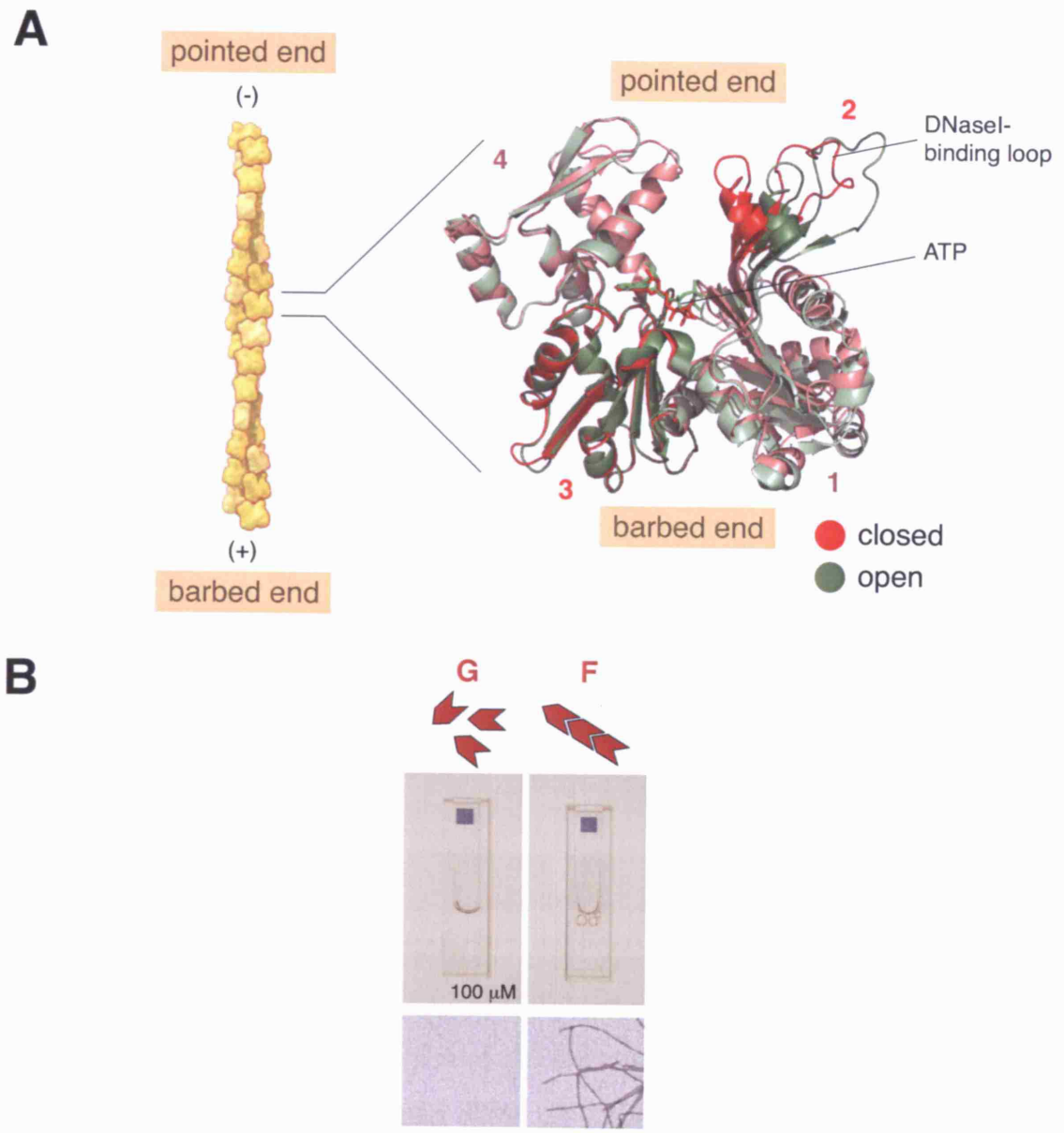

Figure 1.1 Structures of monomeric and polymeric actin. (**A**) Left, schematic representation of the actin filament (taken from Pollard and Borisy, 2003) with two-stranded helical arrangement of the actin protomers. The filament ends are labelled. Right, superposition of the actin monomer in the closed (red; generated from pdb file 2BTF; Schutt et al., 1993) and open (green; generated from pdb file 1HLU; Chik et al., 1996) conformations with directionality in the filament indicated. The actin subdomains are colour-coded: subdomain 1, residues 1-32, 70-144, and 338-372; subdomain 2, residues 33-69; subdomain 3, residues 145-180, and 270-337; subdomain 4, residues 181-269 with subdomains 1 and 4 in pale colours (Kabsch et al., 1985 and 1990). The main chains of subdomains 4 have been superimposed. ATP is bound in both structures, but the closed and open states are thought to represent different conformations adopted by ATP- and ADP-actin, respectively (see text). The side of actin facing the viewer in this orientation is referred to as the "front" while the bottom is named the "base" in this thesis. (**B**) Appearance of purified rabbit skeletal muscle actin. Top, addition of salt and ATP polymerises actin, as seen by an increased viscosity of the actin solution at 100 μM. Bottom, negatively stained actin filaments are visible by transmission electron microscopy (microscopy images by Rose Watson, LRI).

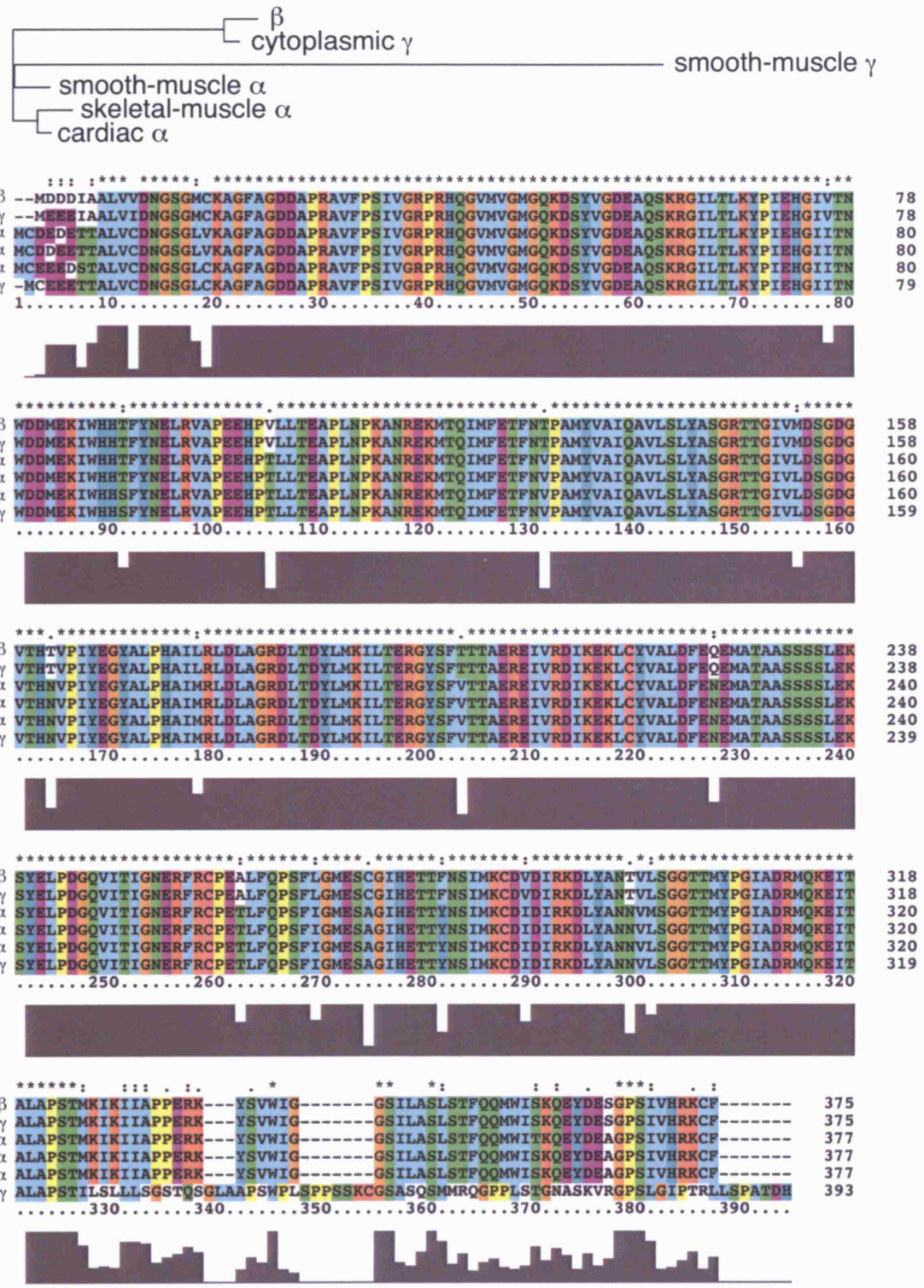

Figure 1.2 Actin isoforms. Phylogramme and multiple sequence alignment of the mouse actin isoforms (β actin, accession number NP_031419; cytoplasmic γ actin, NP_033739; smooth-muscle γ actin, NM_009610; skeletal-muscle α actin, P68134; cardiac-muscle α actin, NP_033738; smooth-muscle α actin, NP_031418), generated with ClustalW (Chenna et al., 2003) and ClustalX (Thompson et al., 1997), respectively. The distances to the closest nodes are β actin, 0.00733; cytoplasmic γ actin, 0.00333; smooth-muscle γ actin, 0.14109; smooth-muscle α actin, 0.00752; skeletal-muscle α actin, 0.00752; cardiac-muscle α actin, 0.00309. The identities of β actin to cytoplasmic γ, smooth-muscle γ, skeletal-muscle α, cardiac-muscle α and smooth-muscle α actin are 98%, 80%, 93%, 93% and 93%, respectively. The histogramme indicates conservation.

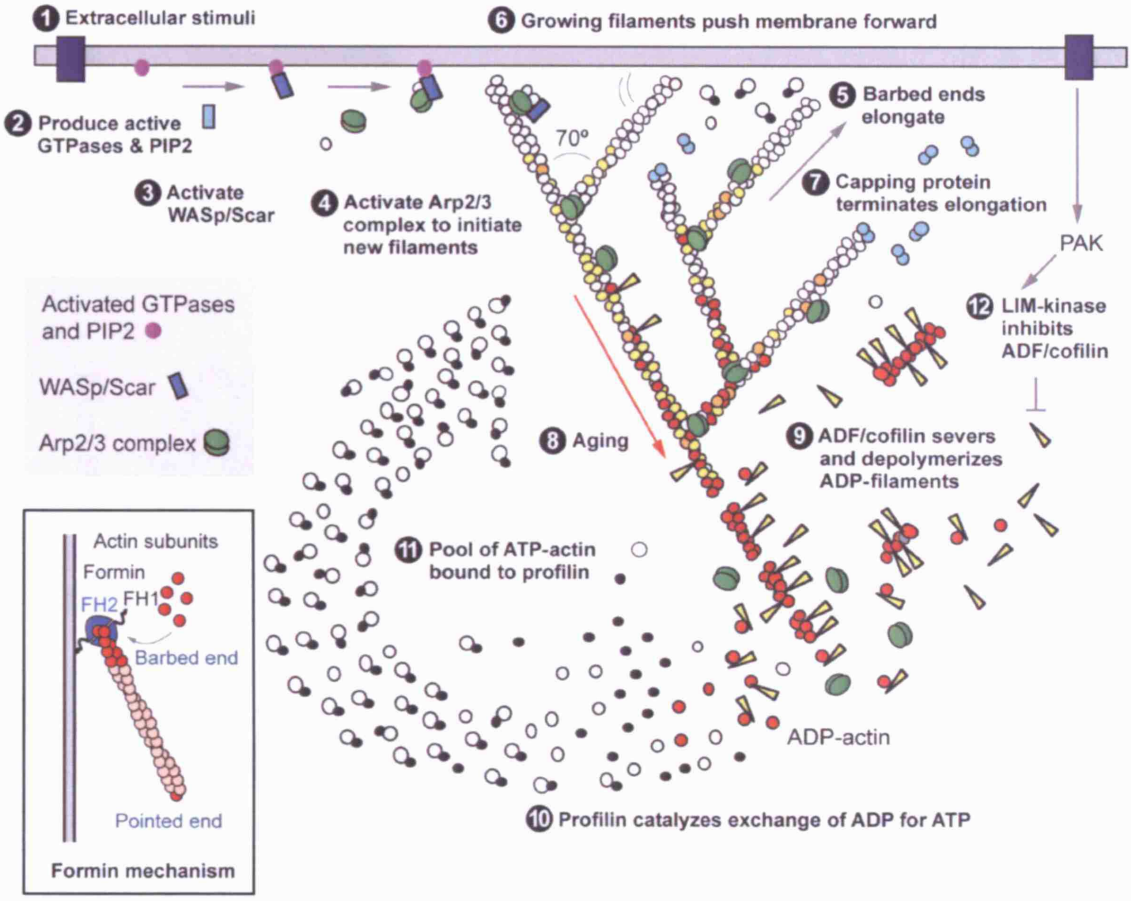

Figure 1.3 Regulation of actin dynamics according to the dendritic nucleation model for F-actin assembly at the leading edge of motile cells. The regulators shown mediate multiple actin-mediated processes. ATP-actin is shown in white, ADP-P_i-actin in yellow and ADP-actin in red. Profilin is represented by black ellipsoids, capping protein by pairs of blue circles and ADF/cofilin by yellow wegdes. (1) An extracellular signal activates plasma-membrane receptors, resulting (2) in the activation of Rho-family GTPases and PI(4,5)P_2 production, both of which (3) cooperate to activate nucleation-promoting factors such as WASP/Scar proteins that (4) activate Arp2/3-complex and (inset) formin-mediated actin-filament assembly. (5) Actin filament elongation proceeds until (7) the barbed end is capped. (8) ATP hydrolysis by actin marks aging filaments. (9) ADP-F-actin is depolymerised with the assistance of ADF/cofilin. (10) Profilin catalyses the exchange of ADP for ATP on actin and provides a buffering system for actin monomers that are eventually fed into newly assembled actin filaments. Signalling through Rho-family GTPases activates p21-activated kinase (PAK) and Rho kinases (ROCK; not shown) that (12) phosphorylate and activate LIM kinase (LIMK). LIMK phosphorylates and inactivates ADF/cofilin, thereby stablising existing filaments. ROCK-LIMK-ADF/cofilin signalling and formin-mediated actin assembly contribute to G-actin depletion that results in the activation of SRF upon growth-factor mediated activation of RhoA. The figure was taken from Pollard, 2007.

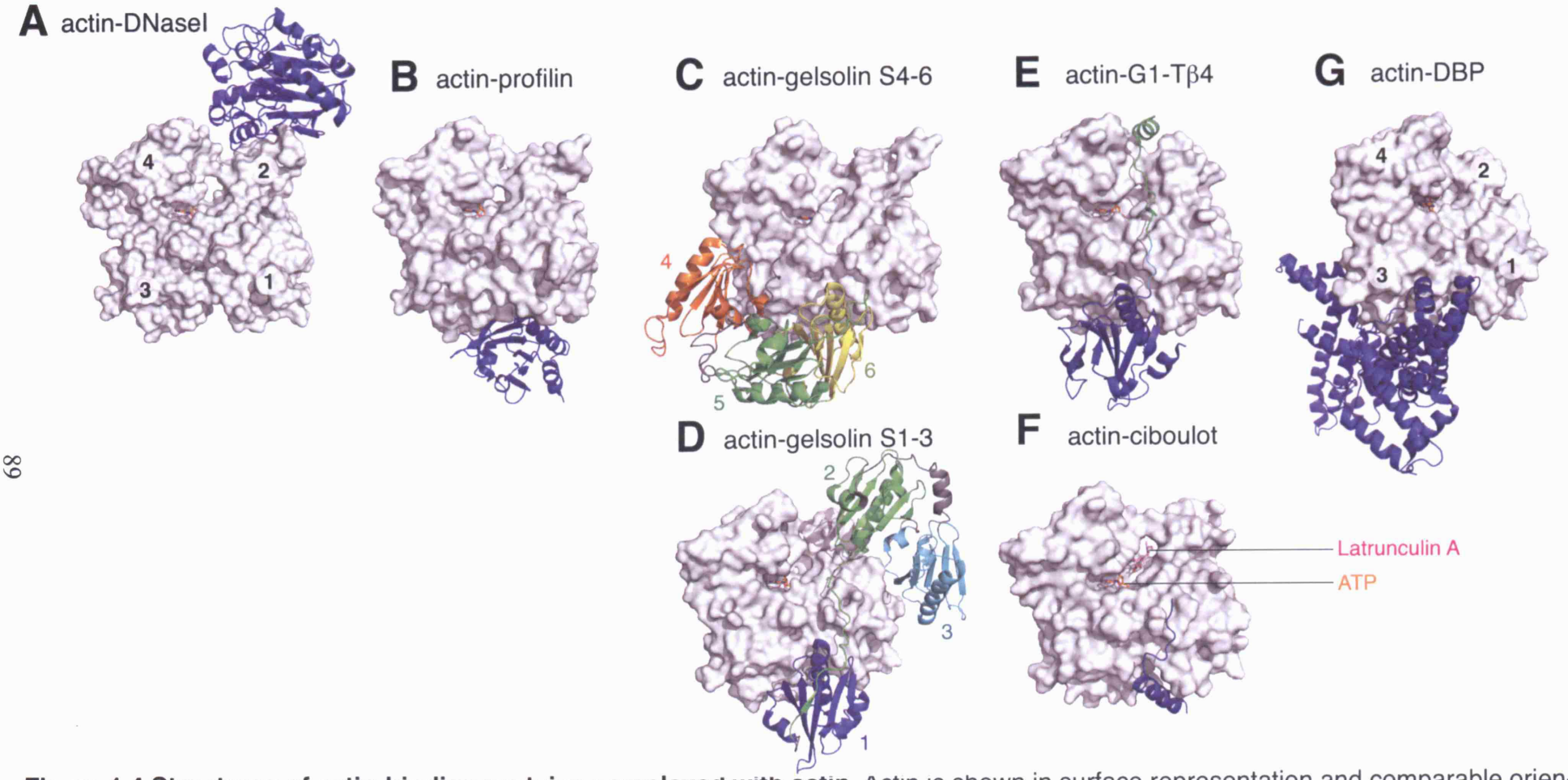

Figure 1.4 Structures of actin-binding proteins complexed with actin. Actin is shown in surface representation and comparable orientations with subdomains indicated in (A), actin-binding proteins as cartoons. (**A**) Actin-DNaseI (produced from pdb file 1ATN; Kabsch et al., 1990). (**B**) Actin-profilin (2BTF; Schutt et al., 1993). (**C**) Actin-gelsolin S4-6 (1H1V; segments indicated by colours; Robinson et al, 1999). (**D**) Actin-gelsolin S1-3 (1RGI; segments segments indicated by colours; Burtnick et al., 2004). (**E**) Actin-(gelsolin S1-thymosin β4) (1T44; Irobi et al., 2004). (**F**) Actin-ciboulot (1SQK; Hertzog et al., 2004). (**G**) Actin-vitamin-D binding protein (1KXP; Otterbein et al., 2002).

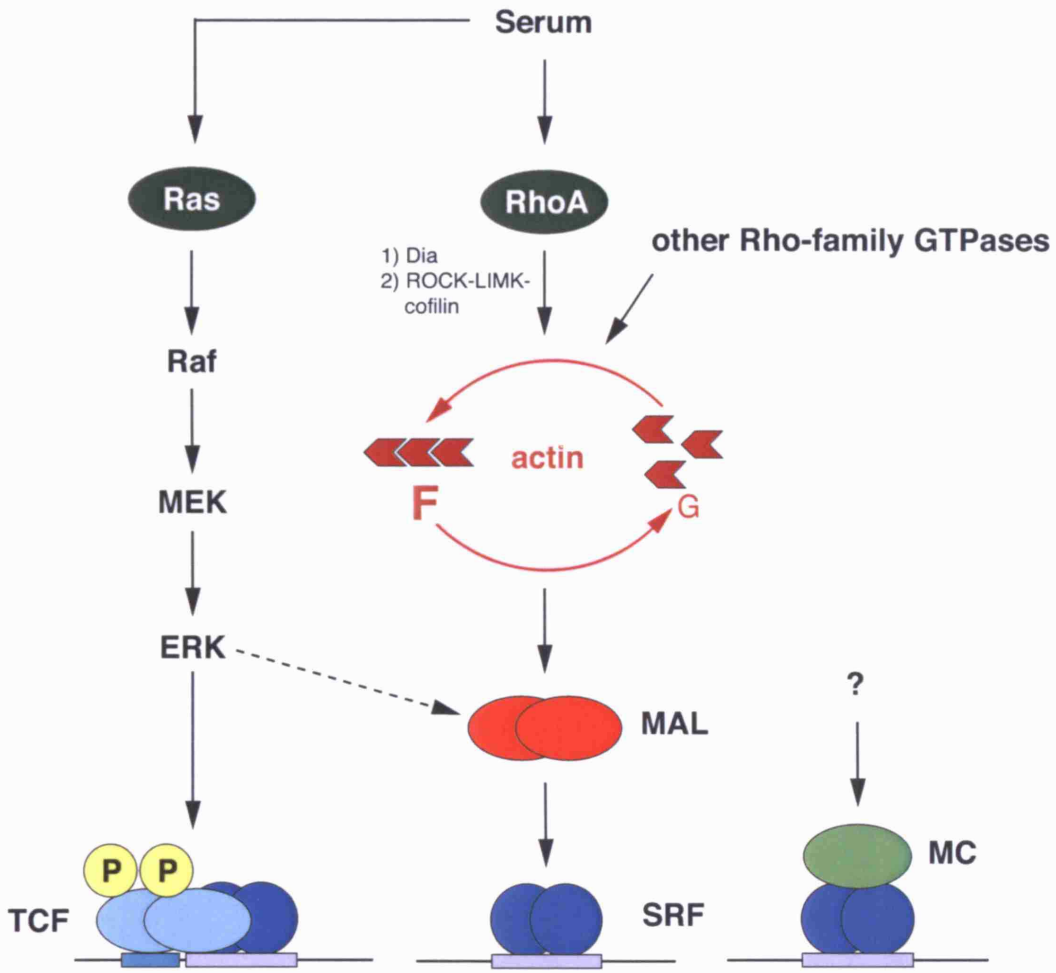

Figure 1.5 Competing cofactors link SRF to different signalling pathways. Ternary complex factors (TCFs) bind SRF at one set of SRF target genes, which are characterised by an ETS site adjacent to the SRE. TCFs are targets of Ras-Raf-MEK-ERK-dependent phosphorylation, by which they become activated. Another set of SRF target genes is controlled through myocardin-family proteins: the myocardin-related transcription factors (MRTFs) MAL and MAL16 and myocardin (MC). MAL and MAL16, referred to as MAL in this figure, are controlled by Rho-actin signalling. Two RhoA-effector branches control SRF-activity in the RhoA-actin signalling pathway: 1) formin-mediated F-actin assembly and 2) stabilisation of F-actin through the ROCK-LIMK-cofilin pathway. Rho and ERK signalling contribute to MAL phophorylation. See text for details.

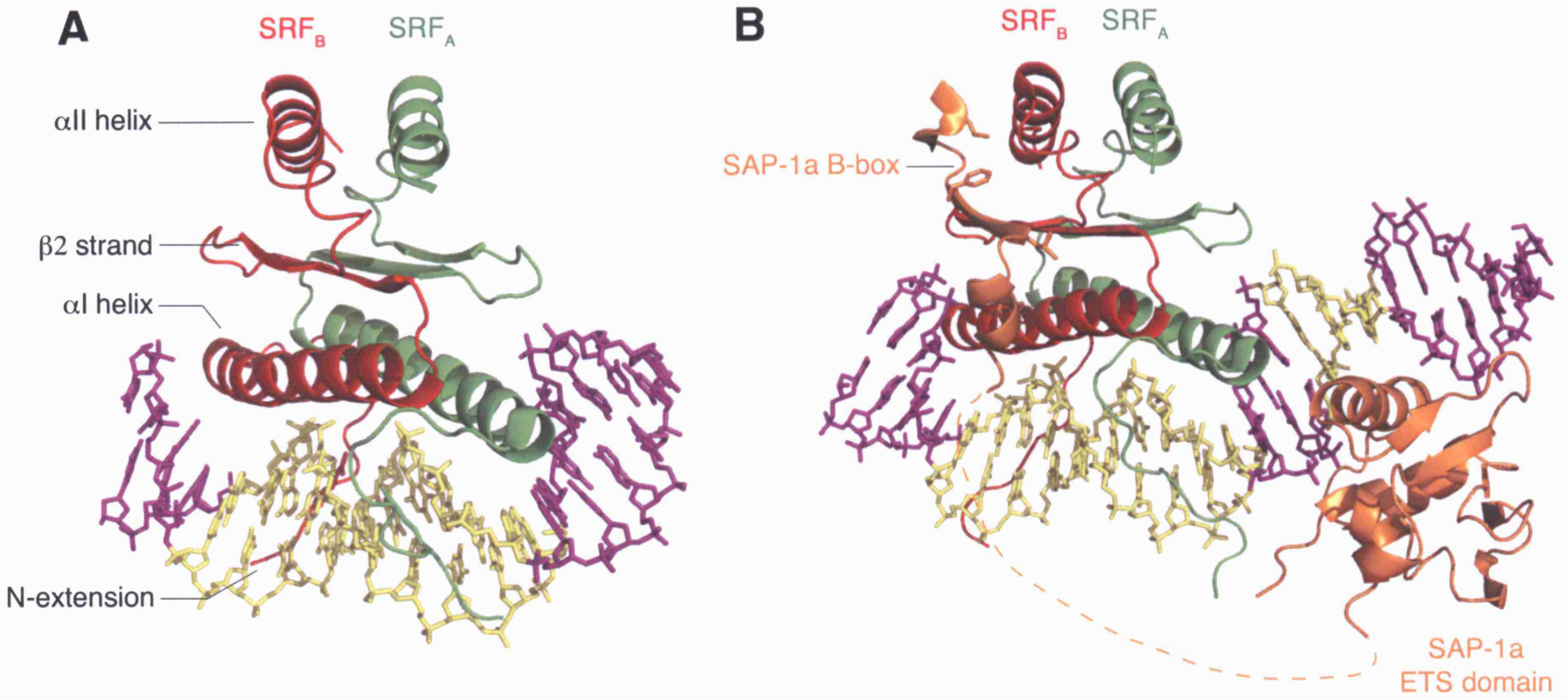

Figure 1.6 SRF Structures. (**A**) Structure representation of the SRF DNA binding domain complexed to SRE DNA, produced from pdb file 1SRS (Pellegrini et al., 1995). SRF molecules in the SRF dimer are shown as cartoon in red and green, respectively. DNA in stick representation is shown in purple with SRE sequence in yellow. Key structural elements of SRF are indicated. The colouring scheme is adapted from Pellegrini et al., 1995. (**B**) Structure representation of the SAP-1a–SRF–DNA ternary complex, produced from pdb file 1HBX (Hassler et al., 2001). Orientation and colouring of the complex is equivalent to (A). SAP-1a is shown in orange with the B-box–ETS domain linker, which is not resolved in the crystal structure, indicated as dashed line. Indeed, it is unclear whether the B-box and the ETS domain derive from the same molecule (T. Richmond, personal communication). Key hydrophobic residues that mediate SRF binding are shown as sticks. The core of the ETS site is shown in yellow.

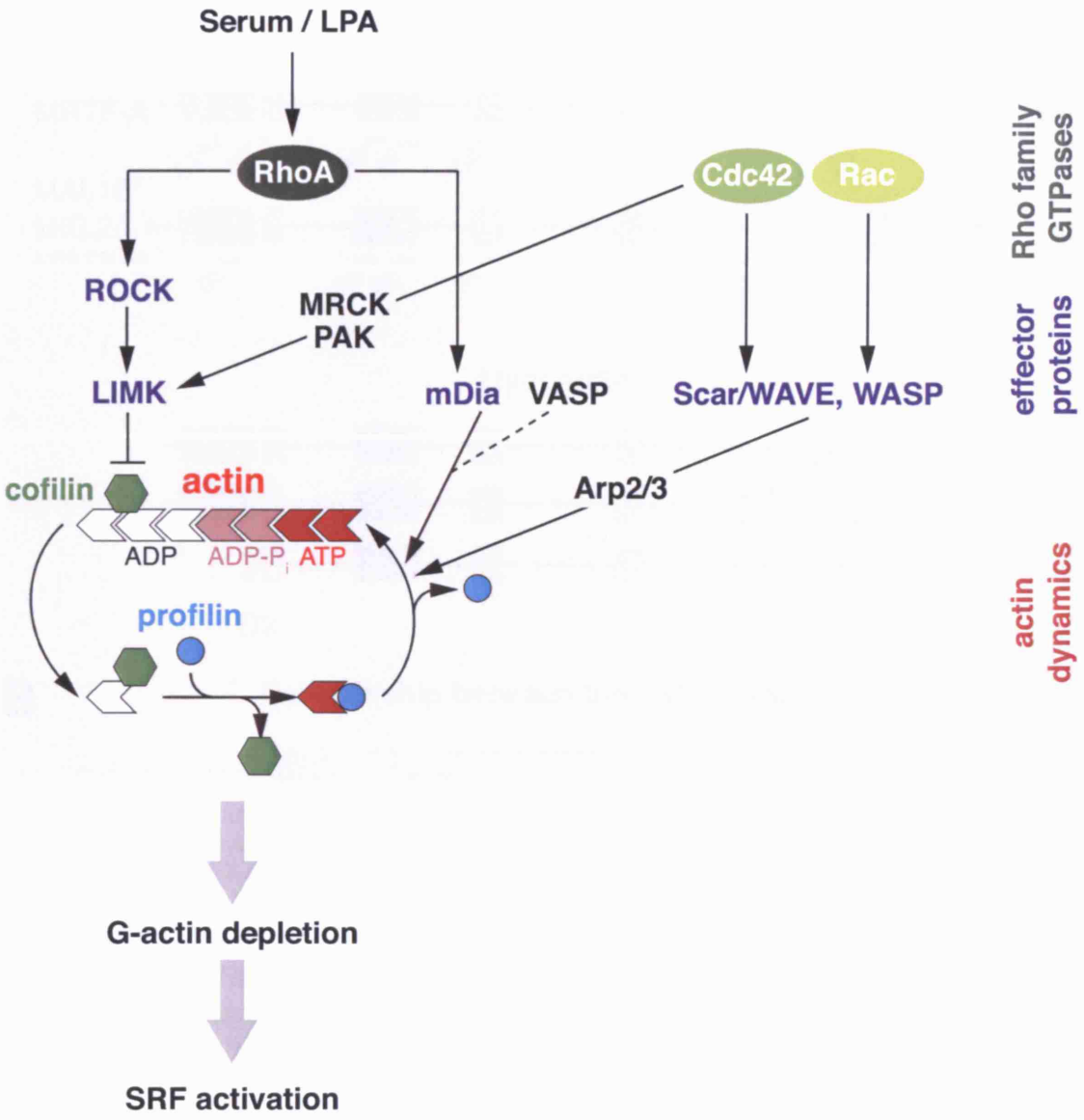

Figure 1.7 Active Rho family GTPases deplete the cellular G-actin pool. Rho-GTPase effector proteins promote the assembly of F-actin, either by stabilisation of existing filaments through the ROCK-LIMK-cofilin signalling axis or de-novo actin assembly through formin- or Arp2/3-mediated actin nucleation. Myotonic dystrophy kinase-related Cdc42-binding kinases (MRCKs) are Cdc42 effectors; p21-activated kinase (PAK) is an effector of both Cdc42 and Rac and activates LIMK. Both MRCKs and PAK activate LIMK (reviewed in Zhao and Manser, 2005). Thymosin β4 and gelsolin are not shown for simplicity. G-actin depletion activates SRF-mediated transcription.

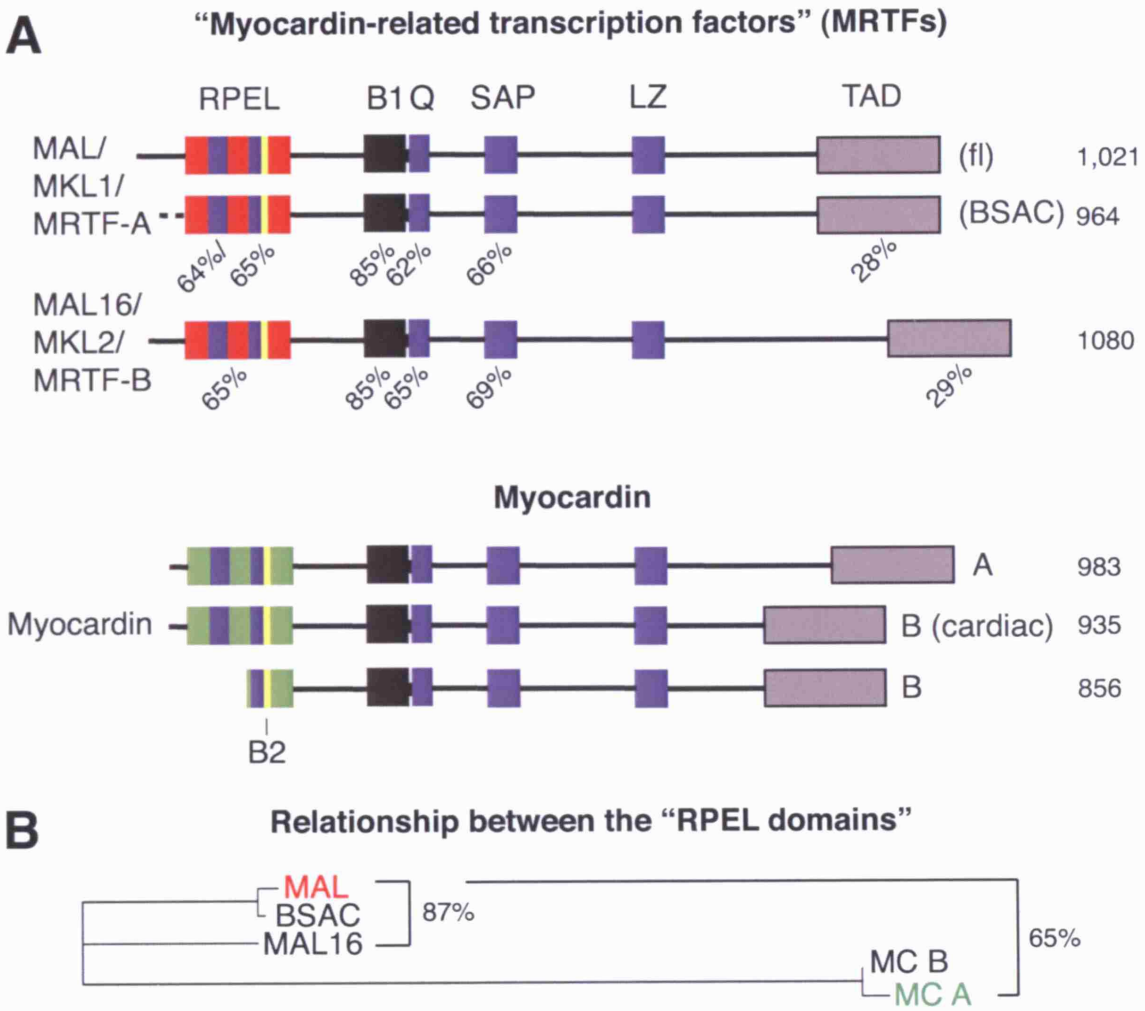

Figure 1.8 Domain organisation of proteins of the myocardin family of SRF cofactors. (**A**) The myocardin family is represented by myocardin (MC) itself and myocardin-related transcription factors (MRTFs). The mouse proteins are shown. Alternative splicing and differential translation-start sites generate two MAL and three myocardin isoforms. RPEL, RPEL motif; B2 and B1, basic regions; Q, Q-rich region; SAP, SAP (SAF-A/B, acinus, pias) domain; LZ, leucine zipper; TAD, transcription activation domain. MAL, accession code EDL04588; BSAC, AAM94258 ; MAL16, NP_705816; MC A, NM_145136; MC B, NM_146386. A myocardin isoform lacking RPEL1 and most of RPEL2 is generated from an mRNA containing an alternative second exon (Creemers et al., 2006). The length of the proteins is indicated in amino acids. RPEL motifs are shown in red for MAL proteins and green for myocardin. The indicated percentages denote identity between the MRTFs and myocardin B, the founding member of the family (Wang and Olson, 2004). The percentages given for the RPEL domain, as defined by PFAM (Finn et al., 2006), were calculated using ClustalW (Chenna et al., 2003). When compared across the entire sequence length, MAL and MAL16 are 42% identical; MAL and MC A or B are 34 and 35% identical, respectively, and MAL16 and MC A or B are 32 and 34% identical, respectively, as calculated by ClustalW. (**B**) Phylogramme documenting the relationship between the RPEL domains (as defined by PFAM) of the mouse proteins, generated by ClustalW. Distances to the closest nodes are: MAL, 0.00682; BSAC, 0.00227; MAL16, 0.06136; MC A, 0; MC B, 0.00909. Percentages indicate identity between RPEL domains. The MC isoform studied in the present thesis is MC A.

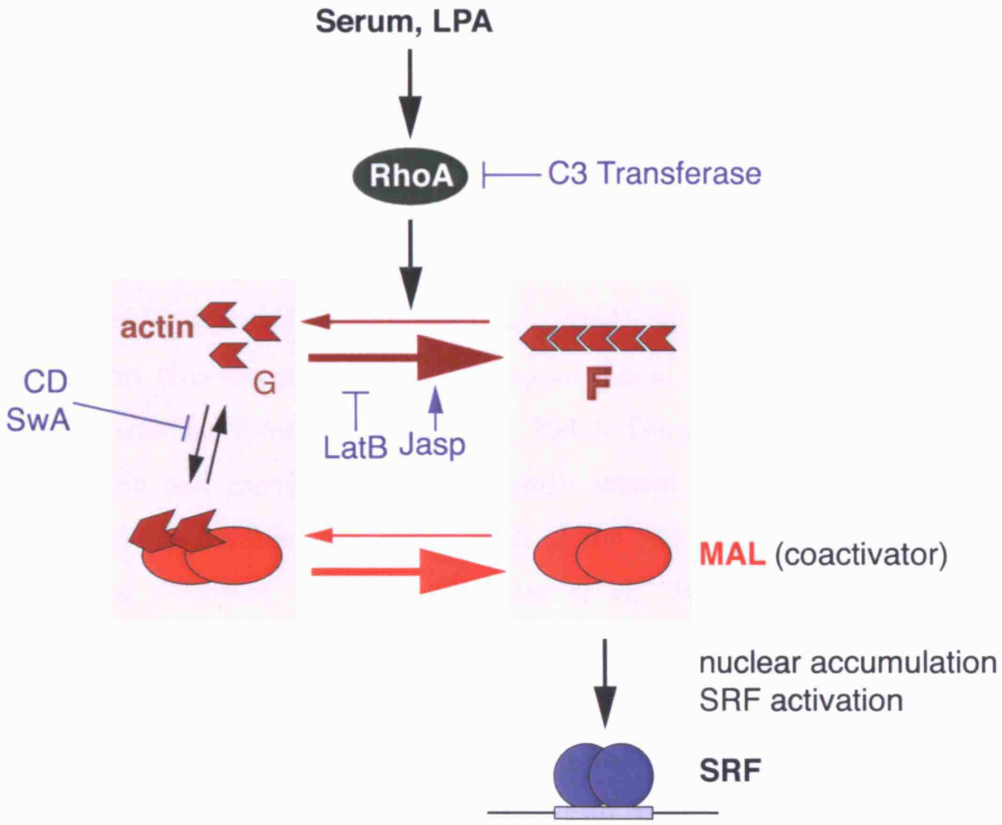

Figure 1.9 Depletion of the G-actin pool activates the SRF-coactivator MAL. According to a simple titration model, the bulk of MAL is complexed with G-actin in quiescent cells. Upon serum stimulation, RhoA effectors accumulate F-actin at the expense of G-actin, which results in a net dissociation of MAL-actin complexes, nuclear accumulation of MAL and SRF activation. For simplicity, active MAL is shown as being not bound to actin. Rho-actin signalling might re-organise the MAL-actin complex rather than completely dissociate it. Agents that interfere with Rho-actin signalling are shown in blue: C3 transferase inactivates Rho GTPases by ADP-ribosylation; cytochalasin D (CD) and swinholide A (SwA) dissociate the MAL-actin complex (see Chapter 2) ; jasplakinolide (Jasp) stabilises F-actin; latrunculin B (LatB) sequesters actin monomers, thereby increasing the G-actin concentration. Overexpression of wild-type or nonpolymerisable actin, like LatB application, blocks MAL activation by serum, whereas expression of mutant actin derivatives that stabilise F-actin activates MAL (not shown). See text for details.

2 The MAL RPEL domain as actin-binding regulatory unit

2.1 Aims

Processes that lead to the depletion of the cellular G-actin pool have long been known to activate SRF. These include stabilisation of actin filaments by treatment of cells with the F-actin binding drug jasplakinolide (Sotiropoulos et al., 1999), overexpression of components of the actin-filament nucleation or elongation machinery (Copeland and Treisman, 2002; Grosse et al., 2003), activation of the ROCK-LIMK-cofilin pathway (Geneste et al., 2002; Sotiropoulos et al., 1999) or expression of actin mutants that stabilise F-actin (Posern et al., 2002). The discovery of MAL, a G-actin binding protein and member of the myocardin-related transcription factor (MRTF) family of SRF-coactivators, has filled much of the gap in understanding of the link between actin dynamics and SRF (Miralles et al., 2003). Previous work in our laboratory has demonstrated that the N-terminal RPEL domain of MAL is required for interaction with actin and that actin binding is critical for MAL regulation (Miralles et al., 2003). Although insightful, the actin-binding studies have been complicated by an initial uncertainty about the translation start site of MAL. Actin binding was initially studied with MAL(met), whose translation start site was predicted to be the first in-frame ATG codon. Later analysis of the full mRNA including its 5'-UTR revealed that the open reading frame extends beyond the ATG codon and encodes another RPEL motif. The full-length MAL protein, whose translation is initiated at or just 5' of a leucine codon, is 92 amino acids longer at the N-terminus and contains three RPEL motifs (Miralles et al., 2003), compared to MAL(met), which lacks RPEL motif 1. Furthermore, it remained unclear whether MAL directly interacts with actin or whether another factor is required. My initial aim was to define a unit sufficient to confer nucleocytoplasmic regulation on MAL. I then planned to characterise the interaction of the full-length variant of MAL with actin and investigate whether a third protein is required. Since actin-binding studies had been limited to co-immunoprecipitation, I also set out to characterise the MAL-actin interaction using purified components.

2.2 The RPEL repeat mediates nucleocytoplasmic shuttling of MAL

To address the contribution of the RPEL domain to the localisation of MAL, I fused the MAL RPEL domain to the heterologous pyruvate kinase protein (MAL(2-

204)-PK, Figure 2.2 A, Kalderon et al., 1984). This fragment was chosen on the basis of sequence conservation and secondary structure prediction: A190 and I191 form a hydrophobic unit that is conserved across the myocardin family and, together with an α-helix that is predicted to end at I192, mark the end of conservation C-terminal to RPEL motif 3 (Figure 2.1). Eleven amino acids that follow further C-terminal and are predicted to be unstructured were included as a linker. Pyruvate kinase forms a tetramer of 4 x 60 kDa that is strictly excluded from the cell nucleus (Figure 2.2 B, Kalderon et al., 1984). MAL(2-204)-PK displayed predominantly cytoplasmic localisation in serum-starved cells and accumulated in the nucleus upon serum stimulation or treatment with the SRF-activating actin-binding drugs cytochalasin D (CD) or jasplakinolide (Jasp), similarly to the full-length protein. Interestingly, block of Crm1-mediated nuclear export by application of the antifungal antibiotic leptomycin B (LMB) resulted in nuclear accumulation of MAL(2-204)-PK, as was observed for MAL (Vartiainen et al., 2007). This indicates that the MAL RPEL domain contains regulatory elements responsible for nuclear import and export of MAL and that it sufficient to mediate nucleocytoplasmic shuttling in serum-starved cells. Nuclear MAL(2-204)-PK in serum-stimulated cells relocalised to the cytoplasm upon treatment of cells with latrunculin B (LatB) or attenuation of signalling by serum washout. Serum-induced nuclear accumulation of MAL(2-204)-PK was blocked by co-expression of C3 transferase, which ADP-ribosylates and inactivates Rho (Hill et al., 1995), or expression of non-polymerisable β-actin R62D (Posern et al., 2002). Mutation of the first and most conserved arginine residue in each of the RPEL motifs, which virtually abolishes actin binding (xxx mutant; Section 2.3.2.5), resulted in constitutively nuclear MAL(2-204)-PK (Figure 2.2). Actin-regulated nuclear accumulation of MAL and MAL(2-204)-PK was dependent on the B2 region, a putative nuclear import signal in MAL. MAL and MAL(2-204)-PK derivatives containing both the xxx and ΔB2 mutation were predominantly cytoplasmic, indicating that the B2 region controls MAL localisation downstream of actin binding. These observations are in agreement with the RPEL domain acting as a G-actin sensor that controls MAL subcellular localisation.

2.3 The RPEL domain of MAL is sufficient for actin binding

The work presented in the previous section has defined a functional RPEL domain as the unit for further biochemical investigations. To address whether the RPEL domain is sufficient for actin binding, I performed large-scale GST affinity sedimentation

experiments using recombinant MAL(2-261) with an N-terminal GST-His-S-tag. Amino acid 261 as C-terminal boundary of the construct was chosen because the same context has been used for previous studies of MAL(met) (Posern et al., 2004). The GST-fusion protein was produced in *E. coli*, immobilised to glutathione-sepharose, washed thoroughly and probed with high-salt extract readily obtained in large quantities from suspension HeLa cells. Upon binding and washing, the bait was cleaved from its affinity tag using GST-3C protease (Figure 2.3 A). Co-eluting proteins were detected following SDS-PAGE and Coomassie brilliant blue staining. The wild-type RPEL domain recruited large amounts of a protein of a molecular mass between 30 and 45 kDa (Figure 2.3 B). Using mass spectrometry, this was identified as actin. Only small quantities of actin were retained by the xxx mutant of the RPEL domain (see Section 2.3.2.5 for further actin-binding analysis of this mutant). No other proteins were found to specifically co-elute with actin under the conditions used. Therefore, the interaction of actin with MAL is direct, although it remains possible that additional proteins other than actin interact with the RPEL domain.

2.3.1 The MAL RPEL domain sequesters G-actin with high apparent affinity

2.3.1.1 MAL interacts with both beta- and alpha-actin

In-vitro actin binding studies can be greatly facilitated by the use of skeletal-muscle α actin, which is readily obtained in large quantities from rabbit skeletal muscle. To investigate whether MAL also interacts with skeletal-mucle actin, I performed co-immunoprecipitation experiments. C-terminally HA-tagged MAL was co-expressed with N-terminally FLAG-tagged β or α actin (Figure 2.4 A). Using an anti-FLAG affinity resin, I could specifically co-immunoprecipitate MAL-HA with both FLAG-β or -α actin. No MAL-HA was precipitated in the absence of FLAG-actins. Recovery of MAL-HA with the β and α isoforms of actin was comparable. I therefore proceeded to purify MAL(2-261) without affinity tag and skeletal-muscle α actin (Figure 2.4 B and C). Where purified actin is used in experiments described in this thesis, the isoform employed is skeletal-muscle α actin.

2.3.1.2 MAL sequesters G-actin and does not bind actin filaments

Previous actin-MAL co-immunoprecipitation studies with nonpolymerisable β actin R62D and actin-binding drugs as well as detergent extraction experiments demonstrated that MAL interacts with G-actin (Miralles et al., 2003). No binding of MAL to F-actin was observed (Miralles et al., 2003). To address G- and F-actin binding properties of MAL with purified components, I performed actin co-sedimentation / sequestering experiments (Figure 2.5 A). MAL is incubated with different concentrations of polymerised actin. Actin filaments are then sedimented by ultracentrifugation, and equivalent amounts of supernatants and pellets are analysed by SDS-PAGE and Coomassie brilliant blue staining. MAL was never found in the pellets together with F-actin, confirming that it is not an actin-filament binding protein. Instead, MAL clearly increased the amount of actin in the supernatants, demonstrating that MAL binding blocks actin polymerisation. The amount of sequestered G-actin was very similar when actin polymerisation was induced after co-incubation of G-actin with MAL. MAL therefore effectively prevents re-incorporation of dissociated actin monomers into treadmilling actin filaments. Analysis of the binding reactions after either 30 min or 20 h indicated that more than 30 min were required to reach binding equilibrium.

2.3.1.3 MAL binds actin with high apparent affinity

I exploited the incompatibility of MAL-actin interaction with actin polymerisation to estimate the affinity of MAL for actin (Hertzog et al., 2002). To quantitatively analyse the effect of MAL binding on actin polymerisation, I modified skeletal muscle α actin with pyreneiodoacetamide, which covalently couples to a reactive cysteine residue at penultimate position 374 (Kouyama and Mihashi, 1981). The pyrenyl-actin polymerisation assay relies on weak fluorescence of G-actin and a large increase in fluorescence intensity upon actin polymerisation. The critical concentration of actin was estimated as 0.27 μM, based on the actin concentration at which regression lines describing pyrenyl G- and F-actin fluorescence over a range of actin concentrations intersect (see Section 7.14.4 in Chapter 7; Materials and Methods). A construct comprising gelsolin segments 4-6 (gelsolin S4-6), which sequesters an actin monomer (Way et al., 1989, see Section 1.2.2.4), was used as a positive control and a MAL construct lacking the RPEL domain (MAL(187-261)) as a negative control. Increasing amounts of MAL(2-261) or gelsolin(S4-6) led to complete inhibition of actin

polymerisation at similar concentrations, whereas MAL(187-261) did not block F-actin assembly (Figure 2.5 B). This was consistent with an apparent K_d of 24 nM for MAL-actin and an apparent K_d of 76 nM for gelsolin(S4-6)-actin, in good agreement with published observations (Way et al., 1989). The high-affinity MAL-actin interaction suggests that MAL should be able to effectively compete for actin with other G-actin binding proteins, especially the highly expressed profilin, which binds to G-actin with about 0.1 μM affinity, sequestering the majority of the cellular G-actin pool (Buss et al., 1992; Perelroizen et al., 1996). Co-immunoprecipitation experiments demonstrated that profilin and MAL do not bind to actin simultaneously, and therefore competition for actin must occur (Posern et al., 2004). A set of experiments addressing the role of RPEL motifs in actin binding by MAL will be presented in Chapter 4.

2.3.2 MAL stably associates with three molecules of actin

It is noteworthy that supernatants obtained in actin sequestering assays appear to contain larger amounts of actin than MAL, although different sensitivity to Coomassie staining might also contribute. This suggests that MAL binds more than one molecule of actin. To analyse the composition of the MAL-actin complex more closely, I performed gel filtration chromatography using a column calibrated with globular proteins of known molecular masses. Surprisingly, MAL(2-261) eluted at a volume corresponding to 111 kDa, about three times the molecular mass expected theoretically (29 kDa) and observed in SDS-PAGE (between 30 and 45 kDa) (Figure 2.4 B and see below in Figure 2.7), suggesting that the pure MAL N-terminus adopts an extended conformation, multimerises or does both. Therefore, I first investigated the properties of the isolated MAL RPEL domain.

2.3.2.1 The MAL RPEL domain is monomeric and extended

I employed dynamic light scattering (DLS) to determine the apparent size of MAL(2-261), termed the hydrodynamic radius, which corresponds to the radius of a hypothetical hard sphere with diffusion properties identical to those of the molecule studied (Malvern Instruments, 2005). The hydrodynamic radius of MAL(2-261) was determined as 8.79 nm, which corresponds to a molecular mass of 107.6 kDa, assuming globularity of the protein (Figure 2.6 A). Interestingly, this value is very similar to the apparent molecular mass determined by gel filtration. The apparent size as measured by

DLS does not consider effects of solvation, non-globularity and tumbling of the molecules studied. I therefore employed static light scattering (SLS) to determine the actual molecular mass of MAL(2-261). In SLS, the time-averaged intensity of scattered light produced by the macromolecule is proportional to the product of the mass-average molecular mass and the concentration (Malvern Instruments, 2005). The molecular mass can be determined on the basis of the Rayleigh equation, which describes the relationship between the intensity of scattered light and the molecular mass (Equation 2.1).

$$\frac{Kc}{R_\theta} = \frac{1}{M} + 2A_2c$$

Equation 2.1 Rayleigh Equation. K, optical constant; R_0, Rayleigh ratio of the scattered to incident light intensity; M, mass-average molecular mass; A_2, second virial coefficient; c, sample concentration.

Linear regression of a plot of Kc/R_0 versus c (the Debye plot, Figure 2.6 B) revealed a mass-average molecular mass M of 34 kDa, which is the inverse of the intercept value. This is very close to the molecular mass expected for monomeric MAL(2-261). The slope of the regression function corresponds to the second virial coefficient A_2. A_2 is an expression of the interaction strength of the molecule with the solvent. A negative value for A_2, -3.08×10^{-6} for MAL(2-261), indicates that the molecules tend to crystallise or aggregate. Indeed, purified derivatives of the MAL aminoterminus, especially shorter ones, showed moderate aggregation when stored at 4 °C for prolonged periods.

2.3.2.2 The MAL RPEL domain is largely unstructured

Light scattering and gel filtration suggest that MAL(2-261) assumes an extended conformation that might arise from long regions devoid of secondary structure. To investigate this, I purified a set of MAL aminotermini for analysis by circular dichroism (CD) spectroscopy (reviewed in Pelton and McLean, 2000, Figure 2.6 C). Purification of MAL(2-204), the RPEL domain in the same context as used in the pyruvate kinase fusion protein described above (Section 2.2), generated a stable proteolysis fragment identified as MAL(2-199) by mass spectrometry and N-terminal Edman sequencing (see Figure 5.1 in Chapter 5). MAL(2-199) and the equivalent construct of BSAC, which has a shorter N-terminus (see Figure 1.8 in Chapter 1 and Figure 2.1), were generated. CD

spectroscopy, kindly performed by Dr. Bernard O'Hara (Birkbeck College, London) revealed that the RPEL domain is largely unstructured with average proportions of unordered regions estimated as 71%, 68% and 54% for MAL(2-261), MAL(2-199) and BSAC(2-142), respectively. While the estimated average helical content ranged from 10-27%, the proportions of β-strand were estimated from 5-10% and those of turns from 10-13%. This is in agreement with secondary structure prediction (Figure 2.1) and the fact that MAL(2-261) co-purifies with *E. coli* DnaK (see Figure 2.4 B and Section 7.11.1 in Chapter 7; Materials and Methods). The relative increase of secondary structure with decreasing size of the RPEL domain indicates that regions preceding and following the RPEL motifs are largely unordered.

2.3.2.3 The MAL RPEL domain stably binds three actin molecules

Having investigated the molecular nature of the isolated RPEL domain, I next turned to the analysis of the MAL-actin complex. G-actin alone eluted at 45 kDa (Figure 2.7). To analyse the molecular mass of the MAL-actin complex, I coupled actin sequestering assays with gel filtration chromatography. 10 μM MAL were co-incubated with 30 μM (unmodified) G-actin. Any unbound actin was polymerised and sedimented by ultracentrifugation. Equivalent amounts of total samples, supernatants and pellets were subjected to SDS-PAGE and Coomassie brilliant blue staining (Figure 2.7, left). Supernatants were analysed by gel filtration (Figure 2.7, right). The MAL-actin complex eluted at a volume corresponding to a molecular mass of 252 kDa, which suggests the presence of three molecules of actin (Figure 2.7). To corroborate the stoichiometry of the MAL-actin complex, I attempted to supershift the MAL-actin complex with DNaseI. DNaseI, a globular protein of about 30 kDa, forms a 1:1 complex with G-actin, interacting with the DNaseI-binding loop in actin subdomain 2 and blocking actin polymerisation (Kabsch et al., 1990, see Figure 1.1 in Chapter 1). A MAL(2-261)-actin-DNaseI complex was prepared from 10 μM MAL(2-261), 30 μM actin and 30 μM DNaseI. An actin-DNaseI complex eluted with an apparent molecular mass of 77 kDa, consistent with a 1:1 stiochiometry (Figure 2.8 A). The MAL-containing complex eluted with an apparent molecular mass of 358 kDa, compatible with the presence of 3 actin molecules and 3 molecules of DNaseI (Figure 2.7). Therefore, DNaseI does not compete with MAL for actin binding.

These observations show that the MAL RPEL domain can form a 1:3 complex with actin that is resistant to subsequent actin polymerisation and centrifugation and stable in gel filtration chromatography.

2.3.2.4 The effects of actin-binding drugs on the MAL-actin complex re-capitulate their action on actin-SRF signalling

Actin-binding drugs have distinct effects on SRF activation. LatB, which increases the cellular G-actin pool by sequestering actin monomers, blocks serum-induced activation of SRF. Conversely, CD, jasplakinolide (Jasp), and swhinholide A (SwA) activate SRF in the absence of upstream stimuli (Sotiropoulos et al., 1999, see Section 1.2.6 in Chapter 1). Previous GST affinity precipitation and co-immunoprecipitation experiments suggested that actin-binding drugs might act by disrupting the MAL-actin complex or prevent its formation (Miralles et al., 2003; Posern et al., 2004). To resolve this question, I included these drugs in the gel filtration experiments. LatB increased the yield of the MAL-actin complex (Figure 2.7). The virtual loss of actin filaments as documented by the accompanying actin sequestering assay indicates that the increased yield is likely to be due to an increase in the amount of G-actin available for MAL binding. LatB did not affect MAL-actin complex stoichiometry. Conversely, CD, Jasp and SwA blocked MAL-actin complex formation (Figure 2.7). The actin sequestering assay shows that filaments formed in the presence of CD and Jasp, which is in agreement with known properties of these drugs (see Section 1.2.6 in Chapter 1). SwA blocked actin polymerisation by non-covalently cross-linking two actin molecules with the dimer eluting at 80 kDa (see Section 1.2.6.3 in Chapter 1).

2.3.2.5 Actin binding is sensitive to mutations in the RPEL motifs

I next attempted to generate mutant derivatives of full-length MAL that are unable to interact with actin. Previous MAL-actin interaction studies (by co-immunoprecipitation, GST affinity precipitation, native gel electrophoresis and yeast-two-hybrid analysis) have highlighted the importance of the R and P residues of the two RPEL motifs of MAL(met) for actin binding (Miralles et al., 2003; Posern et al., 2004). For the nomenclature of mutant MAL derivatives, I will refer to the "R" position as position 1 and the following one as position 2. I generated the equivalent mutants of the

full-length variant of MAL. In MAL-123-2A, I exchanged each amino acid at position 2, which is arginine for RPEL1, to alanine. The arginine residue at position 1 represents the most conserved residue of the entire RPEL motif. It is likely that it is critically involved in RPEL motif functionality. I therefore generated a second mutant, MAL xxx, in which I replaced the conserved R residue for A in all three RPEL motifs. Neither MAL(2-261)-123-2A nor MAL(2-261) xxx were able to form complexes with actin that were stable enough to resist actin polymerisation and subsequent gel filtration (Figure 2.7). The elution behaviour of the small amount of actin retained by MAL(2-261)-123-2A indicates that an unstable complex was formed but dissociated during chromatography. This is not observed for MAL(2-261) xxx, indicating that MAL-123-2A exhibits higher residual affinity for actin than MAL xxx. This difference becomes even more apparent in GST affinity precipitation experiments, where the amount of actin recruited by GST-MAL(2-261)-123-2A is still substantial compared to the wild-type protein whereas GST-MAL(2-261) xxx is largely defective in retaining actin from total NIH3T3 cell lysate (Figure 2.7, inset).

Based on pyrenyl-actin polymerisation assays, gel filtration analysis, light scattering studies, and GST affinity sedimentation experiments, I conclude that the monomeric aminoterminus of MAL stably binds three molecules of actin.

2.3.2.6 TMR modification of C374 destabilises the MAL-actin interaction

A block of actin polymerisation is desirable for an *in*-vitro analysis of the MAL-actin complex. Modification of actin with the fluorophore tetramethylrhodamine (TMR) at C374 achieves this and has recently resulted in the first crystal structure of uncomplexed actin (Otterbein et al., 2001). To test the feasibility of this approach for studying the MAL-actin complex, I generated TMR-actin and performed gel filtration chromatography of MAL(2-261) with TMR-actin in the same way as described above for complexes with non-modified actin. While a MAL-actin complex with apparent 1:3 stoichiometry was readily detectable, a much smaller shift of MAL was observed with TMR-actin (Figure 2.8 B). The elution volume of the TMR-actin-containing complex corresponds to an apparent molecular mass of 131 kDa while MAL(2-261) eluted with an apparent molecular mass of 114 kDa. The difference of less than a unit of TMR-actin (apparent molecular mass 46 kDa) indicates that MAL cannot engage in a stable complex with TMR-actin. A complex appears to have formed, as indicated by the absorption shoulder preceding the 131 kDa peak and the MAL(2-261):TMR-actin ratio

in the corresponding fraction, but this complex did not resist gel filtration. I therefore conclude that the TMR moiety of TMR-actin interferes with MAL binding.

2.3.2.7 MAL is likely to bind at the subdomain 1-3 interface of actin

The data above show that cytochalasin D, swinholide A, jasplakinolide and actin polymerisation interfere with MAL binding while latrunculin B or DNaseI do not negatively affect MAL-actin complex formation. Previous work indicated that profilin and MAL compete for actin binding (Posern et al., 2004). To gain preliminary insights into the surface that MAL occupies on the actin molecule, available structural models were grouped according to their compatibility with the MAL-actin complex (Figure 2.9). Latrunculin B occupies the interdomain cleft of actin (Morton et al., 2000). DNaseI binds a loop in actin subdomain 2 (Kabsch et al., 1990). Strikingly, actin-binding agents that interfere with the MAL-actin complex, including actin itself, modify or occupy the cleft formed between actin subdomains 1 and 3 at the base of the molecule (Holmes et al., 1990; Klenchin et al., 2005; Otterbein et al., 2001; Schutt et al., 1993). It is therefore likely that MAL targets this region of actin. Crystallographic studies of the MAL-actin interaction are presented in Chapter 5.

2.4 Summary

The MAL RPEL domain contains regulatory elements that mediate both nuclear import and export and can confer actin-regulated nucleocytoplasmic shuttling on a heterologous protein such as pyruvate kinase. MAL directly interacts with both β and skeletal muscle α actin and does not require any other protein for actin binding. The isolated MAL RPEL domain is monomeric, extended and largely unstructured. It effectively engages with three actin molecules, blocking their ability to polymerise. The actin-binding drugs cytochalasin D, jasplakinolide and swinholide A activate SRF by directly interfering with the MAL-actin interaction. MAL-actin complex formation is, however, insensitive to latrunculin B. This clearly establishes that actin-binding drugs have a specific effect on actin-SRF signalling. Structural information available for complexes of actin with actin-binding proteins and drugs suggest that MAL binding involves the cleft formed between actin subdomains 1 and 3 at the base of the actin molecule.

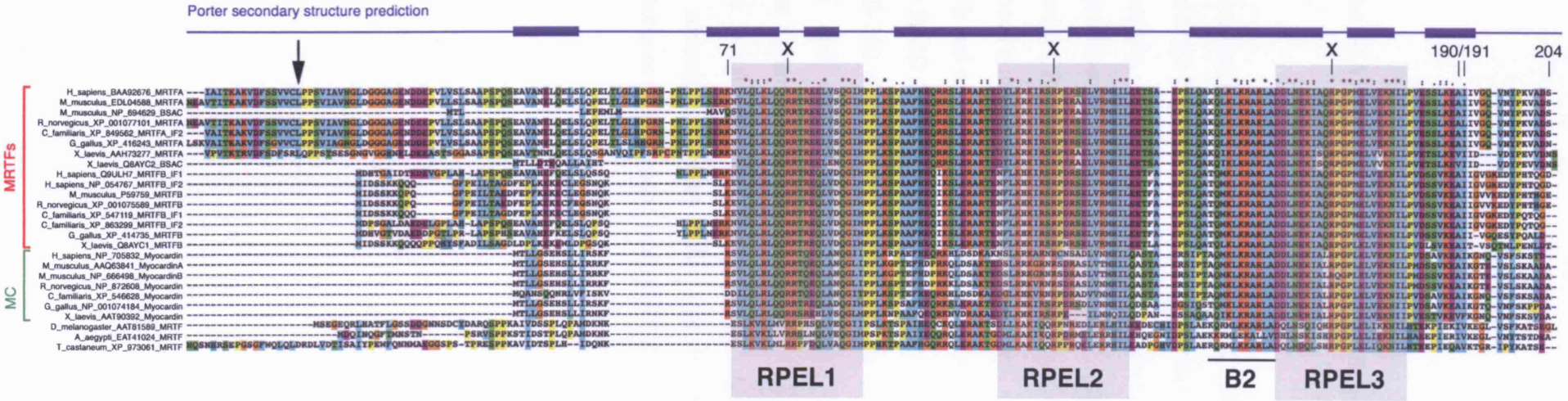

Figure 2.1 Amino acid alignment of the N-termini of myocardin family members. Accession numbers and predicted orthologues are indicated. The RPEL motifs as defined by PFAM (Finn et al., 2006) at the beginning of this study are shaded in grey. The leucine residue, at which MAL / MRTF-A translation is likely to be initiated (position 1 of full-length MAL mainly used in this study), is marked by an arrow. The last position of MAL / MRTF-A shown is serine 204. The B2 basic region is indicated. "x" denotes the positions of the first and most conserved arginine residues in the RPEL motifs (R81, R125 and R169 in mouse MAL / MRTF-A) that were mutated, as described later in this and subsequent chapters. A secondary structure prediction obtained for mouse MAL / MRTF-A from Porter (Pollastri et al., 2005; http://distill.ucd.ie/porter/) is shown. The sequence alignment was obtained using ClustalX (Thompson et al., 1997). Red bracket indicates MRTFs, green one myocardin. The last three sequences in this alignment represent insect proteins.

Figure 2.2 The MAL RPEL domain is sufficient to confer nucleocytoplasmic shuttling.

see overleaf

(**A**) Schematic representation of MAL(2-204)-PK. (**B**) Immunofluorescence microscopy of MAL and MAL(2-204)-PK in NIH3T3 fibroblasts. Cells were transfected with the indicated derivatives, serum-starved and stimulated as indicated (FCS, foetal calf serum; CD, cytochalasin D; Jasp, jasplakinolide; LatB, latrunculin B; LMB, leptomycin B). Treatment with CD, Jasp, LatB and LMB was for 30 min. LatB was added 30 min after cells had been stimulated with FCS. For serum washout, cells were stimulated with 15% FCS for 1 h and re-starved with 0.5% FCS for 1 h. Where indicated, C3 transferase (C3) or β-actin R62D (R62D) were co-expressed. See text for nomenclature of mutant derivatives. 150-200 cells were scored according to predominantly nuclear (N), pan-cellular (N/C) and predominantly cytoplasmic (C) MAL or MAL(2-204)-PK localisation. See Figure 8.1 for an explanation of the localisation scoring system. Bars in pairs show localisation of MAL (left) and MAL(2-204)-PK (right). (**C**) Representative micrographs with MAL and PK derivatives shown in green and endogenous F-actin or co-expressed β-actin R62D in red.

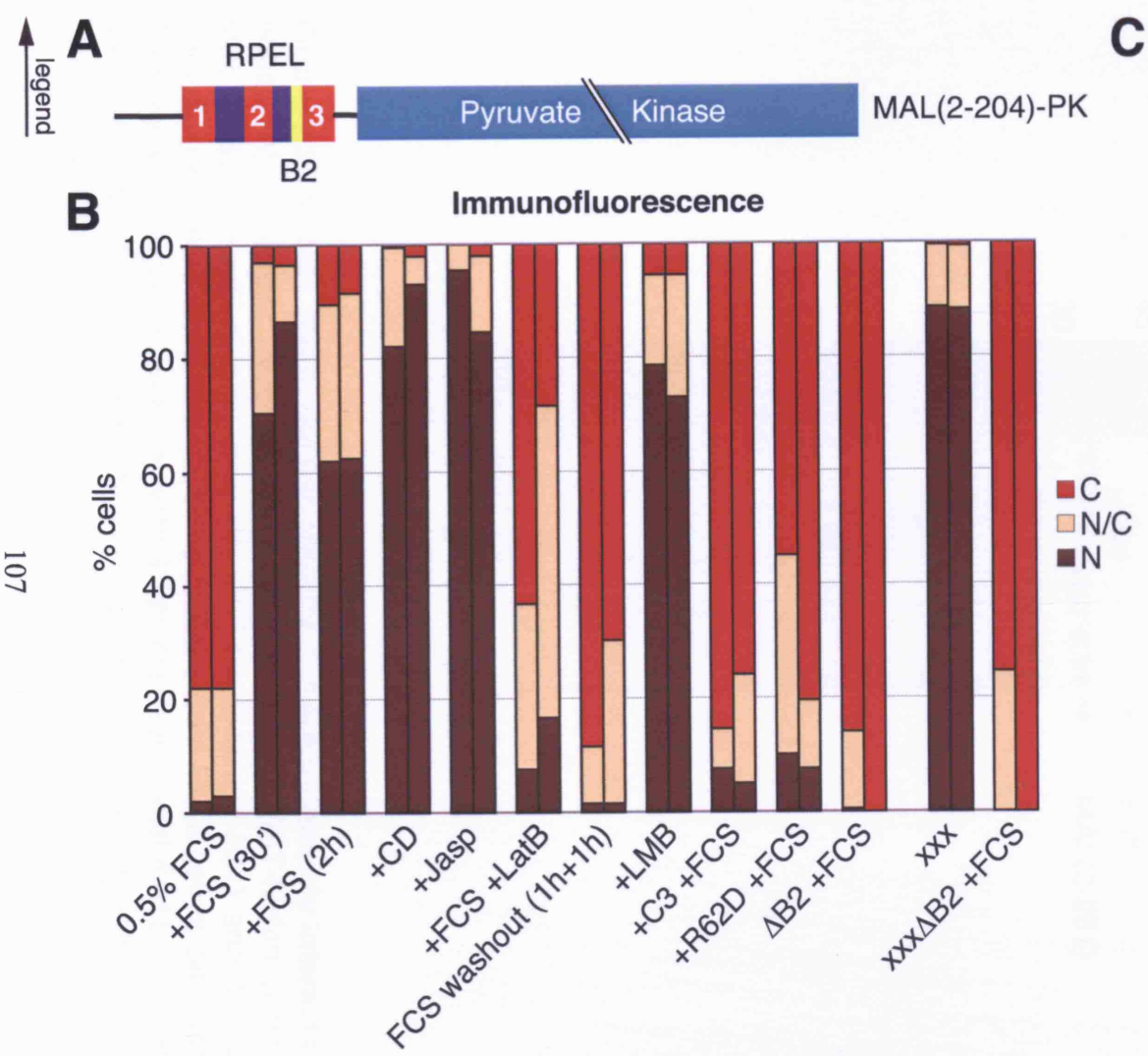

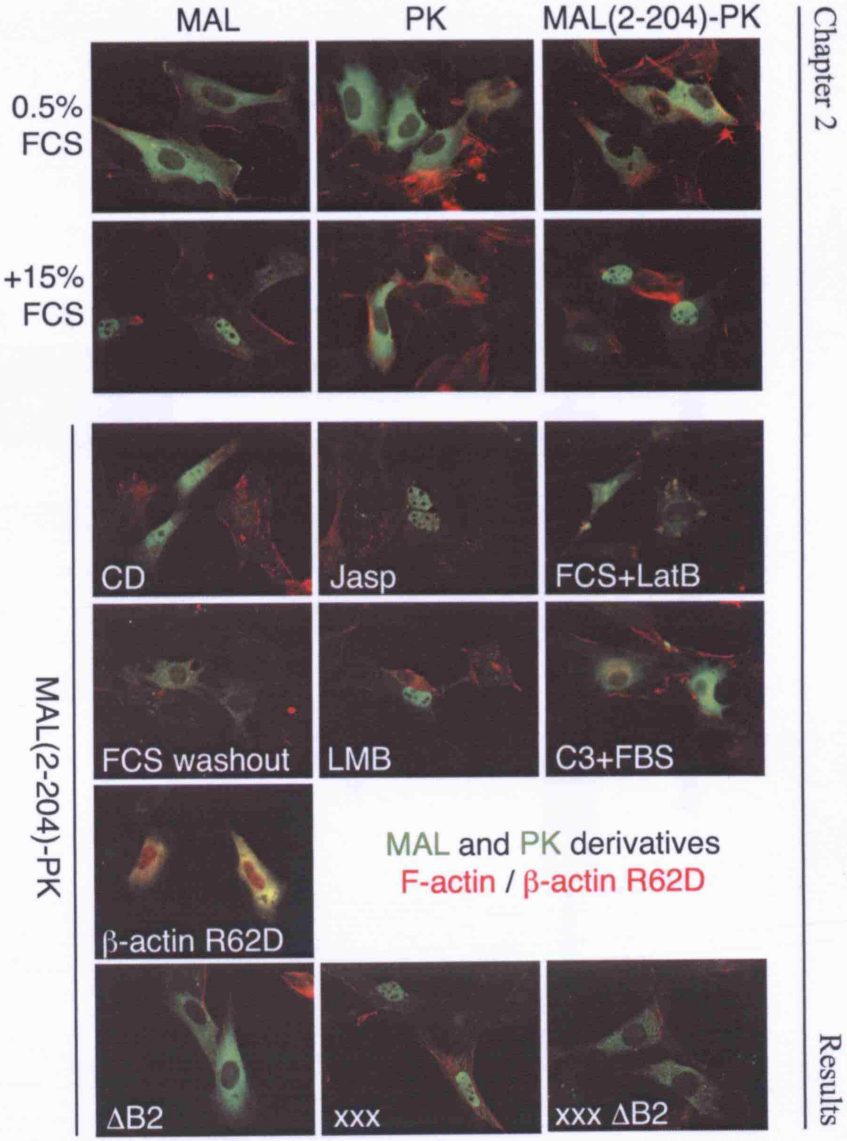

Figure 2.2 MAL (left bars) and MAL(2-204)-PK (right bars)

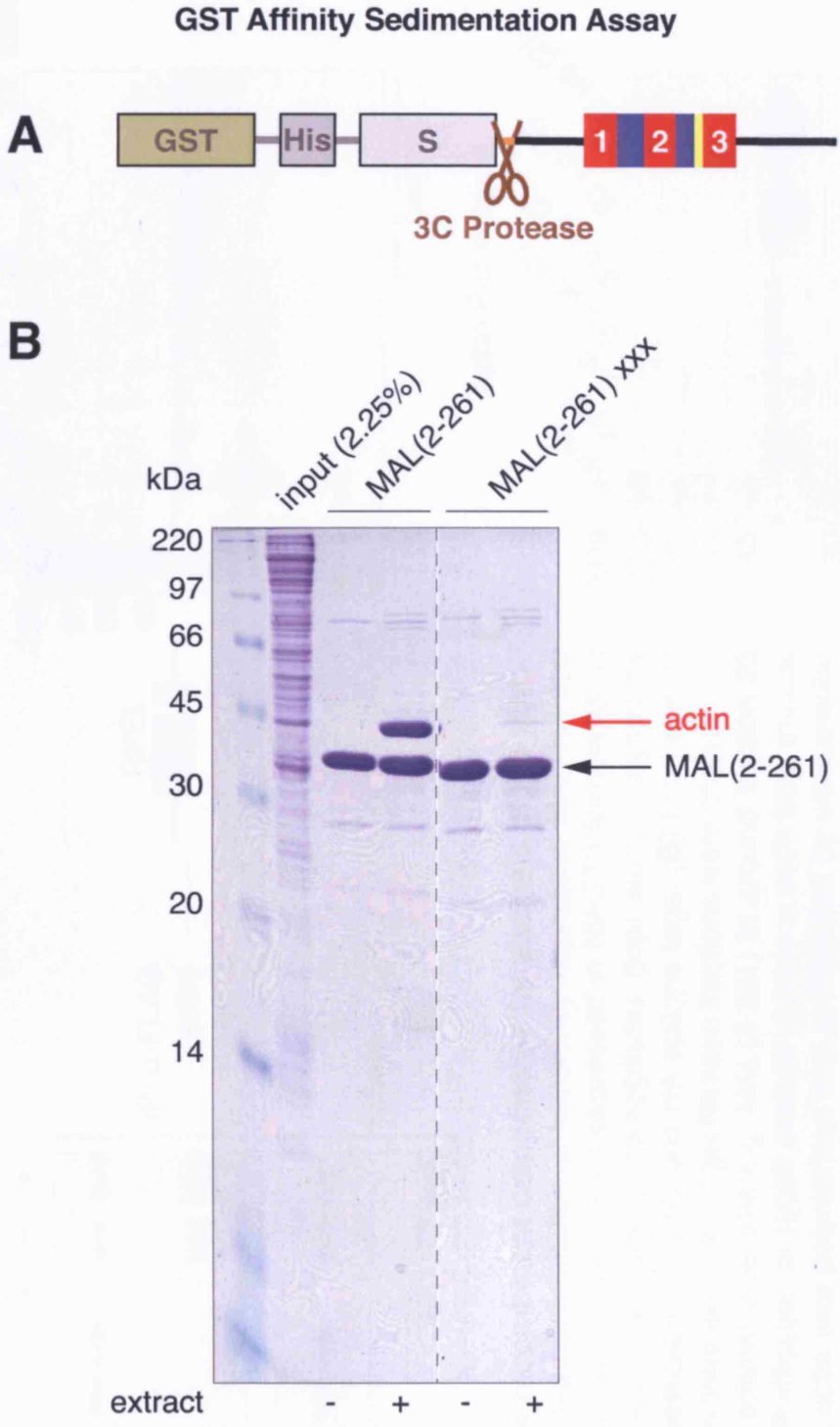

Figure 2.3 The MAL RPEL domain directly and autonomously interacts with actin. (**A**) Schematic representation of recombinant GST-fusion protein of MAL(2-261) generated in E. coli. (**B**) GST-His-S-MAL(2-261) and its mutant derivative xxx were used to immobilise proteins from HeLa cell nuclear extract. Proteins were eluted by cleavage with 3C protease and analysed by SDS-PAGE and Coomassie brilliant blue staining. The proteins migrating between 66 and 97 kDa are bacterial and murine chaperones.

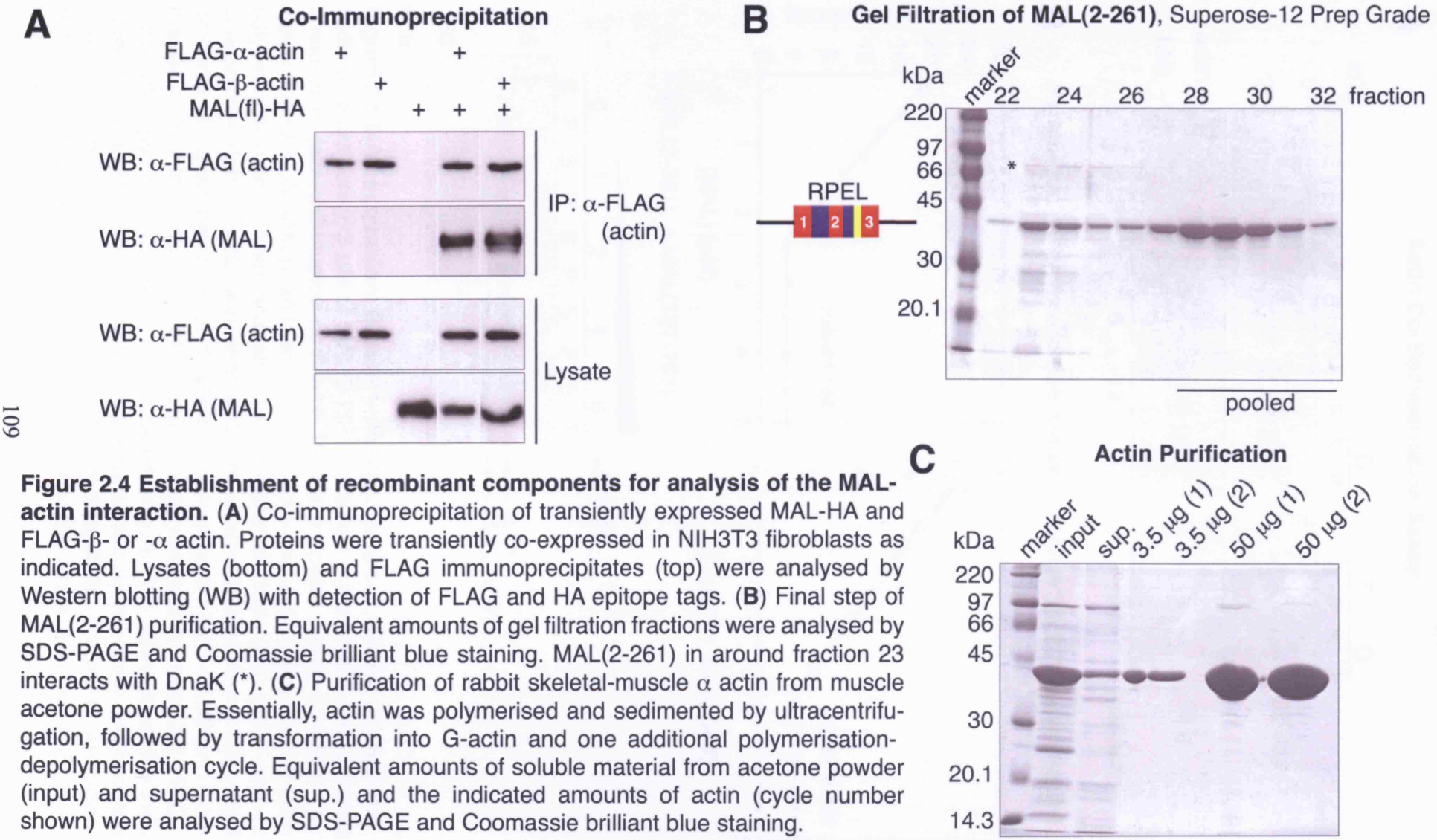

Figure 2.4 Establishment of recombinant components for analysis of the MAL-actin interaction. (**A**) Co-immunoprecipitation of transiently expressed MAL-HA and FLAG-β- or -α actin. Proteins were transiently co-expressed in NIH3T3 fibroblasts as indicated. Lysates (bottom) and FLAG immunoprecipitates (top) were analysed by Western blotting (WB) with detection of FLAG and HA epitope tags. (**B**) Final step of MAL(2-261) purification. Equivalent amounts of gel filtration fractions were analysed by SDS-PAGE and Coomassie brilliant blue staining. MAL(2-261) in around fraction 23 interacts with DnaK (*). (**C**) Purification of rabbit skeletal-muscle α actin from muscle acetone powder. Essentially, actin was polymerised and sedimented by ultracentrifugation, followed by transformation into G-actin and one additional polymerisation-depolymerisation cycle. Equivalent amounts of soluble material from acetone powder (input) and supernatant (sup.) and the indicated amounts of actin (cycle number shown) were analysed by SDS-PAGE and Coomassie brilliant blue staining.

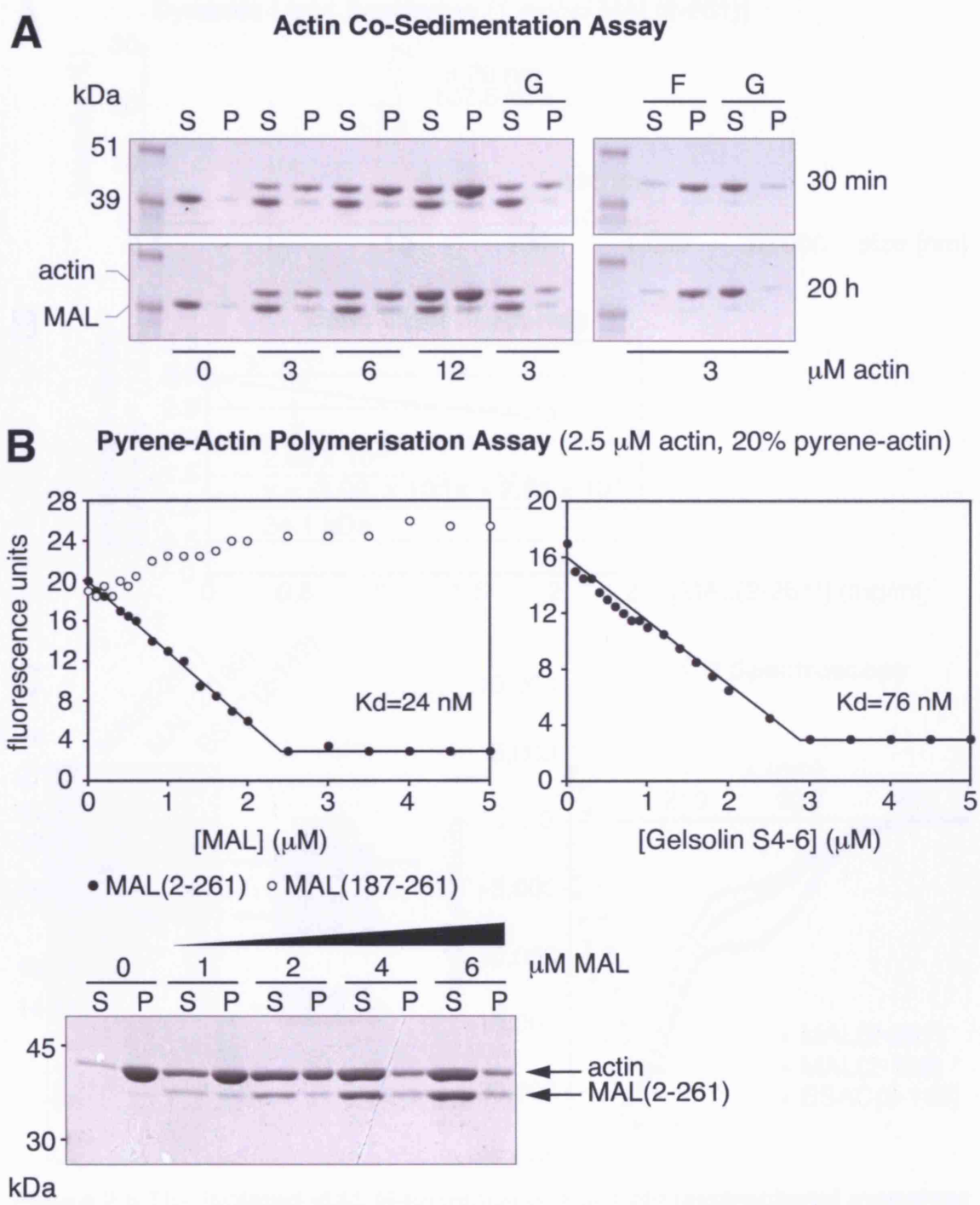

Figure 2.5 MAL sequesters G-actin with high apparent affinity. (**A**) Actin co-sedimentation assay. 3 μM of MAL(2-261) were co-incubated with the indicated amounts of (skeletal-muslce α) F-actin for the specified times. Controls: co-incubation of 3 μM MAL(2-261) with 3 μM G-actin followed by induction of actin polymerisation and further incubation for the indicated times (left) and F-actin or G-actin only (right). F-actin was sedimented by ultracentrifugation and equivalent amounts of supernatants (S) and pellets (P) analysed by SDS-PAGE and Coomassie brilliant blue staining. (**B**) Pyrene-actin polymerisation assay. 2.5 μM G-actin (20% pyrene-actin) were co-incubated with varying amounts of the indicated proteins. Actin polymerisation was induced and pyrene-actin fluorescence measured at binding equilibrium. The apparent dissociation constants are shown. Bottom, analysis of the pyrene-actin polymerisation assay with MAL(2-261) by ultracentrifugation as in (A).

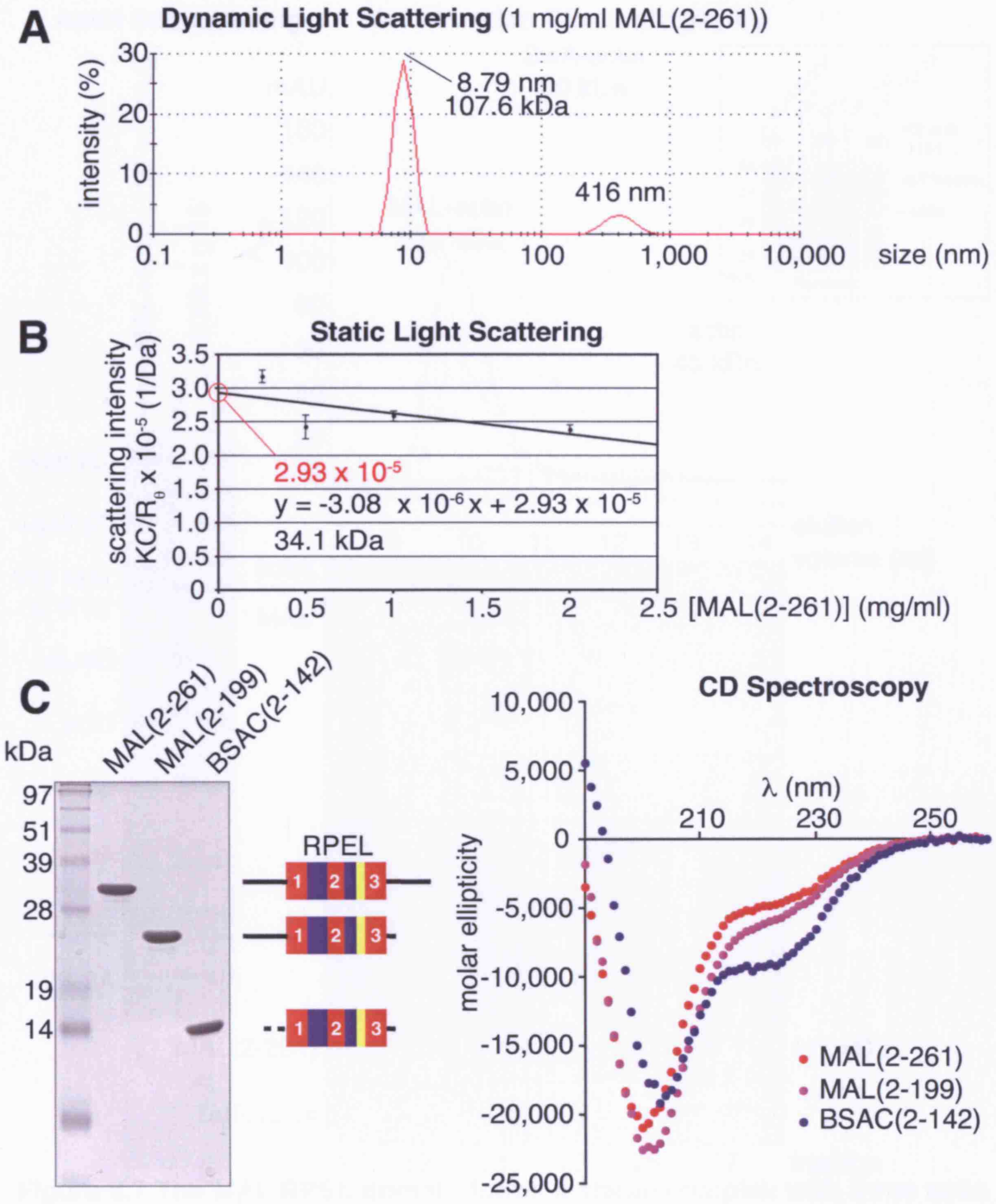

Figure 2.6 The isolated MAL N-terminus is a largely unstructured monomer with an extended conformation. (**A**) Dynamic light scattering of MAL(2-261). The peak corresponding to a hydrodynamic radius of 416 nm is likely due to particles in the buffer. (**B**) Debye plot documenting static light scattering of MAL(2-261) at concentrations of 0.25, 0.5, 1.0 and 2.0 mg/ml. The reciprocal of the intercept of the linear regression function with the y-axis corresponds to the mass-average molecular mass and its slope to the second virial coefficient A_2. n=2 measurements of the same set of samples with SD. (**C**) The indicated protein derivatives (Coomassie-brilliant blue stained SDS-PAGE gel and schematic representation on the left) were subjected to CD spectroscopy (right). The negative peak of molar ellipticity at 202 nm is indicative of a random-coil arrangement. Average secondary-structure parameters are: MAL(2-261), 71% unordered, 10% helix, 10% turn; MAL(2-199), 68% unordered, 18% helix, 5% strand, 11% turn; BSAC(2-142), 54% unordered, 27% helix, 7% strand, 13% turn.

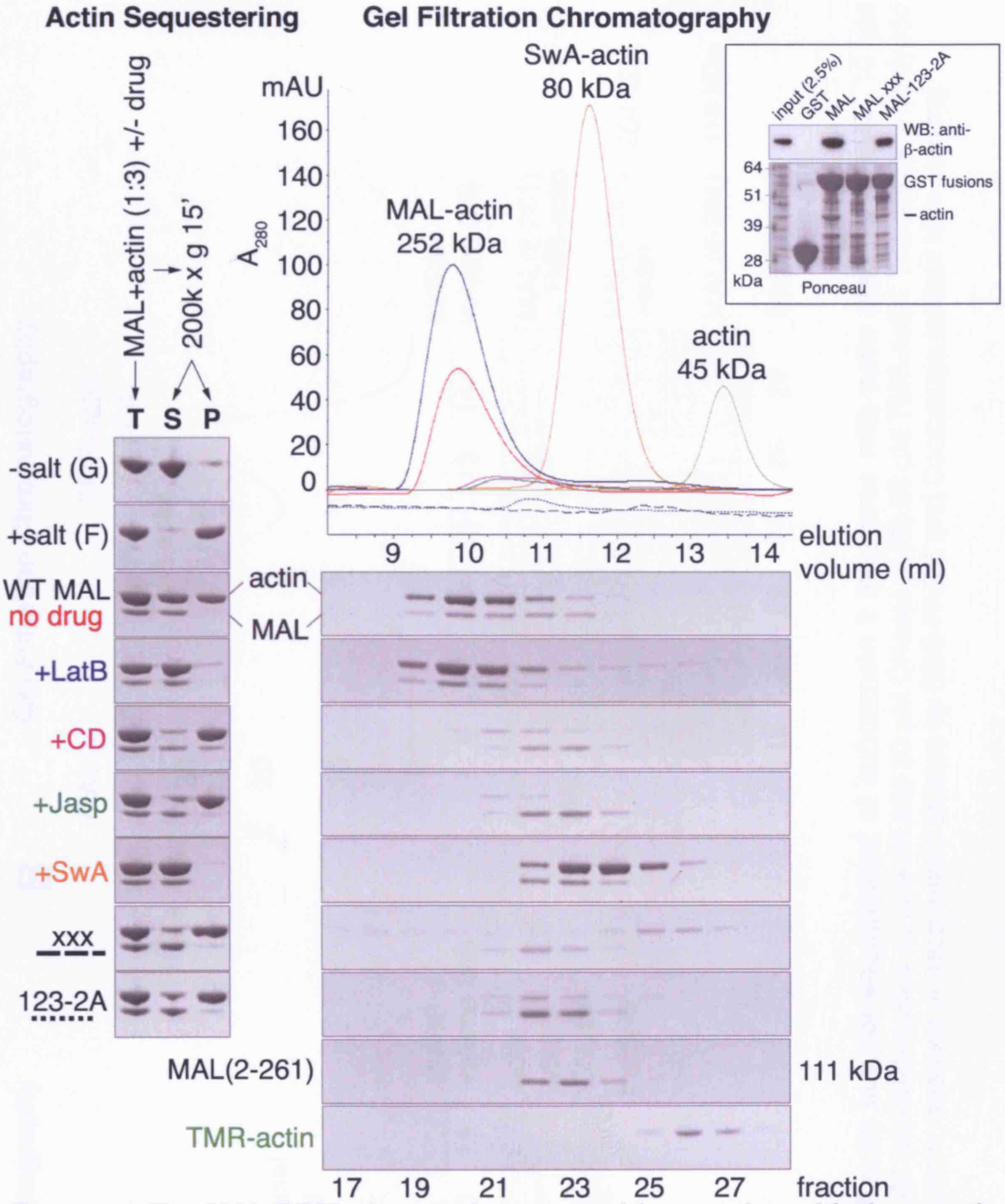

Figure 2.7 The MAL RPEL domain forms a stable complex with three actin molecules that is sensitive to SRF-activating actin-binding drugs and mutation of RPEL motifs. 10 µM MAL(2-261) were incubated with 30 µM (skeletal-muslce α) G-actin with and without drug (LatB, latrunculin B; CD, cytochalasin D; Jasp, jasplakinolide; SwA, swinholide A). Unbound actin was polymerised by salt addition and removed by ultracentrifugation (sequestering assay, analysed by SDS-PAGE and Comassie brilliant blue staining, on the left: T, total sample; S, supernatant; P, pellet). Supernatants were analysed on a calibrated gel filtration column. Eluates were collected in 500 µl fractions and analysed by SDS-PAGE and Coomassie staining. For analysis of actin only, actin was rendered nonpolymerisable by modification with tetramethylrhodamine (TMR; Otterbein et al., 2001). Apparent molecular masses were determined via the elution volumes. **Inset:** Actin recruitment from total NIH3T3 cell extract by indicated derivatives of GST-MAL(2-261). WB, Western blot with detection of β actin; Ponceau stain of membrane to show GST-fusion proteins.

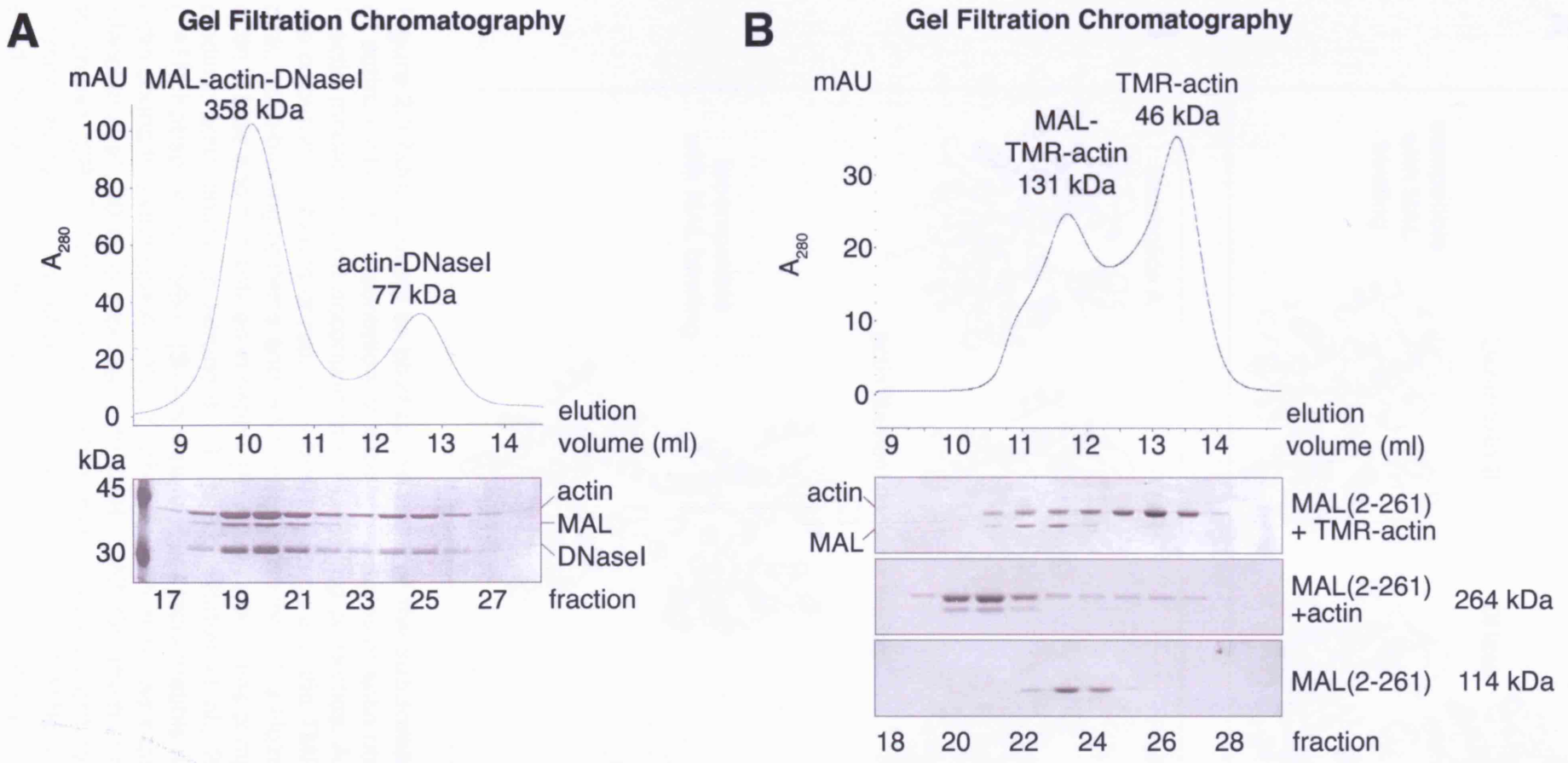

Figure 2.8 C-terminal modification of actin but not engagement of subdomain 2 interferes with actin binding to MAL. 10 μM MAL(2-261) were incubated with (**A**) 30 μM (skeletal-muslce α) G-actin and 30 μM DNaseI or (**B**) 30 μM TMR-actin. The complex analysed as in Figure 2.7. Top, chromatograms; bottom, analysis of fractionated eluates by SDS-PAGE and Coomassie brilliant blue staining.

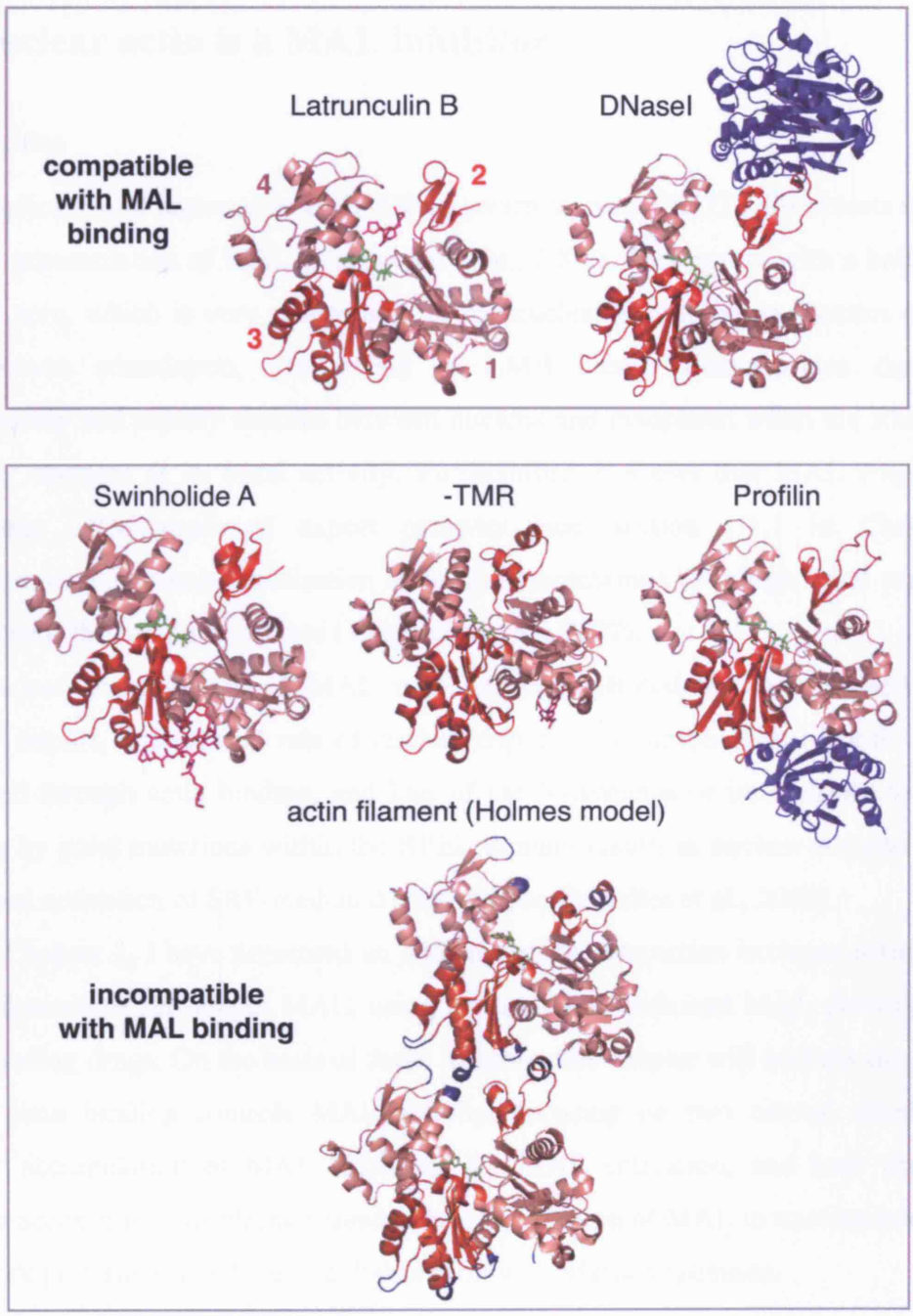

Figure 2.9 MAL is likely to bind at the base of the subdomain 1-3 interface of actin. Ribbon representation of known structures of actin complexes and an F-actin model grouped according to MAL-binding properties. Actin subdomains are coloured in shades of red, actin-binding drugs and the TMR modification in pink, actin-binding proteins and actin-actin contacts in the Holmes model of F-actin in blue and nucleotides in green. (**A**) Actin assemblies compatible with MAL binding: actin bound to latrunculin B (1ESV; Morton et al., 2000) or DNaseI (1ATN; Kabsch et al., 1990). (**B**) Actin assemblies incompatible with MAL binding: actin bound to swinholide A (1YXQ; only one actin molecule shown for simplicity; Klenchin et al., 2005) or modified with TMR (1J6Z; Otterbein et al., 2001), bound to profilin (2BTF; Schutt et al., 1993) and F-actin according to the Holmes filament model (Holmes et al., 1990; two protomers of TMR-actin (1J6Z) modelled into approximate arrangement in one strand; C-terminal residue modelled).

3 Nuclear actin is a MAL inhibitor

3.1 Aims

Application of leptomycin B (LMB) to serum-starved NIH3T3 fibroblasts results in nuclear accumulation of MAL (Vartiainen et al., 2007). This occurs with a half time of about 1 min, which is very comparable to the nuclear-accumulation kinetics observed upon serum stimulation. The effect of LMB clearly demonstrates that MAL continuously and rapidly shuttles between nucleus and cytoplasm when the RhoA-actin pathway operates at its basal activity. Furthermore, it shows that MAL employs the ubiquitous CRM1-mediated export pathway (see Section 1.1.1 in Chapter 1). Cytoplasmic steady-state localisation of MAL is maintained by a high basal export rate that exceeds the basal import rate (Vartiainen et al., 2007).

Nuclear accumulation of MAL may be accomplished by an increased rate of nuclear import, a decreased rate of nuclear export or a combination of both. MAL is regulated through actin binding, and loss of the N-terminus or interference with actin binding by point mutations within the RPEL domain results in nuclear accumulation of MAL and activation of SRF-mediated transcription (Miralles et al., 2003).

In Chapter 2, I have presented an analysis of the interaction between actin and the RPEL domain of full-length MAL, using actin-binding deficient MAL derivatives and actin-binding drugs. On the basis of these insights, this chapter will address the levels at which actin binding controls MAL activity, focusing on two central questions: is nuclear accumulation of MAL sufficient for MAL activation, and how does actin binding accomplish cytoplasmic steady-state localisation of MAL in unstimulated cells? The work presented was done in collaboration with Maria Vartiainen.

3.2 Evidence for inhibition of MAL activity by a nuclear MAL-actin interaction

Dissociation of the MAL-actin complex by various means not only accumulates MAL in the nucleus but also activates SRF-mediated transcription (Miralles et al., 2003; Sotiropoulos et al., 1999). Actin might therefore also play a role in MAL regulation at the transcriptional level. Furthermore, given that MAL constantly shuttles through the nucleus, how is it prevented from engaging in productive transcription in the absence of

activating signals? Efficient nuclear export of MAL certainly represents an important mechanism to avoid the formation of active MAL-SRF transcription complexes.

Is nuclear accumulation of MAL sufficient to activate SRF-mediated transcription? This question was partially addressed by earlier work by our laboratory (Posern et al., 2002), though in a different context: a previous report proposed that actin is exported from the cell nucleus via the CRM1 pathway (Wada et al., 1998). To test whether nuclear accumulation of actin directly affects SRF-target gene activity, the effect of LMB on basal and induced SRF activity was studied using an SRF-luciferase reporter and RNase protection assay monitoring the transcription of an exogenous and the endogenous *Fos* gene (Posern et al., 2002). No influence of LMB on SRF activity was observed. Note also that LMB had no effect on the steady-state localisation of actin (Posern et al., 2002). A later study identified exportin 6 as a *bona-fide* nuclear export receptor of actin (see Section 1.2.5.1 in Chapter 1). In retrospect, we can conclude that nuclear accumulation of MAL via LMB treatment is likely not to be sufficient for the activation of SRF-mediated transcription.

However, because of the broad substrate range of CRM1 (reviewed in Hutten and Kehlenbach, 2007), application of LMB cannot resolve this question conclusively. To specifically accumulate MAL in the nucleus in the absence of an activating stimulus, I transiently expressed a MAL derivative bearing the heterologous nuclear localisation signal (NLS) of SV40 (simian virus 40) large T antigen at its C-terminus (MAL-NLS, Figure 3.1 A, Kalderon et al., 1984) in NIH3T3 fibroblasts.

MAL-NLS was found predominantly nuclear in about 50% and pan-cellular in approximately 25% of transfected, serum-starved cells (Figure 3.1 B). MAL-NLS was substantially more nuclear than wild-type MAL, which is predominantly cytoplasmic in about 90% of the cells. The actin-binding deficient derivatives of MAL introduced in Chapter 2 showed pronounced nuclear localisation: MAL xxx was predominantly nuclear in about 90% of the cells whereas MAL-123-2A showed a localisation more comparable to that of MAL-NLS, although it hardly ever appeared predominantly cytoplasmic. Despite its clearly enhanced nuclear localisation at basal conditions, MAL-NLS failed to activate an SRF luciferase reporter more potently than wild-type MAL in serum-starved cells (Figure 3.1 C). Under the identical conditions, both MAL xxx and MAL-123-2A strongly activated the SRF reporter (Figure 3.1 C and D). The activation of the SRF reporter by low doses of cytochalasin D (CD) such as 0.5 μM can be

sensitised by expression of MAL. I exploited this observation to ask whether the release from actin can activate MAL-NLS. Indeed, both MAL and MAL-NLS, but not MAL xxx, were stimulated by CD (Figure 3.1 C). Therefore, nuclear accumulation of MAL is not sufficient to activate SRF unless MAL is additionally released from its complex with actin.

3.3 A nuclear RPEL domain activates MAL-NLS

Based on the observations presented in the previous section, we proposed the existence of an inhibitory MAL-actin interaction in the nucleus. To further test this idea, I attempted to sequester nuclear actin by expressing a nuclear RPEL domain (MAL(2-261)-NLS), which should efficiently compete with MAL for actin binding (Figure 3.2 A). Both MAL(2-261)-NLS and its actin-binding deficient xxx derivative localised to the nucleus in virtually 100% of transfected serum-starved cells (Figure 3.2 B). MAL(2-261)-NLS, but not its xxx derivative, potentiated MAL-NLS-induced SRF reporter activity (Figure 3.2 C, right). A weak reporter activation by MAL(2-261)-NLS was also observed without co-expression of MAL-NLS, likely through the activation of endogenous MAL (Figure 3.2 C, left). These observations further support a role of nuclear actin in the inhibition of MAL activity.

3.4 Nuclear accumulation of MAL is not sufficient to activate MAL-dependent SRF target genes

I next tested whether nuclear accumulation of endogenous MAL by LMB is sufficient to induce the MAL-dependent SRF target genes *Vcl*, *Cyr61*, *Srf* and *Acta2* (*smooth-muscle α actin*) in serum-starved NIH3T3 fibroblasts. Following the isolation of RNA 30, 60 and 90 min upon stimulation of the cells with CD, serum (FCS) or treatment with LMB, the relative mRNA levels of these targets were quantified by reverse-transcription and real-time PCR (Figure 3.3). CD and FCS induced these genes potently. LMB treatment, however, failed to do so: at the time points of maximal induction by CD or FCS, mRNA abundance was only moderately increased (Figure 3.3, orange highlights). Of these cases, only the 1.7-fold induction of *Srf* by LMB was found to be significant ($p=0.0257$; confidence interval, 95%) in an unpaired t test for statistical significance. The moderate LMB-induced activity of MAL-dependent SRF target genes might reflect a titration of actin occurring upon concentration of MAL in the nucleus

and a consequential weak activation of MAL transcriptional activity. It is consistent with a subtle effect of LMB on the basal activity of an SRF reporter gene (Posern et al., 2002; Vartiainen et al., 2007). The primarily TCF-controlled SRF target genes *Egr1* and *Fos* were strongly induced by FCS but not by the MAL-specific activator CD or LMB (Figure 3.3). In conclusion, LMB-induced nuclear accumulation of endogenous MAL is not sufficient to activate MAL-dependent SRF target genes.

3.5 Nuclear accumulation of MAL is sufficient for its association with target genes

Actin might inhibit MAL activity at the level of MAL-SRF-DNA ternary complex formation or otherwise repress the activation of a MAL-actin-SRF complex on DNA (Figure 3.4 A). To distinguish between these scenarios, I performed chromatin immunoprecipitation (ChIP), asking whether nuclear accumulation of MAL is sufficient for its promoter association *in vivo*. Serum-starved cells were stimulated with CD or FCS to activate MAL or treated with LMB to accumulate MAL in the nucleus without activation. MAL activation and LMB treatment both recruited MAL to promoters of MAL-dependent SRF target genes (*Vcl*, *Cyr61*, *Srf*) but not to *Gapdh*. With LMB, a target gene enrichment of 6.4, 4.9 and 3.8-fold compared to serum-starved cells was observed for *Vcl*, *Cyr61* and *Srf*, respectively. Therefore, nuclear accumulation of MAL, whereas not sufficient for SRF activation, suffices for association of MAL with its target genes without the induction of RhoA-actin signalling. This suggests that repression of MAL occurs downstream of MAL-SRF-DNA ternary complex formation. Abrogation of actin binding through mutating the RPEL motifs does not show an actin-dependent effect on MAL-SRF-DNA ternary complex formation in electrophoretic mobility shift assays, further supporting the above conclusion (Figure 8.2 in Chapter 8).

The observations described in this section provide clear but indirect evidence for the presence of actin on MAL-dependent SRF target genes in their inactive state. I attempted to directly study the association of actin with these genes using chromatin immunoprecipitation against actin. So far, I was unable to obtain interpretable data. Recovery of target genes was generally low, likely due to the low effectiveness of commercially available actin antibodies, and the presence of non-MAL dependent genes such as *Gapdh* in the chromatin immunoprecipitates. (Note that *Gapdh* was not recovered in anti-MAL and anti-SRF ChIPs.) Gene recovery in anti-actin

immunoprecipitations might be attributable to the presence of actin in basal transcriptional machineries on actively transcribing genes and chromatin remodelling complexes (see Section 1.2.5 in Chapter 1). Furthermore, one might speculate that any potential removal of actin from inhibitory MAL-actin complexes on SRF target genes is accompanied by the recruitment of actin with active RNA polymerase II. Further analysis is necessary and under way to understand the mechanism of actin-mediated repression of MAL transcriptional activity.

3.6 MAL interacts with actin in both the cytoplasm and the nucleus

The experiments described above strongly suggest the existence of a nuclear MAL-actin complex. We sought to directly visualise MAL-actin interactions to gain insights into temporal and spatial parameters of MAL regulation by actin. To this end, Maria Vartiainen developed a Förster resonance energy transfer (FRET) assay. In this assay, MAL-green fluorescent protein (MAL-GFP) or its derivatives were co-expressed with N-terminally MYC-tagged β actin in NIH3T3 fibroblasts. Following treatment, the cells were fixed, and the exogenous actin was labelled with Cy3-coupled anti-MYC antibodies.

FRET refers to radiation-less energy transfer from the excited (donor) fluorophore to the second (acceptor) fluorophore, given that the emission spectrum of the donor and the excitation spectrum of the acceptor fluorophores overlap significantly. FRET occurs only if both fluorophores are in close, direct proximity of each other and can therefore be used as a readout for direct protein-protein interactions (see, for example, Larijani et al., 2003). In the experimental setup, GFP was excited and therefore used as the donor fluorophore, whereas Cy3 served as the acceptor fluorophore (Figure 3.5 A). FRET was measured by fluorescence lifetime imaging (FLIM) of the donor fluorophore. FRET efficiencies were calculated as measures for MAL-actin interaction.

FRET between MAL and actin was readily detected in serum-starved cells, demonstrating that both proteins interact *in vivo* (Figure 3.5 B). Importantly, FRET between MAL and actin was clearly apparent in the nucleus upon LMB treatment of the cells. This directly documents the existence of the nuclear MAL-actin complex postulated above. Treatment of cells with latrunculin B (LatB), which sequesters actin

monomers, thereby increasing the cellular G-actin concentration, significantly increased the FRET efficiency. Application of CD or introduction of the xxx mutation into the RPEL domain virtually abolished MAL-actin FRET. These observations are in good agreement with *in-vitro* experiments presented in Chapter 2: LatB increased the yield of the MAL-actin complex in gel filtration chromatography whereas CD or mutation of the RPEL motifs abolished actin binding by MAL (see Figure 2.7 in Chapter 2). Serum stimulation resulted in a significant drop in FRET efficiency, indicating that the MAL-actin complex is, at least partially, dissociated upon induction of RhoA-actin signalling (Figure 3.5 B). At the 10-min time point upon serum stimulation used here, MAL-actin FRET did not drop to efficiencies as low as upon CD treatment or mutation of the RPEL motifs. After 10 min of serum stimulation, the MAL-actin interaction recovered (Vartiainen et al., 2007). This suggests that the drop in MAL-actin interaction upon serum stimulation is very rapid and transient or that the MAL-actin complex never fully dissociates. Further experiments presented in the next chapter will be discussed in this context.

3.7 Actin binding is required for nuclear export of MAL

Several lines of evidence suggest that actin binding is able to block nuclear import of MAL, at least when G-actin concentrations are higher than they are in serum-starved NIH3T3 fibroblasts (Vartiainen et al., 2007). Inactivation of Rho GTPases by co-expression of C3 transferase, application of LatB or overexpression of wild-type or non-polymerisable actin all block LMB-induced nuclear accumulation of MAL. However, LatB is unable to restore cytoplasmic localisation of MAL after CRM1 has been blocked by LMB (Vartiainen et al., 2007).

To address the role of actin in nuclear export of MAL, Maria Vartiainen devised a fluorescence-loss in photobleaching (FLIP) assay to assess the dynamic localisation of MAL in living cells expressing MAL-GFP. The FLIP assay essentially measures the extent to which MAL travels through the cytoplasm even though it appears nuclear: while the cytoplasm is repeatedly photobleached, the nuclear fluorescence of MAL-GFP is measured (Figure 3.6 A). A decay of GFP-fluorescence intensity indicates that the protein of interest spends some time in the cytoplasm. The nuclear fluorescence of GFP, which can be expected to diffuse freely between nucleus and cytoplasm, was readily diminished by cytoplasmic photobleaching (Figure 3.6 B). Conversely, the nuclear

fluorescence of a protein that should never leave the nucleus, Ran-binding protein 1 with a mutated nuclear export signal (RanBP1 ΔNES), was virtually insensitive to cytoplasmic photobleaching (Figure 3.6 B). The nuclear bleaching kinetics of MAL-GFP in the presence of LMB were very similar to those observed for RanBP1 ΔNES, indicating that inactivation of CRM1 is sufficient to entirely block nuclear export of MAL. Therefore, unlike for several other transcriptional regulators such as STATs (see Section 1.1.1 in Chapter 1), no parallel export pathway appears to operate in the case of MAL. In the presence of the actin-binding drugs CD, swinholide A (SwA) or jasplakinolide (Jasp), all of which dissociate the MAL-actin complex (see Chapter 2), the bleach rates indicated that nuclear export of MAL-GFP is inefficient, suggesting that dissociation of the MAL-actin complex blocks nuclear export of MAL. In serum-stimulated cells, nuclear export occurred inefficiently but nevertheless with a higher rate than in cells that were treated with actin-binding drugs (Figure 3.6 B). Serum stimulation may affect the MAL-actin complex less severely than the application of actin-binding toxins. The bleaching kinetics observed for the actin-binding defective MAL derivative xxx (see Chapter 2) were virtually indistinguishable from those seen for MAL-GFP in CD-treated cells, strongly supporting the conclusion that actin binding targets MAL for nuclear export. An alternative mutant derivative of MAL that is defective for actin binding, 123-2A (see Chapter 2), behaved very similarly in this assay. One should note that MAL-123-2A-GFP displayed a nuclear steady-state localisation similar to that of MAL xxx-GFP, while its C-terminally HA-tagged counterpart was significantly more cytoplasmic (see Figure 3.1 B, Vartiainen et al., 2007).

Given that MAL xxx and MAL-123-2A retain a residual ability to interact with actin (see Figure 2.7 in Chapter 2), we tested the effect of actin overexpression on the bleaching kinetics of these mutants in the FLIP assay, seeking to "rescue" their actin-binding deficiencies. The bleach rate of MAL xxx increased significantly when actin was overexpressed, and this was sensitive to CD treatment. These observations clearly established a role of nuclear actin in targeting MAL for CRM1-mediated nuclear export. While MAL xxx essentially remained nuclear upon overexpression of actin, MAL-123-2A relocalised to the cytoplasm under the identical settings (Vartiainen et al., 2007). This is in line with MAL-123-2A retaining a higher residual actin avidity than MAL xxx (see Figure 2.7 in Chapter 2).

3.8 Summary

This chapter has highlighted that a nuclear MAL-actin interaction inhibits MAL activity at two levels: that of nucleocytoplasmic transport and that of SRF co-activation. Actin binding in the nucleus targets MAL for efficient nuclear export. The actin-binding deficient RPEL motif mutants of MAL (xxx and 123-2A), which I characterised biochemically in the preceding chapter, are nuclear and transcriptionally active in serum-starved cells. However, nuclear accumulation of MAL in the absence of activating signals is not sufficient to activate an SRF reporter gene or MAL-dependent SRF target genes. Nuclear MAL associates with its target genes, but remains inactive unless its interaction with actin is abrogated. MAL-actin interaction can be directly visualised by Förster resonance energy transfer (FRET), which shows that serum stimulation transiently dissociates the MAL-actin complex. Under the conditions used, no FRET was detected for MAL xxx and actin, demonstrating that the *in-vitro* observations presented in Chapter 2 can be translated into the *in-vivo* cellular system. Inhibition of MAL transcriptional activity most likely occurs downstream of MAL-SRF-DNA ternary complex formation, raising the possibility that actin acts as co-repressor on DNA.

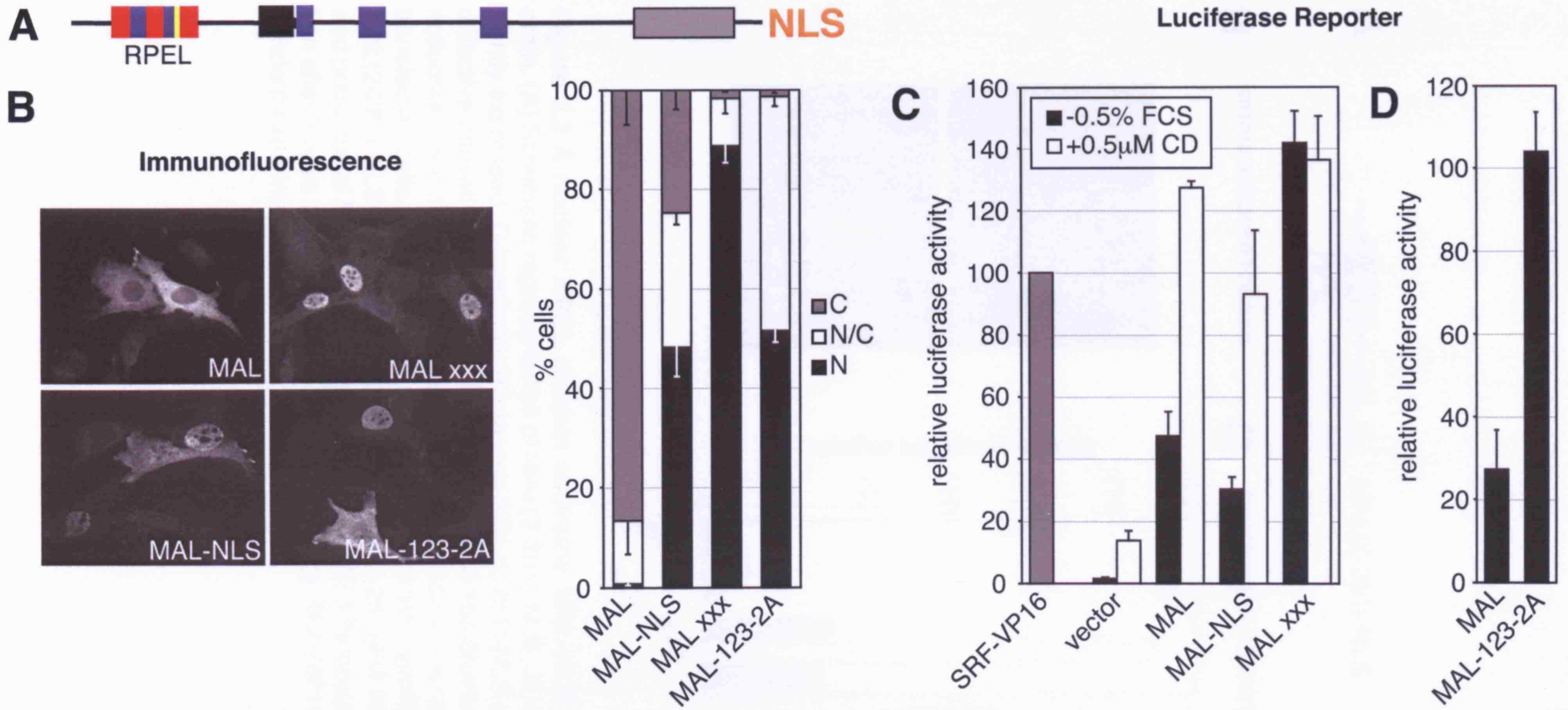

Figure 3.1 Nuclear accumulation of MAL is not sufficient to activate SRF-mediated transcription. (**A**) Schematic representation of MAL-NLS. For domains, see Figure 1.8. (**B**) Localisation of the indicated transiently expressed, C-terminally HA-tagged MAL derivatives in serum-starved NIH3T3 fibroblasts detected by immunofluorescence microscopy. Left, representative micrographs; right, quantitation of immunofluorescence microscopy: localisation was scored in 200 cells (N, nuclear; N/C, pan-cellular; C, cytoplasmic; n=3 independent experiments; error bars, SEM; see Figure 8.1 for an explanation of the localisation scoring system). (**C**) and (**D**) Activation of an SRF luciferase reporter by expression of the indicated MAL derivatives under the indicated conditions. Reporter activation is normalised to that conferred by SRF-VP16 (100%). n=3 independent experiments; error bars, SEM.

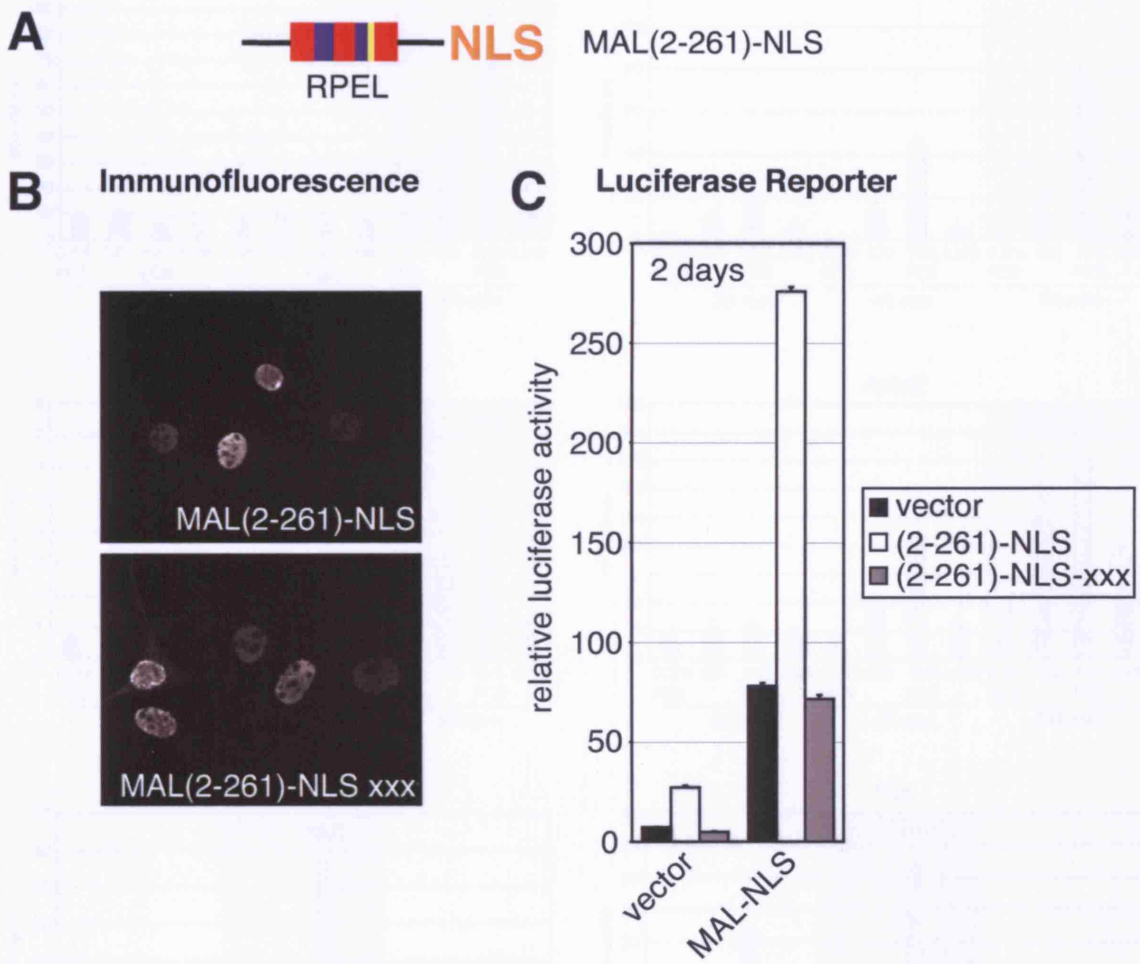

Figure 3.2 A nuclear RPEL domain activates MAL-NLS by competing for actin. (**A**) Schematic representation of MAL(2-261)-NLS. (**B**) Localisation of transiently expressed, C-terminally HA-tagged MAL(2-261)-NLS and its actin-binding defective derivative xxx in serum-starved NIH3T3 fibroblasts detected by immunofluorescence microscopy. Both constructs localise to the nucleus in virtually all transfected cells. (**C**) Activation of an SRF luciferase reporter by expression of MAL(2-261)-NLS constructs (180 ng pEF-MAL(2-261)-HA-NLS) in the absence and presence of MAL-NLS in serum-starved NIH3T3 fibroblasts. Reporter activation after 2 days is normalised to that conferred by SRF-VP16 (100%). n=3 independent experiments; error bars, SEM.

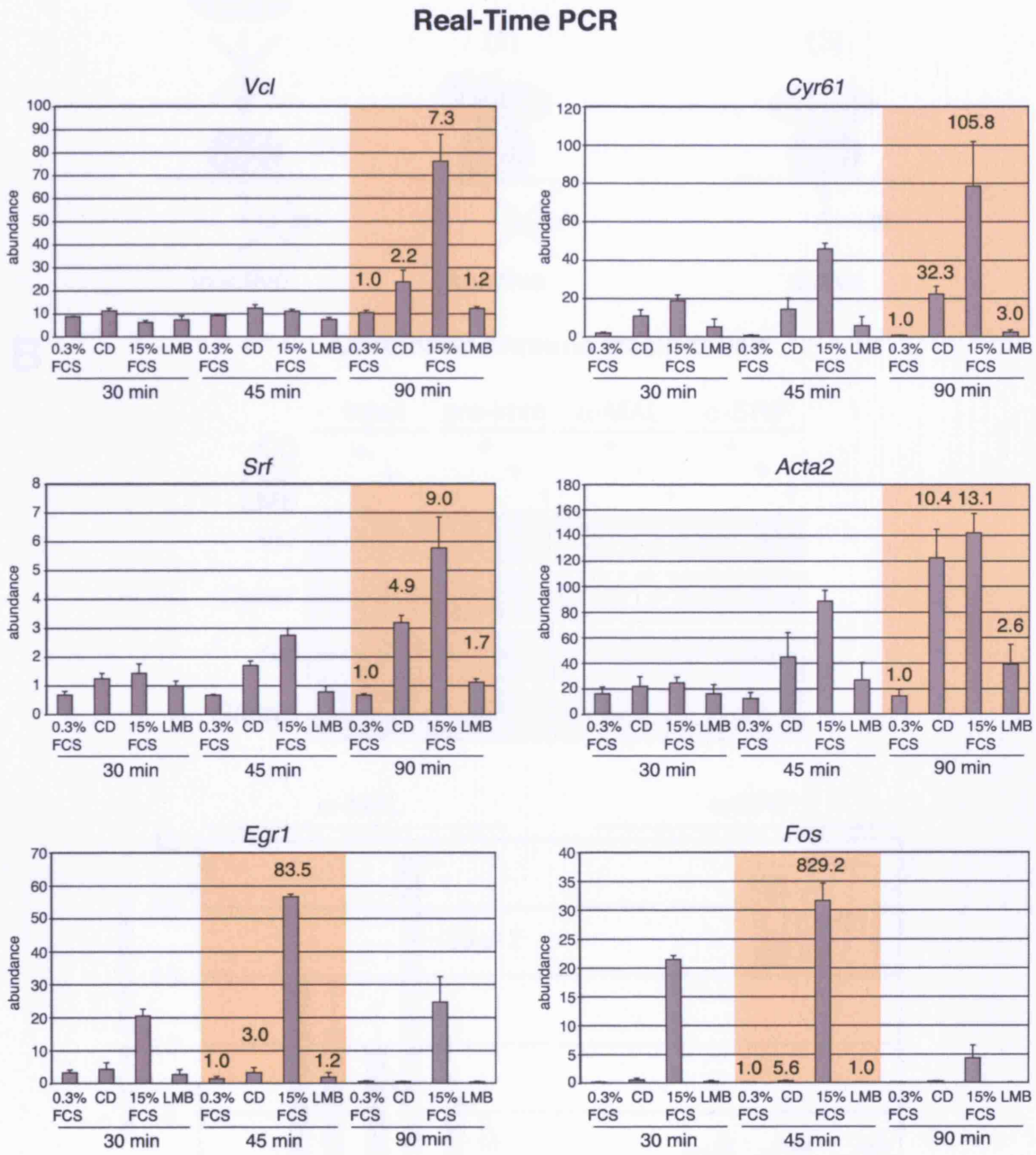

Figure 3.3 LMB does not activate MAL-dependet SRF target genes. NIH3T3 fibroblasts were serum-starved for 2 days and then stimulated with CD, FCS or LMB for 30, 45 or 90 minutes. RNA was isolated and the mRNA abundance of the indicated SRF target gene mRNAs analysed by quantitative RT-PCR using the ΔΔCt method (see Chapter 7, Materials and Methods). Relative abundances obtained after normalisation for *Gapdh* message are shown. The time points of maximal message abundane are shaded. Data represent 3 independent experiments with SEM. The mean values for fold induction calculated from the mean relative abundances are indicated above the bars at time points of maximal message abundance.

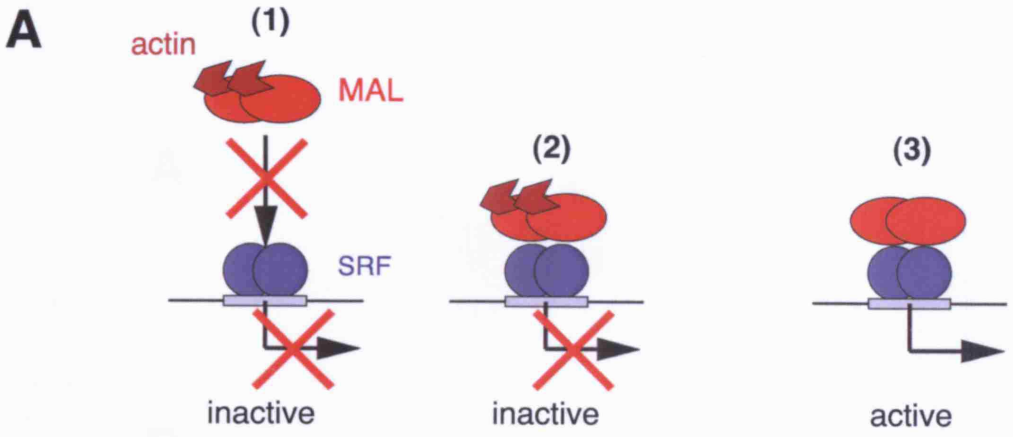

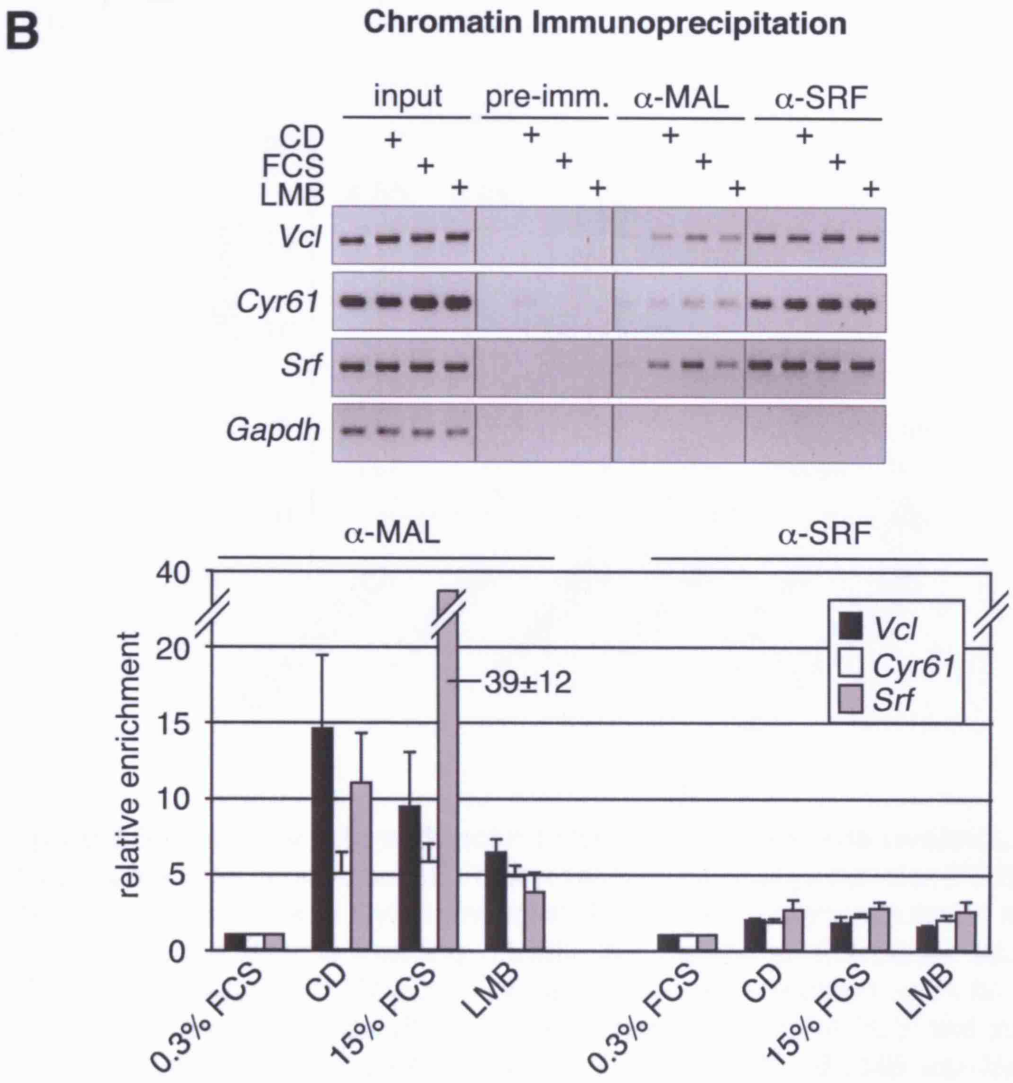

Figure 3.4 Nuclear accumulation of MAL allows its association with target genes. (**A**) Models for inhibition of MAL activity by actin: 1, inhibition of MAL-SRF-DNA ternary complex formation; 2, inhibition of transcription activation downstream of MAL-SRF-DNA ternary complex formation; 3, active MAL-SRF-DNA complex. (**B**) Chromatin immunoprecipitates of MAL or SRF from NIH3T3 fibroblasts under the indicated conditions were analysed by semiquantitative PCR (top) and quantitative real-time PCR (bottom) to detect the promoter regions of the indicated genes. Relative enrichment refers to target gene recovery from serum-starved cells. Pre-imm., pre-immune serum. Data are from three independent experiments; error bars, SEM.

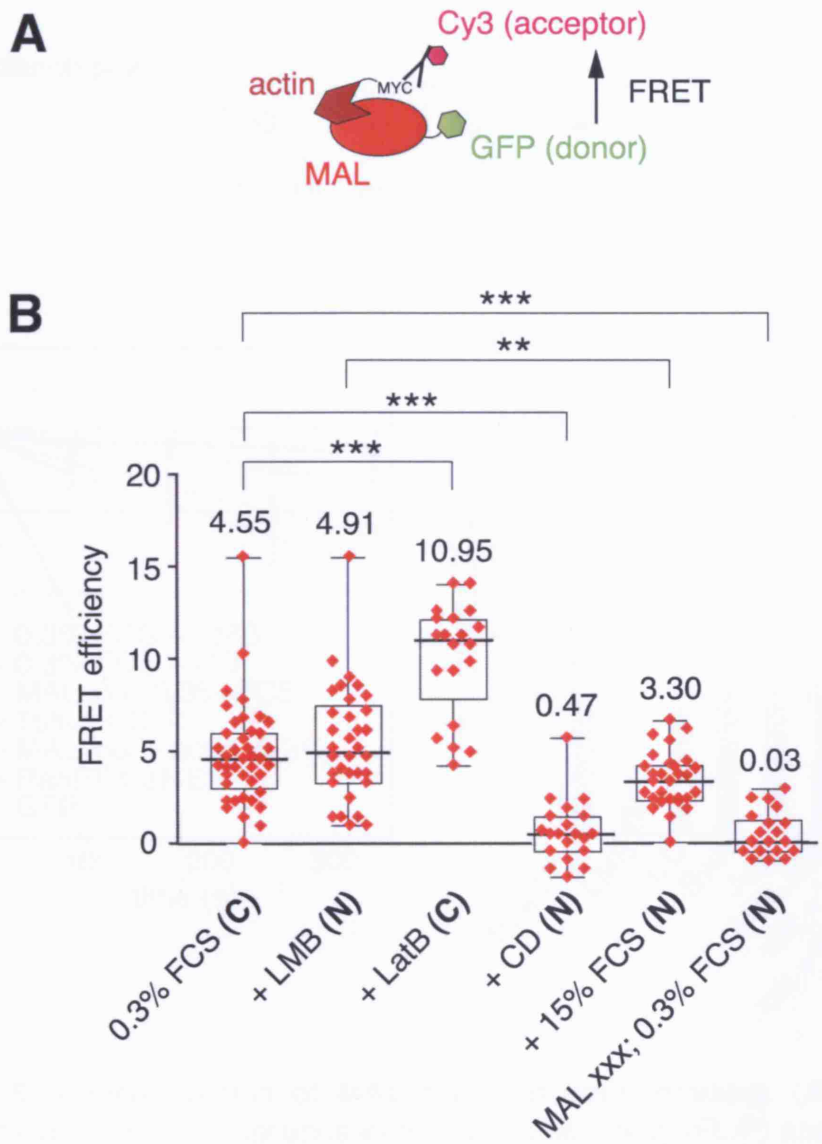

Figure 3.5 MAL interacts with actin in both cytoplasm and nucleus.
(**A**) Schematic representation of Förster resonance energy transfer (FRET) using MAL-GFP as donor and Cy3-immunolabelled, epitope-tagged actin as acceptor. In fluorescence lifetime imaging (FLIM), the lifetime of the donor fluorophore (GFP) is measured. (**B**) Detection of the MAL-actin interaction by FLIM. NIH3T3 fibroblasts were serum-starved with media containing 0.3% FCS and treated as indicated. Treatment with 2 μM CD, 0.3 μM LatB and 20 nM LMB was for 30 min. Serum stimulation with 15% FCS was for 10 min. FRET efficiencies are shown as box-and-whisker plots with median (>20 cells per condition; Mann-Whitney test, ***$p < 0.0005$; **$p < 0.005$). The localisation of MAL-GFP under the given conditions is indicated in bold (C, cytoplasmic; N, nuclear). See Vartiainen et al., 2007, supplementary online material, for donor and acceptor intensity images and lifetime maps.
The data were obtained by Maria Vartiainen.

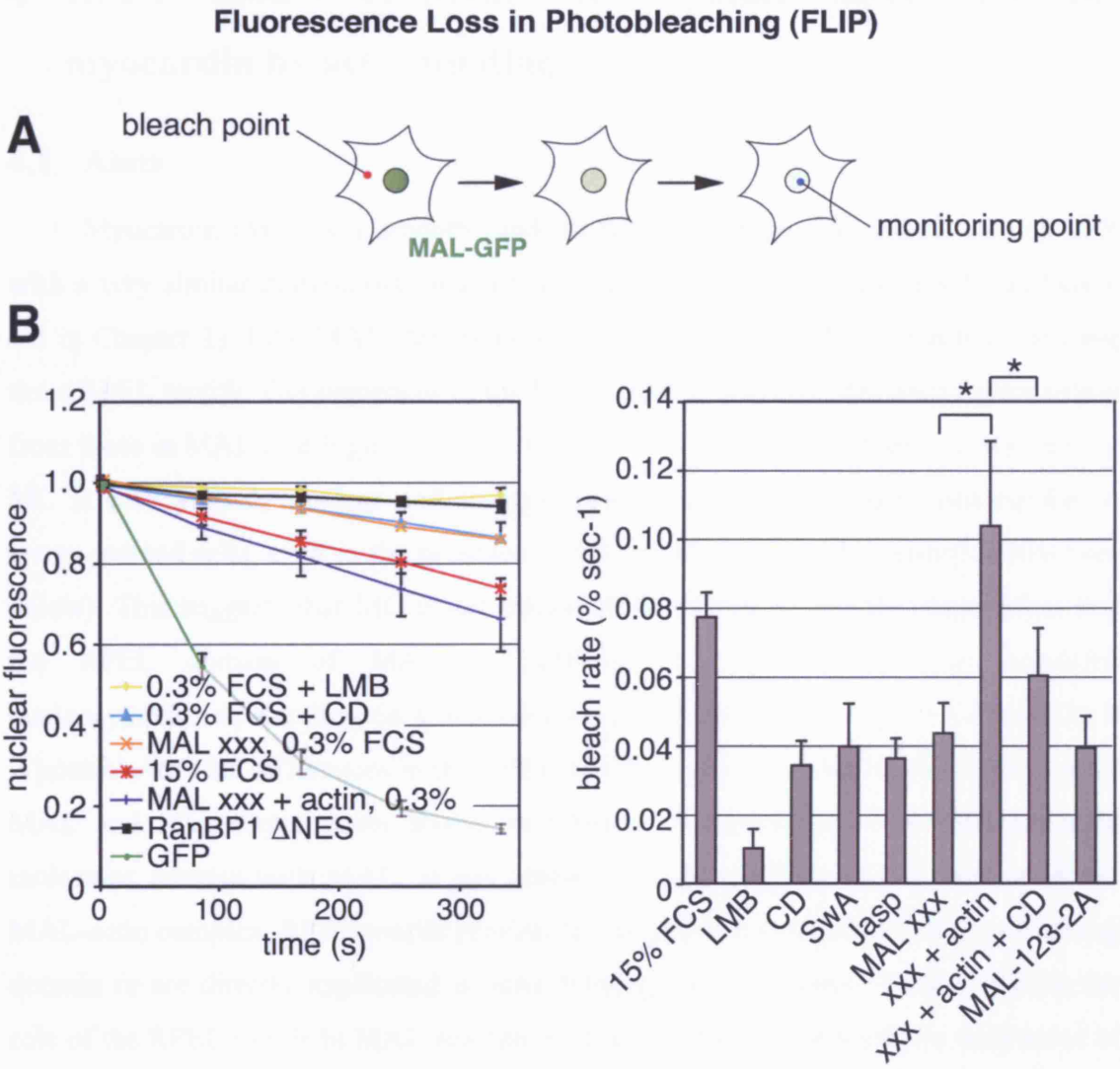

Figure 3.6 Nuclear export of MAL requires actin binding. (**A**) Schematic representation of the fluorescence loss in photobleaching (FLIP) assay. The fluorescence signal of nuclear MAL-GFP is indicated in green. The cytoplasm is bleached repeatedly (red point) while the nuclear fluorescence is measured (blue point) over time. (**B**) Left, decay kinetics of nuclear fluorescence for the indicated constructs and conditions. Right, initial bleach rates determined from the data on the left. Data of three independent experiments are from at least 10 cells per condition (error bars, SD; Student's t test, *$p < 0.05$).
The data were obtained by Maria Vartiainen.

4 RPEL motifs cooperate to regulate MAL but not myocardin by actin binding

4.1 Aims

Myocardin (MC) is a smooth- and cardiac-muscle specific coactivator of SRF with a very similar domain organisation to that of MAL (see Section 1.4.3 and Figure 1.8 in Chapter 1). Like MAL, MC possesses an N-terminal RPEL domain comprising three RPEL motifs. The sequences of the RPEL motifs, however, deviate to some extent from those in MAL (see Figure 1.8 B in Chapter 1, Figure 2.1 in Chapter 2 and below). MC is constitutively nuclear and strongly potentiates SRF-mediated transcription in serum-starved cells, even in the presence of C3 transferase, which inactivates Rho (see below). This suggests that MC is not controlled by RhoA. Given the observation that the RPEL domain of MAL is sufficient to confer Rho-actin regulated nucleocytoplasmic shuttling on a heterologous protein (see Figure 2.2 in Chapter 2), it is possible that the differences in the RPEL motifs account for differential regulation of MAL and MC. Experiments shown in Chapter 2 demonstrate that multiple actin molecules interact with MAL. It has remained open whether, in the context of the MAL-actin complex, RPEL motifs provide the structural framework of an actin-binding domain or are directly implicated in actin binding. In this chapter, I shall address the role of the RPEL motifs in MAL regulation, functionally comparing them with those of MC. I will show that the RPEL domain of MC binds actin weakly and does not link myocardin to RhoA via actin binding. Exploiting this observation, I generated MAL-MC chimaeras to gain insights into how actin binding regulates MAL activity.

4.2 The RPEL domains account for differential regulation of MAL and myocardin

MC appears nuclear in serum-starved NIH3T3 fibroblasts (Figure 4.1), in agreement with previous observations (Wang et al., 2001a). I have shown in Chapter 2 that the RPEL domain of MAL is sufficient to confer Rho-actin regulated nucleocytoplasmic shuttling on pyruvate kinase, which on its own is a strictly cytoplasmic protein (see Section 2.2 in Chapter 2). To test whether RPEL domain of MC is sufficient to confer nuclear localisation, I fused it to pyruvate kinase in a context equivalent to that of MAL(2-204) (Figure 4.1 A; compare to Figure 2.2 in Chapter 2).

Like MC, the fusion protein MC(2-150)-PK was predominantly nuclear in more than 90% of the transfected cells (Figure 4.1 B and C). Serum stimulation and latrunculin B (LatB) treatment did not affect the nuclear localisation of either MC or MC(2-150)-PK. Coexpression of non-polymerisable β-actin derivative R62D (Posern et al., 2002), however, resulted in a moderate re-localisation of both MC and MC(2-150)-PK to the cytoplasm, suggesting that the MC RPEL domain may, in principle, bind to actin (Figure 4.1 B and C).

To address to what extent the RPEL domains determine differential regulation of MAL and MC, I reciprocally exchanged them between the two proteins, generating a MAL protein with a MC N-terminus (MC-N123-MAL) and MC protein with a MAL N-terminus (MAL-N123-MC) (Figure 4.2 A). I then evaluated the subcellular localisation of the protein chimaeras by immunofluorescence microscopy and their ability to activate an SRF reporter gene in serum-starved NIH3T3 fibroblasts. For the latter, I also co-expressed C3 transferase to inactivate Rho (Hill et al., 1995), asking whether reporter activation was dependent on Rho. MC-N123-MAL, like MC, was predominantly nuclear (Figure 4.2 B). Both proteins potently activated the SRF reporter to very similar extent, and this was not dependent on functional Rho (Figure 4.2 C). Conversely, MAL-N123-MC was predominantly cytoplasmic in serum-starved cells; it moderately activated the SRF reporter in a Rho-dependent manner, as did MAL (Figure 4.2 B and C). This shows that the RPEL domains are responsible for the differential regulation of MAL and MC.

4.3 Myocardin does not shuttle between nucleus and cytoplasm

How is nuclear localisation of MC in serum-starved cells brought about? It is possible that, like MAL, MC also shuttles through the nucleus, its nuclear localisation reflecting enhanced import and/or decreased export rates compared to MAL. Using the fluorescence loss in photobleaching assay introduced in the previous chapter, we assessed the dynamic nucleocytoplasmic shuttling properties of MC and the chimaeras in comparison with MAL. In this assay, the decay of nuclear fluorescence of a test protein fused to GFP was monitored during photobleaching of the cytoplasm (see Figure 3.6 A in Chapter 3 for a schematic representation of the assay). A MC-GFP fusion protein localised to the nucleus; its bleaching rate was slower than that of MAL-GFP in serum-stimulated or cytochalasin D (CD)-treated cells, and very similar to that

of MAL-GFP in the presence of leptomycin B (LMB), which blocks Crm1-dependent nuclear export (Figure 4.3; see also Figure 3.6 B in Chapter 3). Like MC itself, MC-N123-MAL-GFP was not appreciably bleached and therefore not exported from the nucleus. MAL-N123-MC-GFP was cytoplasmic in serum-starved cells, accumulating in the nucleus upon CD treatment or serum stimulation. When nuclear, its nuclear export rate was comparable to that of MAL (Figure 4.3). In conclusion, MC is nuclear because it is not exported from the nucleus. The RPEL domain appears to be entirely responsible for the differential shuttling behaviours of MAL and MC. This does not, however, rule out the possibility that the RPEL domains cooperate with functional elements that are conserved between MAL and MC to control nucleocytoplasmic shuttling.

4.4 MAL and MC RPEL domains bind actin differentially

Actin binding is essential for coupling MAL localisation to Rho signalling. I tested whether regulation of MAL but not MC by Rho signalling is a consequence of differential actin-binding properties of their RPEL domains. In GST affinity sedimentation assays, GST-MAL(2-261) efficiently recruited endogenous β-actin from a total cell lysate (Figure 4.4 A). Actin recruitment by GST-MC(2-209) was substantially less efficient and was further weakened in the presence of the non-ionic detergent Triton X-100 at 0.5% (Figure 4.4 A). To test whether differential actin binding to MAL and MC occurs in a cellular environment, we used Förster resonance energy transfer (FRET) detected by fluorescence lifetime imaging microscopy (FLIM; see Figure 3.5 A in Chapter 3 for an explanation of the assay). In this assay, FRET between MAL-GFP and Cy3-immunolabelled MYC-β-actin could be readily detected with FRET efficiencies of 4.55 and 4.91 (see Figure 3.5 B in Chapter 3) in serum-starved or LMB-treated cells, respectively (Vartiainen et al., 2007). In contrast, we did not observe FRET for MC-GFP and actin under identical conditions: here, the FRET efficiency (0.5, Figure 4.5 B) was very similar to that observed for MAL in the presence of CD (0.47) or for the actin-binding deficient MAL derivative xxx (0.47) (see Figure 3.5 B in Chapter 3 and Vartiainen et al., 2007).

In summary the differential regulatory properties of MAL and MC are associated with differences in the actin-binding properties of their RPEL domains *in vitro* and *in vivo*.

4.5 The isolated RPEL motif is an actin-binding element

Gel filtration chromatography resolves a MAL-actin complex that contains three actin molecules (see Figure 2.7 in Chapter 2). According to a simple model, the RPEL motif might constitute an actin-binding unit, and each of the RPEL motifs might be occupied by a single actin molecule in this complex. Considering this hypothesis, I investigated the basis for the differential actin-binding characteristics of the MAL and MC RPEL domains, analysing the properties of the individual RPEL motifs.

Phylogenetic analysis shows that each of the three MAL RPEL motifs is more closely related to the corresponding motifs in the other family members, MAL16 and MC, than to the other motifs in MAL (Figure 4.5). RPEL1 and RPEL2 are most divergent between MAL and MC, while RPEL3 is relatively conserved.

I first performed GST affinity sedimentation assays using GST fusions of the individual RPEL motifs as baits. The peptides fused to GST were chosen to encompass 32 amino acids, spanning the RPEL motif as defined by PFAM (http://pfam.sanger.ac.uk/, Finn et al., 2006) with 5 amino acids on either side (see Figure 4.5 A) to minimise a potential effect of incomplete folding. In order to achieve a high sensitivity, I omitted detergent throughout all steps of the experiment. Under these conditions, GST fusions of MAL RPEL1 or RPEL2 efficiently recruited β-actin from cell lysates, while MAL RPEL3 recovered β-actin inefficiently (Figure 4.6). I also introduced point mutations into the RPEL motifs, initially exchanging the their first and most conserved arginine residues (R81, R125, R169 in RPEL motifs 1, 2 and 3, respectively) to alanine (referred to as R->A hereafter). These exchanges are identical to the ones of the actin-binding deficient and constitutively active MAL derivative xxx (see Chapter 2). In the GST affinity sedimentation assay, the MAL RPEL1 R->A substitution greatly reduced but did not abolish interaction with actin, whereas the analogous substitutions in RPEL2 and RPEL3 had a much greater effect (Figure 4.6). A more severe, charge reversal mutation in MAL RPEL1, RR81/82DD, blocked its interaction of actin in this assay. In contrast to MAL, MC RPEL1 and RPEL2 did not recover detectable amounts of β-actin in this assay. MC RPEL3, however, appeared to bind actin similarly to MAL RPEL3 (Figure 4.6).

Because GST affinity sedimentation involves washing of immobilised protein complexes to reduce non-specific background binding, the assay essentially measures

the off-rates of molecular interactions. To determine RPEL-actin binding affinities quantitatively under conditions of solution binding equilibrium, I established a fluorescence anisotropy assay (Lundblad et al., 1996). The assay exploits the fact that larger molecules or complexes, in this case RPEL-actin complexes, show a lower mobility in solution resulting from Brownian motion than smaller molecules or complexes, for the purposes of this analysis RPEL peptides (see Figure 4.7 A for a schematic representation of the assay). To measure peptide mobility, I used RPEL peptides that were N-terminally fluorescein- (FITC-)labelled. In fluorescence anisotropy assays, linearly polarised light is used to selectively excite a population of fluorophores whose absorption transition vectors are aligned parallel to the electric vector of the light waves. As a consequence, these fluorophores reach their excited, high-energy state, which has a fluorophore-specific lifetime. Fluorescence is measured when the fluorophores are in the process of re-adopting their ground energy state. Within the time window of the fluorophore lifetime, the molecular entities which the fluorophore is coupled to will have changed their orientation as a result of Brownian motion and a function of molecular size and shape. The emitted fluorescence signal is of different average polarisation than the polarisation of the light used for excitation. Polarisation (or, alternatively, anisotropy, another measure of directional homogeneity of a sample) hence is a function of molecular size (Lundblad et al., 1996). A preparation of free FITC-RPEL peptide will show a lower degree of anisotropy than a preparation of FITC-RPEL peptide in complex with actin. Increases in anisotropy occurring upon complex formation are proportional to the amount of complex and can therefore be used for affinity measurements.

Since the aim was to obtain affinity information at quasi-physiological salt concentrations, I needed to circumvent the problem of actin polymerisation by using latrunculin B (LatB). To this end, G-actin was saturated with LatB. Any unbound actin was polymerised by raising the salt concentration to 100 mM NaCl and 3 mM $MgCl_2$ and the ATP concentration to 0.7 mM. Polymerised actin or precipitates were removed by ultracentrifugation and the concentration of LatB-actin measured.

Increasing amounts of non-polymerisable LatB-actin were titrated into binding reactions containing a constant amount of FITC-RPEL peptides. The RPEL peptide sequences used were identical to those fused to GST for the above experiment. The fluorescence anisotropy at 525 nm was measured, and the equilibrium dissociation

constants derived as described in Materials and Methods (Chapter 7). MAL RPEL1 and RPEL2 bound actin with comparable affinities of 5.4 ± 0.5 μM and 2.3 ± 0.2 μM, respectively (Figure 4.7 B). MAL RPEL3 bound three to seven times weaker with a K_d of only 18.8 ± 1.0 μM. The R->A mutation decreased the affinities of MAL RPEL1 and RPEL2 for actin to 16.4 ± 2.1 μM and 15.0 ± 3.3 μM, respectively, and reduced the affinity of MAL RPEL3 below the detection limit, as did the RPEL1 charge reversal mutation. Actin bound to MC RPEL1 with a K_d of 15.4 ± 0.8 μM, three-fold lower than to MAL RPEL1, but strikingly, binding of actin to MC RPEL2 was undetectable under the assay conditions. The affinity of MC RPEL3, K_d = 16.6 ± 0.2 μM, was very similar to that of MAL RPEL3 (Figure 4.7 B). Taken together, these data demonstrate that the RPEL motif constitutes a G-actin-binding element with a wide range of affinities for actin. Each MAL RPEL motif binds actin. The binding analysis for MC RPEL peptides suggests that the different properties of the MAL and MC RPEL domains may reflect differences in the affinities of their RPEL motifs for actin.

4.6 The three RPEL motifs functionally cooperate in MAL regulation

I next used the insights gained from the actin binding analysis to address the functional significance of RPEL motifs for MAL regulation. To this end, I introduced the R->A mutation into each of the RPEL motifs, generating single (x23; 1x3; 12x), double (1xx; x2x; xx3), and triple (xxx) MAL RPEL domain mutants (Figure 4.8 A). The proteins were expressed in NIH3T3 cells and analysed for their subcellular localisation and potential to activate an SRF reporter in serum-starved cells (Figure 4.8 B and C).

Under serum-starved conditions, wild-type MAL was found detectably nuclear (N+N/C) in less than 10% of the cells. The R->A mutations within RPEL1, RPEL2 and RPEL3 increased this value to 25%, 40%, and 70% of the cells, respectively. Compared to single RPEL mutants, all double RPEL mutants displayed a much stronger tendency to accumulate in the nucleus, and MAL 1xx and xxx were virtually indistinguishable, with 90% of cells displaying predominantly nuclear localisation (Figure 4.8 B). Following serum stimulation, all proteins were predominantly nuclear in >80% of the cells (data not shown). The ability of these mutants to activate the SRF reporter correlated well with the proportion of cells displaying appreciable nuclear accumulation (Figure 4.8 C). I used co-expression of C3 transferase to assess Rho-dependence of the MAL mutants in the activation of the SRF reporter gene. Single R->A mutations

reduced reporter dependence on Rho, with mutation of RPEL3 showing the greatest effect, and double substitutions further decreased Rho-dependence. Therefore, the integrity of all three RPEL motifs is required for MAL regulation.

The alanine-substituted MAL RPEL1 and RPEL2 peptides both retain an affinity for actin similar to that of MAL RPEL3. The weaker effect of RPEL1 or RPEL2 mutation on MAL regulation compared to RPEL3 mutation might reflect this. To analyse the role of actin binding to RPEL1 more thoroughly, I introduced the RPEL1 charge reversal mutation, which effectively abolishes actin binding *in vitro*, into MAL (MAL-1^{DD}; see Figure 4.9 A). MAL-1^{DD} was more severely deregulated than MAL x23: it was cytoplasmic in only 30% of the cells, pan-cellular in about 60%, and nuclear in approximately 10% and activated the SRF reporter more strongly (Figure 4.9 B and C). I used a similar approach with MAL RPEL2, in this case precisely exchanging it for MC RPEL2, which does not bind actin detectably *in vitro* (MAL-2^{MC}; see Figure 4.9 A). This mutant also exhibited deregulation, with nuclear localisation in 20% of the cells, and most of the remainder displaying pan-cellular localisation (Figure 4.9 B). Expression of MAL-2^{MC} strongly activated the SRF reporter and greatly reduced the dependence of the reporter activity on functional Rho (Figure 4.9 C).

These results demonstrate that the three MAL RPEL motifs functionally cooperate, with even the weakest actin-binding motif, RPEL3, playing an important role in MAL regulation. Mutations in any single MAL RPEL motif are sufficient to cause deregulation of its subcellular localisation and reporter activation, provided such mutations are sufficient to effectively abolish RPEL-actin interaction *in vitro*. Taken together, the results suggest that MAL regulation involves assembly of higher order actin-MAL complexes.

4.7 The RPEL1-RPEL2 unit specifies differential regulation of MAL and MC

The different actin-binding affinities of MAL and MC RPEL1 and RPEL2 suggest that the reason for differential regulation of MAL and MC might reside in the region comprising these two RPEL motifs. Indeed, the observation above that substitution of MAL RPEL2 by that of MC results in substantial deregulation of MAL subcellular localisation and activity is consistent with this idea. To address the role of

the RPEL motifs in MC localisation more systematically, I generated a series of MAL-MC chimaeras, in which increasing extents of N terminal sequences were reciprocally exchanged, with cross-over points in the centre of the RPEL-RPEL linker sequence (see Figure 4.10 A for nomenclature). The chimaeras were analysed for their subcellular localisation and their ability to activate an SRF reporter in serum-starved cells (Figure 4.10 B and C), and their nuclear export rates were analysed using the FLIP assay (Figure 4.11; see also Figure 4.3).

I first used the chimaeras to map which RPEL domain sequences are necessary to specify the nuclear localisation of MC (Figure 4.10 A, left). Replacement of the MAL N-extension (those sequences N-terminal to RPEL1) by that of MC had a slight effect on MAL regulation, with an increased number of cells showing pan-cellular localisation. However, replacement of the MAL N-extension and RPEL1 by the corresponding MC sequences resulted in its profound de-regulation: MC-N1-MAL was nuclear in about 70% and pan-cellular in almost all of the remaining cells, and it strongly activated the SRF reporter independently of functional Rho (Figure 4.10 B and C). In the FLIP assay, MC-N1-MAL exhibited a slightly increased bleach rate compared to MC and MC-N123-MAL, indicating that it was weakly susceptible to export (Figure 4.11). Further substitution of the MAL RPEL domain with MC sequences increased the proportion of cells with predominantly nuclear protein, and allowed strong activation of the SRF reporter in a Rho-independent manner. Taken together with the properties of the MAL-2^{MC} mutant presented in Figure 4.9, these results suggest that MC RPEL1 and RPEL2 sequences play an important role in determining its nuclear localisation.

To determine which parts of the RPEL domain specify MAL-like regulation, I replaced MC RPEL domain sequences with the corresponding sequences from MAL (Figure 4.10 A, right). Replacement of the MC N-extension with that of MAL had little effect on MC subcellular localisation or its ability to activate the SRF reporter (Figure 4.10 B and C). Substitution of the MC N-extension and RPEL1 sequences with those of MAL had a greater impact: most cells expressed MAL-N1-MC throughout nucleus and cytoplasm, and, as with MAL, SRF reporter activation was now substantially Rho-dependent. Replacement of the MC N-extension, RPEL1 and RPEL2 by the equivalent sequences from MAL conferred authentic MAL-like regulation on MC, both at the level of steady-state subcellular localisation and SRF reporter activation. MAL-N12-MC

accumulated in the nucleus upon LMB treatment, indicating that it shuttles continuously through the nucleus, and analysis of its nuclear export rates by FLIP indicated that it behaves very similarly to intact MAL or MAL-N123-MC upon serum or CD stimulation (Figure 4.11).

I finally tested whether substitution of MC RPEL2 by that of MAL is sufficient to confer MAL-like regulation on MC (Figure 4.12 A). The resulting mutant, MC-2^{MAL}, behaved effectively identically to MC itself, both at the level of subcellular localisation and SRF reporter activation (Figure 4.12 B and C). These results show that the regulatory properties of MAL require the integrity of its RPEL1-RPEL2 unit, consistent with the analysis presented in Figure 4.10.

Taken together, the behaviour of MAL-MC chimaeras demonstrates that the different regulatory behaviours of MAL and MC are both specified by the identity of their RPEL1-RPEL2 unit.

4.8 The functional significance of RPEL3 depends on its context

The results presented above show that the different regulatory behaviours of MAL and MC are specified by the identity of their RPEL1-RPEL2 unit. The data also suggest that although both MAL RPEL3 and MC RPEL3 bind actin with a similar low affinity, actin binding by RPEL3 is functionally relevant only in the context of MAL. To test this idea, I examined the functional significance of RPEL3 R->A mutations, which abolish actin binding *in vitro*. The R->A mutation of MAL RPEL3 induced strong deregulation of MAL both at the level of localisation and reporter activation, as described above, while the analogous mutation of MC RPEL3, affected neither MC nuclear localisation nor its ability to activate the SRF reporter (Figure 4.13). In contrast, the MC RPEL3 mutation caused pronounced deregulation in the context of MAL-N12-MC: while the intact protein behaved very similarly to MAL, its RPEL3 R->A derivative was nuclear in almost 40% of the cells, pan-cellular in 50-60%, and cytoplasmic in only 10%, and strongly activated the SRF reporter. These results show that RPEL3 is functionally interchangeable between MAL and MC, and suggest that its ability to confer regulation depends on the identity of the RPEL1-RPEL2 unit N-terminal to it. Mutation of both RPEL motifs 1 and 2 (MAL xx3; see Figure 4.8) results in a comparable degree of

deregulation, which suggests that it is the ability of the RPEL1-RPEL2 unit to bind actin determines whether actin binding to RPEL3 is significant for MAL regulation.

4.9 RPEL3 is dispensable for formation of the 1:3 MAL-actin complex observed in gel filtration

It is tempting to speculate that the presence of three RPEL motifs in MAL directly relates to the 1:3 stoichiometry observed for the MAL-actin complex in gel filtration chromatography (see Chapter 2). To analyse the contribution of the RPEL motifs to overall MAL-actin complex stoichiometry, I produced recombinant MAL RPEL-domain constructs containing the R->A mutation in all possible combinations in the context of MAL(2-261). To assess molecular masses of the complexes of these proteins with actin, I performed gel filtration chromatography analogous to the experiment presented in Figure 2.7 in Chapter 2 (Figure 4.14).

I evaluated apparent MAL-actin complex stoichiometries based on the apparent molecular masses obtained from the elution volumes of the RPEL domains alone and in complex with actin. Performing this comparison separately for each mutant RPEL domain minimised the possibility of interpreting any potential change in conformation or secondary structure content resulting from the R->A mutation as a function of stoichiometry.

In agreement with previous observations (see Chapter 2), wild-type MAL(2-261) formed a complex of an apparent molecular mass consistent with the presence of three actin molecules, while mutation of all three RPEL motifs effectively abolished actin binding (Figure 4.14 A). If viewed with an expectation of a simple beads-on-a-string model of actin binding to RPEL motifs as autonomous actin-binding units, the mutation of one or two RPEL motifs had surprising effects on MAL-actin stoichiometry. While the single RPEL mutants x23 and 12x still bound three actin molecules, MAL(2-261) 1x3 apparently bound only two. Moreover, double RPEL mutant derivatives of the RPEL domain showed a range of binding properties: no actin complex was resolved for MAL(2-261) xx3; the x2x mutant bound three actin molecules, and the 1xx derivative eluted in complex with two actin molecules. The increased ratio of MAL:actin intensities reflected different stoichiometries of the 1x3 and 1xx derivatives of MAL(2-261) and actin (Figure 4.14 B).

These observations require some critical discussion at this point. The comparison of actin binding in gel filtration chromatography with that in GST affinity sedimentation assays (see Figure 2.7 in Chapter 2) shows that gel filtration is very stringent. Gel filtration only resolves MAL-actin complexes of considerable avidity, which can resist the change of binding equilibrium imposed by polymerisation of excess actin and its removal during the complex preparation and the subsequent chromatography procedure. Given that MAL RPEL3 is the RPEL motif with the weakest affinity for actin (K_d = 18.8 ± 1.0 μM, see Section 4.5) and that no actin binding is observed for MAL(2-261) xx3 in gel filtration, I suggest that the stringency of the gel filtration assay is too high to detect actin binding to MAL RPEL3. It is possible that cooperative effects account for actin being bound to RPEL3 in the context of MAL(2-261). However, the apparent 1:3 stoichiometry of the 12x derivative and actin make this rather unlikely. I cannot rule out that cooperative actin binding may partially "rescue" the actin binding defects caused the R->A mutations. This would mean that the impact of these mutations might not be detectable by gel filtration. For this reason, these observations should be interpreted with care.

Alternatively, we reasoned that it is possible that the RPEL1-RPEL2 unit is sufficient to form a 1:3 complex. In this complex, RPEL2 might represent a *bona-fide* actin-binding element as the 1x3 mutant only binds two actin molecules. It is likely that RPEL1 can somehow recruit two actin molecules to MAL. Consistent with that, the 1xx derivative still binds two actin molecules. Given that actin can interact with itself in a multitude of ways, we speculated that RPEL1 recruits a second actin molecule through actin-actin interactions. This cooperativity between the two actin molecules might occur reciprocally and might also involve an actin molecule bound to RPEL2, which may explain why the x23 derivative still binds three actin molecules. It is noteworthy that, as a consequence of this model, MAL would almost certainly be able to engage in actin complexes of a theoretical stoichiometry of at least 1:4 (see Chapter 6; Discussion). Indeed, this reasoning is strongly supported by structural studies that are presented in the next chapter.

4.10 Summary

In this chapter, I have outlined the actin-binding and regulatory properties of MAL and MC. Differences between the N-terminal RPEL domains define the distinct regulatory behaviours of MAL, which exhibits Rho-dependent nucleocytoplasmic

shuttling, and MC, which is confined to the nucleus. The MAL RPEL domain exhibits greater affinity for actin than that of MC, both *in vivo* and *in vitro*. Loss of actin binding accounts for Rho-independent activity of MC. Individual RPEL motifs represent actin-binding elements with varying affinities. While MAL RPEL1 and 2 bind actin relatively strongly, MAL RPEL3 binds actin weakly. MC RPEL1 binds actin weakly whereas no actin binding was detected for MC RPEL2 under the settings used. MC RPEL3 displays an affinity for actin that is comparable with that of MAL RPEL3. Chimaera and point-mutant studies show that all three RPEL motifs functionally cooperate to regulate nucleocytoplasmic transport and activity of MAL. Mutation of RPEL3 had a particularly strong deregulatory effect on MAL. The identity of the RPEL1-RPEL2 unit defines the regulatory properties of MAL and MC, while RPEL3 is exchangeable between MAL and MC and functions in a context-dependent manner. These observations can be rationalised by the determined RPEL-actin affinities. Gel filtration chromatography suggests that RPEL motifs and possibly another actin-binding site within the RPEL domain but outside the RPEL motifs cooperate in actin binding. We speculate that positive cooperativity in MAL-actin binding represents the molecular basis for the functional cooperation of RPEL motifs in MAL regulation.

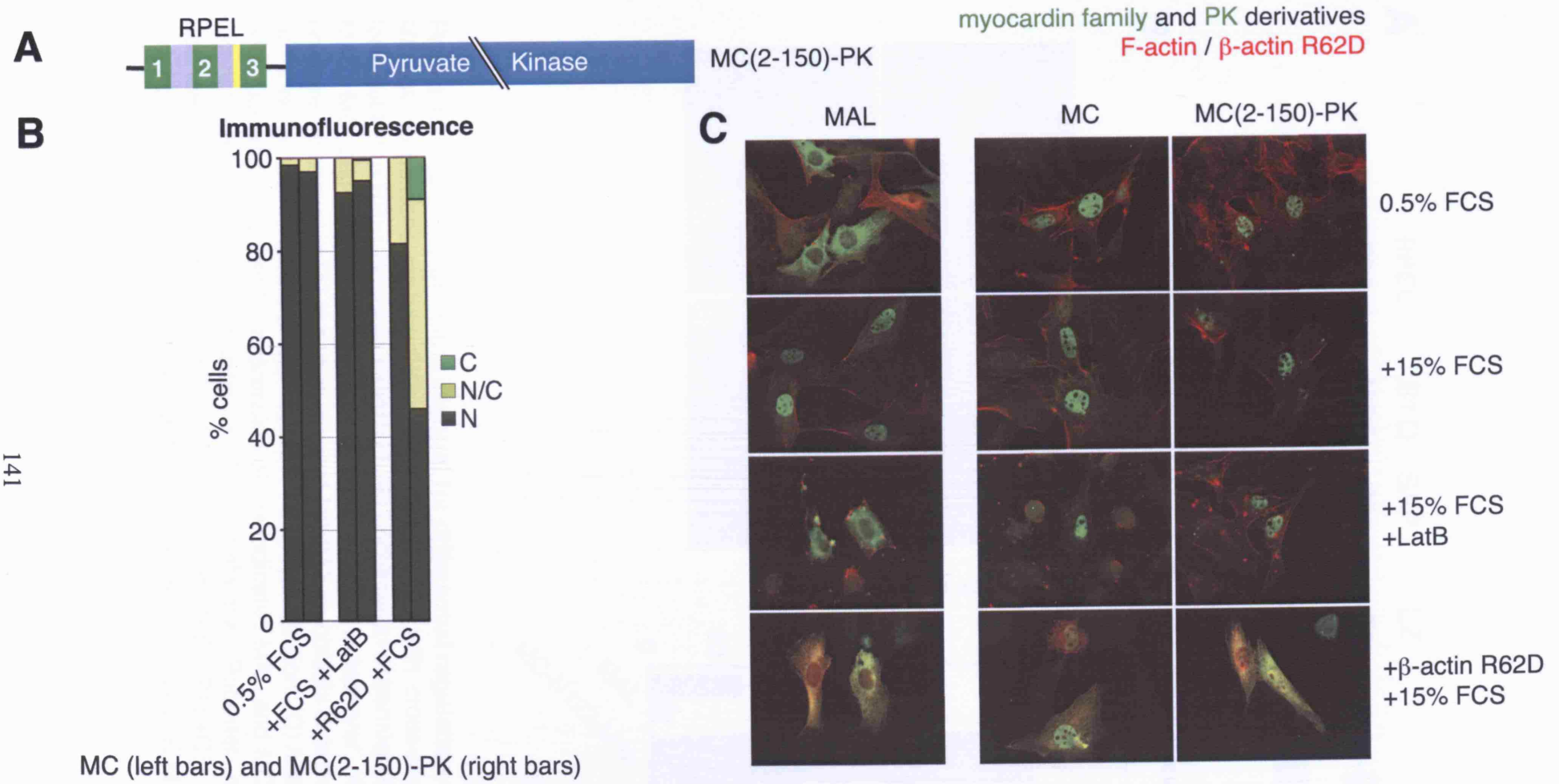

Figure 4.1 The myocardin RPEL domain is sufficient to confer nuclear localisation. (**A**) Schematic representation of MC(2-150)-PK. (**B**) Immunofluorescence microscopy of MC and MC(2-150)-PK: localisation was scored in 150-200 cells (N, nuclear; N/C, pan-cellular; C, cytoplasmic. (**C**) Representative micrographs of the data in (B) with localisation of MAL shown for comparison. See Figure 2.2 for the equivalent experiment with MAL and further details.

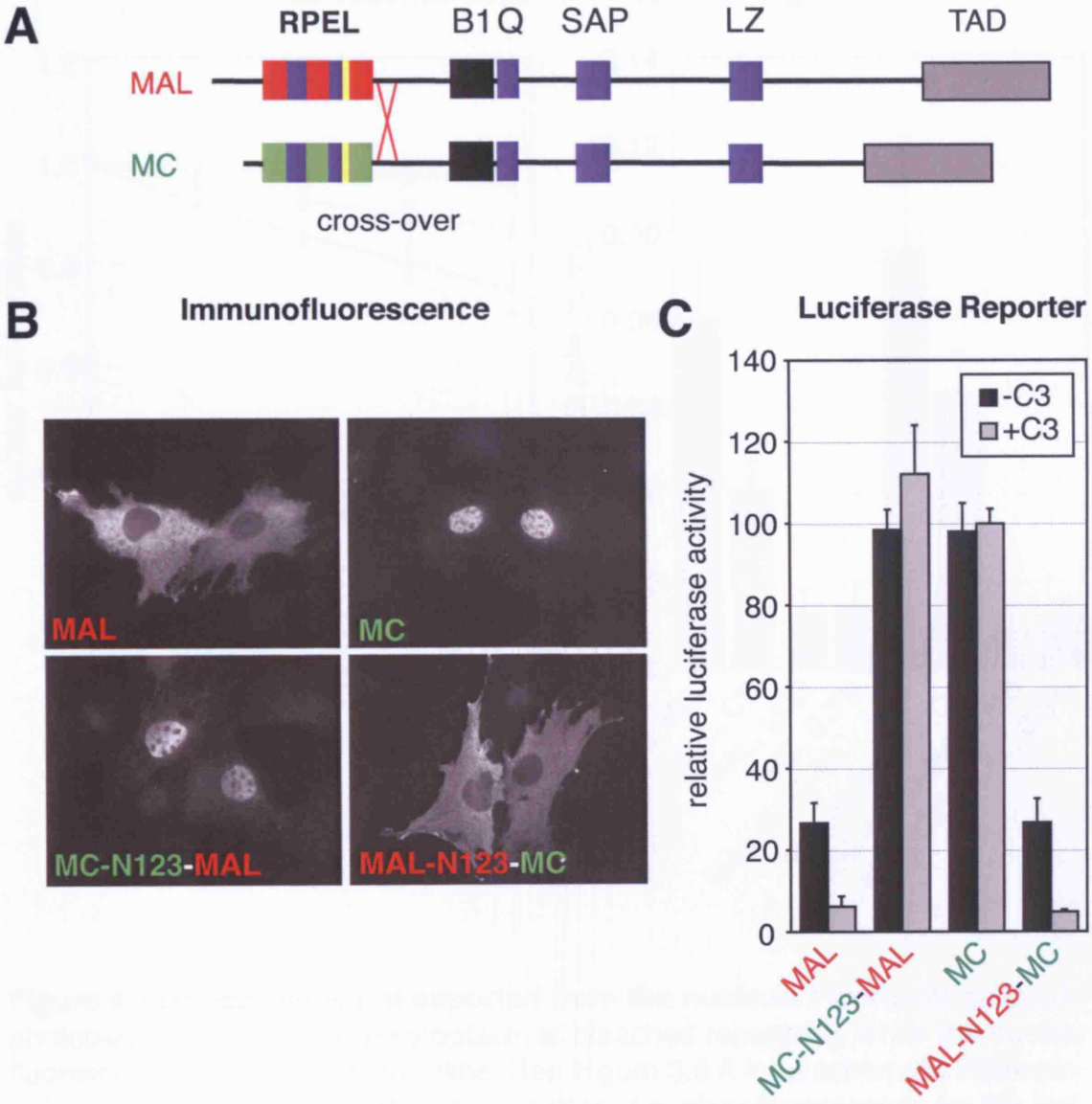

Figure 4.2 The RPEL domains account for differential regulation of MAL and MC. (**A**) Schematic representation of MAL and MC with cross-over point C-terminal to the RPEL domains indicated. (**B**) Localisation of transiently expressed MAL, MC and chimaeras generated by reciprocal cross-over of the RPEL domains as shown in (A) in serum-starved NIH3T3 fibroblasts detected by immunofluorescence microscopy. See Figure 4.10 for quantitation. (**C**) Activation of an SRF luciferase reporter by expression of the indicated MAL and MC derivatives without and with co-expression of C3 transferase. Reporter activation is normalised to that conferred by SRF-VP16 or SRF-VP16+C3 transferase, respectively (100%). n=3 independent experiments; error bars, SEM.

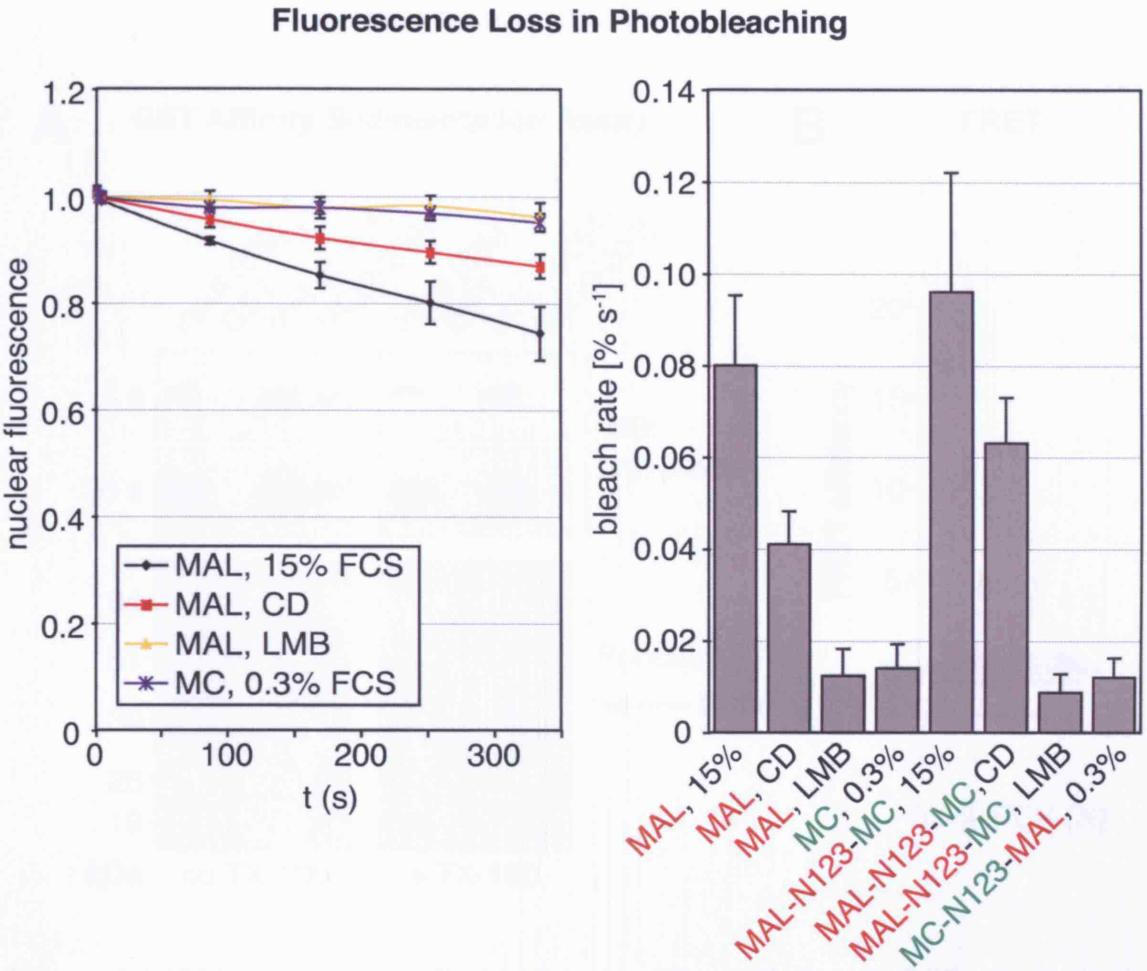

Figure 4.3 Myocardin is not exported from the nucleus. Fluorescence loss in photobleaching (FLIP). The cytoplasm is bleached repeatedly while the nuclear fluorescence is measured over time. See Figure 3.6 A for a schematic representation of the FLIP assay. Left, decay kinetics of nuclear fluorescence for the indicated constructs and conditions. Right, initial bleach rates determined from decay kinetics of nuclear fluorescence. Data of three independent experiments are from at least 10 cells per condition (error bars, SD).
The data were obtained by Maria Vartiainen.

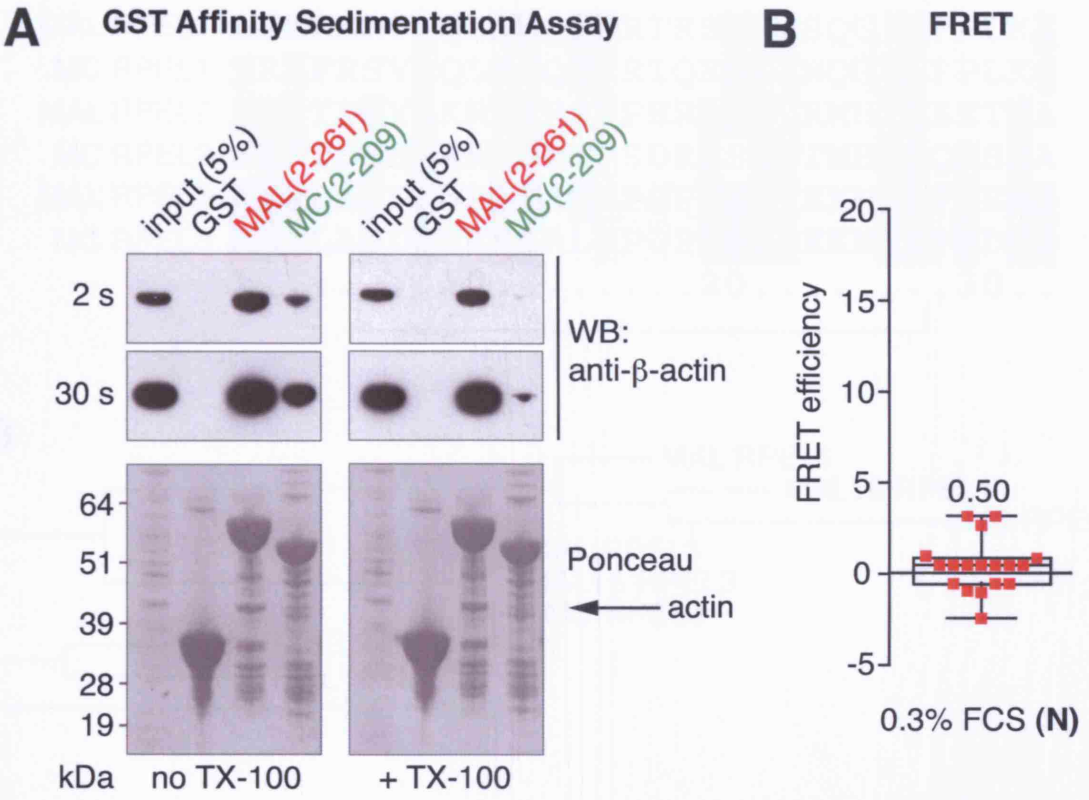

Figure 4.4 MAL and myocardin bind actin differentially. (**A**) GST affinity sedimentation assay. The indicated GST fusion proteins were used to immobilise endogenous actin from a total NIH3T3 cell lysate in the absence or presence of 0.5% TX-100. WB, Western blot with detection of β actin (2 exposures shown); Ponceau stain of membrane to show GST fusion proteins. (**B**) Förster resonance energy transfer (FRET) analysis of the interaction between MC-GFP (donor) and Cy3-immunolabelled MYC-β-actin (acceptor). See Figure 3.5 A for a schematic representation of the FRET assay. FRET efficiencies in serum-starved cells are shown as box-and-whisker plot with median (18 cells). "N" indicates nuclear localisation of MC-GFP. See Figure 3.5 B for FRET between MAL and actin, which can be directly compared to the data shown here as these experiments were done in parallel.
The data in (B) were obtained by Maria Vartiainen.

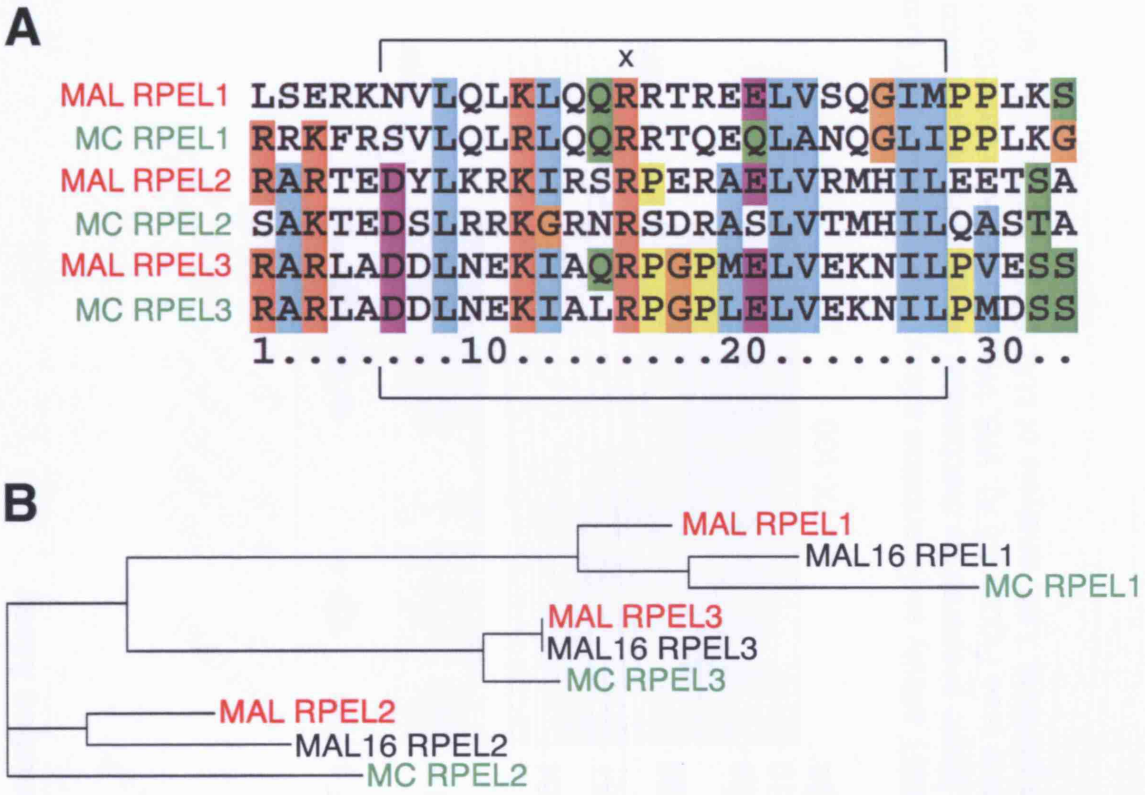

Figure 4.5 Sequence relationship between the RPEL motifs of mouse MC and MRTFs. (**A**) Multiple sequence alignment of RPEL motifs of mouse MAL and MC, generated by ClustalX (1.81) (Thompson et al., 1997). The brackets indicate the RPEL motif as defined by PFAM at the beginning of this study (Finn et al., 2006). "x" denotes the first and most conserved R residue of the RPEL motif targeted by the R->A mutation. (**B**) Corresponding phylogramme also containing MAL16, generated by ClustalW (Chenna et al., 2003). The phylogramme is based on the RPEL motifs as defined by PFAM and shown in (A). Distances to the closest nodes are: MAL RPEL1, 0.06250; MAL16 RPEL1, 0.07468; MC RPEL1, 0.19805; MAL RPEL2, 0.08807; MAL16 RPEL2, 0.13920; MC RPEL2, 0.24148; MAL RPEL3, 0.0; MAL16 RPEL3, 0.0; MC RPEL3, 0.05114.

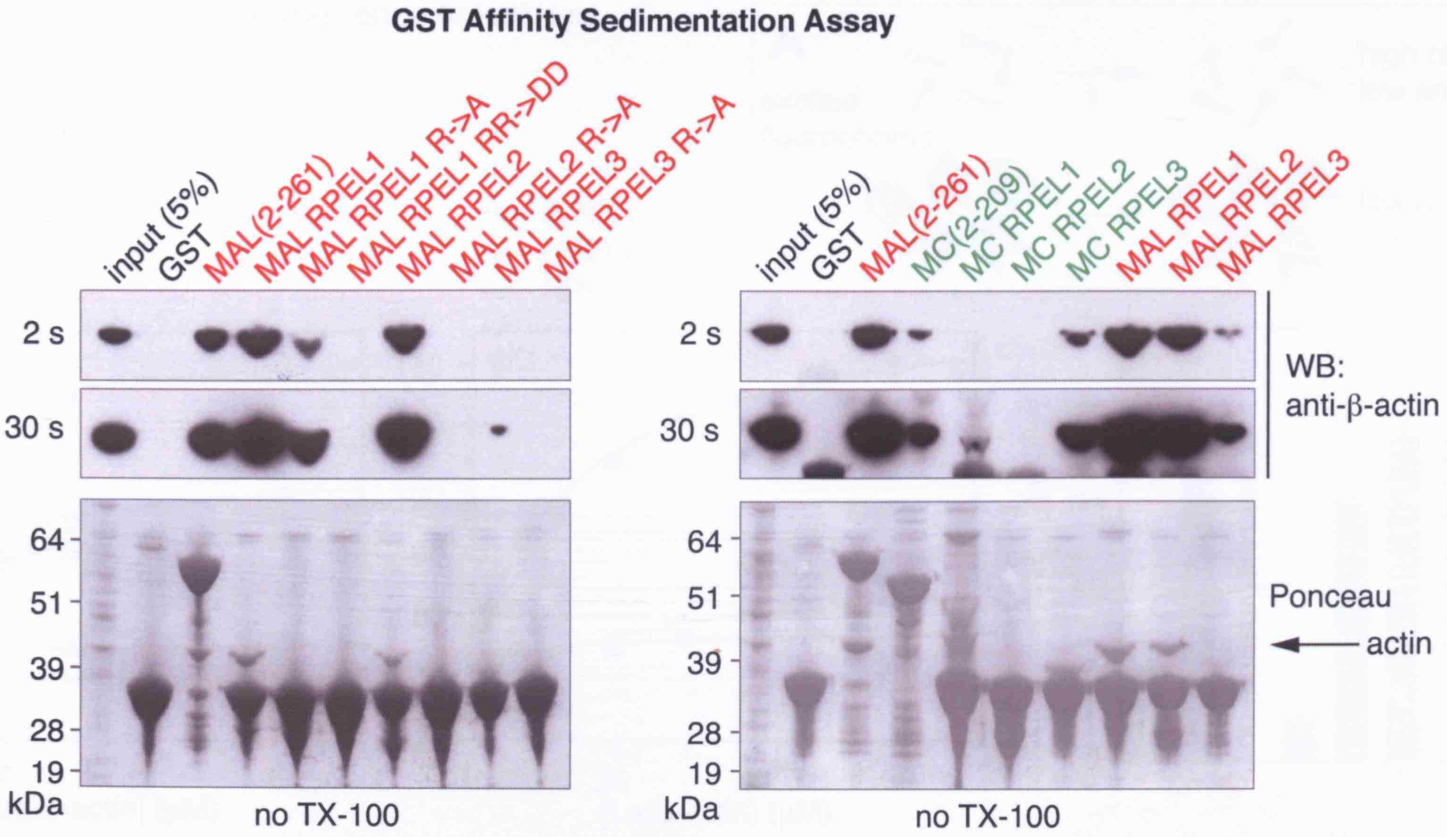

Figure 4.6 The isolated RPEL motif is an actin-binding element. GST affinity sedimentation assay. The indicated GST fusion proteins were used to immobilise endogenous actin from a total NIH3T3 cell lysate prepared by mechanical shearing in the absence of TX-100. RPEL motifs were as defined by PFAM plus 5 amino acids on either side (see Figure 4.5 A). WB, Western blot with detection of β actin (2 exposures shown); Ponceau stain of membrane to show GST fusion proteins. Left, analysis of MAL RPEL motifs; right, analysis of MC RPEL motifs with MAL derivatives for direct comparison.

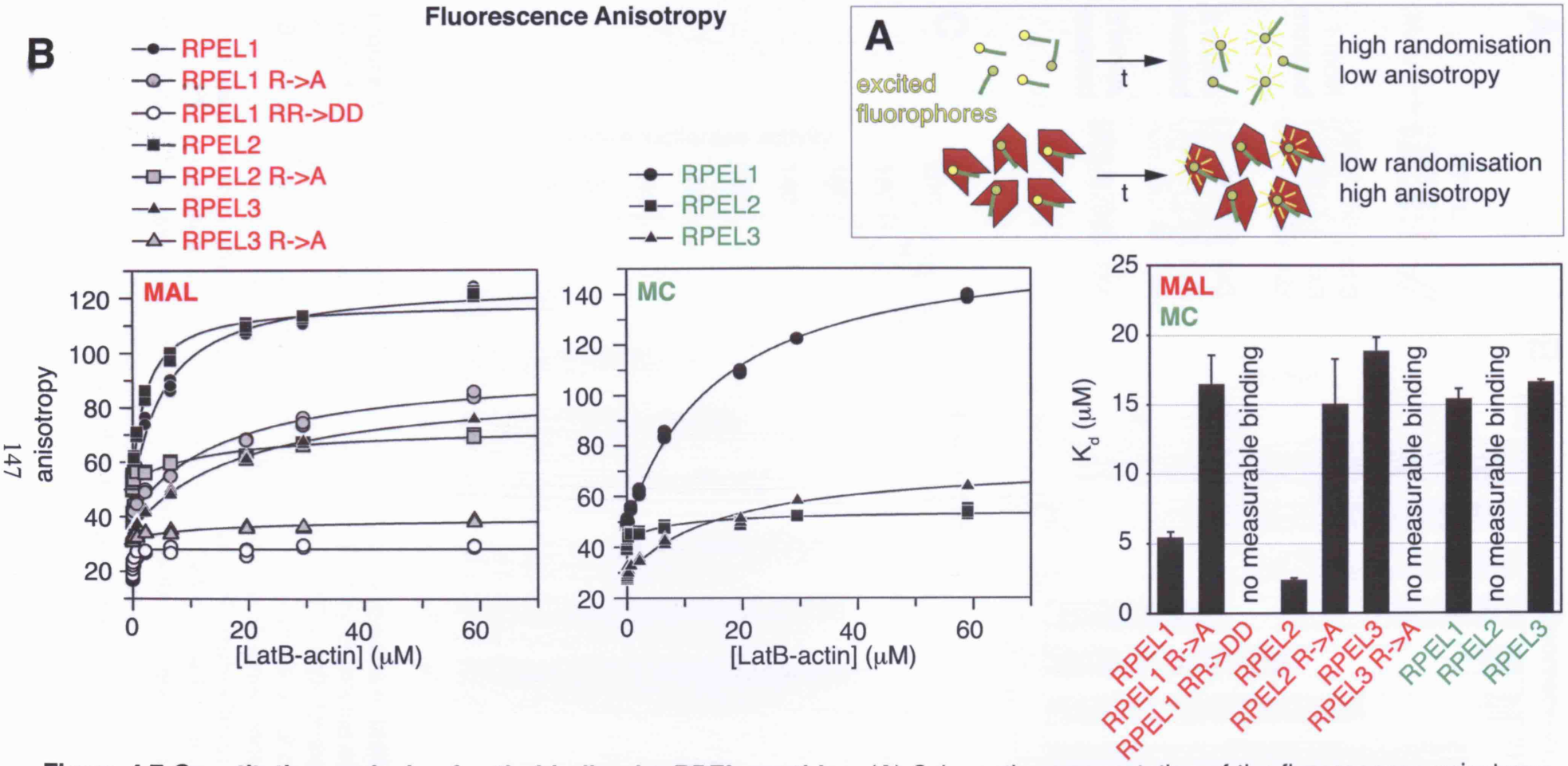

Figure 4.7 Quantitative analysis of actin binding by RPEL peptides. (**A**) Schematic representation of the fluorescence anisotropy assay. Actin is shown in red and RPEL peptides in green with excited fluorophores indicated in yellow (left) and by rays (right). See text for further explanation. (**B**) Anisotropy of indicated FITC-conjugated RPEL peptides at 0.5 μM measured over a range of latrunculin B-(LatB-)-actin concentrations (skeletal-muslce α isoform). Right, plot of equilibrium dissociation constants (K_d) of RPEL-actin interactions as determined by non-linear regression (n=3 parallel experiments; error bars, SD).

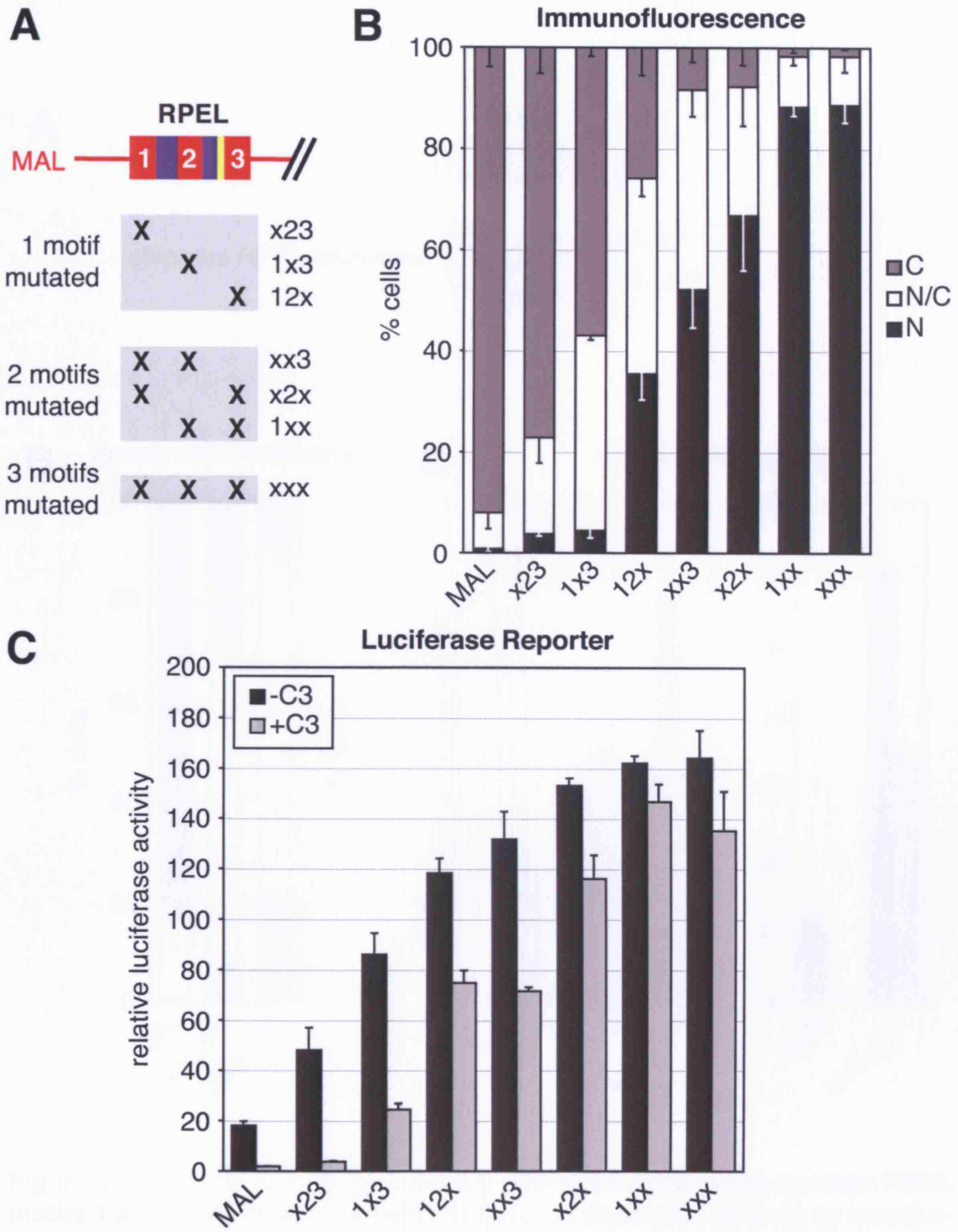

Figure 4.8 The three RPEL motifs functionally cooperate in MAL regulation. (**A**) Schematic representation of generated mutants by exchange of the first and most conserved arginine residue in the indicated RPEL motifs for alanine (R->A). (**B**) Localisation of transiently expressed MAL derivatives as shown in (A) in serum-starved NIH3T3 fibroblasts detected by immunofluorescence microscopy. Localisation was scored in 200 cells (N, nuclear; N/C, pan-cellular; C, cytoplasmic; n=3 independent experiments; error bars, SEM). See Figure 8.5 for representative micrographs. (**C**) Activation of an SRF luciferase reporter by expression of the indicated MAL derivatives without and with co-expression of C3 transferase. Reporter activation is normalised to that conferred by SRF-VP16 or SRF-VP16+C3 transferase, respectively (100%). n=3 independent experiments; error bars, SEM.

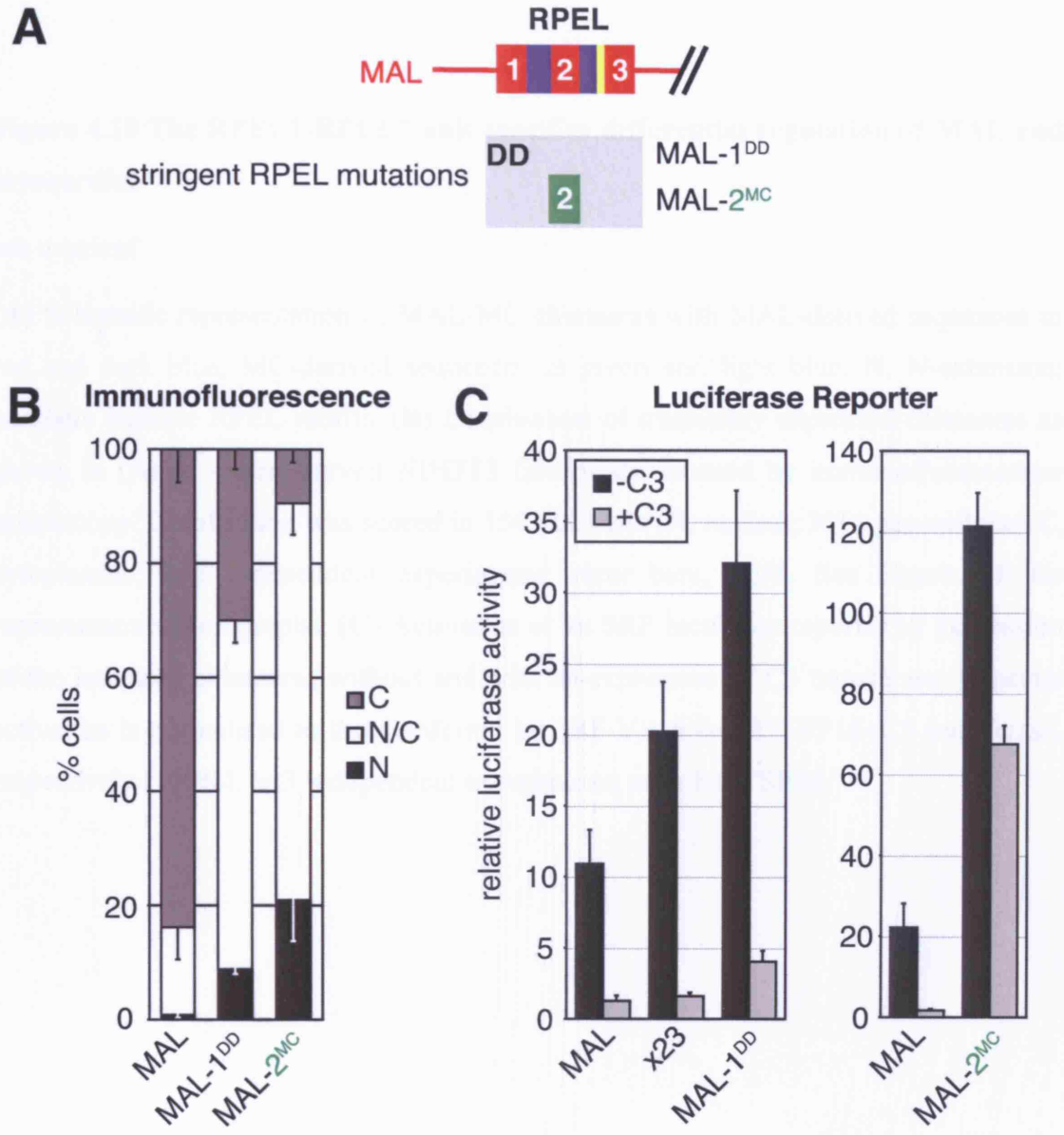

Figure 4.9 Analysis of MAL derivatives with more stringently mutated RPEL motifs 1 and 2. (**A**) Schematic representation of generated mutants by introduction of the RR81/82DD mutation into RPEL1 or exchange of MAL RPEL2 by that of MC. (**B**) Localisation of transiently expressed MAL derivatives as shown in (A) in serum-starved NIH3T3 fibroblasts detected by immunofluorescence microscopy. Localisation was scored in 150-200 cells (N, nuclear; N/C, pan-cellular; C, cytoplasmic; n=3 independent experiments; error bars, SEM. See Figure 8.5 for representative micrographs. (**C**) Activation of an SRF luciferase reporter by expression of the indicated MAL derivatives without and with co-expression of C3 transferase. Reporter activation is normalised to that conferred by SRF-VP16 or SRF-VP16+C3 transferase, respectively (100%). n=3 independent experiments; error bars, SEM.

Figure 4.10 The RPEL1-RPEL2 unit specifies differential regulation of MAL and myocardin.

see overleaf

(**A**) Schematic representation of MAL-MC chimaeras with MAL-derived sequences in red and dark blue, MC-derived sequences in green and light blue. N, N-extension; numbers indicate RPEL motifs. (**B**) Localisation of transiently expressed chimaeras as shown in (A) in serum-starved NIH3T3 fibroblasts detected by immunofluorescence microscopy. Localisation was scored in 150-200 cells (N, nuclear; N/C, pan-cellular; C, cytoplasmic; n=3 independent experiments; error bars, SEM. See Figure 8.6 for representative micrographs. (**C**) Activation of an SRF luciferase reporter by expression of the indicated chimaeras without and with co-expression of C3 transferase. Reporter activation is normalised to that conferred by SRF-VP16 or SRF-VP16+C3 transferase, respectively (100%). n=3 independent experiments; error bars, SEM.

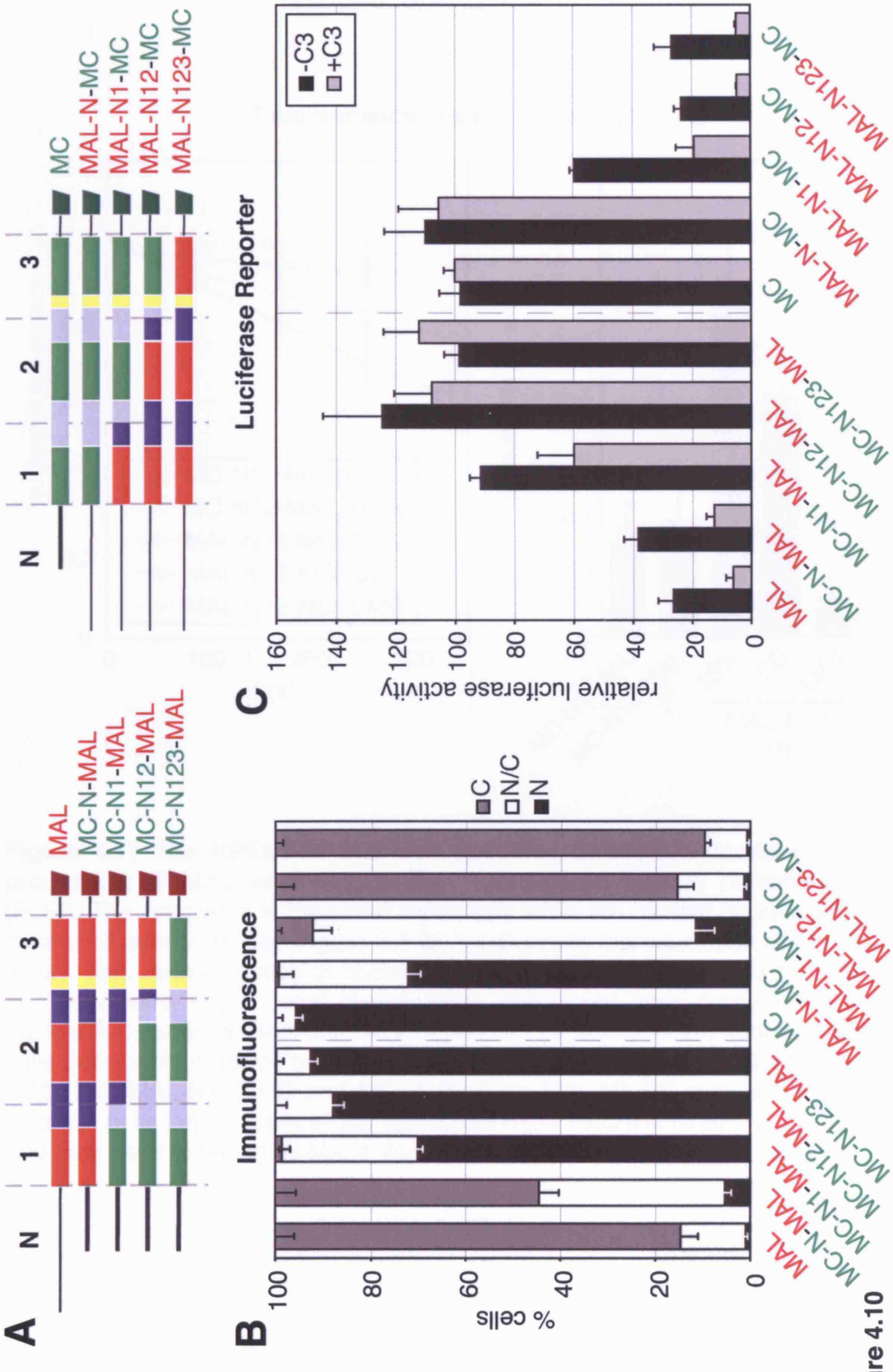
A
N
1
2
3
MAL
MC-N-MAL
MC-N1-MAL
MC-N12-MAL
MC-N123-MAL
MC
MAL-N-MC
MAL-N1-MC
MAL-N12-MC
MAL-N123-MC
legend
B
Immunofluorescence
% cells
C
N/C
N
C
Luciferase Reporter
-C3
+C3
relative luciferase activity
MAL
MC-N-MAL
MC-N1-MAL
MC-N12-MAL
MC-N123-MAL
MC
MAL-N-MC
MAL-N1-MC
MAL-N12-MC
MAL-N123-MC

Figure 4.10

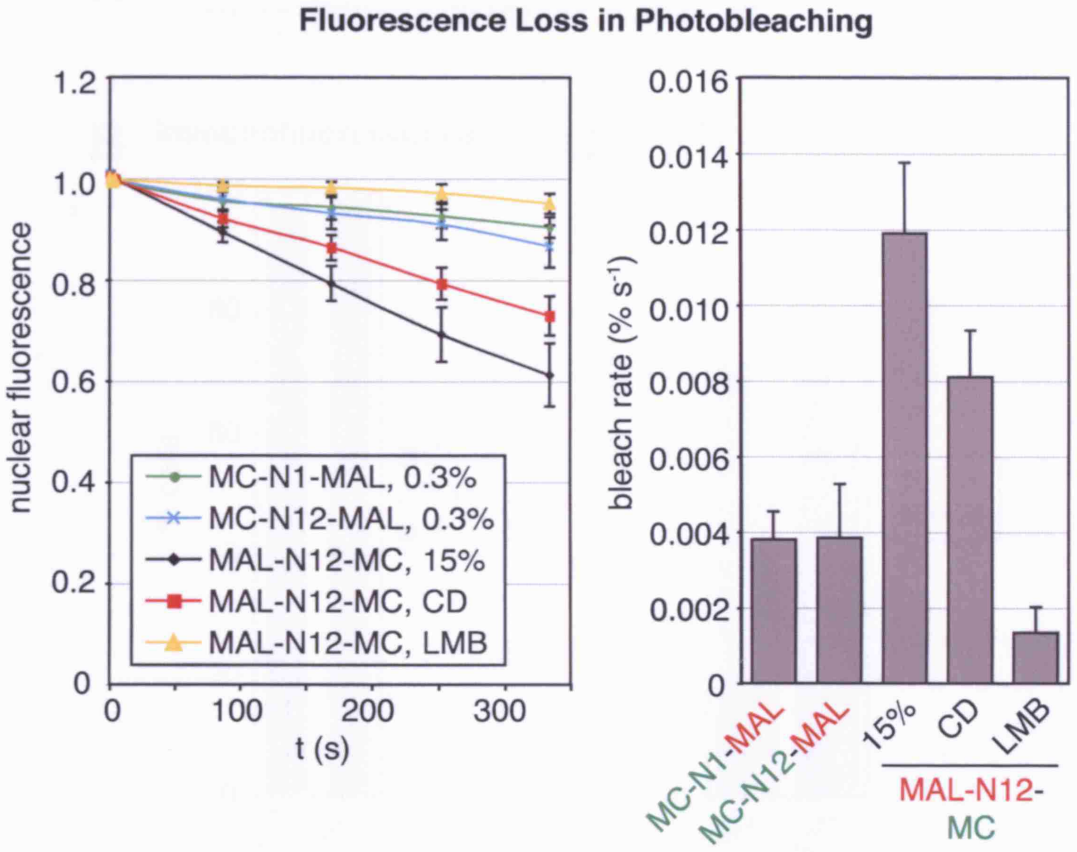

Figure 4.11 The RPEL1-RPEL2 unit specifies differential nuclear export properties of MAL and myocardin. Fluorescence loss in photobleaching (FLIP). The cytoplasm is bleached repeatedly while the nuclear fluorescence is measured over time. See Figure 3.6 for a schematic representation of the FLIP assay. Left, decay kinetics of nuclear fluorescence for the indicated constructs and conditions. Right, initial bleach rates determined from decay kinetics of nuclear fluorescence. Data of three independent experiments are from at least 10 cells per condition (error bars, SD). See Figure 4-3 for the parallel analysis of MAL, MC, MAL-N123-MC and MC-N123-MAL. MAL-N1-MC was not analysed because of its largely pan-cellular localisation (see Figure 4.10 B).
The data were obtained by Maria Vartiainen.

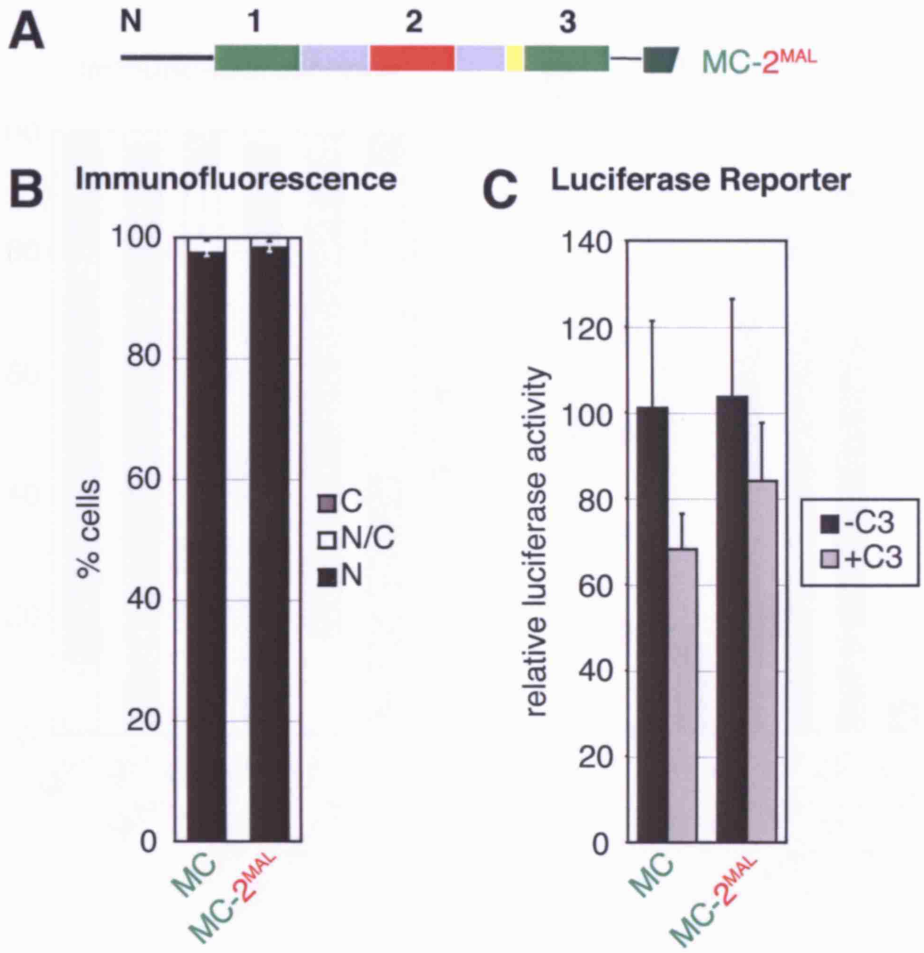

Figure 4.12 MAL RPEL2 is not sufficient to confer MAL-like regulation on myocardin. (**A**) Schematic representation of MC-2^{MAL} with RPEL motif 2 of MAL shown in red. (**B**) Localisation of transiently expressed MC and MC-2^{MAL} in serum-starved NIH3T3 fibroblasts detected by immunofluorescence microscopy. Localisation was scored in 150-200 cells (N, nuclear; N/C, pan-cellular; C, cytoplasmic; n=3 independent experiments; error bars, SEM. See Figure 8.6 for representative micrographs. (**C**) Activation of an SRF luciferase reporter by expression of MC and MC-2^{MAL} without and with co-expression of C3 transferase. Reporter activation is normalised to that conferred by SRF-VP16 or SRF-VP16+C3 transferase, respectively (100%). n=3 independent experiments; error bars, SEM.

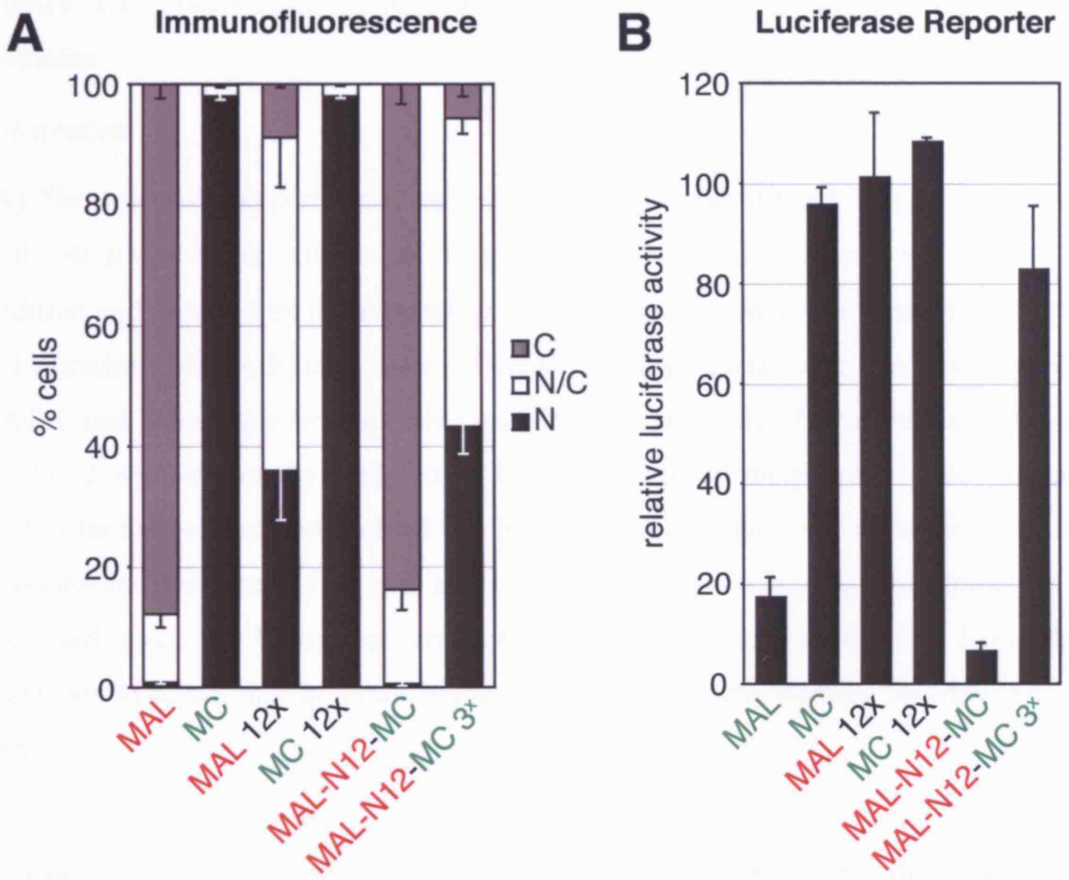

Figure 4.13 The functional significance of RPEL3 depends on its context. (**A**) Localisation of indicated transiently expressed MAL and MC derivatives in serum-starved NIH3T3 fibroblasts detected by immunofluorescence microscopy. Localisation was scored in 150-200 cells (N, nuclear; N/C, pan-cellular; C, cytoplasmic; n=3 independent experiments; error bars, SEM. "3x" indicates that the R->A mutation has been introduced into MC RPEL3 in the given context. See Figure 8.6 for representative micrographs. (**B**) Activation of an SRF luciferase reporter by expression of the indicated MAL and MC derivatives. Reporter activation is normalised to that conferred by SRF-VP16 (100%). n=3 independent experiments; error bars, SEM.

Figure 4.14 Analysis of actin binding stoichiometries of mutant MAL RPEL domains.

see overleaf

(**A**) The analysis was performed as in Figure 2.7: 10 μM MAL(2-261) were incubated with 30 μM (skeletal-muscle α) G-actin. Unbound actin was polymerised by salt addition and removed by ultracentrifugation. Supernatants were analysed on a calibrated gel filtration column. Eluates were collected in 500 μl fractions and analysed by SDS-PAGE and Coomassie brilliant blue staining. For analysis of actin alone, actin was modified with tetramethylrhodamine (TMR) to render it nonpolymerisable. Apparent molecular masses were determined via the elution volumes and are shown for the RPEL domains and their complexes with actin. The apparent actin binding stoichiometries are indicated in red. (**B**) Equivalent amounts of the peak fractions analysed by SDS-PAGE and Coomassie staining. Note the higher ratios of MAL:actin staining for MAL 1x3 and 1xx.

A basis for the observed stoichiometry effects is suggested by structural studies presented in the following chapter, Chapter 5. The observations may be explained by direct and likely water-mediated contacts between actin molecules in the RPEL domain-actin complex. Cooperative effects may result from these actin-actin interactions.

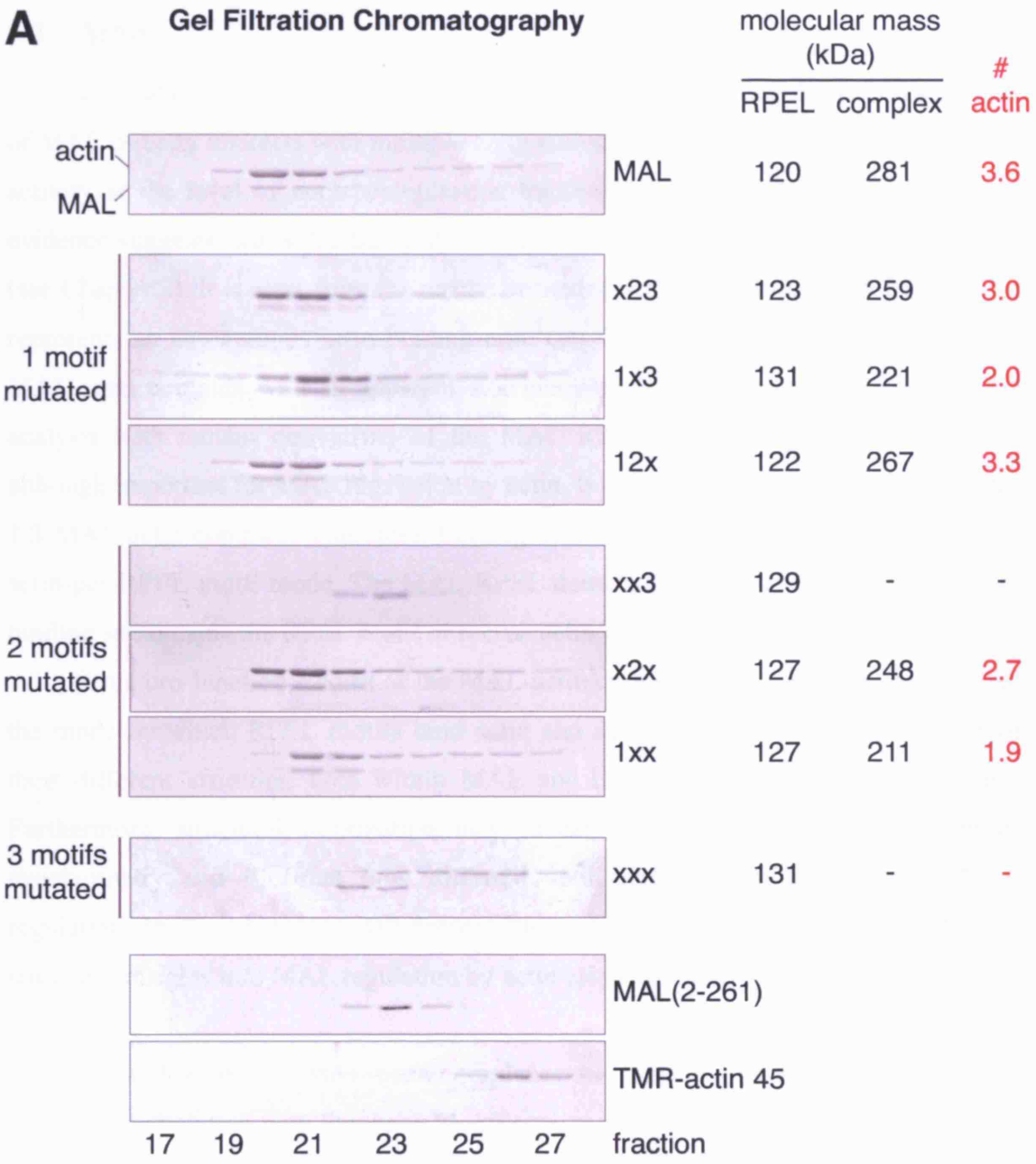

legend

Figure 4.14

5 Structure-function analysis of the MAL-actin interaction

5.1 Aims

The data presented in the preceding three chapters show that the full-length form of MAL directly interacts with multiple actin molecules in a manner that controls MAL activity at the level of nucleocytoplasmic transport and transcription. Circumstantial evidence suggests that MAL binds at the base of the subdomain 1-3 interface of actin (see Chapter 2). It is clear from the results presented in Chapter 4 that each RPEL motif represents an autonomous actin-binding unit. Gel filtration chromatography resolves a MAL-actin complex with an apparent stoichiometry of 1:3. However, a gel filtration analysis with mutant derivatives of the MAL RPEL domain suggests that RPEL3, although important for MAL regulation by actin, is dispensable for the formation of this 1:3 MAL-actin complex. Therefore, binding of actin may not occur via a simple one-actin-per-RPEL-motif mode. The MAL RPEL domain may contain an additional actin-binding site outside the RPEL motif or recruit actin via actin-actin interactions.

Structure-function studies of the MAL-actin complex have the potential to reveal the mode by which RPEL motifs bind actin and shed light on the molecular basis of their different affinities, both within MAL and between myocardin-family proteins. Furthermore, structural information may reveal the basis of MAL-actin complex stoichiometry and illustrate how different actin-binding sites cooperate in MAL regulation. In this chapter, I will present the current state of ongoing efforts to gain structural insights into MAL regulation by actin using X-ray crystallography.

Crystallography of MAL-actin complexes and all structural analyses shown were done in collaboration with Stephane Mouilleron, a crystallographer in Neil McDonald's laboratory at the Institute. Of the work presented, I established and routinely prepared MAL/RPEL-actin complexes for crystallisation and was involved in the initial screens. Stephane performed the majority of the crystallisation screens, all of the optimisation work at the crystallisation stage, collected the X-ray diffraction data and solved the crystal structures. Where analyses were done primarily by Stephane, this is indicated in the legends. I also acknowledge Stephane's assistance in preparing the figures that contain structural representations.

I will present three MAL-actin crystal structures and initial functional analyses carried out on the basis of the obtained structural information. A more detailed interpretation of the structures in the context of the results described in the preceding chapters will be given in Chapter 6 (Discussion).

5.2 Defining the approaches for MAL-actin crystallisation

5.2.1 Defining a suitable MAL crystallisation construct

The first 204 amino acids of MAL are sufficient to confer nucleocytoplasmic shuttling on the heterologous pyruvate kinase protein or GFP (see Section 2.2 in Chapter 2). Therefore, this fragment represents an interesting module for structural studies. To generate a suitable MAL crystallisation construct, I initially expressed and purified MAL(2-204). During the purification, a stable proteolysis product accumulated (Figure 5.1). Using mass spectrometry and N-terminal Edman sequencing, the fragment was determined to represent MAL(2-199). I consequently generated recombinant MAL(2-199), which was stable during purification (see Figure 2.6 C). Since MAL(2-261) can be generated without major signs of C-terminal degradation, I also used this derivative for initial crystallisation trials.

Additionally, we set out to crystallise RPEL peptides complexed to G-actin, since these interact autonomously with actin monomers (see Section 4.5 in Chapter 4).

5.2.2 Crystallisation trials for the MAL RPEL domain

Dissociation of actin from MAL may result in MAL adopting a particular conformation that is compatible with nuclear import but not nuclear export. It would be interesting to compare MAL in its actin-free and actin-bound states to gain direct insights into the regulatory roles of the MAL-actin interaction. I extensively screened crystallisation conditions for the isolated MAL N-terminus, using both MAL(2-261) and MAL(2-199). These experiments failed to reveal any suitable crystallisation conditions, and only clear drops, precipitate and spherulites were observed (data not shown). Circular dichroism (CD) spectroscopy and gel filtration chromatography presented in Chapter 2 (see Section 2.3.2) demonstrated that the MAL N-terminus is largely unordered and flexible. This offers a likely explanation for the failure of the RPEL domain to crystallise.

Including a binding partner frequently increases the crystallisability of the protein of interest by restricting its intrinsic flexibility and thereby generating a more rigid scaffold, which is a prerequisite for the formation of crystalline arrays of molecules. Therefore, the MAL-actin complex might crystallise more readily than MAL on its own. I will next describe how we established the crystallisation of several MAL-actin complexes.

5.2.3 Establishing crystallisation of the MAL-actin complex

5.2.3.1 Overcoming the obstacle of actin polymerisation

The polymerisation of actin represents a major obstacle for its crystallisation. The fact that binding of the RPEL domain blocks actin polymerisation (see Section 2.3.1.2 in Chapter 2) provides a promising basis for a crystallographic analysis of the MAL-actin complex. I initially generated a MAL-actin complex by mixing MAL(2-261) and G-actin in a 1:3 molar ratio, inducing polymerisation and removing the excess actin that polymerised by ultracentrifugation, analogous to the preparation of complexes for analysis by gel filtration (see Figure 2.7 in Chapter 2). Following its purification by gel filtration chromatography, the MAL-actin complex was concentrated to obtain a preparation suitable for crystallisation screens. I noted, however, that during concentration actin polymerised, as apparent from the increased viscosity of the preparation. Therefore, at high actin concentration, the binding equilibrium appears to shift toward actin filaments, very much to the disadvantage of the MAL-actin complex.

Consequently, actin polymerisation had to be blocked by additional means. The work presented in Chapter 2 has fleshed out two approaches to potentially address this problem. Firstly, modification of actin with tetramethylrhodamine (TMR) efficiently blocks actin polymerisation and renders uncomplexed actin crystallisable (Otterbein et al., 2001). We initially used TMR-actin for crystallisation (see Sections 5.2.4.1 and 5.2.4.3 below). Further biochemical studies, however, soon revealed that covalent TMR linkage to actin destabilises the MAL-actin interaction substantially (see Section 2.3.2.6 in Chapter 2). Secondly, we considered latrunculin as a polymerisation-blocking agent for MAL-actin complex crystallisation. Latrunculin was successfully used in previous structural studies of actin and its binding partners (see, for example, Hertzog et al., 2004; Morton et al., 2000). Gel filtration chromatography presented in Chapter 2 (Figure 2.7) demonstrated that latrunculin-B binding to actin is compatible with, and

may even promote, MAL-actin complex formation. Latrunculin A (LatA) is likely to bind actin with higher affinity than latrunculin B (LatB) (see Section 1.2.6.1 in Chapter 1; Introduction). To assess which of these latrunculins would best serve our purposes, I tested the potential of LatA and LatB to inhibit actin polymerisation in actin sedimentation assays (Figure 5.2). G-actin was incubated with increasing amounts of either LatA or LatB followed by induction of actin polymerisation. G- and F-actin were separated by ultracentrifugation and their relative ratios analysed by SDS-PAGE. Both LatA and LatB potently blocked actin polymerisation with similar efficiencies at the conditions used (Figure 5.2). Since large quantities of LatB are more easily available commercially than of LatA, we used LatB for structural studies.

5.2.4 Establishment of MAL-actin complexes for crystallisation

5.2.4.1 RPEL peptide-TMR-actin complexes

Work presented in Chapter 4 demonstrates that the RPEL motif represents an autonomous actin-binding unit (see Section 4.5). Since, of all three MAL RPEL motifs, RPEL1 appeared to most efficiently recruit actin from NIH3T3 cell lysate (see Figure 4.6 in Chapter 4), we initially sought to crystallise TMR-actin with a 32-amino acid RPEL1 peptide in the same context as the peptides used for actin-binding studies presented in Chapter 4 (see Section 4.5). TMR-actin was co-incubated with a 2-fold molar excess of RPEL1 peptide, purified by gel filtration chromatography and concentrated to 5.7 mg/ml. We then screened 1152 buffer conditions to identify crystallisation conditions for the protein preparation. Crystals were observed under two very similar screening conditions and further optimised. The optimised condition under which crystalline plates were obtained was very similar to that under which uncomplexed TMR-actin was previously described to crystallise (Otterbein et al., 2001). The structure was solved by molecular replacement using the coordinates of TMR-actin (PDB file 1J6Z, Otterbein et al., 2001) as molecular model. We did not observe any electron density apart from that which accounted for actin, indicating that the complex of TMR-actin and RPEL1 did not form or dissociated during purification or crystallisation. The subsequent finding that the TMR moiety interferes with MAL binding offers an obvious explanation for this (see Section 2.3.2.6 in Chapter 2).

5.2.4.2 RPEL peptide-LatB-actin complexes

Because TMR group on actin interferes with MAL binding, we turned to using LatB-actin for all subsequent peptide studies. LatB-actin was prepared as described in Chapters 4 (see Section 4.5) and 7 (Materials and Methods; see Section 7.13.4) and mixed with a three-fold molar excess of peptide at various concentrations, typically 6 and 12 mg/ml (Figure 5.3 A). A precipitate became apparent, especially at the higher protein concentrations. This was likely to represent actin, based on the amounts of actin in the total samples and the supernatants upon ultracentrifugation of the preparations. We reasoned that this might merely increase the peptide:actin ratio and proceeded with crystallisation trials. Peptide-actin complexes were prepared for all three MAL RPEL peptides.

We obtained crystals suitable for X-ray diffraction for the complexes of RPEL1 and RPEL2 with LatB-actin (Figure 5.4 E). Crystals typically reached their maximum size within two weeks. The optimised crystals were analysed (ESRF, ID42) and the structures solved by molecular replacement at resolutions of 2.35 and 1.45 Å for RPEL1 and RPEL2 complexes, respectively (see Table 8.1 in Chapter 8; Appendix, for data collection and refinement statistics). To-date, no crystals grew from LatB-RPEL3 preparations.

5.2.4.3 RPEL domain-TMR-actin complexes

Gel filtration chromatography of TMR-actin-MAL preparations suggests that the TMR moiety generally destabilises the MAL-actin complex (see Section 2.3.2.6 in Chapter 2). However, previous preliminary observations raised the possibility that TMR-actin engages in a 1:1 complex with the RPEL domain. Therefore, complexes of TMR-actin and the MAL RPEL domain, both in the context of MAL(2-261) and MAL(2-199), were initially prepared by adding the proteins in a 1:1 molar ratio (Figure 5.3 B). Dynamic light scattering confirmed the presence of a single molecular entity in these preparations. Despite intensive screening across 1152 conditions, we did not identify any crystallisation condition for the complex of TMR-actin and MAL(2-261). However, for the complexes prepared with MAL(2-199), we obtained two conditions under which small, elongated crystals formed. Because of their colour, the presence of TMR-actin was immediately apparent. The conditions were clearly different from those under which we previously obtained TMR-actin crystals (see Figure 5.4 A for

comparison). Therefore, it was likely that in these crystals, TMR-actin was bound to MAL. Through optimisation work, which involved preparation of more highly concentrated complexes, refinement of the crystallisation condition and microseeding, larger crystals (10 x 10 x 200 µm) that were part of "sea-urchin like" assemblies (Figure 5.4 B) were recovered and analysed at the European Synchrotron Radiation Facility (ESRF) in Grenoble, France (microfocusing beamline ID23-2). The diffraction of these crystals was limited to about 6 Å. Therefore, these crystals did not meet the requirements for a structural analysis. CD spectroscopy strongly suggested that MAL(2-199) contains unstructured regions (see Section 2.3.2.2 in Chapter 2). These are likely to hamper the formation of good-quality protein crystals. Therefore, our next aim was to re-define the N-terminal boundary of the MAL crystallisation construct.

The residues preceding RPEL motif 1 are predicted to be devoid of secondary structure (see Figure 2.1 in Chapter 2). This is likely to be the case since the shorter BSAC variant of the RPEL domain displays a higher relative helix content and a lower degree of disorder, as shown by CD spectroscopy (see Section 2.3.2.2 and Figure 2.6 in Chapter 2). We therefore proceeded using a MAL contruct, MAL(67-199), lacking the first 66 amino acids. MAL(67-199) was readily expressed under the previously established expression conditions and largely resistant against proteolysis during its purification. The apparent molecular mass of a complex of MAL(67-199) and actin was consistent with the 1:3 stoichiometry observed for longer derivatives of the MAL N-terminus (Figure 5.5).

Crystallisation trials with 1:1 preparations of MAL(67-199) and TMR-actin identified eight initial crystallisation conditions out of 1152. Further optimisation yielded much larger crystals, however, the crystals appeared twinned (Figure 5.4 C, left) and were therefore not suitable for X-ray diffraction since it is close to impossible to resolve the contribution of differently oriented crystal lattices to the overall diffraction pattern. Microseeding and further variation of precipitant concentration and pH did not markedly improve the crystal quality. We therefore performed an additive screen, choosing a single crystallisation condition to be supplied with different agents thought to affect protein-protein and protein-solvent interactions and water structure, including detergents, salts, non-covalent cross-linkers and organic solvents ('Additive Screen', Hampton Research). The addition of 4% acetonitrile had a striking effect on crystal morphology: instead of numerous interconnected rods, we observed large, cubic

monocrystals that were untwinned in their early stages of growth (Figure 5.4 C, right). These crystals were analysed by X-ray diffraction (ESRF, ID23-1), and the data used to determine a 3.4-Å structure by molecular replacement, using the coordinates of the TMR-actin structure we obtained previously (see Section 5.2.4.1). This structure quickly revealed the presence of three actin molecules in the MAL-TMR-actin complex. Although no 1:3 stoichiometry was observed for complexes of the MAL RPEL domain and TMR-actin by gel filtration (see Section 2.3.2.6 in Chapter 2), a complex containing three actins might still prevail under the high protein concentration used for crystallography or be favoured in the context of crystal packing. This finding was important because it indicated that the 1:1 protein ratio for complex setup was suboptimal. Therefore, all subsequent complexes of MAL(67-199) and actin, either TMR-actin or LatB-actin (see Figure 5.3 C), were prepared using a three-fold molar excess of actin over MAL as described in Chapter 7 (Materials and Methods).

5.2.4.4 RPEL domain-LatB-actin complexes

We decided to focus on the crystallisation of MAL(67-199) with LatB-actin rather than TMR-actin because of the negative effect of TMR on the MAL-actin interaction.

In the screening stage, MAL(67-199)-LatB-actin crystals grew readily in 10 out of 1152 conditions. Crystallisation conditions were similar to those under which we previously observed crystallisation of MAL(67-199)-TMR-actin complexes. Typically, crystals grew within one to two weeks, and their size appeared to positively correlate with the concentration of the protein preparations up to 25 mg/ml, which was the maximum concentration tested (Figure 5.4 D). The maximum diffraction of the optimised crystals was limited to 7 Å (X-ray home source) or 4.5 Å (ESRF, ID23-1).

To further optimise the diffraction of these crystals, we aimed to shrink the volume of the crystal unit cells by dehydration, an approach that has been shown to, in some cases, dramatically improve diffraction (Heras and Martin, 2005). Dehydration was achieved by serial transfer of the crystals into solutions containing higher concentrations of precipitant (PEG 3350) and ethylene glycol while allowing for air dehydratation of these solutions (see Figure 5.6). This procedure reproducibly shifted the diffraction limit to about 3 Å (at both the X-ray home source and the ESRF),

eventually allowing for the crystal structure of the MAL(67-199)-LatB-actin complex to be solved at a resolution of 2.9 Å by molecular replacement.

5.3 Structures

I will subsequently present the structures of the RPEL motif peptides and LatB-actin, followed by a description of a preliminary structure of the RPEL domain with LatB-actin. A summary of the data collection and refinement statistics is given in Chapter 8; Appendix (Table 8.1).

5.3.1 Structures of RPEL1 and RPEL2 peptides with LatB-actin

5.3.1.1 Overall description of the RPEL-actin interactions

Both the RPEL1 and RPEL2 peptides bind at the base of the actin molecule in its "classical" view with actin subdomain 1 at the lower right and subdomain 4 at the upper left, (Figure 5.7). The conformations of the peptides are very comparable, and they follow similar yet distinct trajectories on the actin molecule. Molecular contacts are shown in Figures 5.7 and 5.8 and summarised in Figure 5.10. The N-terminal part of the RPEL peptides contains an α helix of two turns ("helix 1"), which, mainly via hydrophobic interactions, docks onto the hydrophobic cleft present between actin subdomains 1 and 3 (Figure 5.7, see Dominguez, 2004, for a discussion of this region of actin). Following the C-terminal end of helix 1, the main chain adopts an unfolded but well-ordered segment of 4 amino acids, the "connector", which contains the first and most conserved arginine residue of the RPEL motif and contacts actin mainly via polar interactions. A second, short helix of less than two turns ("helix 2") contacts a hydrophobic region of actin at the base of subdomain 3 that we termed the "subdomain-3 platform" (Figure 5.7). For both peptides, the polypeptide chain that directly follows helix 2 proceeds underneath the actin-proximal side of the helix, thereby becoming sandwiched between helix 2 and the subdomain-3 platform. Helix 2 and residues emanating from the subsequent unstructured region establish hydrophobic contacts with the subdomain-3 platform.

5.3.1.2 Detailed description of the RPEL-actin interactions

Helix 1 provides three well-conserved key side chains for interaction with actin: L74, K77 and L78 in RPEL1 and L118, K121 and I122 in RPEL2 (Figure 5.8 and Figure 5.10). The portion of the hydrophobic cleft of actin that interacts with helix 1 is defined by the actin residues I345, L346 and L349. In the RPEL1-LatB-actin structure, the ε-amino group of K77 forms a hydrogen bond with main chain carbonyl group of G146 in actin. This interaction is conserved in RPEL2, where the corresponding lysine residue, K121, establishes an equivalent contact. K121 also adopts an alternative conformation with an occupancy of 50%. In the alternative orientation, the ε-amino group forms a salt bridge with the side-chain carboxyl group of E167 of actin.

Likewise, key hydrophobic residues that mediate the helix 2-subdomain-3 platform interactions are conserved between the two RPEL motifs: L87, I92 and M93 in RPEL1 and L131, I136 and L137 in RPEL2 (Figure 5.8 and Figure 5.10). Hydrophobicity of the subdomain-3 platform is conferred by the actin residues I289, Y166, L171 and Y169. Only L87 in RPEL1 and L131 in RPEL2 are contributed by helix 2, which spans residues 84-90 in RPEL1 and 128-134 in RPEL2. The other two conserved hydrophobic side chains contacting the subdomain-3 platform (I92 and M93 of RPEL1 and I136 and L137 of RPEL2) are contributed by the "unstructured" region that follows helix 2 (Figure 5.8 and Figure 5.10; the term "unstructured" is put in quotation marks because, strictly speaking, these residues are structured, but they lack the common secondary-structure elements helix or strand). Closer inspection of the main-chain hydrogen bonds reveals that the "unstructured" region is stabilised by hydrogen bonds that extend from the end of helix 2: the main-chain carbonyl groups of residues L87 in RPEL1 and L131 in RPEL2 engage in hydrogen bonds with the main-chain amino groups of the two hydrophobic amino acids that contact the subdomain-3 platform (I92 and M93 in RPEL1 and I136 and L137 in RPEL2) and the preceding amino acid (Figure 5.9). Therefore, the "unstructured" region also "caps" helix 2.

Helix 2 itself appears to become oriented by the core glutamate residues of the RPEL motif, E86 in RPEL1 and E130 of RPEL2, which extend from helix 2 and establish a conserved hydrogen bond with the main-chain amino group of the non-conserved residue three positions N-terminal to these glutamates (Figure 5.8 and Figure 5.10).

The helix1-helix2 connector mediates mainly electrostatic RPEL-actin interactions via the conserved RR or RP unit of the RPEL core: R81 and R82 in RPEL1 and R125 and P126 in RPEL2 (Figure 5.8 and Figure 5.10). For both peptides, the first and most conserved arginine residue of the entire motif extends toward the actin molecule, engaging in numerous electrostatic interactions and hydrogen bonds via its guanidinium group. Two of these interactions are conserved between RPEL1 and RPEL2: firstly, and most strikingly, both R81 and R125 are in close proximity to the aromatic side chain of Y169 of actin and in an orientation compatible with a cation-π interaction. Arginine residues are relatively frequently found involved in this type of interaction, in which the guanidinium group engages the de-localised electrons of the aromatic side group (Gallivan and Dougherty, 1999). Secondly, both R81 and R125 form hydrogen bonds with the main-chain carbonyl group at position E167 of actin. Additionally, the arginine residues engage in RPEL-specific interactions. In RPEL1, R81 forms an intra-RPEL hydrogen bond with the main-chain carbonyl group of L78. This contact is not present in RPEL2. There, R125 establishes a salt bridge with the main-chain carboxyl group of the ultimate C-terminal actin residue, F375, via its guanidinium group (Figure 5.8 and Figure 5.10). This is unusual since actin's ultimate C-terminal residue is rarely resolved in crystal structures. Another example where F375 is visible in a crystal structure is the complex of gelsolin segment 1 with skeletal muscle actin (McLaughlin et al., 1993). In addition to its electrostatic interaction with the arginine, F375 might become oriented by a solvent molecule (2-(n-morpholino)-ethanesulfonic acid, MES) present within its vicinity in the complex. Since the MES molecule is specific to the RPEL2-LatB-actin crystallisation condition, it is absent from the RPEL1 structure.

For both RPEL motifs, a role for amino acids immediately following the most conserved arginine residue in RPEL-actin interactions are apparent. P126 in RPEL2 is likely to contribute a hydrophobic component to the RPEL2-actin interaction while presumably guiding the main chain of the peptide by introducing a bend into the peptide chain (Figure 5.8 and Figure 5.10). P126 will restrict conformational flexibility in the helix1-helix2 connector. RPEL1 has an arginine residue, R82, at the equivalent position. R82 extends into the opposite direction of R81 (Figure 5.8, left). Its guanidinium group establishes a hydrogen bond with the hydroxyl oxygen of Y166 and the side-chain carboxyl group of E167 in actin. Since an arginine is absent at the equivalent position in

RPEL2, E167 is in a different rotamer conformation in RPEL2 and can establish an intra-RPEL salt bridge with K121 (see above).

The hydroxyl group of Y169 of actin, the residue involved in the cation-π interaction described above, engages in two additional conserved interactions with both RPEL peptides: it forms hydrogen bonds with the main chain at RPEL1 positions R82 and R84 and RPEL2 positions P126 and R128, acting both as hydrogen donor and acceptor (Figure 5.8 and Figure 5.10).

It is notable that, especially in the region of the connector, the peptide chain of RPEL2 is more closely positioned toward subdomain 1 than the peptide chain of RPEL1 (see Figure 5.7 C and D). The explanation for this is likely to lie in the interactions that the connector side chains engage in. In the case of RPEL2, R125 is attracted by the ultimate C-terminal residue of actin, which emanates from subdomain 1 (Figure 5.8, right). This interaction is absent in the RPEL1-actin complex, in which close approach of the connector to actin subdomain 3 may result from the interaction of R82 with Y166 and E167 of actin (Figure 5.8, left).

The interaction potential of the guanidinium groups of arginines appears to be fully used in both RPEL1- and RPEL2-actin complexes. The structure provides a simple rationale for the finding that alanine substitution of the first and most conserved arginine residues has a stronger impact of MAL-actin complex stability than the exchange of the following amino acid (see Section 2.3.2.5 in Chapter 2).

The crystal structures allow us to relate direct interactions between RPEL motifs and actin to the sequence conservation across all known RPEL motifs. As I will address in the next chapter, this analysis strongly suggests that the RPEL motif primarily represents and actin-binding motif.

5.4 A structure of the RPEL domain with actin

We determined the structure of MAL(67-199) with LatB-actin at a resolution of 2.9 Å. Although crystallographic refinement of this structural model is still in progress, we can draw some preliminary conclusions from it. In the future, we will aim towards improving this structure by optimising the preparation of the MAL-actin complex,

collecting higher-resolution data and altering the refinement procedures. Therefore, the following observations should be considered as tentative results.

5.4.1 Description of the RPEL domain-actin structure

Strikingly, of the 133 amino acids of MAL present in the crystallisation construct, MAL(67-199), only 56 (42%) are ordered. These encompass MAL residues L67 to I122, 16 of which (29%) have no side chains accounted for by the electron density (Figure 5.11). The remaining 77 amino acids of the MAL construct (58%) are absent and therefore presumably disordered. This includes the basic region, B2, postulated to represent a nuclear import signal in MAL (see Section 2.2 in Chapter 2, Miralles et al., 2003; Vartiainen et al., 2007) and RPEL3, which might represent the most downstream actin-controlled regulatory site in MAL (see Chapter 4 and Chapter 5; Discussion). Therefore, this structure cannot directly address the contribution of these components to MAL regulation.

A representation of the RPEL domain-LatB-actin structure is shown in Figure 5.11. Both the TMR-actin and LatB-actin structures contain three actin molecules (actins 1, 2 and 3) in an identical relative arrangement (data for TMR-actin complex not shown). In the discussion that follows, I will describe the contacts established by the actin molecules based on the structure obtained with LatB-actin.

5.4.1.1 Actin 1

Actin 1 interacts with the RPEL domain via RPEL1, and the general mode of its docking onto MAL is effectively identical to that observed for the RPEL1-LatB-actin structure (Figure 5.11 and Figure 5.12 A). However, the two structures differ from each other in a number of aspects. (1) In the RPEL domain-LatB-actin structure, an additional contact is made by K71 of MAL, the first residue N-terminal to RPEL1 as defined by PFAM (http://pfam.sanger.ac.uk/, Finn et al., 2006): K71 establishes a hydrogen bond with S348 of actin via its ε-amino group while its long aliphatic chain appears to contribute to the hydrophobic core of the helix 1-actin interface (Figure 5.12 A). (2) The poor electron density for this side chain at the given resolution does not allow us to unequivocally conclude whether the hydrogen bond between K77 in RPEL1 and the main-chain carbonyl group at position G146 of actin is present in the RPEL

domain-actin structure. (3) A hydrogen bond between the guanidinium group of R81 and the main-chain amino group of L78, which is present in the RPEL1-LatB-actin structure, is not discernable in the MAL(67-199)-LatB-actin structure. (4) A hydrogen bond between the hydroxyl oxygen of Y169 of actin and the main-chain amino group of R84 in RPEL1 appears to be absent in the MAL(67-199)-LatB-actin structure. Instead, Y169 appears to form a hydrogen bond with the guanidinium group of R81 (Figure 5.12 A).

5.4.1.2 Actin 2

Two proline residues C-terminal to RPEL1 in MAL, P94 and P95, introduce a sharp bend into the direction of the main chain of MAL (Figure 5.12 B). The following 7 amino acids lack a classical secondary structure, and another proline residue at position 99 contributes in to the dramatic change in main-chain directionality. The bend positions an α-helix, "helix 3", whose N-terminal boundary is marked by MAL residue 103. The second actin molecule ("actin 2") is bound to residues 97-102 and the N-terminal portion of helix 3 up to residue 110 (Figure 5.11 and Figure 5.12 B). This region corresponds to the linker between RPEL motifs 1 and 2. An aspartate side chain, D25, of actin forms an electrostatic contact with the main-chain amino groups of A100 and A101 in MAL. The short side chains of alanine at these positions in MAL may minimise any potential interference with this main-chain contact. P99 and F102 of MAL engage in hydrophobic contacts with actin 2 that mainly involve I341 and I345 (Figure 5.12 B). Furthermore, Q105, R106 and L109, which emanate from helix 3 in MAL, establish hydrophobic contacts with the hydrophobic cleft of actin. The polar amide group of Q105 and the guanidinium group of R106 point away from the hydrophobic surface. Besides the interactions mediated by D25 of actin, two further polar interactions between MAL and actin 2 are apparent. The main-chain amino group of S98 of MAL forms a hydrogen bond with the main-chain carbonyl group of G23 of actin, and the hydroxyl group of S108 of MAL establishes a hydrogen bond with the main-chain carbonyl group of G146.

The relative orientation between actins 1 and 2 can be roughly described by a translation of actin 1 along an axis that is perpendicular to its face, i.e., the subdomains in actin 2 become positioned closest to the identical subdomains in actin 1, respectively (Figure 5.11). Although the parallel arrangement of actins 1 and 2 is striking, no

obvious direct contacts between them are apparent although protein-solvent contacts are likely to dominate. Since at the given resolution no water molecules can be discerned, we cannot draw any conclusions about the role of water-mediated hydrogen bonds.

5.4.1.3 Actin 3

Compared to actins 1 and 2, actin 3 is located on the opposite side of the MAL chain in the complex (Figure 5.11). At 2.9 Å resolution, only a limited number of direct MAL-actin 3 contacts can be reliably pinpointed (Figure 5.12 C). R111, which is five amino acids N-terminal of the PFAM-defined RPEL2 motif, makes an electrostatic interaction with D25 of actin 3. R111 itself is oriented by an electrostatic intra-MAL interaction of its guanidinium group with the side-chain carboxyl group of E115. A second interaction of actin 3 is mediated by Q90, which extends from helix 2 of MAL and establishes a hydrogen bond with the main-chain amino group of M305. Q90 itself is oriented by an intra-MAL interaction with the guanidinium group of R82 in RPEL1, a contact that does not appear in the RPEL1-actin structure and might therefore be induced by actin 3. Another potential contact between MAL and actin 3 is established by Q80, whose terminal amino group is placed close to (3.01 Å) the main-chain carbonyl group of S239 in actin 3. The region corresponding to helix 1 of RPEL2 is poorly resolved in the current crystal structure, i.e., for the residues at positions corresponding to residues 3 to 7 of helix 1 in RPEL2 (see Figure 5.10), only the main chain is discernable. The following residues are absent (see Figure 5.11). Therefore, no significant interaction occurs between this region and actin 3 in the crystal. The helical conformation of the preceding sequence (helix 3) could explain the lack of contact between actin 3 and this region of MAL.

5.4.1.4 Direct contacts between actins 1 and 3

We did not observe any direct contacts between actins 1 and 2. However, actin 3 contacts actin 1 directly (Figure 5.13 A). K336 and Y337 of actin 3 establish electrostatic interactions and hydrogen bonds, respectively, with D288 at the base of subdomain 3 of actin 1. Furthermore, V30 of actin 3 and I287 of actin 1 form a hydrophobic contact. The residues of actin 3 that contact actin 1 reside within a helix of actin subdomain 1 and are in close proximity to the nucleotide-binding cleft. K336 establishes a hydrogen bond with the adenine ring of the nucleotide (Figure 5.13), and

Y337 takes part in a water-mediated network of hydrogen bonds that spans the nucleotide-binding cleft of actin (Vorobiev et al., 2003). Superposition of ATP-actin3 with the structure of uncomplexed ATP-actin rendered nonpolymerisable by an A204E/P243K mutation ("AP-actin", Rould et al., 2006) demonstrates that the interaction with actin 1 does not grossly affect the conformation of K336 and Y337 of actin 3 (Figure 5.13 B). In the ADP state of AP-actin, K336 and Y337 are oriented very similarly (not shown, Vorobiev et al., 2003).

5.5 Structure-based functional analysis of the MAL-actin interaction

The structures of RPEL motifs 1 and 2 have largely expanded our understanding of the MAL-actin interaction. In this section, I will present our initial experiments to test the validity of the MAL/RPEL-actin structures. Upon obtaining the structure of the RPEL domain with actin, we set out to analyse its implications for actin binding, using fluorescence anisotropy, and MAL regulation, using immunofluorescence microscopy and SRF luciferase reporter assays. The preliminary results presented here do not yet take into account the more comprehensive insights gained by comparing all of the obtained MAL-actin and RPEL-actin structures with each other. Future work will continue to address the implications of the observed interactions for MAL regulation.

5.5.1 Initial structure-based actin binding analysis for RPEL1

For an initial analysis, I used a fluorescence anisotropy assay to study actin binding by mutant derivatives of the RPEL1 peptide (see Section 4.5 in Chapter 4 for description of the assay). This was done in parallel with the analysis of MAL and MC RPEL peptides presented in Chapter 4 (see Figure 4.7). Therefore, the following results are directly comparable to the results presented in the preceding chapter.

Two hydrophobic amino acids in helix 1, L74 and L78, and one hydrophobic amino acid in helix 2, I92, were exchanged for alanine. While RPEL1 bound with an affinity of K_d = 5.4 ± 0.5 μM in the fluorescence anisotropy assay, no binding was detected for the L74A L78A I92A mutant peptide, indicating that hydrophobic interactions are indeed critical for actin binding (Figure 5.14). More subtle mutations will be required to discern specific contributions of helix-1 and helix-2 mediated RPEL-actin contacts.

Interestingly, many actin-binding proteins contain a hydrophobic amino acid at the position equivalent to K71 in RPEL1, which is seen to establish both hydrophobic and polar interactions with actin in the MAL(67-199)-LatB-actin complex (see Figure 5.12 A). We therefore wondered whether exchanging K71 for a hydrophobic amino acid would stabilise the RPEL1-actin interaction. This would open an interesting perspective for obtaining structural insights into the otherwise weak RPEL3-actin contact. Indeed, a K71I derivative of RPEL1 bound actin with an affinity of K_d = 1.7 ± 0.1 μM in the fluorescence anisotropy assay (Figure 5.14). Of all the RPEL peptides studied to-date, the RPEL1 K71I peptide displays the highest affinity for actin.

5.5.2 Interference with helix 1 function results in MAL de-regulation

Although we currently do not have any direct structural information for RPEL3, the RPEL1- and RPEL2-actin structures allow predictions to be made regarding the low-affinity RPEL3-actin interaction. The validity of this comparison is illustrated by the fact that the exchange of R169 in RPEL3 for alanine strongly affects actin binding (see Section 4.5 in Chapter 4). It is therefore likely that RPEL3 establishes similar contacts with actin as RPEL motifs 1 and 2. To test the significance of hydrophobic interactions of helix 1 with actin, I exchanged its first two actin-binding hydrophobic amino acids for alanine in each of the three RPEL motifs. The mutant derivatives were expressed in NIH3T3 fibroblasts and their localisation in serum-starved cells analysed by immunofluorescence microscopy (Figure 5.15).

Wild-type MAL was cytoplasmic in about 90% of the cells. Its localisation was unaffected by the helix-1 mutation in RPEL 1 (L74A L78A). However, the equivalent mutation in RPEL motifs 2 and 3 resulted in substantial de-regulation: nuclear localisation of the mutants was detected in about 15% and pan-cellular localisation in 50-70% of the cells (Figure 5.15). To increase the stringency of the RPEL1 mutation, I additionally substituted K71, which extends from helix 1 and contacts actin in the MAL(67-199)-LatB-actin structure, with alanine. MAL K71A L74A L78A showed pronounced de-regulation, being nuclear in nearly 10% and distributed pan-cellularly in approximately 40% of the cells. Additional mutation of I92 did not potentiate this deregulatory effect. Exchange of only K71 for alanine or methionine had no effect on MAL localisation. The synergy of K71 with hydrophobic amino acids in helix 1 may reflect a contribution of K71 to actin recruitment, however, a more detailed actin-

binding analysis will be necessary to understand this effect. Note that there is no lysine at the position equivalent to K71 in the BSAC splice variant of MAL (see Figure 2.1 in Chapter 2).

In conclusion, these preliminary experiments show that hydrophobic contacts between actin and each of the three RPEL motifs are critical for MAL regulation. The observation confirm the effects of RPEL motif mutations seen previously, including the relative resistance of MAL regulation to mutations in RPEL1 (see Section 4.6 in Chapter 4).

5.5.3 The relevance of the RPEL1-2 linker for MAL regulation is currently unclear

The binding of actin 2 to the RPEL1-2 linker was a surprise. As for RPEL motifs 1 and 2, the mode of actin 2 binding involves hydrophobic contacts between an α helix (helix 3) and the hydrophobic cleft of actin. The presence of actin 2 offers an explanation for some of the MAL-actin stoichiometries observed in gel filtration experiments with RPEL domain derivatives that contain RPEL motif mutations (see Section 4.9 in Chapter 4). For example, an RPEL domain with impaired function of RPEL motifs 2 and 3 ("1xx") is still capable of binding two actin molecules (see Figure 4.14 in Chapter 4). In this complex, one actin molecule is likely to be bound by RPEL1 since additional abrogation of RPEL1 function ("xxx") abolishes actin binding in the gel filtration assay. The second actin molecule may represent actin 2, which appears to be recruited by an actin-RPEL1 contact, possibly through water-mediated actin 1-actin 2 interactions (see Chapter 6 for a more detailed discussion).

To characterise the RPEL1-2 linker interaction, I asked whether a 16-amino acid RPEL1-2 linker peptide encompassing residues L96 to R111 was sufficient to bind actin. Since we do not have any evidence for a MAL-actin interaction involving the sequences between RPEL motifs 2 and 3, I used an RPEL2-3 linker peptide spanning the entire sequence between the PFAM-defined RPEL motif, residues E138 to A159, as a control. Using the fluorescence anisotropy assay, I did not observe any measurable actin binding by the RPEL1-2 linker peptide, suggesting that it is not able to bind actin autonomously (Figure 5.16). I cannot, however, rule out that this results from misfolding of the peptides. An interesting possibility is that actin binding by the

RPEL1-2 linker depends on actin-actin interactions, and the gel filtration analysis does indeed suggest this. This will be further discussed in Chapter 6 (Discussion). I did not detect actin binding by the RPEL2-3 linker peptide in the fluorescence-anisotropy assay.

In order to address the functional relevance of actin 2, I introduced point mutations into the RPEL1-2 linker, aiming to perturb its interaction with actin. F102 was exchanged for asparagine: this retains side chain length but introduces polarity at the hydrophobic position (F102N). I also mutated three key residues in the RPEL1-2 linker-actin interaction, F102, Q105 and L109 for alanine (F102A Q105A L109A). These MAL derivatives were expressed in NIH3T3 fibroblasts and their localisation observed under serum-starved conditions. Neither of the two RPEL1-2 linker mutations had any substantial effect on MAL localisation (Figure 5.15). The RPEL1-2 linkers diverge significantly between MAL and MC. In Chapter 4, I showed that the unit encompassing RPEL motifs 1 and 2 is responsible for differential regulation of MAL and MC. It is therefore possible that the RPEL1-2 linker contributes to this effect. The positions of the double alanine in MAL, A100 and A101, are occupied by threonine and glutamate in MC. In MC, the presence of a negative charge in this region might interfere with the main-chain contact established by D25 of actin in this region (see Section 5.4.1). Furthermore, the position equivalent to Q105 is occupied by proline in MC, which would certainly disrupt the helix that is present in this region in MAL (helix 3). I generated one mutant MAL derivative, AA100/101TE Q105P, reflecting these differences between MAL and MC. This derivative behaved very similarly to wild-type MAL when tested in the immunofluorescence assay. This questions the physiological relevance of actin binding by the RPEL1-2 linker, although we cannot exclude the possibility that the mutations fail to effectively abolish actin binding. This might be especially the case if actin 2 were recruited to MAL via a relatively strong interaction with actin 1. A complete analysis will also require studying the effect of these mutations at the level of transcriptional activity (see Chapter 6; Discussion).

The previous study of MAL-MC chimaeras showed that both RPEL1 and RPEL2 are required for MAL-like regulation of the MRTFs (see Section 4.7 in Chapter 4). However, in the absence of any structural information, I arbitrarily placed the cross-over points for RPEL motif exchange into the centre of the RPEL-RPEL linkers. Therefore, the actin-2 binding site was split when RPEL1 was transferred. In remains

possible that the behaviours of MAL-MC chimaeras are partially a consequence of RPEL1-2 linker disruption. To test this hypothesis and thereby further address the functional relevance of actin-2 binding, I generated two new MAL-MC chimaeras. MC-N-41-MAL contains the N-extension and RPEL1 of MC while its RPEL1-2 linker is preserved. Conversely, MAL-N-110-MC contains the N-extension, RPEL1 and the RPEL1-2 linker of MAL (Figure 5.17 A and B). I expressed the derivatives and analysed their localisation in serum-starved NIH3T3 fibroblasts (Figure 5.17 C).

MC-N-41-MAL localised very similarly to MC-N1-MAL, in which the linker was disrupted by the RPEL1 transfer (Figure 5.17 C). The RPEL1-2 linker was not able to, together with MAL RPEL1, confer MAL-characteristic localisation and activity onto MC: MAL-N-110-MC and MAL-N1-MC localised very similarly.

In conclusion, the contribution of the RPEL1-2 linker to MAL regulation remains obscure. It is likely that actin 2 represents one of the actin molecules in the MAL-actin complex resolved by gel filtration (see Figure 2.7 in Chapter 2), however, more experiments are necessary to understand its function.

5.5.4 Initial functional analysis of actin 3

5.5.4.1 Implications of direct MAL-actin 3 interactions for MAL regulation

MAL makes a very limited set of discernable direct contacts with actin 3. These, involve hydrogen bonds by R111, Q90 and Q80 of MAL, which are distributed across almost the entire length of the MAL fragment observed in the structure (see Section 5.4.1). Each of these side chains establishes contacts with the main chain of actin 3. To address whether these contacts are functionally relevant, I exchanged each of the implicated MAL residues for alanine and assessed the effect of the mutations on MAL regulation, analysing the localisation of the MAL derivatives in serum-starved NIH3T3 fibroblasts. MAL Q80A and Q90A localised like the wild-type protein, being predominantly cytoplasmic in approximately 90% of the cells (Figure 5.15). The R111A derivative, however, appeared predominantly nuclear in about 10% and pan-cellular in approximately 50% of the cells. In MC, the residue at the position equivalent to R111 is a serine. MAL R111S displays very similar distribution compared to MAL R111A. We thus conclude that R111 contributes to MAL regulation.

5.5.4.2 Contribution of R111 to actin binding by RPEL2

R111 has a helical context in the MAL(67-199)-LatB-actin structure. R111 also represents the ultimate N-terminal amino acid of the RPEL2 peptide used for crystallisation; however, it is not part of the "canonical" RPEL motif as defined by PFAM. In the RPEL2-LatB-actin complex, R111 is contributed by an extended portion of the peptide, forming a salt bridge with the side chain of D25 in actin (Figure 5.18 A). Because of the two different interactions R111 establishes in the two different structures, it is difficult to conclude why exactly the exchange of R111 results MAL de-regulation. Depending on whether the region R111 emanates from is helical or lacks secondary structure, R111 might establish different contacts.

To analyse the effect of R111 on actin binding by RPEL2, I re-addressed the RPEL2-actin affinity, using two additional RPEL2 peptides in fluorescence anisotropy experiments. One peptide encompassed an additional seven amino acids N-terminal to R111 (RPEL2+N) to potentially facilitate the formation of a helix as seen in the MAL(67-199)-LatB-actin structure (see Section 5.4.1 and Figure 5.12 C). Another peptide, synthesised in the same context as the previously studied 32-amino acid RPEL2 peptide, included an R111A mutation (Figure 5.18 B). RPEL2 bound LatB-actin with an affinity of K_d = 2.2 ± 0.2 µM (Figure 5.18 C), which is very comparable to the previously measured affinity for RPEL2 (K_d = 2.3 ± 0.2 µM; see Section 4.5 in Chapter 4). The affinity was not affected by the additional N-terminal amino acids: RPEL2+N bound actin with a K_d of 2.1 ± 0.4 µM. However, exchange of R111 for alanine decreased the affinity to K_d = 7.8 ± 0.5 µM. Therefore, R111 makes a contribution to actin binding, at least in the context of the RPEL2 peptide. The additional N-terminal seven amino acids might be unable to form a helix in the absence of an actin contact in this region. The most straightforward conclusion from this experiment and the crystal structures would be to disregard the R111-D25 interaction as an experimental artefact. However, we cannot exclude the possibility that, when extending from a non-helical peptide chain, the R111-D25 salt bridge can occur in a MAL-actin complex (see Chapter 6; Discussion). Indeed, the substitution of R111 for alanine or serine has a deregulating effect on MAL (see Figure 5.15).

5.6 Summary

In this chapter, I have presented our initial approach for the determination of MAL-actin structures by X-ray crystallography, which posed obstacles at each stage of the process, which had to be overcome. These include protein production, MAL-actin complex formation, crystal optimisation, optimisation of diffraction quality and structure determination. I have described the crystal structures of three MAL-actin complexes: RPEL1 and RPEL2 bound to LatB-actin and that of a complex between MAL(67-199) and LatB-actin.

Both RPEL motifs 1 and 2 contact actin via three conserved structural elements: helix 1 binds the hydrophobic cleft at the subdomain 1-3 interface of actin; helix 2 engages in hydrophobic interactions with the subdomain-3 platform at the base of actin subdomain 3, and a connector between the two helices, which adopts an extended conformation and makes several, mainly polar contacts with actin.

The complex of the RPEL domain with LatB-actin contains three actin molecules. The RPEL1-actin ("actin 1") contact site in the context of the RPEL domain shares the general features of the RPEL1 peptide-actin interaction. However, the predicted critical regulatory sites, the basic B2 region of MAL and RPEL3, are absent from this crystal structure. Surprisingly, the structure shows an actin molecule ("actin 2") bound to the sequence that links RPEL motifs 1 and 2. Indirect, water-mediated hydrogen bonds between actins 1 and 2 are likely. A third actin molecule ("actin 3") establishes MAL-actin contacts across multiple sites along the determined MAL-main chain and directly binds actin 1. Actin binding by MAL RPEL1 is sensitive to mutations of hydrophobic amino acids that contact actin. Preliminary functional studies show that interference with helix-1 mediated RPEL-actin interactions in each of the three RPEL motifs interferes with MAL regulation. Although the RPEL1-2 linker binds actin in the context of the RPEL domain, it is not sufficient to interact with actin. So far, functional studies did not suggest any role of the RPEL1-2 linker for MAL regulation. Future work will address the contribution of structural elements of the RPEL motif for RPEL-actin interactions and elucidate the functional significance of the interactions observed in the MAL(67-199)-LatB-actin structure.

In the next chapter, Chapter 6, I will, among other points, discuss the crystal structures in the light of the results presented in Chapters 2 to 4 and draw parallels between the mode by which RPEL motifs and other actin-binding proteins engage with actin. I will also present a working model for MAL regulation by actin and discuss how

features of the crystal structures might support this model or open new hypotheses for how MAL might act as a sensor of the cellular G-actin concentration and respond to growth-factor induced G-actin depletion.

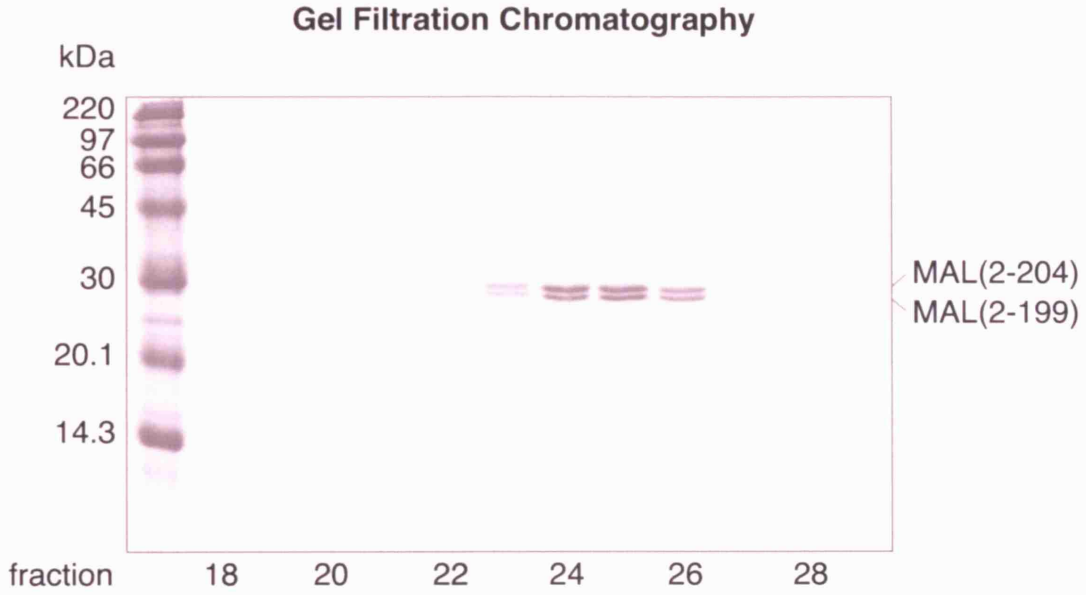

Figure 5.1 Identification of a suitable C-terminal boundary for MAL crystallisation constructs. MAL(2-204) was expressed and purified as described in Chapter 7; Materials and Methods. The last purification step entailed gel filtration chromatography on a Superose-12 column: fractions of 500 μl were collected of which 10 μl each were subjected to SDS-PAGE. The faster migrating protein fragment was identified as MAL(2-199) by mass spectrometry and N-terminal Edman sequencing.

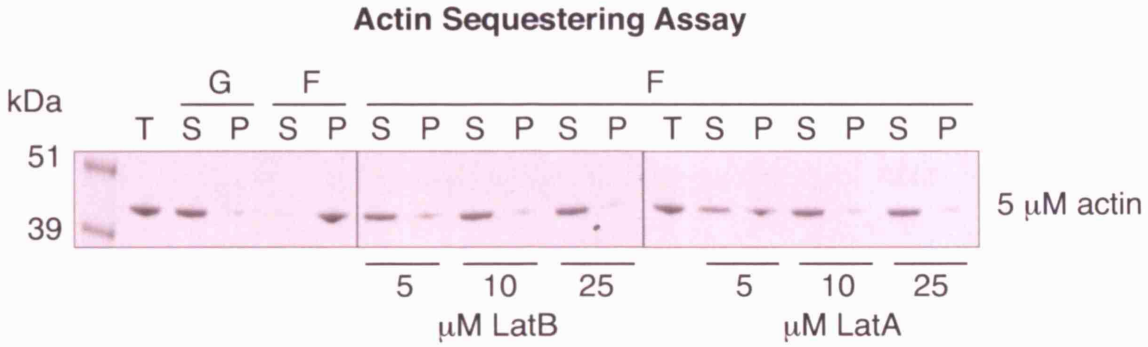

Figure 5.2 Latrunculins sequester actin monomers from polymerisation with similar efficiency. (Skeletal-muslce α) G-actin at a concentration of 5 μM was incubated for 45 min with the indicated amounts of latrunculin B (LatB) or latrunculin A (LatA) before actin polymerisation was initiated and allowed to proceed for 30 min. F-actin was separated from G-actin by ultracentrifugation and equivalent amounts of supernatants and pellets analysed by SDS-PAGE and Coomassie brilliant blue staining.

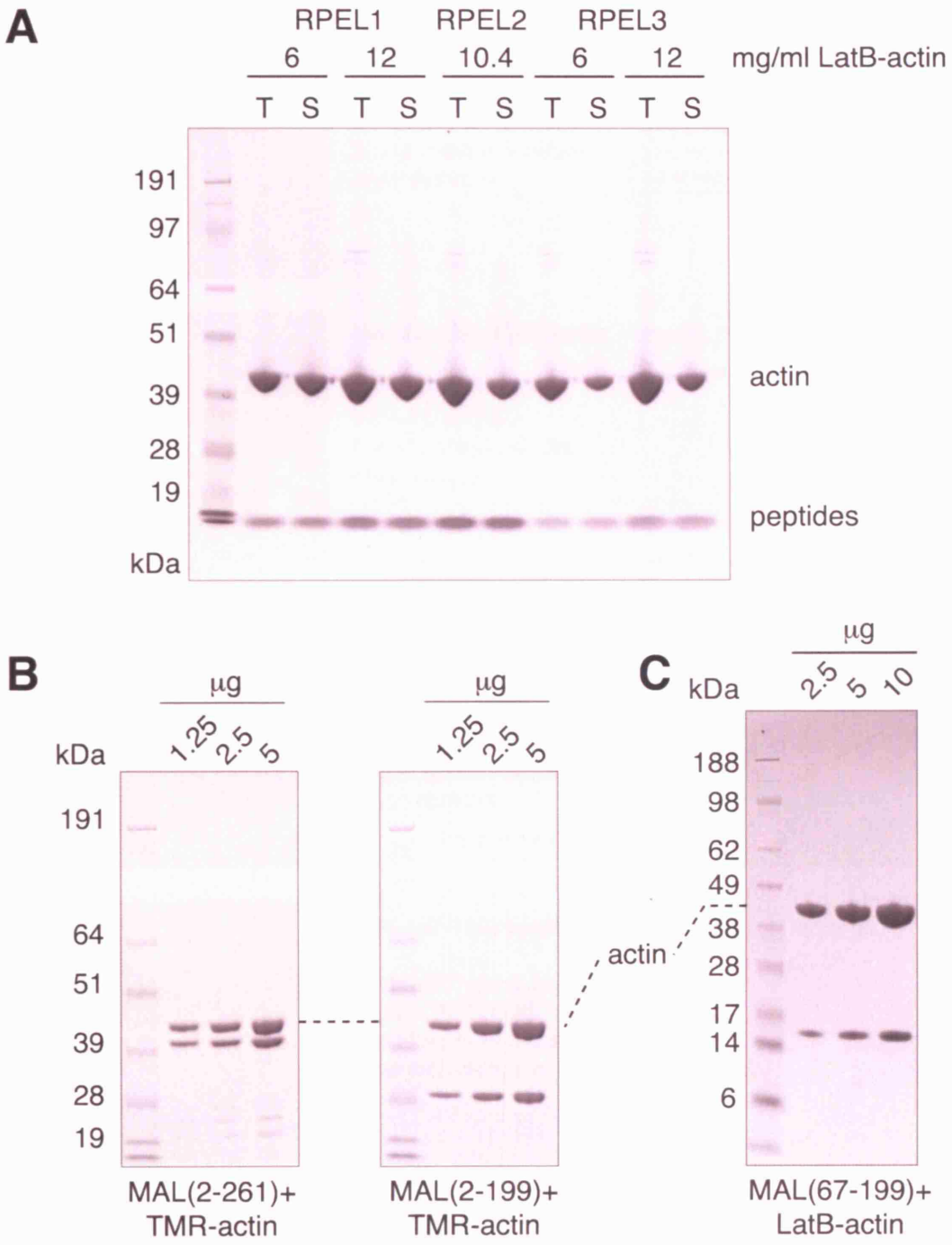

Figure 5.3 Preparation of MAL-actin complexes for crystallisation. (**A**) Complexes of latrunculin B- (LatB-)actin (skeletal-muslce α isoform) and RPEL peptides. LatB-actin at the indicated concentrations was mixed with a three-fold molar excess of the indicated peptides. After co-incubation, the samples were ultracentrifuged to remove precipitate. 0.5 µl of the total samples (T) and supernatants (S) were subjected to SDS-PAGE (in MOPS-based buffer) and Coomassie brilliant blue staining. (**B**) Complexes of TMR-actin with MAL(2-261) and MAL(2-199). (**C**) Complex of LatB-actin with MAL(67-199). MAL derivatives were mixed with an equimolar amount of TMR-actin (B) or a three-fold molar excess of LatB-actin (C). The indicated amounts were subjected to SDS-PAGE (B, in MOPS-based buffer; C, in MES-based buffer) and Commassie brilliant blue staining. See Chapter 7 (Materials and Methods) for details on complex preparation.

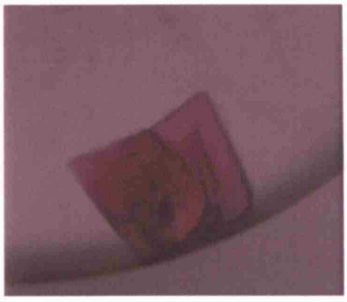

A

TMR-actin (-RPEL1); 5.7 mg/ml

0.1 M Tris-HCl pH 7.5
30% PEG 2000 MME
0.3 M calcium acetate
cryo: paraton

condition for TMR-ADP-actin crystals
(Otterbein et al., 2001):
0.01 M Tris-HCl pH 7.0
22% PEG 2000 MME
0.2 M calcium acetate

B

MAL(2-199)-TMR-actin; 7 mg/ml; microseeding

0.1 M BTP pH 8.5
28% PEG 3350
0.3 M sodium nitrate
cryo: paraton

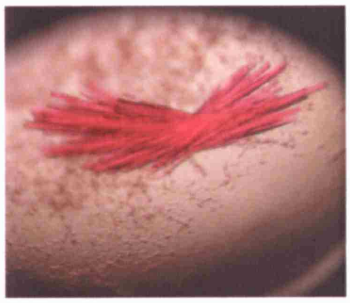

C

MAL(67-199)-TMR-actin
25 mg/ml

0.1 M BTP pH 7.5
20.5% PEG 3350
0.2 M sodium sulfate
cryo: paraton

+ 4% acetonitrile →

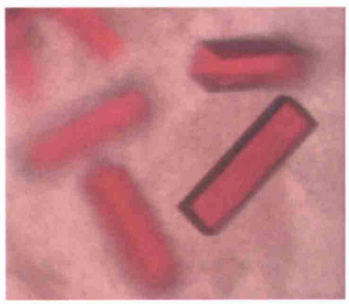

D

MAL(67-199)-LatB-actin; 25 mg/ml

0.1M BTP pH 8.25
20.5% PEG3350
0.4 M sodium nitrate
cryo with dehydration (see Figure 5.6)

E

MAL RPEL1-LatB-actin
12 mg/ml

0.1 M sodium cacodylate pH 6.5
0.15 M potassium thiocyanate
15% PEG 6000
cryo: 20% glycerol

RPEL2-LatB-actin
10.4 mg/ml

MES pH 6.0
20.5% PEG 6000
cryo: 20% glycerol

Figure 5.4 MAL-actin complex crystals. After optimisation, crystals of the indicated complexes were obtained under the conditions shown. Cryoprotectants are indicated.
Crystallogenesis was performed by Stephane Mouilleron.

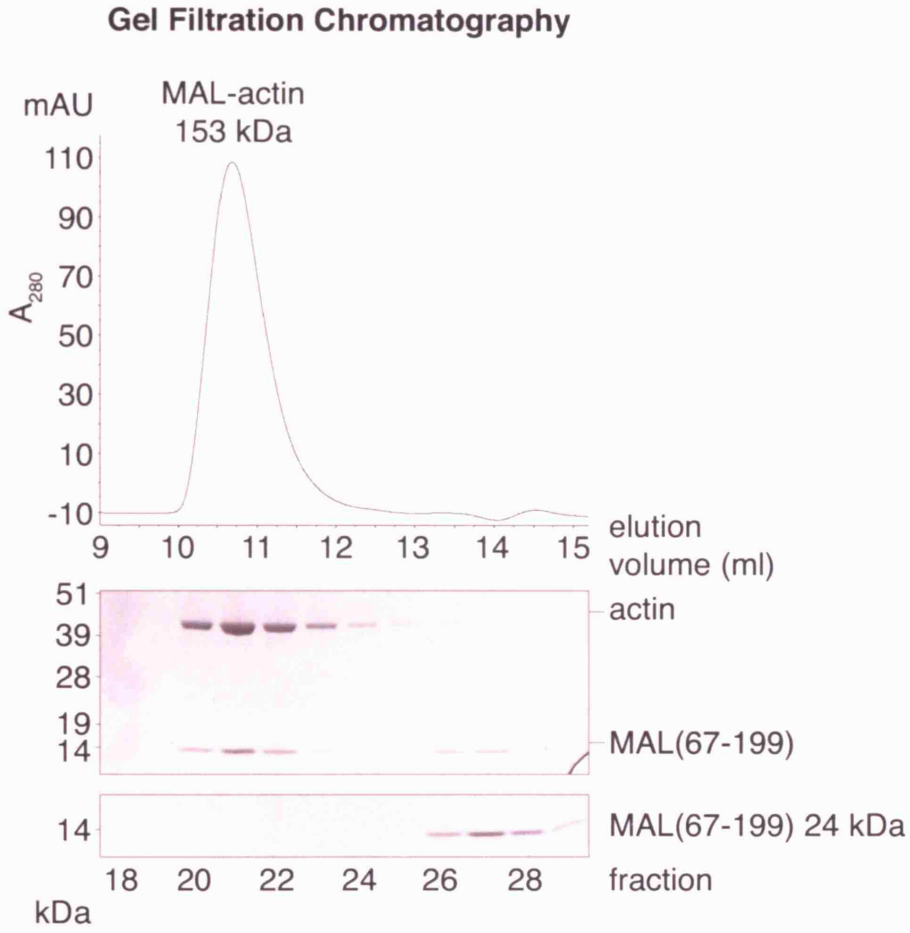

Figure 5.5 MAL(67-199) forms a stable complex with three actin molecules. 10 µM MAL(67-199) were incubated with 30 µM (skeletal-muslce α) G-actin. The complex was prepared as shown in Figure 2.7 and analysed by gel filtration chromatography. Top, chromatogram; bottom, analysis of fractionated eluates by SDS-PAGE and Coomassie brilliant blue staining.

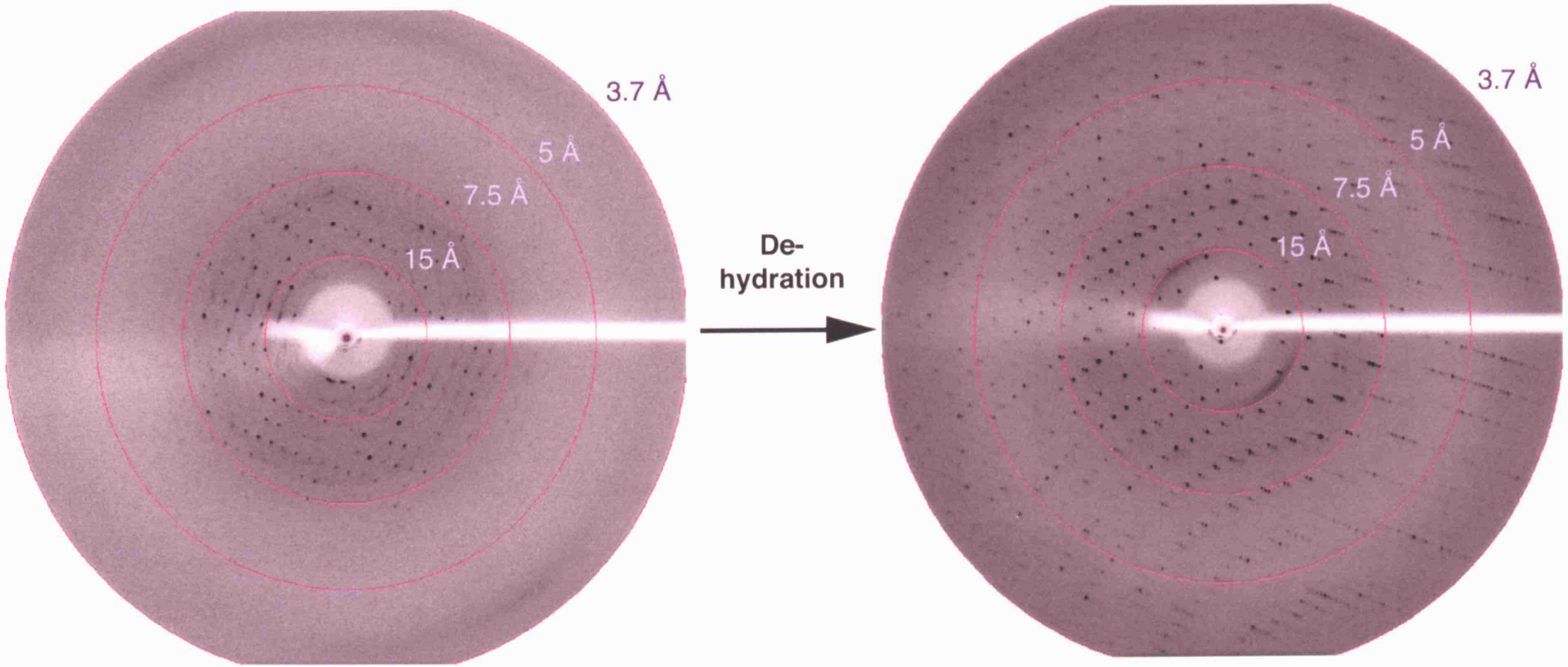

Figure 5.6 Dehydration vastly improves X-ray diffraction by MAL(67-199)-LatB-actin crystals. MAL(67-199)-LatB-actin crystals grown in 0.1 M BTP pH 8.25, 20% PEG 3350; 0.2 M sodium nitrate were placed into the crystallisation butter containing 25% PEG 3350 and 20% ethylene glycol for 15 min. The crystals were then transferred into the equivalent buffer containing 30% PEG 3350 and 10% ethylene glycol, and air dehydration was allowed to proceed for several hours while ensuring that crystals were recovered before PEG 3350 precipitated. The crystals were then directly frozen in liquid nitrogen analysed by X-ray diffraction at the home X-ray source.
The experiment was carried out by Stephane Mouilleron.

Figure 5.7 RPEL motifs 1 and 2 bind actin in a similar mode.

see overleaf

(**A**) Representation of the RPEL1-actin interaction. Left, "classical" actin front view; right, view onto the base of the actin subdomain 1-3 interface. Actin subdomains are indicated. Latrunculin B carbons are shown in pink and those of ATP in orange. (**B**) As (A) for the RPEL2-actin interaction. A MES molecule occupies a pocket at the actin subdomain 1-3 interface. (**C**) Superposition of the RPEL1-actin and RPEL2-actin structural models shown in (A) and (B). The hydrophobic cleft and the subdomain-3 platform of actin are indicated. (**D**) Close-up view of (C) with nomenclature of the structural components of the RPEL peptides and key residues indicated.

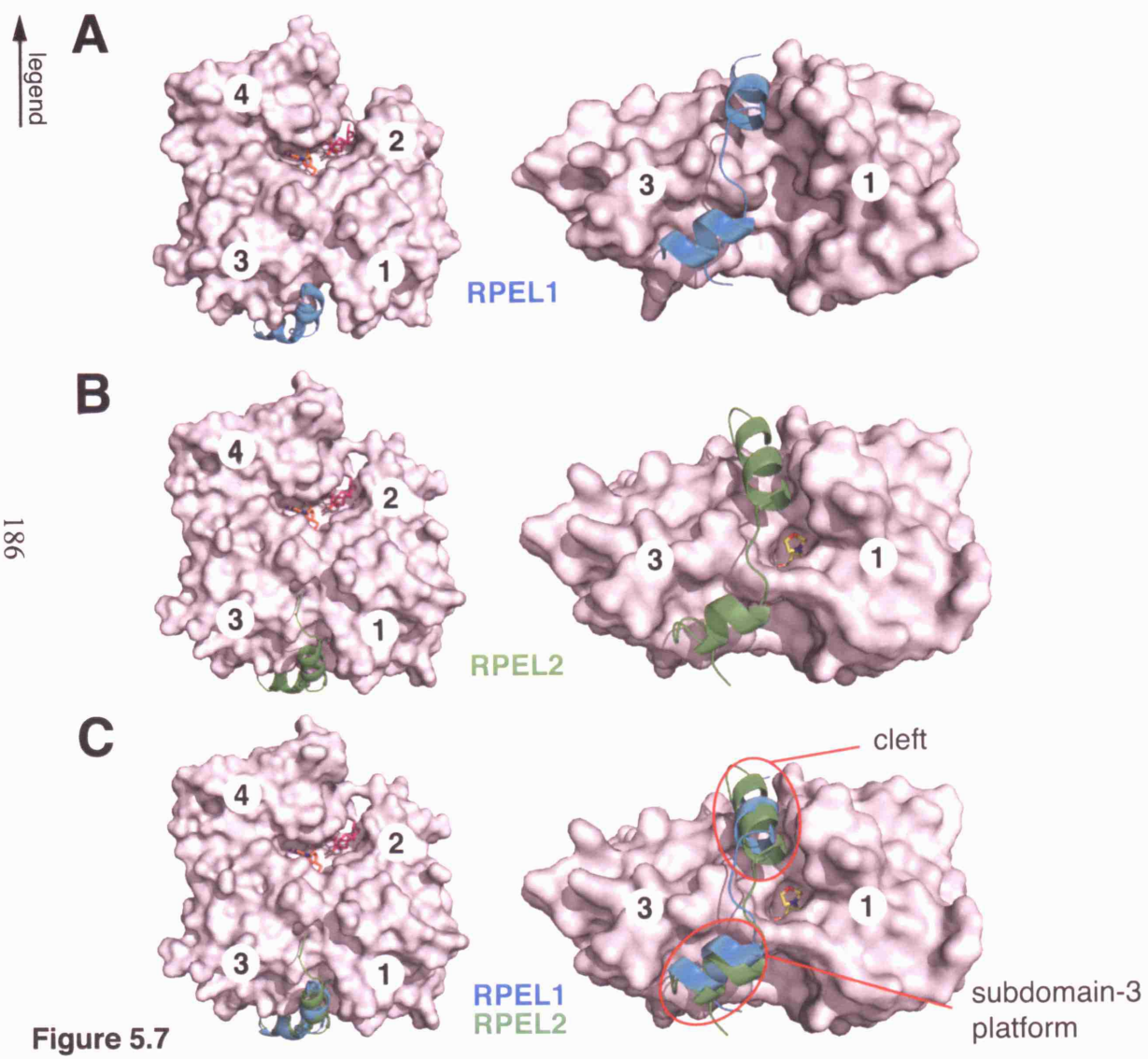
legend
A
4
2
3
1
RPEL1
3
1
B
4
2
3
1
RPEL2
3
1
C
4
2
3
1
RPEL1
RPEL2
cleft
3
1
subdomain-3
platform
D
RPEL1
RPEL2
HELIX 1
L74
L118
L78
I122
CONNECTOR
3
R81
R125
L87
L131
I92
I136
1
HELIX 2
M93
L137

Figure 5.7

Figure 5.8 Interactions of RPEL1 and RPEL2 with actin.

see overleaf

The RPEL1-actin interaction is shown on the left and that of RPEL2 on the right. Hydrogen bonds and electrostatic interactions are indicated. The side chains of T83 and R84 in RPEL1 and E127 and R128, whose main chains engage in hydrogen bonds, are not shown for simplicity.

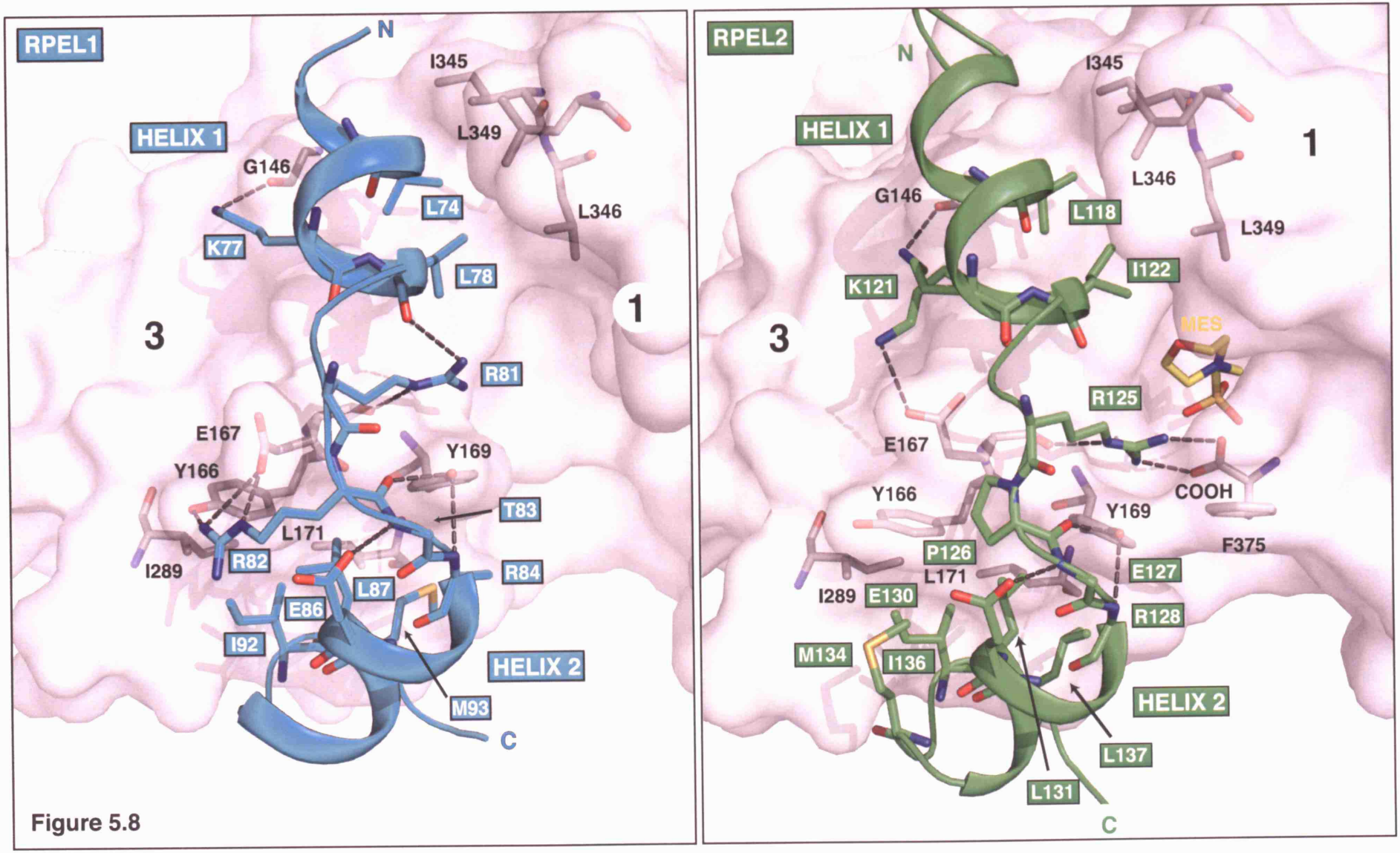
legend
RPEL1
N
I345
L349
L346
HELIX 1
G146
L74
K77
L78
1
3
R81
E167
Y169
Y166
T83
L171
R82
I289
R84
L87
E86
I92
HELIX 2
M93
C
RPEL2
N
I345
HELIX 1
1
L346
G146
L118
L349
K121
I122
MES
3
R125
E167
COOH
Y166
Y169
F375
P126
L171
E127
I289
E130
R128
M134
I136
HELIX 2
L137
L131
C

Figure 5.8

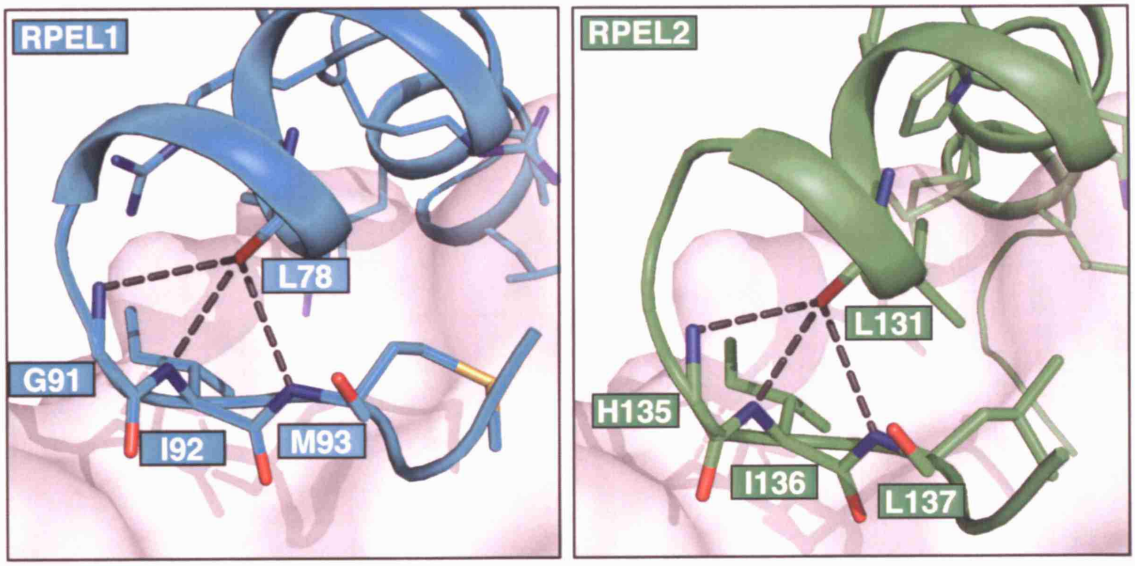

Figure 5.9 The segment which follows helix 2 of the RPEL peptides is stabilised by hydrogen bonds. Hydrogen bonds involving the main-chain carbonyl groups of the indicated residues (L78 and L131) in helix 2 stabilise the following non-helical segment. Three consecutive residues of the non-helical segment are involved. The side chain of H135 in RPEL2 is not shown for simplicity.

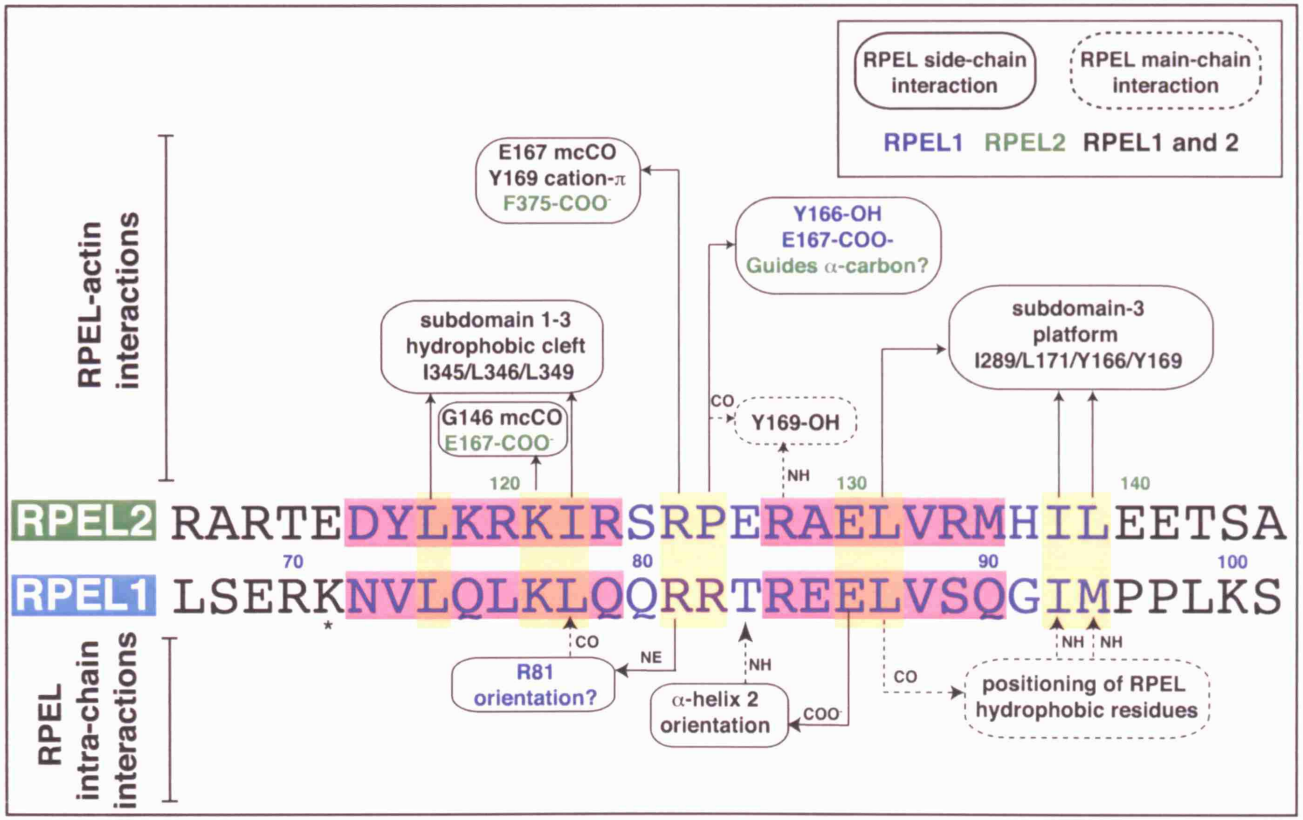

Figure 5.10 Diagram representing interactions observed in the RPEL-actin structures. Helices 1 and 2 are highlighted in pink and residues that maintain conserved interactions with actin (labelled above sequences) or within the RPEL motif (labelled below sequences) in yellow. Rounded rectangles with solid lines indicate side-chain mediated interactions while those with dashed lines describe main-chain interactions. Interactions that are conserved between RPEL motifs 1 and 2 are shown in black and RPEL1- and RPEL2-specific ones in blue and green, respectively. CO, carbonyl group; COO^-, carboxyl group; OH, hydroxyl group; NH, amino group; mcCO, main-chain carbonyl group. See Figure 5.8 for the corresponding structural representations. In a MAL(67-199)-LatB-actin structure shown later in this chapter (see Figures 5.11 and 5.12), K71 of RPEL1 (indicated by *) interacts with actin. Compare to Figure 6.4 in Chapter 6 for sequence conservation across all known RPEL motifs. The interaction map was provided by Stephane Mouilleron.

Figure 5.11 Overview of the latrunculin B-MAL(67-199) crystal structure.

see overleaf

The three actin molecules are shown in blue, yellow and green, respectively, and MAL in purple. N- and C-termini of the resolved MAL fragment and actin subdomains are indicated. The colour-coded sequence indicates the extent to which the amino acids of MAL(67-199) are accounted for by the electron density; RPEL motifs as defined by PFAM (Finn et al., 2006) are shaded in grey. The 'GPGS' sequence preceding L67 derives from the MAL(67-199) expression construct.

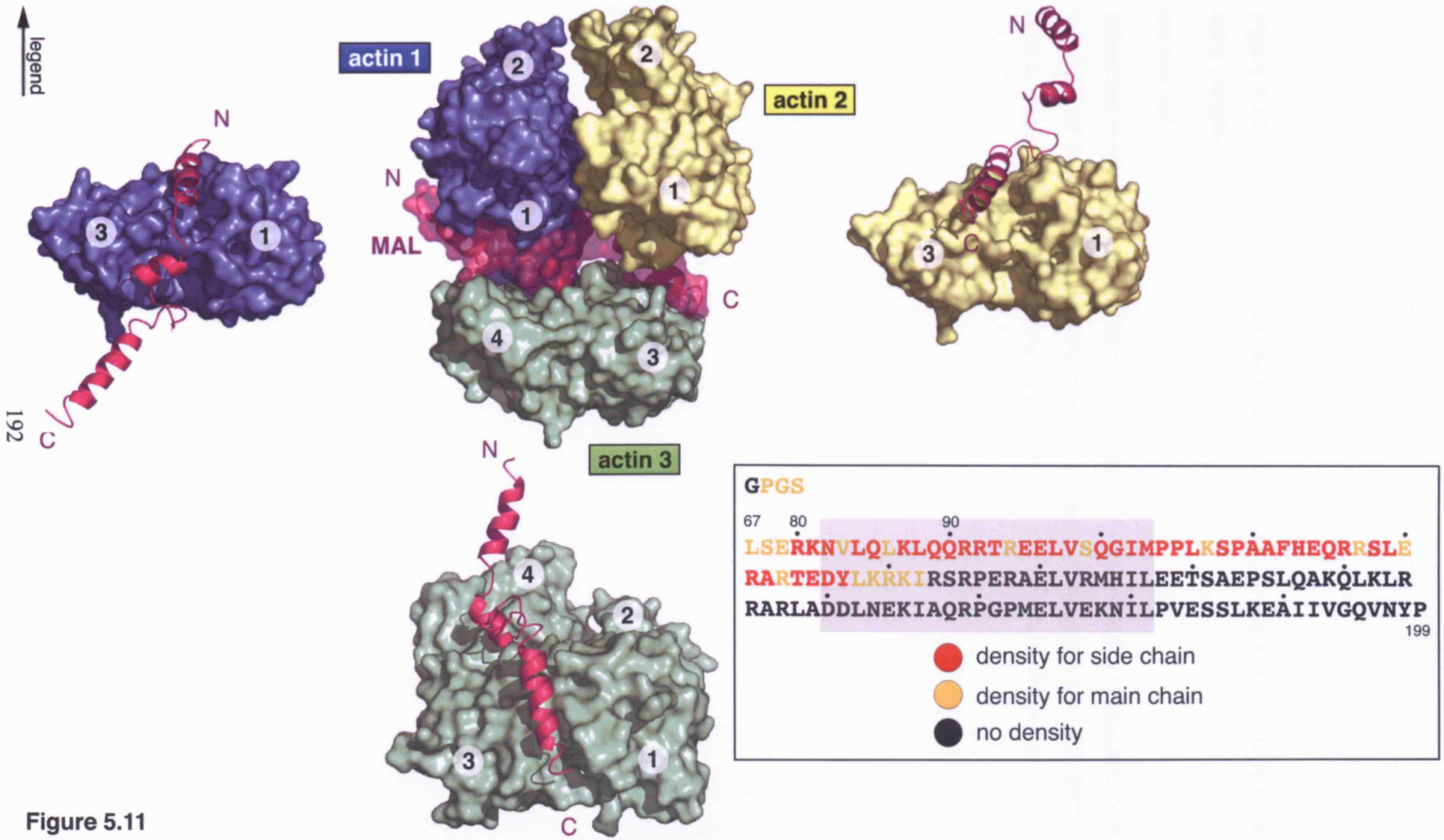
legend
N
C
192
actin 1
actin 2
actin 3
MAL
N
C
GPGS
67 80 90
LSERKNVLQLKLQQRRTREELVSQGIMPPLKSPAAFHEQRRSLE
RARTEDYLKRKIRSRPERAELVRMHILEETSAEPSLQAKQLKLR
RARLADDLNEKIAQRPGPMELVEKNILPVESSLKEAIIVGQVNYP
199
density for side chain
density for main chain
no density

Figure 5.11

Figure 5.12 Interactions of the three actin molecules in the MAL(67-199)-LatB-actin complex.

see overleaf

Interacting residues of actin are labelled in black and those of MAL in magenta. A100 and A101 of MAL, whose main-chain atoms engage in hydrogen bonds with D25 of actin 2, are not labelled. Actin colours and numbering are identical to Figure 5.11.

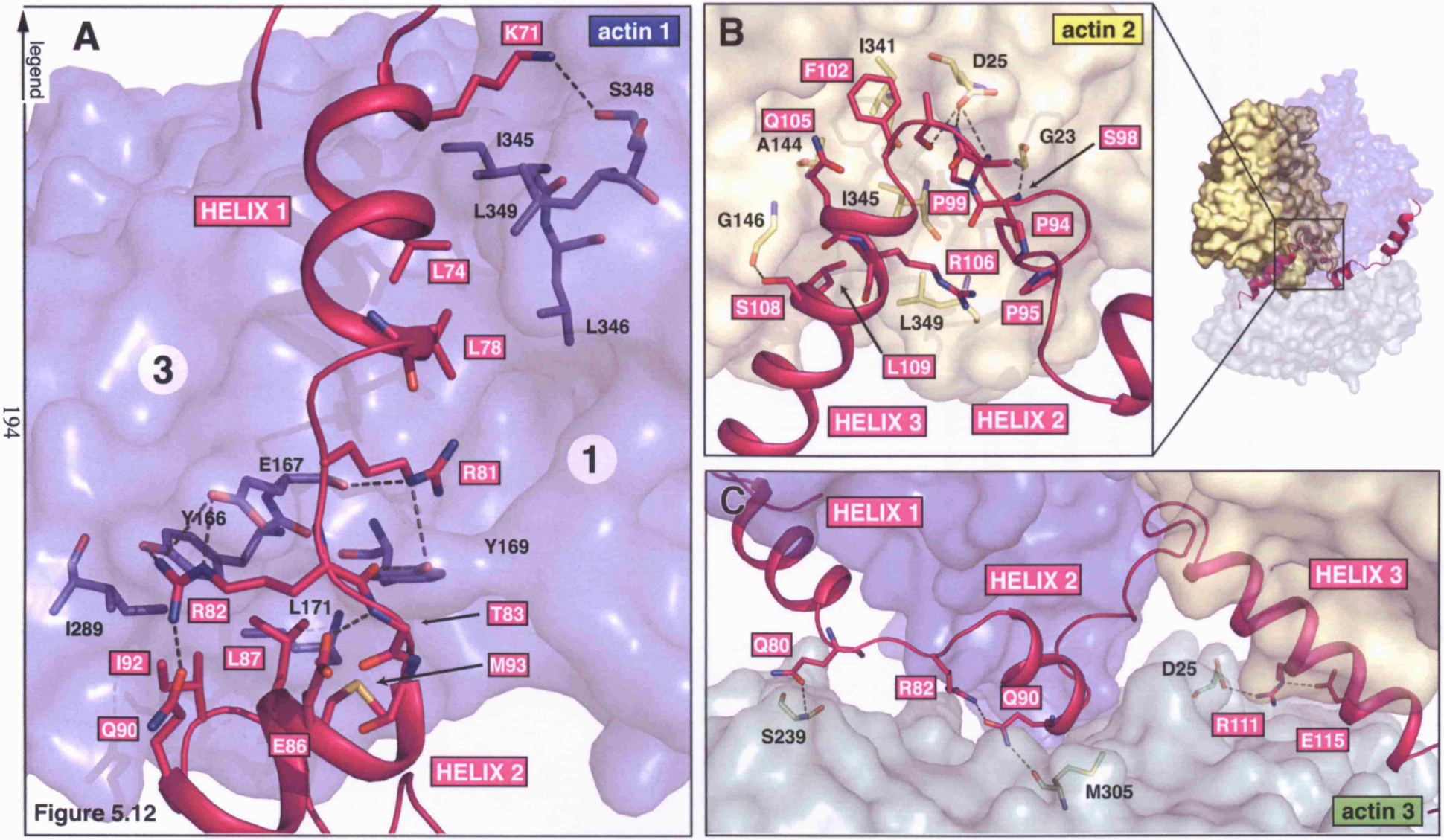
A
legend
actin 1
K71
S348
I345
HELIX 1
L349
L74
L346
L78
3
1
E167
R81
Y166
Y169
I289
R82
L171
T83
I92
L87
M93
Q90
E86
HELIX 2
B
actin 2
I341
D25
F102
Q105
A144
G23
S98
I345
P99
G146
P94
R106
S108
L349
P95
L109
HELIX 3
HELIX 2
C
HELIX 1
HELIX 2
HELIX 3
Q80
D25
R82
Q90
R111
E115
S239
M305
actin 3

Figure 5.12

Figure 5.13 Direct interaction between actins 1 and 3 in the MAL(67-199)-LatB-actin complex.

see overleaf

(**A**) Cartoon representation of the MAL(67-199)-LatB-actin complex with colours as in Figure 5.15. The enlargement shows direct contacts between the indicated residues in actin 1 and actin 3. (**B**) Superposition of actin 3 (green; ATP in orange and element colours) and uncomplexed ATP-AP-actin (ATP in grey and element colours, 2HF4, Rould et al., 2006; Whitehurst et al.). The side chains of relevant residues are shown.

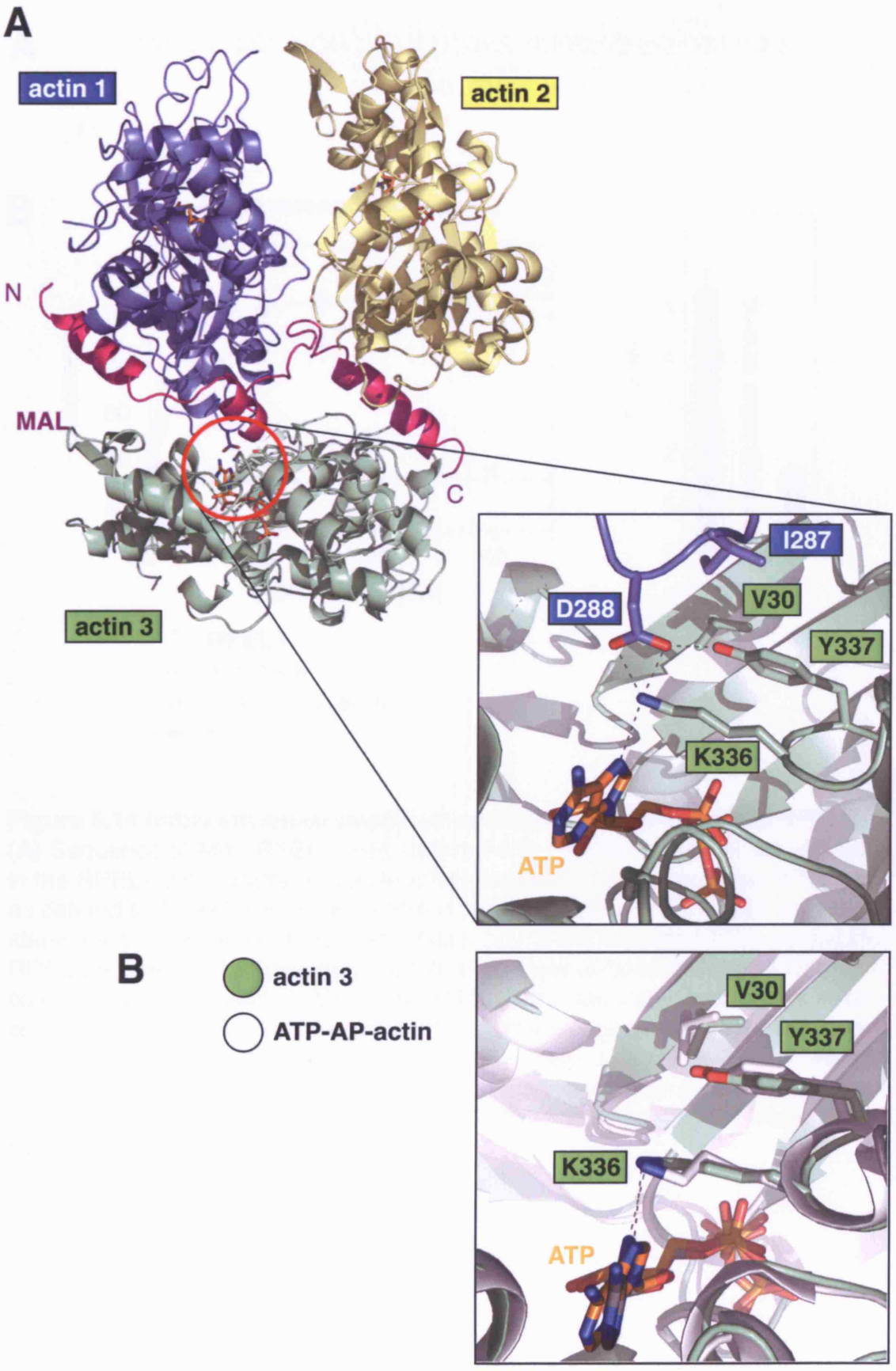

legend

Figure 5.13

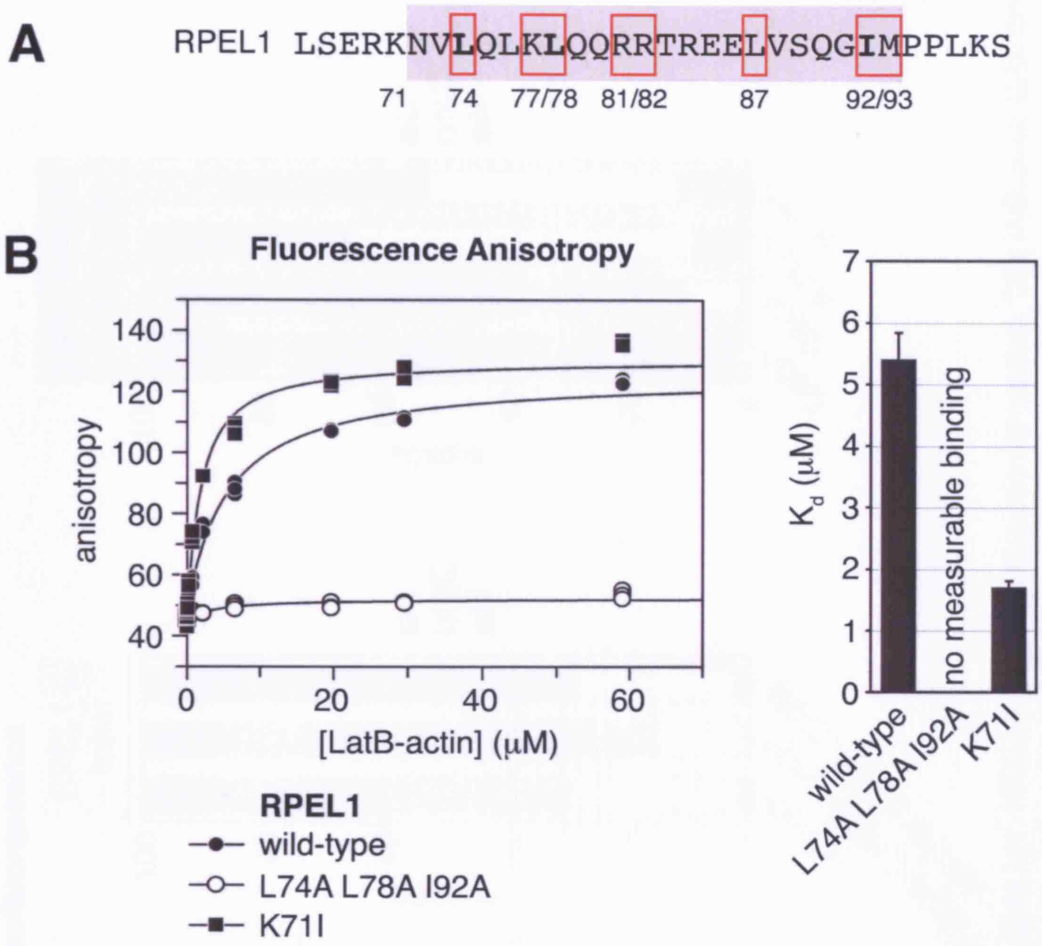

Figure 5.14 Initial structure-based actin-binding analysis of MAL RPEL1. (**A**) Sequence of MAL RPEL1. Key amino acids making direct contact with actin in the RPEL1-actin crystal structure are indicated by red boxes. The RPEL motif as defined by PFAM (Finn et al., 2006) is shaded in grey. Amino acids mutated to alanine are shown in bold. (**B**) Left, anisotropy of the indicated FITC-conjugated RPEL peptides at 0.5 μM measured over a range of latrunculin B- (LatB-)actin concentrations (skeletal-muslce α isoform). Right, plot of equilibrium dissociation constants (K_d) of RPEL-actin interactions as determined by non-linear regression (n=3 parallel experiments; error bars, SD). The data for wild-type RPEL1 are from Figure 4.7 B; these were obtained in parallel to the other data shown here and are displayed for comparison. See Figure 4.7 A for a schematic representation of the fluorescence anisotropy assay.

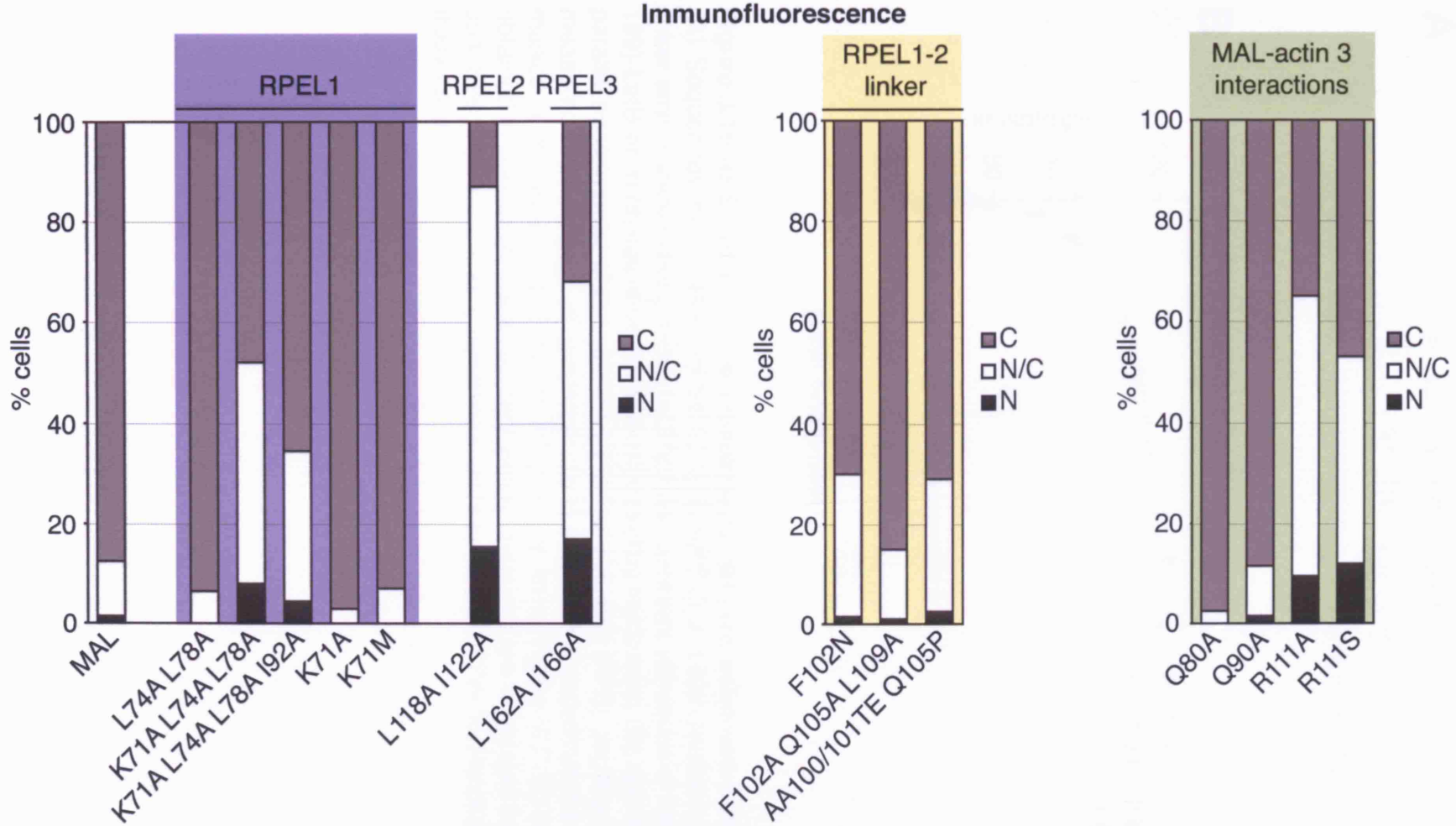

Figure 5.15 An initial analysis of MAL regulation based on the MAL(67-199)-latrunculin B-actin structure. The indicated MAL derivatives were expressed in NIH3T3 fibroblasts, which were serum-starved and subjected to immunofluorescence microscopy. Localisation was scored in 200 cells (N, nuclear; N/C, pan-cellular; C, cytoplasmic; see Figure 8.1 for an explanation of the localisation scoring system). Colour coding refers to colours of actins 1, 2 and 3 in Figure 5.11.

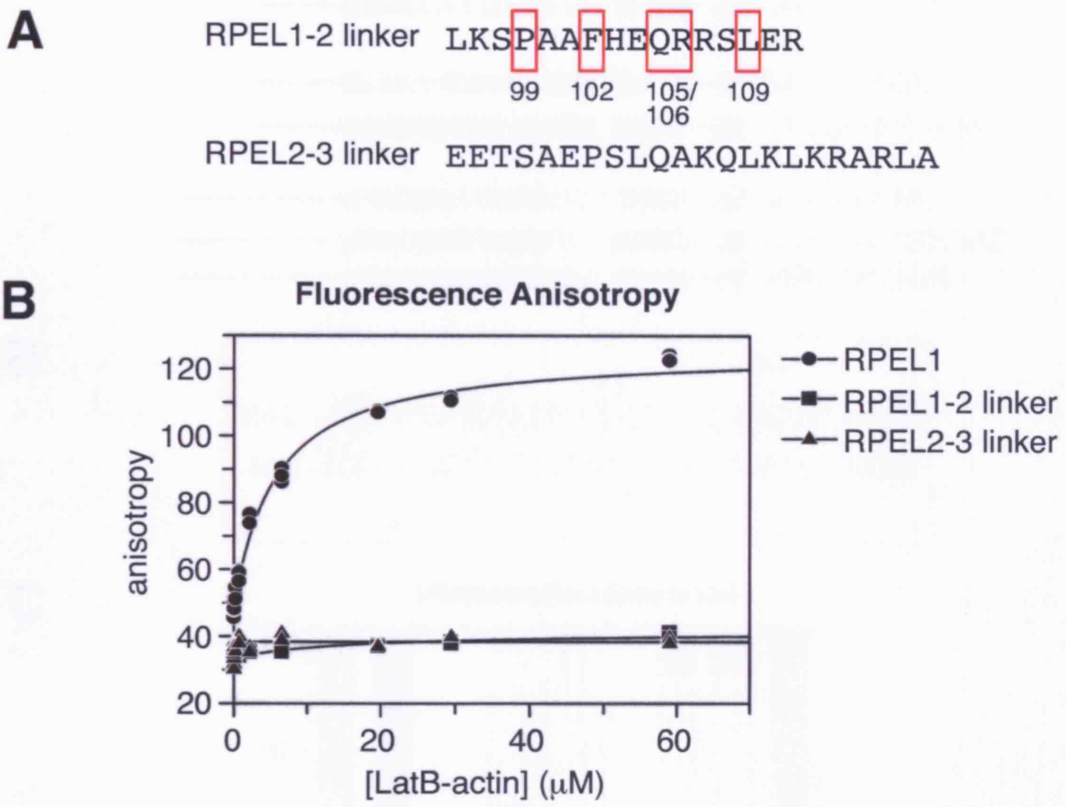

Figure 5.16 RPEL-RPEL linker peptides do not bind actin autonomously. (**A**) Sequences of the MAL RPEL1-2 and RPEL2-3 linker peptides. RPEL1-2 linker amino acids making direct hydrophobic contacts with actin in the MAL(67-199)-LatB-actin crystal structure are indicated by red boxes. (**B**) Anisotropy (n=3 parallel experiments) of the indicated FITC-conjugated RPEL peptides at 0.5 μM measured over a range of latrunculin B- (LatB-)actin concentrations (skeletal-muslce α isoform). The data for RPEL1 are from Figure 4.7 B; these were obtained in parallel to the other data shown here and are displayed for comparison. See Figure 4.7 A for a schematic representation of the fluorescence anisotropy assay.

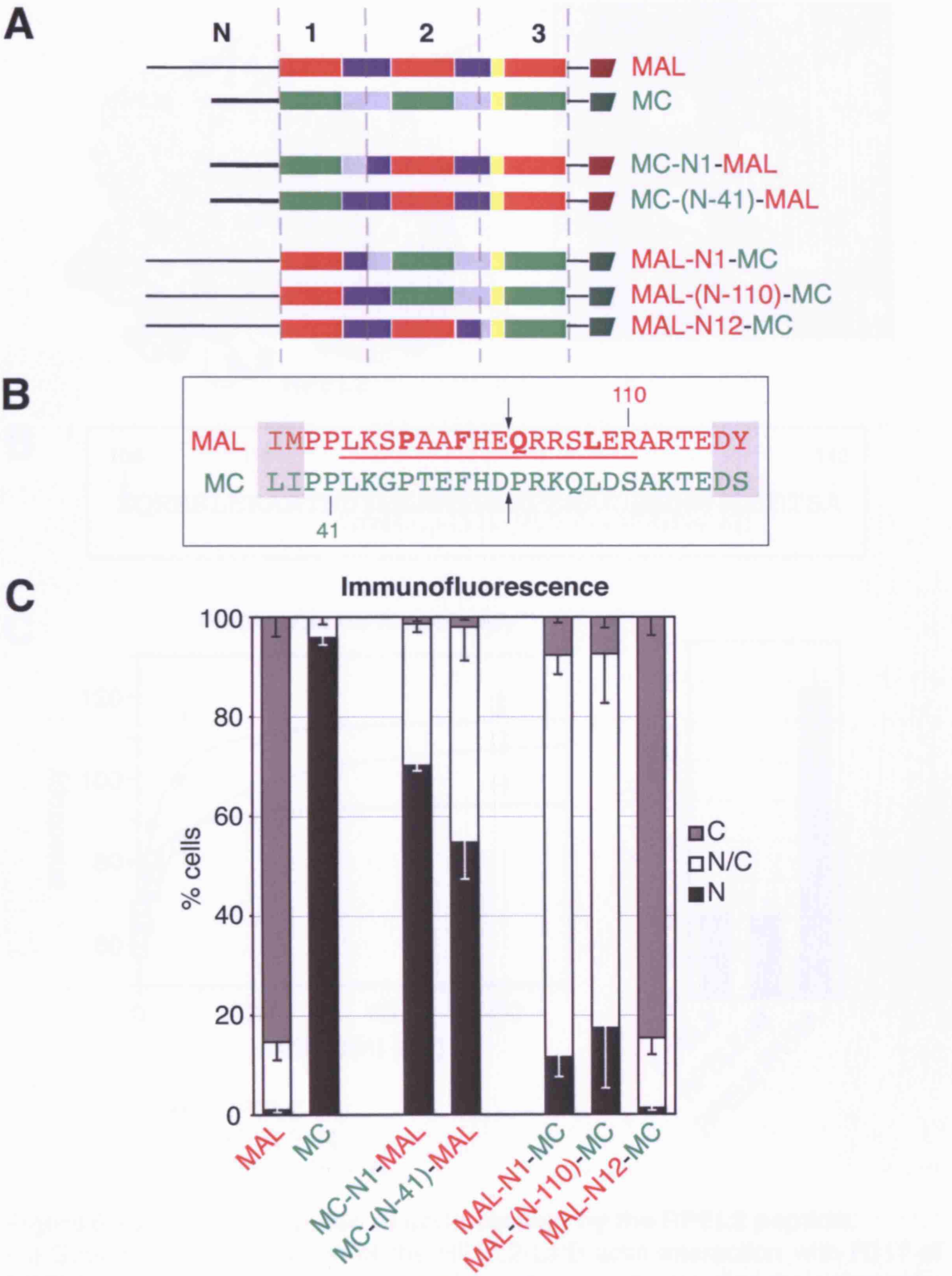

Figure 5.17 Disruption of the RPEL1-2 linker does not contribute to the regulatory behaviours of the MAL-MC chimaeras studied previously.
(**A**) Schematic representation of MAL-MC chimaeras with MAL-derived sequences in red and dark blue, MC-derived sequences in green and light blue. N, N-extension; numbers indicate RPEL motifs. (**B**) Sequences of the MAL (red) and MC (green) RPEL1-2 linkers. The arrows indicate the previous cross-over positions. Residues defined as RPEL motif by PFAM are shaded in grey. (**C**) Localisation of transiently expressed chimaeras as shown in (A) in serum-starved NIH3T3 fibroblasts, scored in 200 cells (N, nuclear; N/C, pan-cellular; C, cytoplasmic; see Figure 8-1 for an explanation of the localisation scoring system).

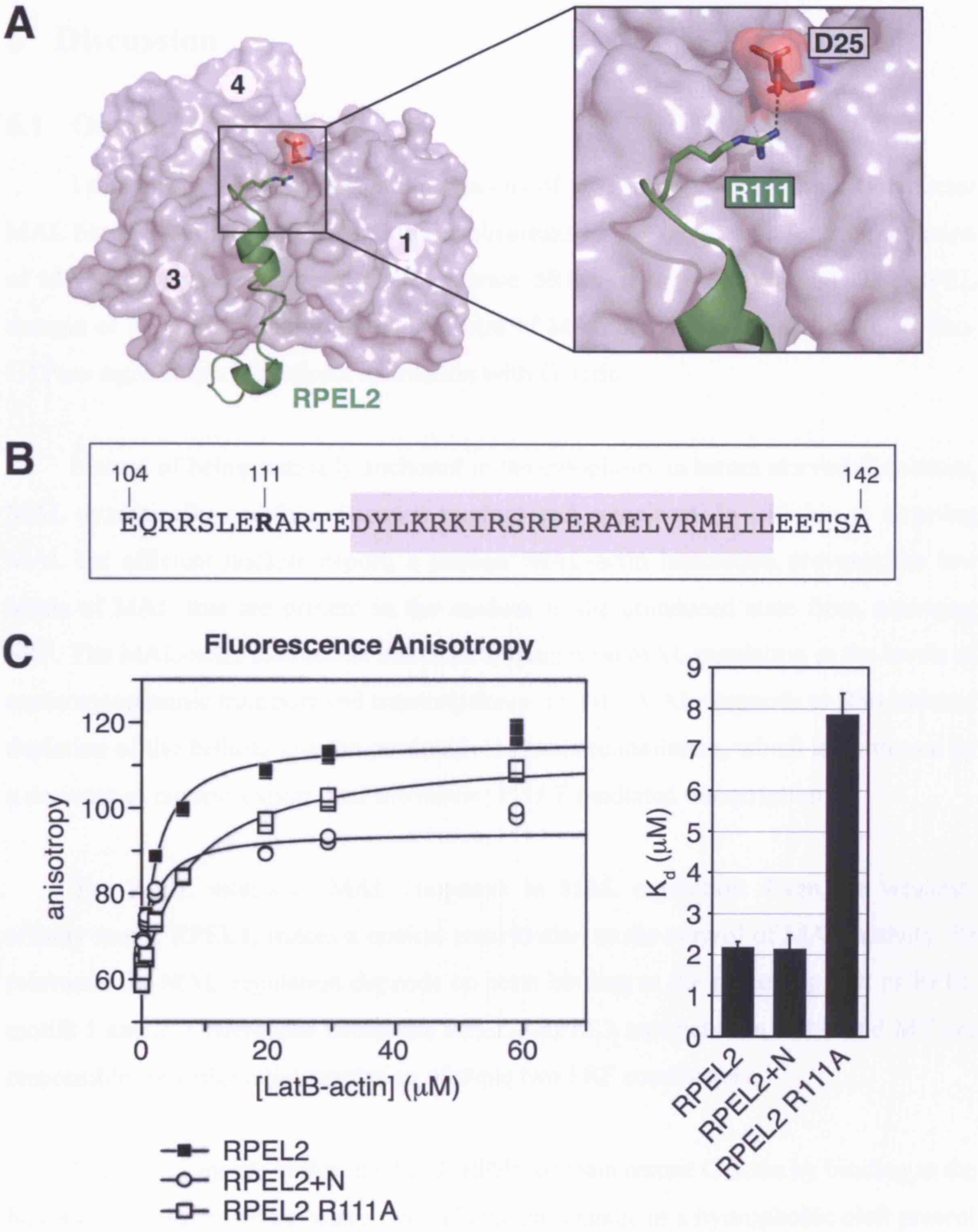

Figure 5.18 R111 contributes to actin binding by the RPEL2 peptide.
(**A**) Structural representation of the RPEL2-LatB-actin interaction with R111 of RPEL1 and D25 of actin shown as sticks and coloured according their elements. (**B**) Sequence of the RPEL2 peptides: RPEL2, residues 111-142; RPEL2+N, residues 104-142. The RPEL2 sequence as defined by PFAM (Finn et al., 2006) is shaded in grey. (**C**) Left, anisotropy of the indicated FITC-conjugated RPEL peptides at 0.5 μM measured over a range of LatB-actin concentrations (skeletal-muslce α isoform). Right, plot of equilibrium dissociation constants (K_d) of RPEL-actin interactions as determined by non-linear regression (n=3 parallel experiments; error bars, SD). Note that the longer RPEL2+N peptide shows a smaller anisotropy change upon actin binding. See Figure 4.7 A for a schematic representation of the fluorescence anisotropy assay.

6 Discussion

6.1 Outline

I this thesis, I have presented an analysis of the mode by which the SRF cofactor MAL binds G-actin and addressed the implications of this interaction for the regulation of MAL activity, i.e. its potential to activate SRF-mediated transcription. The RPEL domain of MAL is an important determinant of MAL activity as it links MAL to Rho-GTPase signalling via its direct interaction with G-actin.

Instead of being statically anchored in the cytoplasm, in serum-starved fibroblasts, MAL dynamically circulates between nucleus and cytoplasm. In addition to targeting MAL for efficient nuclear export, a nuclear MAL-actin interaction prevents the low levels of MAL that are present in the nucleus in the uninduced state from activating SRF. The MAL-actin interaction therefore impinges on MAL regulation at the levels of nucleocytoplasmic transport and transcriptional activity. MAL responds to Rho-induced depletion of the cellular G-actin pool with nuclear accumulation, which is conferred by a decrease in nuclear export, and activation of SRF-mediated transcription.

The RPEL motifs of MAL cooperate in MAL regulation. Even the weakest-affinity motif, RPEL3, makes a critical contribution to the control of MAL activity. Its relevance for MAL regulation depends on actin binding to the preceding unit of RPEL motifs 1 and 2. Differences within the RPEL1-RPEL2 unit between MAL and MC are responsible for differential regulation of these two SRF coactivators.

The RPEL motifs within the MAL RPEL domain recruit G-actin by binding to the base of the actin molecule, using two helices that engage in a hydrophobic cleft present at the actin subdomain 1-3 interface and a site on the base of subdomain 3, termed the subdomain-3 platform, respectively. An extended segment connecting the two helices, the connector, mainly contributes polar contacts to the RPEL-actin interaction. The RPEL domain contains a previously unanticipated actin-binding site in the linker between RPEL motifs 1 and 2.

The data presented in the previous chapters support a model in which the MAL RPEL domain acts as a sensor of the G-actin concentration and a regulatory device that

mediates nucleocytoplasmic transport and controls activity of MAL. The G-actin sensor function of MAL is likely to involve the formation of higher-order MAL-actin complexes. The control of MAL by unpolymerised actin represents an example of a non-cytoskeletal function of the versatile actin protein.

In this chapter, I will discuss aspects of the MAL-actin interaction and present a model in which the formation of higher-order MAL-actin complexes controls MAL activity. The structural insights into MAL-actin binding will be discussed in the context of known modes of interaction between actin and its binding partners. I will outline how our current knowledge of the MAL-actin interaction supports a hypothesis by which cooperative engagement of G-actin with MAL controls MAL nucleocytoplasmic transport and activity. Future experiments will be addressed throughout this chapter.

The structural analysis presented in this chapter was performed in collaboration with Stephane Mouilleron from Neil McDonald's laboratory at the Institute.

6.2 The MAL RPEL domain is a regulatory device that binds multiple actin molecules

6.2.1 The MAL RPEL domain binds multiple actin molecules

The RPEL domain of full-length MAL directly binds G-actin without the need of an additional cofactor, efficiently sequestering the actin molecules it engages from polymerisation. The absence of F-actin binding activity is an important feature of a G-actin sensor such as the RPEL domain (see Section 2.3.1.2 in Chapter 2). In isolation, the RPEL domain is largely unstructured. Strictly speaking, the MAL N-terminus should therefore not be referred to as domain since it does not fulfil the domain definition as "independently folding structural unit". When I use the term "RPEL domain" in this thesis, it should be understood from its historic context. Rather than providing structural support to a folded actin-binding domain, RPEL motifs directly represent the actin-binding units (see Section 4.5 in Chapter 4). This means that the RPEL motif has a status of an autonomous actin-binding motif, similar to the short WH2 motif found in multiple actin-binding proteins. It is possible that secondary structure in MAL is induced upon actin binding, similarly to thymosin β4 (see Section 1.2.2.2 in Chapter 1; Introduction).

A MAL-actin complex containing three actin molecules was detected by gel filtration chromatography. Since the formation of this complex does not require a functional third RPEL motif, additional, non-RPEL-actin interactions must occur. Structural data presented in Chapter 5 identified another actin-binding site between RPEL motifs 1 and 2. Therefore, to our current knowledge, the RPEL domain of MAL contains four actin-binding sites. Gel filtration chromatography is too stringent to resolve a 1:4 MAL-actin complex, and stabilisation of the RPEL3-actin interaction by structure-based mutagenesis might facilitate the analysis of these higher-order MAL-actin complexes.

6.2.2 The MAL RPEL domain suffices for regulating nucleocytoplasmic shuttling of MAL

The RPEL domain of the full-length MAL protein is sufficient to confer nucleocytoplasmic shuttling properties on heterologous proteins such as pyruvate kinase (PK) or GFP, demonstrating that it contains both nuclear import and export signals. RPEL-domain mediated localisation is controlled through actin binding.

It should be noted that the cytoplasmic steady-state localisation of the RPEL domain-PK fusion protein was more sensitive to their expression level than that of intact, full-length MAL (data not shown). The same was the case for RPEL domain-GFP fusion proteins (Maria Vartiainen, personal communication). Since MAL regulates SRF-mediated transcription of *actin* genes (see Sections 1.2.7 and 1.3.3 in Chapter 1; Introduction), MAL overexpression may increase actin expression. Consequentially, higher G-actin concentrations might maintain regulation of MAL. Because the MAL(2-204)-PK derivative lacks regions required for activation of MAL-mediated, SRF-dependent transcription, it is possible that its transient expression does not elicit this potential homeostasis mechanism. However, it also remains possible that the expression sensitivity is a consequence of the fusion.

6.2.3 Actin-binding drugs act through interference with the MAL-actin complex

Some uncertainty has previously remained regarding the mechanism through which actin-binding drugs (see Section 1.2.6 in Chapter 1; Introduction) activate or

inhibit MAL-dependent, SRF-mediated transcription. The *in-vitro* analysis presented in Chapter 2 demonstrates unequivocally that these actin-binding drugs act at the level of MAL-actin complex formation rather than 'non-specifically' in response to cytoskeletal stress.

Latrunculin B (LatB) is compatible with MAL-actin binding, and it even increases the yield of the MAL-actin complex in the gel filtration analysis. It is likely that the apparent stabilisation of the MAL-actin complex by LatB merely results from an increased availability of unpolymerised actin competent to bind MAL. The use of recombinant, purified non-polymerisable actin mutants such as R62D (Posern et al., 2002) or blocking agents such as DNaseI without and with LatB in quantitative actin-binding assays such as fluorescence anisotropy should resolve this question. Conversely, in the presence of cytochalasin D (CD), swinholide A (SwA) or jasplakinolide (Jasp), MAL-actin complex formation is strongly impaired. The impact of these actin-binding drugs on the MAL-actin complex correlate with their specific effects on actin-MAL-SRF signalling: CD, SwA and Jasp activate MAL-dependent, SRF-mediated transcription, whereas LatB blocks serum-induced MAL activity by preventing changes in the cellular G-actin concentration through sequestering actin monomers.

It is clear from structural studies presented in Chapter 5 that at least SwA blocks the MAL-actin interaction by competing with MAL for actin binding (see Section 6.6.7). There is no structural information available for CD; however, it is likely that the basis for its action is competition with MAL for actin. Clearly, Jasp disrupts the MAL-actin complex, but it was initially chosen for the stabilisation of actin filaments, which MAL is unable to bind. CD is widely used as actin-depolymerising agent, however, even at high concentration over actin, it failed to block actin polymerisation. The effects of cytochalasins on the actin cytoskeleton are various: they include G-actin binding, filament barbed-end capping and nucleation of actin filaments (see Section 1.2.6.2 in Chapter 1; Introduction). The failure of CD to block actin polymerisation in these experiments may reflect that functions other than actin depolymerisation dominate *in vitro*, at least under the conditions used.

6.3 Multiple levels of MAL regulation by actin

It is striking that actin binding impinges simultaneously on nucleocytoplasmic transport and transcriptional activity of MAL. This is especially apparent in the analysis

of mutant derivatives of MAL in which the actin-binding activities of the RPEL motifs are impaired (see Chapter 4). In these experiments, nuclear localisation of MAL derivatives strongly correlates with their potential to activate an SRF reporter gene. However, it is clear that actin controls MAL activity at the levels of nucleocytoplasmic transport and transcription, because nuclear accumulation of MAL is not sufficient to activate SRF-mediated transcription unless the MAL-actin interaction is released (see Chapter 2).

6.3.1 Regulation of MAL activity through the control of nuclear import and export

Under basal activity of the Rho-actin signalling pathway, MAL constantly and rapidly shuttles between nucleus and cytoplasm, employing the ubiquitous CRM1-mediated nuclear export machinery (Figure 6.1, Vartiainen et al., 2007). Nucleocytoplasmic shuttling is a common phenomenon observed for multiple signal transducers that respond to extracellular signals (see Section 1.1.1 in Chapter 1; Introduction). In the case of Smad proteins, for example, nucleocytoplasmic shuttling is observed even under conditions in which the TGF-β pathway is active, although the export rate is slowed down (Section 1.1.1.3 in Chapter 1; Introduction for more information on TGF-β signalling). An interpretation for this is that Smads require the constant passage through the cytoplasm to sense the activation status of their cognate receptors.

What is the functional significance of MAL shuttling? One might argue that MAL needs to sense the G-actin concentration in the cytoplasm. This hypothesis is particularly attractive because actin is efficiently exported from the nucleus by exportin 6 (Stuven et al., 2003). Therefore, the concept of an equilibrium between G- and F-actin might not be transferable to the nuclear compartment. However, this idea does not hold true in practice: even in cells in which CRM1-mediated nuclear export is blocked by application of leptomycin B (LMB), MAL remains responsive to serum stimulation (Vartiainen et al., 2007). Therefore, it is likely that the nuclear and cytoplasmic actin pools communicate with each other. Despite the action of exportin 6, alterations in the dynamics of the actin polymerisation cycle might be reflected in the nucleus. There is evidence in support of this hypothesis: (1) the nuclear actin concentration may be in the low micromolar range, which is compatible with actin polymerisation (see Section

1.2.5.1 in Chapter 1; Introduction). (2) A recent report suggests that approximately 20% of all nuclear actin is present in actin filaments that turn over rapidly (McDonald et al., 2006).

So if MAL can respond to decreasing G-actin levels in the nucleus, what is the advantage of shuttling at all? Confining the bulk population of MAL to the cytoplasm certainly contributes to ensuring that MAL is inactive unless the Rho-actin pathway is activated. Actin binding does promote nuclear export of MAL and can, at least under certain conditions, inhibit its nuclear import (Figure 6.1 A). Changes in actin binding upon Rho activation result in the re-establishment of a new steady state that is characterised by nuclear localisation of MAL through an inhibition of nuclear export (Figure 6.1 B). Simple regulation at the level of nuclear import would reduce the number of regulatory steps to one. The regulation of nuclear export appears to confer an additional level of control to the nuclear localisation of inducible signal transducers. In fact, in the case of MAL, the basal nuclear import rate is so high that regulation occurs almost entirely via the block of nuclear export. One could speculate that dynamic shuttling of signal transducers provides a fail-safe mechanism for the control of subcellular localisation whose resistance to failure exceeds that of a simple mechanism of cytoplasmic retention. Redundancy of control at multiple levels is frequently observed in regulatory mechanisms, for example receptor tyrosine kinases (RTKs): interdependent activating mechanisms observed across several RTKs include ligand-induced receptor dimerisation, (auto-)phosphorylation of the activation loop and autophosphorylation-induced release of autoinhibitory interactions mediated by a juxtamembrane region, and these activities are counteracted or modulated by protein tyrosine phosphatases, growth-factor induced endocytosis of the receptors and their recycling or degradation (reviewed in Schlessinger, 2003). Given that MAL constantly and rapidly shuttles between nucleus and cytoplasm in NIH3T3 fibroblasts, nuclear accumulation is most rapidly and "economically" achieved by blocking nuclear export of MAL. In addition, one might speculate that MAL serves cytoplasmic functions that are independent of its role as a gene regulator.

6.3.2 Regulation of MAL activity through the control of transcriptional activity

Nuclear accumulation of MAL is not sufficient for the activation of MAL-dependent, SRF-mediated transcription. This is apparent both in SRF gene reporter assays and for the transcription of endogenous MAL target genes (see Section 3.4 in Chapter 3). Dissociation of the MAL-actin complex, however, suffices for the activation of SRF by MAL. This establishes that a nuclear MAL-actin interaction not only targets MAL for nuclear export, but also restrains MAL from engaging in productive transcription unless Rho is activated (Figure 6.1). Given that MAL constantly shuttles between nucleus and cytoplasm, low nuclear concentrations of MAL will prevail in serum-starved cells. One can therefore regard the block of MAL activity in the nucleus as a "safety net", ensuring that nuclear MAL-actin complexes do not activate SRF-mediated transcription. MAL localisation remains predominantly nuclear up to around 6 h upon serum stimulation when MAL-dependent transcriptional activity is low (Miralles et al., 2003; Vartiainen et al., 2007, see also Chapter 3). This might reflect actin binding in the nucleus, which indeed recovers rapidly, within minutes after serum stimulation (Miralles et al., 2003; Vartiainen et al., 2007). Furthermore, a significant proportion of MAL appears constitutively nuclear in MDA-MB-231 human breast cancer cells; however, its transcriptional activity is potentiated by CD treatment (Cristina Perez-Sanchez and Souhila Medjkane, personal communication). Therefore, it is likely that some cell types solely rely on the role of nuclear actin as a MAL inhibitor at the level of transcription.

Treatment of NIH3T3 fibroblasts with LMB results in a low, reproducible but not statistically significant activation of an SRF reporter and a number of SRF target genes (see Section 3.4 in Chapter 3). This low activation might reflect the dynamic nature of the MAL-actin interaction. Higher nuclear concentrations of MAL with essentially unchanged concentrations of free nuclear actin may shift the MAL-actin complex binding equilibrium somewhat more closely toward a form of MAL that is (partially) free of actin and therefore active.

6.3.2.1 Potential mechanisms for inhibition of MAL-dependent transcription by actin

Actin may inhibit productive MAL-dependent transcription in several possible ways. According to a simple model, actin may block the incorporation of MAL into a ternary complex with SRF and DNA. This model is unlikely since nuclear accumulation of MAL by LMB treatment is sufficient to recruit MAL to promoters of MAL-dependent SRF target genes. Yet, these genes do not become activated unless the MAL-actin complex is disengaged.

In addition, loss of actin binding and consequentially increased baseline-transcriptional activity does not necessarily correlate with an increased MAL-SRF-DNA-complex formation in electrophoretic mobility shift assays (EMSAs) (see Section 8.1 and Figure 8.3 in Chapter 8; Appendix). For example, mutation of RPEL3 by alanine substitution of its first and most conserved arginine residue results in an increased nuclear steady-state localisation of MAL and activation of SRF-mediated transcriptional activity in serum-starved cells (see Section 4.6 in Chapter 4), but there is no substantial increase of ternary complex formation observed in the EMSA experiments. MAL xxx, in which all three RPEL motifs were mutated, behaves similarly (see Figure 8.3 in Chapter 8; Appendix). Deletion of the RPEL domain largely increases the formation of MAL-SRF-DNA complexes in this assay, however, CD treatment, which reliably disrupts MAL-actin complexes, does not (see Section 8.1 in Chapter 8, Miralles et al., 2003; Zaromytidou, 2007). In addition, deletion of the RPEL domain of MC also increases its potential to form complexes with SRF and DNA in the EMSA analysis (Zaromytidou, 2007). The RPEL domain may therefore inhibit MAL-SRF-DNA complex formation in a manner that is independent of actin binding. Different DNA-binding assays would help to resolve this question.

Therefore, when bound to MAL on DNA, actin may serve as a transcriptional co-repressor. Actin may, for example, recruit gene-regulatory proteins that repress transcription, either directly or at the level of chromatin structure. Alternatively, actin may prevent recruitment of factors that are necessary for active transcription, for example components of the basal transcriptional machinery. Myocardin has been reported to recruit histone acetyltransferases and histone deacetylases which modulate myocardin-regulated smooth-muscle gene expression (Cao et al., 2005).

At this stage, it is important to directly test whether an actin-MAL-SRF-DNA complex can form. I have attempted chromatin immunoprecipitation (ChIP) against actin to recover MAL-dependent SRF target genes. However, gene recovery was weak and not limited to MAL/SRF target genes. One limiting factor for these experiments is the efficiency by which endogenous actin can be immunoprecipitated with the antibodies that are currently available. I have also attempted to introduce epitope-tagged exogenous β-actin, however, this approach did not solve the problem of immunoprecipitation efficiency. This is not surprising since transiently expressed actin has to compete with the overwhelmingly abundant endogenous actin, whose cytoplasmic concentrations in non-muscle cells are estimated as 65-300 μM (see Section 1.2.1 in Chapter 1; Introduction). The recruitment of a wide variety of genes with actin antibodies is not unexpected since actin is part of all three RNA-polymerase complexes and present in chromatin-remodelling machineries as well as nascent RNA complexes (see Section 1.2.5 in Chapter 1; Introduction).

Optimisation of the ChIP procedure with an appropriate actin antibody is required. Alternatively, and possibly more promisingly, one could consider using actin-binding proteins that bind actin with high affinity without interfering with the MAL-actin interaction for ChIP. One good candiate would be DNaseI, which one would have to produce recombinantly in a DNA-binding and DNase-activity deficient form.

To overcome the challenge posed by the presence of actin in multiple gene-associated complexes, it would be worth considering sequential ChIP approaches that, in a first step, recover promoters via immobilisation of SRF and, secondly, actin. It would be interesting to observe changes in the actin recruitment upon induction of Rho-actin-MAL signalling. It is, however, possible that the detection of a MAL-actin dissociation becomes, at least partially, masked by the recruitment of actin with RNA polymerase II in these experiments since actin is a component of the basal transcriptional machinery (see Section 1.2.5.2 in Chapter 1; Introduction).

Future approaches should also include DNA affinity sedimentation assays, using a biotinylated SRE oligonucleotide bound onto a streptavidin-conjugated matrix to purify DNA-SRF-MAL complexes. It will be interesting to ask whether actin specifically co-purifies with these assemblies.

6.4 RPEL motifs in myocardin-family proteins

6.4.1 Myocardin is not linked to Rho signalling because its RPEL domain does not bind actin

The MAL-related SRF coactivator myocardin (MC) is not linked to Rho-GTPase signalling and constitutively active when expressed in a number of cell lines, including NIH3T3 fibroblasts (see Section 1.4.3.1 in Chapter 1; Introduction). Myocardin is genuinely nuclear since it is not exported from the nucleus and therefore does not shuttle like MAL (see Section 4.3 in Chapter 4). The RPEL domain of myocardin displays low avidity for actin, and this appears to underlie the differential regulation of MAL and MC. The regulatory behaviours of MAL and MC can be reciprocally switched by mutual exchange of their RPEL domains, providing another example for how swapping of modular protein domains can re-wire signalling pathways (Bhattacharyya et al., 2006; Pawson and Nash, 2003). The MC RPEL domain is sufficient to confer constitutive nuclear localisation on heterologous proteins such as pyruvate kinase and GFP (see Section 4.2 in Chapter 4 and Guettler et al., 2007). These observations further underline the importance of the RPEL domain for MAL regulation and suggest that, rather than being controlled in fundamentally different ways, MAL and MC are differentially regulated because of differences in their RPEL domains that are reflected in actin binding.

What is the functional advantage of uncoupling SRF activation from Rho-actin signalling in muscle cells via MC? The specialised role of actin in differentiated muscle cells might impinge on the actin polymerisation cycle in a way that might interfere with growth factor signalling via the actin cytoskeleton. Indeed, actin filaments are stabilised in muscle cells, as documented by their relative resistance to the actin-depolymerising drugs cytochalasin D or latrunculin B (for references, see Wang et al., 2005), which rely on actin filament turnover. Filament stabilisation in muscle cells is, for example, conferred by the actin-filament binder tropomyosin, which inhibits ADF/cofilin activity (Ono and Ono, 2002). Maintenance of smooth and cardiac muscle identity may require myocardin as an actin-independent SRF co-activator.

6.4.2 RPEL motifs bind actin with a range of affinities

Fluorescence anisotropy and GST affinity sedimentation experiments show that RPEL motifs represent actin-binding structures with a range of affinities for actin. The actin-RPEL interactions tested occur with dissociation constants in the low micromolar range. While MAL RPEL1 and RPEL2 bind with relatively high affinity, binding of RPEL3 to actin is much weaker. The reason for differential actin binding by MAL and MC lies in RPEL motifs 1 and 2: MC RPEL1 binds actin substantially more weakly than MAL RPEL1, and I did not detect any actin binding for MC RPEL2 under the conditions used. RPEL motifs 3 of both MAL and MC bind with similar, relatively low affinity. This is reflected at the level of sequence conservation between the RPEL motifs of MAL and MC: while RPEL motifs 1 and 2 are relatively divergent between MAL and MC, RPEL motifs 3 are very similar (see Figure 4.5 in Chapter 4). The conservation of RPEL3 in MC is puzzling since MC does not appear to be regulated by actin, at least in our system: it remains possible that other, unknown regulatory factors interact with RPEL3, and it will be interesting to identify such proteins.

6.4.3 RPEL motifs cooperate in MAL regulation

Each of the MAL RPEL motifs participates in MAL regulation, but their contributions are different. Provided that the mutations introduced are of sufficient severity to disrupt the RPEL-actin interaction, mutation of RPEL1 has a substantially weaker de-regulating effect than mutation of the other two RPEL motifs. The sensitivity of MAL regulation to mutation of RPEL3 is particularly striking, especially when bearing in mind that RPEL3 represents the weakest actin binder among all three RPEL motifs of MAL (see Sections 4.5 and 4.6 in Chapter 4). The fact that combined mutation of RPEL motifs results in a stronger de-regulation of MAL than any single-RPEL motif mutation indicates that the RPEL motifs cooperate to control MAL activity. Given that MC is not controlled by actin because of its deviating RPEL domain, I generated a set of MAL-MC chimaeras to study the relationship between RPEL motifs in MAL regulation (see Figure 4.10 in Chapter 4). This was especially useful before we obtained the structure since I could regard MC as a "naturally occurring mutant derivative" of MAL.

6.4.4 The RPEL1-2 unit specifies differential regulation between MAL and MC

A careful analysis of MAL-MC chimaeras indicates that differential regulation of MAL and MC is conferred by differences in RPEL motifs 1 and 2, which bind actin more weakly than their counterparts in MAL (see Sections 4.5 and 4.7 in Chapter 4). Exchange of the N-terminus up to including RPEL1 of MAL for the equivalent region of MC is sufficient to de-regulate MAL. However, the conversion of MC into a protein that is regulated in a MAL-like manner requires transfer of both MAL RPEL motifs 1 and 2. Transfer of only MAL RPEL2 into MC is not sufficient to change the regulatory behaviour of MC. This indicates that an intact unit of MAL RPEL motifs 1 and 2 is necessary for Rho-dependent regulation. The experiments performed so far do not directly reveal any contribution of the RPEL1-2 linker to MAL regulation, although this will be tested more thoroughly since the linker contains an unexpected actin contact site. Functionally, RPEL3 is interchangeable between MAL and MC. MAL-MC chimaeras reveal that RPEL3 contributes to MAL regulation only when preceded by an intact unit of RPEL motifs 1 and 2 competent to bind actin.

The functional and biochemical data suggest that occupancy of RPEL3 would be most sensitive to changes in the G-actin concentration (see Chapter 4).

6.5 A model for MAL regulation by actin

Based on biochemical and functional experiments, we propose a working model by which cooperative engagement of actin with its RPEL domain regulates MAL activity (Figure 6.2). This model, a refined version of the titration model introduced in Chapter 1 (see Section 1.4.3.5 and Figure 1.9; Introduction), aims to explain how MAL can sensitively monitor cellular G-actin levels and respond to growth-factor induced depletion of the actin monomer pool by nuclear accumulation and activation of SRF-mediated transcription.

We propose that actin is recruited to MAL by an initial high-affinity interaction, possibly involving RPEL1. Actin-actin interactions and/or allosteric effects of actin on the secondary structure of MAL may promote the recruitment of further actin molecules into the MAL-actin complex via lower-affinity actin-binding sites. According to the simplest model, low-affinity interaction of actin with RPEL3 that is dependent on actin

binding to higher-affinity binding sites may confer the ultimate regulatory step, i.e. the promotion of nuclear export and, provided that the G-actin concentration is very high, a block of nuclear import. The latter might occur through masking of the B2 region directly preceding RPEL3. We propose that at the G-actin concentrations prevailing in resting cells, there is a significant probability that all of the MAL RPEL motifs can bind actin (Figure 6.2). Given the high basal import rate of MAL (Vartiainen et al., 2007), this complex might be a substrate for both nuclear import and export factors. Alternatively, if actin binding to RPEL3 were indeed able to block nuclear import of MAL, shuttling might be conferred by a dynamic interaction of actin with RPEL3 or changes in the conformation of this MAL-actin complex. The elucidation of the underlying mechanism will require further work. Upon depletion of the G-actin pool following Rho activation, it is binding of actin to RPEL3, the weakest actin binder, that would be affected first. Dissociation of actin from RPEL3 would confer an inhibition of nuclear export. Positive cooperativity in actin binding might confer a robust, switch-like response of MAL to a growth-factor induced drop in the G-actin concentration while rendering the system insensitive to subtle fluctuations in actin dynamics (see discussion in the following section).

6.5.1 Examples of positive cooperativity in biological systems

In this section, I will give examples of biological systems that are regulated through positive cooperativity. I will illustrate common principles of these scenarios and speculate that similar mechanisms could be operating to control to MAL activity by actin binding.

6.5.1.1 Oxygen binding by hemoglobin

A prominent example for positive cooperativity in biological systems is the binding of oxygen by hemoglobin (Perutz, 1978). Positive cooperativity of oxygen binding to four subunits of hemoglobin, each of which coordinates one oxygen molecule, maximises the efficiency of oxygen uptake in the lungs. In the target tissues, where the oxygen partial pressure is only fivefold lower than in the lungs, the cooperative nature of oxygen coordination ensures that oxygen is efficiently and completely released. Cooperativity can be expressed by the Hill coefficient, which is 1

in the absence of cooperativity and lies above or below 1 for positive or negative cooperativity, respectively (Weiss, 1997).

6.5.1.2 WASP activation by phosphoinositides

Many signalling proteins contain an "output" domain that, in isolation, confers constitutive activity. Activation of signalling proteins frequently entails the release of autoinhibition. For this to occur, an "input" signal is sensed by a regulatory component of the signalling protein (Bhattacharyya et al., 2006; Pawson and Nash, 2003). This can be, for example, a posttranslational modification, protein-protein interaction or binding of a second messenger. An example from the area of actin regulation referred to earlier is the activation of the Arp2/3 complex by N-WASP (see Section 1.2.3.1 in Chapter 1; Introduction). In this context, the output domain of N-WASP is the Arp2/3-complex binding region, whose activity is inhibited by an intramolecular interaction between its N-terminal autoregulatory domain and a C-terminal, so-called VCA region. There are numerous activation scenarios for N-WASP, which include binding of the active Rho family GTPases Cdc42 or Rac to a GTPase-binding domain or polyproline ligands to a proline-rich region to release the closed conformation (see Section 1.2.3.1 in Chapter 1; Introduction). One further mechanism of N-WASP activation is binding of phosphatidylinositol(4,5)-bisphosphate, $PI(4,5)P_2$, to a polybasic motif. Since the polybasic motif is involved in autoinhibitory interactions, phospholipid binding releases the autoinhibited state of N-WASP. Interestingly, binding of multiple $PI(4,5)P_2$ molecules occurs with a high degree of positive cooperativity that correlates with the density of positive charge in the polybasic motif (Papayannopoulos et al., 2005). In essence, the polybasic motif of N-WASP senses the local concentration, or density, of $PI(4,5)P_2$, responding to its increase above a certain threshold it in a sharp, "all-or-nothing-", switch-like manner. Cooperativity-controlled switches may provide resistance to "leaky" activation caused by signal fluctuations below the switch-inducing threshold. This appears particularly important in systems with a relatively high degree of basal activator levels such as in the example of $PI(4,5)P_2$, whose levels vary by only ±50% (see Papayannopoulos et al., 2005). The active state of WASP is stabilised by tyrosine phosphorylation (Torres and Rosen, 2003).

6.5.1.3 Engineering of cooperative signalling switches

A recent study illustrates how multiple autoregulatory interactions within N-WASP, can confer positive cooperativity and switch-like behaviour (Dueber et al., 2007). The authors coupled multiple SH3 domains to the N-terminus of the N-WASP VCA region and numerous SH3 ligand peptide sequences to the C-terminus. Cooperativity correlated with the number of interactions, provided their individual affinities were moderate ($K_d \approx 10$ μM). Multiple higher-affinity regulatory interactions ($K_d \approx 0.1$ μM) rendered the synthetic switch nonactivatable. This illustrates how cooperativity between moderate-affinity interaction sites can generate an ultrasensitive switch-like behaviour (Dueber et al., 2007).

6.5.1.4 Binding of the λ repressor to its operator site in the gene control of phage λ

A case for positive cooperativity in gene regulation is constituted by the control of gene expression through the λ repressor in the bacteriophage λ (see Ptashne, 2004, for a comprehensive illustration of this system). In the lysogenic state of the phage, high levels of the λ repressor achieve repression of genes required for the switch to the lytic lifestyle of phage λ. Proteolytic cleavage of the λ repressor induces lysis. I will briefly discuss the λ-repressor system since it provides an outstanding paradigm for the relationship between binding site affinities and positive cooperativity.

The promoters of two genes in the phage λ chromosome, *cI* and *cro*, share parts of a tripartite operator with three operator sites, O_R1, O_R2 and O_R3 (Figure 6.3 A). The two genes are transcribed in opposite directions. The *cI* gene encodes λ repressor while the *cro* gene product is a critical component for the lytic programme of phage λ. The λ repressor consists of an N- and a C-terminal globular domain, both of which are connected to each other by a flexible linker. λ repressor molecules dimerise in a parallel fashion, and the dimers bind DNA via their N-terminal globular domains. Binding of a λ repressor dimer to O_R2 promotes RNA polymerase recruitment for transcription of *cI* while blocking transcription of *cro*. Hypothetical binding of the λ repressor to only O_R3 would be compatible with transcription of *cro* but not *cI*. Engagement of the repressor with O_R1 only would turn both genes off (Figure 6.3A).

The three operator sites have different affinities for λ repressor: O_R1 binds the λ repressor with highest affinity while the affinities of O_R2 and O_R3 are about ten times lower. Because of that, at low repressor concentration, O_R1 would be the first site to become occupied by the repressor. Positive cooperativity immediately recruits a λ repressor dimer to O_R2. This is conferred by an interaction of the C-terminal globular domains of λ repressors bound to O_R2 and O_R1. Therefore, a repressor dimer bound to O_R1 helps another dimer to bind O_R2. The repressor bound to O_R2 cooperates with RNA polymerase to transcribe its own gene. In the lysogenic state, the repressor will occupy O_R1 and O_R2 most of the time. This system entails three examples of positive cooperativity: between repressor monomers, repressor dimers and between repressor dimers and RNA polymerase (Figure 6.3 A).

At high λ repressor concentrations, the repressor will also occupy O_R3, thereby shutting off its own expression. In the context of the intact operator, the repressor binds independently to O_R3 since the C-terminal domains of the repressor dimer bound to O_R2 lean toward O_R1. That is why O_R3 only becomes occupied at high repressor concentrations. However, if O_R1 is rendered unable by mutation to bind repressor, binding of λ repressor to O_R2 cooperates with O_R3 occupancy, illustrating that cooperativity occurs in an "alternate pairwise" manner (Figure 6.3 A, discussed in Ptashne, 2004).

A plot of the efficiency of *cro* gene repression versus the repressor concentration results is a sigmoidal curve, which is indicative of positive cooperativity (Figure 6.3 B, see Ptashne, 2004). Starting from the highest repressor levels, a substantial decrease in repressor concentration remains without effect on gene repression. This is brought about by positive cooperativity in repressor binding to O_R1 and O_R2 and renders the system resistant against random fluctuations of the repressor concentration. Only when the repressor concentration drops about fivefold, repression is released in a switch-like manner over a small window of repressor concentration (see Ptashne, 2004). As in the other examples mentioned above, systems based on positive cooperativity translate an analog signal, in this case repressor concentration, into a robust, digital "all-or-nothing" response. In a simple single-site (high-affinity) operator-repressor system, the switch-like response of the repression state to the repressor concentration would be lost, and a much larger drop in repressor concentration would be required to lift repression (Figure 6.3 B, see Ptashne, 2004).

The combinatorial regulation of the interferon-β (IFN-β) enhancer by a multi-transcription factor complex represents another example of functional and biochemical cooperativity in gene regulation (see Section 1.1.2.1 in Chapter 1; Introduction).

6.5.2 Positive cooperativity in the regulation of MAL by actin?

In the case of MAL, nuclear accumulation and activation of SRF-mediated transcription can be regarded as the output activity. The input is provided by the concentration of G-actin, which may be sensed by cooperative engagement of the RPEL domain with actin. Conversely to the $PI(4,5)P_2$-N-WASP system, but more similarly to the λ-repressor system, MAL becomes activated by a decrease in the ligand (G-actin) concentration. Within 10 minutes upon serum stimulation, the pool of G-actin accessible through staining with the G-actin specific agent DNaseI drops by about 30% (Vartiainen et al., 2007). It is possible that the actual decrease in the concentration of G-actin is higher at earlier time points and that, due to the limited sensitivity of the assay, 30% represents an underestimate of the change. We speculate that G-actin recruitment to the RPEL domain occurs with positive cooperativity and that this confers resistance of the Rho-actin-MAL-SRF system to fluctuations in the cellular G-actin concentration while allowing for a "switch-like" activation of MAL once the G-actin concentration has dropped below a certain threshold. The affinities of the MAL RPEL motifs for actin may be in the critical range that is necessary for MAL to respond to changes in the growth-factor induced G-actin concentration. Because of its substantially lower affinity for actin, the G-actin threshold level for activation is higher for myocardin than it is for MAL.

6.5.2.1 Does the RPEL domain-actin interaction exhibit positive cooperativity?

I should note first that, as of today, we cannot give any quantitative measure of cooperativity for the MAL-actin interaction. However, several lines of circumstantial evidence strongly suggest that cooperative actin binding does indeed occur. (1) RPEL motifs cooperate in the regulation of MAL activity (see Section 4.6 in Chapter 4). (2) The mutation of RPEL motifs changes actin-binding stoichiometries in a way that is incompatible with independent RPEL-mediated actin binding events (see Section 4.9 in Chapter 4). For example, MAL 1xx recruits two actin molecules in the stringent gel filtration assay. In the same assay, MAL x2x still binds three actin molecules. Mutation

of all three RPEL motifs (MAL xxx), however, results in a complete loss of actin binding as detected by gel filtration. (3) Cooperativity in actin binding may explain the apparent discrepancy between the fluorescence anisotropy results, which show that individual RPEL motifs recruit actin with micromolar affinity, and the nanomolar affinity of the intact MAL RPEL domain previously estimated from actin polymerisation inhibition studies (see Section 2.3.1.3 in Chapter 2 and Section 4.5 in Chapter 4). (4) We observe direct actin-actin interactions in the MAL(67-199)-LatB-actin complex and predict the presence of indirect, water-mediated contacts (see Section 5.4 in Chapter 5). The flexibility of the only partially folded RPEL domain peptide chain may facilitate actin-actin interactions, similarly (in functional terms) to how the flexible linker between the globular domains of the λ repressor allows for cooperation of repressor molecules bound to different operator sites (see Section 6.5.1.4). It is also possible that a first actin binding event induces structural changes in MAL that facilitate binding of other actin molecules.

The model predicts that in its active state, MAL does not necessarily need to be devoid of actin. Interestingly, this might be supported by the Förster resonance energy transfer analysis of the MAL-actin interaction (see Chapter 2 and Vartiainen et al., 2007). The FRET signal detected between MAL and actin does not drop to the low levels seen upon treatment of the cells with cytochalasin D, at least at the earliest time point that can be captured in the assay used. This might reflect a changed MAL-actin complex stoichiometry, although this effect may also be explained by dissociation of part of the MAL pool from actin.

Functional cooperativity between multiple actin-binding motifs or domains has previously been observed in many F-actin regulatory proteins such as gelsolin (Selden et al., 1998), skeletal muscle myosin (Conibear and Geeves, 1998) and the non-receptor tyrosine kinase Arg (Wang et al., 2001b). The actin-MAL interaction appears unique in that functional cooperation occurs between G-actin binding sites, and the actin-binding partner is the target, not the regulator.

We will use the fluorescence anisotropy assay to study whether actin binding to MAL constructs that contain multiple actin-binding sites involves positive cooperativity. It will be interesting to ask whether a peptide encompassing RPEL1 and the RPEL1-2 linker, the unit occupied by two actin molecules in the MAL(67-199)-LatB-actin structure, binds actin with positive cooperativity. Fluorescently conjugated

RPEL-domain constructs will be generated to study the entire RPEL domain of MAL by fluorescence anisotropy. This will entail chemical modification of the RPEL domain and its purification to achieve a complete fluorophore conjugation. These experiments will allow for a more direct comparison of the apparent affinities by which isolated RPEL motifs and RPEL motifs in the context of the RPEL domain recruit actin. It will be insightful to modulate the affinities of actin-binding sites and study the effects on actin binding and MAL regulation.

6.6 Structural insights explain aspects of RPEL motif function

6.6.1 Key actin-binding residues are conserved across RPEL motifs

The PFAM database currently contains 180 RPEL motifs of species ranging from fungi to mammals (http://pfam.sanger.ac.uk/, Finn et al., 2006). There are two families of RPEL-motif containing proteins (see Section 1.4.3.2.1.1 in Chapter 1; Introduction). Our direct, structural insights into the RPEL-actin interaction now allow us to relate the conservation of these RPEL motifs to actin binding. A representation of the relative frequencies of amino acids at certain positions of the RPEL motif, generated by "HMM Logo" (Schuster-Bockler et al., 2004), shows that across all RPEL motifs in the PFAM database, the residues whose side chains contact actin are very conserved (Figure 6.4; see also Figures 5.8 and 5.10 in Chapter 5). This is, however, not the case for residues that engage in conserved interactions via their main chains. The side-chain conservation suggests that the primary function of the RPEL motif is actin binding. Structural insights also allow us to rationalise the molecular basis of different affinities between RPEL motifs and actin and observations that document competition of other actin-binding agents with MAL for actin binding.

6.6.2 Differential actin binding by MAL and MC RPEL motifs 1 and 2 can be rationalised structurally

Relating the sequence of the MC RPEL domain to the RPEL-actin crystal structures suggests that only a few differences account for differential actin binding and regulation of MAL and MC (Figure 6.4).

The MAL-actin crystal structures do not immediately offer an obvious explanation for the lower affinity of MC RPEL1 compared to that of MAL RPEL1 (see Section 4.5 in Chapter 4). Position 77 in MAL RPEL1 is a lysine, which establishes both hydrophobic and polar contacts with actin; the equivalent position in MC is occupied by an arginine (Figure 6.4; see also Figure 5.8, left, in Chapter 5). Arginine may functionally substitute in the hydrogen bond that K77 establishes with the main chain of actin, although we cannot rule out a negative effect on actin binding. Another case of divergence between RPEL motifs 1 of MAL and MC occurs in the glutamate of the RPEL core sequence (E86 in MAL RPEL1), which is replaced by glutamine in MC. This exchange is likely to preserve the intra-RPEL hydrogen bond mediated by the glutamate side chain in MAL. The structure of MAL(67-199) provides another potential factor in determining different affinities: there, K71 of MAL establishes a hydrogen bond with S348 of actin (see Figure 5.12 A in Chapter 5). The equivalent amino acid in MC is an arginine (Figure 6.4). Furthermore, mutation of K71 in the context of mutations of hydrophobic amino acids in helix 1 has a deregulatory effect on MAL (see Section 5.5.2 in Chapter 5). It should be noted, however, that a lysine at this position is only found in RPEL1 and does therefore not represent a conserved RPEL-actin contact.

These observations clearly suggest that the affinity difference between MAL and MC RPEL1 results from the sum of multiple subtle deviations in the RPEL motif sequences.

Functional divergence between RPEL motifs 2 of MAL and MC is more pronounced than that between RPEL motifs 1: no binding between MC RPEL2 and actin was detected by GST affinity sedimentation and fluorescence anisotropy assays (see Section 4.5 in Chapter 4). The RPEL core glutamate, E130 in MAL RPEL2, is replaced by serine in MC (Figure 6.4). Serine would be unable to mediate the intra-RPEL interaction that is likely to orient helix 2 (see Figures 5.8, right, and 5.10 in Chapter 5). Additionally, the position equivalent to I122 is occupied by a glycine in MC: a direct hydrophobic contact would be lost, and additionally, glycine at this position might interfere with the stability of helix 1 since it allows for a high degree of main-chain flexibility. Helix-1 interactions with the hydrophobic cleft are critical for MAL regulation. Furthermore, the position of the proline residue of the "RP" dyad in MAL RPEL2 is occupied by serine in MC RPEL2. The polar serine side chain would

abolish possible hydrophobic contacts that are mediated by proline in this region (see Figure 5.8, right, in Chapter 5).

To further test whether actin binding represents the sole determinant for differential regulation of MAL and MC, it would be interesting to specifically and reciprocally interconvert MAL and MC by targeting the candidate residues responsible for differential regulation through both gain and loss-of-function approaches.

6.6.3 The reason for the relatively low affinity of MAL RPEL3 for actin is likely to involve general folding of the RPEL motif

All key residues that are involved in direct RPEL-actin interactions for RPEL motifs 1 and are conserved in RPEL3 (Figure 6.4). Why then is the affinity of MAL RPEL3 by almost one order of magnitude lower that of RPEL1 or RPEL2? The explanation for this has to lie outside the conserved set of amino acids that establish direct contacts with actin. Two residues that directly follow the "RP" dyad of RPEL3, G127 and P128, are likely to be responsible for this effect. P128 is found a position equivalent to those that mark the beginning of helix 2 in RPEL motifs 1 and 2. Proline very likely interferes with the formation of this helix. Because glycine lacks a side chain, it can introduce flexibility while proline introduces a bend into the amino acid chain. Thus, the "GP" unit might alter the main chain and thereby interfere with the positioning of helix 2 onto the subdomain-3 platform. A GP-induced kink in the RPEL main chain might override the contribution of the RPEL core glutamate in orienting helix 2.

Future experiments will address the contribution of each functional element of the RPEL motif in actin binding, using the fluorescence anisotropy assay. This will also contribute to resolving questions regarding the basis of the different affinities of RPEL motifs for actin.

6.6.4 Interference of the TMR group with MAL binding and its implications for biochemical MAL-actin binding studies

Modification of actin with tetramethylrhodamine (TMR) at C374 substantially destabilises the MAL-actin interaction (see Section 2.3.2.6 in Chapter 2). The structures reveal the basis for this observation: TMR occupies the hydrophobic cleft, thereby sterically impairing the interaction of helix 1 and the connector of the RPEL motif with actin (Figure 6.5 A). A certain flexibility in the orientation of TMR might allow MAL to bind, but with lower avidity. This is in line with observations made in gel filtration experiments that suggest a destabilised interaction of MAL with TMR-actin (see Section 2.3.2.6 in Chapter 2). In this context, it is interesting to note that MAL(67-199)-TMR-actin crystals are very sensitive to manipulation (Stephane Mouilleron, personal communication).

C374 is a common target for experimental modification of actin with fluorophores to study actin polymerisation and protein interactions that actin engages in. I have initially set out to study MAL-actin interaction using actin modified with 7-chloro-4-nitrobenzeno-2-oxa-1,3-diazole chloride (NBD-actin, Detmers et al., 1981). Although NBD modification of actin occurs on K372 at the base of subdomain 1, the modification procedure entails previous blockage of C374 with N-ethylmaleimide. Although N-ethylmaleimide is much smaller than TMR, we cannot rule out interference with MAL binding. Initial measurements for MAL-NBD-actin complexes indicated that MAL binds ATP- and ADP-actin with comparable affinities. Future studies will employ the fluorescence anisotropy assay introduced in Chapter 4 to re-address this question.

6.6.5 Competition between MAL and profilin for actin

Overexpression of profilin potentiates SRF-mediated transcription in NIH3T3 fibroblasts (Sotiropoulos et al., 1999). This is likely to occur through direct competition between MAL and profilin for actin, as suggested by co-immunoprecipitation experiments (Posern et al., 2004). The RPEL1- and RPEL2-actin structures offer a direct explanation for competition between MAL and profilin. Profilin also binds at the base of the subdomain 1-3 interface of actin (Schutt et al., 1993, Figure 6.5 B). It should be noted that profilin's mode of actin binding is fundamentally different from that of the RPEL motif, as profilin does not insert a helix into the hydrophobic cleft (Figure 6.5 B; see also Section 1.2.2.1 in Chapter 1; Introduction). Yet, binding of the RPEL peptides

would cause a strong steric hindrance to profilin binding, mainly via the helix 1-2 connector and helix 2.

6.6.6 Suggestions for the mechanism of G-actin sequestration by MAL

The MAL-actin interaction sequesters actin from polymerisation, and the RPEL-actin structures may provide part of the molecular basis for this. Both MAL RPEL1 and RPEL2 dock onto regions that are implicated in actin-actin contacts within the Holmes model of the actin filament (Figure 6.5 C, Holmes et al., 1990). These sites include regions on actin that are contacted by the connector region and helix 2 of the RPEL motif. It is interesting to note that numerous actin binders of the WH2-motif protein family, such as WASP and ciboulot, promote actin assembly, in contrast to thymosin β4, which inhibits it (Hertzog et al., 2004). Thus, interaction of an α helix with the hydrophobic cleft of actin cannot be sufficient to sequester actin monomers. In the case of thymosin β4, an additional interaction with the subdomain 2-4 interface is responsible for conferring a block of actin polymerisation (Hertzog et al., 2004, and see Section 1.2.2.2 in Chapter 1). One might speculate that the equivalent role in MAL is adopted by the helix 2-subdomain-3 platform interaction.

Sequestration of G-pyrene-actin by full-length MAL is very efficient. However, preliminary experiments suggest that RPEL peptides are unable to inhibit actin polymerisation in the pyrene-actin polymerisation assay, even at high peptide concentrations (data not shown). Therefore, we have to consider the possibility that the way actin binds in the context of the RPEL domain is critical for G-actin sequestration.

It remains possible that the pyrene fluorophore interferes with RPEL binding, especially since it is coupled to the same cysteine residue in actin as tetramethylrhodamine (TMR), which interferes with MAL binding (see Section 2.3.2.6 in Chapter 2 and Figure 6.5 A). Yet, the interference may be less severe since the pyrene fluorophore, which consists of four fused benzene rings, is less bulky than the TMR moiety. Since the arrangement of actin molecules in the MAL(67-199)-actin structure is very packed (see Figure 5.11 in Chapter 5), it is conceivable that steric hindrance of actin polymerisation caused by MAL is not limited to the RPEL-actin contacts shown in Figure 5.8.

6.6.6.1 Does MAL control actin dynamics in vivo?

It is unlikely that the ability of MAL to sequester G-actin has a direct effect on actin dynamics since its cellular concentrations is probably low. To test this hypothesis, I raised an antibody specific to the RPEL domain of all mammalian paralogues of MAL. This antibody will be used to measure the concentration of MAL by quantitative Western blotting.

6.6.7 Competition between MAL and swinholide A for actin

Swinholide A blocks MAL-actin complex formation by direct competition with MAL for actin (see Section 2.3.2.4 in Chapter 2). Superposition reveals a striking steric clash between helices 1 of the RPEL1 and RPEL2 peptides and swinholide A, which inserts a side group of its macrolide ring into the hydrophobic cleft between actin subdomains 1 and 3 (Figure 6.5 D, Klenchin et al., 2003). No structural information is available for cytochalasin D. It is possible that cytochalasin D, and perhaps jasplakinolide, also compete with the RPEL motif for actin binding, similarly to swinholide A.

6.7 RPEL motifs bind actin via a conserved mechanism

The WH2 motif is a ubiquitous actin-binding motif (reviewed in Paunola et al., 2002), and numerous structures of WH2-motif containing proteins bound to actin were solved previously. These comprise the WH2 motif of Arp2/3-complex activators such as WASP (Wiskott-Aldrich Syndrome Protein, Chereau et al., 2005), WAVE2 (WASP-family verprolin homologous protein 2, Chereau et al., 2005) and WIP (WASP-Interacting Protein, Chereau et al., 2005), the G-actin binder MIM (Missing-In-Metastasis, Lee et al., 2007) and the actin-sequestering protein ciboulot (Hertzog et al., 2004) (see Section 1.2.2.2 in Chapter 1; Introduction for more information on some of these proteins). Comparison with these structures reveals that the helix 1-actin interaction of the RPEL motifs is very similar to the way WH2 motifs bind actin. In all these cases, an α-helix targets the hydrophobic cleft of actin, providing four key residues, which we named A to D (Figure 6.6).

Similarities to the mode by which RPEL motifs bind actin are not restricted to the WH2-motif family of actin-binding proteins. Multiple structures of the actin-

severing and capping protein gelsolin (see Section 1.2.2.4 in Chapter 1; Introduction) in complex with actin (Burtnick et al., 2004; McLaughlin et al., 1993; Robinson et al., 1999) show that gelsolin also contacts the hydrophobic cleft of actin by a helix-1 like interaction (Figure 6.7 A). The crystal structure of vitamin-D binding protein (Otterbein et al., 2002), a potent actin-sequestering protein (see Section 1.2.2.6 in Chapter 1; Introduction), reveals a striking similarity with the RPEL motif-actin interaction (Figure 6.7 B). Although separated by approximately 100 amino acids, two helices of DBP equivalent to those of helix 1 and helix 2 in the RPEL motif contact the hydrophobic cleft and the subdomain-3 platform of actin, respectively. Unlike in the RPEL motif, where two hydrophobic residues that contact the subdomain-3 platform of actin extend from a region that lacks secondary structure, the equivalent side chains of DBP extend from a helical context (Figure 6.7 B). Inspection of residues that dock the helices onto actin shows that three positions, A, C and D and even two hydrophobic contacts mediated by helix 2 (and the following non-helical segment) are conserved (Figure 6.7 B and Figure 6.8). The hydrophobic amino acids of DBP occupy almost identical positions in the RPEL motifs and DBP. At position D, a lysine residue, K207, forms a hydrogen bond with the main chain of actin (Figure 6.7 B).

Roberto Dominguez recently proposed that the hydrophobic cleft of actin, and an adjacent region he termed the hydrophobic "pocket", represents a "hotspot" for interactions with many actin-binding proteins (Dominguez, 2004). According to this hypothesis, binding of the cleft may represent an efficient mechanism for specifically targeting G-actin, provided that the hydrophobic interaction is extensive enough, as, for example, in thymosin β4, or interfering with the stability of F-actin, for example in gelsolin and possibly ADF/cofilin (discussed in Dominguez, 2004).

6.7.1 Actin-binding side chains are conserved despite different directionalities of helix binding in the hydrophobic cleft of actin

In the different structures, the helices equivalent to helix 1 of the RPEL motifs dock onto the cleft in different main-chain directionalities: in the "classical" actin view (see Figure 1.1 A in Chapter 1; Introduction), helices of gelsolin segment 1, DBP and the RPEL motifs run from the front to the back of the actin molecule ("forward") while those of WH2 motifs run in the opposite direction ("reverse") (see Dominguez, 2004) (Figure 6.8 A). Nevertheless, the spacing of the amino acids critical for actin binding is

conserved independently of the helix orientation. Positions A, B and C are mostly occupied by hydrophobic amino acids (although position B is marked by lysines in RPEL motifs) while those at position D correspond to the first and most conserved arginine residue of the RPEL motif. Interestingly, across all the proteins compared, many of the hydrophobic contacts mediated by positions A, B and C within these helices are conserved (Figure 6.8). Gelsolin segment 1 and DBP are exceptional in that they present conserved interacting residues only at positions B or C, but not both (Figure 6.8 B). Moreover, even a positively charged residue at position D is present in all of these proteins except for MIM and gelsolin segment 1 (Figure 6.8 B). The aspartate side chain at position D in gelsolin, however, interacts with actin.

6.7.2 Does MAL affect nucleotide exchange on actin?

The WH2 motifs of WASP, WAVE, WIP and MIM as well thymosin β4 inhibit nucleotide exchange on actin, possibly by interfering with the dynamics of the nucleotide-binding cleft of actin (Chereau et al., 2005). It would be interesting to test whether binding of RPEL motifs to actin also affects nucleotide exchange.

6.8 Discussion of the RPEL domain-actin structure and its possible implications for MAL regulation

6.8.1 Analysis of actin 2

The MAL(67-199)-LatB-actin structure explains why an RPEL domain in which both RPEL motifs 2 and 3 have been mutated (1xx) still recruits two actin molecules (see Section 4.9 in Chapter 4). One actin molecule is bound to RPEL1 ("actin 1"), but a second one ("actin 2") occupies a previously unanticipated site between RPEL motifs 1 and 2, termed the RPEL1-2 linker (see Section 5.4.1.2 and Figure 5.12 B in Chapter 5). Although at the current resolution of the data no water molecules are visible, it is likely that numerous water-mediated contacts exist between these two actin molecules. Since no autonomous actin binding by the RPEL1-2 linker peptide was detected, recruitment of actin 2 to the RPEL domain is likely to involve cooperation with actin 1 (see Section 5.5.3 in Chapter 5). We attempted to crystallise an RPEL1-2 linker peptide bound to LatB-actin; however, we did not obtain any crystals. Non-autonomous actin binding by the linker might explain this.

Another confirmation of the presence of both actin 1 and actin 2 in solution comes from a superposition of the DNaseI-actin complex onto the MAL(67-199)-LatB-actin structure (Figure 6.9). The incorporation of three molecules of DNaseI into the MAL-actin complex is sterically possible. While the biochemical evidence for actin 2 is convincing, its functional relevance awaits elucidation. In a first step, we will address whether mutation of the RPEL1-2 linker changes the stoichiometry of the MAL-actin complex.

6.8.2 Analysis of actin 3

Because the stoichiometry of the MAL-actin complex is sensitive to mutation of RPEL2 (see Section 4.9 in Chapter 4), it is likely that the 1:3 complex observed in the MAL(67-199)-LatB-actin structure does not precisely represent the 1:3 complex we observe in gel filtration chromatography in regard to actin binding by RPEL2. In the crystal structure, the regions of RPEL2 whose mutation affects MAL-actin stoichiometry are not resolved (see Figure 5.11 in Chapter 5). Superposition of the MAL chains in the MAL(67-199)-LatB-actin and RPEL2-LatB-actin structures shows that actin 3 would clash with an actin molecule bound to RPEL2 (Figure 6.10). Instead, the orientations of the two actin molecules in this representation appear to be related by a rotation of about 10° along an axis connecting subdomains 1 and 3 of the actin molecule. The direct interaction between actins 1 and 3 (see Section 5.4.1.4 in Chapter 5) might be a main contributor to the orientation of actin 3. It is possible that the orientation in which actin 3 has been captured in the crystal structure represents an effect of crystal packing (see Figures 5.11 and 5.12 C in Chapter 5). We cannot, however, exclude the possibility that the interactions of actin 3 observed in the crystal structure are of physiological relevance. The hydrogen bonds maintained by Q80 and Q90 with actin 3 appear to play no major role for MAL regulation (see Section 5.5.4.1 in Chapter 5). In fact, they appear disengaged in the superposition of the MAL(67-199)-LatB-actin and RPEL2-LatB-actin structures (Figure 6.10; compare to Figure 5.12 C in Chapter 5). In contrast, the interaction between actin bound to RPEL2 and R111 seems to be maintained in the superposition.

Since the spacing of RPEL motifs does not vary across the RPEL domain, it is conceivable that an actin-actin interaction similar to that between actin molecules 1 and 3 in the MAL(67-199)-LatB-actin complex might occur between actins bound to

RPEL2 and RPEL3 (see Figures 5.11, 5.12 and 5.13 in Chapter 5). One can imagine that, if an actin molecule were bound to RPEL3, it would interact with actin bound to RPEL2, thereby reaching across the RPEL2-3 linker, similarly to how actin 3 in the MAL(67-199)-LatB-actin structure faces the entire length of the MAL fragment. This interaction could mask the B2 box, the proposed nuclear import signal of MAL, which acts downstream of actin (see Section 2.2 in Chapter 2). B2 masking might be dynamic and therefore allow for the observed high basal import rate of MAL (see Chapter 3). According to a cooperativity model, actin-actin interactions within a MAL-actin complex would, conceptually, be equivalent to interactions between λ repressor dimers bound to different operator sites (see Section 6.5.1.4).

It will be necessary to address the effect of the actin-actin interactions, since they might be critical for the cooperation of RPEL motifs in MAL regulation. Site-directed mutagenesis of actin and corresponding functional studies will help to resolve this issue.

We will also undertake an electron-microscopy analysis of the MAL-actin-DNaseI complex in cooperation with Carolyn Moores (Birkbeck College, London). This will help to distinguish between crystallisation-induced MAL-actin and actin-actin interactions and those that indeed occur in solution. Electron microscopy will also have the potential to detect higher-stoichiometry MAL-actin complexes.

Future studies will also take a crystallographic approach to addressing the question of whether the observed actin-MAL and actin-actin contacts in the MAL(67-199)-LatB-actin structure represent *bona-fide* interactions or are induced during crystallisation. The use of DNaseI-actin instead of LatB-actin for MAL-actin complex crystallisation has the potential to generate different crystal-packing interactions.

The crystallisation of higher-order MAL-actin complexes with actin occupying all RPEL motifs provides an interesting problem for the future. The use of DNaseI-actin in crystallisation may contribute to achieving this goal. Other approaches will entail site-directed mutagenesis to stabilise RPEL-actin interactions within RPEL-domain crystallisation constructs. Candidate residues are the amino acids corresponding to K71 in RPEL1, whose exchange for isoleucine stabilised the RPEL1-actin interaction (see Section 5.5.1 in Chapter 5). Stabilisation of the RPEL3-actin interaction might be achievable by exchanging the "GP" unit following the "RP" dyad of RPEL3 for the corresponding residues of RPEL motifs 1 and 2 (see Section 6.6.3 and Figure 6.4). However, these mutagenesis approaches will require an extensive prior analysis of the

RPEL-actin interactions, which will be performed using the fluorescence anisotropy assay.

6.9 Contribution of RPEL1 to MAL regulation

The exchange of the MAL N-extension and RPEL1 by the equivalent region of MC (MC-N1-MAL) resulted in a degree of MAL deregulation which exceeded that caused by point mutations (R81A and RR81/82DD) in RPEL1 (see Sections 4.6 and 4.7 in Chapter 4). This might be due to contributions of residues outside the RPEL motif. We cannot exclude the possibility that the sequence spanning the N-extension and RPEL1 of MC contains determinants that actively confer nuclear localisation of MC. In fact, this region contains residues necessary for the activation of MEF2-mediated transcription by MC (Creemers et al., 2006; see also Section 1.4.3.2.1 in Chapter 1; Introduction). Deletion of the N-extension (MAL Δ1-66) moderately increased baseline nuclear localisation of MAL and its ability to activate the SRF reporter (see Figure 8.4 in Chapter 8; Appendix). I did, however, not detect any interaction of the isolated N-extension (MAL(2-66)) with actin in GST affinity sedimentation experiments (data not shown). Furthermore, MAL(67-199) and actin form a complex with an apparent stoichiometry of 1:3 (see Figure 5.5 in Chapter 5). The BSAC splice variant of MAL, which deviates from MAL in sequences preceding RPEL1 (see Figure 1.8 in Chapter 1; Introduction and Figure 2.1 in Chapter 2), also displays a somewhat higher baseline activity and slightly increased tendency to localise to the nucleus in serum-starved NIH3T3 fibroblasts (see Figure 8.4 in Chapter 8; Appendix). Residues outside the PFAM-defined RPEL motif may somehow contribute to MAL regulation without being required for actin binding.

MAL(met) lacks RPEL1 since its translation start site corresponds to M93 in full-length MAL. When expressed in NIH3T3 fibroblasts, it showed a substantial degree of deregulation, both at the level of localisation and SRF reporter activation (see Figure 8.4 in Chapter 8; Appendix). Deregulation of MAL(met) is more severe than that of RPEL1 point mutants presented in Chapter 4 (see Section 4.5). The higher tendency of nuclear localisation and increased basal activity of MAL(met) underlines the contribution of RPEL1 to MAL regulation, although it is clear from this experiment and the analysis presented in Chapter 4 that loss of RPEL1 does not completely abolish MAL regulation by actin. MAL(met) clearly retains a certain degree of Rho-dependence (see Figure 8.4

in Chapter 8; Appendix). An explanation for this might be a potential stabilisation of the RPEL2-actin interaction by R111, which binds D25 of actin in the context of the RPEL2 peptide. I should note that previous results obtained with MAL(met) questioned the importance of RPEL1, given that MAL(met) appeared regulated as the full-length variant of MAL (Miralles et al., 2003; Posern et al., 2004). We later found that the MAL(met) variant used for the previous studies contained a K154R exchange, which appeared to override the loss of RPEL1 at the level of MAL regulation. It would be interesting to elucidate the basis for this observation.

A translocation between chromosomes 22 and 13 (t(1;22)(p13,q13)) results in two different fusion proteins in which the RNA-binding protein RBM15 (also called OTT) becomes fused to the N-terminus of MAL (Ma et al., 2001; Mercher et al., 2001). In one of those, RPEL1 is lost whereas in the other, the full RPEL domain is retained. Either of the fusion proteins is associated with acute megakaryoblastic leukaemia (AML). Both OTT-MAL variants are nuclear when expressed in NIH3T3 fibroblasts, potently activating SRF-mediated transcription. Actin-binding studies suggest that both OTT-MAL variants do not bind actin (Guido Posern, personal communication). It is currently unclear whether loss of actin binding of OTT-MAL contributes to OTT-MAL activity and leukaemogenesis.

6.10 Perspective

We know through biochemical and structural evidence that MAL has the potential to bind up to four actin molecules, three of which are complexed to one RPEL motif each and one is bound to the RPEL1-2 linker. Future work will elucidate the mechanism by which RPEL motifs cooperate in regulating MAL activity.

In the immediate future, we will focus on crystallising the MAL-actin complex with an actin molecule bound to RPEL3. This will require the stabilisation of the MAL-RPEL3 interaction through mutation of the RPEL motif and/or the use of DNaseI to block actin polymerisation while potentially allowing for favourable crystal-packing interactions to occur. Additionally, one might consider destabilisation of actin 3-MAL interactions observed in the current MAL-actin crystal structure.

Parallel biochemical studies will directly address whether actin binding to MAL is cooperative, as strongly predicted by the current insights. We will test how modulation

of actin-binding site affinities and expression of mutant actin derivatives that cannot engage in the actin-actin interactions observed crystallographically affects the response of MAL to decreased G-actin concentrations. It will be interesting to monitor the occupancy of actin-binding sites within the RPEL domain of MAL *in vivo*, especially RPEL3. A possible way to tackle this challenge would be to combine site-directed mutagenesis of MAL with a sensitive FRET-based analysis of the MAL-actin interaction in real time. Additionally, site-specific *in-vivo* crosslinking approaches may prove insightful in the detection of MAL-actin interactions and their changes upon induction of Rho-actin-MAL-SRF signalling. Future work will also have to address the molecular nature of the nuclear import and export signals of MAL and how, mechanistically, they confer actin-controlled nucleocytoplasmic shuttling of MAL. Furthermore, the mechanism by which a nuclear MAL-actin interaction inhibits transcriptional activity of MAL remained unclear and poses an interesting question for future studies.

This combined approach will resolve how MAL can sensitively yet robustly respond to a growth-factor induced depletion of the cellular G-actin pool.

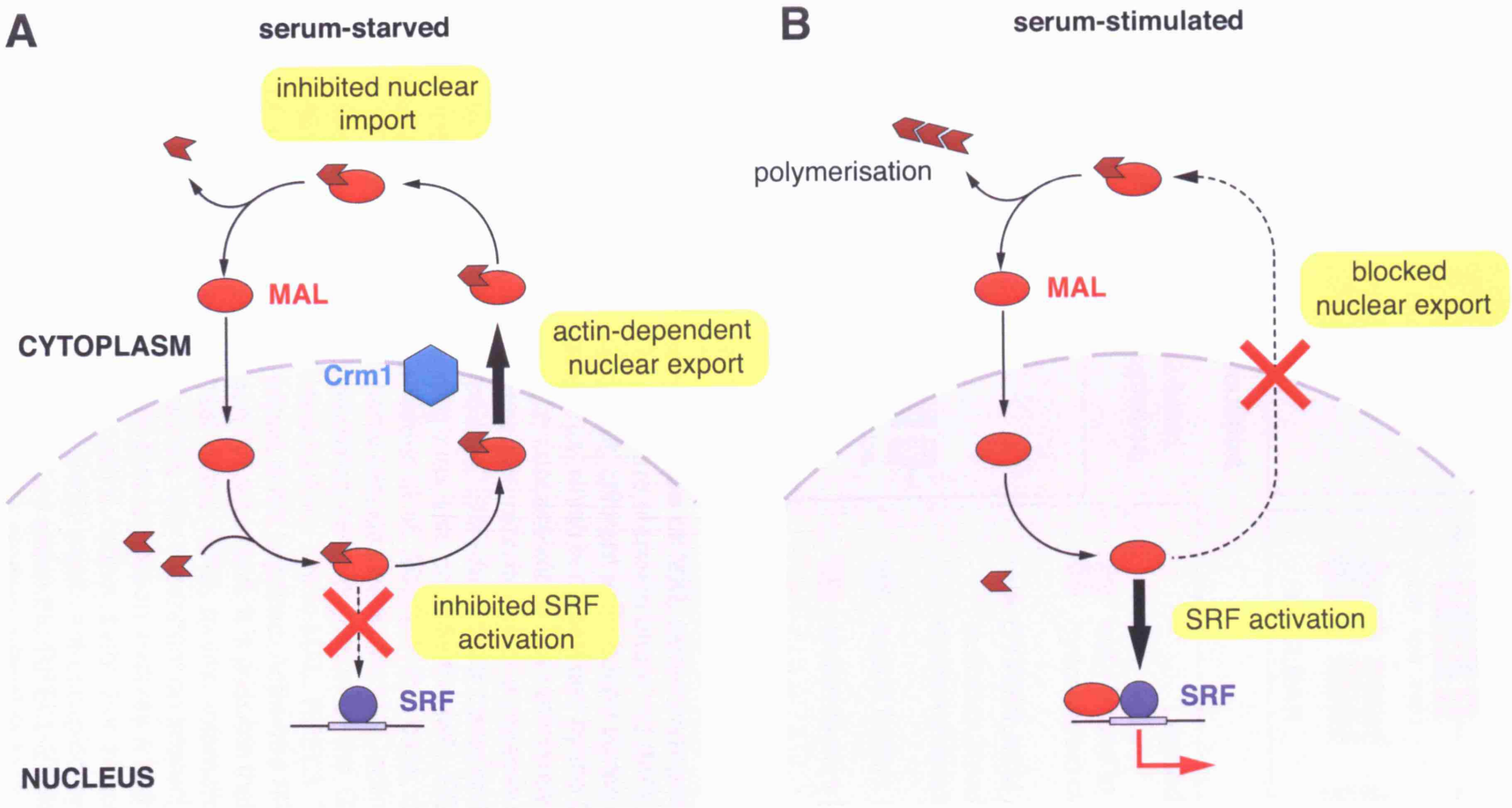

Figure 6.1 Multiple levels of MAL regulation by actin. (**A**) In serum-starved NIH3T3 fibroblasts, MAL (bright red) constantly and rapidly shuttles between nucleus and cytoplasm. Actin (dark red) binding targets MAL for efficient, CRM1-dependent nuclear export, resulting in cytoplasmic steady-state localisation of MAL. Nuclear actin prevents SRF (dark blue) activation by the low levels of MAL passing through the nucleus. (**B**) Upon induction of RhoA signalling, G-actin levels decrease, and a change in MAL-actin interaction blocks nuclear export of MAL. MAL accumulates in the nucleus and activates SRF-mediated transcription.

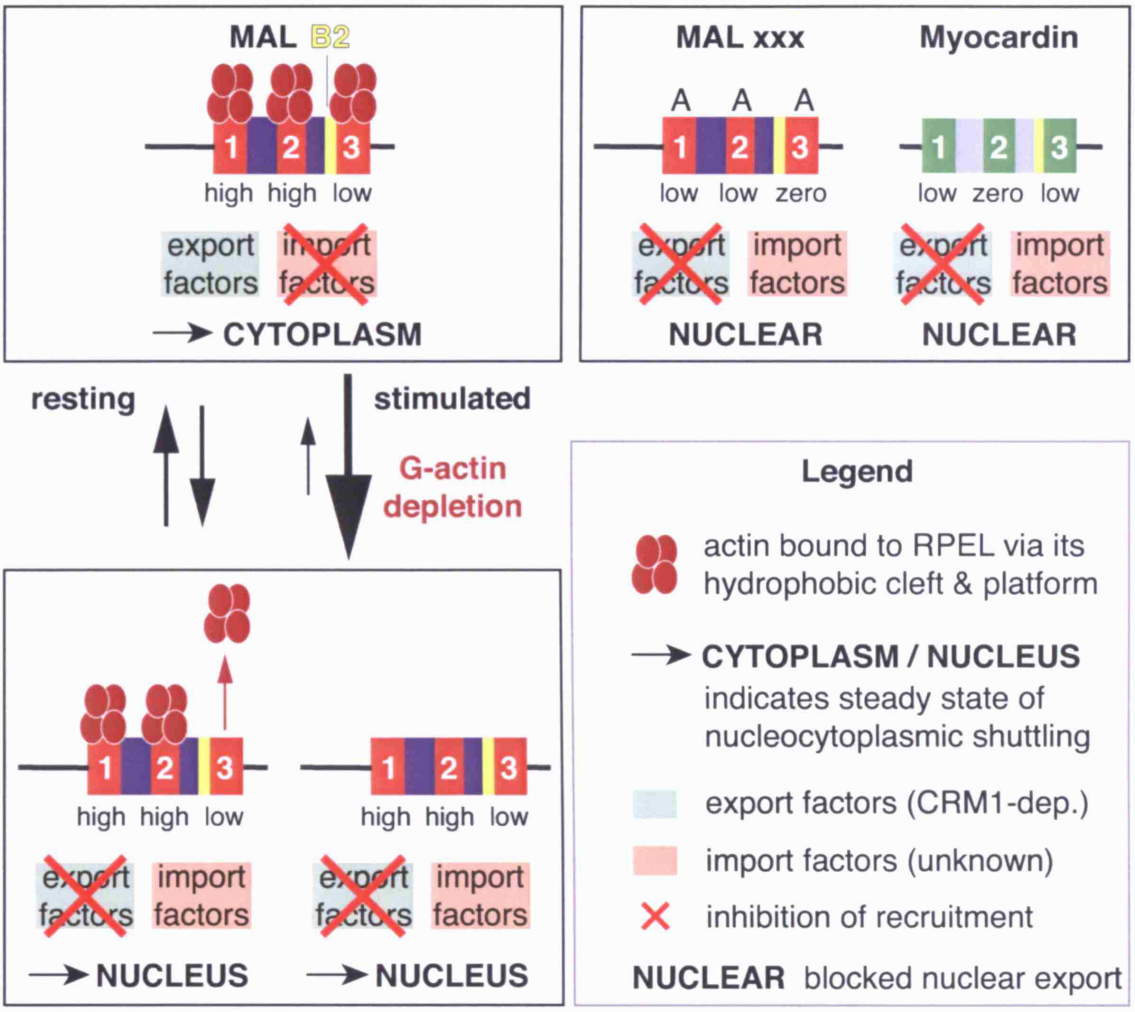

Figure 6.2 A model for the regulation of MAL nucleocytoplasmic shuttling and activity by actin. RPEL motifs are shown in bright red (MAL) or green (MC) with relative affinities indicated. Left, different actin-bound states of MAL are in a dynamic equilibrium with each other, which is determined by the G-actin concentration. Top, in resting cells, actin concentrations are sufficiently high to ensure occupancy of RPEL3, actin-dependent recruitment of a putative export factor to MAL and inhibition of MAL-mediated, SRF-dependent transcription. At high G-actin concentration, actin binding may also occlude the MAL B2 nuclear import signal adjacent to RPEL3 (Vartiainen et al., 2007). In this case, dynamic binding of actin to RPEL3 or conformational changes within the MAL-actin complex might confer shuttling. Bottom, in stimulated cells, depletion of the G-actin pool first affects binding of actin to its lowest-affinity site in MAL, RPEL3. This results in a block of nuclear export while import is not impaired. Actin-free MAL would represent a substrate of nuclear import but not export. It is possible that, in active MAL, actin remains bound to a subset of the RPEL motifs. Interaction of actin with RPEL3 of MAL confers regulation in a way dependent on interaction of actin with the RPEL1-RPEL2 unit. It is likely that regulation involves a higher-order actin-MAL complex formed through positive cooperativity. For simplicity, the figure shows a complex in which all three RPEL motifs are occupied by actin; the functional relevance of the actin-binding site within the RPEL1-2 linker still needs to be elucidated. In contrast, MC, or actin binding-defective MAL RPEL mutants, display very weak actin binding and are therefore insensitive to the G-actin concentration; they are substrates for import but not export. Differential regulation of MAL and MC is conferred by differential actin binding to RPEL motifs 1 and 2.

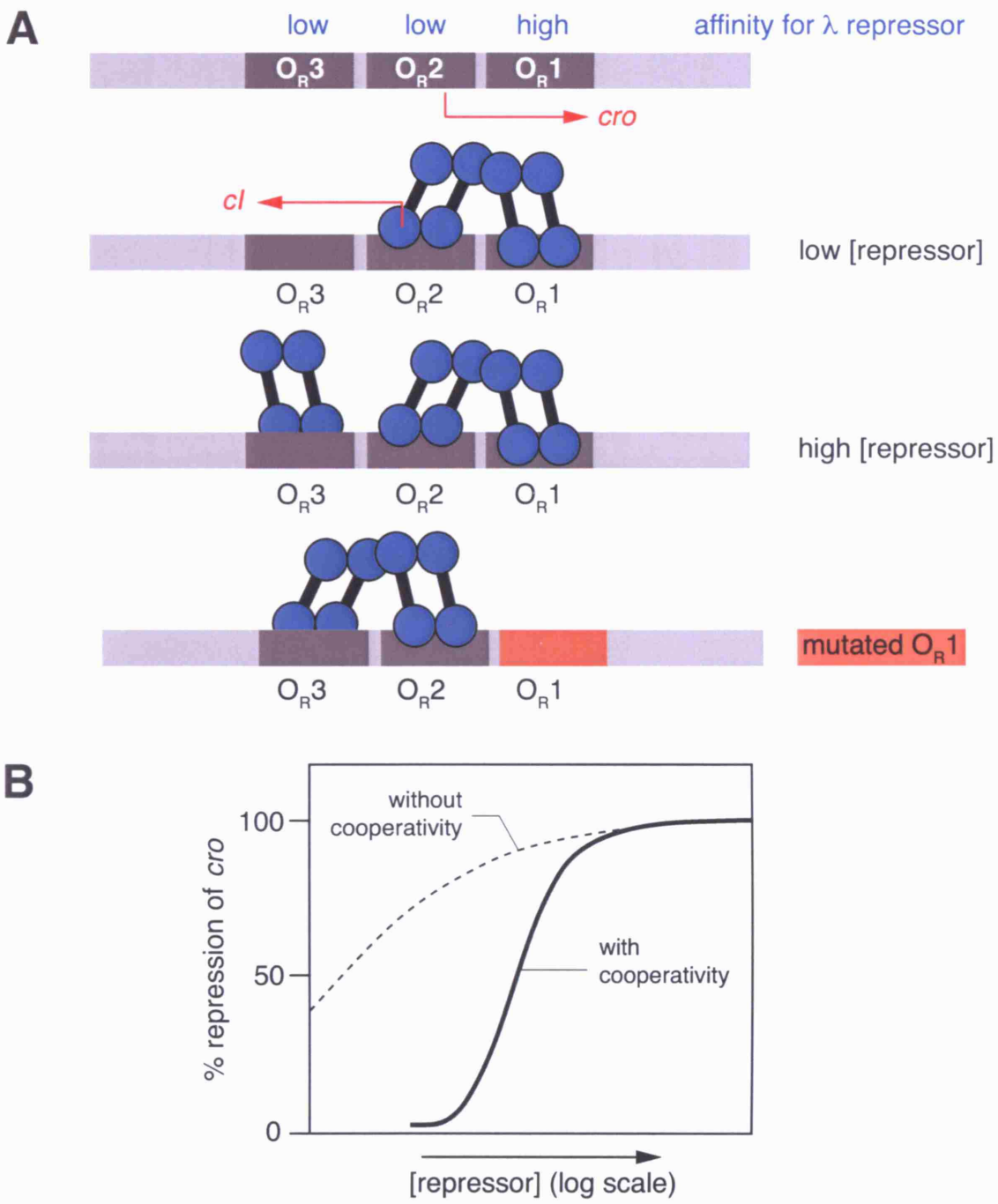

Figure 6.3 Positive cooperativity in the recruitment of λ repressor to operator sites in phage λ. (**A**) DNA is shown in light grey and operators in dark grey. Red arrows indicate gene transcription. λ repressor, in blue, consists of an N- and a C-terminal globular domain connected by a flexible linker and forms dimers, which bind DNA. At low repressor concentrations, λ repressor binds to O_R1, and this immediately recuits another repressor dimer to the low-affinity O_R2 site through repressor-interaction mediated positive cooperativity. Binding of repressor to O_R2 helps RNA polymerase bind to transcribe cI, the gene encoding λ repressor. The low-affinity O_R3 site is only occupied at high repressor concentrations. Mutation of O_R1 (red) results in positive cooperativity in repressor binding to O_R2 and O_R3. (**B**) Plot of repression of cro versus repressor concentration: the solid line represents the multi-site operator-repressor system of phage λ while the dased line illustrates a single-site operator-repressor system. See text for details. Concept of the figure adapted from Ptashne, 2004.

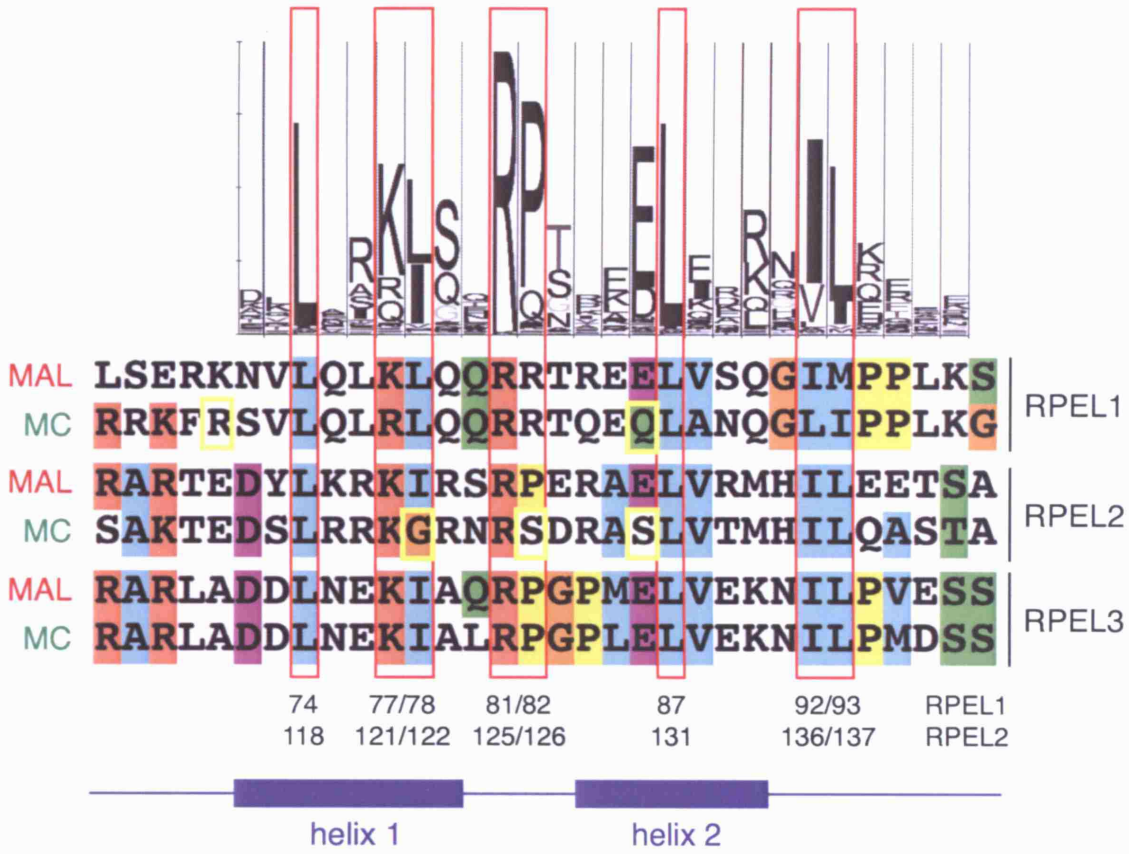

Figure 6.4 Sequence conservation within the RPEL motifs reflects actin binding. Bottom, sequence alignment of mouse MAL and myocardin (MC) generated by ClustalX (Thompson et al., 1997) with helices 1 and 2 observed in the RPEL-actin crystal structures indicated in blue. Top, HMM Logo representation reflecting sequence conservation across all 180 RPEL motifs present in the PFAM database to-date (Schuster-Bockler et al., 2004; Finn et al., 2006). Key amino acids making direct contact with actin in the RPEL1- and RPEL2-actin crystal structures are indicated by red boxes and positions below the sequences. Candidate residues for explaining differential actin binding by MAL and MC RPEL motifs are highlighted in yellow. See text for details. Compare with Figure 5.10 in Chapter 5 for direct RPEL-actin contacts.

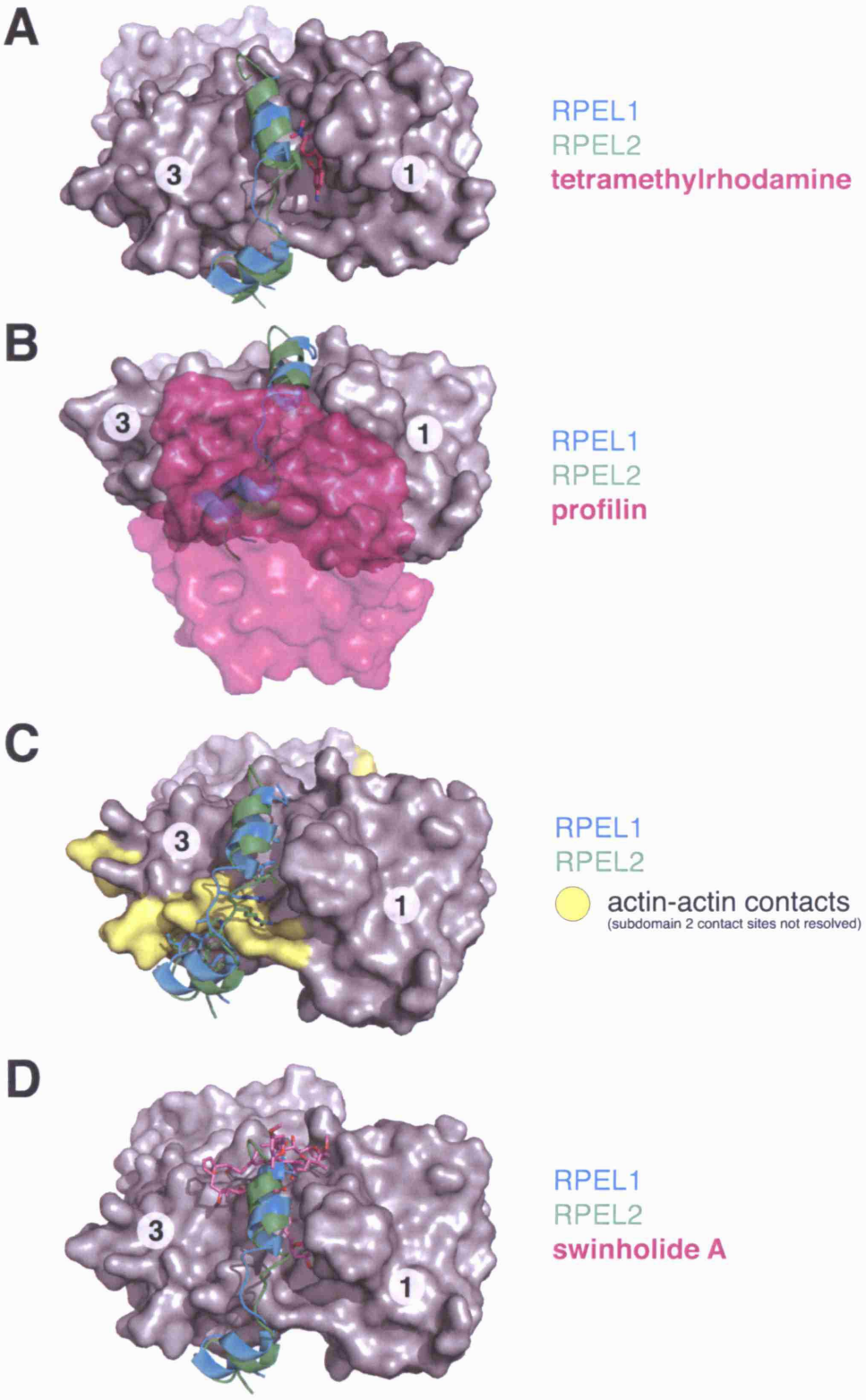

Figure 6.5 Steric clashes of tetramethylrhodmine, profilin, F-actin, and swinholide A with the RPEL-actin interaction. Competition of RPEL1 and RPEL2 with (**A**) tetramethylrhodamine coupled to C374 (1J6Z; Otterbein et al., 2001), (**B**) profilin (2BTF; Schutt et al., 1993), (**C**) actin-actin contacts in the Holmes filament model (Holmes et al., 1990) and (**D**) swinholide A (1YXQ; only one actin molecule shown for simplicity; Klenchin et al., 2005). The RPEL side chains that directly contact actin are shown in (B) for reference; see Figure 5.8 in Chapter 5 for details and numbering.

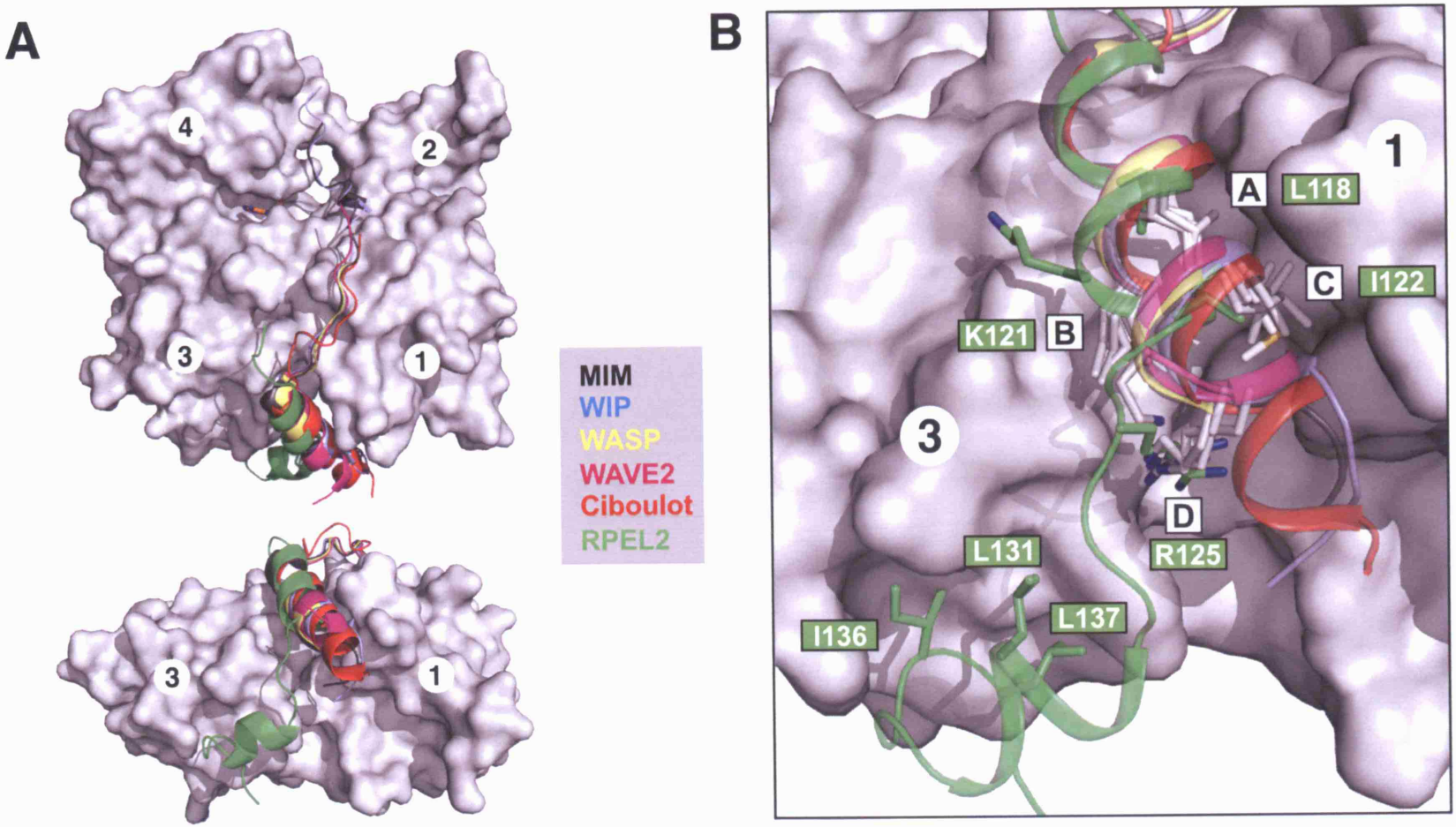

Figure 6.6 WH2 motifs and RPEL motifs target the hydrophobic cleft of actin via a conserved set of interactions. (**A**) Superposition of the indicated WH2 domains and RPEL2 bound to actin (top, "classical" front view of actin; bottom, view onto the base of the subdomain 1-3 interface of actin. (**B**) Detailed view of (A). RPEL2 residue numbers and the nomenclature of the conserved positions of interaction (A-D) are indicated. Colouring is identical to (A).
The analysis was done by Stephane Mouilleron.

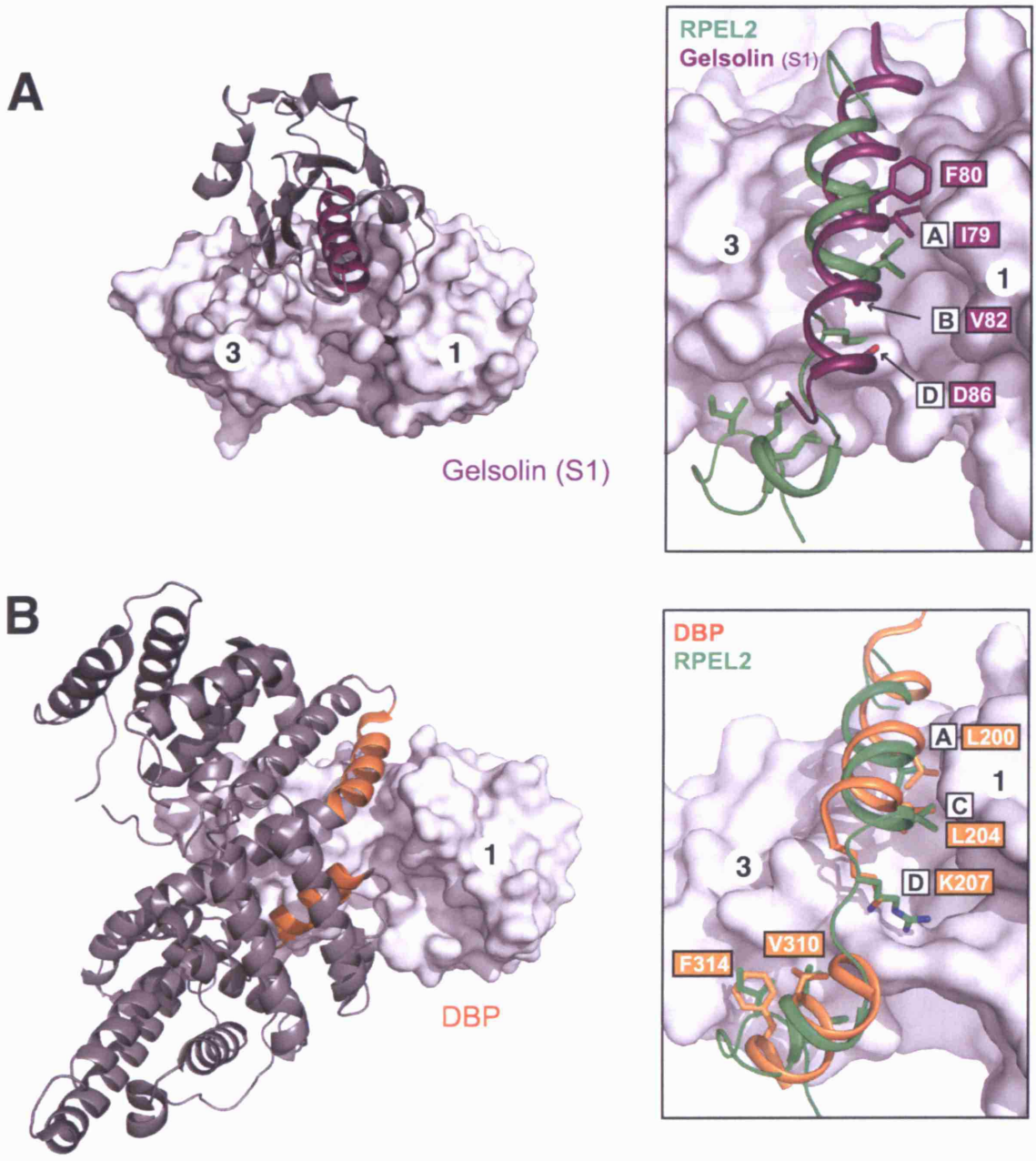

Figure 6.7 Similarities in the interactions of gelsolin, vitamin-D binding protein and RPEL motifs with actin. (**A**) Superposition of gelsolin segment 1 (1EQY; McLaughlin et al., 1993) and MAL RPEL 2 bound to actin: left, view onto the base of the actin molecule; right, detailed view with conserved interactions indicated. The helix in gelsolin that corresponds to helix 1 of the RPEL motif is shown in purple. (**B**) Superposition of vitamin D-binding protein (DBP; 1KXP; Otterbein et al., 2002) and MAL RPEL2, equivalent to (A). Note that, like the RPEL motif, DBP docks onto actin via two helices; one targets the hydrophobic cleft while the other binds the subdomain-3 platform of actin. Even a polar interaction corresponding to R125 in RPEL2 occurs in DBP via K207. The residue nomenclature introduced in Figure 6.6 is shown.
The analysis was done by Stephane Mouilleron.

A

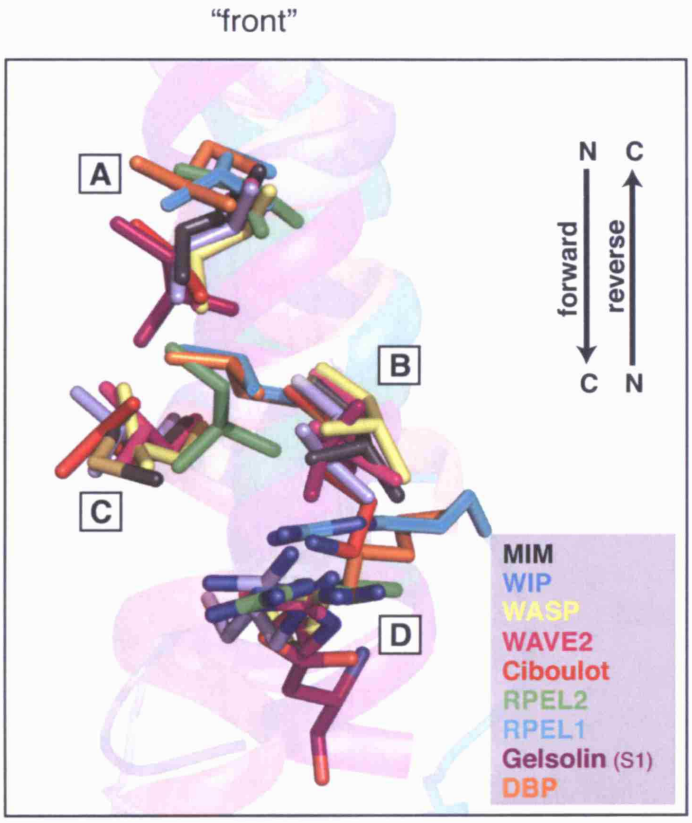

B

	WASP	WIP	WAV E2	MIM	Ciboulot	RPEL1	RPEL2	Gelsolin	DBP
	2A3Z	2A41	2A40	2D1K	1SQK	-	-	1EQY	1KXP
domain	WH2	WH2	WH2	WH2	WH2/Tβ4	RPEL	RPEL	-	-
helix orientation	reverse	reverse	reverse	reverse	reverse	forward	forward	forward	forward
A	I438	I40	I443	I735	L22	L74	L118	I79	L200
	-	-	-	-	-	-	-	-	-
	-	-	-	-	-	-	-	-	-
B	L435	L37	L440	L732	K19	K77	K121	V82	-
C	L434	L36	L439	M731	L18	L78	I122	-	L204
	-	-	-	-	-	-	-	-	-
	-	-	-	-	-	-	-	-	-
D	R431	R33	R436	-	(K19)	R81	R125	D86	K207

Figure 6.8 Helices that target the hydrophobic cleft of actin bind in different directionalities. (**A**) Structural alignment of the helices that correspond to helix 1 of the RPEL motifs in the indicated proteins. The relationship between the helix termini and their directionalities is indicated by arrows. The "front" (see Figure 1.1 A for definition) of the actin molecule would correspond to the top of the figure. (**B**) Table corresponding to the structural alignment in (A) with equivalent amino acids indicated (WASP, WIP, WAVE2 and MIM, Chereau et al., 2005; ciboulot, Hertzog et al., 2004; gelsolin segment 1, McLaughlin et al., 1993; DBP, Otterbein et al., 2002). D86 of gelsolin (segment 1 numbering) is of the opposite charge to amino acids present at this position in many other actin-binding proteins, but it interacts with actin (see Figure 6.5). The classification of positions A, B, C and D was done according to the positions of the amino-acid side chains.
The analysis was done by Stephane Mouilleron.

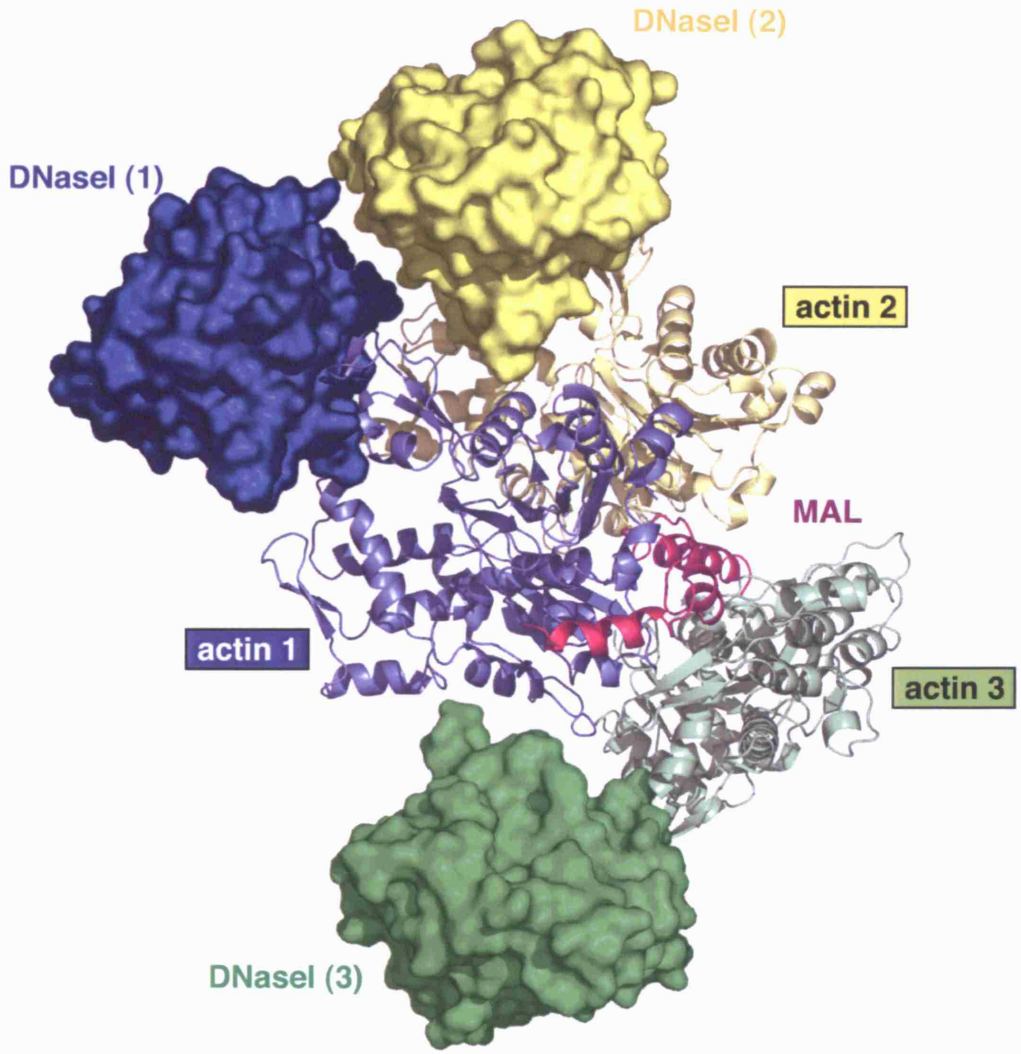

Figure 6.9 Superposition of DNaseI-actin onto the MAL(67-199)-LatB-actin crystal structure. The actin molecules of the DNaseI-actin structure (1ATN, Kabsch et al., 1990) were superimposed onto those of the MAL(67-199)-LatB-actin structure. Actin molecules superimposed onto actins 1, 2 and 3 are coloured as in Figure 5.11 in Chapter 5. The corresponding DNaseI molecules are shown in surface representation and more intense colours. Note that there is no steric clash between the DNaseI molecules.

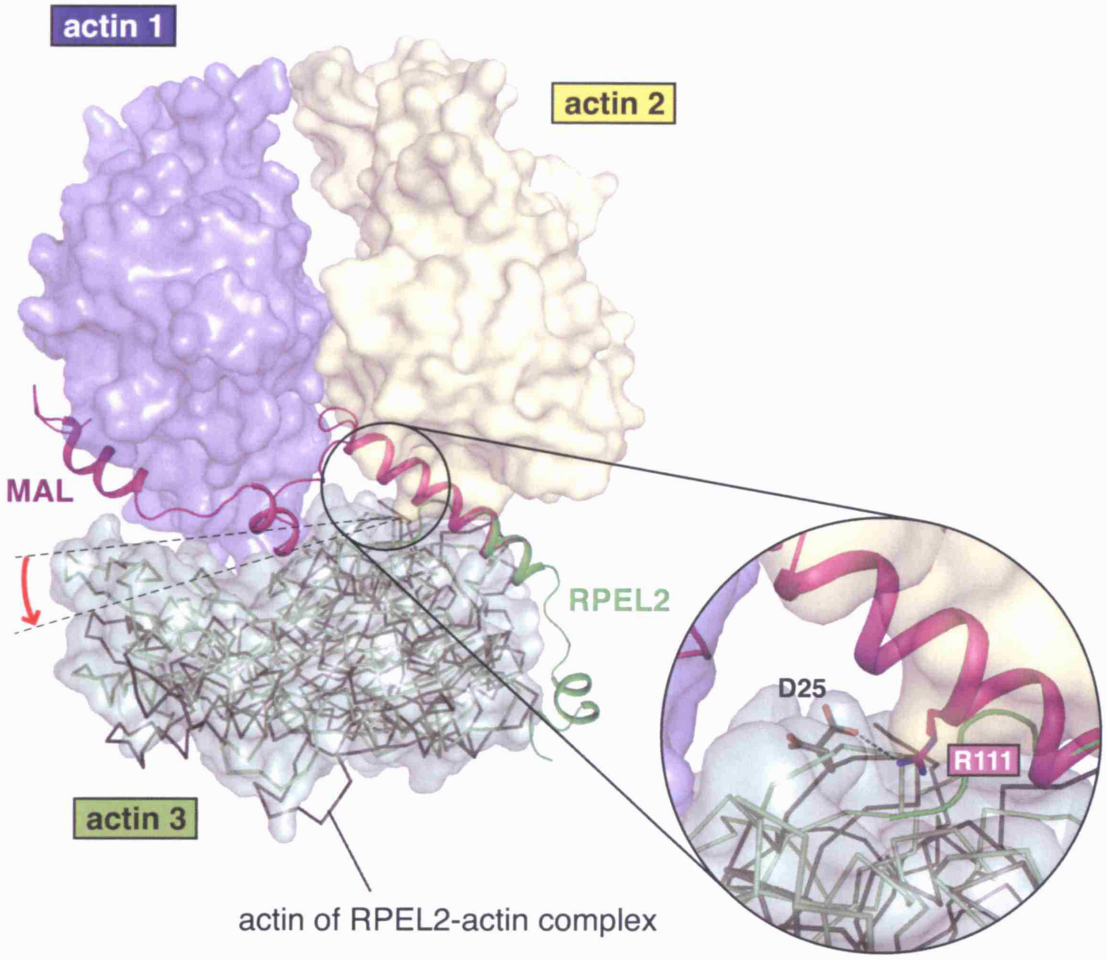

Figure 6.10 Superposition of the MAL(67-199)-LatB-actin and RPEL2-LatB-actin structures. Helix 1 of the RPEL2-LatB-actin structure was superimposed onto the end of helix 3 of the MAL(67-199)-LatB-actin structure. Actin 3 of the MAL(67-199)-LatB-actin complex and actin bound to RPEL2 are shown as α-carbon trace in light and dark green, respectively. Actin 3 is also shown in surface representation. The spatial relationship of the two actin molecules can be approximated by a rotation indicated by the red arrow. Note that an interaction between Q80 and Q90 of MAL and actin bound to RPEL 2 would be impossible due to the rotation (see Figure 5.12 for comparison). The interaction of R111 of MAL and this actin molecule could, at least theoretically, occur (see inset). See text for details.
The superposition was done by Stephane Mouilleron.

7 Materials and Methods

7.1 Chemicals and reagents

Most chemicals were obtained from Sigma, Merck and Roche unless stated otherwise. A list of the most commonly used reagents and materials follows. Method-specific reagents are described in the relevant sections.

Acrylamide/Bisacrylamide 37.5:1 solution	AMRESCO
ATP (disodium salt)	Sigma
Agarose	Invitrogen
Ammonium persulphate	Sigma
Ampicillin	Sigma
Benzamidine	Sigma
Bromophenol Blue	BioRad
BSA (acetylated)	Sigma
Chloramphenicol	Boehringer Mannheim
Complete protease inhibitor cocktail tablets	Roche
Coomassie Brilliant Blue	BioRad
Cytochalasin D	Calbiochem
Dithiothreitol (DTT)	Calbiochem
Dimethyldichlorosilane solution	BDH
Dimethyl sulfoxide (DMSO)	Fisher Scientific
Ethidium bromide	Boehringer Mannheim
Glycogen	Boehringer Mannheim
Isopropyl-β-D-thiogalactopyranoside (IPTG)	MP Biomedicals
Jasplakinolide	Calbiochem
Kanamycin	Sigma
Latrunculin A	Sigma
Latrunculin B	Calbiochem
Leupeptin	Sigma
β-mercaptoethanol	Sigma
Milk powder	Marvel

PROTRAN® nitrocellulose transfer membrane	Whatman
dNTPs	Pharmacia
Orange G	Sigma
3MM paper	Whatman
Phenylmethyl-sulfonyl fluoride (PMSF)	Sigma
Poly(dIdC)•poly(dIdC)	Amersham
Protein assay reagent	BioRad
Protein electrophoresis marker (SeeBlue Plus2 Prestained Standard)	Invitrogen
Revidue ^{32}P dNTPs	Amersham
Slide-A-Lyzer dialysis cassettes	Pierce
Spermidine	Sigma
Swinholide A	Calbiochem
TEMED	Sigma
Trizma-base	Sigma
Triton X-100	Sigma
Tween® 20	Sigma
Xylene cyanol	Biorad

Restriction enzymes were obtained from New England Biolabs (NEB) and used as recommended by the manufacturer. Additional enzymes used were purchased from the following companies:

Biotaq Red DNA polymerase	Bioline
Calf intestinal alkaline phosphatase	NEB
Proofstart DNA polymerase	Qiagen
Proteinase K	Gibco BRL
RNase inhibitor	Boehringer Mannheim

Enzymes were used with the buffers supplied by the manufacturer where applicable.

7.2 Buffers and solutions

Buffers and solutions were prepared with deionised water (Milli-Q plus system, Millipore) and, where necessary, sterile-filtered using a 0.2 μm vaccum-driven filtration system (Millipore). A list of the most commonly used solutions follows. Method-specific buffers and solutions are described in the respective sections.

PBS	0.17 mM NaCl
	3 mM KCl
	1 mM Na_2HPO_4
	1.8 mM KH_2PO_4 pH 7.4
TBE	89 mM Tris Base
	89 mM boric acid
	2 mM EDTA
TE	10 mM Tris-HCl pH 8.0
	1 mM EDTA pH 8.0
TEN	10 mM Tris-HCl pH 7.5
	1 mM EDTA pH 7.5
	100 mM NaCl

7.3 Expression vectors

Protein expression in mammalian cells

MAL, actin and derivatives were expressed from the following vectors:

pEF-FLAG	derived from EF.plink (Hill et al., 1995); produces an N-terminal FLAG epitope tag
pEF-MYC	derived from EF.plink (Hill et al., 1995); produces an N-terminal MYC epitope tag

pEF-HA	derived from EF.plink (Hill et al., 1995); produces two C-terminal HA epitope tags

Protein expression in reticulocyte lysate in vitro translation systems

SRF(120-265) was expressed from the following vector:

pFTX5	derived from T7Plink (Howell and Hill, 1997); produces an N-terminal Myc epitope tag

Protein expression in E. coli

GST-fusion proteins were expressed from the following vectors:

pET-41a	Novagen (contains an enterokinase site)
pET-41a-3CΔ	modified from pET-41a by replacement of the enterokinase site with a 3C protease site and deletion of all restriction endonuclease sites 5' of *BamHI*

7.4 Oligonucleotides

Oligonucleotides were synthesised by the Cancer Research UK oligonucleotide synthesis service or Sigma Genosys. All oligonucleotides were deprotected and desalted. Lyophilised oligonucleotides were dissolved in water to final concentrations of 20 or 100 μM in TE, pH 8.0 and stored at -20 °C.

7.5 Peptides

Peptides (Table 7.1) were synthesised and HPLC (high-performance liquid chromatography)-purified by the Cancer Research UK Protein and Peptide Chemistry Laboratory. Peptides were synthesised with an N-terminal amino group, unless N-terminally modified, and a C-terminal carboxyl group. N-terminal fluorescein labels were linked to peptides via ε-aminohexanoic acid (EAhx). Lyophylised peptides were dissolved in 10 mM Tris-HCl pH 8.0, 10 mM NaCl (unlabelled peptides) or Mg^{2+}-F-buffer containing 0.7 mM ATP (fluorescein-conjugated peptides; see Section 7.13.1 for buffer) and insoluble material removed by centrifugation. Peptide solutions were snap-frozen in liquid nitrogen for storage at -80 °C.

peptide name	peptide sequence
MAL RPEL1 (67-98)	LSERKNVLQLKLQQRRTREELVSQGIMPPLKS
MAL RPEL2 (111-142)	RARTEDYLKRKIRSRPERAELVRMHILEETSA
MAL RPEL3 (155-186)	RARLADDLNEKIAQRPGPMELVEKNILPVESS
MAL RPEL1-2 linker (96-111; 16 aa)	LKSPAAFHEQRRSLER
FITC-MAL RPEL1 (32 aa) wild-type	LSERKNVLQLKLQQRRTREELVSQGIMPPLKS
R81A	LSERKNVLQLKLQQ**A**RTREELVSQGIMPPLKS
R81/82DD	LSERKNVLQLKLQQ**DD**TREELVSQGIMPPLKS
L74A L78A I92A	LSERKNV**A**QLK**A**QQRRTREELVSQG**A**MPPLKS
K71A L74A L78A I92A	LSER**A**NV**A**QLK**A**QQRRTREELVSQG**A**MPPLKS
K71A L74A L78A RR81/82AA I92A	LSER**A**NV**A**QLK**A**QQ**AA**TREELVSQG**A**MPPLKS
K71I	LSER**I**NVLQLKLQQRRTREELVSQGIMPPLKS
FITC-MAL RPEL1-2 linker (96-111; 16 aa)	LKSPAAFHEQRRSLER
FITC-MAL RPEL2 (32 aa) wild-type	RARTEDYLKRKIRSRPERAELVRMHILEETSA
R125A	RARTEDYLKRKIRS**A**PERAELVRMHILEETSA
R111A	**A**ARTEDYLKRKIRSRPERAELVRMHILEETSA
FITC-MAL RPEL2+N (104-142; 39 aa)	EQRRSLERARTEDYLKRKIRSRPERAELVRMHILEETSA
FITC-MAL RPEL2-3 linker (138-159; 22 aa)	EETSAEPSLQAKQLKLKRARLA
FITC-MAL RPEL3 (32 aa) wild-type	RARLADDLNEKIAQRPGPMELVEKNILPVESS
R169A	RARLADDLNEKIAQ**A**PGPMELVEKNILPVESS
FITC-MC RPEL1 (32 aa)	RRKFRSVLQLRLQQRRTQEQLANQGLIPPLKG
FITC-MC RPEL2 (32 aa)	SAKTEDSLRRK**G**RNRSDRASLVTMHILQASTA

peptide name	peptide sequence
FITC-MC RPEL3 (32 aa)	RARLADDLNEKIALRPGPLELVEKNILPMDSS

Table 7.1 Peptides used in this study.

Mutations are indicated in bold.

7.6 Bacterial manipulations

7.6.1 Bacterial strains

DH5α	Invitrogen; used for plasmid propagation and cloning procedures
JM110	Stratagene; used for production of unmethylated DNA
BL21 (DE3)	Invitrogen; used for expression of recombinant proteins
Rosetta (DE3) pLysS	Novagen; used for expression of MAL- and MC-derived proteins and GST-3C protease

7.6.2 Bacterial media

LB media	1% w/v Bacto-tryptone, 0.5% w/v Bacto-yeast extract, 1% w/v NaCl
LB agar	1% w/v Bacto-tryptone, 0.5% w/v Bacto-yeast extract, 1% w/v NaCl, 1.5% w/v Bacto-agar

In accordance with plasmid antibiotic resistance markers, liquid media and LB agar plates were supplemented with 100 µg/ml ampicillin, 30 µg/ml kanamycin, or 34 µg/ml chloramphenicol or combinations of those for selection.

7.6.3 Preparation of electrocompetent *E. coli*

A single *E. coli* colony grown on LB agar was inoculated in 15 ml of LB media and grown overnight at 37 °C and 200 rpm. 10 ml of saturated culture was transferred into 1 l of LB medium. Cells were grown at 37 °C with shaking at 200 rpm until they reached OD_{600} = 0.5 (± 0.03). The culture was chilled on ice for 20 min, and cells were collected by centrifugation at 3,000 xg for 15 min at 4 °C. The pellet was re-suspended in 1 l of ice-cold 10% glycerol and incubated on ice for 20 min. The wash, centrifugation and incubation steps were repeated twice, reducing the pellet re-suspension volume first to 100 and then to 4 ml. The bacterial suspension was divided into 50 µl aliquots in pre-chilled microcentrifuge tubes and snap-frozen in liquid nitrogen before storage at -80 °C.

7.6.4 Transformation of *E. coli* by electroporation

50 µl of electrocompetent *E. coli* were thawed on ice and mixed with purified DNA dissolved in water or TE, typically up to 1 µg, or 5 µl out of 10 µl of DNA obtained from a ligation reaction (see Section 7.7.4.5) after purification. The cell-DNA mixture was transferred into an ice-cold electroporation cuvette (0.2 cm gap, Geneflow) and subjected to an electric pulse of 2.5 kV (capacitance, 25 µF; resistance s, 200 Ω) using a BioRad Gene pulser with a pulse controller. 450 µl of LB media were immediately added to the cell suspension, which was incubated at 37 °C for 1 h. Cells were then plated on LB plates containing the appropriate concentration of antibiotic, depending on antibiotic resistance markers of plasmids. For propagation of plasmid DNA, cells were streaked with an inculation loop. For ligation samples and propagation of low-copy number plasmids, the complete cell suspension was plated.

7.7 Nucleic acid manipulations and recombinant DNA techniques

7.7.1 Purification of plasmid DNA

A single *E. coli* colony grown on LB agar with the appropriate antibiotics was inoculated in 5 or 10 ml (small-scale preparation, miniprep) or 200 ml (large-scale preparation, maxiprep) of antibiotic-supplemented LB media and grown overnight at 37 °C and 200 rpm. Miniprep DNA was isolated by the Cancer Research UK Equipment

Park miniprep service using a Qiagen Biorobot 9600. Maxiprep DNA was isolated using a Plasmid Maxi Kit (Qiagen) according to the manufacturer's instructions.

7.7.2 Quantitation of nucleic acids

Concentrations of double-stranded DNA and RNA were determined by measuring absorption at 260 nm using a ND-1000 UV/Vis spectrophotometer (NanoDrop Technologies). One A_{260} unit corresponds to 50 µg/ml double stranded DNA and 40 µg/ml RNA. Nucleic acid purity was assessed by measuring sample absorption at 280 nm. An A_{260}/A_{280} ratio of ≥ 1.8 but ≤ 2.0 indicates pure DNA whereas A_{260}/A_{280} ratio of ≥ 2.0 indicates pure RNA.

7.7.3 Agarose gel electrophoresis

1-3% agarose gels were prepared in 1x TBE with 0.5 µg/ml ethidium bromide. Samples were supplemented with 5x DNA loading buffer. Gels were run in 1x TBE with at 100-150 V for the required times, using 100 bp and 1kb DNA ladders (New England Biolabs, NEB) as markers. DNA was visualised on a White/2UV Transilluminator (Ultra-Violet Products, UVP).

5x DNA loading buffer	0.01 % w/v Orange G
	30 % glycerol in TE pH 8.0

7.7.4 Recombinant DNA techniques

cDNA fragments, obtained either by restriction endonuclease digestion of a previously generated plasmid or PCR and subsequent restriction endonuclease cleavage of sites introduced with the PCR primers, were ligated into appropriately restriction-endonuclease digested vectors. Generated constructs were verified by DNA sequencing.

7.7.4.1 Polymerase chain reaction (PCR)

PCR was used to amplify cDNA for subcloning and the generation of mutant derivatives by site-directed mutagenesis. ProofStart DNA polymerase (Qiagen) was used because of its high proofreading activity and a chemical modification that reduces primer degradation during PCR setup. Oligonucleotide primers were designed

according to their purpose and desired melting temperature, and restriction endonuclease sites and point mutations were introduced as required.

Components of standard 50 µl PCRs were:

- 1 µl of 10 ng/µl template DNA
- 0.5 µl each of 100 µM forward and reverse primers
- 0.6 µl dNTPs (25 mM each)
- 2.5 units of ProofStart DNA polymerase (1 µl, Qiagen)
- 5 µl 5x PCR buffer
- ad 50 µl H_2O

PCRs were carried out in a Biometra TRIO-thermoblock thermal cycler.

DNA was amplified using the following standard programme:

95 °C	5 min (initial melting and enzyme activation)	
95 °C	1 min	⎫
50-60 °C	30 s - 1 min	⎬ x 30-35 cycles
72 °C	1-2 min	⎭
72 °C	3 min	
4 °C	∞	

PCR products were purified as described below (see Section 7.7.4.4).

7.7.4.2 Restriction endonuclease digestion

Restriction endonuclease reactions were performed for 1 to 2 h as instructed by the manufacturer. Up to 5 µg of DNA were used in a 50 µl reaction.

7.7.4.3 Dephosphorylation of DNA fragment ends

To prevent re-ligation of vectors without insert, 5′ phosphate groups were removed from restriction-endonuclease digested vectors using calf intestinal alkaline phosphatase (CIP; NEB). 0.5 µl of the enzyme were added to the restriction endonuclease digestion reaction, followed by incubation for 30 min - 1 h at 37 °C and DNA fragment purification.

7.7.4.4 Purification of DNA fragments generated by enzymatic reactions

DNA fragments generated by PCR, restriction endonuclease digestion or 5'-dephosphorylation were purified using the QIAquik or MinElute PCR product purification kits (Qiagen) unless several DNA species were generated. In this case, DNA was resolved by agarose gel electrophoresis (see Section 7.7.3) and desired fragments extracted from the gel using the QIAquik or MiniElute Gel Extraction kits (Qiagen) according to the manufacturer's instructions.

7.7.4.5 DNA ligation

Relative concentrations of vector and insert DNA were assessed by agarose gel electrophoresis (see Section 7.7.3). DNA ligations reactions were performed in 15 µl, using approximately 250 - 500 ng of restriction-endonuclease digested and 5'-dephosphorylated vector DNA, a 3-fold molar excess of insert DNA and 280 units of T4 DNA ligase in 1x T4 DNA ligase buffer (NEB). Reactions were incubated at 16 °C overnight, purified by ethanol precipitation (see Section 7.7.6) and taken up in 10 µl of H_2O, of which 5 µl were used for electrotransformation of *E. coli* DH5α (see Section 7.6.4). Transformed *E. coli* were plated on LB agar plates and colonies screened for the desired constructs upon small-scale DNA isolation (miniprep) by restriction endonuclease digestion and/or DNA sequencing.

7.7.4.6 Site-directed mutagenesis and insertions

Mutations were introduced into RPEL domains by modifying the corresponding cDNA sequences, which lie 5' of unique *BamHI* restriction endonuclease sites in both the MAL and MC cDNA. The 5' cloning sites were *BamHI* for pEF-MAL-HA and *NcoI* for pEF-MC-HA whereas their 3' cloning site were *XbaI* (Figure 7.1). Primers were designed to contain the desired mutations with typically 12-15 nonmodified nucleotides on either side of the change to achieve annealing (Table 7.2). Fragments to be subcloned were generated in two successive PCRs, extending the primer into either direction using primers that anneal across or beyond the 5' and 3' *NcoI* or *BamHI* restriction nuclease sites: the product of the first PCR was purified, and all of it was used as "megaprimer" in the second PCR. If the yield of the second PCR was low, a third PCR was performed on the product of the second PCR to amplify the product, using the flanking primers. The resulting DNA fragment was purified, *BamHI*- or

NcoI+BamHI-digested and purified again (see Section 7.7.4.4). pEF-MAL-HA was *BamHI*-digested and 5'-dephosphorylated whereas pEF-MC-HA was digested with *BamHI+XbaI* or *NcoI+XbaI*. Only the vector backbone obtained upon *NcoI+XbaI*-digestion of pEF-MC-HA was 5'-dephosphorylated. The fragments were purified and ligated as described above (see Sections 7.7.4.4 and 7.7.4.5).

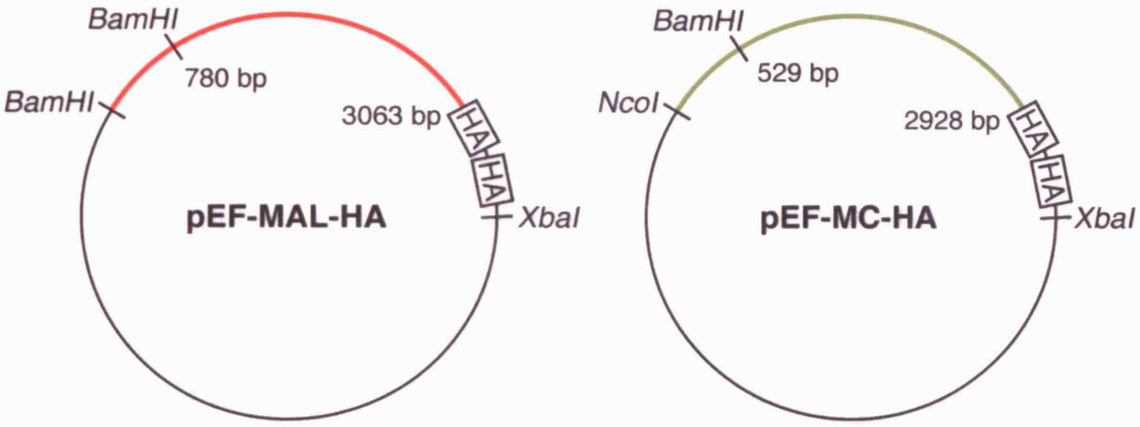

Figure 7.1 pEF-MAL-HA and pEF-MC-HA plasmids.

Coding sequences for MAL and MC are indicated in red and green, respectively with commonly used restriction endonuclease sites. The regions encoding the RPEL domains are contained within the indicated *BamHI-BamHI* and *NcoI-BamHI* fragments of MAL and MC, respectively.

Insertions or mutations of larger stretches of DNA were introduced essentially in the same way. For modifications extending over stretches larger than could be incorporated into a single oligonucleotide primer, a double-stranded fragment containing the mutation/insertion with sequences 5' and 3' of it that match the template was generated by extension of an overlapping primer pair in a single annealing – polymerisation cycle. The product was used in two successive PCRs like a primer containing a point mutation (see above).

RPEL domain chimaeras between MAL and MC were generated using primers corresponding to the cross-over points and that contained both MAL- and MC-derived cDNA sequences (Table 7.2). These primers were used in two successive PCRs similar to the introduction of point mutations except that the templates for these PCRs were pEF-MAL-HA in one and pEF-MC-HA in the other PCR. The chimaeric cDNA fragments were subcloned as described for point mutants. Cross-over points between MAL and MC for chimaeras shown in Figure 4.10, Chapter 4, were placed directly 3' to the codons encoding P66 (N-extension), E104 (up to including RPEL1), A148 (up to

including RPEL2), L187 (up to including RPEL3) in MAL and the equivalent sites in MC (Table 7.2).

plasmid	description
pEF-MAL-HA	full-length mouse MAL cloned by Francesc Miralles (Miralles et al., 2003); subcloned as *BamHI-XbaI* fragment as shown in Figure 7.1; produces protein with 2 C-terminal HA tags
MAL x23	R81A (reverse oligonucleotide g ttc ctc ccg ggt ccg AGC ctg ctg gag ctt c)
MAL 1x3	R125A (reverse oligonucleotide gc tct ctc ggg AGC gga acg gat ctt c)
MAL 12x	R169A (forward oligonucleotide gaa aag att gca cag GCT cct ggc ccc atg)
MAL xx3	R81A R125A
MAL x2x	R81A R169A
MAL 1xx	R125A R169A
MAL xxx (123-1A)	R81A R125A R169A; described as MAL-123-1A in Vartiainen et al., 2007
MAL-1^{DD}	RR81/82DD (reverse oligonucleotide g ttc ctc ccg ggt GTC GTC ctg ctg gag ctt c)
MAL-2^{MC}	RPEL motif 2 of MAL, as defined by PFAM at the onset of this study (amino acids 116-137) was substituted for the equivalent region of RPEL motif 2 of MC (amino acids 62-83) using the primer pair GAG CGG GCC AGG ACC GAG gat tcc ctg agg cgc aag ggc aga **aac agg tcc gac cgt gcc ag** (forward) and GG CTC AGC CGA GGT CTC TTC gag aat gtg cat agt aac cag **gct ggc acg gtc gga cct gtt** (reverse) to generate a megaprimer by annealing and extension (MAL sequence capitalised; annealing sequences in bold).
MAL-123-2A	R82A P126A P170A (R82A, reverse oligonucleotide g ttc ctc ccg ggt AGC ccg ctg ctg gag ctt c; P126A, reverse oligonucleotide ctc tgc tct ctc GGC ccg gga acg gat; P170A, forward oligonucleotide att gca cag agg GCT ggc ccc atg gag)
MAL L74A L78A	forward oligonucleotide cgg aag aat gtg GCT cag ttg aag GCT cag cag cgg cgg
MAL K71A L74A L78A	forward oligonucleotide ctt agt gag cgg GCT aat gtg GCT cag ttg aag GCT cag cag cgg cgg
MAL K71A L74A L78A I92A	forward oligonucleotide g gtg agc caa ggg GCT atg ccg cct ttg for introduction of I92A exchange
MAL K71A	forward oligonucleotide ctt agt gag cgg GCT aat gtg ctg cag
MAL K71M	forward oligonucleotide ctt agt gag cgg ATG aat gtg ctg cag
MAL L118A I122A	forward oligonucleotide g acc gag gac tat GCT aaa cgg aag GCT cgt tcc cgg ccc
MAL L162A I166A	forward oligonucleotide ctg gct gat gac GCT aat gaa aag GCT gca cag agg cct g
MAL F102N	forward oligonucleotide g aaa agc ccc gct gca AAT cat gag cag ag
F102A Q105A L109A	forward oligonucleotide gc ccc gct gca GCT cat gag GCT aga aga agc GCT gag cgg gcc ag

MAL AA100/101TE Q105P	forward oligonucleotide ct ttg aaa agc ccc ACC GAG ttt cat gag CCA aga aga agc ctg
MAL Q80A	forward oligonucleotide g ttg aag ctc cag GCT cgg cgg acc cgg
MAL Q90A	forward oligonucleotide gaa ctg gtg agc GCT ggg atc atg ccg
MAL R111A	forward oligonucleotide ga aga agc ctg gag GCT gcc agg acc gag
MAL R111S	forward oligonucleotide ga aga agc ctg gag TCC gcc agg acc gag
MAL ΔRPEL	Δ67-186 (PFAM ± 5 aa); reverse oligonucleotide gat agc ctc ctt cag tgg agg taa att ggg
MAL Δ1-186	forward oligonucleotide tat *ggatcc* ctg aag gag gct atc att gtg (*BamHI*)
MAL ΔB2 (WT, xxx)	Δ149-159 (see Miralles et al., 2003); reverse oligonucleotide gc aat ctt ttc att gag gtc atc ggc ctg gag cga agg ctc agc
pEF-FLAG-MAL(2-204)-PK (WT, xxx, ΔB2)	region encoding MAL residues 2-204 cloned as *BamHI-BamHI* fragment between sequences coding for FLAG tag and chicken pyruvate kinase; amplified using forward oligonucleotide EF+ and reverse oligonucleotide tat *ggatcc* act gtc tgc tac ctt tgg g; pEF-FLAG-PK obtained from Francesc Miralles (1270 bp corresponding to PK subcloned as *BamHI-EcoRI* fragment)
pEF-FLAG-MC(2-150)-PK	region encoding MC residues 2-150 cloned as *BamHI-BamHI* fragment between sequences coding for FLAG tag and chicken pyruvate kinase; amplified using forward oligonucleotide tat *ggatcc* aca ctc ctg ggg tct gaa c and reverse oligonucleotide tat *ggatcc* tgc atc tgc tgc ctt gga g; pEF-FLAG-PK obtained from Francesc Miralles (1270 bp corresponding to PK subcloned as *BamHI-EcoRI* fragment)
pEF-MAL-HA-NLS	The nuclear localisation signal of SV40 large T antigen was fused to the C-terminus of MAL-HA. A *BclI-XbaI* fragment was produced using forward oligonucleotide tat *t gat ca*g ttt gat att ctt att cag and reverse oligonucleotide tat *tctaga* cta **CAC CTT CCG CTT TTT CTT AGG CGG** CCC tgc ata gtc cgg gac gtc ata g (NLS sequence in bold capital letters, Gly codon capitalised).
pEF-MAL(2-261)-HA-NLS (WT, xxx)	MAL(2-261) cloned as *BamHI-XbaI* fragment, amplified using forward oligonucleotide EF+ and reverse oligonucleotide tat *tctaga* cta **CAC CTT CCG CTT TTT CTT AGG CGG** CCC tgc ata gtc cgg gac gtc ata ggg ata GCC cgc ata gtc agg aac atc gta tgg gta CCC atc cgg agc cat tgg gag ttg (NLS sequence in bold capital letters, Gly codons capitalised); produces protein with 2 C-terminal HA tags followed by the nuclear localisation signal of SV40 large T antigen
pEF-MC-HA	mouse MC, transcript variant A (accession number NM_145136; obtained by Francesc Miralles by RT-PCR from mouse cardiac RNA), cloned as *NcoI-XbaI* fragment as shown in Figure 7.1; produces fusion protein with 2 C-terminal HA tags

MAL-N-MC	Amino acids 1-16 of MC were exchanged for amino acids 2-66 of MAL using reverse oligonucleotide gac tga tcg gaa ctt cct tct TGG AGG TAA ATT GGG GTT CC (MAL sequence capitalised).
MAL-N1-MC	Amino acids 1-50 of MC were exchanged for amino acids 2-104 of MAL using reverse oligonucleotide c act atc caa ttg ttt tct cgg CTC ATG AAA TGC AGC GGG G (MAL sequence capitalised).
MAL-N12-MC	Amino acids 1-94 of MC were exchanged for amino acids 2-148 of MAL using reverse oligonucleotide c tct ttt gag ctt cat ctg agc GGC CTG GAG CGA AGG CTC (MAL sequence capitalised).
MAL-N123-MC	Amino acids 1-133 of MC were exchanged for amino acids 2-187 of MAL using reverse oligonucleotide c agt acc ttt tat agc ctc ttt CAG GCT GGA CTC CAC AGG (MAL sequence capitalised).
MC-N-MAL	Amino acids 2-66 of MAL were exchanged for amino acids 1-16 of MC using reverse oligonucleotide CAC ATT CTT CCG CTC ACT AAG aat cag caa aga gtg ttc aga c (MAL sequence capitalised).
MC-N1-MAL	Amino acids 2-104 of MAL were exchanged for amino acids 1-50 of MC using reverse oligonucleotide G CTC CAG GCT TCT TCT CTG gtc atg gaa ttc agt tgg acc (MAL sequence capitalised).
MC-N12-MAL	Amino acids 2-148 of MAL were exchanged for amino acids 1-94 of MC using reverse oligonucleotide CT CCT CAG CTT CAG CTG CTT agt tgg aat gga cct ttc tgc (MAL sequence capitalised).
MC-N123-MAL	Amino acids 2-187 of MAL were exchanged for amino acids 1-133 of MC using reverse oligonucleotide CC CAC AAT GAT AGC CTC CTT cac gga aga atc cat cgg c (MAL sequence capitalised).
MC-2^{MAL}	RPEL motif 2 of MC, as defined by PFAM at the onset of this study (amino acids 62-83) was substituted for the equivalent region of RPEL motif 2 of MAL (amino acids 116-137) using the primer pair caa ttg gat agt gcc aag act gaa GAC TAT TTG AAA CGG AAG ATC CGT **TCC CGG CCC GAG AGA GCA G** (forward) and ga cct ttc tgc cgt gga ggc ttg CAG AAT GTG CAT CCT GAC CAG CTC **TGC TCT CTC GGG CCG GGA** (reverse) to generate a megaprimer by annealing and extension (MAL sequence capitalised; annealing sequences in bold).
MC 12x	R115A (forward oligonucleotide g aag atc gct ctc GCT cca ggg ccc ttg)
MAL-N12-MC 3^{x}	R169A (MAL numbering) in the context of MAL-N12-MC
MC-(N-41)-MAL	Amino acids 2-95 of MAL were exchanged for amino acids 1-41 of MC using reverse oligonucleotide G AAA TGC AGC GGG GCT TTT CAA tgg cgg tat taa gcc ttg gtt ag (MAL sequence capitalised).

MAL-(N-110)-MC	Amino acids 1-56 of MC were exchanged for amino acids 2-110 of MAL using reverse oligonucleotide g gga atc ttc agt ctt ggc act CTC CAG GCT TCT TCT CTG CTC (MAL sequence capitalised).
pEF-BSAC-HA	obtained from Francesc Miralles; cloned as *BamHI-XbaI* fragment (as MAL; see Figure 7.1)
pEF-MAL Δ1-66	forward oligonucleotide tat *ggatcc* ctt agt gag cgg aag aat g
pEF-FLAG-MAL	obtained from Francesc Miralles (Miralles et al., 2003)
pEF-FLAG-MAL(met)	obtained from Francesc Miralles (Miralles et al., 2003); K154R exchange corrected by Maria Vartiainen
pEF-FLAG-β-actin	human; obtained from Guido Posern (Posern et al., 2002); cloned as *NcoI-XbaI* fragment
pEF-FLAG-α-actin	mouse skeletal-muslce α actin; obtained from Guido Posern; cloned as *NcoI-XbaI* fragment
pEF-MYC-β-actin R62D	human; obtained from Guido Posern (Posern et al., 2002); cloned as *NcoI-XbaI* fragment
pET-41a-3CΔ-MAL(2-261) (WT and RPEL mutant derivatives)	region encoding MAL residues 2-261 cloned as *BamHI-EcoRI* fragment; amplified using forward oligonucleotide EF+ and reverse oligonucleotide tat *gaattc* tta atc cgg agc cat tgg gag
pET-41a-3CΔ-MAL(187-261)	region encoding MAL residues 187-261 cloned as *BamHI-EcoRI* fragment; amplified using forward oligonucleotide tat *ggatcc* ctg aag gag gct atc att gtg and reverse oligonucleotide tat *gaattc* tta atc cgg agc cat tgg gag
pET-41a-3CΔ-MAL(2-199)	region encoding MAL residues 2-199 cloned as *BamHI-XhoI* fragment; amplified using forward oligonucleotide EF+ and reverse oligonucleotide tat *ctcgag* tta tgg gta att tac ctg gcc
pET-41a-3CΔ-MAL(67-199)	region encoding MAL residues 67-199 cloned as *BamHI-XhoI* fragment; amplified using forward oligonucleotide tat *ggatcc* ctt agt gag cgg aag aat g and reverse oligonucleotide tat *ctcgag* tta tgg gta att tac ctg gcc
pET-41a-3CΔ-BSAC(2-142)	region encoding BSAC residues 2-142 cloned as *BamHI-XhoI* fragment; amplified using forward oligonucleotide tat *ggatcc* act ctg ctg gag cct g and reverse oligonucleotide tat *ctcgag* tta tgg gta att tac ctg gcc
pET-41a-3CΔ-MAL RPEL1 (WT, R81A, RR81/82DD)	region encoding MAL residues 67-98 (PFAM ± 5 aa) cloned as *BamHI-EcoRI* fragment; amplified using forward oligonucleotide tat *ggatcc* ctt agt gag cgg aag aat g and reverse oligonucleotide tat *gaattc* cta gct ttt caa agg cgg cat g
pET-41a-3CΔ-MAL RPEL2 (WT, R125A)	region encoding MAL residues 111-142 (PFAM ± 5 aa) cloned as *BamHI-EcoRI* fragment; amplified using forward oligonucleotide tat *ggatcc* cgg gcc agg acc gag g and reverse oligonucleotide tat *gaattc* cta agc cga ggt ctc ttc cag
pET-41a-3CΔ-MAL RPEL3 (WT, R169A)	region encoding MAL residues 155-186 (PFAM ± 5 aa) cloned as *BamHI-EcoRI* fragment; amplified using forward oligonucleotide tat *ggatcc* aga gcc agg ctg gct gat g and reverse oligonucleotide tat *gaattc* cta cag gct gga ctc cac agg

pET-41a-3CΔ-MC (2-209)	region encoding MC residues 2-209 cloned as *BamHI-XhoI* fragment; amplified using forward oligonucleotide tat *ggatcc* aca ctc ctg ggg tct gaa c and reverse oligonucleotide tat *ctcgag* tta ctg gga ggc tgc atc att c
pET-41a-3CΔ-MC RPEL1	region encoding MC residues 13-44 (PFAM ± 5 aa) cloned as *BamHI-EcoRI* fragment; amplified using forward oligonucleotide tat *ggatcc* aga agg aag ttc cga tca gtc and reverse oligonucleotide tat *gaattc* tta acc ttt cag tgg cgg tat taa g
pET-41a-3CΔ-MC RPEL2	region encoding MC residues 57-88 (PFAM ± 5 aa) cloned as *BamHI-EcoRI* fragment; amplified using forward oligonucleotide tat *ggatcc* agt gcc aag act gaa gat tcc and reverse oligonucleotide tat *gaattc* tta tgc cgt gga ggc ttg gag
pET-41a-3CΔ-MC RPEL3	region encoding MC residues 101-132 (PFAM ± 5 aa) cloned as *BamHI-EcoRI* fragment; amplified using forward oligonucleotide tat *ggatcc* aga gcc cgc ctt gca gat g and reverse oligonucleotide tat *gaattc* tta gga aga atc cat cgg cag aat g
pET-41a-gelsolin S4-6	obtained from Guido Posern; region encoding human gelsolin S4-6 subcloned as *BamHI-HindIII* fragment

Table 7.2 Expression plasmid constructs used in this study.

Mutations were introduced by mutagenesis oligos that were designed to span across and anneal 5' and 3' to the codons to be changed. Mutagenesis PCRs were performed on templates of MAL or MC (or their derivatives), typically in pEF-HA. Flanking primers used to extend the mutagenesis oligo in either direction were EF+ (forward oligonucleotide annealing 5' of the MCS: ttctcaagcctcagacagtgg), cc agg atc cgg agc cat tg (reverse oligonucleotide spanning across the unique *BamHI* site in MAL) or tat *gga tcc* tgt aga gcc ctg ggg (reverse oligonucleotide containing *BamHI* corresponding to the unique *BamHI* site in MC) unless specified otherwise. To generate MC constructs with MAL-derived N-terminal sequences, the forward oligonucleotide tat *gcc atg* gcc ccc cct tcc gtc att gct g was used to introduce the 5'-*NcoI* restriction site. To generate MAL constructs with MC-derived N-terminal sequences, the forward oligonucleotide tat *ggatcc* atg aca ctc ctg ggg tct g was used to introduce the 5'-*BamHI* restriction site (see Figure 7.1.) Restriction endonuclease sites are shown in italics; STOP codons are underlined. Where no vector name is listed, the vector is pEF-HA.

7.7.5 DNA sequencing

All newly generated constructs were confirmed by DNA sequencing. Sequencing reactions contained 150-200 ng of plasmid, 3.2 pmol of the appropriate primer and 8 µl of dirhodamine big dye terminator cycle mix (BDT versions 1.1 or 3.1; Perkin Elmer) in a 20 µl reaction.

Thermal cycling was as follows:

96 °C	5 min		
96 °C	30 s	]	
50 °C	15 s	}	x 25 cycles
72 °C	4 min	]	
4 °C	∞		

The products were purified by ethanol precipitation (see Section 7.7.6). Fragments were detected by the sequencing service of the Cancer Research UK Equipment Park, using an ABI PRISM 377 DNA sequencer. DNA sequences were analysed using 4Peaks and DNA Strider software.

7.7.6 Ethanol precipitation

DNA in a 20 µl sample was precipitated by addition of 0.5 µl of 0.5 M EDTA, 2 µl of 3 M NaOAc pH 5.2 and 50 µl of 96% ethanol at room temperature for 30 min. DNA precipitates were sedimented by centrifugation at 13,000 rpm in an Eppendorf 5415 R tabletop centrifuge for 30 min at 4 °C, washed with 70 µl of 70% ethanol and speed-vac dried. Volumes were adjusted accordingly for different sample sizes.

7.8 Mammalian cell culture

7.8.1 Cell lines

NIH3T3 mouse fibroblasts (Treisman Laboratory, Cancer Research UK) were used for all cell culture experiments.

7.8.2 Cell culture media and solutions

E4*	equivalent to Dulbecco's MEM
Foetal calf serum (FCS)	Gibco BRL
Opti-MEM I	reduced serum medium; Invitrogen

5x Versene*	1 g/l EDTA; 8 g/l NaCl; 0.2 g/l KCl; 1.16 g/l Na_2HPO_4; 0.2 g/l KH_2PO_4; 1.5 ‰ phenol red; pH 7.2
Trypsin/Versene*	0.25% (w/v) trypsin in 5x versene
*Cancer Research UK media production	

7.8.3 Cell culture conditions

Cells were cultured in E4 supplemented with 10% FCS on tissue culture grade plastic dishes (Corning Incorporated and Beckton Dickinson) in a Forma Scientific incubator at 37 °C and 10% CO_2. Media were warmed to 37 °C in a water bath before addition to cells. To detach cells from the dish, cells were washed once with Versene and then incubated with trypsin/Versene for 1-2 minutes at 37 °C. Cells were serum-starved with E4 containing 0.3% or 0.5% FCS for the times indicated in the relevant sections.

7.8.4 Transient transfection with lipofectamine reagent

NIH3T3 cells were transfected using Lipofectamine reagent (Invitrogen) according to the manufacturer's instructions. Cells were seeded 1 day before transfection, in 24-well dishes for luciferase assays, 6-well dishes for immunofluorescence microscopy, 6-cm dishes for electrophoretic mobility shift assays, and 10-cm dishes for co-immunoprecipitations. DNA was added to half the indicated volume of Opti-MEM and Lipofectamine to the other half (see Table 7.3). DNA and Lipofectamine solutions were mixed by vortexing and incubated at room temperature for 30 min. Cells were washed once with Opti-MEM prior to addition of the indicated volumes of Opti-MEM (see Table 7.3) and incubated with the transfection mixture for 4 h. The transfection mixture was then replaced with E4 containing serum at an experiment-dependent concentration.

plate	cells / plate or well	total amount of DNA	vol. lipofectamine	vol. Opti-MEM I for transf. mix	vol. Opti-MEM I on cells
24-well	3×10^4	0.2 µg	0.6 µl	40 µl	0.2 ml
6-well	1.5×10^5	1 µg	3 µl	200 µl	1 ml
6 cm	3.5×10^5	2 µg	6 µl	400µl	1.6 ml
10 cm	1×10^6	2-4 µg	10 µl	1000 µl	4 ml

Table 7.3 Transfection of NIH3T3 fibroblasts with lipofectamine.

7.9 Luciferase reporter assays

The following quantities of plasmids were routinely used for transfections performed as described in Section 7.8.4: 8 ng p3D.ALuc (SRF reporter), 20 ng ptkRL, 40 ng pMLV.SRF-VP16, 2 ng C3 transferase, and 10 ng of MAL or MC constructs in pEF-HA or pEF-FLAG. The amount of pEF-MAL(2-261)-HA-NLS (WT or xxx) used for luciferase reporter assays was 180 ng. The total amount of DNA used for transfections for luciferase reporter assays typically was 200 ng, achieved by filling up with empty pEF-HA. Where necessary, the amounts of MAL or MC expression constructs were varied to achieve comparable expression levels of the derivatives to be compared. Cells were serum-starved with E4 containing 0.5% FCS upon removal of the transfection mixture. If required, cells were serum-stimulated or treated with the indicated drugs 15 h after media change post transfection for 7 h unless stated otherwise and lysed in 40 µl of passive lysis buffer (Promega) after a single wash with PBS. The PBS wash step was omitted if cells were treated with cytoskeletal toxins to minimise loss of cells. 20 µl of the lysate were transferred into white flat-bottom 96-well polystyrene dishes (Matrix Technology) to perform dual-luciferase assays (Promega). 50 µl of Luciferase Assay Reagent II (Promega) were added and luminescence measured with an MLX Microtiter© plate luminometer (Dynex Technologies) using Revelation software (version 3.2). Luciferase luminescence was quenched and renilla luciferase luminescence elicited by addition of 50 µl of Stop&Glo Reagent (Promega). Renilla luminescence was measured in the same way. Luciferase luminescence values were normalised to renilla luciferase luminescence. All normalised values were

expressed relative to the reporter activity observed upon co-expression of SRF-VP16, which was considered 100%. Values obtained under C3-transferase co-expression were normalised to luciferase reporter activation by SRF-VP16 with C3 transferase co-expression. Data shown are from 3 independent experiments with SEM.

7.9.1 Mammalian reporter plasmids

p3D.ALuc	a derivative of the 3D.ACAT SRF reporter (Mohun et al., 1987) with firefly luciferase in place of the CAT sequence; contains a synthetic promoter with 3 copies of the *Fos* SRF binding site with *Xenopus* type 5 actin TATA box and transcription start site. Constructed by O. Geneste (Geneste et al., 2002)
ptkRL	renilla luciferase controlled by the thymidine kinase promoter (Geneste et al., 2002); an internal reference controlling for transfection efficiencies, cell number and non-specifc effects on the SRF reporter
pMLV.SRF-VP16	a constitutively active SRF derivative used for relative normalisation (Dalton and Treisman, 1992)

7.10 Immunofluorescence microscopy

Cells in 6-well dishes with 2 coverslips per well were transfected as described in Section 7.8.4 (using 100 ng pEF-MAL-HA, pEF-BSAC-HA, pEF-MC-HA, pEF-MAL(2-261)-HA-NLS and derivatives; 50 ng pEF-FLAG-MAL and derivatives; 10 ng pEF-FLAG-MAL(2-204)-PK and derivatives; 10 ng pEF-MC(2-150)-PK; 50 ng pEF-MYC-β-actin R62D). The total amount of DNA used for transfections for immunofluorescence microscopy was 1 μg, achieved by filling up with empty pEF-HA. Cells were serum-starved for 20 h and then treated with 15% FCS, 2 μM CD, 0.1 μM Jasp, 0.3 μM LatB or 20 nM LMB (Calbiochem) as indicated and fixed with 4% formaldehyde or paraformaldehyde in PBS at 37 °C for 10 min. Following fixation, cells were washed once with PBS and stored at 4 °C if necessary before staining. Cells were permeabilised with 0.2% TX-100 in PBS for 10 min. Nonspecific sites were

blocked by incubation with immunofluorescence blocking solution (10% FCS; 1% fish skin gelatin; PBS) for 1 h. Staining was carried out at room temperature on Parafilm (SPI Supplies) in closed plastic dishes containing moist filter paper to prevent samples from drying out (see Table 7.4 for staining reagents). Coverslips were placed with the cell side onto 30 µl drops of the appropriate staining solution. Incubation with primary and secondary antibodies (see Table 7.4) was for 1 h in immunofluorescence blocking solution, respectively, with one washing step in between. For washing, coverslips were dipped into PBS for 5 s. Co-staining of actin filaments with conjugated FITC-phalloidin was together with the secondary antibody (see Table 7.4). After incubation with the secondary antibody, cells were washed once in PBS and stained for DNA using DAPI in PBS for 5 min (see Table 7.4). Coverslips were then washed once with PBS followed by a very brief wash step in water to remove salts and mounted on microscope glass slides with Mowiol. Mowiol was dried overnight at room temperature. The samples were kept in the dark whenever possible after application of fluorescent conjugates to minimise photobleaching. Microscopic samples were stored at -20 °C if kept for longer periods of time.

For preparation of Mowiol mounting medium, 6 ml glycerol, 2.4 g Mowiol 4-88 (Calbiochem), 12 ml Tris-HCl pH 8.5 and 6 ml H_2O were mixed at 50 °C until homogenous. The solution was filtered through a 0.45 µm syringe filter. 2.5% (w/v) 1,2-diazabicyclo-[2.2.2]octane anti-fade reagent (Dabco, Sigma) were added. 1 ml aliquots were stored at -20 °C.

Cells were imaged using a Zeiss Axiovert microscope equipped with a Hamamatsu ORCA-ER digital camera and Smart Capture software (Vysis UK). MAL localisation was scored as predominantly cytoplasmic (C), predominantly nuclear (N) or pan-cellular (N/C) in 100-200 cells in 3 independent experiments with SEM.

primary antibodies			
antibody	**specificity**	**species**	**concentration**
FLAG (F7425; Sigma)	FLAG	rabbit	1/500
12CA5 HA (Roche)	HA	mouse	1/200
MYC (9E10; CR-UK)	MYC	mouse	1/200
MAL22 (MRTF-A) C-19	MAL22	goat	1/100

secondary antibodies			
antigen	**conjugate**	**species**	**concentration**
mouse IgG (Jackson Labs)	Cy3	donkey	1/500
rabbit IgG (Jackson Labs)	Cy3	donkey	1/500
rabbit IgG (Jackson Labs)	Cy2	donkey	1/200
goat IgG (Molecular Probes)	Alexa 488	donkey	1/200

cell staining reagents		
reagent	**cell component**	**concentration**
phalloidin toxin, FITC-conjugated (Molecular Probes)	F-actin	1/200
phalloidin toxin, Texas Red-conjugated (Molecular Probes)	F-actin	1/200
4',6-diamidino-2-phenylindole stain (DAPI; Molecular Probes)	DNA	300 nM

Table 7.4 Reagents for immunofluorescence microscopy.

7.11 Protein Expression and Purification

7.11.1 Expression and purification of recombinant MAL and MC proteins and gelsolin S4-6

E. coli Rosetta (DE3) pLysS were transformed with the expression plasmid. A single clone was selected, and a pre-culture was grown overnight at 37 °C. LB medium was supplemented with 1% glucose as additional carbon source to avoid induction due to overgrowth. 1/200 volume was used to inoculate the expression culture. Expression was induced at OD_{600}=0.6 by addition of 0.5 mM IPTG and performed for 5 h at 25 °C. Cells were pelleted for 30 min at 4,000 xg, and the pellet was resuspended in a small volume of bacterial lysis buffer without detergent. Cells were then frozen on dry ice and stored at -80 °C until processed further.

Bacterial lysis buffer	50 mM Tris-HCl pH 7.5 300 mM NaCl 1% TX-100 5 mM DTT 10 mM EDTA 1 mM PMSF 15 µg/ml benzamidine
PMSF	100 mM stock in isopropanol (stored at -20 °C)
Benzamidine	10 mg/ml stock in H_2O (stored at -20 °C)

Lysis buffer was added to the frozen suspension to a final volume of 50 ml per litre of culture. Cytoplasmic lysozyme was released upon thawing, which greatly facilitated the lysis. To shear the liberated DNA, cells were sonicated 4 times for 1 min each at maximum energy with intervening chilling on ice, using a SANYO Soniprep 150 MSE sonicator. Insoluble material was pelleted by centrifugation at 30,000 xg for 30 min, using a Beckman JA-25.50 or JLA-16.250 rotor in a Beckman Coulter Avanti J-25 centrifuge. GST fusion proteins were bound to glutathione-agarose (Sigma) or glutathione-sepharose 4B (GE Healthcare) for 2-4 h at 4 °C (1 ml resin per litre of culture). The resin was transferred to a column and washed with 10 CV of wash buffer 1, wash buffer 2, 10 CV of ATP wash buffer to remove a DnaK contaminant (MAL and MC only) and equilibrated in equilibration buffer. Washes were done using a Chromabond vacuum manifold for 12 columns (Machery Nagel) connected to a Capex L2C vacuum pump (Charles Austen Pumps) and the corresponding columns.

Wash buffer 1	50 mM Tris-HCl pH 7.5 300 mM NaCl 1 mM DTT

Wash buffer 2	50 mM Tris-HCl pH 7.5 500 mM NaCl 1 mM DTT
ATP wash buffer	50 mM Tris-HCl pH 7.5 50 mM KCl 20 mM $MgCl_2$ 5 mM ATP 1 mM DTT
Equilibration buffer	50 mM Tris-HCl pH 7.5 100 mM NaCl 1 mM DTT

The GST moiety was cleaved from MAL and MC proteins by overnight incubation at 4 °C with 100 µg of GST-3C protease per ml of resin. Gelsolin S4-6 was cleaved overnight using biotin-factor Xa (Roche) according to the manufacturer's instructions. The cleaved protein was eluted with 2 CV of equilibration buffer. Biotin-factor Xa was removed using streptavidin-agarose (Fluka). Following concentration to 1-2 ml in Vivaspin 6 or Vivaspin 20 concentrators (Vivascience), the protein was subjected to gel filtration chromatography into 10 mM Tris-HCl pH 8.0; 10 mM NaCl on Superose-12 (GE Healthcare) using an ÄKTA FPLC system (GE Healthcare). Peak fractions were pooled and concentrated. Proteins (see Table 7.5) were concentrated using VivaSpin 6 and VivaSpin 500 concentrators (5,000 MWCO; PES; Vivascience), snap-frozen in liquid nitrogen and stored at -80 °C. Mass spectrometry and N-terminal Edman sequencing to validate the boundaries of the produced constructs was performed by the Cancer Research UK mass spectrometry service.

protein	theoretical MW (Da)	molar extinction coeff. ε_{280} ($M^{-1}cm^{-1}$)	abs. 0.1% (=1 g/l)
MAL(2-261)	28663.2	2980	0.104
MAL(2-199)	22296.4	2980	0.134
MAL(67-199)	15753.2	2980	0.189
BSAC(2-142)	16600.3	2980	0.180
Gelsolin S4-6	38187.7	65890	1.725

Table 7.5 Parameters of expressed and purified MAL proteins.

Parameters were calculated by *ProtParam* (http://expasy.org/tools/protparam.html), which uses the Edelhoch method (Edelhoch, 1967) for calculation of extinction coefficients but the method of Pace et al. (Pace et al., 1995) for determination of extinction coefficients of tyrosine and tryptophane.

7.11.2 Expression and purification of GST-3C protease

GST-3C protease (in pGEX-2T; kind gift by Phil Knowles) was expressed in Rosetta (DE3) pLysS for 20 h at 25 °C, following induction of expression by addition of 0.1 mM IPTG into the culture grown at 37 °C to OD_{600}=0.6 (Brown et al., 1999). The GST fusion protein was purified essentially as described above for MAL but eluted with 100 mM reduced glutathione (Sigma), followed by dialysis into 50 mM Tris-HCl pH 8.0; 150 mM NaCl; 10% glycerol; 1 mM DTT. The protein was concentrated to about 10 mg/ml using a VivaSpin 6 concentrator (5,000 MWCO; PES; Vivascience) and snap-frozen in liquid nitrogen and stored at -80 °C.

7.11.3 Purification of rabbit skeletal muscle actin

Rabbit skeletal muscle actin was purified essentially as described (Feuer et al., 1948; Spudich and Watt, 1971). All steps were carried out at 4 °C unless stated otherwise, and quantities correspond to about 500 g of muscle tissue. White muscle from rabbit hind legs was minced several times until homogenous. The homogenate was vigorously stirred in the following solutions for the indicated times and drained by filtering trough 4 layers of gauze in between the washing steps:

2 l 10 mM KCl	10 min
2 l 50 mM $NaHCO_3$	10 min
3 l 1 mM EDTA	10 min

The homogenate was split into parts corresponding to about 250 g muscle weight, which were washed as follows:

3.5 l H_2O	5 min (swelling occurs)
3.5 l H_2O	5 min; then bring to room temperature
3.5 l cold acetone	as briefly as possible
2 volumes acetone	10 min at room temperature
2 volumes acetone	10 min at room temperature
2 volumes acetone	10 min at room temperature

The washed homogenate was dried overnight spread out on 3MM Whatman paper in a fume hood and then stored at -20 °C until further use.

Actin was extracted from acetone powder as follows: 10 g of dried acetone powder were hydrated to 200 ml of ice-cold storage G-buffer containing 0.15 mM PMSF and stirred for 1 h on ice. Low temperature and low salt were to minimise troponin and tropomyosin contamination. The hydrated powder was filtered through 4 layers of gauze and the filtrate, containing the extracted actin, collected. The remaining homogenate was extracted once more with 100 ml of storage G-buffer. The pooled filtrates were centrifuged for 90 min at 27,000 xg and 0 °C using a Beckman JLA-16.250 rotor in a Beckman Coulter Avanti J-25 centrifuge to pellet insoluble material.

G-actin was polymerised for 1 to 2 h under slow stirring upon adjusting to 1 mM ATP, 2 mM $MgCl_2$ and 50 mM KCl. Contaminating F-actin binding proteins such as cofilin, troponin and tropomyosin were removed by addition of solid KCl to 600 mM and powerful stirring for 1 to 1.5 h. Polymerised actin was pelleted by centrifugation at 100,000 xg for 1.5 h (34,000 rpm; Beckman Type 50.2 Ti rotor; Beckman Coulter Optima L-100 XP ultracentrifuge). The pellets were re-suspended in storage G-buffer containing 0.5 mM ATP and 1 mM DTT to a total volume of about 30 ml, followed by thorough Dounce homogenisation (60-100 x) on ice, avoiding the introduction of air bubbles. Actin was then dialysed against 2 l of storage G-buffer for 2 to 3 days with daily buffer changes. The ATP concentration was 0.5 mM in the first and 0.2 mM in the last dialysis step. Upon dialysis, insoluble or residual polymerised actin was removed

by ultracentrifugation at 100,000 xg for 30 min. Actin at 5-6 mg/ml was snap-frozen in liquid nitrogen and stored at -80 °C.

Actin concentration was measured spectrophotometrically at 290 nm using a molar extinction coefficient of ε_{290}=26,600 $M^{-1}cm^{-1}$. Although actin was stored as Ca^{2+}-actin, all biochemical experiments have been performed with Mg^{2+}-actin, which represents the physiologically relevant species. The experiment with gelsolin S4-6 was performed in the presence of $CaCl_2$.

Storage G-buffer	5 mM Tris-HCl pH 8.0
	0.2 mM $CaCl_2$
	0.2 mM ATP
	0.5 mM DTT

7.12 Protein analysis

7.12.1 Concentration determination of proteins and peptides

Concentrations were calculated via the Lambert-Beer law (Equation 7.1):

$$A = \varepsilon \, c \, l$$

Equation 7.1 Lambert-Beer law. A, absorption; ε, molar extinction coefficient in M^{-1} cm^{-1}; c, concentration in M; l, cell path length in cm.

Peptide concentration was measured using an Agilent 8453 UV/Vis spectrophotometer and 100 µl quartz cuvettes (Hellma) with a pathlength of 0.3 cm. Absorption of the peptide bond was measured at 215 nm and the concentration calculated using ε_{215}=1,000 M^{-1} cm^{-1} per peptide bond. For fluorescein-labelled peptides, absorption of the fluorophore at 492 nm was exploited to calculate the concentration, using ε_{492}=83,000 M^{-1} cm^{-1} (Information from Invitrogen/Molecular Probes handbook for fluorescein-5-maleimide, product number F150). Concentrations of MAL were measured at 280 nm using a ND-1000 UV/Vis spectrophotometer (NanoDrop Technologies). See Table 7.5 for molar extinction coefficients of recombinant proteins. To avoid interference through absorption by ATP, absorption of actin was measured at 290 nm and concentration calculated using ε_{290}=26,600 M^{-1} cm^{-1}.

7.12.2 SDS-PAGE

Proteins were separated according to their size by SDS-polyacrylamide gel electrophoresis (SDS-PAGE) using a minigel apparatus (ATTA) essentially as described by Laemmli, 1970. 9% gels were used to resolve MAL, 12% gels to resolve actin and MAL(2-261) and 16% gels to resolve small RPEL domain derivatives. The gel mix was prepared as shown in Table 7.6 and poured between two assembled glass plates. The surface was overlaid with water to ensure an even, air-free polymerisation interface. Following polymerisation of the acrylamide, the water was removed, the stacking gel mix was poured on top of the resolving gel and a plastic comb was inserted between the plates to generate the wells.

	resolving gel			**stacking gel**
percentage	9%	12%	16%	
40% acrylamide/ bisacrylamide (37.5:1)	3.38 ml	4.5 ml	6.0 ml	1.27 ml
1 M Tris-HCl pH 8.8	5.65 ml	5.65 ml	5.65 ml	-
1 M Tris-HCl pH 6.8	-	-	-	1.25 ml
10 % (w/v) SDS	150 µl	150 µl	150 µl	100 µl
water	5.62 ml	4.5 ml	3.0 ml	6.37 ml
50 % Glycerol	-	-	-	0.9 ml
10 % (w/v) APS	150 µl	150 µl	150 µl	100 µl
TEMED	15 µl	15 µl	15 µl	10 µl

Table 7.6 Composition of denaturing gels for SDS-PAGE.

After polymerisation of the stacking gel, the comb and plastic seals were removed and the electrophoresis apparatus assembled. Wells were rinsed with 1x SDS running buffer to remove polyacrylamide residuals from the wells. Alternatively, especially if samples were to be subjected to mass spectrometry, pre-cast NuPAGE® Novex Bis-Tris 4-12% gradient gels (Invitrogen) were used with the provided MOPS- and MES-based running buffers according to the manufacturer's instructions.

The samples were boiled for 5 min in SDS sample buffer to denature proteins, allowed to cool down and centrifuged briefly at maximum speed in a tabletop centrifuge (Biofuge Pico, Heraeus Instruments) to ensure their complete recovery. Protein

molecular weight markers (either RPN756 Rainbow marker, GE Healthcare or SeeBlue Plus2 Prestained Standard, Invitrogen) were used in all experiments. Gels were run at 120-180 V in SDS running buffer until the dye front was about to exit the gel. After SDS-PAGE, gels were either subjected to Western blotting (see Section 7.12.3) or stained with Coomassie brilliant blue. For that, gels were immersed in Coomassie staining solution for 30 min and then subjected to multiple de-staining cycles under slow shaking with a paper tissue to absorb liberated Coomassie. De-staining was achieved either in Coomassie de-staining solution or by boiling in water.

1x SDS running buffer	192 mM glycine 25 mM Tris base 0.1% SDS
4x SDS sample buffer	200 mM Tris-HCl pH 6.8 8% SDS 40% glycerol 10% β-mercaptoethanol trace bromophenol blue
Coomassie staining solution	prepared from 2% Coomassie R250 in methanol and 3% acetic acid just prior to use
Coomassie de-staining solution	10% acetic acid 40% methanol

7.12.3 Western blotting

Following SDS-PAGE, proteins were transferred onto a PROTRAN® nitrocellulose membrane (Whatman). Gel and membrane were sandwiched between two layers of Whatman 3MM paper, one on either side. Protein transfer was performed using a Mini Trans-Blot Cell (Biorad) containing an ice pack for 2 h at 200 mA per transfer unit. After the transfer, the membrane was stained using Ponceau S to assess protein loading and transfer, de-stained in water and incubated in Western blot blocking solution for 30 minutes at room temperature to saturate the membrane with protein and

minimise non-specific binding of the antibody. The membrane was then incubated with the primary antibody (Table 7.7) in Western blot blocking solution for 1 h at room temperature or overnight at 4 °C on a shaker. The membrane was then washed three times for 5 min with PBS-Tween prior to incubation with a secondary antibody conjugated to horseradish peroxidase (HRP; Table 7.7) in PBS-Tween for 45 min. The membrane was then washed again three times for 5 min with PBS-Tween, and the HRP activity was detected with ECL Western blotting detection reagents (GE Healthcare). Equal volumes of ECL solutions A and B were mixed and applied to the membrane for 1 min. Excess liquid was removed, and the membrane exposed to ECL Hyperfilm (GE Healthcare). Primary antibodies directly coupled to HRP were applied to the membrane in Western blot blocking solution for 1 h at room temperature. After that, the steps following the incubation with secondary antibodies described above were followed.

Transfer buffer	192 mM glycine 25 mM Tris base 10% methanol
PBS-Tween	PBS 0.1% Tween® 20 (polyethylene glycol sorbitan monolaurate)
Western blot blocking solution	PBS-Tween® 20 5% dry milk powder
Ponceau S solution	2% (w/v) Ponceau S 30% (v/v) trichloroacetic acid

primary antibodies			
antibody	**specificity**	**species**	**concentration**
FLAG (F7425; Sigma)	FLAG	rabbit	1/500
M2 FLAG (Sigma)	FLAG	mouse	1/2000
M2 FLAG-HRP (Sigma)	FLAG	mouse	1/2000
3F10 HA-HRP (Roche)	HA	rat	1/750
AC-15 β-actin (Sigma)	β-actin	mouse	1/500
B-5-1-2 α-tubulin	α-tubulin	mouse	1/2500

secondary antibodies			
antigen	**conjugate**	**species**	**concentration**
rabbit IgG (DAKO)	HRP	goat	1/4000
mouse IgG (DAKO)	HRP	goat	1/4000

Table 7.7 Antibodies used for protein detection by Western blotting.

7.12.4 Light scattering

Light scattering experiments were performed using the Zetasizer Nano ZS (Malvern Instruments) and the manufacturer's support software. 50 µl samples were measured at 25 °C in 100 µl quartz cuvettes (Hellma) with a pathlength of 0.3 cm. MAL(2-261) was diluted in 10 mM Tris-HCl pH 8.0, 10 mM NaCl. Viscosity (0.8766 cP) and refractive index (1.3303) of the solvent were calculated by the software. Dynamic light scattering at an angle of 90° was measured over a period of 60 s at a MAL(2-261) concentration of 1 mg/ml. For static light scattering, toluene was used as standard. Static light scattering at an angle of 173° was measured for MAL(2-261) dilutions of 0.25, 0.5, 1 and 2 mg/ml.

7.12.5 Circular dichroism (CD) spectroscopy

CD spectroscopy of MAL N-termini was kindly performed by Dr. Bernard O'Hara (Birkbeck College, London).

Three spectra were collected from 10 mM Tris-HCl pH 8.0, 10 mM NaCl in a 0.01cm path-length quartz cell using a CD spectropolarimeter at 25 °C. Processing of spectra was carried out using the program CDTool (Lees et al., 2004); spectra were

smoothed and averaged; buffer and sample spectra were subtracted to accomplish baseline correction; the resulting spectra were shifted to bring ellipticity values within the region of 263-267 nm to zero and scaled.

The spectra were analysed using three popular methods, the ridge regression method as implemented in the program CONTINLL (Provencher and Glockner, 1981), the self-consistent method as implemented in SELCON3 (Sreerama and Woody, 1993) and the variable selection method implemented in CDSSTR (Johnson, 1999). The programs were accessed through Dichroweb (Lobley et al., 2002). Analyses were conducted using reference set 7, which contains the largest number of reference proteins, and which allows analysis over the largest wavelength range, 190-240 nm. The values for average secondary structure content obtained by the three algorithms were averaged.

7.13 Actin manipulations

7.13.1 Frequently used actin buffers

Mg^{2+}-G-buffer	2 mM Tris-HCl pH 8.0
	0.3 mM $MgCl_2$
	0.2 mM EGTA
	0.2 mM ATP
	0.5 mM DTT
20x initiation buffer	2 M NaCl
	60 mM $MgCl_2$
	10 mM ATP
Mg^{2+}-F-buffer	2 mM Tris-HCl pH 8.0
	100 mM NaCl
	3 mM $MgCl_2$
	0.2 mM EGTA
	0.2 mM ATP
	0.5 mM DTT

7.13.2 Pyrene-modification of actin

Rabbit skeletal muscle actin was conjugated on C374 with pyrene as described previously (Kouyama and Mihashi, 1981). Actin in storage G-buffer (see Section 7.11.3) was dialysed against pyrene labelling F-buffer overnight and diluted to 1 mg/ml. Actin was reacted with 4- to 7-fold molar excess of N-(1-pyrene)iodoacetamide (Invitrogen; added from 10 mM stock in DMF) for 24 h at 4 °C in the dark. Precipitated dye was pelleted and removed by a brief centrifugation at maximum speed (16,100 xg) in an Eppendorf 5415 R tabletop centrifuge. F-actin was pelleted by centrifugation for 1 h at 100,000 xg using a Beckman TLA 120.2 rotor with Beckman 11 x 44 mm polycarbonate tubes in a Beckman TL-100 tabletop ultracentrifuge. The F-actin pellet was resuspended in G-buffer to 5-6 mg/ml by Dounce homogenisation on ice and dialysed against storage G-buffer for 2 to 3 days with daily buffer changes to depolymerise actin and remove unconjugated dye. Upon dialysis, insoluble or residual polymerised actin were removed by centrifugation at 100,000 xg for 30 min using a Beckman TLA 120.2 rotor with Beckman 11 x 44 mm polycarbonate tubes. Pyrene-actin concentration was measured spectrophotometrically at 290 nm using a molar extinction coefficient of ε_{290}=26,600 $M^{-1}cm^{-1}$ upon correction of A_{290} by subtraction of A_{344}*0.127. The labelling efficiency was determined by measuring the pyrene concentration, using a molar extinction coefficient for pyrene of ε_{344}=22,000 $M^{-1}cm^{-1}$.

Pyrene labelling F-buffer	5 mM Tris-HCl pH 8.0
	100 mM NaCl
	3 mM $MgCl_2$
	0.2 mM $CaCl_2$
	1 mM ATP

Pyrene-actin was snap-frozen in liquid nitrogen and stored at -80 °C.

7.13.3 TMR-modification of actin

Rabbit skeletal muscle actin was conjugated on C374 with tetramethylrhodamine (TMR) as described previously (Otterbein et al., 2001). Actin at about 5 mg/ml in G-buffer was fully reduced by addition of 10 mM DTT. DTT was then removed by extensive dialysis of the protein against TMR-labelling G-buffer. Dialysed actin was reacted with a 3-fold molar excess of tetramethylrhodamine-5-

maleimide (single isomer; Invitrogen; added from fresh 30 mM stock in DMF) at 4 °C overnight under stirring in the dark. The reaction was stopped by addition of 5 mM DTT. Unconjugated actin was polymerised for 1 h upon addition of 20x initiation buffer (see Section 7.13.1). The reaction was briefly centrifuged at maximum speed (16,100 xg) in an Eppendorf 5415 R tabletop centrifuge to remove precipitated excess dye. F-actin was pelleted by a 30-min centrifugation at 100,000 xg using a Beckman TLA 120.2 rotor with Beckman 11 x 44 mm polycarbonate tubes in a Beckman TL-100 tabletop ultracentrifuge. Unconjugated dye was separated from TMR-actin by passing the reaction over an Econo-Pac 10DG column (BioRad) equilibrated in Mg^{2+}-G-buffer (see Section 7.13.1). TMR-actin was concentrated to around 10 mg/ml using a 10,000 MWCO VivaSpin 2 concentrator with a PES membrane (VivaScience), snap-frozen in aliquots in liquid nitrogen and stored at -80 °C.

TMR-labelling G-buffer	2 mM MOPS pH 7.0
	0.2 mM $CaCl_2$
	0.2 mM ATP
	de-gassed

7.13.4 Preparation of latrunculin B-actin

Rabbit skeletal muscle actin was dialysed overnight into Mg^{2+}-G-buffer (see Section 7.13.1) to convert Ca^{2+}-actin into Mg^{2+}-actin and its concentration measured. A 10-fold molar excess of latrunculin B (LatB; Calbiochem) was added from a 50 mM LatB stock solution in DMSO. The solution was mixed immediately to prevent actin precipitation due to high local concentrations of DMSO and incubated overnight at 4 °C. Any uncomplexed actin was polymerised for 1 h at 4 °C upon addition of 20x initiation buffer (see Section 7.13.1). Actin filaments and any insoluble material were removed by centrifugation at 200,000 xg for 15 min at 4 °C, using a Beckman TLA 120.2 rotor with Beckman 11 x 44 mm polycarbonate tubes or a Beckman TLA 100 rotor with Beckman 7 x 20 mm polycarbonate tubes in a Beckman TL-100 tabletop ultracentrifuge. LatB-actin was stored for short periods (not longer than one week) at 4 °C.

If required, for example for crystallisation (see Section 7.15), LatB-actin was concentrated using a 5,000 or 10,000 MWCO VivaSpin 500 or VivaSpin 2 concentrator

with a PES membrane (VivaScience), followed by another step of ultracentrifugation as above. The LatB-actin concentration was measured using a blank sample prepared from the dialysis buffer, DMSO and 20x initiation buffer.

7.14 Actin-binding assays

7.14.1 Co-immunoprecipitation

10^6 NIH3T3 fibroblasts were plated on 10 cm dishes and transiently transfected on the following day as described in Section 7.8.4, using 1 µg of pEF-FLAG-actin and 1 µg of pEF-MAL-HA. On the next day, cells were serum-starved by exchanging the media containing 10% FCS for media with 0.5% FCS. On the next day, cells were washed with ice-cold PBS and scraped off the plate upon addition of 500 µl ice-cold immunoprecipitation buffer per plate. The lysates were transferred into microcentrifuge tubes and centrifuged for 10 min at maximum speed (16,100 xg) in an Eppendorf 5415 R tabletop centrifuge at 4 °C. 500 µl of the cleared lysates were subjected to immunoprecipitation in a total volume of 1 ml immunoprecipitation buffer after removal of an input sample. 30 µl of anti-FLAG M2 agarose (Sigma) were added per reaction. Binding was performed for 2 h at 4 °C, followed by three of washes with 750 µl immunoprecipitation buffer (not containing protease inhibitors) each and sedimentation of the resin at 500 xg in an Eppendorf 5415 R tabletop centrifuge at 4 °C. After washing, the resin was suspended in 50 µl 2x SDS sample buffer. One volume of 2x SDS sample buffer was also added to the input material. The samples were boiled and subjected to SDS-PAGE (see Section 7.12.2) and Western blotting (see Section 7.12.3).

Immunoprecipitation buffer	50 mM Tris-HCl pH 8.0 100 mM NaCl 1% TX-100 1 mM DTT Complete protease inhibitor cocktail (Roche)

7.14.2 Actin co-sedimentation assays

Rabbit skeletal muscle actin in Mg^{2+}-G-buffer (see Section 7.13.1) was polymerised by addition of 20x initiation buffer (see Section 7.13.1) and incubation for 30 min at room temperature. Final actin concentrations were 3, 6 and 12 µM. MAL(2-261) was added to the F-actin preparations at a final concentration of 3 µM in a final volume of 50 µl. After co-incubation for 30 min or 20 h at room temperature, the preparations were ultracentrifuged for 30 min at 200,000 xg and 4 °C, using a TLA 100 rotor with Beckman 7 x 20 mm polycarbonate tubes in a Beckman TL-100 tabletop ultracentrifuge to sediment F-actin. The protein pellets were taken up in 50 µl of 1x SDS sample buffer. Equivalent volumes of supernatant and pellet samples (4 µl) were analysed by SDS-PAGE (see Section 7.12.2) and Coomassie brilliant blue staining.

7.14.3 GST affinity sedimentation assays

GST fusion proteins were expressed in *E. coli* and isolated essentially as described in Section 7.11.1. Typically, 30 µl hydrated glutathione-agarose (Sigma) or glutathione-sepharose 4B (GE Healthcare) were saturated with GST or the GST fusion protein by co-incubation with 2 ml of lysate. The resin was washed three times with bacterial lysis buffer and once with ATP wash buffer (see Section 7.11.1) and equilibrated in GST affinity sedimentation buffer. Total NIH3T3 cell extract was generated by lysis in GST affinity sedimentation buffer through syringing and removal of insoluble material by centrifugation for 10 min at maximum speed (16,100 xg) in an Eppendorf 5415 R tabletop centrifuge at 4 °C. An equivalent of a confluent 150 mm dish of NIH3T3 cells was used for 2 binding reactions. Binding was for 2 h in GST affinity sedimentation buffer, supplemented with 0.5% TX-100 where indicated. The resin was washed 3 times in the respective binding buffer without protease inhibitors and suspended in 50 µl 2x SDS sample buffer. One volume of 2x SDS sample buffer was also added to the input material. The samples were boiled and typically 10 µl of final sample volume subjected to SDS-PAGE (see Section 7.12.2) and Western blotting (see Section 7.12.3).

GST affinity sedimentation buffer	50 mM Tris-HCl pH 8.0 100 mM NaCl 3 mM $MgCl_2$ 0.2 mM EGTA 0.5% TX-100 where indicated 1 mM DTT Complete protease inhibitor cocktail (Roche)

The GST affinity sedimentation experiment shown in Figure 2.3; Chapter 2, was performed with a nuclear-enriched extract of suspension-cultured HeLa-cells, which were available in large quantities from the Cancer Research UK fermentation service. Extracts were produced essentially as described (see, for example, Stuven et al., 2003). Cells (15 ml pellet volume) were broken by hypotonic lysis in 20 ml of 20 mM Tris-HCl pH 7.5, 1 mM $MgCl_2$, 0.5 mM EGTA, 2 mM β-mercaptoethanol and protease inhibitors, followed by dounce homogenisation. Cell nuclei were sedimented by centrifugation in 50-ml Falcon tubes for 5 min at 3000 xg using a Beckman GS-6KR centrifuge. The supernatants (low-salt cytoplasmic extracts) were used to study binding of nuclear transport receptors (not addressed in the present thesis). The nuclear pellets were taken up in 50 ml 20 mM Tris-HCl pH 7.5, 1 mM $MgCl_2$, 0.5 mM EGTA, 1 mM sodium vanadate, 5 mM NaF, 10 mM β-glycerolphosphate, 2 mM β-mercaptoethanol and protease inhibitors. 500 mM NaCl and 10 mM $MgCl_2$ were added to extract nuclear proteins. DNA was sheared by sonication for 1 min at maximum energy on ice, using a SANYO Soniprep 150 MSE sonicator. The obtained preparation was cleared by ultracentrifugation at 100,000 xg for 1 h at 4 °C and 100 mM sucrose were added for storage purposes. GST fusion proteins were immobilised onto glutathione-agarose (Sigma) and washed as described above. 30 µl of glutathione-affinity resin saturated with GST fusion protein were used per binding reaction. Binding to GST fusion proteins was performed for 2 h at 4 °C in 20 mM Tris-HCl pH 7.5, 150 mM NaCl, 5 mM $MgCl_2$, 0.25 mM EGTA, 0.2 mM ATP, 1 mM sodium vanadate, 5 mM NaF, 10 mM β-glycerolphosphate, 2 mM β-mercaptoethanol and protease inhibitors. After binding, the resin was washed three times with the binding buffer lacking protease and phosphatase inhibitors. One resin volume of wash buffer and 1 µg of GST-3C protease were added per reaction, and proteolysis of the affinity tag was allowed to proceed

overnight at 4 °C. 5 µl of free glutathione-agarose were added to completely remove GST-3C protease. The material not bound to the resin was recovered, and the resin washed once more with 30 µl wash buffer for efficient elution. The corresponding supernatants were pooled, and 20 µl were subjected to analysis by SDS-PAGE and Coomassie brilliant blue staining (see Section 7.12.2).

7.14.4 Pyrene-actin polymerisation assays

Rabbit skeletal muscle G-actin (2.5 µM, 20% pyrene-labelled; see Section 7.13.2) was incubated for 30 min with the protein to be tested) in Mg^{2+}-G-buffer (see Section 7.13.1; containing 0.2 mM DTT) or the equivalent amount of buffer (10 mM Tris-HCl pH 7.5, 10 mM NaCl, 1 mM DTT). The total reaction volume was 60 µl. For measurements with gelsolin S4-6, G-buffer contained 0.2 mM $CaCl_2$ instead of $MgCl_2$ and EGTA. Actin polymerisation was then initiated by addition of 20x initiation buffer (see Section 7.13.1). Endpoint pyrene fluorescence was measured 2 h after initiation of actin polymerisation using a CytoFluor Series 4000 plate reader and the corresponding software (PerSeptive Biosystems; excitation, 360 nm, 20 nm bandwidth; emission, 395 nm, 25 nm bandwidth; gain 60; 5 reads per well) and black 96-well polystyrene plates (Costar 3915, Corning). All steps were carried out at room temperature. For measurement of the critical actin concentration (C_c), actin at concentrations ranging from 0 to 7 µM (20% pyrene-labelled) was maintained as G-actin (in Mg^{2+}-G-buffer) or polymerised by addition of 20x initiation buffer. The fluorescence intensities were measured as described above and the C_c estimated as 0.27 µM from the actin concentration at the intercept of the regression lines (fluorescence units vs. actin concentration) obtained for G- and F-actin.

Apparent affinities were calculated as described (Hertzog et al., 2002) using Equation 7.2. For this, the fluorescence intensities measured at saturating doses of MAL/gelsolin S4-6 (no further drop in pyrene fluorescence intensity with further increase in concentration of actin-binding protein) were set to 0 and all other values normalised accordingly. The maximum normalised fluorescence intensity at 0 µM MAL/gelsolin S4-6 corresponded to an F-actin concentration of 2.23 µM (2.5 µM – C_c) whereas the lowest fluorescence intensity corresponded to an F-actin concentration of 0 µM and a corresponding concentration of unassembled, non-polymerised actin of 2.5 µM. The data were analysed by linear regression.

$$K_d = \frac{([ABP_{total}] - ([A_u] - C_c)) \times C_c}{[A_u] - C_c}$$

Equation 7.2 Calculation of an apparent MAL-actin affinity by pyrene-actin polymerisation assays. K_d, dissociation constant; $[ABP_{total}]$, total MAL/gelsolin S4-6 concentration; $[A_u]$, concentration of unassembled (non-polymerised) actin ($[A_u] = C_c + [ABP\text{-}A] - [A_{total}] - [F\text{-actin}]$ where C_c, critical concentration of actin; [ABP-A], concentration of the actin-binding protein-actin complex; $[A_{total}]$, total actin concentration).

7.14.5 Actin sequestering and analytical gel filtration assays

10 µM of MAL(2-261) and mutant derivatives were incubated with 30 µM of rabbit skeletal muscle G-actin in Mg^{2+}-G-buffer for 30 min in a total volume of 300 µl. For the DNaseI supershift experiment, 30 µM DNaseI (Worthington) was included in the binding reaction. Drug concentrations were 30 µM swinholide A, 300 µM cytochalasin D, 60 µM jasplakinolide and 300 µM latrunculin B. Free polymerisable actin was polymerized by adding 1/20 volume of 20x initiation buffer (see Section 7.13.1) and removed by ultracentrifugation at 200,000 xg for 15 min using a Beckman TLA 120.2 rotor with Beckman 11 x 44 mm polycarbonate tubes in a Beckman TL-100 tabletop ultracentrifuge. Equivalent amounts (1.5 µl) of total sample, supernatant and pellet were subjected to SDS-PAGE and Coomassie brilliant blue staining (actin sequestering assay). Supernatants were subjected to gel filtration chromatography on a calibrated Superose 12 column (GE Healthcare) in Mg^{2+}-F-buffer (see Section 7.13.1) containing 0.2 mM ATP but no DTT, as this affects the baseline absorbance at 280 nm during the course of the experiment. 30 µM non-polymerizable TMR-actin or 10 µM MAL(2-261) only were used as controls. Eluates were collected in 500 µl fractions of which 10 µl each were resolved by 12% or 4-12% SDS-PAGE followed by Coomassie brilliant blue staining (see Section 7.12.2). Apparent molecular masses of MAL-actin complexes were derived from the elution volumes. The gel filtration column was calibrated for every separate experiment, using a gel filtration standard (BioRad) under conditions identical to those of the experiments.

7.14.6 Fluorescence anisotropy

Fluorescence anisotropy was measured in a total volume of 50 µl in Mg^{2+}-F-buffer (2 mM Tris-HCl pH 8.0; 100 mM NaCl; 3 mM $MgCl_2$; 0.2 mM EGTA; 0.7 mM

ATP; 0.5 mM DTT). The reactions were set up at room temperature in microcentrifuge tubes or 96-well plates. FITC-conjugated peptides (see Section 7.5) were used at a concentration of 0.5 µM. LatB-actin (see Section 7.13.4) was added at a concentration range of 1 nM up to 59 µM, typically in 3-fold concentration steps and two 1½-fold concentration steps for the highest concentration points. Reactions were transferred into black 348-well flat-bottom polysterene plates with a non-binding surface (3654; Corning). The plates were read after a minimal co-incubation period of 5 h at room temperature to ensure the establishment of a binding equilibrium, using a Safire^2 microplate reader (Tecan) in fluorescence polarisation mode and its Magellan software (version 5.03). Settings employed were excitation, 470 nm; emission, 525 nm; excitation bandwidth, 20 nm; emission bandwidth, 20 nm; optimal gain; 10 reads; time between move and flash, 10 ms; integration time, 40 µs; lag time, 0; automatically determined z-position. Anisotropy (A) was calculated by the Magellan software using a G-factor of 1.2041 and the formula $A = (I_{parallel}-I_{perpendicular})/(I_{parallel}+2I_{perpendicular})$. $I_{parallel}$ and $I_{perpendicular}$ denote the fluorescence intensities parallel and perpendicular to the excitation plane, respectively. The anisotropy values displayed in Figure 4.7; Chapter 4, were obtained after multiplication of the calculated anisotropy values by 100. Non-linear regression to determine K_d values was done with GraFit version 4 (Erithacus Software) using Equation 7.3 (Heyduk and Lee, 1990):

$$A = A_f + (A_b - A_f)\left(\frac{\frac{1}{K_d}[R_t] + \frac{1}{K_d}[L_t] + 1 - \sqrt{\left(\frac{1}{K_d}[R_t] + \frac{1}{K_d}[L_t] + 1\right)^2 - 4\left(\frac{1}{K_d}\right)^2 [R_t][L_t]}}{2\frac{1}{K_d}[R_t]}\right)$$

Equation 7.3 Non-linear regression analysis of fluorescence anisotropy. A, measured value for anisotropy; A_f and A_b, anisotropy values corresponding to free and bound peptide, respectively; $[R_t]$ and $[L_t]$, total peptide ("receptor") and total LatB-actin ("ligand") concentrations, respectively; K_d, dissociation constant.

7.15 Crystallisation

7.15.1 Preparation of RPEL domain - actin complexes

TMR-actin was generated as described in Section 7.13.3 and LatB-actin as described in Section 7.13.4. TMR-actin was dialysed overnight into Mg^{2+}-G-buffer (see Section 7.13.3). Both TMR-actin and LatB-actin were concentrated using VivaSpin 500

or VivaSpin 2 concentrators containing a PES membrane with a MWCO of 5000 or 10,000 (VivaScience). A typical concentration of the concentrated actin stocks was 1.5 mM. MAL RPEL-domain derivatives were expressed and purified as described in Section 7.11.1. RPEL-domain derivatives in 10 mM Tris-HCl pH 8.0, 10 mM NaCl were concentrated in the same way as actin, typically to around 1 mM.

TMR-actin complexes with MAL(2-261) and MAL(2-199) were prepared in Mg^{2+}-G-buffer. For complexes with MAL(67-199), the final NaCl concentration was adjusted to 100 mM before the addition of MAL because MAL(67-199) tended to precipitate at the low salt concentration in G-buffer. MAL and TMR-actin were mixed in a molar ratio of 1:1 (MAL:TMR-actin) at final concentrations between 6 and 25 mg ml.

LatB-actin complexes were prepared in 2 mM Tris-HCl pH 8.0, 3 mM $MgCl_2$, 100 mM NaCl, 0.7 mM ATP, 0.5 mM DTT. The higher $MgCl_2$ and ATP concentrations were due to the induction of actin polymerisation during the generation of LatB-actin, which requires the addition of 20x initiation buffer (see Section 7.13.1). MAL(67-199) were mixed in a molar ratio of 1:3 (MAL:LatB-actin) at final concentrations between 6 and 25 mg/ml.

Both types of complexes were allowed to form for at least 1 h, but typically overnight, at 4 °C. Before setting up the crystallisation, the complex preparations were ultracentrifuged for 5 min at 200,000 xg and 4 °C using a Beckman TLA 120.2 or TLA 100 rotor with Beckman 11 x 44 mm or 7 x 20 mm polycarbonate tubes in a Beckman TL-100 tabletop ultracentrifuge to remove any residual F-actin or precipitate. See Figure 5.3 in Chapter 5 for an illustration of complex preparation.

7.15.2 Preparation of RPEL peptide - LatB-actin complexes

LatB-actin was generated and concentrated as described in Sections 7.13.1 and 7.15.1. RPEL-motif peptides (see Section 7.5) were dissolved in 2 mM Tris-HCl pH 8.0, 3 mM $MgCl_2$, 100 mM NaCl, 0.7 mM ATP, 0.5 mM DTT and quantified as described in Section 7.12.1. Typical peptide stock concentrations were between 2 and 3 mM. LatB-actin complexes were prepared in 2 mM Tris-HCl pH 8.0, 3 mM $MgCl_2$, 100 mM NaCl, 0.7 mM ATP, 0.5 mM DTT at final concentrations between 6 and 12 mg/ml,

using a three-fold molar excess of peptide over LatB-actin (see Figure 5.3 in Chapter 5). A precipitate become apparent upon the addition of peptides to the actin preparation, especially at higher protein concentration, and this was likely to be actin. The precipitate was removed by ultracentrifugation as described in Section 7.15.1. Since crystals formed, complex preparation was not further optimised. See Figure 5.3 in Chapter 5 for an illustration of complex preparation.

7.15.3 Crystallisation and structure determination

Crystallisation was performed at 20 °C by sitting-drop vapour diffusion. For initial screening, a range of commercially available screening kits was used: "Index Screen HT", "Salt RX Screen HT", and "Crystal Screen HT" by Hampton Research; "Classics Lite", "The Pegs", "The MPD" and "The AmSO4" by Qiagen, and "Clear Strategy I", "Clear Strategy II", "PACT Premier" and "pH Clear" by Molecular Dimensions. Crystal screens were mostly set up in 96-well format with 100 µl of precipitant in the reservoir and 200-nl drops in a 1:1 protein:precipiant ratio, using a "Mosquito Crystal" robot (TTP Labtech).

Optimisation the crystals of a given complex involved refinement of the crystallisation condition, microseeding, additive screening, and dehydration, of which all steps after complex preparation were performed by Stephane Mouilleron (see Figures 5.4 and 5.6 in Chapter 5 for an illustration of the optimisation process and cryoprotection).

Diffraction data were obtained by Stephane Mouilleron and colleagues of the Structural Biology Laboratory, using a rotating-anode X-ray source at the London Research Institute or facilities of the European Synchrotron Radiation Facility (ESRF) in Grenoble, France. The structures were solved by molecular replacement by Stephane Mouilleron (see Chapter 5 for more information).

7.16 Gene expression analysis by quantitative real-time RT-PCR

About 10^6 NIH3T3 cells were plated on 10-cm dishes, serum-starved (0.3% FCS) from the following day on for 2 days and stimulated for 30, 45 and 90 minutes with 1 µM cytochalasin D, 15% FCS or 50 nM LMB (LC Laboratories).

Total RNA was isolated using TRI Reagent (Helena Biosciences): 500 µl were added per plate, and the cells were immediately scraped from the dish and transferred into screw-cap tubes. The homogenates were kept at room temperature for 5 min to permit complete dissociation of nucleoprotein complexes. The samples were supplemented with 100 µl of chloroform and shaken vigorously for 15 s. After 10 min of incubation at room temperature, the samples were centrifuged at 12,000 xg for 15 min at 4 °C in an Eppendorf 5415 R tabletop centrifuge to achieve phase separation. RNA was precipitated from the aqueous phase by addition of 250 µl isopropanol and incubation for 5-10 min at room temperature. RNA was sedimented by centrifugation at 12,000 xg for 8 min and washed with 75% ethanol followed by pelleting at 12,000 xg for 5 min. Pellets were air-dried and dissolved in 80 µl H_2O. RNA was quantified spectrophotometrically at 260 nm (see Section 7.7.2).

RNA was used for cDNA synthesis with the SuperScript III First Strand Synthesis system and random hexamer primers (Invitrogen):

Components of 10 µl reactions were:

2 µg RNA
1 µl random hexamers (50 ng/µl)
1 µl dNTPs (10 mM)
ad 10 µl with H_2O

Priming was performed at 65 °C for 5 min followed by incubation on ice for 5 min. The reaction was then supplemented with

2 µl 10x reaction buffer (200 mM Tris-HCl pH 8.4; 500 mM KCl)
4 µl 25 mM $MgCl_2$
2 µl 0.1 M DTT
1 µl RNase Inhibitor (40 U/µl; Roche)
1 µl SuperScript III reverse transcriptase (200 U/µl)

and cDNA synthesis performed as follows:

1	10 min	25 °C
2	30 min	50 °C
3	5 min	85 °C (termination of the reaction)
4	5 min	4 °C

Amounts of cDNA corresponding to 100 ng of RNA were used in SYBR-Green based real-time PCR (Invitrogen).

Components of 20 µl PCRs were:

1 µl template cDNA
1 µl forward primer (10 µM)
1 µl reverse primer (10 µM)
10 µl SYBR Green reaction mix
7 µl H_2O

PCR cycling was as follows:

1	50 °C	2 min	
2	95 °C	10 min	
3	95 °C	15 s	
4	60 °C	1 min	go to 3 (40 cycles total)

Amplification thresholds were chosen to lie in the linear range of the semi-log amplification plot (lg ΔR_n vs. cycle number, where ΔR_n denominates the fluorescence intensity of the PCR product). Relative abundances of template cDNA were calculated by the comparative C_T ($\Delta\Delta C_T$) method, normalising to the abundance of the *Gapdh* cDNA: relative abundance = $2^{-C_T(target)} / 2^{-C_T(Gapdh)} * 100$, where C_T denominates the threshold cycle at which ΔR_n crosses the threshold. Fold induction was calculated by normalising all relative abundances to relative abundances under serum-starved conditions, which were considered as 1 (in Vartiainen et al., 2007). SEM values were calculated from relative abundances or fold induction values of three independent experiments. Gene-specific primers were as follows:

*Vcl*_for: AGCCCAGATGCTTCAGTCAGA

*Vcl*_rev: GGTCAGATGTGCCAGAAAGGA

*Srf*_for: TTCCCGTCCGAGGAAACAT

*Srf*_rev: GGCTCTTTTGACCCAGACCAT

*Cyr61*_for: AATCGCAATTGGAAAAGGCA

*Cyr61*_rev: TGAAAAGAACTCGCGGTTCG

*Acta2*_for: ACTGGGACGACATGGAAAAG

*Acta2*_rev: GTTCAGTGGTGCCTCTGTCA

*Egr1*_for: ATTGATGTCTCCGCTGCAGATC

*Egr1*_rev: TCAGCAGCATCATCTCCTCCA

*Fos*_for: TTCCTACTACCATTCCCCAGCC

*Fos*_rev: GATCTGCGCAAAAGTCCTGTG

*Gapdh*_for: TCTTGTGCAGTCCCAGCCT

*Gapdh*_rev: CAATATGGCCAAATCCGTTCA

7.17 Chromatin immunoprecipitation

Chromatin immunoprecipitation (ChIP) assays were performed essentially as described (Alberts et al., 1998; Miralles et al., 2003). About 10^7 NIH3T3 cells were plated on a 15-cm dish and serum-starved (0.3% FCS) on the next day for 1 day. Cells were stimulated for 10 min with 2 µM CD, 15% FCS or 50 nM LMB (LC Laboratories) and cross-linked for 10 min at 37 °C upon addition of 1% formaldehyde to the media. Cells were washed with ice-cold PBS, scraped from the plate in 1 ml of ice-cold PBS containing protease inhibitors (Complete protease inhibitor cocktail, Roche; 100 µM PMSF) and collected by 5 min of centrifugation at 500 xg, using a Beckman GS-6KR centrifuge. The cell pellet was re-suspended in 2.5 ml of buffer A (see below for buffers) and rotated for 10 min at 4 °C. Crude nuclei were pelleted by centrifugation for 5 min at 500 xg, washed with 2.5 ml of buffer A without detergent and taken up in 400 µl of buffer B. Nuclear extracts were snap-frozen in liquid nitrogen and stored at -80 °C if necessary. DNA was sheared to between 200 and 1,000 basepairs by sonicating for 90 s (BioRuptor water bath sonicator with reflectors and aluminium rings to define the depth of the samples in the waterbath; 3 cycles of 30 s medium intensity sonication followed by 30 s pause) in 15-ml polypropylene (orange cap) Falcon tubes with 1.2 ml of nuclear lysate (from 3 plates). Care was taken to avoid precipitation of SDS due to low temperature. Debris was removed by centrifugation and supernatants of identical

conditions pooled. Supernatants were diluted 10-fold in IP buffer to obtain chromatin solution, of which 100 µl were removed for input analysis. The chromatin solution was pre-cleared for 30 min with proteinA/G-sepharose (30 µl / 4 ml chromatin solution) pre-adsorbed with BSA and sonicated salmon sperm DNA (20 µg DNA / 100 µl sepharose in IP buffer with 1 mg/ml BSA). Sepharose was removed by centrifugation and the supernatants subjected to immunoprecipitation using 10 µl pre-immune rabbit serum, 10 µl anti-MAL rabbit serum (Miralles et al., 2003), or 4 µg anti-SRF antibody (Santa Cruz Biotechnology; sc-335) for 1 h. Immune complexes were collected with pre-adsorbed proteinA/G-sepharose (30 µl / 4 ml chromatin solution) for 45 min. Immobilised immune complexes were washed twice for 3-5 min with 5 ml of each of the wash buffers (wash buffers 1-3). Immune complexes were then washed 4 times with 5 ml of TE pH 8.0 for 3-5 min each and eluted with 500 µl of ChIP elution buffer in 2 steps of 250 µl each by incubating the resin for 15 min at room temperature. 4 volumes (400 µl) of elution buffer were added to the input material. Upon adjustment to 200 mM NaCl, cross-links were reversed overnight at 65 °C in input and IP samples. Proteolysis was performed for 1 h at 45 °C upon addition of 10 mM EDTA, 40 mM Tris-HCl pH 6.5 and 1 µl of proteinase K (20 mg/ml). DNA was recovered by phenol-chloroform extraction and ethanol precipitation.

For phenol-chloroform extraction, 1 volume (500 µl) of saturated phenol:chloroform (1:1; lower phase) was added to the samples in screw-cap tubes and the solutions mixed by brief vortexing. The samples were then centrifuged for 10 min at maximum speed in a tabletop centrifuge (Biofuge Pico, Heraeus Instruments) to achieve phase separation. The aqueous phases were transferred to new screw-cap tubes. To remove traces of phenol, the samples (aqueous phases) were mixed with equal volumes of chloroform and centrifuged for 10 min as described above. The aqueous phases were then transferred to new tubes and subjected to ethanol precipitation, essentially as described in Section 7.7.6. However, no more EDTA was added to the samples. To visualise the precipitate, 2-4 µg of glycogen (Sigma) were added before precipitation. The recovered DNA was dissolved in 80 µl of TE pH 8.0.

ChIP buffer A	5 mM Hepes pH 8.0 85 mM KCl 0.5% NP40 Complete protease inhibitor cocktail (Roche)
ChIP buffer B	50 mM Tris-HCl pH 8.1 1% SDS 10 mM EDTA Complete protease inhibitor cocktail (Roche)
ChIP IP buffer	16.7 mM Tris-HCl pH 8.1 167 mM NaCl 0.01% SDS 1.2 mM EDTA 1.1% TX-100 Complete protease inhibitor cocktail (Roche)
ChIP wash buffer 1	20 mM Tris-HCl pH 8.1 150 mM NaCl 0.1% SDS 2 mM EDTA 1% TX-100
ChIP wash buffer 2	20 mM Tris-HCl pH 8.1 300 mM NaCl 0.1% SDS 2 mM EDTA 1% TX-100

ChIP wash buffer 3	10 mM Tris-HCl pH 8.1
	0.25 M LiCl
	1 mM EDTA
	1% deoxycholate
	1% NP40
ChIP elution buffer	1% SDS
	0.1 M $NaHCO_3$

SYBR-Green based real-time PCR (Invitrogen) was performed using 5 dilutions (undiluted to 1:625) of a 5-fold dilution series of chromatin solution for calibration and to derive arbitrary abundance units (arbitrary abundances from dilution series: undiluted, 100; 1:5, 20; 1:25, 4; 1:125, 0.8; 1:625, 0.2). The same chromatin solution was used in all experiments for calibration. PCR setup was as follows:

Components of 20 µl PCRs were:

2 µl template DNA
1 µl forward primer (10 µM)
1 µl reverse primer (10 µM)
10 µl SYBR Green reaction mix
6 µl H_2O

PCR cycling was as follows:

1	50 °C	2 min	
2	95 °C	5 min	
3	95 °C	30 s	
4	52 °C	30 s	
5	72 °C	30 s	go to 3 (45 cycles total)

Primers used were as follows:

*Vcl*_for: CTGGCGCTGCCTGAGGTGAGGATAT

*Vcl*_rev: AGGGATTGCGACCGGATTCCCGAAC

*Cyr61*_for: ATGCCTTGTGGTTGGATAACAGAGG

*Cyr61*_rev: CCAGATGGTGAATCAGACACCAGAC

*Srf*_for: GGCTCCACTGTTCCTTTAAGGAGTTGGC

*Srf*_rev: CCCCCATATAAAGAGATACAATGTTTCCTTT

*Gapdh*_for: CCCTGCTTATCCAGTCCTAGCTCAAGG

*Gapdh*_rev: CTCGGGAAGCAGCATTCAGGTCTCTGG

Relative enrichment was calculated by setting arbitrary abundances under serum-starved conditions to 1 and expressing arbitrary abundances from all other conditions relative to that.

7.18 Electrophoretic mobility shift assays (EMSAs)

7.18.1 Generation of EMSA DNA probes

Probes were generated by PCR and labelled by incorporation of [α^{32}P] dCTP.

Components of 20 µl PCRs were:

- 2 µl 10x Biotag buffer (Bioline)
- 1 µl 15 mM $MgCl_2$
- 2 µl 500 µM d(G, A and T)TP
- 2 µl 200 µM dCTP
- 4 µl [α^{32}P] dCTP (10 µCi/µl)
- 2 µl 7 µM P10 (forward) primer
- 2 µl 7 µM P11 (reverse) primer
- 1 µl 50 ng/µl template plasmid: Fos.WT, pF711 (Treisman, 1985)
- 2.5 µl H_2O
- 0.5 µl BioTaq polymerase (1 U/µl)

PCRs were carried out in a Biometra TRIO-thermoblock thermal cycler.

Thermal cycling was:

1	95 °C	2 min	
2	95 °C	1 min	]
3	65 °C	1 min	} x 30 cycles
4	72 °C	1 min	]
5	72 °C	5 min	
6	4 °C	∞	

The PCR product was precipitated by addition of an equal volume of 5 M NH_4OAc and 8 volumes of 95% ethanol and incubation at -20 °C for at least 1 h. To visualise the precipitate, 2-4 µg of glycogen (Sigma) were added before precipitation. The DNA precipitate was pelleted (see Section 7.7.6), washed with 200 µl 70% ethanol and dissolved in 12 µl TE. 6 µl of EMSA loading buffer were added, and the sample applied onto a 7% non-denaturing polyacrylamide gel. The gel was run at 170 V for about 2 h and then exposed to MXB Film (Kodak) for 1-2 min to identify the position of the probe on the gel. The probe was excised from the gel and extracted overnight by incubation with 300 µl probe extraction buffer at 37 °C. Another round of extraction was performed with 150 µl probe extraction buffer at 37 °C for 1 h. The two samples of extracted probe were pooled and the probe precipitated with 2-2.5 volumes (900 µl) of ethanol at -20 °C for at least 1 h, washed with 70% ethanol, air dried and then dissolved in 50-100 µl TEN (see Section 7.2). The radiolabelled probe was quantitated by Cerenkov counting of 1 µl of the product, using a Beckman LS 6500 scintillation counter. For quantitation, the decay factor of the ^{32}P dCTP stock was calculated: decay factor (^{32}P) = $e^{(-0.0485 \times t)}$ with t being the time in days passed after the indicated assay date. This was then used to calculate the concentration of the probe in ng/µl via determination of the specific activity in cpm/pg using Equation 7.4:

$$\textit{specific}\ \text{activity (cpm/pg)} = \frac{40\ (\mu\text{Ci}) \times 10^6\ (\text{Cerenkov cpm}/\mu\text{Ci}) \times \text{decay factor}}{20\ (\mu\text{l}) \times 40\ (\text{pmol}/\mu\text{l}) \times 330\ (\text{pg/pmol}) \times 4\ (\text{dNTPs})}$$

Equation 7.4 Quantitation of EMSA probe. Cpm on the left side of the equation are obtained by scintillation counting. Cpm/µCi refer to the efficiency of the counter.

The concentration of the probe was adjusted to 0.5 – 1 ng/µl with TEN.

EMSA loading buffer	60% glycerol
	10 mM EDTA
	0.01% w/v xylene cyanol
	0.01% w/v bromophenol blue
Probe extraction buffer	0.4 M NH_4OAc
	1 mM EDTA

7.18.2 Preparation of cell lysates for EMSA

NIH3T3 cells on a 6-well dish were transfected with 2 µg of the indicated pEF-MAL-HA derivatives as described in Section 7.8.4 and serum-starved with media containing 0.5% FCS immediately after transfection. On the following day, cells were washed with ice-cold PBS and lysed by addition of ice-cold EMSA lysis buffer. The cells were scraped off the plate, transferred into microcentrifuge tubes and centrifuged for 10 min at maximum speed in an Eppendorf 5415 R tabletop centrifuge at 4 °C. The cleared lysates were snap-frozen in aliquots in liquid nitrogen and stored at -80 °C.

EMSA lysis buffer	20 mM HEPES, pH 7.9
	10% glycerol
	400 mM KCl
	0.4% TX-100
	10 mM EGTA
	5 mM EDTA
	1 mM DTT
	Complete protease inhibitor cocktail

7.18.3 In-vitro transcription / translation

SRF(120-265) was produced by *in-vitro* transcription translation, using the TNT® coupled transcription / translation system (Promega).

Components of the 50 µl *in-vitro* reaction were:

25 µl reticulocyte lysate

2 µl TNT reaction buffer

1 µl T7 TNT RNA polymerase

0.5 µl amino acid mix lacking leucine

0.5 µl amino acid mix lacking methionine

1 µl 1 µg/µl template (pFTX5-SRF(120-265); see Section 7.3)

20 µl H_2O

The reaction was performed for 60 min at 30 °C, upon which it was frozen down in aliquots in liquid nitrogen and stored at -80 °C.

7.18.4 EMSA analysis

Two glass plates (19 x 20 cm), one of which coated with 2% dimethyldichlorosilane solution to minimise sticking of the gel to the glass surface, were assembled with 1.5 mm plastic spacers and sealed with electrical tape. Non-denaturing polyacrylamide gel mix (50 ml; Table 7.8) was applied between the plates, and a 1.5 mm plastic comb was inserted between the plates to generate the wells. 4% gels were used for analysis of full-length MAL from cell extracts and 7% gels for purification of the DNA probe (see Section 7.18.1).

Non-denaturing polyacrylamide gels		
percentage	4%	7%
40% (w/v) acrylamide	6 ml	10.5 ml
1 x TBE	3 ml	3 ml
H_2O	50 ml	45.5 ml
10 % (w/v) APS	58 µl	58 µl
TEMED	700 µl	700 µl

Table 7.8 Composition of non-denaturing gels for EMSA.

After polymerisation of the gel, the comb and tape were removed and the electrophoresis apparatus (Cambridge) assembled. The wells were rinsed with 0.5x TBE

to remove polyacrylamide residuals from the wells. The gel was pre-run at 170 V for 1-2 h in 0.5 x TBE at room temperature prior to sample loading.

EMSA binding reactions contained 2 µl of total cell lysate, 1 µl of *in-vitro* transcription / translation reaction containing the SRF DNA binding domain (SRF(120-265)) and 5 µl 2x DBB in a final volume of 9 µl. The binding reactions were incubated on ice for 5 min before addition of 1 µl of 1 ng/µl radiolabelled DNA probe and further incubation for 15 min at room temperature. EMSA loading buffer was added to the samples, which were then subjected to electrophoresis at 170 V in 0.5 x TBE at room temperature for approximately 3 h until the xylene cyanol dye had migrated half-way through the gel. Gels were transferred onto 3MM Whatman paper and dried at 80 °C for 45 min using a gel drier. The radiolabelled DNA probe was visualised by overnight exposure to KODAK Biomax Film at -80 °C.

2x DBB	20 mM Tris-HCl, pH 7.9 100 mM NaCl 2 mM EDTA 1 mM DTT 100 ng/ml BSA 50-200 ng/µl poly(dI-dC)•poly(dI-dC)

poly(dI-dC)•poly(dI-dC) (GE Healthcare)
A 1 mg/ml solution in TEN was heated to 72 °C for 5-10 min to separate the strands and allowed to adopt double-stranded configuration for 30 min at room temperature. DNA fragments of 200-400 bp were generated by 3 cycles of 30 s medium intensity sonication followed by 30 s pause, using a BioRuptor water bath sonicator. For sonication, the solution was transferred into a 15-ml polypropylene Falcon tube.

7.19 Life-cell imaging, photobleaching and Förster resonance energy transfer

Life cell imaging, fluorescence loss in photobleaching (FLIP) and Förster resonance energy transfer (FRET) were carried out by Maria Vartiainen as described (Vartiainen et al., 2007).

7.20 Software

Data were analysed using Microsoft Excel and figures generated with Adobe Photoshop and Illustrator. Statisitical analysis was performed with GraphPad Prism (GraphPad Software, Inc.), version 4.0 c or Microsoft Excel. Structural representations were generated with MacPyMol (Delano, 2002).

8 Appendix

This section does not address any particular questions and merely contains supplementary information to further illustrate analyses presented in the previous chapters. The sections and figures shown here are not necessarily related to each other but referred to in the Results and Discussion sections of this thesis (Chapters 2-6).

8.1 The inhibitory role of the MAL N-terminus on ternary complex formation is not attributable to actin binding to the RPEL domain

It was previously observed that the N-terminus of MAL inhibits MAL-SRF-DNA ternary complex formation in electrophoretic mobility shift assays (EMSAs) (Miralles et al., 2003; Zaromytidou, 2007). Ternary complex formation with MAL is weak, but deletion of the N-terminal 172 amino acids of MAL (MAL ΔN, Miralles et al., 2003) largely increases the efficiency of ternary complex formation. Furthermore, ternary complex formation with MAL(met), which lacks RPEL1, occurs more readily (Miralles et al., 2003).

To address whether the inhibitory effect of the N-terminus of MAL on ternary complex formation reflects actin binding, I performed an EMSA assay from cells transiently expressing MAL, the MAL derivatives with mutant RPEL domains described in Chapter 4 (x23, 1x3, 1xx, xx3, x2x, xx3 and xxx; see Section 4.6 and Figure 4.8), a MAL derivative with an internal deletion of the RPEL motifs (MAL ΔRPEL (RPEL motifs as defined by PFAM (http://pfam.sanger.ac.uk/, Finn et al., 2006) ± 5 amino acids on either side) and MAL Δ1-186. Furthermore, cells expressing MAL were treated with cytochalasin D (CD) prior to lysis, and 10 μM CD were maintained in all subsequent steps of the analysis. Application of CD efficiently accumulates MAL in the nucleus and activates SRF-mediated transcription due to MAL-actin complex disruption (Miralles et al., 2003, see also Chapter 2).

In agreement with previous observations, MAL bound SRF and DNA with low efficiency (Figure 8.3). Complex formation was strongly increased when the entire N-terminus (Δ1-186) or the RPEL motifs (ΔRPEL) were deleted. A moderate increase of complex formation was observed for RPEL mutant derivatives of MAL, in agreement with previous observations (Zaromytidou, 2007). The continued presence of CD during the experiment had no effect on SRF and DNA binding by MAL. The observed weak

effects of RPEL mutations on complex formation with SRF and DNA are therefore unlikely to be due to actin binding. In agreement with this, the RPEL domain of myocardin (MC), which is not regulated through Rho-actin signalling and binds actin weakly (see Chapter 4), also exerts a negative effect on ternary complex formation with SRF and DNA in EMSAs (Zaromytidou, 2007). The RPEL domain might play additional roles in regulating MAL activity. Furthermore, we cannot rule out that the inhibitory effect of the MAL N-terminus is specific to this type of assay.

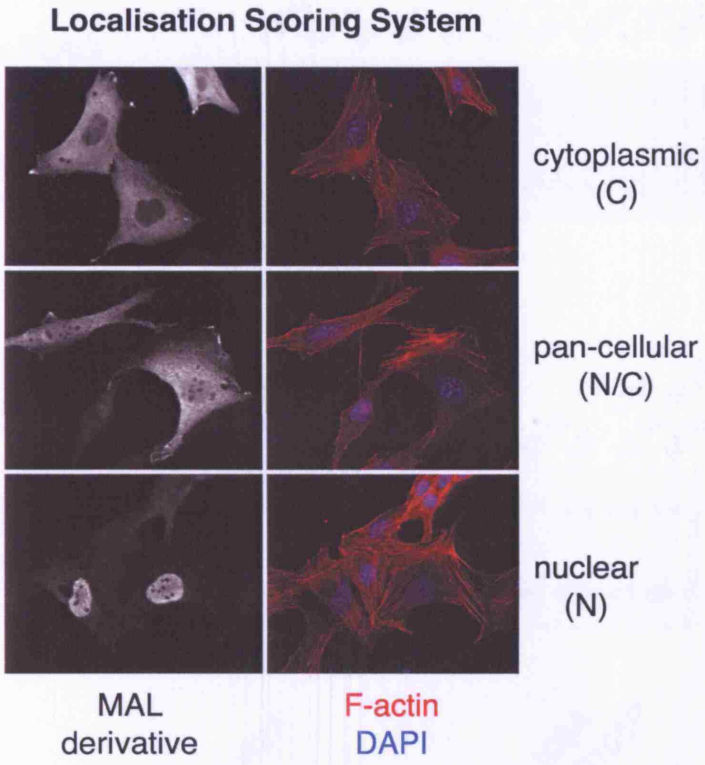

Figure 8.1 Scoring system for subcellular localisation of myocardin-family derivatives in NIH3T3 fibroblasts. Cells were transiently transfected with C-terminally HA-tagged MAL derivatives and serum-starved. MAL derivatives were detected by immunofluorescence labelling of the HA tag and microscopy. Examples for cytoplasmic, pan-cellular and nuclear localisation are shown. For quantitation, 150-200 cells were counted per condition.

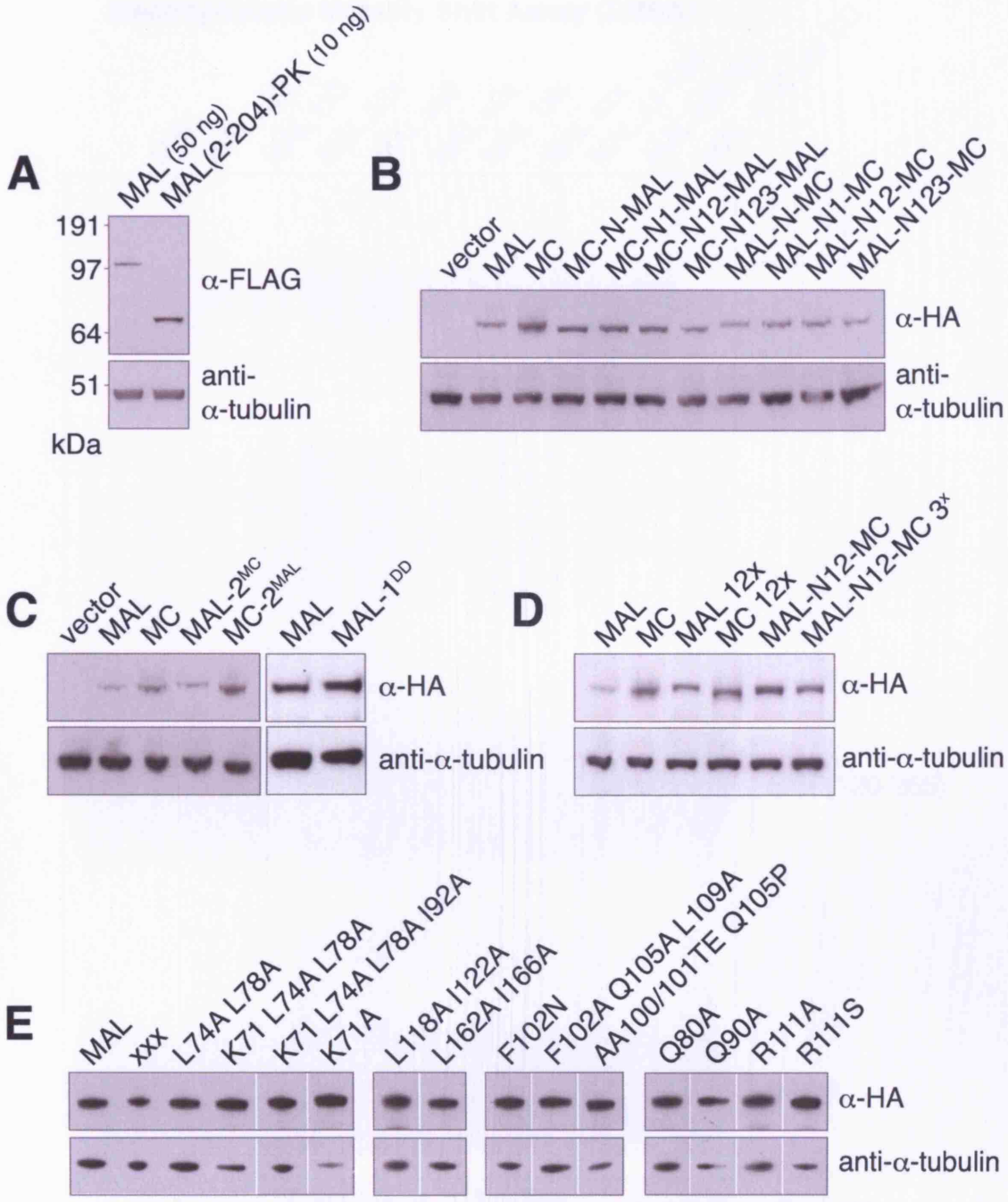

Figure 8.2 Expression levels of the used MAL derivatives. NIH3T3 cells in a 24-well dish were transfected with the indicated constructs. Relative amounts of DNA were identical to those used for immunofluorescence microscopy and luciferase reporter assays. Expression levels were assessed by Western blotting against the FLAG or double-HA tags as indicated. α-tubulin was detected as loading control. **(A)** FLAG-MAL and FLAG-MAL(2-204)-PK. (**B**) MAL-MC chimaeras (see Figure 4.10). (**C**) Reciprocal RPEL2 exchange (see Figures 4.9 and 4.12) and MAL-1^{DD} (see Figure 4.9) (**D**) RPEL3 mutation in different contexts (see Figure 4.13). (**E**) Structure-based MAL mutants (see Figure 5.15; relevant lanes selected from a larger comparison of 34 constructs analysed simultaneously and exposed to the same film). For expression of R->A RPEL-motif mutants used in Chapter 4, see Figure 8.3. See Vartiainen et al., 2007, supplementary online material, for expression levels of MAL-NLS, MAL-123-2A and MAL(2-261)-NLS derivatives.

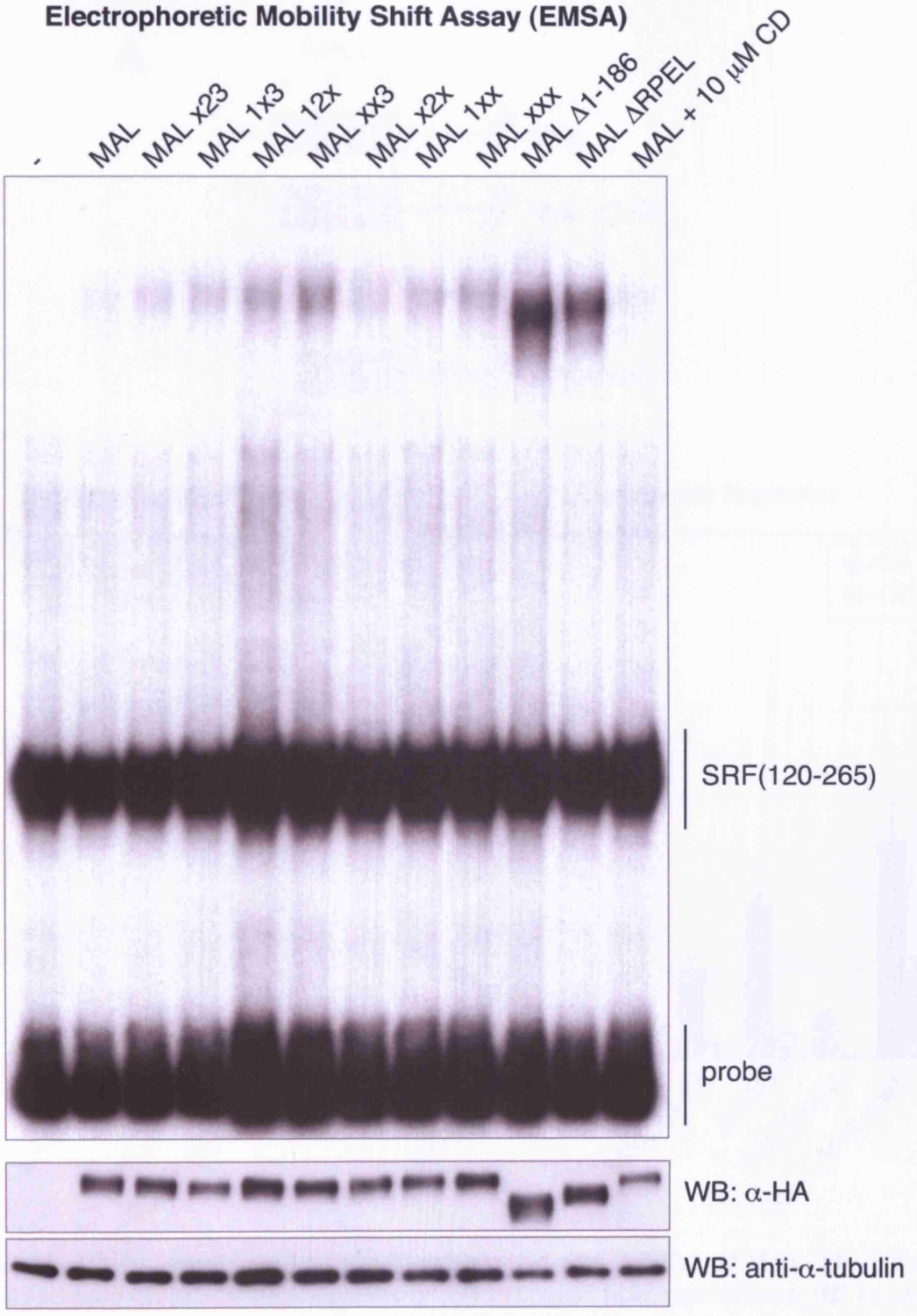

Figure 8.3 Analysis of MAL-SRF-DNA ternary complex formation by MAL derivatives with mutations in the RPEL motifs. The indicated MAL derivatives (see Figure 4.8 and text for nomenclature) were transiently expressed in NIH3T3 fibroblasts and analysed by EMSA using a radiolabelled DNA probe of the Fos SRE and in-vitro translated, exogenous SRF-DNA binding domain (SRF(120-265)). Top, autoradiograph of native gel; bottom, Western-blot (WB) analysis of the expression levels of the indicated C-terminally HA-tagged MAL derivatives. α-tubulin was detected as loading control. The cells were serum-starved before lysis. Cytochalasin-D (CD) stimulation was for 30 min at 2 μM; 10 μM CD were maintained in this sample throughout the experiment.

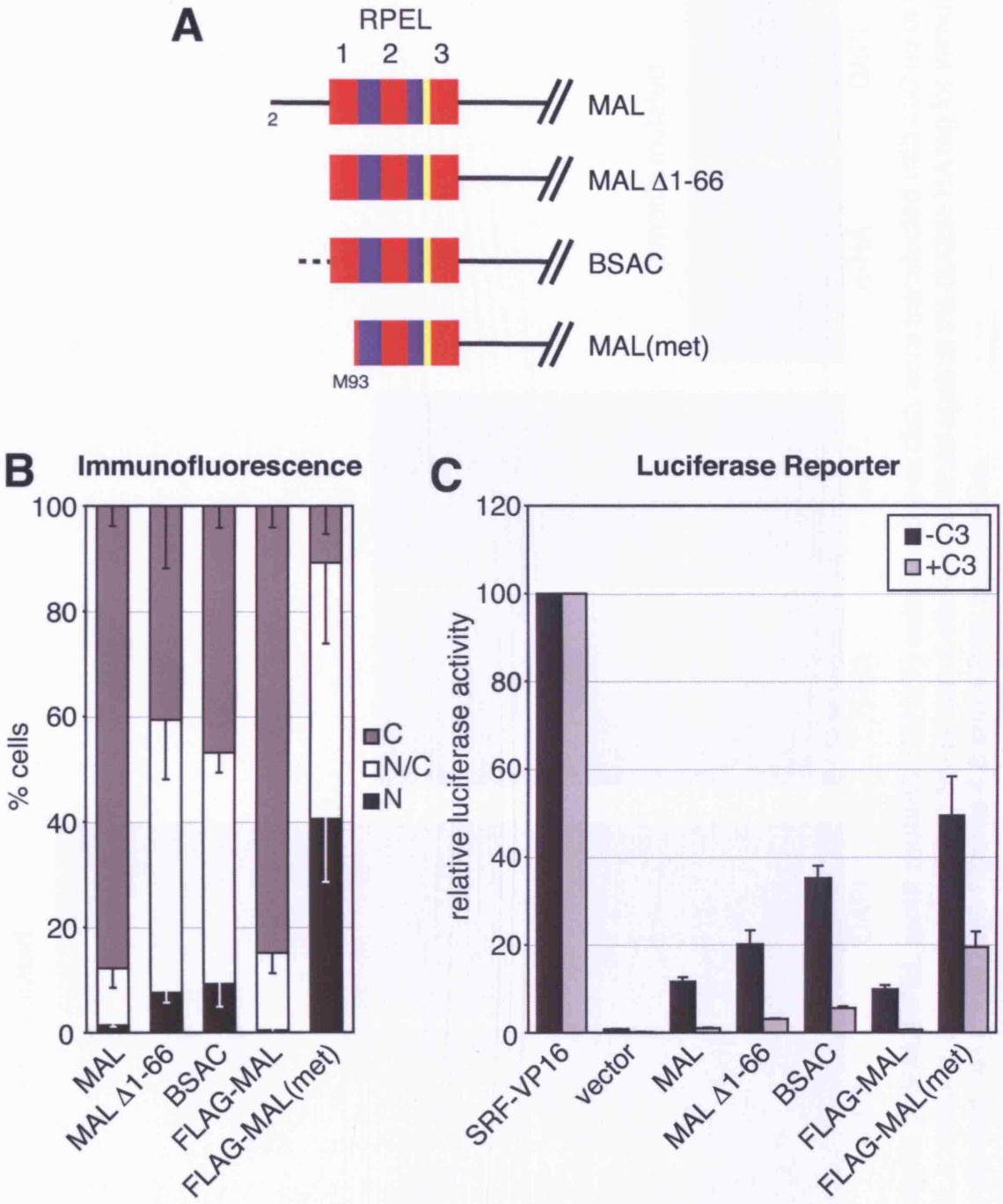

Figure 8.4 Regulatory role of the N-extension and RPEL1 of MAL. (**A**) Schematic representation of the N-termini of the indicated MAL derivatives. (**B**) Localisation of transiently expressed MAL derivatives as shown in (A) in serum-starved NIH3T3 fibroblasts detected by immunofluorescence microscopy. Localisation was scored in 124-200 cells (N, nuclear; N/C, pan-cellular; C, cytoplasmic; n=3 independent experiments; error bars, SEM). (**C**) Activation of an SRF luciferase reporter by expression of the indicated MAL derivatives without and with co-expression of C3 transferase. Reporter activation is normalised to that conferred by SRF-VP16 (100%). n=3 independent experiments; error bars, SEM.
The previously studied MAL(met) variant contained a K154R exchange and appeared regulated very similarly to MAL (Miralles et al., 2003). This mutation was corrected for in the present MAL(met) construct.

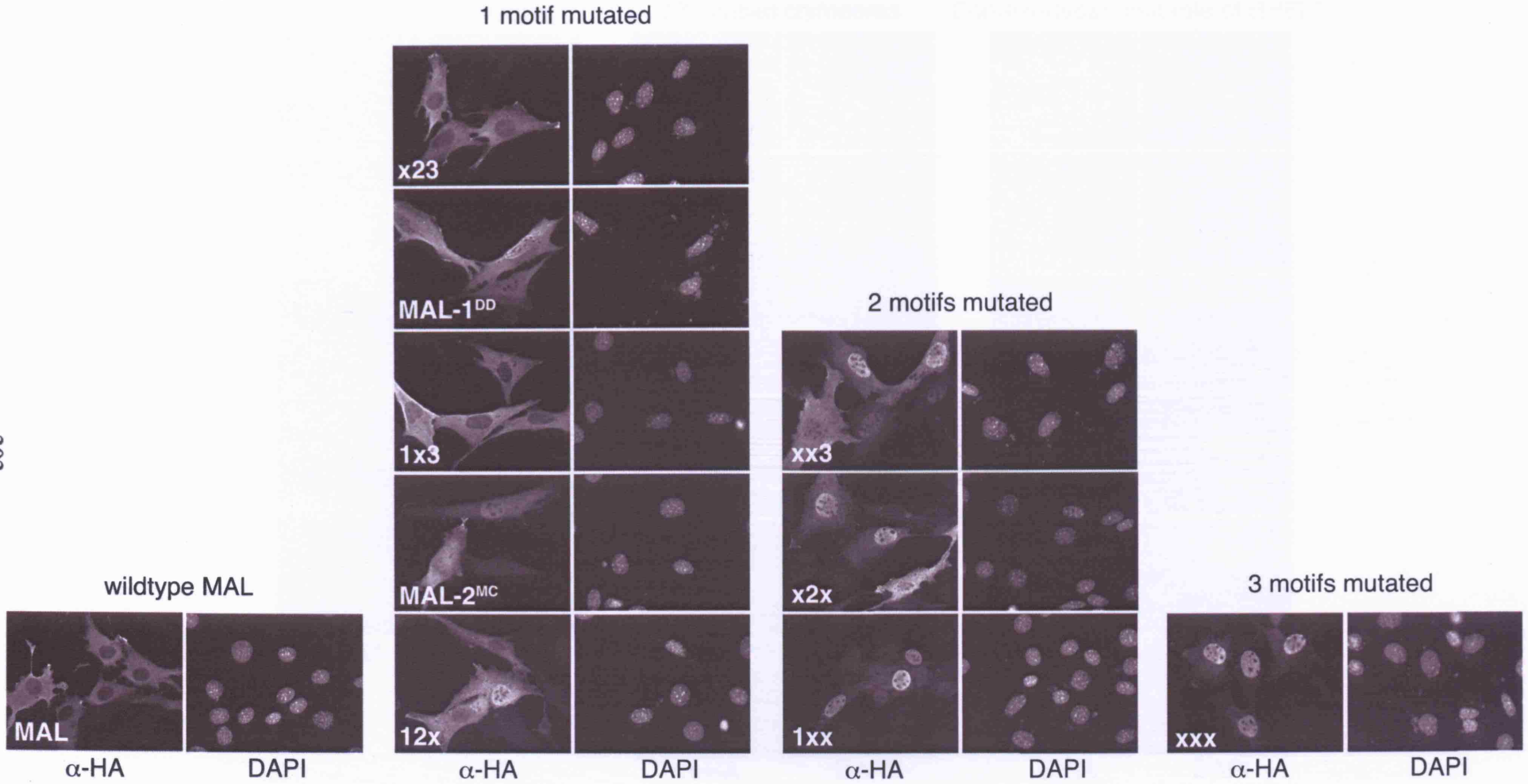

Figure 8.5 Representative micrographs of MAL RPEL motif mutants. NIH3T3 cells in a 6-well dish were transfected with 100 ng of the indicated C-terminally HA-tagged MAL constructs and maintained in 0.5% serum. Cells were stained against the double HA tag for immunofluorescence. DAPI was used to counterstain cell nuclei. See Figures 4.8 and 4.9 for quantitation.

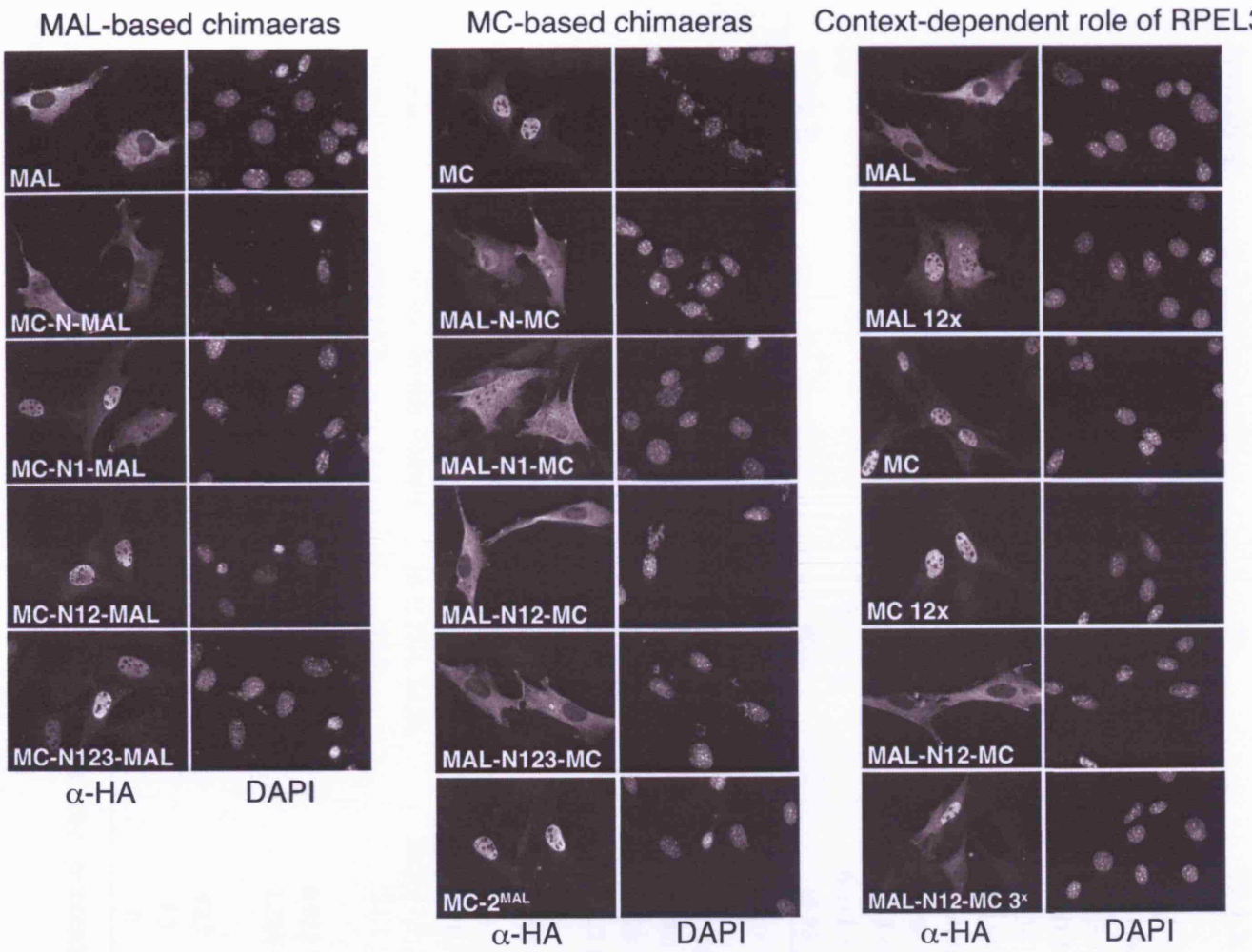

Figure 8.6 Representative micrographs of MAL-MC chimaeras. NIH3T3 cells in a 6-well dish were transfected with 100 ng of the indicated C-terminally HA-tagged constructs and maintained in 0.5% serum. Cells were stained against the double HA tag for immunofluorescence. DAPI was used to counterstain cell nuclei. See Figures 4.10, 4.12 and 4.13 for quantitation.

Data Collection Statistics		
Protein	RPEL1 - Actin	RPEL2 - Actin
Ligand	ATP, Latrunculin B	ATP, Latrunculin B
Space group	$P2_1$	$P2_12_12_1$
Unit cell dimensions (Å)		
a, b, c	59.0, 53.0, 166.3	54.9, 55.5, 138.7
α, β, γ	90, 90.1, 90	90, 90, 90
Resolution (Å)[a]	2.35 (2.48-2.35)	1.45 (1.53-1.45)
Beamline	ESRF ID 14-1	ESRF ID 14-1
Wavelength (Å)	0.934	0.934
No. unique reflections	37,426	69,166
Average redundancy	2.8 (2.9)	3.4 (4.0)
Completeness (%)	86.7 (72.3)	91.2 (90.1)
R_{merge} (%)	0.07 (0.57)	0.05 (0.49)
I/σ	9.1 (1.3)	6.6 (1.3)
Wilson B	45.2	16.53
Refinement Statistics		
Resolution (Å)[a]	50-2.35 (2.41-2.35)	50 - 1.45 (1.48-1.45)
No. reflections	35,522	65,593
R_{work} (%)	19.2 (27.2)	18.0 (28.1)
R_{free} (%)	24.2 (31.2)	22.6 (22.8)
No. atoms		
Protein	5,963	3,230
Ligands	128	84
Waters	198	291
Average B-factors (proteins, ligands, waters)	36.1; 27.4; 34.56	20.2; 17.7; 31.5
Mean B factor (all atoms) (Å^2)	35.9	21.1
r.m.s.d. from ideal values		
Bonds (Å)	0.020	0.022
Angles (°)	2.245	2.284
Ramachandran plot (%)		
Allowed	88.7	92.7
Generously allowed	10.1	7.3
Disallowed	1.2	0

Table 8.1 Data collection and refinement statistics for the presented crystal structures of RPEL1 and RPEL2 with LatB-actin.

Numbers in parentheses are values in the highest resolution shell.
Structure determination and refinement were done by Stephane Mouilleron.

References

Aberle, H., Bauer, A., Stappert, J., Kispert, A., and Kemler, R. (1997). beta-catenin is a target for the ubiquitin-proteasome pathway. Embo J *16*, 3797-3804.

Affolter, M., Montagne, J., Walldorf, U., Groppe, J., Kloter, U., LaRosa, M., and Gehring, W. J. (1994). The Drosophila SRF homolog is expressed in a subset of tracheal cells and maps within a genomic region required for tracheal development. Development *120*, 743-753.

Alberti, S., Krause, S. M., Kretz, O., Philippar, U., Lemberger, T., Casanova, E., Wiebel, F. F., Schwarz, H., Frotscher, M., Schutz, G., and Nordheim, A. (2005). Neuronal migration in the murine rostral migratory stream requires serum response factor. Proc Natl Acad Sci U S A.

Alberts, A. S. (2001). Identification of a carboxyl-terminal diaphanous-related formin homology protein autoregulatory domain. J Biol Chem *276*, 2824-2830.

Alberts, A. S., Geneste, O., and Treisman, R. (1998). Activation of SRF-regulated chromosomal templates by Rho-family GTPases requires a signal that also induces H4 hyperacetylation. Cell *92*, 475-487.

Allen, P. B., Greenfield, A. T., Svenningsson, P., Haspeslagh, D. C., and Greengard, P. (2004). Phactrs 1-4: A family of protein phosphatase 1 and actin regulatory proteins. Proc Natl Acad Sci U S A *101*, 7187-7192.

Allen, P. G. (2003). Actin filament uncapping localizes to ruffling lamellae and rocketing vesicles. Nat Cell Biol *5*, 972-979.

Alvarez-Buylla, E. R., Pelaz, S., Liljegren, S. J., Gold, S. E., Burgeff, C., Ditta, G. S., Ribas de Pouplana, L., Martinez-Castilla, L., and Yanofsky, M. F. (2000). An ancestral MADS-box gene duplication occurred before the divergence of plants and animals. Proc Natl Acad Sci U S A *97*, 5328-5333.

Amann, K. J., and Pollard, T. D. (2001). The Arp2/3 complex nucleates actin filament branches from the sides of pre-existing filaments. Nat Cell Biol *3*, 306-310.

Andrianantoandro, E., and Pollard, T. D. (2006). Mechanism of actin filament turnover by severing and nucleation at different concentrations of ADF/cofilin. Mol Cell *24*, 13-23.

Arai, A., Spencer, J. A., and Olson, E. N. (2002). STARS, a striated muscle activator of Rho signaling and serum response factor-dependent transcription. J Biol Chem *277*, 24453-24459.

Aravind, L., and Koonin, E. V. (2000). SAP - a putative DNA-binding motif involved in chromosomal organization. Trends Biochem Sci *25*, 112-114.

Arber, S., Barbayannis, F. A., Hanser, H., Schneider, C., Stanyon, C. A., Bernard, O., and Caroni, P. (1998). Regulation of actin dynamics through phosphorylation of cofilin by LIM-kinase. Nature *393*, 805-809.

Arsenian, S., Weinhold, B., Oelgeschlager, M., Ruther, U., and Nordheim, A. (1998). Serum response factor is essential for mesoderm formation during mouse embryogenesis. Embo J *17*, 6289-6299.

Ayadi, A., Zheng, H., Sobieszczuk, P., Buchwalter, G., Moerman, P., Alitalo, K., and Wasylyk, B. (2001). Net-targeted mutant mice develop a vascular phenotype and up-regulate egr-1. Embo J *20*, 5139-5152.

Bamburg, J. R. (1999). Proteins of the ADF/cofilin family: essential regulators of actin dynamics. Annu Rev Cell Dev Biol *15*, 185-230.

Bear, J. E., Svitkina, T. M., Krause, M., Schafer, D. A., Loureiro, J. J., Strasser, G. A., Maly, I. V., Chaga, O. Y., Cooper, J. A., Borisy, G. G., and Gertler, F. B. (2002). Antagonism between Ena/VASP proteins and actin filament capping regulates fibroblast motility. Cell *109*, 509-521.

Belmont, L. D., Orlova, A., Drubin, D. G., and Egelman, E. H. (1999). A change in actin conformation associated with filament instability after Pi release. Proc Natl Acad Sci U S A *96*, 29-34.

Bernales, S., Papa, F. R., and Walter, P. (2006). Intracellular signaling by the unfolded protein response. Annu Rev Cell Dev Biol *22*, 487-508.

Bershadsky, A. D., Gluck, U., Denisenko, O. N., Sklyarova, T. V., Spector, I., and Ben-Ze'ev, A. (1995). The state of actin assembly regulates actin and vinculin expression by a feedback loop. J Cell Sci *108 (Pt 3)*, 1183-1193.

Besant, P. G., Tan, E., and Attwood, P. V. (2003). Mammalian protein histidine kinases. Int J Biochem Cell Biol *35*, 297-309.

Bettinger, B. T., Gilbert, D. M., and Amberg, D. C. (2004). Actin up in the nucleus. Nat Rev Mol Cell Biol *5*, 410-415.

Bhattacharyya, R. P., Remenyi, A., Yeh, B. J., and Lim, W. A. (2006). Domains, Motifs, and Scaffolds: The Role of Modular Interactions in the Evolution and Wiring of Cell Signaling Circuits. Annu Rev Biochem.

Blanchoin, L., Amann, K. J., Higgs, H. N., Marchand, J. B., Kaiser, D. A., and Pollard, T. D. (2000). Direct observation of dendritic actin filament networks nucleated by Arp2/3 complex and WASP/Scar proteins. Nature *404*, 1007-1011.

Blanchoin, L., and Pollard, T. D. (2002). Hydrolysis of ATP by polymerized actin depends on the bound divalent cation but not profilin. Biochemistry *41*, 597-602.

Blessing, C. A., Ugrinova, G. T., and Goodson, H. V. (2004). Actin and ARPs: action in the nucleus. Trends Cell Biol *14*, 435-442.

Blikstad, I., Markey, F., Carlsson, L., Persson, T., and Lindberg, U. (1978). Selective assay of monomeric and filamentous actin in cell extracts, using inhibition of deoxyribonuclease I. Cell *15*, 935-943.

Bohnsack, M. T., Stuven, T., Kuhn, C., Cordes, V. C., and Gorlich, D. (2006). A selective block of nuclear actin export stabilizes the giant nuclei of Xenopus oocytes. Nat Cell Biol *8*, 257-263.

Boquet, I., Boujemaa, R., Carlier, M. F., and Preat, T. (2000). Ciboulot regulates actin assembly during Drosophila brain metamorphosis. Cell *102*, 797-808.

Bos, J. L., Rehmann, H., and Wittinghofer, A. (2007). GEFs and GAPs: critical elements in the control of small G proteins. Cell *129*, 865-877.

Boxer, L. M., Prywes, R., Roeder, R. G., and Kedes, L. (1989). The sarcomeric actin CArG-binding factor is indistinguishable from the c-fos serum response factor. Mol Cell Biol *9*, 515-522.

Bremer, A., Henn, C., Goldie, K. N., Engel, A., Smith, P. R., and Aebi, U. (1994). Towards atomic interpretation of F-actin filament three-dimensional reconstructions. J Mol Biol *242*, 683-700.

Brown, N. R., Noble, M. E., Endicott, J. A., and Johnson, L. N. (1999). The structural basis for specificity of substrate and recruitment peptides for cyclin-dependent kinases. Nat Cell Biol *1*, 438-443.

Bubb, M. R., Senderowicz, A. M., Sausville, E. A., Duncan, K. L., and Korn, E. D. (1994). Jasplakinolide, a cytotoxic natural product, induces actin polymerization and competitively inhibits the binding of phalloidin to F-actin. J Biol Chem *269*, 14869-14871.

Bubb, M. R., Spector, I., Bershadsky, A. D., and Korn, E. D. (1995). Swinholide A is a microfilament disrupting marine toxin that stabilizes actin dimers and severs actin filaments. J Biol Chem *270*, 3463-3466.

Burtnick, L. D., Koepf, E. K., Grimes, J., Jones, E. Y., Stuart, D. I., McLaughlin, P. J., and Robinson, R. C. (1997). The crystal structure of plasma gelsolin: implications for actin severing, capping, and nucleation. Cell *90*, 661-670.

Burtnick, L. D., Urosev, D., Irobi, E., Narayan, K., and Robinson, R. C. (2004). Structure of the N-terminal half of gelsolin bound to actin: roles in severing, apoptosis and FAF. Embo J *23*, 2713-2722.

Buss, F., Temm-Grove, C., Henning, S., and Jockusch, B. M. (1992). Distribution of profilin in fibroblasts correlates with the presence of highly dynamic actin filaments. Cell Motil Cytoskeleton *22*, 51-61.

Caldwell, J. E., Heiss, S. G., Mermall, V., and Cooper, J. A. (1989). Effects of CapZ, an actin capping protein of muscle, on the polymerization of actin. Biochemistry *28*, 8506-8514.

Cao, D., Wang, Z., Zhang, C. L., Oh, J., Xing, W., Li, S., Richardson, J. A., Wang, D. Z., and Olson, E. N. (2005). Modulation of smooth muscle gene expression by association of histone acetyltransferases and deacetylases with myocardin. Mol Cell Biol *25*, 364-376.

Carlier, M. F. (1991). Actin: protein structure and filament dynamics. J Biol Chem *266*, 1-4.

Carlier, M. F., Laurent, V., Santolini, J., Melki, R., Didry, D., Xia, G. X., Hong, Y., Chua, N. H., and Pantaloni, D. (1997). Actin depolymerizing factor (ADF/cofilin)

enhances the rate of filament turnover: implication in actin-based motility. J Cell Biol *136*, 1307-1322.

Carlier, M. F., and Pantaloni, D. (1986). Direct evidence for ADP-Pi-F-actin as the major intermediate in ATP-actin polymerization. Rate of dissociation of Pi from actin filaments. Biochemistry *25*, 7789-7792.

Carlier, M. F., Pantaloni, D., Evans, J. A., Lambooy, P. K., Korn, E. D., and Webb, M. R. (1988). The hydrolysis of ATP that accompanies actin polymerization is essentially irreversible. FEBS Lett *235*, 211-214.

Carlsson, L., Nystrom, L. E., Sundkvist, I., Markey, F., and Lindberg, U. (1977). Actin polymerizability is influenced by profilin, a low molecular weight protein in non-muscle cells. J Mol Biol *115*, 465-483.

Carson, J. A., Fillmore, R. A., Schwartz, R. J., and Zimmer, W. E. (2000). The smooth muscle gamma-actin gene promoter is a molecular target for the mouse bagpipe homologue, mNkx3-1, and serum response factor. J Biol Chem *275*, 39061-39072.

Cesari, F., Brecht, S., Vintersten, K., Vuong, L. G., Hofmann, M., Klingel, K., Schnorr, J. J., Arsenian, S., Schild, H., Herdegen, T., *et al.* (2004). Mice deficient for the ets transcription factor elk-1 show normal immune responses and mildly impaired neuronal gene activation. Mol Cell Biol *24*, 294-305.

Chan, A. Y., Bailly, M., Zebda, N., Segall, J. E., and Condeelis, J. S. (2000). Role of cofilin in epidermal growth factor-stimulated actin polymerization and lamellipod protrusion. J Cell Biol *148*, 531-542.

Chang, F., Drubin, D., and Nurse, P. (1997). cdc12p, a protein required for cytokinesis in fission yeast, is a component of the cell division ring and interacts with profilin. J Cell Biol *137*, 169-182.

Charvet, C., Houbron, C., Parlakian, A., Giordani, J., Lahoute, C., Bertrand, A., Sotiropoulos, A., Renou, L., Schmitt, A., Melki, J., *et al.* (2006). New role for serum response factor in postnatal skeletal muscle growth and regeneration via the interleukin 4 and insulin-like growth factor 1 pathways. Mol Cell Biol *26*, 6664-6674.

Chen, C. Y., Croissant, J., Majesky, M., Topouzis, S., McQuinn, T., Frankovsky, M. J., and Schwartz, R. J. (1996). Activation of the cardiac alpha-actin promoter depends upon serum response factor, Tinman homologue, Nkx-2.5, and intact serum response elements. Dev Genet *19*, 119-130.

Chenna, R., Sugawara, H., Koike, T., Lopez, R., Gibson, T. J., Higgins, D. G., and Thompson, J. D. (2003). Multiple sequence alignment with the Clustal series of programs. Nucleic Acids Res *31*, 3497-3500.

Chereau, D., Kerff, F., Graceffa, P., Grabarek, Z., Langsetmo, K., and Dominguez, R. (2005). Actin-bound structures of Wiskott-Aldrich syndrome protein (WASP)-homology domain 2 and the implications for filament assembly. Proc Natl Acad Sci U S A *102*, 16644-16649.

Chik, J. K., Lindberg, U., and Schutt, C. E. (1996). The structure of an open state of beta-actin at 2.65 A resolution. J Mol Biol *263*, 607-623.

Cobaleda, C., Schebesta, A., Delogu, A., and Busslinger, M. (2007). Pax5: the guardian of B cell identity and function. Nat Immunol *8*, 463-470.

Conibear, P. B., and Geeves, M. A. (1998). Cooperativity between the two heads of rabbit skeletal muscle heavy meromyosin in binding to actin. Biophys J *75*, 926-937.

Cooper, J. A. (1987). Effects of cytochalasin and phalloidin on actin. J Cell Biol *105*, 1473-1478.

Copeland, J. W., and Treisman, R. (2002). The Diaphanous-related Formin mDia1 Controls Serum Response Factor Activity through its Effects on Actin Polymerization. Mol Biol Cell *13*, 4088-4099.

Costello, P. S., Nicolas, R. H., Watanabe, Y., Rosewell, I., and Treisman, R. (2004). Ternary complex factor SAP-1 is required for Erk-mediated thymocyte positive selection. Nat Immunol *5*, 289-298.

Coue, M., Brenner, S. L., Spector, I., and Korn, E. D. (1987). Inhibition of actin polymerization by latrunculin A. FEBS Lett *213*, 316-318.

Cox, J. S., and Walter, P. (1996). A novel mechanism for regulating activity of a transcription factor that controls the unfolded protein response. Cell *87*, 391-404.

Creemers, E. E., Sutherland, L. B., Oh, J., Barbosa, A. C., and Olson, E. N. (2006). Coactivation of MEF2 by the SAP domain proteins myocardin and MASTR. Mol Cell *23*, 83-96.

Czisch, M., Schleicher, M., Horger, S., Voelter, W., and Holak, T. A. (1993). Conformation of thymosin beta 4 in water determined by NMR spectroscopy. Eur J Biochem *218*, 335-344.

Dalton, S., and Treisman, R. (1992). Characterization of SAP-1, a protein recruited by serum response factor to the c-fos serum response element. Cell *68*, 597-612.

De Cesare, D., Fimia, G. M., and Sassone-Corsi, P. (1999). Signaling routes to CREM and CREB: plasticity in transcriptional activation. Trends Biochem Sci *24*, 281-285.

De La Cruz, E. M., Ostap, E. M., Brundage, R. A., Reddy, K. S., Sweeney, H. L., and Safer, D. (2000). Thymosin-beta(4) changes the conformation and dynamics of actin monomers. Biophys J *78*, 2516-2527.

Dedova, I. V., Nikolaeva, O. P., Safer, D., De La Cruz, E. M., and dos Remedios, C. G. (2006). Thymosin beta4 induces a conformational change in actin monomers. Biophys J *90*, 985-992.

Delano, W. L. (2002). The PyMol Molecular Graphics System.

DerMardirossian, C., and Bokoch, G. M. (2005). GDIs: central regulatory molecules in Rho GTPase activation. Trends Cell Biol *15*, 356-363.

Derynck, R., and Zhang, Y. E. (2003). Smad-dependent and Smad-independent pathways in TGF-beta family signalling. Nature *425*, 577-584.

Detmers, P., Weber, A., Elzinga, M., and Stephens, R. E. (1981). 7-Chloro-4-nitrobenzeno-2-oxa-1,3-diazole actin as a probe for actin polymerization. J Biol Chem *256*, 99-105.

DiDonato, J. A., Hayakawa, M., Rothwarf, D. M., Zandi, E., and Karin, M. (1997). A cytokine-responsive IkappaB kinase that activates the transcription factor NF-kappaB. Nature *388*, 548-554.

Disanza, A., Steffen, A., Hertzog, M., Frittoli, E., Rottner, K., and Scita, G. (2005). Actin polymerization machinery: the finish line of signaling networks, the starting point of cellular movement. Cell Mol Life Sci *62*, 955-970.

Domanski, M., Hertzog, M., Coutant, J., Gutsche-Perelroizen, I., Bontems, F., Carlier, M. F., Guittet, E., and van Heijenoort, C. (2004). Coupling of folding and binding of thymosin beta4 upon interaction with monomeric actin monitored by nuclear magnetic resonance. J Biol Chem *279*, 23637-23645.

Dominguez, R. (2004). Actin-binding proteins--a unifying hypothesis. Trends Biochem Sci *29*, 572-578.

Dong, J., Feldmann, G., Huang, J., Wu, S., Zhang, N., Comerford, S. A., Gayyed, M. F., Anders, R. A., Maitra, A., and Pan, D. (2007). Elucidation of a universal size-control mechanism in Drosophila and mammals. Cell *130*, 1120-1133.

dos Remedios, C. G., Chhabra, D., Kekic, M., Dedova, I. V., Tsubakihara, M., Berry, D. A., and Nosworthy, N. J. (2003). Actin binding proteins: regulation of cytoskeletal microfilaments. Physiol Rev *83*, 433-473.

Du, J., and Frieden, C. (1998). Kinetic studies on the effect of yeast cofilin on yeast actin polymerization. Biochemistry *37*, 13276-13284.

Du, K. L., Chen, M., Li, J., Lepore, J. J., Mericko, P., and Parmacek, M. S. (2004). Megakaryoblastic leukemia factor-1 transduces cytoskeletal signals and induces smooth muscle cell differentiation from undifferentiated embryonic stem cells. J Biol Chem *279*, 17578-17586.

Dubois, E., Bercy, J., and Messenguy, F. (1987). Characterization of two genes, ARGRI and ARGRIII required for specific regulation of arginine metabolism in yeast. Mol Gen Genet *207*, 142-148.

Dueber, J. E., Mirsky, E. A., and Lim, W. A. (2007). Engineering synthetic signaling proteins with ultrasensitive input/output control. Nat Biotechnol *25*, 660-662.

Edelhoch, H. (1967). Spectroscopic determination of tryptophan and tyrosine in proteins. Biochemistry *6*, 1948-1954.

Edgar, B. A. (2006). From cell structure to transcription: Hippo forges a new path. Cell *124*, 267-273.

Elder, P. K., Schmidt, L. J., Ono, T., and Getz, M. J. (1984). Specific stimulation of actin gene transcription by epidermal growth factor and cycloheximide. Proc Natl Acad Sci U S A *81*, 7476-7480.

Escalante, R., and Sastre, L. (1998). A Serum Response Factor homolog is required for spore differentiation in Dictyostelium. Development *125*, 3801-3808.

Etienne-Manneville, S., and Hall, A. (2002). Rho GTPases in cell biology. Nature *420*, 629-635.

Etkin, A., Alarcon, J. M., Weisberg, S. P., Touzani, K., Huang, Y. Y., Nordheim, A., and Kandel, E. R. (2006). A role in learning for SRF: deletion in the adult forebrain disrupts LTD and the formation of an immediate memory of a novel context. Neuron *50*, 127-143.

Fagerlund, R., Melen, K., Kinnunen, L., and Julkunen, I. (2002). Arginine/lysine-rich nuclear localization signals mediate interactions between dimeric STATs and importin alpha 5. J Biol Chem *277*, 30072-30078.

Farina, K. L., Huttelmaier, S., Musunuru, K., Darnell, R., and Singer, R. H. (2003). Two ZBP1 KH domains facilitate beta-actin mRNA localization, granule formation, and cytoskeletal attachment. J Cell Biol *160*, 77-87.

Favot, L., Gillingwater, M., Scott, C., and Kemp, P. R. (2005). Overexpression of a family of RPEL proteins modifies cell shape. FEBS Lett *579*, 100-104.

Feuer, G., Molnar, F., Pettko, E., and Straub, F. B. (1948). Studies on the composition and polymerization of actin. Hung Acta Physiol *1*, 150-163.

Finn, R. D., Mistry, J., Schuster-Bockler, B., Griffiths-Jones, S., Hollich, V., Lassmann, T., Moxon, S., Marshall, M., Khanna, A., Durbin, R., *et al.* (2006). Pfam: clans, web tools and services. Nucleic Acids Res *34*, D247-251.

Fischer, U., Huber, J., Boelens, W. C., Mattaj, I. W., and Luhrmann, R. (1995). The HIV-1 Rev activation domain is a nuclear export signal that accesses an export pathway used by specific cellular RNAs. Cell *82*, 475-483.

Fleige, A., Alberti, S., Grobe, L., Frischmann, U., Geffers, R., Muller, W., Nordheim, A., and Schippers, A. (2007). Serum response factor contributes selectively to lymphocyte development. J Biol Chem.

Fomproix, N., and Percipalle, P. (2004). An actin-myosin complex on actively transcribing genes. Exp Cell Res *294*, 140-148.

Fraser, A. G., Kamath, R. S., Zipperlen, P., Martinez-Campos, M., Sohrmann, M., and Ahringer, J. (2000). Functional genomic analysis of C. elegans chromosome I by systematic RNA interference. Nature *408*, 325-330.

Frey, S., Richter, R. P., and Gorlich, D. (2006). FG-rich repeats of nuclear pore proteins form a three-dimensional meshwork with hydrogel-like properties. Science *314*, 815-817.

Frischknecht, F., Moreau, V., Rottger, S., Gonfloni, S., Reckmann, I., Superti-Furga, G., and Way, M. (1999). Actin-based motility of vaccinia virus mimics receptor tyrosine kinase signalling. Nature *401*, 926-929.

Fristrom, D., Gotwals, P., Eaton, S., Kornberg, T. B., Sturtevant, M., Bier, E., and Fristrom, J. W. (1994). Blistered: a gene required for vein/intervein formation in wings of Drosophila. Development *120*, 2661-2671.

Fukata, Y., Amano, M., and Kaibuchi, K. (2001). Rho-Rho-kinase pathway in smooth muscle contraction and cytoskeletal reorganization of non-muscle cells. Trends Pharmacol Sci *22*, 32-39.

Gallivan, J. P., and Dougherty, D. A. (1999). Cation-pi interactions in structural biology. Proc Natl Acad Sci U S A *96*, 9459-9464.

Gauthier-Rouviere, C., Cavadore, J. C., Blanchard, J. M., Lamb, N. J., and Fernandez, A. (1991). p67SRF is a constitutive nuclear protein implicated in the modulation of genes required throughout the G1 period. Cell Regul *2*, 575-588.

Geneste, O., Copeland, J. W., and Treisman, R. (2002). LIM kinase and Diaphanous cooperate to regulate serum response factor and actin dynamics. J Cell Biol *157*, 831-838.

Ghosh, M., Song, X., Mouneimne, G., Sidani, M., Lawrence, D. S., and Condeelis, J. S. (2004). Cofilin promotes actin polymerization and defines the direction of cell motility. Science *304*, 743-746.

Gille, H., Sharrocks, A. D., and Shaw, P. E. (1992). Phosphorylation of transcription factor p62TCF by MAP kinase stimulates ternary complex formation at c-fos promoter. Nature *358*, 414-417.

Gilman, M. Z., Wilson, R. N., and Weinberg, R. A. (1986). Multiple protein-binding sites in the 5'-flanking region regulate c-fos expression. Mol Cell Biol *6*, 4305-4316.

Gineitis, D., and Treisman, R. (2001). Differential usage of signal transduction pathways defines two types of serum response factor target gene. J Biol Chem *276*, 24531-24539.

Giovane, A., Pintzas, A., Maira, S. M., Sobieszczuk, P., and Wasylyk, B. (1994). Net, a new ets transcription factor that is activated by Ras. Genes Dev *8*, 1502-1513.

Goldschmidt-Clermont, P. J., Machesky, L. M., Doberstein, S. K., and Pollard, T. D. (1991). Mechanism of the interaction of human platelet profilin with actin. J Cell Biol *113*, 1081-1089.

Görlich, D., and Kutay, U. (1999). Transport between the cell nucleus and the cytoplasm. Annu Rev Cell Dev Biol *15*, 607-660.

Görlich, D., Seewald, M. J., and Ribbeck, K. (2003). Characterization of Ran-driven cargo transport and the RanGTPase system by kinetic measurements and computer simulation. Embo J *22*, 1088-1100.

Graham, R., and Gilman, M. (1991). Distinct protein targets for signals acting at the c-fos serum response element. Science *251*, 189-192.

Greenberg, M. E., Greene, L. A., and Ziff, E. B. (1985). Nerve growth factor and epidermal growth factor induce rapid transient changes in proto-oncogene transcription in PC12 cells. J Biol Chem *260*, 14101-14110.

Greenberg, M. E., Hermanowski, A. L., and Ziff, E. B. (1986). Effect of protein synthesis inhibitors on growth factor activation of c-fos, c-myc, and actin gene transcription. Mol Cell Biol *6*, 1050-1057.

Greenberg, M. E., and Ziff, E. B. (1984). Stimulation of 3T3 cells induces transcription of the c-fos proto-oncogene. Nature *311*, 433-438.

Grosse, R., Copeland, J. W., Newsome, T. P., Way, M., and Treisman, R. (2003). A role for VASP in RhoA-Diaphanous signalling to actin dynamics and SRF activity. Embo J *22*, 3050-3061.

Grueneberg, D. A., Natesan, S., Alexandre, C., and Gilman, M. Z. (1992). Human and Drosophila homeodomain proteins that enhance the DNA-binding activity of serum response factor. Science *257*, 1089-1095.

Guillemin, K., Groppe, J., Ducker, K., Treisman, R., Hafen, E., Affolter, M., and Krasnow, M. A. (1996). The pruned gene encodes the Drosophila serum response factor and regulates cytoplasmic outgrowth during terminal branching of the tracheal system. Development *122*, 1353-1362.

Han, Z., Li, X., Wu, J., and Olson, E. N. (2004). A myocardin-related transcription factor regulates activity of serum response factor in Drosophila. Proc Natl Acad Sci U S A *101*, 12567-12572.

Harding, H. P., Zhang, Y., and Ron, D. (1999). Protein translation and folding are coupled by an endoplasmic-reticulum-resident kinase. Nature *397*, 271-274.

Harvey, K., and Tapon, N. (2007). The Salvador-Warts-Hippo pathway - an emerging tumour-suppressor network. Nat Rev Cancer *7*, 182-191.

Hassler, M., and Richmond, T. J. (2001). The B-box dominates SAP-1-SRF interactions in the structure of the ternary complex. Embo J *20*, 3018-3028.

Hayden, M. S., and Ghosh, S. (2004). Signaling to NF-kappaB. Genes Dev *18*, 2195-2224.

Heiss, S. G., and Cooper, J. A. (1991). Regulation of CapZ, an actin capping protein of chicken muscle, by anionic phospholipids. Biochemistry *30*, 8753-8758.

Heras, B., and Martin, J. L. (2005). Post-crystallization treatments for improving diffraction quality of protein crystals. Acta Crystallogr D Biol Crystallogr *61*, 1173-1180.

Herrera, R. E., Shaw, P. E., and Nordheim, A. (1989). Occupation of the c-fos serum response element in vivo by a multi-protein complex is unaltered by growth factor induction. Nature *340*, 68-70.

Hertzog, M., van Heijenoort, C., Didry, D., Gaudier, M., Coutant, J., Gigant, B., Didelot, G., Preat, T., Knossow, M., Guittet, E., and Carlier, M. F. (2004). The beta-thymosin/WH2 domain; structural basis for the switch from inhibition to promotion of actin assembly. Cell *117*, 611-623.

Hertzog, M., Yarmola, E. G., Didry, D., Bubb, M. R., and Carlier, M. F. (2002). Control of actin dynamics by proteins made of beta-thymosin repeats: the actobindin family. J Biol Chem *277*, 14786-14792.

Heyduk, T., and Lee, J. C. (1990). Application of fluorescence energy transfer and polarization to monitor Escherichia coli cAMP receptor protein and lac promoter interaction. Proc Natl Acad Sci U S A *87*, 1744-1748.

Higgs, H. N. (2005). Formin proteins: a domain-based approach. Trends Biochem Sci *30*, 342-353.

Higgs, H. N., Blanchoin, L., and Pollard, T. D. (1999). Influence of the C terminus of Wiskott-Aldrich syndrome protein (WASp) and the Arp2/3 complex on actin polymerization. Biochemistry *38*, 15212-15222.

Hill, C. S., Marais, R., John, S., Wynne, J., Dalton, S., and Treisman, R. (1993). Functional analysis of a growth factor-responsive transcription factor complex. Cell *73*, 395-406.

Hill, C. S., Wynne, J., and Treisman, R. (1994). Serum-regulated transcription by serum response factor (SRF): a novel role for the DNA binding domain. Embo J *13*, 5421-5432.

Hill, C. S., Wynne, J., and Treisman, R. (1995). The Rho family GTPases RhoA, Rac1, and CDC42Hs regulate transcriptional activation by SRF. Cell *81*, 1159-1170.

Hofmann, W. A., Stojiljkovic, L., Fuchsova, B., Vargas, G. M., Mavrommatis, E., Philimonenko, V., Kysela, K., Goodrich, J. A., Lessard, J. L., Hope, T. J., *et al.* (2004). Actin is part of pre-initiation complexes and is necessary for transcription by RNA polymerase II. Nat Cell Biol *6*, 1094-1101.

Holmes, K. C., Angert, I., Kull, F. J., Jahn, W., and Schroder, R. R. (2003). Electron cryo-microscopy shows how strong binding of myosin to actin releases nucleotide. Nature *425*, 423-427.

Holmes, K. C., Popp, D., Gebhard, W., and Kabsch, W. (1990). Atomic model of the actin filament. Nature *347*, 44-49.

Howell, M., and Hill, C. S. (1997). XSmad2 directly activates the activin-inducible, dorsal mesoderm gene XFKH1 in Xenopus embryos. Embo J *16*, 7411-7421.

Hu, P., Wu, S., and Hernandez, N. (2004). A role for beta-actin in RNA polymerase III transcription. Genes Dev *18*, 3010-3015.

Huang, J., Wu, S., Barrera, J., Matthews, K., and Pan, D. (2005). The Hippo signaling pathway coordinately regulates cell proliferation and apoptosis by inactivating Yorkie, the Drosophila Homolog of YAP. Cell *122*, 421-434.

Huttelmaier, S., Zenklusen, D., Lederer, M., Dictenberg, J., Lorenz, M., Meng, X., Bassell, G. J., Condeelis, J., and Singer, R. H. (2005). Spatial regulation of beta-actin translation by Src-dependent phosphorylation of ZBP1. Nature *438*, 512-515.

Hutten, S., and Kehlenbach, R. H. (2007). CRM1-mediated nuclear export: to the pore and beyond. Trends Cell Biol *17*, 193-201.

Huxley, H. E. (1963). Electron Microscope Studies on the Structure of Natural and Synthetic Protein Filaments from Striated Muscle. J Mol Biol *7*, 281-308.

Ichetovkin, I., Han, J., Pang, K. M., Knecht, D. A., and Condeelis, J. S. (2000). Actin filaments are severed by both native and recombinant dictyostelium cofilin but to different extents. Cell Motil Cytoskeleton *45*, 293-306.

Inman, G. J., Nicolas, F. J., and Hill, C. S. (2002). Nucleocytoplasmic shuttling of Smads 2, 3, and 4 permits sensing of TGF-beta receptor activity. Mol Cell *10*, 283-294.

Irobi, E., Aguda, A. H., Larsson, M., Guerin, C., Yin, H. L., Burtnick, L. D., Blanchoin, L., and Robinson, R. C. (2004). Structural basis of actin sequestration by thymosin-beta4: implications for WH2 proteins. Embo J *23*, 3599-3608.

Isenberg, G., Aebi, U., and Pollard, T. D. (1980). An actin-binding protein from Acanthamoeba regulates actin filament polymerization and interactions. Nature *288*, 455-459.

Iyer, D., Belaguli, N., Fluck, M., Rowan, B. G., Wei, L., Weigel, N. L., Booth, F. W., Epstein, H. F., Schwartz, R. J., and Balasubramanyam, A. (2003). Novel phosphorylation target in the serum response factor MADS box regulates alpha-actin transcription. Biochemistry *42*, 7477-7486.

Iyer, D., Chang, D., Marx, J., Wei, L., Olson, E. N., Parmacek, M. S., Balasubramanyam, A., and Schwartz, R. J. (2006). Serum response factor MADS box serine-162 phosphorylation switches proliferation and myogenic gene programs. Proc Natl Acad Sci U S A *103*, 4516-4521.

Jaffe, A. B., and Hall, A. (2005). Rho GTPases: biochemistry and biology. Annu Rev Cell Dev Biol *21*, 247-269.

Janknecht, R., Ernst, W. H., Pingoud, V., and Nordheim, A. (1993). Activation of ternary complex factor Elk-1 by MAP kinases. Embo J *12*, 5097-5104.

Janknecht, R., and Nordheim, A. (1992). Elk-1 protein domains required for direct and SRF-assisted DNA-binding. Nucleic Acids Res *20*, 3317-3324.

Jockusch, B. M., Schoenenberger, C. A., Stetefeld, J., and Aebi, U. (2006). Tracking down the different forms of nuclear actin. Trends Cell Biol *16*, 391-396.

Johansen, F. E., and Prywes, R. (1993). Identification of transcriptional activation and inhibitory domains in serum response factor (SRF) by using GAL4-SRF constructs. Mol Cell Biol *13*, 4640-4647.

Johnson, W. C. (1999). Analyzing protein circular dichroism spectra for accurate secondary structures. Proteins *35*, 307-312.

Kabsch, W., Mannherz, H. G., and Suck, D. (1985). Three-dimensional structure of the complex of actin and DNase I at 4.5 A resolution. Embo J *4*, 2113-2118.

Kabsch, W., Mannherz, H. G., Suck, D., Pai, E. F., and Holmes, K. C. (1990). Atomic structure of the actin:DNase I complex. Nature *347*, 37-44.

Kalab, P., Weis, K., and Heald, R. (2002). Visualization of a Ran-GTP gradient in interphase and mitotic Xenopus egg extracts. Science *295*, 2452-2456.

Kalderon, D., Roberts, B. L., Richardson, W. D., and Smith, A. E. (1984). A short amino acid sequence able to specify nuclear location. Cell *39*, 499-509.

Karakozova, M., Kozak, M., Wong, C. C., Bailey, A. O., Yates, J. R., 3rd, Mogilner, A., Zebroski, H., and Kashina, A. (2006). Arginylation of beta-actin regulates actin cytoskeleton and cell motility. Science *313*, 192-196.

Kashina, A. S. (2006). Differential arginylation of actin isoforms: the mystery of the actin N-terminus. Trends Cell Biol *16*, 610-615.

Kerkhoff, E. (2006). Cellular functions of the Spir actin-nucleation factors. Trends Cell Biol *16*, 477-483.

Kim, E., Waters, S. H., Hake, L. E., and Hecht, N. B. (1989). Identification and developmental expression of a smooth-muscle gamma-actin in postmeiotic male germ cells of mice. Mol Cell Biol *9*, 1875-1881.

Kislauskis, E. H., Zhu, X., and Singer, R. H. (1994). Sequences responsible for intracellular localization of beta-actin messenger RNA also affect cell phenotype. J Cell Biol *127*, 441-451.

Klenchin, V. A., Allingham, J. S., King, R., Tanaka, J., Marriott, G., and Rayment, I. (2003). Trisoxazole macrolide toxins mimic the binding of actin-capping proteins to actin. Nat Struct Biol *10*, 1058-1063.

Klenchin, V. A., King, R., Tanaka, J., Marriott, G., and Rayment, I. (2005). Structural basis of swinholide A binding to actin. Chem Biol *12*, 287-291.

Knoll, B., Kretz, O., Fiedler, C., Alberti, S., Schutz, G., Frotscher, M., and Nordheim, A. (2006). Serum response factor controls neuronal circuit assembly in the hippocampus. Nat Neurosci *9*, 195-204.

Kobielak, A., and Fuchs, E. (2004). Alpha-catenin: at the junction of intercellular adhesion and actin dynamics. Nat Rev Mol Cell Biol *5*, 614-625.

Kolappan, S., Gooch, J. T., Weeds, A. G., and McLaughlin, P. J. (2003). Gelsolin domains 4-6 in active, actin-free conformation identifies sites of regulatory calcium ions. J Mol Biol *329*, 85-92.

Korn, E. D. (1982). Actin polymerization and its regulation by proteins from nonmuscle cells. Physiol Rev *62*, 672-737.

Kouyama, T., and Mihashi, K. (1981). Fluorimetry study of N-(1-pyrenyl)iodoacetamide-labelled F-actin. Local structural change of actin protomer both on polymerization and on binding of heavy meromyosin. Eur J Biochem *114*, 33-38.

Kovar, D. R., Harris, E. S., Mahaffy, R., Higgs, H. N., and Pollard, T. D. (2006). Control of the assembly of ATP- and ADP-actin by formins and profilin. Cell *124*, 423-435.

Kozma, R., Ahmed, S., Best, A., and Lim, L. (1995). The Ras-related protein Cdc42Hs and bradykinin promote formation of peripheral actin microspikes and filopodia in Swiss 3T3 fibroblasts. Mol Cell Biol *15*, 1942-1952.

Krause, M., Dent, E. W., Bear, J. E., Loureiro, J. J., and Gertler, F. B. (2003). Ena/VASP proteins: regulators of the actin cytoskeleton and cell migration. Annu Rev Cell Dev Biol *19*, 541-564.

Kukalev, A., Nord, Y., Palmberg, C., Bergman, T., and Percipalle, P. (2005). Actin and hnRNP U cooperate for productive transcription by RNA polymerase II. Nat Struct Mol Biol *12*, 238-244.

Kuwahara, K., Barrientos, T., Pipes, G. C., Li, S., and Olson, E. N. (2005). Muscle-specific signaling mechanism that links actin dynamics to serum response factor. Mol Cell Biol *25*, 3173-3181.

Kuwahara, K., Teg Pipes, G. C., McAnally, J., Richardson, J. A., Hill, J. A., Bassel-Duby, R., and Olson, E. N. (2007). Modulation of adverse cardiac remodeling by STARS, a mediator of MEF2 signaling and SRF activity. J Clin Invest *117*, 1324-1334.

Laemmli, U. K. (1970). Cleavage of structural proteins during the assembly of the head of bacteriophage T4. Nature *227*, 680-685.

Landschulz, W. H., Johnson, P. F., and McKnight, S. L. (1988). The leucine zipper: a hypothetical structure common to a new class of DNA binding proteins. Science *240*, 1759-1764.

Lanford, R. E., and Butel, J. S. (1984). Construction and characterization of an SV40 mutant defective in nuclear transport of T antigen. Cell *37*, 801-813.

Lang, P., Gesbert, F., Delespine-Carmagnat, M., Stancou, R., Pouchelet, M., and Bertoglio, J. (1996). Protein kinase A phosphorylation of RhoA mediates the morphological and functional effects of cyclic AMP in cytotoxic lymphocytes. Embo J *15*, 510-519.

Larijani, B., Allen-Baume, V., Morgan, C. P., Li, M., and Cockcroft, S. (2003). EGF regulation of PITP dynamics is blocked by inhibitors of phospholipase C and of the Ras-MAP kinase pathway. Curr Biol *13*, 78-84.

Lassing, I., and Lindberg, U. (1985). Specific interaction between phosphatidylinositol 4,5-bisphosphate and profilactin. Nature *314*, 472-474.

Lazarides, E., and Lindberg, U. (1974). Actin is the naturally occurring inhibitor of deoxyribonuclease I. Proc Natl Acad Sci U S A *71*, 4742-4746.

Lee, S. H., Kerff, F., Chereau, D., Ferron, F., Klug, A., and Dominguez, R. (2007). Structural basis for the actin-binding function of missing-in-metastasis. Structure *15*, 145-155.

Lee, T. C., Chow, K. L., Fang, P., and Schwartz, R. J. (1991). Activation of skeletal alpha-actin gene transcription: the cooperative formation of serum response factor-binding complexes over positive cis-acting promoter serum response elements displaces a negative-acting nuclear factor enriched in replicating myoblasts and nonmyogenic cells. Mol Cell Biol *11*, 5090-5100.

Lees, J. G., Smith, B. R., Wien, F., Miles, A. J., and Wallace, B. A. (2004). CDtool-an integrated software package for circular dichroism spectroscopic data processing, analysis, and archiving. Anal Biochem *332*, 285-289.

Lengsfeld, A. M., Low, I., Wieland, T., Dancker, P., and Hasselbach, W. (1974). Interaction of phalloidin with actin. Proc Natl Acad Sci U S A *71*, 2803-2807.

Levy, D. E., and Darnell, J. E., Jr. (2002). Stats: transcriptional control and biological impact. Nat Rev Mol Cell Biol *3*, 651-662.

Li, J., Zhu, X., Chen, M., Cheng, L., Zhou, D., Lu, M. M., Du, K., Epstein, J. A., and Parmacek, M. S. (2005). Myocardin-related transcription factor B is required in cardiac neural crest for smooth muscle differentiation and cardiovascular development. Proc Natl Acad Sci U S A *102*, 8916-8921.

Li, Q. J., Yang, S. H., Maeda, Y., Sladek, F. M., Sharrocks, A. D., and Martins-Green, M. (2003a). MAP kinase phosphorylation-dependent activation of Elk-1 leads to activation of the co-activator p300. Embo J *22*, 281-291.

Li, S., Chang, S., Qi, X., Richardson, J. A., and Olson, E. N. (2006). Requirement of a myocardin-related transcription factor for development of mammary myoepithelial cells. Mol Cell Biol *26*, 5797-5808.

Li, S., Wang, D. Z., Wang, Z., Richardson, J. A., and Olson, E. N. (2003b). The serum response factor coactivator myocardin is required for vascular smooth muscle development. Proc Natl Acad Sci U S A *100*, 9366-9370.

Lobley, A., Whitmore, L., and Wallace, B. A. (2002). DICHROWEB: an interactive website for the analysis of protein secondary structure from circular dichroism spectra. Bioinformatics *18*, 211-212.

Lopez, M., Oettgen, P., Akbarali, Y., Dendorfer, U., and Libermann, T. A. (1994). ERP, a new member of the ets transcription factor/oncoprotein family: cloning, characterization, and differential expression during B-lymphocyte development. Mol Cell Biol *14*, 3292-3309.

Lorenz, M., Popp, D., and Holmes, K. C. (1993). Refinement of the F-actin model against X-ray fiber diffraction data by the use of a directed mutation algorithm. J Mol Biol *234*, 826-836.

Lundblad, J. R., Laurance, M., and Goodman, R. H. (1996). Fluorescence polarization analysis of protein-DNA and protein-protein interactions. Mol Endocrinol *10*, 607-612.

Lyubimova, A., Bershadsky, A. D., and Ben-Ze'ev, A. (1997). Autoregulation of actin synthesis responds to monomeric actin levels. J Cell Biochem *65*, 469-478.

Lyubimova, A., Bershadsky, A. D., and Ben-Ze'ev, A. (1999). Autoregulation of actin synthesis requires the 3'-UTR of actin mRNA and protects cells from actin overproduction. J Cell Biochem *76*, 1-12.

Ma, Z., Morris, S. W., Valentine, V., Li, M., Herbrick, J. A., Cui, X., Bouman, D., Li, Y., Mehta, P. K., Nizetic, D., *et al.* (2001). Fusion of two novel genes, RBM15 and MKL1, in the t(1;22)(p13;q13) of acute megakaryoblastic leukemia. Nat Genet *28*, 220-221.

Machesky, L. M., Atkinson, S. J., Ampe, C., Vandekerckhove, J., and Pollard, T. D. (1994). Purification of a cortical complex containing two unconventional actins from Acanthamoeba by affinity chromatography on profilin-agarose. J Cell Biol *127*, 107-115.

Machesky, L. M., Mullins, R. D., Higgs, H. N., Kaiser, D. A., Blanchoin, L., May, R. C., Hall, M. E., and Pollard, T. D. (1999). Scar, a WASp-related protein, activates nucleation of actin filaments by the Arp2/3 complex. Proc Natl Acad Sci U S A *96*, 3739-3744.

Maciver, S. K., Pope, B. J., Whytock, S., and Weeds, A. G. (1998). The effect of two actin depolymerizing factors (ADF/cofilins) on actin filament turnover: pH sensitivity of F-actin binding by human ADF, but not of Acanthamoeba actophorin. Eur J Biochem *256*, 388-397.

Mack, C. P., and Owens, G. K. (1999). Regulation of smooth muscle alpha-actin expression in vivo is dependent on CArG elements within the 5' and first intron promoter regions. Circ Res *84*, 852-861.

Maekawa, M., Ishizaki, T., Boku, S., Watanabe, N., Fujita, A., Iwamatsu, A., Obinata, T., Ohashi, K., Mizuno, K., and Narumiya, S. (1999). Signaling from Rho to the actin cytoskeleton through protein kinases ROCK and LIM-kinase. Science *285*, 895-898.

Malvern Instruments, L. (2005). Zetasizer Nano Series User Manual, Issue 2.2.

Mannherz, H. G., Goody, R. S., Konrad, M., and Nowak, E. (1980). The interaction of bovine pancreatic deoxyribonuclease I and skeletal muscle actin. Eur J Biochem *104*, 367-379.

Mannherz, H. G., Kabsch, W., and Leverman, R. (1977). Crystals of skeletal muscle actin: pancreatic DNAase I complex. FEBS Lett *73*, 141-143.

Manning, G., Whyte, D. B., Martinez, R., Hunter, T., and Sudarsanam, S. (2002). The protein kinase complement of the human genome. Science *298*, 1912-1934.

Manseau, L. J., and Schupbach, T. (1989). cappuccino and spire: two unique maternal-effect loci required for both the anteroposterior and dorsoventral patterns of the Drosophila embryo. Genes Dev *3*, 1437-1452.

Marais, R., Wynne, J., and Treisman, R. (1993). The SRF accessory protein Elk-1 contains a growth factor-regulated transcriptional activation domain. Cell *73*, 381-393.

Marg, A., Shan, Y., Meyer, T., Meissner, T., Brandenburg, M., and Vinkemeier, U. (2004). Nucleocytoplasmic shuttling by nucleoporins Nup153 and Nup214 and CRM1-dependent nuclear export control the subcellular distribution of latent Stat1. J Cell Biol *165*, 823-833.

Marinissen, M. J., and Gutkind, J. S. (2005). Scaffold proteins dictate Rho GTPase-signaling specificity. Trends Biochem Sci *30*, 423-426.

Matsubayashi, Y., Fukuda, M., and Nishida, E. (2001). Evidence for existence of a nuclear pore complex-mediated, cytosol-independent pathway of nuclear translocation of ERK MAP kinase in permeabilized cells. J Biol Chem *276*, 41755-41760.

McBride, K. M., Banninger, G., McDonald, C., and Reich, N. C. (2002). Regulated nuclear import of the STAT1 transcription factor by direct binding of importin-alpha. Embo J *21*, 1754-1763.

McDonald, D., Carrero, G., Andrin, C., de Vries, G., and Hendzel, M. J. (2006). Nucleoplasmic beta-actin exists in a dynamic equilibrium between low-mobility polymeric species and rapidly diffusing populations. J Cell Biol *172*, 541-552.

McGough, A., Pope, B., Chiu, W., and Weeds, A. (1997). Cofilin changes the twist of F-actin: implications for actin filament dynamics and cellular function. J Cell Biol *138*, 771-781.

McLaughlin, P. J., Gooch, J. T., Mannherz, H. G., and Weeds, A. G. (1993). Structure of gelsolin segment 1-actin complex and the mechanism of filament severing. Nature *364*, 685-692.

Mercher, T., Coniat, M. B., Monni, R., Mauchauffe, M., Khac, F. N., Gressin, L., Mugneret, F., Leblanc, T., Dastugue, N., Berger, R., and Bernard, O. A. (2001). Involvement of a human gene related to the Drosophila spen gene in the recurrent t(1;22) translocation of acute megakaryocytic leukemia. Proc Natl Acad Sci U S A *98*, 5776-5779.

Messenguy, F., and Dubois, E. (2003). Role of MADS box proteins and their cofactors in combinatorial control of gene expression and cell development. Gene *316*, 1-21.

Meyer, T., Hendry, L., Begitt, A., John, S., and Vinkemeier, U. (2004). A single residue modulates tyrosine dephosphorylation, oligomerization, and nuclear accumulation of stat transcription factors. J Biol Chem *279*, 18998-19007.

Meyer, T., Marg, A., Lemke, P., Wiesner, B., and Vinkemeier, U. (2003). DNA binding controls inactivation and nuclear accumulation of the transcription factor Stat1. Genes Dev *17*, 1992-2005.

Meyer, T., and Vinkemeier, U. (2004). Nucleocytoplasmic shuttling of STAT transcription factors. Eur J Biochem *271*, 4606-4612.

Miano, J. M., Long, X., and Fujiwara, K. (2007). Serum response factor: master regulator of the actin cytoskeleton and contractile apparatus. Am J Physiol Cell Physiol *292*, C70-81.

Miano, J. M., Ramanan, N., Georger, M. A., de Mesy Bentley, K. L., Emerson, R. L., Balza, R. O., Jr., Xiao, Q., Weiler, H., Ginty, D. D., and Misra, R. P. (2004). Restricted inactivation of serum response factor to the cardiovascular system. Proc Natl Acad Sci U S A *101*, 17132-17137.

Minty, A., and Kedes, L. (1986). Upstream regions of the human cardiac actin gene that modulate its transcription in muscle cells: presence of an evolutionarily conserved repeated motif. Mol Cell Biol *6*, 2125-2136.

Miralles, F., Posern, G., Zaromytidou, A. I., and Treisman, R. (2003). Actin dynamics control SRF activity by regulation of its coactivator MAL. Cell *113*, 329-342.

Miralles, F., and Visa, N. (2006). Actin in transcription and transcription regulation. Curr Opin Cell Biol *18*, 261-266.

Mohun, T., Garrett, N., and Treisman, R. (1987). Xenopus cytoskeletal actin and human c-fos gene promoters share a conserved protein-binding site. Embo J *6*, 667-673.

Montagne, J., Groppe, J., Guillemin, K., Krasnow, M. A., Gehring, W. J., and Affolter, M. (1996). The Drosophila Serum Response Factor gene is required for the formation of intervein tissue of the wing and is allelic to blistered. Development *122*, 2589-2597.

Moore, P. B., Huxley, H. E., and DeRosier, D. J. (1970). Three-dimensional reconstruction of F-actin, thin filaments and decorated thin filaments. J Mol Biol *50*, 279-295.

Morton, W. M., Ayscough, K. R., and McLaughlin, P. J. (2000). Latrunculin alters the actin-monomer subunit interface to prevent polymerization. Nat Cell Biol *2*, 376-378.

Moss, J. B., McQuinn, T. C., and Schwartz, R. J. (1994). The avian cardiac alpha-actin promoter is regulated through a pair of complex elements composed of E boxes and serum response elements that bind both positive- and negative-acting factors. J Biol Chem *269*, 12731-12740.

Mueller, C. G., and Nordheim, A. (1991). A protein domain conserved between yeast MCM1 and human SRF directs ternary complex formation. Embo J *10*, 4219-4229.

Muller, J., Oma, Y., Vallar, L., Friederich, E., Poch, O., and Winsor, B. (2005). Sequence and comparative genomic analysis of actin-related proteins. Mol Biol Cell *16*, 5736-5748.

Mullins, R. D., Heuser, J. A., and Pollard, T. D. (1998). The interaction of Arp2/3 complex with actin: nucleation, high affinity pointed end capping, and formation of branching networks of filaments. Proc Natl Acad Sci U S A *95*, 6181-6186.

Murai, K., and Treisman, R. (2002). Interaction of serum response factor (SRF) with the Elk-1 B box inhibits RhoA-actin signaling to SRF and potentiates transcriptional activation by Elk-1. Mol Cell Biol *22*, 7083-7092.

Muscat, G. E., Gustafson, T. A., and Kedes, L. (1988). A common factor regulates skeletal and cardiac alpha-actin gene transcription in muscle. Mol Cell Biol *8*, 4120-4133.

Narita, A., Takeda, S., Yamashita, A., and Maeda, Y. (2006). Structural basis of actin filament capping at the barbed-end: a cryo-electron microscopy study. Embo J *25*, 5626-5633.

Niu, Z., Yu, W., Zhang, S. X., Barron, M., Belaguli, N. S., Schneider, M. D., Parmacek, M., Nordheim, A., and Schwartz, R. J. (2005). Conditional mutagenesis of the murine serum response factor gene blocks cardiogenesis and the transcription of downstream gene targets. J Biol Chem *280*, 32531-32538.

Niwa, R., Nagata-Ohashi, K., Takeichi, M., Mizuno, K., and Uemura, T. (2002). Control of actin reorganization by Slingshot, a family of phosphatases that dephosphorylate ADF/cofilin. Cell *108*, 233-246.

Nobes, C. D., and Hall, A. (1995). Rho, rac, and cdc42 GTPases regulate the assembly of multimolecular focal complexes associated with actin stress fibers, lamellipodia, and filopodia. Cell *81*, 53-62.

Norman, C., Runswick, M., Pollock, R., and Treisman, R. (1988). Isolation and properties of cDNA clones encoding SRF, a transcription factor that binds to the c-fos serum response element. Cell *55*, 989-1003.

Nurrish, S. J., and Treisman, R. (1995). DNA binding specificity determinants in MADS-box transcription factors. Mol Cell Biol *15*, 4076-4085.

Nyman, T., Schuler, H., Korenbaum, E., Schutt, C. E., Karlsson, R., and Lindberg, U. (2002). The role of MeH73 in actin polymerization and ATP hydrolysis. J Mol Biol *317*, 577-589.

Oda, T., Makino, K., Yamashita, I., Namba, K., and Maeda, Y. (2001). The helical parameters of F-actin precisely determined from X-ray fiber diffraction of well-oriented sols. Results Probl Cell Differ *32*, 43-58.

Oh, J., Richardson, J. A., and Olson, E. N. (2005). Requirement of myocardin-related transcription factor-B for remodeling of branchial arch arteries and smooth muscle differentiation. Proc Natl Acad Sci U S A *102*, 15122-15127.

Ohashi, K., Nagata, K., Maekawa, M., Ishizaki, T., Narumiya, S., and Mizuno, K. (2000). Rho-associated kinase ROCK activates LIM-kinase 1 by phosphorylation at threonine 508 within the activation loop. J Biol Chem *275*, 3577-3582.

Olave, I. A., Reck-Peterson, S. L., and Crabtree, G. R. (2002). Nuclear actin and actin-related proteins in chromatin remodeling. Annu Rev Biochem *71*, 755-781.

Ono, S., and Ono, K. (2002). Tropomyosin inhibits ADF/cofilin-dependent actin filament dynamics. J Cell Biol *156*, 1065-1076.

Oriol, C., Dubord, C., and Landon, F. (1977). Crystallization of native striated-muscle actin. FEBS Lett *73*, 89-91.

Ossareh-Nazari, B., Bachelerie, F., and Dargemont, C. (1997). Evidence for a role of CRM1 in signal-mediated nuclear protein export. Science *278*, 141-144.

Otey, C. A., Kalnoski, M. H., Lessard, J. L., and Bulinski, J. C. (1986). Immunolocalization of the gamma isoform of nonmuscle actin in cultured cells. J Cell Biol *102*, 1726-1737.

Otterbein, L. R., Cosio, C., Graceffa, P., and Dominguez, R. (2002). Crystal structures of the vitamin D-binding protein and its complex with actin: structural basis of the actin-scavenger system. Proc Natl Acad Sci U S A *99*, 8003-8008.

Otterbein, L. R., Graceffa, P., and Dominguez, R. (2001). The crystal structure of uncomplexed actin in the ADP state. Science *293*, 708-711.

Pace, C. N., Vajdos, F., Fee, L., Grimsley, G., and Gray, T. (1995). How to measure and predict the molar absorption coefficient of a protein. Protein Sci *4*, 2411-2423.

Page, R., Lindberg, U., and Schutt, C. E. (1998). Domain motions in actin. J Mol Biol *280*, 463-474.

Panne, D., Maniatis, T., and Harrison, S. C. (2007). An atomic model of the interferon-beta enhanceosome. Cell *129*, 1111-1123.

Pantaloni, D., and Carlier, M. F. (1993). How profilin promotes actin filament assembly in the presence of thymosin beta 4. Cell *75*, 1007-1014.

Papayannopoulos, V., Co, C., Prehoda, K. E., Snapper, S., Taunton, J., and Lim, W. A. (2005). A polybasic motif allows N-WASP to act as a sensor of PIP(2) density. Mol Cell *17*, 181-191.

Parlakian, A., Tuil, D., Hamard, G., Tavernier, G., Hentzen, D., Concordet, J. P., Paulin, D., Li, Z., and Daegelen, D. (2004). Targeted inactivation of serum response factor in the developing heart results in myocardial defects and embryonic lethality. Mol Cell Biol *24*, 5281-5289.

Passmore, S., Elble, R., and Tye, B. K. (1989). A protein involved in minichromosome maintenance in yeast binds a transcriptional enhancer conserved in eukaryotes. Genes Dev *3*, 921-935.

Paunola, E., Mattila, P. K., and Lappalainen, P. (2002). WH2 domain: a small, versatile adapter for actin monomers. FEBS Lett *513*, 92-97.

Pawson, T., and Nash, P. (2003). Assembly of cell regulatory systems through protein interaction domains. Science *300*, 445-452.

Pederson, T., and Aebi, U. (2002). Actin in the nucleus: what form and what for? J Struct Biol *140*, 3-9.

Pellegrini, L., Tan, S., and Richmond, T. J. (1995). Structure of serum response factor core bound to DNA. Nature *376*, 490-498.

Pelton, J. T., and McLean, L. R. (2000). Spectroscopic methods for analysis of protein secondary structure. Anal Biochem *277*, 167-176.

Percipalle, P., Fomproix, N., Kylberg, K., Miralles, F., Bjorkroth, B., Daneholt, B., and Visa, N. (2003). An actin-ribonucleoprotein interaction is involved in transcription by RNA polymerase II. Proc Natl Acad Sci U S A *100*, 6475-6480.

Perelroizen, I., Didry, D., Christensen, H., Chua, N. H., and Carlier, M. F. (1996). Role of nucleotide exchange and hydrolysis in the function of profilin in action assembly. J Biol Chem *271*, 12302-12309.

Perutz, M. F. (1978). Hemoglobin structure and respiratory transport. Sci Am *239*, 92-125.

Peterson, C. L., Zhao, Y., and Chait, B. T. (1998). Subunits of the yeast SWI/SNF complex are members of the actin-related protein (ARP) family. J Biol Chem *273*, 23641-23644.

Philimonenko, V. V., Zhao, J., Iben, S., Dingova, H., Kysela, K., Kahle, M., Zentgraf, H., Hofmann, W. A., de Lanerolle, P., Hozak, P., and Grummt, I. (2004). Nuclear actin and myosin I are required for RNA polymerase I transcription. Nat Cell Biol *6*, 1165-1172.

Philippar, U., Schratt, G., Dieterich, C., Muller, J. M., Galgoczy, P., Engel, F. B., Keating, M. T., Gertler, F., Schule, R., Vingron, M., and Nordheim, A. (2004). The SRF

target gene Fhl2 antagonizes RhoA/MAL-dependent activation of SRF. Mol Cell *16*, 867-880.

Pierreux, C. E., Nicolas, F. J., and Hill, C. S. (2000). Transforming growth factor beta-independent shuttling of Smad4 between the cytoplasm and nucleus. Mol Cell Biol *20*, 9041-9054.

Pipes, G. C., Creemers, E. E., and Olson, E. N. (2006). The myocardin family of transcriptional coactivators: versatile regulators of cell growth, migration, and myogenesis. Genes Dev *20*, 1545-1556.

Pipes, G. C., Sinha, S., Qi, X., Zhu, C. H., Gallardo, T. D., Shelton, J., Creemers, E. E., Sutherland, L., Richardson, J. A., Garry, D. J., *et al.* (2005). Stem cells and their derivatives can bypass the requirement of myocardin for smooth muscle gene expression. Dev Biol *288*, 502-513.

Polet, D., Lambrechts, A., Vandepoele, K., Vandekerckhove, J., and Ampe, C. (2007). On the origin and evolution of vertebrate and viral profilins. FEBS Lett *581*, 211-217.

Pollard, T. D. (1986). Rate constants for the reactions of ATP- and ADP-actin with the ends of actin filaments. J Cell Biol *103*, 2747-2754.

Pollard, T. D. (2007). Regulation of actin filament assembly by Arp2/3 complex and formins. Annu Rev Biophys Biomol Struct *36*, 451-477.

Pollard, T. D., and Borisy, G. G. (2003). Cellular motility driven by assembly and disassembly of actin filaments. Cell *112*, 453-465.

Pollastri, G., and McLysaght, A. (2005). Porter: a new, accurate server for protein secondary structure prediction. Bioinformatics *21*, 1719-1720.

Pollock, R., and Treisman, R. (1990). A sensitive method for the determination of protein-DNA binding specificities. Nucleic Acids Res *18*, 6197-6204.

Popp, D., Lednev, V. V., and Jahn, W. (1987). Methods of preparing well-orientated sols of f-actin containing filaments suitable for X-ray diffraction. J Mol Biol *197*, 679-684.

Posern, G., Miralles, F., Guettler, S., and Treisman, R. (2004). Mutant actins that stabilise F-actin use distinct mechanisms to activate the SRF coactivator MAL. Embo J *23*, 3973-3983.

Posern, G., Sotiropoulos, A., and Treisman, R. (2002). Mutant actins demonstrate a role for unpolymerized actin in control of transcription by serum response factor. Mol Biol Cell *13*, 4167-4178.

Posern, G., and Treisman, R. (2006). Actin' together: serum response factor, its cofactors and the link to signal transduction. Trends Cell Biol *16*, 588-596.

Price, M. A., Rogers, A. E., and Treisman, R. (1995). Comparative analysis of the ternary complex factors Elk-1, SAP-1a and SAP-2 (ERP/NET). Embo J *14*, 2589-2601.

Pring, M., Evangelista, M., Boone, C., Yang, C., and Zigmond, S. H. (2003). Mechanism of formin-induced nucleation of actin filaments. Biochemistry *42*, 486-496.

Provencher, S. W., and Glockner, J. (1981). Estimation of globular protein secondary structure from circular dichroism. Biochemistry *20*, 33-37.

Pruyne, D., Evangelista, M., Yang, C., Bi, E., Zigmond, S., Bretscher, A., and Boone, C. (2002). Role of formins in actin assembly: nucleation and barbed-end association. Science *297*, 612-615.

Prywes, R., and Roeder, R. G. (1986). Inducible binding of a factor to the c-fos enhancer. Cell *47*, 777-784.

Prywes, R., and Roeder, R. G. (1987). Purification of the c-fos enhancer-binding protein. Mol Cell Biol *7*, 3482-3489.

Ptashne, M. (2004). A Genetic Switch: Phage Lambda Revisited, third edition edn (Cold Spring Harbor: Cold Spring Harbor Laboratory Press).

Quinlan, M. E., Heuser, J. E., Kerkhoff, E., and Mullins, R. D. (2005). Drosophila Spire is an actin nucleation factor. Nature *433*, 382-388.

Raghunathan, V., Mowery, P., Rozycki, M., Lindberg, U., and Schutt, C. (1992). Structural changes in profilin accompany its binding to phosphatidylinositol, 4,5-bisphosphate. FEBS Lett *297*, 46-50.

Ramanan, N., Shen, Y., Sarsfield, S., Lemberger, T., Schutz, G., Linden, D. J., and Ginty, D. D. (2005). SRF mediates activity-induced gene expression and synaptic plasticity but not neuronal viability. Nat Neurosci *8*, 759-767.

Rando, O. J., Zhao, K., Janmey, P., and Crabtree, G. R. (2002). Phosphatidylinositol-dependent actin filament binding by the SWI/SNF-like BAF chromatin remodeling complex. Proc Natl Acad Sci U S A *99*, 2824-2829.

Resch, G. P., Goldie, K. N., Hoenger, A., and Small, J. V. (2002a). Pure F-actin networks are distorted and branched by steps in the critical-point drying method. J Struct Biol *137*, 305-312.

Resch, G. P., Goldie, K. N., Krebs, A., Hoenger, A., and Small, J. V. (2002b). Visualisation of the actin cytoskeleton by cryo-electron microscopy. J Cell Sci *115*, 1877-1882.

Reuner, K. H., Wiederhold, M., Dunker, P., Just, I., Bohle, R. M., Kroger, M., and Katz, N. (1995). Autoregulation of actin synthesis in hepatocytes by transcriptional and posttranscriptional mechanisms. Eur J Biochem *230*, 32-37.

Reya, T., and Clevers, H. (2005). Wnt signalling in stem cells and cancer. Nature *434*, 843-850.

Ridley, A. J., and Hall, A. (1992). The small GTP-binding protein rho regulates the assembly of focal adhesions and actin stress fibers in response to growth factors. Cell *70*, 389-399.

Ridley, A. J., Paterson, H. F., Johnston, C. L., Diekmann, D., and Hall, A. (1992). The small GTP-binding protein rac regulates growth factor-induced membrane ruffling. Cell *70*, 401-410.

Robinson, R. C., Mejillano, M., Le, V. P., Burtnick, L. D., Yin, H. L., and Choe, S. (1999). Domain movement in gelsolin: a calcium-activated switch. Science *286*, 1939-1942.

Robinson, R. C., Turbedsky, K., Kaiser, D. A., Marchand, J. B., Higgs, H. N., Choe, S., and Pollard, T. D. (2001). Crystal structure of Arp2/3 complex. Science *294*, 1679-1684.

Romero, S., Le Clainche, C., Didry, D., Egile, C., Pantaloni, D., and Carlier, M. F. (2004). Formin is a processive motor that requires profilin to accelerate actin assembly and associated ATP hydrolysis. Cell *119*, 419-429.

Ross, A. F., Oleynikov, Y., Kislauskis, E. H., Taneja, K. L., and Singer, R. H. (1997). Characterization of a beta-actin mRNA zipcode-binding protein. Mol Cell Biol *17*, 2158-2165.

Rossman, K. L., Der, C. J., and Sondek, J. (2005). GEF means go: turning on RHO GTPases with guanine nucleotide-exchange factors. Nat Rev Mol Cell Biol *6*, 167-180.

Rould, M. A., Wan, Q., Joel, P. B., Lowey, S., and Trybus, K. M. (2006). Crystal structures of expressed non-polymerizable monomeric actin in the ADP and ATP states. J Biol Chem *281*, 31909-31919.

Rubinfeld, B., Albert, I., Porfiri, E., Fiol, C., Munemitsu, S., and Polakis, P. (1996). Binding of GSK3beta to the APC-beta-catenin complex and regulation of complex assembly. Science *272*, 1023-1026.

Sablin, E. P., Dawson, J. F., VanLoock, M. S., Spudich, J. A., Egelman, E. H., and Fletterick, R. J. (2002). How does ATP hydrolysis control actin's associations? Proc Natl Acad Sci U S A *99*, 10945-10947.

Safer, D., Elzinga, M., and Nachmias, V. T. (1991). Thymosin beta 4 and Fx, an actin-sequestering peptide, are indistinguishable. J Biol Chem *266*, 4029-4032.

Safer, D., Golla, R., and Nachmias, V. T. (1990). Isolation of a 5-kilodalton actin-sequestering peptide from human blood platelets. Proc Natl Acad Sci U S A *87*, 2536-2540.

Safer, D., Sosnick, T. R., and Elzinga, M. (1997). Thymosin beta 4 binds actin in an extended conformation and contacts both the barbed and pointed ends. Biochemistry *36*, 5806-5816.

Sagot, I., Rodal, A. A., Moseley, J., Goode, B. L., and Pellman, D. (2002). An actin nucleation mechanism mediated by Bni1 and profilin. Nat Cell Biol *4*, 626-631.

Sahai, E., Alberts, A. S., and Treisman, R. (1998). RhoA effector mutants reveal distinct effector pathways for cytoskeletal reorganization, SRF activation and transformation. Embo J *17*, 1350-1361.

Sahai, E., Ishizaki, T., Narumiya, S., and Treisman, R. (1999). Transformation mediated by RhoA requires activity of ROCK kinases. Curr Biol *9*, 136-145.

Sahai, E., and Marshall, C. J. (2002). RHO-GTPases and cancer. Nat Rev Cancer *2*, 133-142.

Sampath, P., and Pollard, T. D. (1991). Effects of cytochalasin, phalloidin, and pH on the elongation of actin filaments. Biochemistry *30*, 1973-1980.

Sasazuki, T., Sawada, T., Sakon, S., Kitamura, T., Kishi, T., Okazaki, T., Katano, M., Tanaka, M., Watanabe, M., Yagita, H., *et al.* (2002). Identification of a novel transcriptional activator, BSAC, by a functional cloning to inhibit tumor necrosis factor-induced cell death. J Biol Chem *277*, 28853-28860.

Scheer, U., Hinssen, H., Franke, W. W., and Jockusch, B. M. (1984). Microinjection of actin-binding proteins and actin antibodies demonstrates involvement of nuclear actin in transcription of lampbrush chromosomes. Cell *39*, 111-122.

Schlessinger, J. (2003). Signal transduction. Autoinhibition control. Science *300*, 750-752.

Schmidt, A., and Hall, A. (2002). Guanine nucleotide exchange factors for Rho GTPases: turning on the switch. Genes Dev *16*, 1587-1609.

Schmierer, B., and Hill, C. S. (2005). Kinetic analysis of Smad nucleocytoplasmic shuttling reveals a mechanism for transforming growth factor beta-dependent nuclear accumulation of Smads. Mol Cell Biol *25*, 9845-9858.

Schratt, G., Philippar, U., Berger, J., Schwarz, H., Heidenreich, O., and Nordheim, A. (2002). Serum response factor is crucial for actin cytoskeletal organization and focal adhesion assembly in embryonic stem cells. J Cell Biol *156*, 737-750.

Schratt, G., Weinhold, B., Lundberg, A. S., Schuck, S., Berger, J., Schwarz, H., Weinberg, R. A., Ruther, U., and Nordheim, A. (2001). Serum response factor is required for immediate-early gene activation yet is dispensable for proliferation of embryonic stem cells. Mol Cell Biol *21*, 2933-2943.

Schuster-Bockler, B., Schultz, J., and Rahmann, S. (2004). HMM Logos for visualization of protein families. BMC Bioinformatics *5*, 7.

Schutt, C. E., Myslik, J. C., Rozycki, M. D., Goonesekere, N. C., and Lindberg, U. (1993). The structure of crystalline profilin-beta-actin. Nature *365*, 810-816.

Schutt, C. E., Rozycki, M. D., Chik, J. K., and Lindberg, U. (1995). Structural studies on the ribbon-to-helix transition in profilin: actin crystals. Biophys J *68*, 12S-17S; discussion 17S-18S.

Sekimoto, T., Imamoto, N., Nakajima, K., Hirano, T., and Yoneda, Y. (1997). Extracellular signal-dependent nuclear import of Stat1 is mediated by nuclear pore-targeting complex formation with NPI-1, but not Rch1. Embo J *16*, 7067-7077.

Sekimoto, T., Nakajima, K., Tachibana, T., Hirano, T., and Yoneda, Y. (1996). Interferon-gamma-dependent nuclear import of Stat1 is mediated by the GTPase activity of Ran/TC4. J Biol Chem *271*, 31017-31020.

Selden, L. A., Kinosian, H. J., Newman, J., Lincoln, B., Hurwitz, C., Gershman, L. C., and Estes, J. E. (1998). Severing of F-actin by the amino-terminal half of gelsolin suggests internal cooperativity in gelsolin. Biophys J *75*, 3092-3100.

Selvaraj, A., and Prywes, R. (2003). Megakaryoblastic leukemia-1/2, a transcriptional co-activator of serum response factor, is required for skeletal myogenic differentiation. J Biol Chem *278*, 41977-41987.

Selvaraj, A., and Prywes, R. (2004). Expression profiling of serum inducible genes identifies a subset of SRF target genes that are MKL dependent. BMC Mol Biol *5*, 13.

Sept, D., and McCammon, J. A. (2001). Thermodynamics and kinetics of actin filament nucleation. Biophys J *81*, 667-674.

Serpinskaya, A. S., Denisenko, O. N., Gelfand, V. I., and Bershadsky, A. D. (1990). Stimulation of actin synthesis in phalloidin-treated cells. Evidence for autoregulatory control. FEBS Lett *277*, 11-14.

Sharrocks, A. D. (2001). The ETS-domain transcription factor family. Nat Rev Mol Cell Biol *2*, 827-837.

Sharrocks, A. D., Gille, H., and Shaw, P. E. (1993). Identification of amino acids essential for DNA binding and dimerization in p67SRF: implications for a novel DNA-binding motif. Mol Cell Biol *13*, 123-132.

Shaw, P. E., Schroter, H., and Nordheim, A. (1989). The ability of a ternary complex to form over the serum response element correlates with serum inducibility of the human c-fos promoter. Cell *56*, 563-572.

Shi, Y., and Massague, J. (2003). Mechanisms of TGF-beta signaling from cell membrane to the nucleus. Cell *113*, 685-700.

Shore, P., and Sharrocks, A. D. (1994). The transcription factors Elk-1 and serum response factor interact by direct protein-protein contacts mediated by a short region of Elk-1. Mol Cell Biol *14*, 3283-3291.

Shore, P., and Sharrocks, A. D. (1995). The MADS-box family of transcription factors. Eur J Biochem *229*, 1-13.

Shuai, K., Stark, G. R., Kerr, I. M., and Darnell, J. E., Jr. (1993). A single phosphotyrosine residue of Stat91 required for gene activation by interferon-gamma. Science *261*, 1744-1746.

Sidrauski, C., Cox, J. S., and Walter, P. (1996). tRNA ligase is required for regulated mRNA splicing in the unfolded protein response. Cell *87*, 405-413.

Sidrauski, C., and Walter, P. (1997). The transmembrane kinase Ire1p is a site-specific endonuclease that initiates mRNA splicing in the unfolded protein response. Cell *90*, 1031-1039.

Simon, K. J., Grueneberg, D. A., and Gilman, M. (1997). Protein and DNA contact surfaces that mediate the selective action of the Phox1 homeodomain at the c-fos serum response element. Mol Cell Biol *17*, 6653-6662.

Siripala, A. D., and Welch, M. D. (2007a). SnapShot: actin regulators I. Cell *128*, 626.

Siripala, A. D., and Welch, M. D. (2007b). SnapShot: actin regulators II. Cell *128*, 1014.

Sjolinder, M., Bjork, P., Soderberg, E., Sabri, N., Farrants, A. K., and Visa, N. (2005). The growing pre-mRNA recruits actin and chromatin-modifying factors to transcriptionally active genes. Genes Dev *19*, 1871-1884.

Skare, P., and Karlsson, R. (2002). Evidence for two interaction regions for phosphatidylinositol(4,5)-bisphosphate on mammalian profilin I. FEBS Lett *522*, 119-124.

Skarnes, W. C., Auerbach, B. A., and Joyner, A. L. (1992). A gene trap approach in mouse embryonic stem cells: the lacZ reported is activated by splicing, reflects endogenous gene expression, and is mutagenic in mice. Genes Dev *6*, 903-918.

Small, E. M., Warkman, A. S., Wang, D. Z., Sutherland, L. B., Olson, E. N., and Krieg, P. A. (2005). Myocardin is sufficient and necessary for cardiac gene expression in Xenopus. Development *132*, 987-997.

Smith, P. G., Roy, C., Zhang, Y. N., and Chauduri, S. (2003). Mechanical stress increases RhoA activation in airway smooth muscle cells. Am J Respir Cell Mol Biol *28*, 436-442.

Sommer, H., Beltran, J. P., Huijser, P., Pape, H., Lonnig, W. E., Saedler, H., and Schwarz-Sommer, Z. (1990). Deficiens, a homeotic gene involved in the control of flower morphogenesis in Antirrhinum majus: the protein shows homology to transcription factors. Embo J *9*, 605-613.

Somogyi, K., and Rorth, P. (2004). Evidence for tension-based regulation of Drosophila MAL and SRF during invasive cell migration. Dev Cell *7*, 85-93.

Sotiropoulos, A., Gineitis, D., Copeland, J., and Treisman, R. (1999). Signal-regulated activation of serum response factor is mediated by changes in actin dynamics. Cell *98*, 159-169.

Soulez, M., Rouviere, C. G., Chafey, P., Hentzen, D., Vandromme, M., Lautredou, N., Lamb, N., Kahn, A., and Tuil, D. (1996). Growth and differentiation of C2 myogenic cells are dependent on serum response factor. Mol Cell Biol *16*, 6065-6074.

Spector, I., Shochet, N. R., Blasberger, D., and Kashman, Y. (1989). Latrunculins--novel marine macrolides that disrupt microfilament organization and affect cell growth: I. Comparison with cytochalasin D. Cell Motil Cytoskeleton *13*, 127-144.

Spector, I., Shochet, N. R., Kashman, Y., and Groweiss, A. (1983). Latrunculins: novel marine toxins that disrupt microfilament organization in cultured cells. Science *219*, 493-495.

Spudich, J. A., and Watt, S. (1971). The regulation of rabbit skeletal muscle contraction. I. Biochemical studies of the interaction of the tropomyosin-troponin complex with actin and the proteolytic fragments of myosin. J Biol Chem *246*, 4866-4871.

Sreerama, N., and Woody, R. W. (1993). A self-consistent method for the analysis of protein secondary structure from circular dichroism. Anal Biochem *209*, 32-44.

Stuven, T., Hartmann, E., and Gorlich, D. (2003). Exportin 6: a novel nuclear export receptor that is specific for profilin.actin complexes. Embo J *22*, 5928-5940.

Sumi, T., Matsumoto, K., and Nakamura, T. (2001). Specific activation of LIM kinase 2 via phosphorylation of threonine 505 by ROCK, a Rho-dependent protein kinase. J Biol Chem *276*, 670-676.

Sun, Q., Chen, G., Streb, J. W., Long, X., Yang, Y., Stoeckert, C. J., Jr., and Miano, J. M. (2006a). Defining the mammalian CArGome. Genome Res *16*, 197-207.

Sun, Y., Boyd, K., Xu, W., Ma, J., Jackson, C. W., Fu, A., Shillingford, J. M., Robinson, G. W., Hennighausen, L., Hitzler, J. K., *et al.* (2006b). Acute myeloid leukemia-associated Mkl1 (Mrtf-a) is a key regulator of mammary gland function. Mol Cell Biol *26*, 5809-5826.

Tanaka, M., and Shibata, H. (1985). Poly(L-proline)-binding proteins from chick embryos are a profilin and a profilactin. Eur J Biochem *151*, 291-297.

ten Dijke, P., and Hill, C. S. (2004). New insights into TGF-beta-Smad signalling. Trends Biochem Sci *29*, 265-273.

Thanos, D., and Maniatis, T. (1995). Virus induction of human IFN beta gene expression requires the assembly of an enhanceosome. Cell *83*, 1091-1100.

Thompson, J. D., Gibson, T. J., Plewniak, F., Jeanmougin, F., and Higgins, D. G. (1997). The CLUSTAL_X windows interface: flexible strategies for multiple sequence alignment aided by quality analysis tools. Nucleic Acids Res *25*, 4876-4882.

Tirion, M. M., ben-Avraham, D., Lorenz, M., and Holmes, K. C. (1995). Normal modes as refinement parameters for the F-actin model. Biophys J *68*, 5-12.

Tobacman, L. S., and Korn, E. D. (1982). The regulation of actin polymerization and the inhibition of monomeric actin ATPase activity by Acanthamoeba profilin. J Biol Chem *257*, 4166-4170.

Tominaga, T., Sahai, E., Chardin, P., McCormick, F., Courtneidge, S. A., and Alberts, A. S. (2000). Diaphanous-related formins bridge Rho GTPase and Src tyrosine kinase signaling. Mol Cell *5*, 13-25.

Torres, E., and Rosen, M. K. (2003). Contingent phosphorylation/dephosphorylation provides a mechanism of molecular memory in WASP. Mol Cell *11*, 1215-1227.

Treisman, R. (1985). Transient accumulation of c-fos RNA following serum stimulation requires a conserved 5' element and c-fos 3' sequences. Cell *42*, 889-902.

Treisman, R. (1986). Identification of a protein-binding site that mediates transcriptional response of the c-fos gene to serum factors. Cell *46*, 567-574.

Treisman, R. (1994). Ternary complex factors: growth factor regulated transcriptional activators. Curr Opin Genet Dev *4*, 96-101.

Treisman, R. (1995). Journey to the surface of the cell: Fos regulation and the SRE. Embo J *14*, 4905-4913.

Treisman, R., Marais, R., and Wynne, J. (1992). Spatial flexibility in ternary complexes between SRF and its accessory proteins. Embo J *11*, 4631-4640.

Tsukazaki, T., Chiang, T. A., Davison, A. F., Attisano, L., and Wrana, J. L. (1998). SARA, a FYVE domain protein that recruits Smad2 to the TGFbeta receptor. Cell *95*, 779-791.

Tullai, J. W., Schaffer, M. E., Mullenbrock, S., Kasif, S., and Cooper, G. M. (2004). Identification of transcription factor binding sites upstream of human genes regulated by the phosphatidylinositol 3-kinase and MEK/ERK signaling pathways. J Biol Chem *279*, 20167-20177.

Urbanek, P., Wang, Z. Q., Fetka, I., Wagner, E. F., and Busslinger, M. (1994). Complete block of early B cell differentiation and altered patterning of the posterior midbrain in mice lacking Pax5/BSAP. Cell *79*, 901-912.

van Tuyn, J., Knaan-Shanzer, S., van de Watering, M. J., de Graaf, M., van der Laarse, A., Schalij, M. J., van der Wall, E. E., de Vries, A. A., and Atsma, D. E. (2005). Activation of cardiac and smooth muscle-specific genes in primary human cells after forced expression of human myocardin. Cardiovasc Res *67*, 245-255.

Vartiainen, M. K., Guettler, S., Larijani, B., and Treisman, R. (2007). Nuclear actin regulates dynamic subcellular localization and activity of the SRF cofactor MAL. Science *316*, 1749-1752.

Vavylonis, D., Kovar, D. R., O'Shaughnessy, B., and Pollard, T. D. (2006). Model of formin-associated actin filament elongation. Mol Cell *21*, 455-466.

Vorobiev, S., Strokopytov, B., Drubin, D. G., Frieden, C., Ono, S., Condeelis, J., Rubenstein, P. A., and Almo, S. C. (2003). The structure of nonvertebrate actin: implications for the ATP hydrolytic mechanism. Proc Natl Acad Sci U S A *100*, 5760-5765.

Wada, A., Fukuda, M., Mishima, M., and Nishida, E. (1998). Nuclear export of actin: a novel mechanism regulating the subcellular localization of a major cytoskeletal protein. Embo J *17*, 1635-1641.

Wallar, B. J., and Alberts, A. S. (2003). The formins: active scaffolds that remodel the cytoskeleton. Trends Cell Biol *13*, 435-446.

Wang, D., Chang, P. S., Wang, Z., Sutherland, L., Richardson, J. A., Small, E., Krieg, P. A., and Olson, E. N. (2001a). Activation of cardiac gene expression by myocardin, a transcriptional cofactor for serum response factor. Cell *105*, 851-862.

Wang, D. Z., Li, S., Hockemeyer, D., Sutherland, L., Wang, Z., Schratt, G., Richardson, J. A., Nordheim, A., and Olson, E. N. (2002). Potentiation of serum response factor activity by a family of myocardin-related transcription factors. Proc Natl Acad Sci U S A *99*, 14855-14860.

Wang, D. Z., and Olson, E. N. (2004). Control of smooth muscle development by the myocardin family of transcriptional coactivators. Curr Opin Genet Dev *14*, 558-566.

Wang, H. R., Zhang, Y., Ozdamar, B., Ogunjimi, A. A., Alexandrova, E., Thomsen, G. H., and Wrana, J. L. (2003a). Regulation of cell polarity and protrusion formation by targeting RhoA for degradation. Science *302*, 1775-1779.

Wang, J., Sanger, J. M., and Sanger, J. W. (2005). Differential effects of Latrunculin-A on myofibrils in cultures of skeletal muscle cells: insights into mechanisms of myofibrillogenesis. Cell Motil Cytoskeleton *62*, 35-47.

Wang, Y., Miller, A. L., Mooseker, M. S., and Koleske, A. J. (2001b). The Abl-related gene (Arg) nonreceptor tyrosine kinase uses two F-actin-binding domains to bundle F-actin. Proc Natl Acad Sci U S A *98*, 14865-14870.

Wang, Z., Wang, D. Z., Hockemeyer, D., McAnally, J., Nordheim, A., and Olson, E. N. (2004). Myocardin and ternary complex factors compete for SRF to control smooth muscle gene expression. Nature *428*, 185-189.

Wang, Z., Wang, D. Z., Pipes, G. C., and Olson, E. N. (2003b). Myocardin is a master regulator of smooth muscle gene expression. Proc Natl Acad Sci U S A *100*, 7129-7134.

Watanabe, M., Masuyama, N., Fukuda, M., and Nishida, E. (2000). Regulation of intracellular dynamics of Smad4 by its leucine-rich nuclear export signal. EMBO Rep *1*, 176-182.

Watanabe, N., Kato, T., Fujita, A., Ishizaki, T., and Narumiya, S. (1999). Cooperation between mDia1 and ROCK in Rho-induced actin reorganization. Nat Cell Biol *1*, 136-143.

Way, M., Gooch, J., Pope, B., and Weeds, A. G. (1989). Expression of human plasma gelsolin in Escherichia coli and dissection of actin binding sites by segmental deletion mutagenesis. J Cell Biol *109*, 593-605.

Wear, M. A., and Cooper, J. A. (2004). Capping protein: new insights into mechanism and regulation. Trends Biochem Sci *29*, 418-428.

Weinhold, B., Schratt, G., Arsenian, S., Berger, J., Kamino, K., Schwarz, H., Ruther, U., and Nordheim, A. (2000). Srf(-/-) ES cells display non-cell-autonomous impairment in mesodermal differentiation. Embo J *19*, 5835-5844.

Weis, K. (2003). Regulating access to the genome: nucleocytoplasmic transport throughout the cell cycle. Cell *112*, 441-451.

Weiss, J. N. (1997). The Hill equation revisited: uses and misuses. Faseb J *11*, 835-841.

Welch, M. D., and Mullins, R. D. (2002). Cellular control of actin nucleation. Annu Rev Cell Dev Biol *18*, 247-288.

Wen, W., Meinkoth, J. L., Tsien, R. Y., and Taylor, S. S. (1995). Identification of a signal for rapid export of proteins from the nucleus. Cell *82*, 463-473.

Wennerberg, K., and Der, C. J. (2004). Rho-family GTPases: it's not only Rac and Rho (and I like it). J Cell Sci *117*, 1301-1312.

Wennerberg, K., Rossman, K. L., and Der, C. J. (2005). The Ras superfamily at a glance. J Cell Sci *118*, 843-846.

Whitehurst, A. W., Wilsbacher, J. L., You, Y., Luby-Phelps, K., Moore, M. S., and Cobb, M. H. (2002). ERK2 enters the nucleus by a carrier-independent mechanism. Proc Natl Acad Sci U S A *99*, 7496-7501.

Witke, W. (2004). The role of profilin complexes in cell motility and other cellular processes. Trends Cell Biol *14*, 461-469.

Wojciak-Stothard, B., and Ridley, A. J. (2003). Shear stress-induced endothelial cell polarization is mediated by Rho and Rac but not Cdc42 or PI 3-kinases. J Cell Biol *161*, 429-439.

Wu, X., Yoo, Y., Okuhama, N. N., Tucker, P. W., Liu, G., and Guan, J. L. (2006). Regulation of RNA-polymerase-II-dependent transcription by N-WASP and its nuclear-binding partners. Nat Cell Biol *8*, 756-763.

Xu, L., Alarcon, C., Col, S., and Massague, J. (2003). Distinct domain utilization by Smad3 and Smad4 for nucleoporin interaction and nuclear import. J Biol Chem *278*, 42569-42577.

Xu, L., Chen, Y. G., and Massague, J. (2000). The nuclear import function of Smad2 is masked by SARA and unmasked by TGFbeta-dependent phosphorylation. Nat Cell Biol *2*, 559-562.

Xu, L., and Massague, J. (2004). Nucleocytoplasmic shuttling of signal transducers. Nat Rev Mol Cell Biol *5*, 209-219.

Xu, Y., Moseley, J. B., Sagot, I., Poy, F., Pellman, D., Goode, B. L., and Eck, M. J. (2004). Crystal structures of a Formin Homology-2 domain reveal a tethered dimer architecture. Cell *116*, 711-723.

Xue, B., Aguda, A. H., and Robinson, R. C. (2007). Models of the actin-bound forms of the {beta}-thymosins. Ann N Y Acad Sci.

Yang, N., Higuchi, O., Ohashi, K., Nagata, K., Wada, A., Kangawa, K., Nishida, E., and Mizuno, K. (1998). Cofilin phosphorylation by LIM-kinase 1 and its role in Rac-mediated actin reorganization. Nature *393*, 809-812.

Yanofsky, M. F., Ma, H., Bowman, J. L., Drews, G. N., Feldmann, K. A., and Meyerowitz, E. M. (1990). The protein encoded by the Arabidopsis homeotic gene agamous resembles transcription factors. Nature *346*, 35-39.

Yarmola, E. G., and Bubb, M. R. (2006). Profilin: emerging concepts and lingering misconceptions. Trends Biochem Sci *31*, 197-205.

Yarmola, E. G., Parikh, S., and Bubb, M. R. (2001). Formation and implications of a ternary complex of profilin, thymosin beta 4, and actin. J Biol Chem *276*, 45555-45563.

Ye, J., Rawson, R. B., Komuro, R., Chen, X., Dave, U. P., Prywes, R., Brown, M. S., and Goldstein, J. L. (2000). ER stress induces cleavage of membrane-bound ATF6 by the same proteases that process SREBPs. Mol Cell *6*, 1355-1364.

Yokoya, F., Imamoto, N., Tachibana, T., and Yoneda, Y. (1999). beta-catenin can be transported into the nucleus in a Ran-unassisted manner. Mol Biol Cell *10*, 1119-1131.

Yoo, Y., Wu, X., and Guan, J. L. (2007). A novel role of the actin-nucleating Arp2/3 complex in the regulation of RNA polymerase II-dependent transcription. J Biol Chem *282*, 7616-7623.

Zaromytidou, A. I. (2007) Molecular sudy of SRF-cofactor interactions, University College London, London.

Zaromytidou, A. I., Miralles, F., and Treisman, R. (2006). MAL and ternary complex factor use different mechanisms to contact a common surface on the serum response factor DNA-binding domain. Mol Cell Biol *26*, 4134-4148.

Zdobnov, E. M., and Apweiler, R. (2001). InterProScan--an integration platform for the signature-recognition methods in InterPro. Bioinformatics *17*, 847-848.

Zhang, S. X., Garcia-Gras, E., Wycuff, D. R., Marriot, S. J., Kadeer, N., Yu, W., Olson, E. N., Garry, D. J., Parmacek, M. S., and Schwartz, R. J. (2005). Identification of direct serum-response factor gene targets during Me2SO-induced P19 cardiac cell differentiation. J Biol Chem *280*, 19115-19126.

Zhao, K., Wang, W., Rando, O. J., Xue, Y., Swiderek, K., Kuo, A., and Crabtree, G. R. (1998). Rapid and phosphoinositol-dependent binding of the SWI/SNF-like BAF complex to chromatin after T lymphocyte receptor signaling. Cell *95*, 625-636.

Zhao, X. H., Laschinger, C., Arora, P., Szaszi, K., Kapus, A., and McCulloch, C. A. (2007). Force activates smooth muscle alpha-actin promoter activity through the Rho signaling pathway. J Cell Sci *120*, 1801-1809.

Zhao, Y., Samal, E., and Srivastava, D. (2005). Serum response factor regulates a muscle-specific microRNA that targets Hand2 during cardiogenesis. Nature *436*, 214-220.

Zhao, Z. S., and Manser, E. (2005). PAK and other Rho-associated kinases--effectors with surprisingly diverse mechanisms of regulation. Biochem J *386*, 201-214.

Zigmond, S. H., Evangelista, M., Boone, C., Yang, C., Dar, A. C., Sicheri, F., Forkey, J., and Pring, M. (2003). Formin leaky cap allows elongation in the presence of tight capping proteins. Curr Biol *13*, 1820-1823.

Zinck, R., Hipskind, R. A., Pingoud, V., and Nordheim, A. (1993). c-fos transcriptional activation and repression correlate temporally with the phosphorylation status of TCF. Embo J *12*, 2377-2387.

The EMBO Journal (2004) 23, 3973–3983 | © 2004 European Molecular Biology Organization | All Rights Reserved 0261-4189/04
www.embojournal.org

THE
EMBO
JOURNAL

Mutant actins that stabilise F-actin use distinct mechanisms to activate the SRF coactivator MAL

Guido Posern[1], Francesc Miralles, Sebastian Guettler and Richard Treisman*

Transcription Laboratory, Cancer Research UK London Research Institute, Lincoln's Inn Fields Laboratories, London, UK

Nuclear accumulation of the serum response factor coactivator MAL/MKL1 is controlled by its interaction with G-actin, which results in its retention in the cytoplasm in cells with low Rho activity. We previously identified actin mutants whose expression promotes MAL nuclear accumulation via an unknown mechanism. Here, we show that actin interacts directly with MAL *in vitro* with high affinity. We identify a further activating mutation, G15S, which stabilises F-actin, as do the activating actins S14C and V159N. The three mutants share several biochemical properties, but can be distinguished by their ability to bind cofilin, ATP and MAL. MAL interaction with actin S14C is essentially undetectable, and that with actin V159N is weakened. In contrast, actin G15S interacts more strongly with MAL than the wild-type protein. Strikingly, the nuclear accumulation of MAL induced by overexpression of actin S14C is substantially dependent on Rho activity and actin treadmilling, while that induced by actin G15S expression is not. We propose a model in which actin G15S acts directly to promote MAL nuclear entry.

The EMBO Journal (2004) **23,** 3973–3983. doi:10.1038/sj.emboj.7600404; Published online 23 September 2004
Subject Categories: signal transduction; chromatin & transcription
Keywords: actin; MAL; MKL1; Rho; SRF

Introduction

Actin has a long history of proposed connections with nuclear events as well as its classical role as a cytoskeletal component. Recent studies suggest potential roles for actin and its relatives in chromatin remodelling, transcription and RNA export (reviewed by Olave *et al*, 2002; Bettinger *et al*, 2004). Among these roles is that played by actin to control its own expression both transcriptionally and at the level of mRNA translation, localisation and stability (for references see Lyubimova *et al*, 1999; Sotiropoulos *et al*, 1999). Autoregulation of actin transcription occurs via a mechanism in which G-actin binds to and controls the activity of MAL/MKL1, a coactivator of the serum response factor (SRF) transcription factor (Miralles *et al*, 2003). SRF, a MADS-box protein, controls a large number of growth factor-inducible and muscle-specific genes through the mutually exclusive association of different SRF cofactors (Murai and Treisman, 2002; Miralles *et al*, 2003; Wang *et al*, 2004), and the expression of many of these genes is thus influenced by G-actin level. In fibroblasts, MAL and its relative MAL16/MKL2 are predominantly cytoplasmic in the absence of Rho signalling, but accumulate in the nucleus upon Rho activation (Cen *et al*, 2003; Miralles *et al*, 2003; Du *et al*, 2004; C Perez-Sanchez, unpublished data). MAL associates with G-actin *in vivo*, and depletion of the G-actin pool upon activation of Rho releases MAL for nuclear import (Sotiropoulos *et al*, 1999; Posern *et al*, 2002; Miralles *et al*, 2003).

Actin mutants have given useful insight into the mechanism by which Rho controls SRF activity. In support of the notion that G-actin is the regulator, the overexpression of nonpolymerising β-actin mutants such as actins R62D, G13R and actin-VP16 inhibits SRF activation and MAL nuclear accumulation (Posern *et al*, 2002). Consistent with this, MAL can be recovered in immunoprecipitates of these mutants and wild-type actin, and their overexpression prevents MAL nuclear accumulation (Miralles *et al*, 2003). It has remained unclear whether MAL interacts directly with G-actin. We also identified two actin mutants, actins S14C and V159N, which stabilise F-actin and whose expression strongly activates SRF (Posern *et al*, 2002). Curiously, however, although cells expressing these mutants accumulate MAL in the nucleus and exhibit an increase in the F-/G-actin ratio, their absolute level of G-actin is if anything slightly increased relative to that of untransfected cells (Posern *et al*, 2002; Miralles *et al*, 2003). We suggested two mechanisms to explain these observations: either the mutants were incapable of interacting with the SRF coactivator (i.e. MAL), allowing its release to the nucleus, or they acted independently of the actin treadmilling cycle to induce its activation (Posern *et al*, 2002).

In this paper, we study the connection between activating actin mutants and SRF activation in the light of our identification of MAL as an actin-regulated SRF coactivator. We show that wild-type actin binds the N-terminal RPEL domain of MAL directly *in vitro*, and identify a new activating actin mutant, actin G15S, in a two-hybrid screen with this domain. All three activating actin mutants, actins G15S, S14C and V159N, share the ability to stabilise F-actin. They all exhibit a decreased ability to bind the C-terminal half of gelsolin, and an enhanced affinity for profilin, suggesting that their structure mimics that of ATP-actin. However, they can also be distinguished biochemically by their ability to interact with nucleotide, cofilin and MAL. Although actin G15S binds MAL more strongly than wild-type actin, the S14C mutation greatly reduces the actin–MAL interaction. Strikingly, the ability of actin S14C to induce MAL nuclear accumulation is strongly dependent on the actin treadmilling cycle and basal Rho

*Corresponding author. Transcription Laboratory, Room 401, Cancer Research UK, PO Box 123, 44 Lincoln's Inn Fields, London WC2A 3PX, UK. Tel.: +44 207 269 3271; Fax: +44 207 269 3093;
E-mail: richard.treisman@cancer.org.uk
[1]Present address: Max-Planck-Institute of Biochemistry, Am Klopferspitz 18, 82152 Martinsried, Germany

Received: 10 May 2004; accepted: 19 August 2004; published online: 23 September 2004

activity, while G15S- and V159N-induced MAL translocation is not. We propose that whereas actin S14C releases MAL from the inhibitory effect of wild-type G-actin by diluting the endogenous G-actin pool, actin G15S (and probably V159N) may act directly to induce MAL nuclear translocation.

Results

Actin interacts directly with the MAL RPEL motifs in vitro

We previously showed that MAL can be recovered in immunoprecipitates of cytoplasmic actin. The interaction was dependent on the integrity of the MAL N-terminal RPEL motifs (Miralles *et al*, 2003). It remained unclear, however, whether this complex involves a direct interaction between MAL and actin or requires additional proteins. To test whether the actin-MAL complex can form *in vitro*, we passed whole-cell extracts over affinity beads comprising MAL RPEL motifs 2 and 3 fused to GST. As controls we used mutant RPEL derivatives containing P→A or R→D mutations in each RPEL motif, which were previously shown to be defective for actin binding *in vivo* (Miralles *et al*, 2003). After extensive washing, bound proteins were eluted using the G-actin-binding drug swinholide A, which competes with MAL for actin binding (Miralles *et al*, 2003). A 42 kDa protein was prominent in the eluate from the wild-type but not mutant GST fusion protein; no other proteins in the 10–300 kDa M_r range bound specifically (Figure 1A). Similar results were obtained when proteins were eluted from the affinity beads by boiling in SDS–PAGE loading buffer (data not shown). An immunoblot experiment confirmed that the 42 kDa protein was indeed β-actin (Figure 1B). Purified β-actin also bound the wild-type but not the mutant MAL affinity beads, and this interaction was resistant to latrunculin B but sensitive to swinholide A (Figure 1C). These results complement previous experiments in which co-immunoprecipitation of MAL and actin was disrupted by cytochalasin D or swinholide A, which also promoted MAL nuclear accumulation, but not by latrunculin B, which did not (Miralles *et al*, 2003).

Some actin-binding proteins strongly discriminate between different nucleotide-bound forms of actin. We therefore tested the nucleotide-binding requirements of actin–MAL interaction using a native gel electrophoresis assay. Wild-type or mutant GST-MAL fusion proteins were mixed with ADP- or AMP-PNP-bound actin, separated on a native gel and actin detected by immunoblotting. Actin–MAL complex formation was detected regardless of the bound nucleotide (Figure 1D). These results show that additional accessory proteins are not required for binding of actin to the MAL RPEL motifs.

Finally, we determined the apparent affinity of the intact RPEL domain, by exploiting its ability to inhibit actin polymerisation (Hertzog *et al*, 2002). We used skeletal muscle α-actin since it is readily purified and recovers MAL as efficiently as β-actin in co-immunoprecipitation experiments (see Supplementary Figure S1). As a positive control, we evaluated gelsolin segments 4–6 (gelsolin(S4–6)). Increasing amounts of the MAL RPEL domain or gelsolin(S4–6) led to complete inhibition of F-actin assembly at comparable concentrations (Figure 1E). The data are consistent with an apparent K_d of 24 nM for MAL–actin, and an apparent K_d of 76 nM for gelsolin(S4–6), in good agreement with published

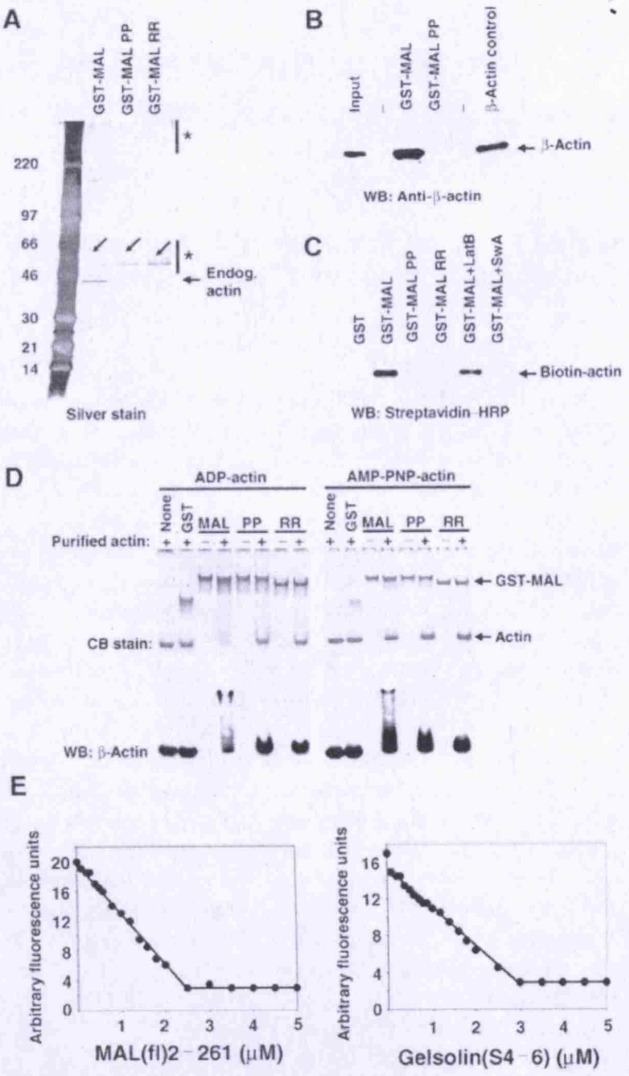

Figure 1 MAL binds directly to actin. (**A**) Actin does not associate with other cellular proteins on the RPEL motif. NIH3T3 cells were lysed by syringing in detergent-free buffer and the high-speed G-actin supernatant was affinity-precipitated using GST-MAL(met)(1–171) or its derivatives PP34/78AA (PP) or RR33/77DD (RR), which carry point mutations in each of the two RPEL motifs. Bound proteins were eluted with 500 nM swinholide A, separated by 6–16% gradient PAGE and detected by silver staining. The diagonal arrows indicate contaminating GST fusion proteins and asterisks mark nonspecifically retained polypeptides. (**B**) Precipitated proteins from a GST-MAL(met)(1–171) affinity precipitation experiment of the type shown in (A) were analysed by immunoblotting with β-actin antibody. (**C**) Affinity precipitation of purified biotinylated nonmuscle actin using GST-MAL(met)(1–171) or its derivatives. Where indicated, 1 μM latrunculin B or 100 nM swinholide A was included in the binding reaction. Bound actin was separated by 12% SDS–PAGE and detected by overlay with peroxidase-conjugated streptavidin. (**D**) Native 6% polyacrylamide gel electrophoresis assay of complex formation between GST-MAL(met)(1–171) derivatives and ADP- or AMP-PNP-loaded nonmuscle actin (left and right panels, respectively), with detection by Coomassie blue (CB) staining or anti-β-actin immunoblot. (**E**) Inhibition of skeletal muscle α-actin polymerisation by MAL(fl)2–261 (left), which contains all three RPEL motifs, and gelsolin(S4–6) (right). Data are mean of two independent experiments.

data (Way *et al*, 1989). Profilin overexpression induces MAL nuclear accumulation and SRF activation (Sotiropoulos *et al*, 1999; Miralles *et al*, 2003), and consistent with this, MAL is not recovered in profilin immunoprecipitates (Supplementary

Figure S1). Thus, high-affinity MAL–actin interaction allows it to compete effectively with profilin for free G-actin.

Identification of actin G15S, a novel MAL-activating protein

To identify cDNAs encoding proteins that interact with the MAL N-terminal region in an unbiased way, we set up a yeast two-hybrid assay. A GAL4 fusion protein containing MAL residues 1–631 was used to screen an NIH3T3 cDNA library, and all cDNAs recovered were counterscreened against a mutant MAL containing RPEL motif point mutations. From 600 000 clones screened, we recovered a mouse γ-actin cDNA containing the mutation G15S and two other cDNAs whose characterisation will be described in full elsewhere. Colony growth and liquid β-galactosidase assays showed that binding of γ-actin G15S to MAL was dependent on the RPEL motifs: it was severely reduced by R→D or P→A mutations at single RPEL motifs, and undetectable upon mutation of both motifs (Figure 2A). Intrigued by this observation, and our previous finding that mutations at the β-actin nucleotide-binding pocket can substantially affect its activity in the SRF activation assay (Posern *et al*, 2002), we tested whether the G15S mutation affects the ability of actin to repress SRF activity. Expression of γ-actin G15S strongly potentiated activity of the SRF reporter gene 3D.A-Luc in serum-starved cells; in contrast, expression of wild-type γ-actin, as with wild-type β-actin, suppressed activation of the reporter following serum stimulation (Figure 2B).

We next introduced the G15S mutation into β-actin. Expression of β-actin G15S also substantially activated expression of the SRF reporter in serum-starved cells, to levels comparable to those achieved by expression of the activating mutants actins S14C and V159N (Figure 2C; Posern *et al*, 2002). Consistent with its ability to activate SRF, β-actin G15S expression induced nuclear accumulation of the SRF coactivator MAL in NIH3T3 cells, but did not itself accumulate in the nucleus (Figure 2D). To allow comparison with our other 'activating' actin mutants, all further studies were performed with β-actin G15S.

Actin G15S stabilises F-actin

Upon transient overexpression in fibroblasts, actins S14C and V159N exhibit properties suggesting that they stabilise F-actin (Posern *et al*, 2002), consistent with structural studies of yeast actin V159N (Belmont and Drubin, 1998; Belmont *et al*, 1999a). We therefore measured intracellular levels of F-actin and G-actin in cells expressing the different actins. Cells were stained with phalloidin, which specifically binds F-actin, or DNase I, which specifically binds G-actin, and staining was quantified in transfected cells relative to untransfected cells in the same population using the FACS

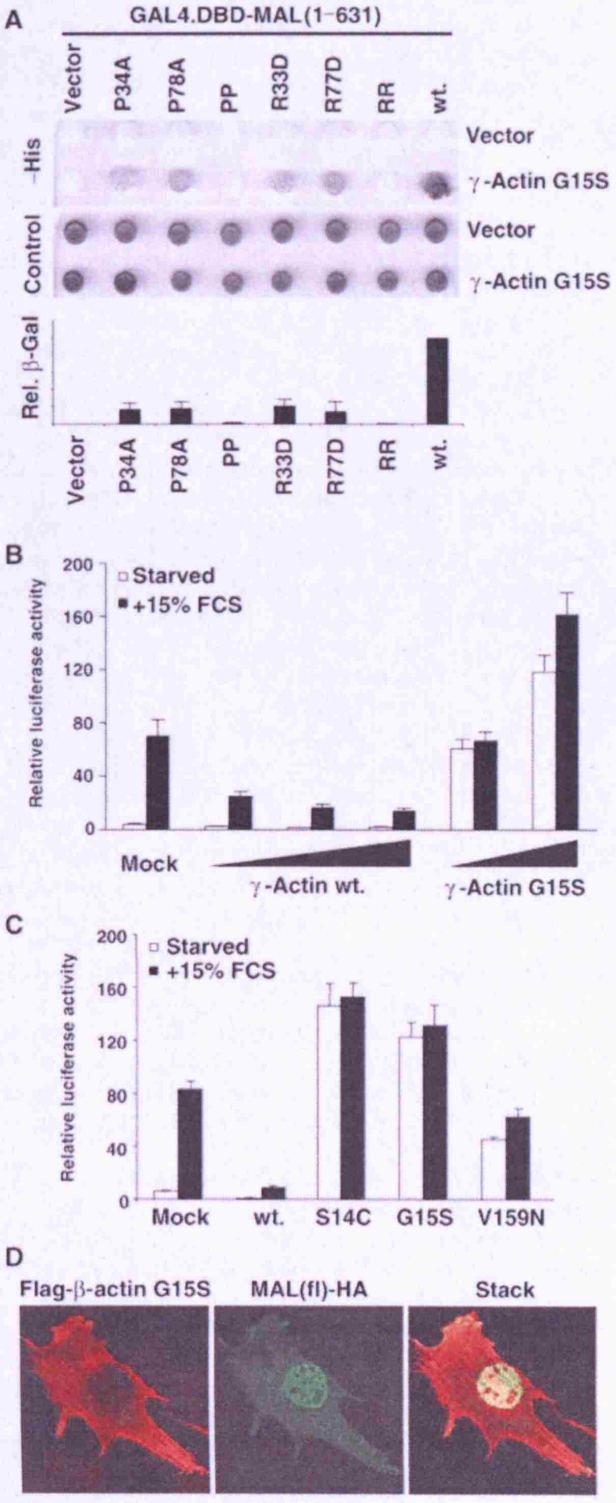

Figure 2 Identification of actin G15S, an activator of MAL and SRF. (**A**) Yeast two-hybrid interactions between γ-actin G15S and MAL(met)(1–631) or mutant derivatives containing point changes in either or both RPEL motifs. Upper panels: *trans*-illuminated images of colony growth on selective (−His) or nonselective (control) medium. Lower histogram: interaction quantification by liquid-culture Gal4-lacZ reporter gene assay (WT γ-actin = 100; error bars: s.e.m.; $n = 3$) (**B**) γ-Actin G15S expression activates SRF. Cells were transfected with SRF reporter 3D.A-Luc (40 ng), together with wild-type γ-actin (100, 250 or 500 ng) or γ-actin G15S (100 or 250 ng), maintained in 0.3% FCS for 40 h and then serum-stimulated where indicated. Data are means of three independent experiments; error bars: s.e.m. (**C**) Reporter activation by β-actin G15S and other β-actin mutants. Cells were transfected with reporter and the indicated β-actin mutants and treated as in (B). (**D**) β-Actin G15S expression induces MAL nuclear accumulation. Cells expressing MAL(fl)-HA (50 ng) and β-actin G15S (500 ng) were processed for immunofluorescence 24 h after transfection. Confocal sections of 0.3 μm thickness show actin G15S (anti-Flag; red) and nuclear accumulation of MAL(fl) (anti-HA; green). The merged picture shows the stack of both actin and MAL sections.

(Geneste *et al*, 2002; Posern *et al*, 2002). Cells expressing wild-type actin exhibit an increase of approximately 40% in both F- and G-actin levels. In this assay, overexpression of actin G15S altered the balance between F- and G-actin in favour of F-actin, as observed previously for actins S14C and V159N (Figure 3A). To corroborate this result, we used detergent extraction and centrifugation to produce F-actin- and G-actin-enriched supernatant and pellet fractions from cells expressing Flag-tagged actin. In this assay, serum stimulation led to increased recovery of wild-type actin in the F-actin fraction (Figure 3B). In contrast, depolymerisation of the cytoskeleton by the actin-binding drugs swinholide A or latrunculin B, or coexpression of C3 transferase or the G-actin-binding protein profilin, caused Flag-actin to accumulate in the G-actin fraction (Figure 3B). Actin G15S was recovered in increased amounts in the F-actin fraction compared to wild-type actin, as were actins S14C and V159N (Figure 3C; Posern *et al*, 2002). Moreover, coexpression of actin G15S and wild-type actin led to an increased recovery of wild-type actin in the F-actin fraction (Figure 3D). These results show that like actins S14C and V159N, actin G15S can copolymerise with wild-type actin to generate F-actin of increased stability.

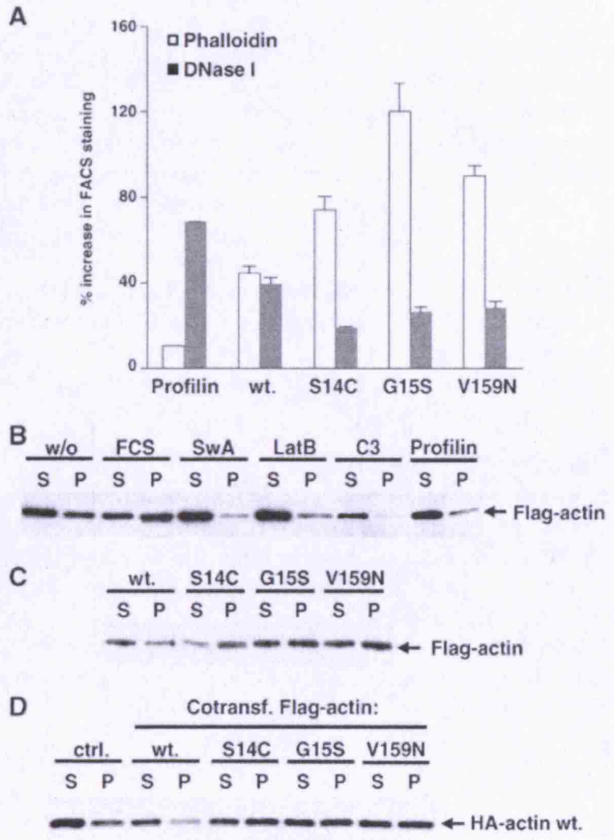

Figure 3 Actin G15S stabilises filament formation. (**A**) Transfected cells expressing the indicated Flag-tagged actins (1 μg) were stained for the Flag epitope and either TRITC-phalloidin (for F-actin) or FITC-DNase I (for G-actin). The FACS was used to quantify mean levels of F- or G-actin in the transfected population relative to those of the untransfected population (error bars: s.e.m.; $n=3$). (**B**) Actin fractionation lysates were prepared from cells expressing wild-type Flag-actin (1 μg) with C3 transferase (50 ng) or profilin (500 ng) coexpression, or treatment with latrunculin B (0.3 μM, 1 h), swinholide A (100 nM, 1 h) or FCS (15%, 10 min) as indicated. Flag-actin in each supernatant (S) and pellet (P) fraction was detected by immunoblotting using anti-Flag antibodies. (**C**) Actin fractionation lysates were prepared from cells expressing the indicated Flag-tagged actin mutants (1 μg) and analysed by anti-Flag immunoblotting as in (B). (**D**) Activating actin mutants copolymerise with and stabilise wild-type F-actin. Actin fractionation lysates were prepared from cells expressing the indicated Flag-tagged actins (1 μg) together with HA-tagged wild-type actin (500 ng), and analysed by anti-HA immunoblot.

Activating actins share altered gelsolin- and profilin-binding properties

To gain insight into the changed conformation of the activating actins, we studied their interaction with different actin-binding proteins, initially focusing on proteins that discriminate between different nucleotide-bound states of the molecule. The C-terminal half of the F-actin severing protein gelsolin, comprising segments 4–6, specifically binds wild-type ADP-bound G-actin (Laham *et al*, 1993). We used the GST-gelsolin(S4–6) fusion protein in pulldown assays with high-speed supernatant extracts of transiently transfected NIH3T3 cells expressing Flag-tagged wild-type or mutant actins. All the activating mutants were recovered inefficiently in comparison to wild-type actin and the nonpolymerisable mutant R62D (Figure 4A, upper); in a control experiment, purified wild-type ADP-actin, but not AMP-PNP-actin, effectively bound GST-gelsolin(S4–6) (Figure 4A, lower). The decreased affinity of the activating actins for GST-gelsolin(S4–6) suggests that their structure does not readily adopt a conformation characteristic of ADP-actin.

We next used the co-immunoprecipitation assay to examine the ability of the mutants to associate with profilin, which favours nucleotide exchange on actin and preferentially binds ATP-actin (see Perelroizen *et al*, 1995; Pollard and Borisy, 2003). Extracts were prepared from cells expressing the Flag-tagged actins, immunoprecipitated using anti-Flag antibodies and recovery of cellular profilin was monitored by immunoblotting. Profilin was recovered in immunoprecipitates of wild-type actin, but not the nonpolymerisable mutant R62D (Figure 4B). In this assay, profilin was more effectively recovered by the activating actin mutants than by the wild-type protein (Figure 4B). Serum stimulation led to a rapid decrease in the recovery of profilin associated with actin (Figure 4B, right).

Taken together, these results suggest that the activating actins cannot enter a conformation readily adopted by ADP-bound wild-type G-actin, and an increased tendency to enter a conformation preferred by ATP-bound wild-type G-actin. In contrast, the nonpolymerising mutant R62D, which retains the ability to inhibit MAL nuclear accumulation, appears to adopt a conformation more characteristic of ADP-bound G-actin.

The activating mutants interact differentially with cofilin and nucleotide

Cofilin binding discriminates in favour of ADP-bound actin (Carlier *et al*, 1997). We therefore also evaluated the ability of the mutant actins to associate with cellular cofilin using the co-immunoprecipitation assay. In contrast to their similar interactions with gelsolin(S4–6) and profilin, however, the activating actins exhibited very different behaviour in this assay: cofilin was efficiently recovered in all the actin immunoprecipitates save that of the activating mutant G15S (Figure 4C).

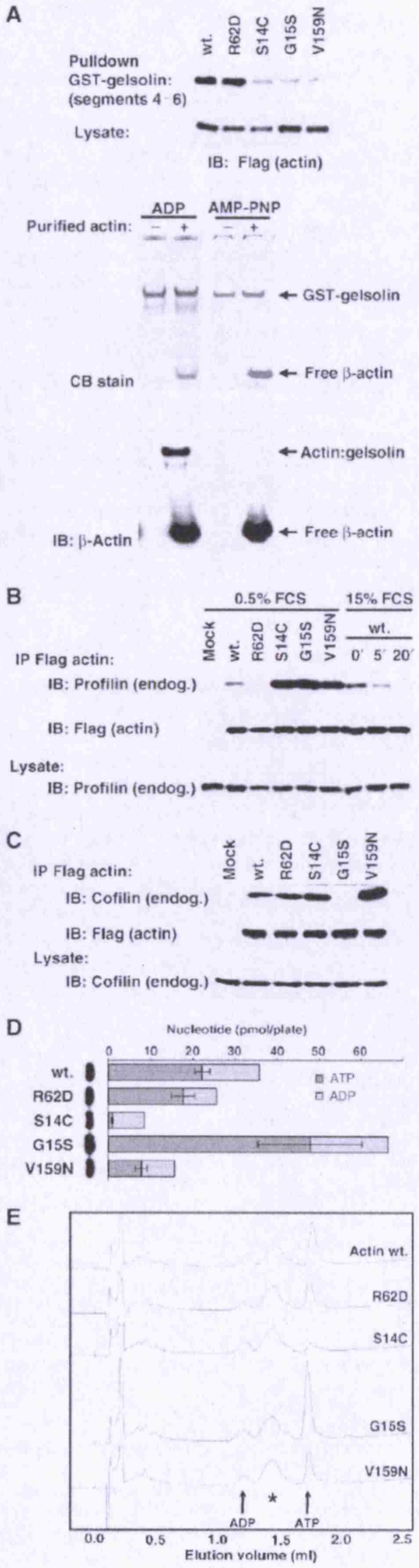

Given that the behaviour of the activating mutants in the gelsolin(S4–6)- and profilin-binding assays suggested that they might adopt an 'ATP-like' conformation more readily than wild-type actin, we next sought to confirm the identity of the nucleotide associated with the different mutants. Each of the actins was recovered from transfected cells by anti-Flag immunoprecipitation (IP) and bound ATP was quantified using a luciferase enzymatic assay (Chen *et al*, 1995; Chen and Rubenstein, 1995; Schuler *et al*, 1999). In this assay, less ATP was recovered with the nonpolymerisable R62D and the activating V159N actin mutants than with wild-type actin, while more ATP was recovered with the activating mutant G15S; in contrast, activating actin S14C was recovered virtually free of ATP (Figure 4D). The relatively high amounts of ADP recovered in these assays may reflect hydrolysis during actin isolation. Essentially identical results were obtained when nucleotide association was evaluated by HPLC assay (Figure 4E; Rosenblatt *et al*, 1995).

Taken together with the results in the preceding section, these data show that although all three activating mutants share a number of properties, they nevertheless can be distinguished biochemically according to their ability to bind nucleotide (S14C defective) and cofilin (G15S defective).

Activating actins also exhibit distinct MAL-binding properties

We next examined the interaction between the activating actins and MAL. Actins were immunoprecipitated from extracts of cells transfected with Flag-tagged actins and recovery of endogenous MAL was assessed by immunoblotting. In this assay, the different activating actins again behaved differently. MAL binding to actin S14C was essentially undetectable; in contrast, actin G15S bound MAL more effectively than wild-type actin (Figure 5A). To increase the sensitivity of the assay, we repeated it, this time overexpressing MAL as well as the actins. Again, MAL binding to actin S14C was undetectable, while actin G15S bound more efficiently than wild-type actin, and V159N less effectively

Figure 4 Activating actin mutants have both shared and distinct properties. (**A**) Activating actins exhibit reduced affinity for the C-terminal half of gelsolin. Upper panel: G-actin supernatants from cells expressing the indicated actins (2 μg) were affinity-precipitated using GST-gelsolin(S4–6), and bound proteins were detected by immunoblotting with anti-Flag antibodies. Lower panels: native gel electrophoresis assay of complex formation between GST-gelsolin(S4–6) and ADP- or AMP-PNP-loaded nonmuscle actin, with detection by Coomassie blue or anti-β-actin immunoblot. (**B**) Interaction of actins with endogenous profilin. Upper panels: Extracts as in (A) were immunoprecipitated with anti-Flag and analysed for profilin (anti-profilin; upper) and actin (anti-Flag; lower). Cells were in 0.5% serum except where stimulated with 15% serum for the indicated times (min). Lower panel: Control immunoblot for profilin in the lysate. (**C**) Interaction of actins with endogenous cofilin. Extracts were prepared and analysed as in (B). (**D**) Nucleotide binding by actin mutants. Actin immunoprecipitates were prepared as in (B), followed by nucleotide determination using the luciferase-based ATP assay. Immunoblot: recovered actin in each sample. Data are mean ± s.e.m. ($n = 4$). (**E**) Nucleotide binding by actin mutants. Actins were prepared as in (D) and nucleotide was identified by Mono-Q anion exchange chromatography. UV absorbance at 254 nm from a representative experiment is shown, with elution volumes for ADP and ATP indicated. The asterisk indicates a nonspecifically recovered component also present in precipitates from mock-transfected cells.

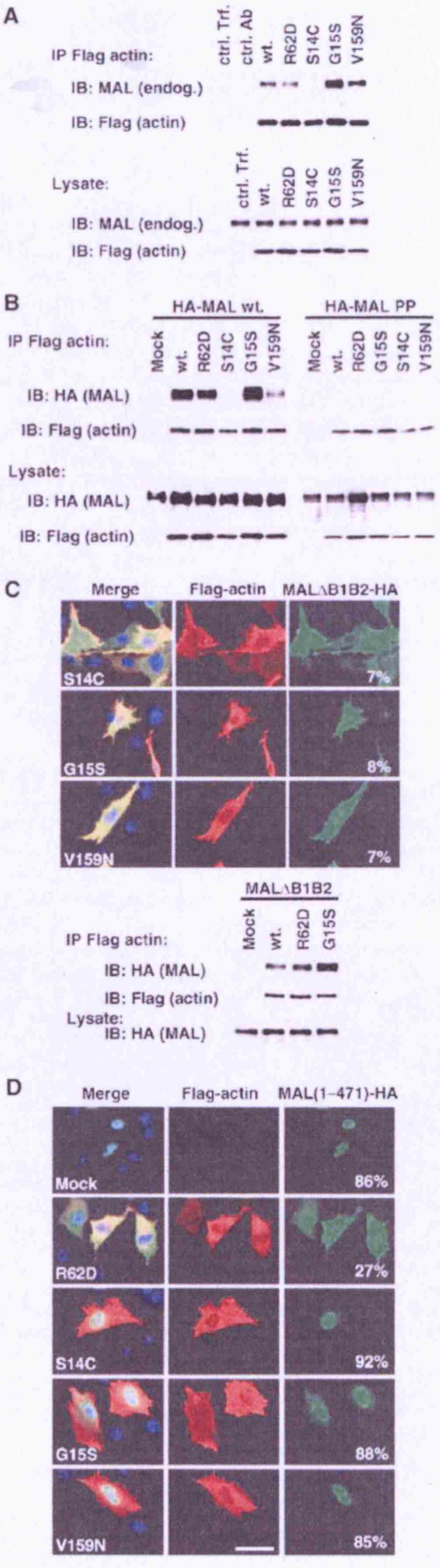

(Figure 5B). Neither wild-type nor mutant actins associated with the MAL mutant PP34/78AA, which carries P→A changes in its RPEL motifs (Figure 5B; Miralles *et al*, 2003). MAL nuclear accumulation in response to serum stimulation is dependent on two basic sequence elements (Miralles *et al*, 2003). MALΔB1ΔB2, which lacks these basic sequences, remained cytoplasmic upon expression of actins S14C, G15S and V159N, indicating that the basic sequences are also required for MAL nuclear accumulation induced by the activating actins (Figure 5C). A control experiment confirmed that MALΔB1ΔB2 nevertheless remains competent to bind wild-type actin as well as the R62D and G15S mutants (Figure 5C).

We previously showed that MAL(1–471), a MAL mutant lacking its C-terminal sequences, which include the dimerisation interface, accumulates in the nucleus under conditions of basal Rho signalling (Miralles *et al*, 2003). Overexpression of nonpolymerisable actin R62D, which binds MAL, is sufficient to relocalise MAL(1–471) to the cytoplasm under these conditions (Figure 5D, top rows). In contrast, none of the activating actins, even actins G15S and V159N, which can interact with MAL, relocalised MAL(1–471) to the cytoplasm (Figure 5D, lower rows). Binding of these actins to MAL is thus incapable of retaining it in the cytoplasm.

MAL activation by actins exhibits differential dependence on actin treadmilling

We previously proposed that activating actin mutants might potentiate SRF activation either because of their inability to bind a putative coactivator (MAL) or because their binding activates it (Posern *et al*, 2002). The different MAL-binding properties of the mutants described above are consistent with the notion that the mutants use different mechanisms to induce MAL nuclear accumulation. To investigate this issue, we tested the dependence of SRF reporter gene activation on basal Rho activity, using C3 transferase coexpression to inactivate endogenous Rho (Hill *et al*, 1995). As previously observed, expression of C3 transferase completely abolished

Figure 5 Interaction of MAL with wild-type and mutant actins. (**A**) Interaction of actins with endogenous MAL from NIH3T3 cells. Upper panels: extracts from cells expressing the indicated Flag-tagged actin mutants (1 μg) were immunoprecipitated with anti-Flag or control antibodies, and analysed for MAL (anti-MAL; upper) and actin (anti-Flag; lower). Lower panels: control immunoblots for MAL (anti-MAL; upper) and actin expression (anti-Flag) in the lysate. ctrl. Trf.: no actin; ctrl. Ab: wild-type actin, anti-HA IP. (**B**) Interaction of actins with overexpressed HA-tagged MAL(met) and HA-MAL(met) PP34/78AA (containing mutated RPEL motifs) (1 μg). Cells were transfected and processed as in (A). Data in lanes 1–3 are from Miralles *et al* (2003). (C) Nuclear accumulation induced by the activating actins requires MAL basic box regions. Upper panels: cells in 0.5% FCS expressing MALΔB1B2-HA (0.1 μg), which lacks the basic regions, and activating actins (1 μg) were fixed and stained for MAL (anti-HA; green), actins (anti-Flag; red) and DNA (Hoechst 33258; blue). Numbers show proportion of cells with predominantly nuclear MAL. Lower panels: control co-immunoprecipitation experiments performed as in (B). (**D**) Overexpression of nonpolymerisable actin R62D, but not the F-actin-stabilising mutants, promotes relocalisation of MAL(met)1–471 to the cytoplasm. Cells expressing HA-tagged MAL(met)1–471 with vector (mock) or Flag-tagged actins were stained and scored as in (C).

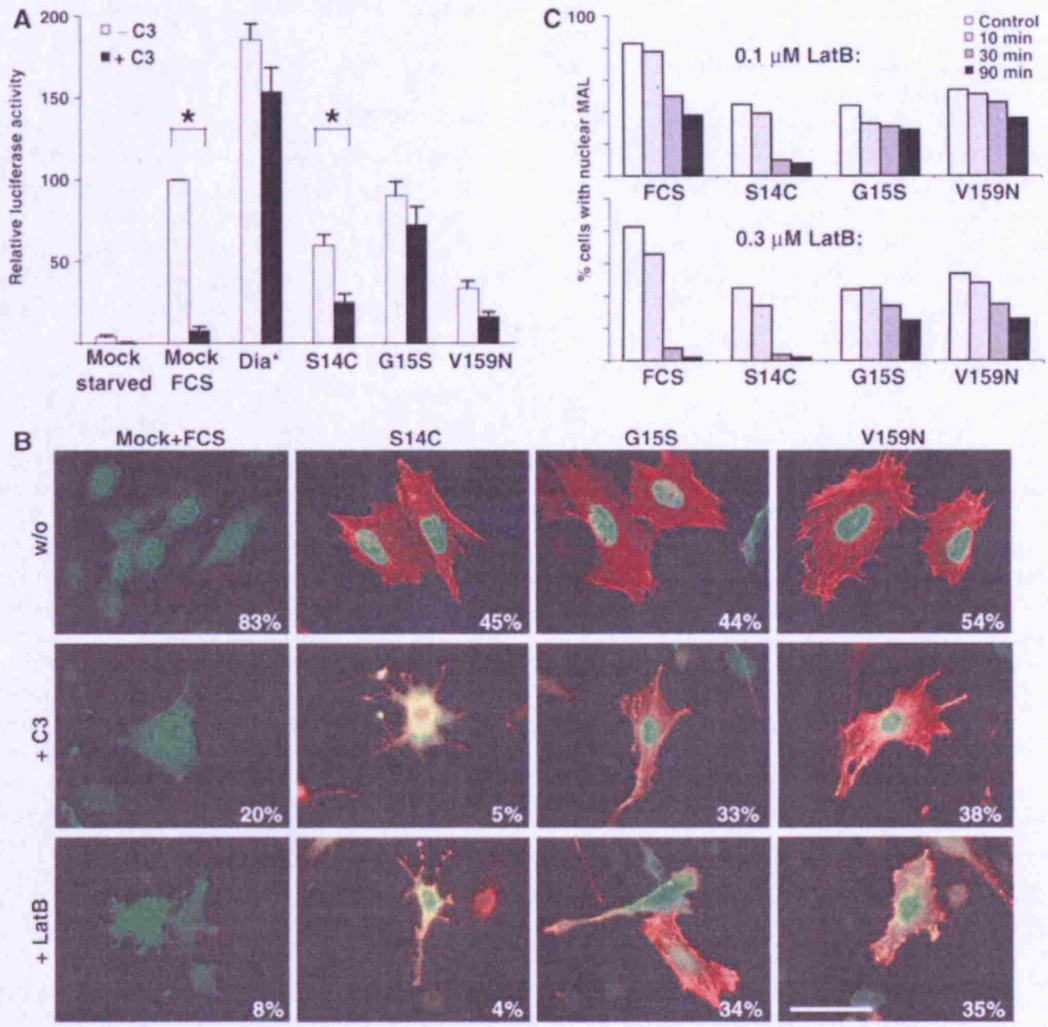

Figure 6 Activating actins exhibit different requirements for actin treadmilling in SRF activation. (**A**) SRF reporter activation by activating actins is differentially sensitive to Rho inactivation. Cells transfected with SRF reporter expressed activating actins (500 ng), C3 transferase (20 ng) and activated mDia (50 ng) as indicated. Data are the mean of four independent experiments (error bars: s.e.m.; asterisks: statistical significance at $P<0.01$, unpaired Student's *t*-test). (**B**) Immunofluorescence analysis of MAL nuclear accumulation induced by serum stimulation or coexpression with activating actin mutants. Cells expressed MAL(met) (50 ng) and activating actins (500 ng), with C3 transferase coexpression (20 ng) or latrunculin B treatment as indicated, and were maintained in 0.5% FCS unless stimulated with 15% FCS for 30 min as indicated. Cells were fixed and stained for MAL (anti-HA; green) and actins (anti-Flag; red). Latrunculin treatment (0.3 μM) was for 30 min prior to staining. Around 100 cells each were analysed and scored for predominantly nuclear MAL staining. (**C**) Kinetics of MAL cytoplasmic reaccumulation. Cells were transfected as in (B) and treated with either 0.1 or 0.3 μM latrunculin B for the times indicated. Data are the mean percentage of predominantly nuclear MAL staining in two independent experiments.

serum-induced activation of the SRF reporter gene, but did not affect its activation by coexpression of an activated mDia mutant (Hill *et al*, 1995; Copeland and Treisman, 2002). Expression of C3 transferase substantially inhibited reporter activation induced by actin S14C expression but had no significant effect upon activation by actin G15S (Figure 6A). In these experiments, the effect of C3 transferase upon activation by actin V159N was of borderline statistical significance, however.

We next tested whether MAL nuclear translocation induced by the activating actins required functional Rho and actin treadmilling. Coexpression of C3 transferase substantially inhibited MAL nuclear accumulation in response to serum stimulation (Figure 6B; Miralles *et al*, 2003). The activating actins induced MAL nuclear accumulation less effectively than serum, with about half of the cell population exhibiting predominantly nuclear fluorescence. Inactivation of Rho by expression of C3 transferase, however, prevented nuclear accumulation of MAL in cells expressing actin S14C, but had little effect on MAL in cells expressing actins V159N and G15S (Figure 6B). To test whether Rho dependence reflected a requirement for actin treadmilling, we used latrunculin B treatment to inhibit actin treadmilling following activation. Although MAL remains in the nucleus for several hours following serum stimulation, treatment with latrunculin B after only 1 h induces its rapid cytoplasmic reaccumulation (Figure 6B and C). In cells expressing actin S14C, nuclear MAL was rapidly redistributed to the cytoplasm following addition of latrunculin B (Figure 6B and C). In contrast, in cells expressing actins G15S and V159N, addition of latrunculin B had little effect on the proportion of cells with nuclear MAL (Figure 6B and C). Expression of C3 transferase or latrunculin B treatment had a more pronounced effect on F-actin staining in cells expressing actin S14C than the other

activating actins (Figure 6B); this may reflect both differential effects of the mutants on F-actin stability and the fact that chronic SRF activation itself appears to increase cellular F-actin level (Schratt *et al*, 2002).

Taken together with the biochemical data, these results show that while the three activating actins all stabilise F-actin, they must use distinct mechanisms to induce MAL nuclear accumulation. The behaviour of actin S14C is consistent with a model in which MAL nuclear accumulation results from replacement of the cytoplasmic G-actin pool by a mutant form incompetent to bind MAL, while that of G15S is consistent with a model in which binding of the actin itself directly promotes nuclear MAL accumulation independent of operation of the actin treadmilling cycle (Figure 7; see Discussion).

A

Properties	S14C	G15S	V159N
F-actin stabilisation	Enhanced	Enhanced	Enhanced
Gelsolin binding	Low	Low	Low
Profilin binding	High	High	High
MAL binding	Low	High	Reduced
Cofilin binding	High	Low	High
Nucleotide binding	Low	Normal	Normal

B

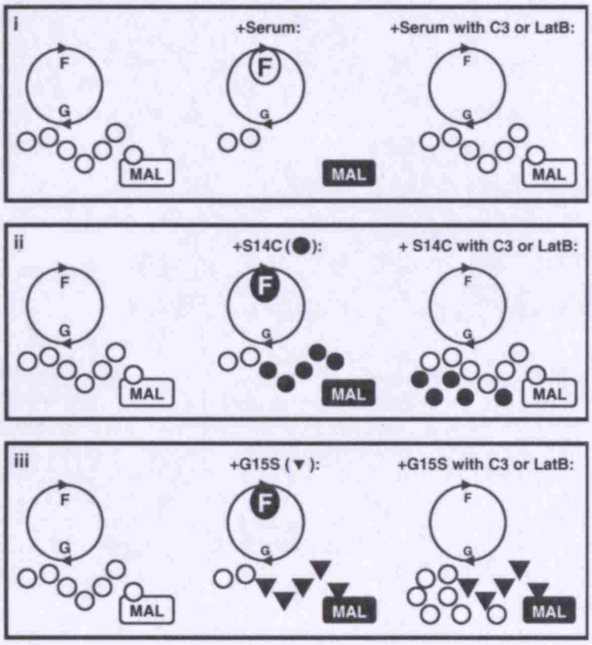

Figure 7 (**A**) Summary of mutant actin properties. Biochemical characteristics of the indicated point mutants are compared to those of the wild-type protein. (**B**) Models for activation of MAL by mutant actins. (i) Normal cells in low serum exhibit a basal actin treadmilling (circle; G: G-actin; F: F-actin). MAL is retained in the cytoplasm (open box) by interaction with G-actin (white circles), which somehow inhibits its nuclear accumulation. Upon serum stimulation, the G-actin pool is depleted and MAL released for nuclear import (black box); blockade of treadmilling by latrunculin B or Rho inactivation prevents this, inhibiting MAL release (open box). (ii) Actin S14C (black circles) stabilises F-actin; its overexpression increases F-actin but does not deplete the G-actin pool. However, actin S14C itself does not effectively bind MAL, which is therefore released for nuclear accumulation (black box). Upon blockade of treadmilling, wild-type G-actin reaccumulates, and MAL is again inhibited (open box). (iii) Actin G15S (black triangles) stabilises F-actin; its overexpression increases F-actin but does not deplete the G-actin pool. Binding of actin G15S to MAL directly promotes MAL nuclear accumulation (black box). MAL therefore remains active upon inhibition of actin treadmilling.

Discussion

We have investigated the functional and physical interaction of wild-type and mutant actins with the SRF coactivator MAL. MAL is a member of two protein families that contain the so-called RPEL motif (interpro IPR004018; pfam PF02755). Integrity of the RPEL motif is required for association with β-actin *in vivo*, and its disruption results in MAL nuclear accumulation (Miralles *et al*, 2003; S Ellis, unpublished data). We find that actin binds directly to MAL through its RPEL motifs *in vitro*, and that this interaction is compatible with binding either to ATP (AMP-PNP) or ADP. The affinity of the actin–MAL interaction (apparent K_d 24 nM) is comparable to gelsolin. This, and the fact that MAL and profilin bind to actin mutually exclusively, is consistent with a model in which MAL competes effectively with profilin for free G-actin. The nonpolymerising actin mutant actin R62D, which nevertheless retains the ability to regulate MAL activity (Posern *et al*, 2002; Miralles *et al*, 2003), has similar MAL-binding properties to the wild-type protein and our studies indicate that it may adopt a structure characteristic of ADP-bound wild-type G-actin.

We have identified a third actin mutant whose overexpression activates rather than inhibits MAL nuclear accumulation and SRF activation. This mutant, actin G15S, shares a number of properties with two other 'activating' actins, actins V159N and S14C, including the ability to stabilise F-actin (Posern *et al*, 2002). The three mutants nevertheless exhibit distinct behaviour in several biochemical assays, including binding to nucleotide, cofilin and MAL (Figure 7A). Our functional studies suggest that these activating mutants use different mechanisms to promote MAL nuclear accumulation, and that interaction of actin G15S with MAL may directly promote MAL nuclear accumulation.

MAL is at least in part regulated by a G-actin titration mechanism in which binding of MAL to G-actin somehow inhibits its nuclear accumulation, perhaps by occluding its nuclear import signals (Figure 7B, i; Miralles *et al*, 2003). How then might expression of F-actin-stabilising actin mutants lead to MAL nuclear accumulation and SRF activation? We previously proposed two nonmutually exclusive mechanisms by which expression of such mutants might lead to activation of SRF regulatory cofactors (MAL at that time remained uncharacterised; Posern *et al*, 2002). One class of mutants might exhibit reduced affinity for MAL but stabilise F-actin. Although expression of such mutants might leave G-actin level substantially unaffected, it would lead to dilution of the wild-type G-actin pool with mutant actin incompetent to interact with MAL, thereby releasing MAL for nuclear import (Figure 7B, ii). Activation by these mutants would require operation of the actin treadmilling cycle to equilibrate with the cellular actin pool, so their ability to drive MAL accumulation and SRF activation would be expected to be heavily dependent on operation of the actin treadmilling cycle. An alternative and more novel type of actin mutation might alter the way in which actin interacts with MAL, such that even when these mutants bind MAL, the complex is somehow actively targeted for nuclear import (Figure 7B, iii). (Note that mutations of this type need not necessarily result in F-actin stabilisation.) Such mutants might mimic the

function of a subpopulation of wild-type actin, which is normally required for MAL nuclear accumulation. Their ability to promote MAL nuclear accumulation directly would obviate any requirement for operation of the actin treadmilling cycle in SRF activation.

The activating actin mutants described here apparently fall into both of the above classes. Actin S14C exhibits substantially reduced interaction with MAL, and actin S14C-induced MAL nuclear accumulation and SRF activation are indeed substantially dependent on actin treadmilling, consistent with the titration model. In contrast, actin G15S retains high-affinity interaction with MAL, and its ability to promote MAL nuclear accumulation and SRF activation is largely independent of actin treadmilling, consistent with the 'direct activation' model (Figure 7B, iii). Actin V159N is also likely to be of this type, even though it exhibits weakened interaction with MAL, since it promotes MAL nuclear accumulation substantially independently of actin treadmilling. We note that although the behaviour of actin S14C is consistent with the titration model, we cannot exclude the possibility that a direct-acting subpopulation of endogenous wild-type actin also remains required for MAL nuclear accumulation upon overexpression of this mutant.

Further experiments are necessary to substantiate the direct activation hypothesis. As yet we have not detected altered interactions between MAL and actin G15S in limited proteolysis experiments (G Posern, unpublished). Moreover, actin G15S does not accumulate in the nucleus, even in the presence of overexpressed MAL, suggesting that although this actin–MAL complex appears targeted for nuclear import, its actin component must either be stripped off during import or immediately re-exported from the nucleus upon MAL entry. Biophysical approaches will allow the dynamics of the interaction between actin and MAL to be studied in living cells.

Our data suggest that mammalian β-actin G15S generates F-actin of increased stability, as previously proposed for yeast actin G15S on the basis that diploid cells expressing both wild-type and G15S actin exhibit increased resistance to latrunculin A (Belmont *et al*, 1999b). The mechanism by which such stabilisation might arise remains obscure, however. Previous studies have shown that the yeast actin V159N generates F-actin that retains structural characteristics of the ADP + P_i F-actin structure even after departure of the hydrolysed phosphate (Belmont *et al*, 1999a). Residues S14 and G15 make intimate contacts with the ATP γ- and β-phosphates, and form part of a loop highly conserved throughout the actin superfamily (Kabsch and Holmes, 1995). ATP hydrolysis may allow S14 to switch to its preferred rotamer, allowing establishment of new hydrogen bonds with R183 in subdomain 4, and thereby transmit conformational changes to distant parts of the molecule (Otterbein *et al*, 2001; Graceffa and Dominguez, 2003). We previously suggested that replacement of serine 14 by cysteine might inhibit such changes (Posern *et al*, 2002). The G15S mutation might also stabilise an ATP-bound actin conformation perhaps through the introduction of new hydrogen bonds between G15S and either R183 or D157 (N McDonald, personal communication), or by constraining the mobility of the conserved loop α-carbon chain. Structural studies might resolve these questions.

The three activating actins share the ability to stabilise F-actin and activate SRF; biochemically, they possess both shared and distinct properties (Figure 7A). Studies of the corresponding yeast mutants also suggest that these mutations are not functionally identical, since the G15S and S14C mutations are recessive lethal, while the V159N mutation remains viable (Chen and Rubenstein, 1995; Belmont and Drubin, 1998; Belmont *et al*, 1999b). Under G-actin conditions, all the mutants share a reduced ability to interact with gelsolin segments S4–S6, and an increased affinity for profilin. These observations suggest that the mutants less readily adopt conformations exclusively available to wild-type ADP-actin, and perhaps more readily enter a conformation accessible to wild-type ATP-actin. Nevertheless, under G-actin conditions, the three mutants exhibit differential affinity for MAL and for cofilin. Unlike actins G15S and V159N, actin S14C exhibits greatly reduced affinity for ATP, consistent with previous studies of the yeast actins S14C and S14A (Chen *et al*, 1995; Chen and Rubenstein, 1995; Schuler *et al*, 1999).

What is the relevance of the activating mutations to the cellular physiology of MAL activation? An exciting possibility is that the actin G15S (and possibly V159N) mutation mimics a directly activating conformation that is adopted by the wild-type protein during normal MAL regulation, either alone or through its association with other proteins. For example, the actin G15S mutation might in some ways be considered equivalent to activating mutations in regulatory GTPases, which lock the proteins in the activated state by inhibiting GTP hydrolysis (Bourne *et al*, 1991). Actin-related proteins (Arps) are involved in protein complexes controlling numerous cytoplasmic and nuclear processes. Moreover, ATP hydrolysis by Arps has been associated with changes in functional state, such as destabilisation of the branching interaction of the arp2/3 complex with F-actin following ATP hydrolysis on arp2 (Le Clainche *et al*, 2003). It might be interesting to test the effect of the G15S mutation on the activity of actin-related proteins.

Materials and methods

Plasmids and proteins

Reporters, and expression plasmids for actins, Rho effectors, C3, profilin and cofilin were described previously (Sotiropoulos *et al*, 1999; Copeland and Treisman, 2002; Miralles *et al*, 2003). MAL(met) residues 1–631 in pGBT9 were used to screen an NIH3T3 cDNA library in pACT2 (Clontech no. ML4009AH) in *Saccharomyces cerevisiae* strain Y190 (Clontech), which allows selection on medium with 15–30 mM 3-aminotriazole and quantification of interactions by liquid culture β-galactosidase assay. Point mutant derivatives of the MAL N-terminal RPEL motifs are as specified in the figure legends. GST-MAL(met)(1–171) and its RPEL mutant derivatives were expressed using pET41. MAL(fl)2–261 (including all three RPEL repeats) and gelsolin(S4–6) (Way *et al*, 1989) were cleaved from appropriate GST fusions and purified by standard techniques.

Transfections and reporter assays

Transient transfections of NIH3T3 cells were carried out using Lipofectamine (Invitrogen) and reporter assays performed as described (Posern *et al*, 2002). Amounts of expression plasmid used are indicated in the figure legends. For co-immunoprecipitation assays, cells were transfected in 10 cm plates with 1 μg of each MAL and actin plasmid; cells were starved for only 24 h prior to lysis in RIPA buffer. For immunofluorescence assays, cells were seeded on coverslips in six-well plates and starved for 24 h following transfection with 50 ng MAL and 0.5 μg actin constructs.

Actin polymerisation assay

Rabbit skeletal α-actin monomers (2.5 μM, 20% pyrene-labelled) were incubated with test protein for 30 min in G buffer (2 mM

Tris–HCl pH 8, 0.3 mM $MgCl_2$, 0.2 mM ATP, 0.2 mM EGTA, 0.2 mM DTT). Critical concentration was estimated as 0.27 μM. For gelsolin measurements, G buffer contained 0.2 mM $CaCl_2$ instead of $MgCl_2$ and EGTA. Actin polymerisation was initiated by addition of 1/20 volume of initiation buffer at room temperature (2 M NaCl, 60 mM $MgCl_2$, 10 mM ATP); end-point pyrene fluorescence was measured 2 h later (Hertzog *et al*, 2002).

Immunoprecipitations and affinity precipitations

For co-immunoprecipitation assays, extracts of half a 10 cm plate were precipitated for 2 h at 4 C in IP buffer (20 mM Tris pH 8.0, 150 mM NaCl, 1 mM EDTA, 5% glycerol, 1% Triton X-100, protease inhibitors) with M2 anti-Flag or anti-HA agarose (Sigma), followed by extensive washing. G-actin supernatant fractions for GST pulldowns, profilin-actin, cofilin-actin and nucleotide determinations were prepared by syringing cells from one 10 cm plate in 500 μl EDTA-free 10 mM Tris pH 8, 50 mM NaCl, 0.2 mM $CaCl_2$ and 0.2 mM DTT containing protease inhibitors (Roche) followed by centrifugation at 436 000 *g*. Precipitations (200 μl) used 20 μl GST-gelsolin(S4–6) beads, or antibodies in the same buffer at 4 C with three washes. Purified biotinylated nonmuscle actin (1 μg, Cytoskeleton Inc.) was affinity-precipitated using 5 μg GST-MAL precoupled to glutathione-agarose beads in 500 μl 10 mM Tris pH 8, 100 mM NaCl, 0.2 mM $CaCl_2$, 0.2 mM DTT, 5% glycerol and 0.5% Triton X-100 supplemented with 1.6 mg/ml dialysed *Escherichia coli* protein lysate (Posern *et al*, 1998). Binding was for 2 h at 4 C, followed by four washes. Following PAGE and transfer to PVDF membrane, biotin-actin was detected by streptavidin–peroxidase conjugate (Sigma). GST-MAL-binding proteins were separated by 6–16% gradient SDS–PAGE and detected by silver staining. Immunoblotting was by standard techniques using anti-Flag peroxidase conjugate (M2, Sigma), anti-HA peroxidase conjugate (3F10, Roche), anti-β-actin (AC15, Sigma), anti-MAL (Miralles *et al*, 2003), anti-cofilin (Cytoskeleton Inc.) and anti-profilin (Immunoglobe, Wuerzburg, Germany).

Native gels

To generate ADP-actin, nonmuscle actin (100 μg and 99% pure, Cytoskeleton Inc.) in G buffer (5 mM Tris pH 8.0, 0.2 mM $CaCl_2$, 0.2 mM DTT) was treated with hexokinase-agarose (Sigma), 5 mM glucose and 0.5 mM ADP for 2 h at 4 C (Ojala *et al*, 2002). AMP-PNP-actin was made by incubation of 100 μg actin with 1.2 mM AMP-PNP for 2 h in G buffer. Following centrifugation at 200 000 *g* for 5 min, the supernatant G-actin fraction was mixed with equimolar amounts of GST fusions in 5 mM Tris pH 8, 0.2 mM $CaCl_2$, 0.2 mM DTT and 0.2 mM ADP or AMP-PNP for 30 min on ice. Samples were loaded with 10% glycerol on prerun 6% native gels in 25 mM Tris, 194 mM glycine, 0.1 mM $CaCl_2$, 0.5 mM DTT, pH 8.0, containing either 0.2 mM ADP or 0.02 mM AMP-PNP. Protein detection was by Coomassie blue staining or immunoblotting.

Nucleotide determination

For nucleotide analysis by luciferase assay (Chen *et al*, 1995; Chen and Rubenstein, 1995; Schuler *et al*, 1999), Flag-actin immunoprecipitate from a 10 cm plate was hydrolysed in 6% perchloric acid (100 μl) and neutralised with 5 M K_2CO_3 (14 μl). The luciferase enzymatic ATP assay (ApoGlow, Cambrex Biosciences) was performed according to the manufacturer's instructions, with ADP determination by conversion to ATP prior to measurement and calibration with nucleotide standards. For nucleotide determination by HPLC (Rosenblatt *et al*, 1995), precipitates were boiled in 130 μl 10 mM Tris pH 7.4 and 8 M urea for 5 min, filtered through 10 kDa microspin columns (Amicon Inc.) and resolved on a Mono-Q 1.6 column (0.1 ml bed) eluted with 100–500 mM NH_4HCO_3 in HPLC-grade water at 6 C (flow rate 0.1 ml/min) on a Pharmacia SMART apparatus. Quantification of the chromatographs was hampered by low sensitivity of ADP detection, but gave essentially the same results as the luciferase-based assay.

FACS analysis, actin fractionation and immunofluorescence

FACS quantification of F-actin or G-actin content, actin fractionation lysates, and immunofluorescence were as described (Geneste *et al*, 2002; Posern *et al*, 2002). Micrographs were taken either by a conventional Zeiss Axioplan II microscope or a Zeiss LSM 510 confocal laser scanning microscope using a Plan-Neofluar ×63 objective. For quantification, 80–120 cells were assessed under each condition for predominantly nuclear MAL staining.

Supplementary data

Supplementary data are available at *The EMBO Journal* Online.

Acknowledgements

We thank members of the laboratory, Michael Way and Caroline Hill for helpful discussions and/or comments on the manuscript. We thank Derek Davies for FACS services and Graham Clark for assistance with F-actin quantification and ATP determinations. GP, FM and SG were supported by fellowships from EMBO, EU and Boehringer Ingelheim Fonds, respectively. This work was funded by Cancer Research UK.

References

Belmont LD, Drubin DG (1998) The yeast V159N actin mutant reveals roles for actin dynamics *in vivo*. *J Cell Biol* **142:** 1289–1299

Belmont LD, Orlova A, Drubin DG, Egelman EH (1999a) A change in actin conformation associated with filament instability after Pi release. *Proc Natl Acad Sci USA* **96:** 29–34

Belmont LD, Patterson GM, Drubin DG (1999b) New actin mutants allow further characterization of the nucleotide binding cleft and drug binding sites. *J Cell Sci* **112:** 1325–1336

Bettinger BT, Gilbert DM, Amberg DC (2004) Actin up in the nucleus. *Nat Rev Mol Cell Biol* **5:** 410–415

Bourne HR, Sanders DA, McCormick F (1991) The GTPase superfamily: conserved structure and molecular mechanism. *Nature* **349:** 117–127

Carlier MF, Laurent V, Santolini J, Melki R, Didry D, Xia GX, Hong Y, Chua NH, Pantaloni D (1997) Actin depolymerizing factor (ADF/cofilin) enhances the rate of filament turnover: implication in actin-based motility. *J Cell Biol* **136:** 1307–1322

Cen B, Selvaraj A, Burgess RC, Hitzler JK, Ma Z, Morris SW, Prywes R (2003) Megakaryoblastic leukemia 1, a potent transcriptional coactivator for serum response factor (SRF), is required for serum induction of SRF target genes. *Mol Cell Biol* **23:** 6597–6608

Chen X, Peng J, Pedram M, Swenson CA, Rubenstein PA (1995) The effect of the S14A mutation on the conformation and thermostability of *Saccharomyces cerevisiae* G-actin and its interaction with adenine nucleotides. *J Biol Chem* **270:** 11415–11423

Chen X, Rubenstein PA (1995) A mutation in an ATP-binding loop of *Saccharomyces cerevisiae* actin (S14A) causes a temperature-sensitive phenotype *in vivo* and *in vitro*. *J Biol Chem* **270:** 11406–11414

Copeland J, Treisman R (2002) The Diaphanous-Related Formin mDia1 controls Serum Response Factor (SRF) activity through its effects on actin polymerisation. *Mol Biol Cell* **13:** 4088–4099

Du KL, Chen M, Li J, Lepore JJ, Mericko P, Parmacek MS (2004) Megakaryoblastic leukemia factor-1 (MKL1) transduces cytoskeletal signals and induces smooth muscle cell differentiation from undifferentiated embryonic stem cells. *J Biol Chem* **17:** 17

Geneste O, Copeland JW, Treisman R (2002) LIM kinase and Diaphanous cooperate to regulate serum response factor and actin dynamics. *J Cell Biol* **157:** 831–838

Graceffa P, Dominguez R (2003) Crystal structure of monomeric actin in the ATP state. Structural basis of nucleotide-dependent actin dynamics. *J Biol Chem* **278:** 34172–34180, Epub 32003 Jun 34117

Hertzog M, Yarmola EG, Didry D, Bubb MR, Carlier MF (2002) Control of actin dynamics by proteins made of beta-thymosin repeats: the actobindin family. *J Biol Chem* **277:** 14786–14792

Hill CS, Wynne JK, Treisman RH (1995) The Rho family GTPases RhoA, Rac1 and CDC42hs regulate transcriptional activation by SRF. *Cell* **81:** 1159–1170

Kabsch W, Holmes KC (1995) The actin fold. *FASEB J* **9:** 167–174

Laham LE, Lamb JA, Allen PG, Janmey PA (1993) Selective binding of gelsolin to actin monomers containing ADP. *J Biol Chem* **268:** 14202–14207

Le Clainche C, Pantaloni D, Carlier MF (2003) ATP hydrolysis on actin-related protein 2/3 complex causes debranching of dendritic actin arrays. *Proc Natl Acad Sci USA* **100:** 6337–6342

Lyubimova A, Bershadsky AD, Ben-Ze'ev A (1999) Autoregulation of actin synthesis requires the 3′-UTR of actin mRNA and protects cells from actin overproduction. *J Cell Biochem* **76:** 1–12

Miralles F, Posern G, Zaromytidou A-I, Treisman R (2003) Actin dynamics control SRF activity by regulation of its coactivator MAL. *Cell* **113:** 329–342

Murai K, Treisman R (2002) Interaction of Serum Response Factor (SRF) with the Elk-1 B-Box inhibits RhoA–actin signalling to SRF and potentiates transcriptional activation by Elk-1. *Mol Cell Biol* **22:** 7083–7092

Ojala PJ, Paavilainen VO, Vartiainen MK, Tuma R, Weeds AG, Lappalainen P (2002) The two ADF-H domains of twinfilin play functionally distinct roles in interactions with actin monomers. *Mol Biol Cell* **13:** 3811–3821

Olave IA, Reck-Peterson SL, Crabtree GR (2002) Nuclear actin and actin-related proteins in chromatin remodeling. *Annu Rev Biochem* **71:** 755–781

Otterbein LR, Graceffa P, Dominguez R (2001) The crystal structure of uncomplexed actin in the ADP state. *Science* **293:** 708–711

Perelroizen I, Carlier MF, Pantaloni D (1995) Binding of divalent cation and nucleotide to G-actin in the presence of profilin. *J Biol Chem* **270:** 1501–1508

Pollard TD, Borisy GG (2003) Cellular motility driven by assembly and disassembly of actin filaments. *Cell* **112:** 453–465

Posern G, Sotiropoulos A, Treisman R (2002) Mutant actins reveal a role for unpolymerised actin in control of transcription by Serum Response Factor. *Mol Biol Cell* **13:** 4167–4178

Posern G, Zheng J, Knudsen BS, Kardinal C, Muller KB, Voss J, Shishido T, Cowburn D, Cheng G, Wang B, Kruh GD, Burrell SK, Jacobson CA, Lenz DM, Zamborelli TJ, Adermann K, Hanafusa H, Feller SM (1998) Development of highly selective SH3 binding peptides for Crk and CRKL which disrupt Crk-complexes with DOCK180, SoS and C3G. *Oncogene* **16:** 1903–1912

Rosenblatt J, Peluso P, Mitchison TJ (1995) The bulk of unpolymerized actin in *Xenopus* egg extracts is ATP-bound. *Mol Biol Cell* **6:** 227–236

Schratt G, Philippar U, Berger J, Schwarz H, Heidenreich O, Nordheim A (2002) Serum response factor is crucial for actin cytoskeletal organization and focal adhesion assembly in embryonic stem cells. *J Cell Biol* **156:** 737–750

Schuler H, Korenbaum E, Schutt CE, Lindberg U, Karlsson R (1999) Mutational analysis of Ser14 and Asp157 in the nucleotide-binding site of beta-actin. *Eur J Biochem* **265:** 210–220

Sotiropoulos A, Gineitis D, Copeland J, Treisman R (1999) Signal-regulated activation of serum response factor is mediated by changes in actin dynamics. *Cell* **98:** 159–169

Wang Z, Wang DZ, Hockemeyer D, McAnally J, Nordheim A, Olson EN (2004) Myocardin and ternary complex factors compete for SRF to control smooth muscle gene expression. *Nature* **428:** 185–189

Way M, Gooch J, Pope B, Weeds AG (1989) Expression of human plasma gelsolin in *Escherichia coli* and dissection of actin binding sites by segmental deletion mutagenesis. *J Cell Biol* **109:** 593–605

Nuclear Actin Regulates Dynamic Subcellular Localization and Activity of the SRF Cofactor MAL

Maria K. Vartiainen,[1]* Sebastian Guettler,[1]* Banafshe Larijani,[2] Richard Treisman[1]†

Actin, which is best known as a cytoskeletal component, also participates in the control of gene expression. We report a function of nuclear actin in the regulation of MAL, a coactivator of the transcription factor serum response factor (SRF). MAL, which binds monomeric actin, is cytoplasmic in many cells but accumulates in the nucleus upon serum-induced actin polymerization. MAL rapidly shuttles between cytoplasm and nucleus in unstimulated cells. Serum stimulation effectively blocks MAL nuclear export, which requires MAL-actin interaction. Nuclear MAL binds SRF target genes but remains inactive unless actin binding is disrupted. Fluorescence resonance energy transfer analysis demonstrates that the MAL-actin interaction responds to extracellular signals. Serum-induced signaling is thus communicated to nuclear actin to control a transcriptional regulator.

Small guanosine 5′-triphosphate (GTP)–binding proteins of the Rho family control the assembly of the actin cytoskeleton in response to extracellular signals. Activation of Rho leads to the accumulation of filamentous actin (F-actin) through both filament stabilization and de novo polymerization with concomitant depletion of cellular levels of monomeric actin (G-actin). In fibroblasts, Rho signaling regulates the subcellular localization and/or activity of MAL, a G-actin–binding SRF coactivator (*1*–*3*). Experiments with actin-binding drugs or actin overexpression have suggested that MAL activity responds to G-actin concentrations (*4*–*6*). Actin-binding drugs have distinct effects on MAL. Serum-induced nuclear accumulation of MAL and SRF activity is inhibited by latrunculin B (LatB), whereas drugs such as cytochalasin D (CD), swinholide A (SwA), and jasplakinolide induce MAL nuclear accumulation and SRF activation in the absence of signals (*1*, *4*). CD and SwA also disrupt MAL-actin interaction in immunoprecipitation and protein-affinity precipitation assays (*1*, *6*), but the role of actin binding in MAL regulation has remained unclear.

We first tested whether interaction with actin retains MAL in the cytoplasm or controls its continuous nucleocytoplasmic shuttling. In unstimulated cells, inactivation of the exportin Crm1 by its specific inhibitory drug leptomycin B (LMB) induced nuclear accumulation of MAL or MAL–green fluorescent protein (GFP), and this required the B2 region of MAL, a putative nuclear import signal (Fig. 1A and fig. S1). This shows that MAL continuously transits through the nucleus and allows investigation of the signaling requirements for its nuclear import in the absence of export. LMB-induced nuclear accumulation of MAL, but not control proteins, was inhibited by the G-actin–sequestering drug LatB and coexpression of C3 transferase, which irreversibly inactivates Rho, wild-type actin, and the nonpolymerizable actin Arg^{62}→Asp^{62} (R62D) mutant (*5*, *7*) (Fig. 1B and fig. S2). Thus, Rho and actin signaling control MAL nuclear import.

LMB-induced MAL-GFP nuclear accumulation was rapid, being effectively complete within 5 min (Fig. 1C and fig. S3) and indicating that basal MAL nuclear export rates must be very high to maintain its cytoplasmic localization (see below). Even the maximum rate of serum-induced MAL-GFP nuclear accumulation was less than this basal import rate, suggesting that increased nuclear import is not the major mechanism of MAL relocalization (Fig. 1C). CD and jasplakinolide, which activate SRF (*4*), induced MAL-GFP nuclear accumulation at a rate comparable to that of LMB (Fig. 1C and fig. S3).

To analyze export directly, we fused MAL to photoactivatable GFP (PAGFP) (*8*, *9*). Fluorescence was activated in the nucleus by focal-plane-restricted multiphoton excitation (*10*), and its subsequent decay measured (Fig. 2A and fig. S4). In resting cells, export of MAL-PAGFP was extremely rapid, with an apparent initial rate of 2.90% s^{-1} (probably an underestimate because the 10-s excitation period is comparable to the decay of nuclear fluorescence), and LMB-sensitive. Export was dramatically reduced after serum stimulation (0.48% s^{-1}) and almost completely inhibited by drugs that induce MAL nuclear accumulation and SRF activation (*1*, *4*), including CD, SwA, and jasplakinolide. MAL-GFP remained nuclear for several hours after serum stimulation; this reflects continued signaling, because MAL reaccumulated in the cytoplasm upon LatB treatment or after serum removal, with an initial rate comparable to that in serum-stimulated cells (Fig. 2B and fig. S5). Thus, nuclear export rather than import represents the major regulatory step in serum-induced nuclear accumulation of MAL.

We next studied the interaction between recombinant MAL and purified actin. Gel filtration resolved a complex with a relative molecular mass of 252,000 and an apparent stoichiometry of 1:3 (Fig. 2C and figs. S6 and S7). Complex formation was insensitive to LatB

[1]Transcription Laboratory, Cancer Research UK, London Research Institute, Lincoln's Inn Fields Laboratories, 44 Lincoln's Inn Fields, London WC2A 3PX, UK. [2]Cell Biophysics Laboratory, Cancer Research UK, London Research Institute, Lincoln's Inn Fields Laboratories, 44 Lincoln's Inn Fields, London WC2A 3PX, UK.

*These authors contributed equally to this work.
†To whom correspondence should be addressed. E-mail: Richard.Treisman@cancer.org.uk

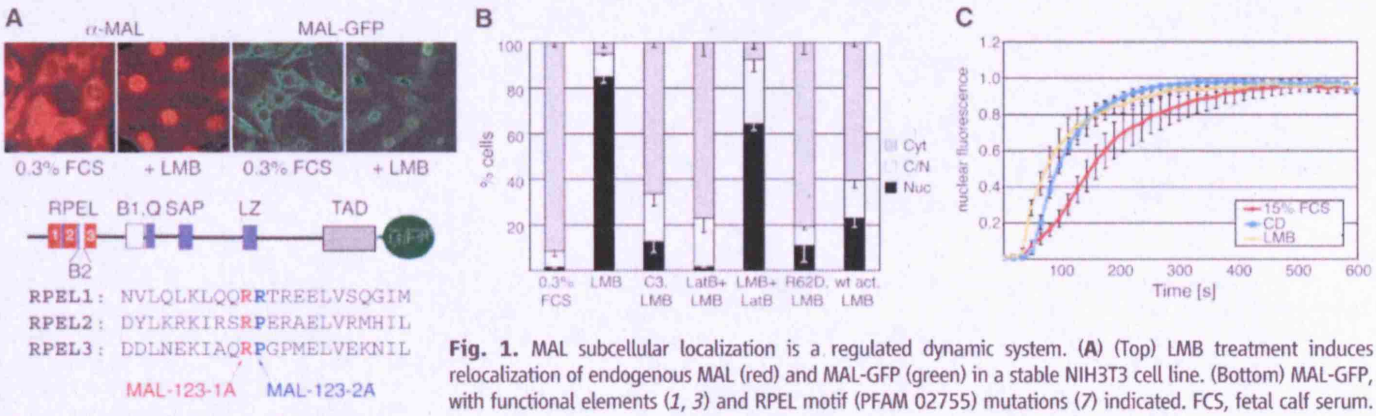

Fig. 1. MAL subcellular localization is a regulated dynamic system. (**A**) (Top) LMB treatment induces relocalization of endogenous MAL (red) and MAL-GFP (green) in a stable NIH3T3 cell line. (Bottom) MAL-GFP, with functional elements (*1*, *3*) and RPEL motif (PFAM 02755) mutations (*7*) indicated. FCS, fetal calf serum. (**B**) Rho-actin signaling is required for MAL nuclear import. Cyt, cytoplasmic; C/N, pancellular; Nuc, nuclear. (100 cells per point; n = 3 independent experiments; error bars indicate SEM). wt, wild type. (**C**) MAL rapidly accumulates in the nucleus (at least 12 cells per condition; error bars, SD).

but blocked by CD, SwA, or jasplakinolide. Substitution of the highly conserved positions 1 or 2 of each RPEL (*7*) motif with alanine (123-1A, 123-2A mutations, Fig. 1A) greatly reduced complex formation. Both gel filtration (Fig. 2C; see fig. S6 for further information) and a less-stringent glutathione *S*-transferase (GST)–MAL pulldown assay (Fig. 2D and fig. S7) indicated that MAL-123-2A exhibited somewhat greater residual affinity for actin than MAL-123-1A did. We used fluorescence loss in photobleaching (FLIP) (*8*) to compare the effect of RPEL mutations on MAL export with that of actin-binding drugs. MAL-123-1A and MAL-123-2A, which are nuclear in unstimulated cells, exhibited low export rates essentially identical to that of the wild-type protein in the presence of drugs that disrupt actin binding (Figs. 2E and 3B and fig. S8). Actin overexpression did not alter the subcellular localization of MAL-123-1A-GFP but slightly increased its export rate in the FLIP assay, which was prevented by CD (Fig. 2E and fig. S8). Actin overexpression redistributed MAL-123-2A to the cytoplasm, consistent with its greater residual affinity for actin, precluding analysis by FLIP (fig. S8). These data show that interaction with actin is required for Crm1-dependent MAL nuclear export.

Although it induced MAL nuclear accumulation, LMB treatment activated neither an SRF reporter nor transcription of the MAL-dependent SRF target genes *Vcl*, *Srf*, *Cyr61*, and *Acta2* in the absence of serum or CD stimulation (Fig. 3A and fig. S9), suggesting that disruption of actin-MAL interaction is required for nuclear MAL to activate SRF; the MAL-independent SRF target

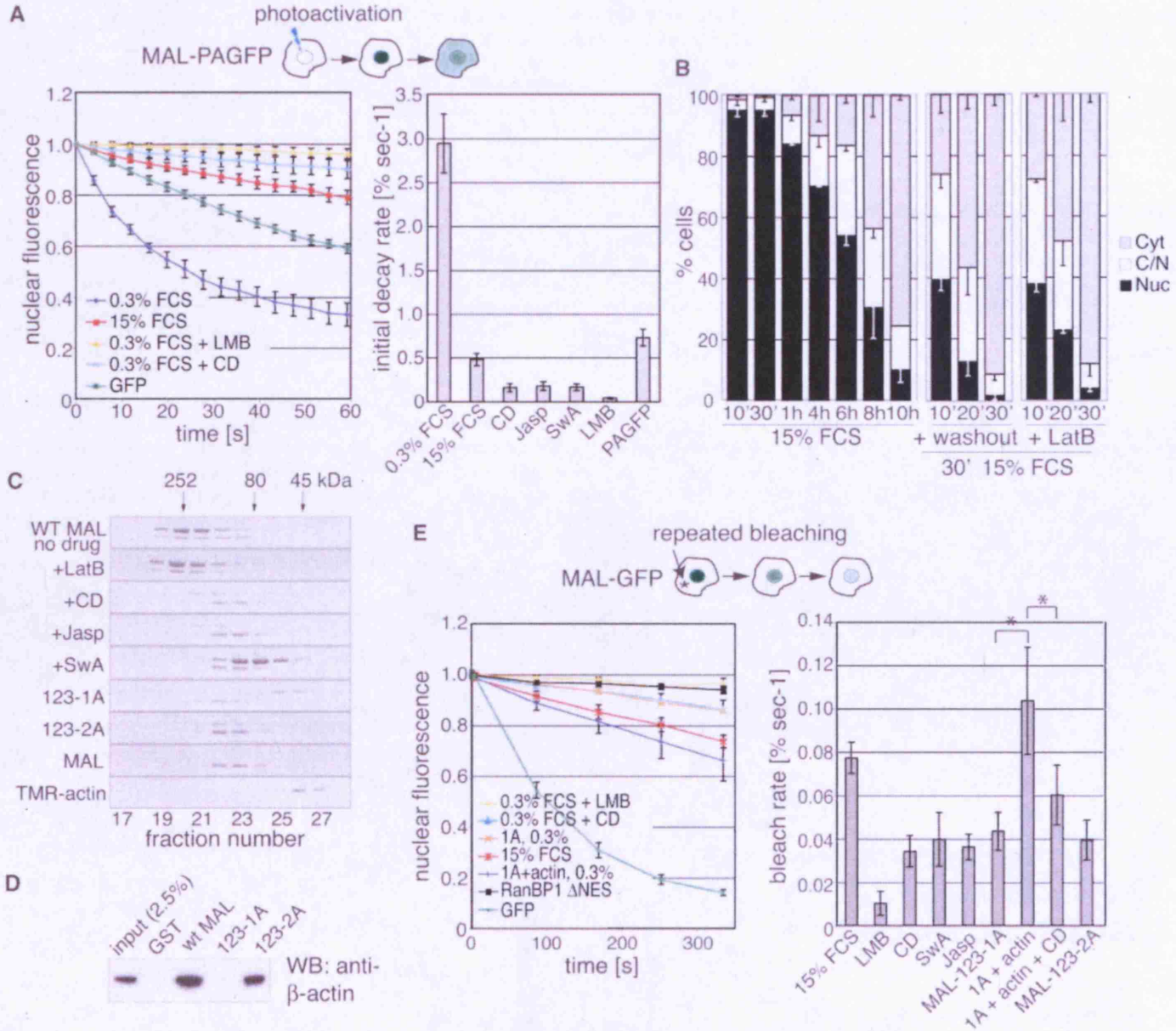

Fig. 2. Actin binding and nuclear export. (**A**) Serum stimulation decreases MAL nuclear export rate. Decay kinetics of nuclear fluorescence after MAL-PAGFP nuclear photoactivation (>10 cells per condition; error bars, SD). (**B**) Nuclear accumulation of MAL-GFP requires continuous signaling. MAL-GFP localization after serum stimulation with or without additional serum washout and LatB treatment. h, hours. $n = 3$; error bars, SEM. (**C**) Sensitivity of a stable MAL-actin complex to actin-binding drugs and RPEL mutations. RPEL domain was bound to G-actin, and apparent molecular masses analyzed by gel filtration. Note that SwA dimerizes actin. Further details are in figs. S6 and S7. (**D**) GST affinity precipitation analysis of MAL-actin interaction. WB, Western blot. GST baits are shown in fig. S7. (**E**) Nuclear export requires interaction with actin. Nuclear export rates of wild-type or mutant MAL-GFP proteins measured by FLIP assay, quantified as in (A) (Student's *t* test, $^*P < 0.05$). Error bars, SEM.

gene Egr1 was unaffected. Consistent with this, CD potentiated activation of an SRF reporter by overexpression of MAL-NLS, which contains a heterologous nuclear import signal and is substantially nuclear-localized, but not activation by the constitutively nuclear MAL-123-1A mutant, which cannot bind actin (Fig. 3B and figs. S8 and S10). MAL-NLS activity was also potentiated by nuclear co-expression of the wild-type MAL RPEL domain (MAL2-261-NLS) but not by its 123-1A derivative, suggesting that MAL-NLS is repressed by actin (Fig. 3B and fig. S10). Consistent with these data, we previously found that NLS-actin expression relocalizes MAL to the nucleus but represses SRF activity (*1*, *5*).

Together these results show that actin, or an actin-dependent cofactor, can repress MAL activity in the nucleus. This appears to occur at the level of gene activation rather than at DNA binding, because in chromatin immunoprecipitation experiments LMB treatment induced a substantial specific increase of MAL recruitment to its target genes *Vcl*, *Cyr61*, and *Srf*, comparable to that induced by CD or serum (Fig. 3C and fig. S11). Nuclear actin might recruit repressors to actin-MAL-SRF complexes or prevent recruitment of transcriptional co-activators. Previous studies have implicated actin in transcriptional control through regulation of RNA polymerases and chromatin-modification and -remodelling complexes (*11*, *12*).

To gain direct insight into actin-MAL interactions in cells, we exploited fluorescence resonance energy transfer (FRET), detected by fluorescence lifetime imaging (*13*). MAL-GFP was used as donor, and Cy3-labeled anti-myc, recognizing co-expressed Myc-actin, as acceptor. Under the assay conditions, the SRF reporter gene remained regulated (fig. S12). In unstimulated cells, FRET was readily detectable between MAL and actin, indicating that they physically interact (Fig. 4A and fig. S13). Treatment with CD reduced this interaction to background level, whereas LatB treatment increased it, consistent with biochemical and functional data (*1*, *6*). In contrast, no FRET was detected between MAL-123-1A and actin. Serum stimulation transiently reduced but did not abolish FRET between wild-type MAL and actin, which returned to its prestimulation level by 30 min (Fig. 4B). Similar results were observed with a MAL-GFP derivative lacking the B2 region, which remained cytoplasmic (Fig. 4B and fig. S1). In contrast, although LMB treatment induced MAL nuclear accumulation in unstimulated cells, it did not affect actin-MAL FRET, which could nevertheless be reduced to background level by CD treatment (Fig. 4A and fig. S12). In LMB-pretreated cells, serum stimulation also transiently reduced but did not abolish nuclear actin-MAL FRET, although recovery was slower than in untreated cells (Fig. 4B; see below). Thus, even when MAL is artificially confined to the nucleus, actin-MAL interaction can respond to serum-induced signals.

In serum-stimulated cells, the reduced but significant actin-MAL FRET, detectable when MAL is entirely nuclear, must reflect generation of a subpopulation of actin-free MAL or reduced actin-binding stoichiometry. It is likely that this reduced interaction at least initially reflects a rapid drop in the availability of G-actin, because total cellular deoxyribonuclease I (DNaseI)–stainable actin exhibited a similarly rapid decrease, followed by a slower recovery to prestimulation level (Fig. 4C). Actin thus interacts with MAL in both nucleus and cytoplasm, and serum-induced signals and actin-binding drugs change this interaction in a way consistent with the functional data. Together, these data provide direct support for our proposal that MAL activation reflects reduced MAL-actin interaction arising from depletion of the cellular G-actin pool (*1*).

We have demonstrated that actin regulates MAL activity at three levels: nuclear import,

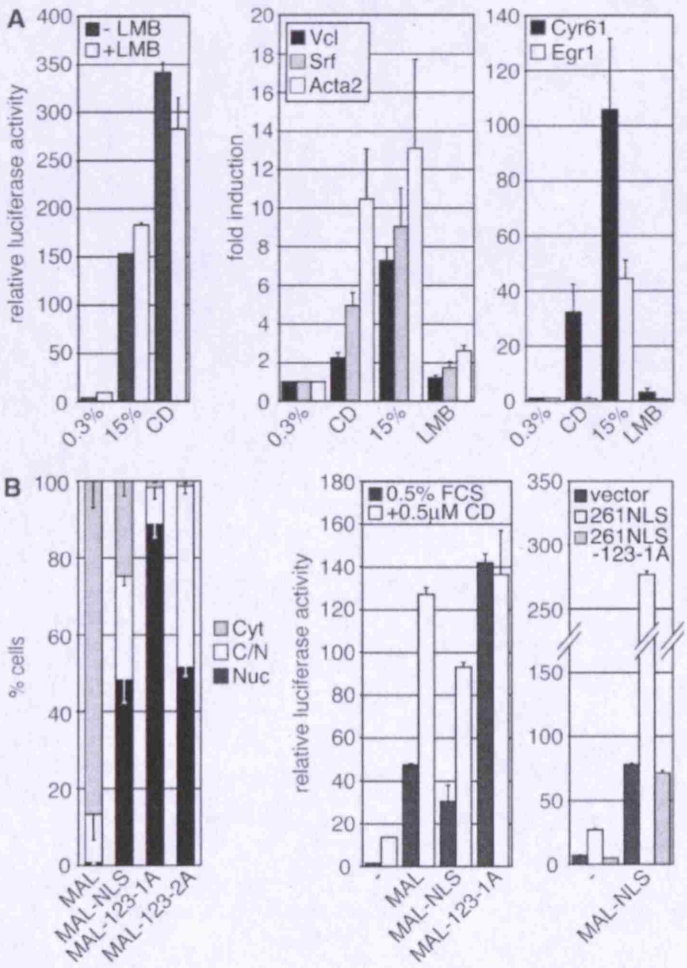

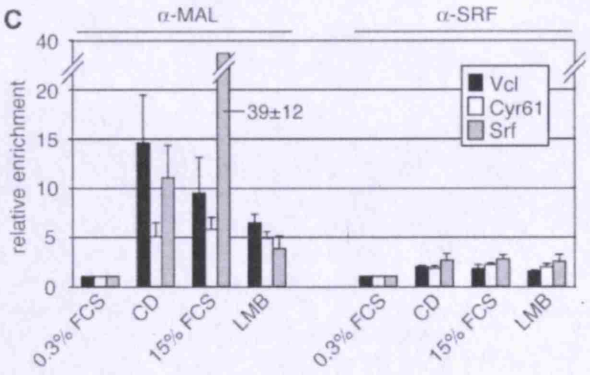

Fig. 3. Nuclear actin represses MAL activity. (**A**) LMB-induced MAL nuclear accumulation does not activate transcription of the SRF reporter (left) or endogenous SRF gene targets (right), measured by quantitative reverse transcription polymerase chain reaction (qRT-PCR). 0.3%, serum-starved cells; 15%, serum-starved cells. $n = 3$; error bars, SEM. (**B**) Disruption of actin binding allows SRF activation by nuclear MAL derivatives. (Left) Localization of MAL derivatives in serum-starved cells. (Right) Activation of MAL-NLS by CD or overexpressed nuclear RPEL domain (261NLS) after 2-day starvation. (**C**) MAL nuclear accumulation allows association with target genes, measured by qPCR analysis of chromatin immunoprecipitates. $n = 3$; error bars, SEM.

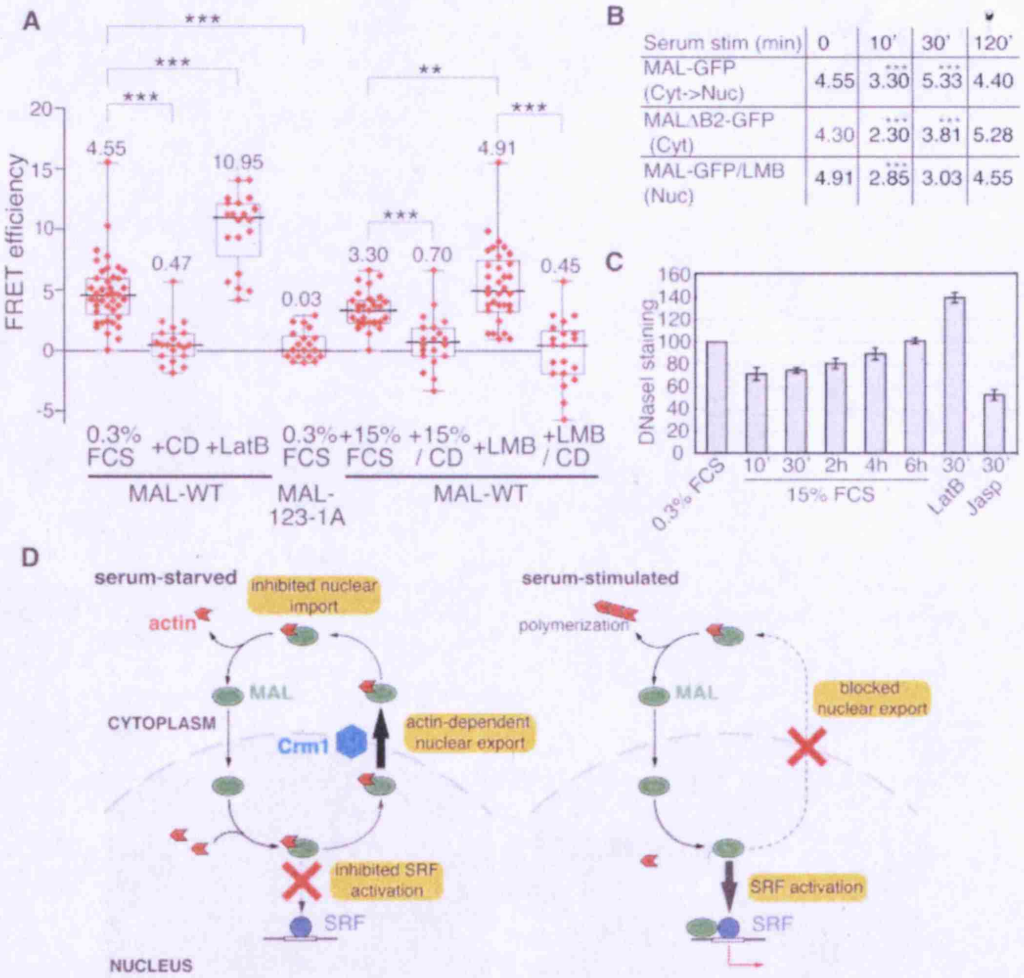

Fig. 4. MAL interacts with actin in both cytoplasm and nucleus. (**A**) Detection of MAL-actin interaction in vivo by FRET and FLIM. FRET efficiencies shown as box-and-whisker plots with median (>20 cells per condition; Mann-Whitney test, ***$P < 0.0005$; **$P < 0.005$). (**B**) Serum stimulation transiently decreases median FRET efficiency (***$P < 0.0005$ relative to previous point). (**C**) Serum stimulation transiently reduces DNAseI-stainable G-actin ($n = 3$; error bars, SD). (**D**) Multiple roles for actin in MAL regulation. In unstimulated cells, high export rates ensure MAL is mainly cytoplasmic, whereas nuclear actin prevents SRF activation. Upon stimulation, decreased export induces nuclear MAL accumulation, and diminished interaction with actin allows SRF activation. Proteins are shown as monomers for simplicity.

nuclear export, and activation of target gene transcription (Fig. 4D). Nuclear actin plays an especially important role in regulation of MAL localization and activity. MAL shuttles continuously between cytoplasm and nucleus, even in unstimulated cells. Serum-induced signals primarily control MAL subcellular localization by reducing the rate of its nuclear export, which requires actin binding and Crm1. However, our preliminary data indicate that recombinant RPEL domain–Crm1 interaction in vitro does not require actin. Perhaps actin instead facilitates interaction of Crm1-MAL complexes with nucleoporins (*14*). Defective nuclear export might explain the ability of some actin mutants to induce MAL nuclear accumulation even though they bind MAL effectively (*6*). Actin overexpression can also inhibit MAL nuclear import, perhaps by masking the B2 nuclear import signal, although this does not appear to play a major point of regulation in the cells studied here. It remains to be seen whether actin enters or exits the nucleus while bound to MAL.

Our data suggest that there must be communication between the cytoplasmic and nuclear actin pools. Other nuclear functions of actin may therefore be sensitive to extracellular signals. Actin-profilin complexes are subject to apparently constitutive export to the cytoplasm via interaction with exportin 6 (*15*), but the mechanisms of actin nuclear import remain obscure, and MAL itself may contribute. It will be interesting to assess how the dynamics of cytoplasmic-nuclear shuttling of actin impinge on MAL subcellular localization and activity in different cell types.

References and Notes

1. F. Miralles, G. Posern, A.-I. Zaromytidou, R. Treisman, *Cell* **113**, 329 (2003).
2. B. Cen *et al.*, *Mol. Cell. Biol.* **23**, 6597 (2003).
3. G. C. Pipes, E. E. Creemers, E. N. Olson, *Genes Dev.* **20**, 1545 (2006).
4. A. Sotiropoulos, D. Gineitis, J. Copeland, R. Treisman, *Cell* **98**, 159 (1999).
5. G. Posern, A. Sotiropoulos, R. Treisman, *Mol. Biol. Cell* **13**, 4167 (2002).
6. G. Posern, F. Miralles, S. Guettler, R. Treisman, *EMBO J.* **23**, 3973 (2004).
7. Single-letter abbreviations for the amino acid residues are as follows: A, Ala; D, Asp; E, Glu; G, Gly; H, His; I, Ile; K, Lys; L, Leu; M, Met; N, Asn; P, Pro; Q, Gln; R, Arg; S, Ser; T, Thr; V, Val; and Y, Tyr.
8. J. Lippincott-Schwartz, G. H. Patterson, *Science* **300**, 87 (2003).
9. G. H. Patterson, J. Lippincott-Schwartz, *Science* **297**, 1873 (2002).
10. B. Schmierer, C. S. Hill, *Mol. Cell. Biol.* **25**, 9845 (2005).
11. F. Miralles, N. Visa, *Curr. Opin. Cell Biol.* **18**, 261 (2006).
12. T. Pederson, U. Aebi, *Mol. Biol. Cell* **16**, 5055 (2005).
13. P. Wu, L. Brand, *Anal. Biochem.* **218**, 1 (1994).
14. D. Engelsma, R. Bernad, J. Calafat, M. Fornerod, *EMBO J.* **23**, 3643 (2004).
15. T. Stuven, E. Hartmann, D. Gorlich, *EMBO J.* **22**, 5928 (2003).

16. We thank P. Jordan and D. Zicha (London Research Institute Light Microscopy); V. Calleja and P. Leboucher for assistance with FRET analysis; B. Schmierer for advice on FLIP and PAGFP; C. Miralles for plasmids and preliminary observations; J. Lippincott-Schwartz and M. Fornerod for plasmids; and C. Hill, M. Way, and laboratory members for technical help, discussions, and comments on the manuscript. This work was funded by Cancer Research UK. M.K.V. is supported by a European Molecular Biology Organization long-term fellowship, and S.G., a fellow of the Studienstiftung des deutschen Volkes, by a Boehringer Ingelheim Fonds predoctoral scholarship. The authors have no conflicting financial interests.

Supporting Online Material

www.sciencemag.org/cgi/content/full/316/5832/1749/DC1
Materials and Methods
Figs. S1 to S13
References

9 February 2007; accepted 27 April 2007
10.1126/science.1141084